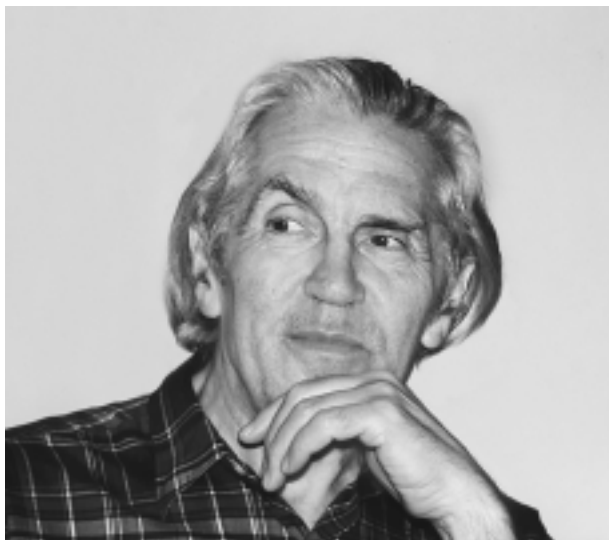


## 70th Birthday of Yuriĭ Antonovich Simonov



On June 6, 2004, Professor Yuriĭ Antonovich Simonov, a prominent theoretical physicist and head of the Laboratory of Theoretical Nuclear Physics at the Institute of Theoretical and Experimental Physics (ITEP, Moscow), celebrated his 70th birthday.

Upon graduating from the Moscow Engineering Physics Institute (MEPI) in 1958, Yu.A. Simonov was immediately invited to work at the Heat Engineering Laboratory (HEL, presently ITEP). At that time, the Theoretical Laboratory at HEL was headed by I.Ya. Pomeranchuk, whose lectures at MEPI, style of conducting scientific seminars, and selfless devotion to science had a profound impact on Simonov.

The independent scientific activities of Simonov began in 1957 with his undergraduate and graduate studies under the supervision of I. Yu. Kobzarev, which were devoted to exploring parity-violating processes. Unfortunately, interesting results that Simonov obtained for circular photon polarization in beta decay and muon capture before the appearance of the well-known articles by Lee and Yang (1957) and his graduation thesis “Neutron Polarization in Muon Capture by Nuclei” remained unpublished.

In 1958–1961, Simonov performed his postgraduate studies under the supervision of K.A. Ter-Martirosyan, who taught him to employ the most advanced formal methods in solving physics problems. At the same time, Simonov was always able to

relate complicated theoretical results to experiments; he was constantly in contact with experimentalists, following one of Pomeranchuk’s precepts: it is necessary to respect experimentalists. On the request of Academician A.I. Alikhanov, Simonov, still a postgraduate student, calculated the propagation of particles in experimental facilities and emulsions; in response to a proposal of Pomeranchuk, he delivered, in 1966, a course of lectures entitled “Methods for Determining Resonance Quantum Numbers”—this was a subject of paramount importance for experimentalists at that time (later on, these lectures were published in the journal *Soviet Physics—Uspekhi*).

Simonov is the author of more than 300 scientific articles, and he was the only author in almost all of the basic ones. By convention, Simonov’s scientific activity can be divided into four periods.

At the first stage, which lasted until 1965, his studies were devoted to the theory of elementary particles and high-energy processes. At that time, theorists gave preference to constructing the theory of elementary-particle interaction without invoking the field-theory formalism—they relied on the unitarity and analyticity of amplitudes. This was precisely the topic of the candidate’s dissertation of Simonov, where he obtained for the first time a new multiple integral representation of amplitudes that generalizes the known formulas of Mandelstam to the case of multileg diagrams. This new representation for amplitudes was derived on the basis of the Bergmann–Weyl integral relations and was highly estimated by mathematicians and physicists. The well-known article written together with A.P. Rudik and devoted to the so-called block method for determining singularities of Feynman diagrams (1963) also belongs to this line of research.

In the same years, Simonov took an active part in studying amplitudes for high-energy scattering by the Regge method. He was the first to calculate the trajectories of Regge poles within the formalism of the Bethe–Salpeter equation. Simonov showed that summation of the asymptotic expressions for Feynman diagrams determines, in the relevant trajectory, only the lowest term in  $g^2$ . The whole trajectory is determined by solving an exact dynamical equation that was derived by Simonov for this purpose in 1964. It is interesting to note that, 40 years later, Simonov,

together with American colleagues, generalized this equation to the case of deep-inelastic scattering in QCD.

In 1965, Simonov, together with Ter-Martirosyan, obtained an important result concerning the asymptotic behavior of particle-production amplitudes (*Nuclear Physics*, 1965), correcting, in that study, the errors of British authors (Polkinghorne and his colleagues). In particular, the amplitude for the production of an extra particle was found there. Among this group of studies, that which concerns the motion of singularities of partial-wave amplitudes in the  $j$  plane (1965) is worthy of particular note—it is thought to be one of the most beautiful in these realms. There, unitarity was used for the first time as a dynamical principle in constructing the theory of branch points in the complex plane of angular momentum. Later on, this principle was extensively used by V.N. Gribov, Pomeranchuk, and Ter-Martirosyan in their basic studies on Reggeon theory.

In 1965, Simonov lost a whole set of completed studies in bootstrap theory; taking this accident as an omen, he decided to switch to a new topic. This marked the beginning of the second stage of Simonov's scientific activity. In this period, Simonov focused on solving three- and many-body problems and on developing the theory of saturation of nuclear forces.

By that time, L.D. Faddeev had completed the derivation of integral equations for the three-body problem, relying on the idea of Skornyakov, Ter-Martirosyan, and Gribov that the characteristics of the three-body problem can be expressed in terms of the two-particle  $S$  matrix.

Simonov proposed an alternative method for solving the three-body problem within the Hamiltonian formalism. For three fermions, he constructed (1965) a complete system of hyperspherical functions, also known as  $K$  harmonics. In terms of these functions, the spectrum and the wave function for a multiparticle system can be found by solving one-dimensional differential equations or equations for partial waves [this was shown in a study performed together with A.M. Badalian (1966)]. In the course of subsequent investigations, it turned out that the method of expansion in hyperspherical functions can be successfully applied both to nuclear and atomic systems and to multi-quark systems. In the latter case, an accuracy higher than 1% in determining baryon masses can be achieved by retaining the lowest harmonic alone. The physical basis for the successful application of the method is that the lowest  $K$  harmonic ensures the smallest number of angular-momentum-excitation quanta, each successive quantum exceeding significantly the energy of a state.

In subsequent years (1967–1970), the method of  $K$  harmonics was successfully generalized to the case of a greater number of particles ( $N > 3$ ), and the binding energies and wave functions for four-nucleon systems were calculated for the first time in 1967. The method of  $K$  harmonics and its modifications were widely used by the groups of A.I. Baz' and Ya.A. Smorodinsky (Moscow), G.F. Filippov (Kiev), V. Vanagas (Vilnius), and R.I. Jibuti (Tbilisi) to calculate the features of complex nuclei.

A general investigation of nuclei and the calculation of their total binding energy revealed an unexpected result: it turned out that the nucleon–nucleon potentials used (as a matter of fact, almost all local potentials) lead to the collapse of nuclei. Together with Calogero, Simonov formulated (1971) necessary and sufficient conditions for stability of nuclei (saturation of nuclear forces). This gave impetus to studying exotic nuclei and to discovering scissor excitations in nuclei (F. Palumbo, 1972). At this stage, it became clear that the saturation of nuclear forces cannot be understood without introducing the internal (quark) structure of nucleons.

The third period (1973–1981) of Simonov's studies was devoted to exploring rigorous relations for multiparticle amplitudes on the basis of unitarity (including three-particle unitarity) and analyticity, which is of paramount importance for multichannel processes. A general theory of multichannel resonances was constructed and applied to various reactions, including  $N\bar{N}$  scattering and annihilation. The discovery of channel-coupling resonances, which arise in the presence of a strong channel coupling, was one of the main results here. These resonances manifest themselves as peaks at the threshold or in the threshold region and may be of importance in analyzing new states recently discovered in the  $D_s^*(0^+, 2317)$  and  $D_s^*(1^+, 2460)$  systems near the  $DK$  and  $D^*K$  thresholds, respectively.

In studying the dynamics of multi-quark bags, Simonov showed in the same period that the puzzling repulsive core in  $NN$  interaction admits reasonable explanation in terms of a six-quark bag, and this led to a complete pattern of phase shifts for  $NN$  scattering (1980). The proposed composite-bag model was then generalized to other hadron–hadron systems and provided a good explanation of experimental data on nucleon interactions with tritium and  $^3\text{He}$ .

Simultaneously, Simonov studied solitons—in particular, the conditions of their stability and quantization. For multidimensional solitons, the conditions of stability were formulated as a generalization of the Derrick theorem (1979). The numerical calculations that Simonov performed together with J. Tjon and L.P. Kok from the Netherlands and A.I. Veselov from ITEP to study soliton excitations and decay in two

and three dimensions (1981) have so far remained second to none.

Since 1981, QCD has become the main region of Simonov's interests. From the outset, he sought to obtain a gauge-invariant formulation both for the Hamiltonian in gluodynamics and for the equations of motion (this seemed impossible at that time). In a study of 1985, Simonov revealed that  $SU(2)$  gluodynamics is similar to a system of interacting rotors in two spaces simultaneously (ordinary and color spaces), solutions in the form of instantons and monopoles corresponding to a symmetric rotor. However, this and the next study, which was devoted to solutions referred to as color-flip solitons, convinced Simonov that the approach based on the use of local Hamiltonians and classical solutions is unable to explain the confinement phenomenon and the structure of the QCD vacuum. In quest of vacuum configurations responsible for confinement, Simonov explored the domain structure of the vacuum, ensembles of dions as instanton chains, and other configurations. Gradually, it became clear to him that only a stochastic pattern of the vacuum can ensure confinement.

However, the heuristic pattern of a stochastic vacuum lacked an adequate formalism. At the same time, Professor H. Dosch from Heidelberg proposed employing a cluster expansion within a simple Abelian model (for the Green's function in averaging over vacuum configurations). An accidental encounter of Simonov and Dosch in Protvino in 1987 resulted in writing the well-known article of the two authors (1988) and in developing the method presently known as the method of vacuum correlation functions.

The idea of a stochastic vacuum changed entirely the pattern of strong interactions and is gradually becoming a basis for modern concepts of the QCD vacuum and hadrons. As far back as 1986, Simonov showed that stochastic fields in a vacuum lead to a linear confinement. A mathematically rigorous proof of this statement was given later in an article written together with Dosch. In this connection, there immediately arose the question of whether it is possible to obtain confinement on the basis of ensembles of classical solutions. Instantons did not lead to confinement, but it remained unclear why this was so. In 1989, Simonov showed that, for the confinement phenomenon to occur, it is necessary that the members of the ensemble have a nonintegral topological charge since integral charges cancel. This ruled out instantons. After that, Simonov considered other configurations (magnetic monopoles and dions) as candidates for this role.

At the Enrico Fermi School in Varenna (1994), Simonov considered in detail dions. The collaboration of ITEP with German physicists from Berlin

(M. Müller-Preussker, M. Ilgenfritz, and D. Ebert) was specially organized for developing this idea. After a few years, it became clear that, because of the presence of long-range forces, dions are strongly distorted by interaction at zero temperature, but they, as well as more complicated configurations, survive in the vacuum and become important at high temperatures. Searches for extraordinary field configurations that would ensure confinement (they are manifested on a lattice and are also explained analytically) are being continued at present (A.I. Veselov, B.V. Martemyanov, and others).

It turned out that the QCD vacuum is populated predominantly by quantum configurations that ensure confinement. Their specific form was found later (they are referred to as gluelumps). They were discovered analytically by Simonov in 2000 and were studied on a lattice earlier.

As a matter of fact, knowledge of the vacuum structure paved the way to constructing the theory of hadrons and to calculating a wide variety of processes.

First of all, it became possible to understand how the deconfining phase transition occurs at finite temperatures and to calculate the transition temperature (1993). Moreover, it was shown that, even under deconfining conditions, color-magnetic fields remain unchanged—only color-electric fields vanish; later on, this effect was confirmed by lattice calculations (earlier, this topic was discussed in the Varenna lectures). Investigations of QCD at nonzero temperatures, which were initiated by Simonov, together with Dosch and H. Pirner, were continued and significantly advanced by N.O. Agasian and his colleagues.

The development of rigorous methods for calculating various nonperturbative effects within the method of vacuum correlation functions was the most important step in constructing the theory of hadrons. A serious obstacle had to be overcome on this path—there were no relativistic gauge-invariant methods of this kind, and it was necessary to create a new formalism. Fortunately, it became possible to formulate a method that combined the proper-time formalism and the formalism of path integrals, which was long ago proposed by Feynman for QED, but which was nowhere used. This revived method, which was called the Fock–Feynman–Schwinger method, is commonly accepted at the present time and is convenient in dealing with gauge fields [two large review articles devoted to the Fock–Feynman–Schwinger method were published by Simonov and Tjon in the journal *Annals of Physics* (1993, 2002)].

The use of the Fock–Feynman–Schwinger representation made it possible to construct relativistic Hamiltonians for hadrons and to calculate, with the aid of these Hamiltonians, the meson and baryon

masses. In 1989, the Regge trajectories for mesons, baryons, and glueballs were obtained analytically within QCD for the first time. However, the slope calculated for the trajectories by using the simplified form of Hamiltonians proved to be different from the string result; in order to remove this discrepancy, Simonov, together with A.Yu. Dubin and A.B. Kaidalov, performed a fundamental investigation (1993), where the authors rigorously took into account string rotation and obtained a correct and universal slope of the trajectories.

It was also of importance to understand how quarks and gluons develop a constituent mass (1989). This mass is generated by quark motion and can be expressed explicitly in terms of the string tension  $\sigma$ . Thereby, the quark model acquired a fundamental basis: a correct slope of Regge trajectories arose and the constituent mass ceased to be an adjustable parameter.

The clarification of the meaning of an arbitrary constant  $C$  that is usually introduced in the hadron mass (or potential) became the next step. In 2001, Simonov showed that this constant is due to the interaction of the quark and antiquark color-magnetic moments with a nonperturbative vacuum field and can be calculated analytically: this constant is negative and is expressed in terms of the string tension.

Within the method of vacuum correlation functions, spin-dependent nonperturbative potentials were calculated by Simonov in 1989 and, later, in 1997 (together with Badalian). This made it possible to perform precision calculations of spin-dependent splitting in mesons and glueballs.

However, QCD is a highly nontrivial field of science, and it became clear before long that, without understanding how the confinement phenomenon affects ordinary perturbative gluon exchange, it would be impossible to make further steps in analyzing hadronic processes and spectroscopy. In 1993, Simonov showed that nonperturbative effects (existence of hybrids) remove the divergence of the strong coupling constant  $\alpha_s$ , which freezes in the infrared region (lectures in Schladming, 1995). Thereby, the freezing effect, which had been merely postulated before that in phenomenological calculations, was explained. The freezing of  $\alpha_s$  also resolves the so-called Linde paradox of the divergence of perturbation-theory series in the deconfining region of QCD. In the Varenna lectures of 1996, Simonov showed that higher loops of the perturbation-theory series do not diverge owing to the presence of nonperturbative color-magnetic fields.

The new understanding of gluon exchanges made it possible to go over to precision analytic calculations of the spectrum and properties of hadrons and to a comparison of the results of such calculations with

experimental data and data from lattice calculations. This new quark theory of hadrons is formulated at an ab initio level—that is, it is derived from the QCD Lagrangian with the aid of vacuum correlation functions. Therefore, it contains a minimal number of parameters: in addition to current quark masses, the theory involves the string tension  $\sigma$  and the QCD scale parameter  $\Lambda$ . All of these parameters are universal and are fixed on the basis of independent results—in particular, in nonperturbative processes and by the slope of Regge trajectories.

The most consistent calculations of the spectra and splittings in the meson sector (for light mesons and heavy quarkonia) were performed by the group of Badalian in the period between 1999 and 2004, the achieved accuracy of the calculations being about 1%. The spectrum of glueballs and the Pomeron trajectory were calculated together with Kaidalov in 1999. The group of Yu.S. Kalashnikova (2001) calculated the spectra of hybrids, attaining good agreement with the results of lattice calculations. Thus, an efficient method for calculating nonperturbative phenomena was developed; previously, only in a limited number of specific cases had it been possible to analyze such phenomena by using QCD sum rules.

Further, there appeared prospects for studying nonperturbative contributions and corrections in processes for which use had previously been made only of perturbative QCD—that is, in the region of high energies and high  $Q^2$ —and in the operator-product expansion. In particular, nonperturbative corrections to the eikonal approximation were obtained (1999) and a nonperturbative description of jet production in the region of small angles was constructed (2002, a review article in the journal *Annals of Physics*). A crucial role of hybrids in some reactions at high energies and in deep-inelastic scattering was established in recent studies of 2003.

Simonov devoted more than 15 years of activity to studying spontaneous chiral-symmetry breaking, yet another problem of great importance in QCD. In all of the existing models—for example, in the instanton model—spontaneous chiral-symmetry breaking has nothing to do with the confinement phenomenon; at the same time, numerous lattice calculations demonstrate that the effect of spontaneous chiral-symmetry breaking disappears together with confinement at the same temperature. Simonov was able to derive an effective Lagrangian from QCD and to establish the relationship between the confinement phenomenon and spontaneous chiral-symmetry breaking. This made it possible to calculate the parameters of spontaneous chiral-symmetry breaking in terms of the string tension. Thereby, it was proven that both phenomena disappear at the same temperature.

Together with V.I. Shevchenko (2002), Simonov gave the first answers to the questions concerning the structure of operator-product expansion (which is a tool of paramount importance in QCD), the parameter of the expansion, and its convergence.

Since 1968, Simonov has actively cooperated with foreign colleagues, including Calogero, Palumbo, and A. Di Giacomo from Italy; Tjon and Bakker from the Netherlands; Dosch and Pirner from Germany; and Gross from the United States.

Twelve theoretical physicists earned their candidate's degrees under Simonov's tutelage. His disciples include I.M. Narodetsky, M.I. Polikarpov, and N.O. Agasian, who are doctors of science.

Simonov is the author of a number of review articles covering problems of topical interest. In 1991,

he was invited to deliver the Kramers Lectures at the University of Utrecht. He was awarded the International Humboldt Prize in 1992 and the First Prize of the 1995 MAIK Nauka Contest. In 2001 and 2002, Simonov delivered a few cycles of lectures at the Jefferson Laboratory (United States). He also lectured at various schools in physics, including those in Varenna (1995), Schladming (1996), Trento (1996), Bukov (1997), Lisbon (1999), and Prague (2000).

At the present time, Simonov continues actively working in the realms of QCD.

The editorial board of the journal *Physics of Atomic Nuclei* heartily congratulates Yu.A. Simonov on the occasion of his birthday and wish him good health and many years of creative activity.

# On the Nature and the Order of the Deconfining Transition in QCD\*

A. Di Giacomo

Dipartimento di Fisica dell'Università Pisa and INFN Sezione di Pisa, Italy

Received May 13, 2004

**Abstract**—The determination of the parameters of the deconfining transition in  $N_f = 2$  QCD and its relevance to the understanding of the mechanism of color confinement are discussed. © 2005 Pleiades Publishing, Inc.

*In honor of Yu.A. Simonov  
on his seventieth birthday*

## 1. INTRODUCTION

Understanding the mechanism by which QCD confines colored particles is one of the most fundamental and challenging problems in field theory [1, 2].

Experiments aimed at detecting the existence of a deconfining transition at high temperature by colliding heavy ions have not yet produced a definite answer [3]. Up to now, the deconfining transition has only been observed in numerical simulations of QCD on a lattice [4]. Identifying a signal of deconfinement is far from trivial in experiments, and it is not easy in lattice simulations either. To be rigorous, confinement means absence of colored particles in asymptotic states. Of course, one cannot check confinement by looking at all asymptotic states. In the quenched approximation, in which dynamical quark loops are neglected, one looks at the static potential acting between a heavy  $Q\bar{Q}$  pair. The criterion for confinement is then the existence of a string tension, which means a linear behavior at large distances

$$V(r) = \sigma r. \quad (1)$$

The static potential is measured on the lattice either in terms of the Wilson loop (parallel transport along a closed path) or, equivalently, in terms of the correlator of Polyakov lines (parallel transport along the time axis). For a Wilson loop of extension  $t$  in the time direction and  $r$  in space,

$$W(r, t) \underset{r, t \rightarrow \infty}{\propto} \exp[-tV(r)]. \quad (2)$$

Confinement Eq. (1) implies the so-called area law

$$W(r, t) \propto \exp[-\sigma r t]; \quad (3)$$

$r, t \rightarrow \infty$  means that they are large compared to the correlation length. The correlator of two Polyakov lines can be written by use of the cluster property,

$$\langle L(r)L^\dagger(0) \rangle \underset{r \rightarrow \infty}{\simeq} C \exp[-\sigma r/T] + |\langle L \rangle|^2. \quad (4)$$

On the other hand,

$$V(r) \simeq -T \ln \langle L(r)L^\dagger(0) \rangle. \quad (5)$$

It is found by numerical simulations that a critical temperature  $T_c$  exists such that, for  $T < T_c$ ,  $\langle L \rangle = 0$ . From Eqs. (4) and (5), confinement Eq. (1) then follows. For  $T > T_c$ ,  $\langle L \rangle \neq 0$  and

$$V(r) \underset{r, t \rightarrow \infty}{\rightarrow} \text{const.} \quad (6)$$

For quenched  $SU(3)$ ,  $T_c/\sqrt{\sigma} \approx 0.65$  [5]. A deconfining phase transition exists at  $T_c \simeq 270$  MeV and the Polyakov line  $\langle L \rangle$  is the order parameter. The symmetry involved is  $Z_3$ , which is broken at  $T > T_c$ , and the transition is order–disorder. Some problems can arise in the continuum limit with the definition [6] of the order parameter  $\langle L \rangle$ , but the main idea looks sound.

The situation is less clear in the more realistic case of full QCD, including dynamical quarks. There,  $Z_3$  is not a symmetry anyhow, being broken by the coupling to the quarks. Moreover, the potential at large distances is not expected to grow with  $r$ , due to the conversion of the potential energy into light  $q\bar{q}$  pairs (string breaking) [7]. One needs then an alternative criterion for confinement, which, however, is not known.

A phase transition is expected anyhow at low quark masses from the low-temperature phase, in which chiral symmetry is spontaneously broken, to a phase in which it is restored: the order parameter for this transition is the chiral condensate  $\langle \bar{\psi}\psi \rangle$ . This transition is indeed observed on the lattice at  $T_c \approx 170$  MeV. A priori restoration of chiral symmetry is

\*This article was submitted by the author in English.

not the same as deconfinement, even if it is physically understandable, e.g., by thinking of a bag model, that confinement can imply chiral symmetry breaking. In the absence of a criterion for confinement, the question of whether chiral and deconfining transitions coincide cannot even be asked. A third symmetry exists, the axial  $U(1)$ , which is broken at low  $T$  as an effect of the anomaly, and it is also expected to be restored at high temperature. In principle, the corresponding transition temperature could be different from that of the other two transitions.

An analysis can be done of the chiral transition based on symmetry arguments and on renormalization group techniques [8]. If the assumption is made that the relevant degrees of freedom at the transition are the pseudoscalar particles, an effective Lagrangian can be written on the basis of symmetry and scale invariance, which describes the density of free energy around the chiral point. For  $N_f \geq 3$ , no infrared stable fixed point exists, so that the transition is expected to be first-order.  $N_f = 2$  is a special case, and the transition can be either weak first-order or second-order. If it is first-order, it is weak first-order also at  $m_q \neq 0$ ; if it is second-order, the transition at  $m_q \neq 0$  is a crossover [8]. What the case is can be investigated by numerical simulations on the lattice, even if up to now [9–11] the results have been rather elusive.

This issue is very important for the understanding of the deconfining phase transition. On the basis of the quenched case mentioned above, the deconfining transition should be order–disorder, and a genuine order parameter should exist labeling the two phases.  $N_c \rightarrow \infty$  arguments suggest, indeed, that the symmetry involved, as well as the mechanism of confinement, should be the same for quenched and unquenched and  $N_c$  independent. If for  $N_f = 2$  the chiral transition is second-order, then the transition for  $m_q \neq 0$  is a crossover, and the deconfining transition is not order–disorder. A first-order chiral transition would instead be consistent with order–disorder and possibly be such up to  $m_q = \infty$ , which is the quenched case.

The order of the transition can be investigated by looking at the volume dependence of the specific heat in numerical simulations, by a technique known as finite size scaling (see Section 2 below). The free-energy density around the phase transition is determined by symmetry arguments [12] up to unknown numerical coefficients in terms of the order parameter. The (pseudo)critical indices determined by looking at the susceptibility of the order parameter must agree with the determination made by looking at the specific heat. Such an agreement is needed to legitimate the choice of the order parameter.

An order parameter  $\langle \mu \rangle$  has been developed and tested [13–15], based on the working hypothesis that the mechanism of confinement is dual superconductivity of the vacuum [2].  $\langle \mu \rangle$  is the vacuum expectation value of an operator  $\mu$  carrying magnetic charge and, unless the Polyakov loop or the chiral condensate is well defined, is independent of  $N_c$ ,  $N_f$  even in the continuum limit.

The critical indices can be investigated by measuring susceptibilities involving  $\mu$ , in particular, the quantity  $\rho = d \ln \langle \mu \rangle / d\tau$ , with  $\tau$  being the reduced temperature

$$\tau = 1 - T/T_c. \quad (7)$$

If they agree with the determination made by use of the specific heat, an additional legitimation results for the order parameter and for the mechanism of confinement by dual superconductivity. Confinement will then be defined in terms of an appropriate symmetry, and the question of whether the deconfining transition and the chiral transitions occur at the same temperature becomes meaningful.

In Section 2, we shall discuss new results on the above issues [16, 17]. In Section 3, we draw some conclusions.

## 2. LATTICE RESULTS AND FINITE SIZE SCALING ANALYSIS

The theory of finite size scaling for higher order and weak first-order phase transitions is based on renormalization group arguments [18, 19], which are expected to hold when, by approaching the transition, the correlation lengths become much larger than the lattice spacing. It allows one to extrapolate to infinite volume results obtained at finite volumes. The extrapolation depends on the (pseudo)critical indices, which can then be determined from the volume dependence, and with them on the order and the universality class of the transition.

The relevant quantities, which are related to derivatives of the free energy and hence to the order of the transition, are the susceptibilities. In the following, we shall consider the susceptibility of the chiral order parameter

$$\chi = \frac{T}{V} \frac{\partial^2}{\partial m^2} \ln Z, \quad (8)$$

the specific heat

$$c_V = \frac{1}{VT^2} \frac{\partial^2}{\partial (1/T)^2} \ln Z, \quad (9)$$

and

$$\rho = \frac{\partial}{\partial \tau} \ln \langle \mu \rangle. \quad (10)$$

The (pseudo)critical indices for weak first-order and second-order  $O(4)$  phase transition

	$\alpha$	$\gamma$	$\nu$	$y_h$
1st order	1	1	1/3	3
$O(4)$ 2nd order	-0.25(1)	1.47(1)	0.75(1)	2.49(1)

All these susceptibilities will depend on the parameters which describe the system, i.e.,  $\beta = 2N_c/g^2$ , with  $g$  being the gauge coupling, and  $ma$ , the bare quark mass in units of the inverse lattice spacing.

The simulation is made on a lattice  $N_t N_s^3$ ,  $N_t \ll N_s$ , of extension  $N_t$  spacings along the time axis and  $N_s$  along the three spatial directions, with periodic boundary conditions (b.c.) in time for bosons and antiperiodic b.c. for fermions.

The temperature is the inverse of the time extension, or

$$T = \frac{1}{N_t a(\beta, ma)}, \quad (11)$$

$a(\beta, ma)$  being the lattice spacing in physical units.

All the susceptibilities as a function of the temperature will have peaks at  $T_c$ , which diverge as the volume  $V \rightarrow \infty$  with a power depending on the order of the transition, specifically on the critical indices. In the usual notation of statistical mechanics, denoting by  $L$  the spatial size of the system,

$$\chi = L^{\gamma/\nu} \Phi_\chi(\tau L^{1/\nu}, mL^{y_h}), \quad (12)$$

$$c_V = c_V^0 + L^{\alpha/\nu} \Phi_c(\tau L^{1/\nu}, mL^{y_h}), \quad (13)$$

$$\rho = L^{1/\nu} \Phi_\mu(\tau L^{1/\nu}, mL^{y_h}). \quad (14)$$

$$\text{Since } T = \frac{1}{N_t a(\beta, ma)},$$

$$\tau = 1 - \frac{a(\beta_c, 0)}{a(\beta, ma)}. \quad (15)$$

In the vicinity of the chiral point, one can expand in powers of  $\beta_c - \beta$  and of  $ma$ , obtaining

$$\tau \propto \beta_c - \beta + Kma \quad (16)$$

with

$$K = - \frac{\partial \ln a}{\partial (ma)} \bigg/ \frac{\partial \ln a}{\partial \beta} \bigg|_{\beta=\beta_c}. \quad (17)$$

In the quenched case, the last term in Eq. (16) is absent.

When the volume of the system becomes large at fixed  $\tau L^{1/\nu}$ , the susceptibilities will certainly tend to a finite limit if the transition is second-order and the free energy is continuous and finite in the neighborhood

of the chiral point. This implies that the powers of  $L$  in front of the susceptibility Eqs. (12)–(14) have to be eliminated by the dependence on  $mL^{y_h}$ , and this means for the three susceptibilities

$$\chi \propto m^{-\gamma/\nu y_h} F_\chi(\tau L^{1/\nu}), \quad (18)$$

$$c_V - c_V^0 \propto m^{-\alpha/\nu y_h} F_c(\tau L^{1/\nu}), \quad (19)$$

$$\rho \propto m^{-1/\nu y_h} F_\rho(\tau L^{1/\nu}). \quad (20)$$

If the transition is weak first-order, the system will behave in the same way for intermediate values of  $L$ , smaller than or equal to the critical correlation length, apart from the different value of the critical indices.

Equations (18)–(20) imply that the maxima of the susceptibilities with respect to  $\tau$  lie on the line of the plane  $(\beta, ma)$  of equation

$$\tau L^{1/\nu} = C, \quad (21)$$

with  $C$  being a constant, or by use of Eq. (16),

$$\beta_c - \beta + Kma - \frac{C}{L^{1/\nu}} = 0. \quad (22)$$

This relation can be tested against the lattice data to determine the value of  $\nu$ . We will discuss the result in the following.

Equations (18)–(20) also imply that the height of the maximum of the susceptibilities is volume independent, whatever the order of the transition, in the limits of the regime in which these equations are obeyed when the transition is first-order.

For a second-order transition, the result is valid for any volume and fits the idea that the transition line in the plane  $(\beta, ma)$  is a crossover.

For a first-order transition, if we cross the transition line at fixed  $ma$ , we expect a behavior typical of a first-order transition, namely, a growth of the peaks of the susceptibilities proportional to the volume. Indeed, for a first-order transition,  $\alpha = \gamma = 1$ ,  $\nu = 1/d = 1/3$ . This behavior will be visible when  $L$  becomes larger than the critical correlation length, and together with it the typical two-peak distribution of the internal energy will appear.

Moreover, if we keep  $mL^{y_h}$  constant, Eqs. (12)–(14) require that the maximum of the peaks again be proportional to a well-defined power of  $L$  depending on the nature of the transition.

The details of the simulations will be reported elsewhere [16, 17]. Here, we only summarize the results.

As a strategy, we assume the critical indices expected for a second-order  $O(4)$  phase transition and, as alternative, those of a first-order transition, and we investigate whether the data are consistent with either of them. A measure of the agreement is the value of  $\chi^2/\text{dof}$ .

In the table, we recall values of the critical indices for the two cases.

We investigate the following:

(i) The position of the peak as a function of mass and volume, which scales according to Eq. (22). The constant  $C$  is compatible with zero within the errors, and there is no further information.

(ii) The peak values of the susceptibilities. They all occur on the same line, within errors. The height of the peak is volume independent at fixed  $ma$  for moderate values of the volume and proportional to an appropriate power of  $(ma)$  Eqs. (18)–(20), which depends on the nature of the transition. The  $\chi^2/\text{dof}$  is compatible with 1 for a first-order transition and much worse typically ( $\chi^2/\text{dof} \approx 10$ ) for  $O(4)$  second-order.

(iii) For low values of  $m$  (e.g.,  $ma = 0.0135$ ), as the volume increases further, a growth of the height of the peak is observed and some sign of bistability is seen in the time histories of the energy density. An increase in the height of the peak by a factor of  $\approx 2$  is observed in going from  $16^3$  to  $32^3$ . This means that there is a transition, and not a crossover. At higher values of  $ma$ , the transition looks weaker and we were not yet able to reach a large enough volume to see a bistability.

(iv) The behavior with respect to volume at fixed  $mL^{y_h}$  is consistent with a first-order transition and disfavors a second-order one: typically,  $\chi^2/\text{dof} \approx 1$  for first-order, and  $\chi^2/\text{dof} \approx 10$  for second-order  $O(4)$ .

Previous investigations of the same system were made on rather small volumes [9–11] or in a less systematic way, and the results were admittedly inconclusive, although a slight psychological preference appeared for a second-order transition. Numerically, our determinations are consistent with the previous ones when done at the same values of the parameters. The details of the simulations and the comparison with previous work will be presented elsewhere [16, 17].

### 3. DISCUSSION

We have obtained substantial preliminary evidence that the chiral transition for  $N_f = 2$  QCD is first-order. This makes the deconfining transition consistent with an order–disorder transition. The disorder parameter  $\langle \mu \rangle$  detecting dual superconductivity of the vacuum provides a determination of the critical indices consistent with the one based on the specific heat, and a transition line consistent with the other

susceptibilities. It can then be used as an order parameter for confinement. The deconfining transition and the chiral transition occur at the same  $T$ . A careful numerical study of the  $U(1)$  axial anomaly across the deconfining transition is under way and will provide a check of the assumption made in [8] that the relevant degrees of freedom at the chiral transition are the pseudoscalar goldstone particles.

### ACKNOWLEDGMENTS

I wish to thank all my collaborators, M. D’Elia, B. Lucini, G. Paffuti, and C. Pica, who contributed substantially to the results presented. Many ideas and motivations also come from discussions and collaboration with Yu.A. Simonov, to whom this paper is dedicated with deep friendship on the occasion of his 70th birthday.

### REFERENCES

1. G. ’t Hooft, Nucl. Phys. B **138**, 1 (1978).
2. G. ’t Hooft, Nucl. Phys. B **190**, 455 (1981).
3. *Proceedings of the International Conference “Quark Matter 2002”*, Nucl. Phys. A **715** (2003).
4. For a review see, e.g., F. Karsch, Nucl. Phys. B (Proc. Suppl.) **83–84**, 14 (2000).
5. Y. Iwasaki *et al.*, Phys. Rev. D **56**, 151 (1997).
6. O. Kaczmarek, F. Karsch, P. Petreczky, and F. Zantow, Phys. Lett. B **543**, 41 (2002).
7. See, e.g., C. De Tar, O. Kaczmarek, F. Karsch, and E. Laerman, Phys. Rev. D **59**, 031501 (1999) and references therein.
8. R. D. Pisarsky and F. Wilczek, Phys. Rev. D **29**, 338 (1984).
9. F. Karsch and E. Laerman, Phys. Rev. D **50**, 6954 (1994).
10. S. Aoki *et al.* (JLQCD Collab.), Phys. Rev. D **57**, 3910 (1998).
11. C. Bernard *et al.*, Phys. Rev. D **46**, 4741 (1992).
12. V. L. Ginzburg and L. D. Landau, Zh. Éksp. Teor. Fiz. **20**, 1064 (1950).
13. L. Del Debbio, A. Di Giacomo, G. Paffuti, and G. Pieri, Phys. Lett. B **355**, 255 (1995).
14. A. Di Giacomo, B. Lucini, L. Montesi, and G. Paffuti, Phys. Rev. D **61**, 034503, 034504 (2000).
15. J. M. Carmona, L. Del Debbio, M. D’Elia, *et al.*, Phys. Rev. D **66**, 011503 (2002).
16. M. D’Elia, A. Di Giacomo, and C. Pica, in preparation.
17. M. D’Elia, A. Di Giacomo, B. Lucini, *et al.*, in preparation.
18. M. E. Fischer and M. N. Barber, Phys. Rev. Lett. **28**, 1526 (1972).
19. E. Brezin, J. Phys. (Paris) **43**, 15 (1982).

## Confinement in the Abelian–Higgs-Type Theories: String Picture and Field Correlators\*

D. V. Antonov<sup>1)</sup> and D. Ebert\*\*

*Institute of Physics, Humboldt University of Berlin, Germany*

Received May 13, 2004; in final form, August 12, 2004

**Abstract**—Field correlators and the string representation are used as two complementary approaches for the description of confinement in the  $SU(N)$ -inspired dual Abelian–Higgs-type model. In the London limit of the simplest,  $SU(2)$ -inspired, model, bilocal electric field-strength correlators have been derived accounting for the contributions to these averages produced by closed dual strings. The Debye screening in the plasma of such strings yields a novel long-range interaction between points lying on the contour of the Wilson loop. This interaction generates a Lüscher-type term, even when one restricts oneself to the minimal surface, as is usually done in the bilocal approximation to the stochastic vacuum model. Beyond the London limit, it has been shown that a modified interaction appears, which becomes reduced to the standard Yukawa one in the London limit. Finally, a string representation of the  $SU(N)$ -inspired model with the  $\Theta$  term, in the London limit, can be constructed. © 2005 Pleiades Publishing, Inc.

### INTRODUCTION

The Stochastic Vacuum Model (SVM) [1] is nowadays commonly recognized as a promising non-perturbative approach to QCD (see [2] for reviews). Within the so-called bilocal or Gaussian approximation, which is well confirmed by the existing lattice data [3, 4], this model is fully described by the irreducible bilocal gauge-invariant field-strength correlator (cumulant),

$$\langle\langle F_{\mu\nu}(x)\Phi(x, x')F_{\lambda\rho}(x')\Phi(x', x)\rangle\rangle.$$

Here,  $F_{\mu\nu} = \partial_\mu A_\nu - \partial_\nu A_\mu - ig[A_\mu, A_\nu]$  stands for the Yang–Mills field-strength tensor,

$$\Phi(x, y) \equiv \frac{1}{N_c} \mathcal{P} \exp \left( ig \int_y^x A_\mu(u) du_\mu \right)$$

is a parallel transporter factor along the straight-line path, and  $\langle\langle \mathcal{O}\mathcal{O}' \rangle\rangle \equiv \langle \mathcal{O}\mathcal{O}' \rangle - \langle \mathcal{O} \rangle \langle \mathcal{O}' \rangle$  with the average defined with respect to the Euclidean Yang–Mills action. It is further convenient to parametrize the bilocal cumulant by the two coefficient functions  $D$  and  $D_1$  [1, 2] as follows:

$$\frac{g^2}{2} \langle\langle F_{\mu\nu}(x)\Phi(x, x')F_{\lambda\rho}(x')\Phi(x', x)\rangle\rangle \quad (1)$$

$$= \hat{1}_{N_c \times N_c} \left\{ (\delta_{\mu\lambda}\delta_{\nu\rho} - \delta_{\mu\rho}\delta_{\nu\lambda}) D((x - x')^2) + \frac{1}{2} [\partial_\mu^x ((x - x')_\lambda \delta_{\nu\rho} - (x - x')_\rho \delta_{\nu\lambda}) + \partial_\nu^x ((x - x')_\rho \delta_{\mu\lambda} - (x - x')_\lambda \delta_{\mu\rho})] D_1((x - x')^2) \right\}.$$

After that, setting for the nonperturbative parts of the  $D$  and  $D_1$  function various ansätze, one can apply the SVM to calculations of the high-energy scattering processes [5] or test these ansätze in lattice experiments [3, 4]. However, from the pure field-theoretical point of view, a challenge remains to derive the coefficient functions analytically. Unfortunately, in QCD, this problem looks too complicated.

To begin with, it is therefore reasonable to derive field-strength correlators not in QCD itself, but rather in some Abelian-type QCD-inspired models, which inherit confinement and allow for its analytic description. These include  $SU(2)$ -inspired [6] and  $SU(3)$ -inspired [7] dual Abelian–Higgs-type theories, as well as 3D compact QED [8]. The bilocal field-strength cumulant in these theories has been studied in [9–11], respectively. In the present minireview, we will briefly survey the results that concern the dual Abelian–Higgs-type theories, as well as their further elaborations performed in [12]. For the sake of simplicity, we will restrict ourselves to the  $SU(2)$ -inspired case, i.e., a simple Dual Abelian–Higgs Model (DAHM), although the  $SU(3)$  generalization is straightforward [10].

\*This article was submitted by the authors in English.

<sup>1)</sup>Permanent address: ITEP, Moscow, Russia; e-mail: antonov@physik.hu-berlin.de

\*\*e-mail: debert@physik.hu-berlin.de

One important fact for further discussion is that, in DAHM, a sector with closed dual strings [13] exists. Such closed strings are short-lived (virtual) objects, whose typical sizes are much smaller than the typical distances between them. This means that, similarly to monopoles in 3D compact QED, closed strings can be treated in the dilute-plasma approximation. Moreover, in the leading (semiclassical) approximation, the interaction of closed dual strings with large open ones, which end up at external quarks, can be disregarded completely. This is precisely the approximation in which field-strength correlators have been evaluated in [9, 10]. A leading correction to these semiclassical expressions, which stems from the interaction of closed strings with open ones, has been found in [12] and will be reviewed below.

The outline of the minireview is as follows. In the next section, we will first mention a correspondence, based on the Abelian projection method, between the DAHM and the  $SU(2)$  QCD, which will be needed for future purposes. Secondly, we will briefly review the main results of a calculation of electric field-strength correlators in the approximation when closed strings are disregarded. In the subsequent section, after a brief review of properties of the grand canonical ensemble of closed strings, we will consider the contribution of these objects to the field-strength correlators. In the same section, we will also discuss two types of corrections to the  $\bar{q}q$  potential—that due to closed strings and that due to the deviation from the London limit. In the last section, we will present a string representation of the  $SU(N)$ -inspired analog of DAHM extended by the  $\Theta$  term. The main results will finally be quoted in the Summary.

ELECTRIC FIELD-STRENGTH CORRELATORS IN THE ABSENCE OF CLOSED STRINGS

*The Model*

To derive from the Lagrangian of  $SU(2)$  gluodynamics an IR effective theory, based on the assumption of condensation of Abelian-projected monopoles, one usually employs the so-called Abelian dominance hypothesis [14]. It states that the off-diagonal (in the sense of the Cartan decomposition) fields can be disregarded, since after the Abelian projection those can be shown to become very heavy and therefore irrelevant to the IR region. The action describing the remaining diagonal fields and Abelian-projected monopoles reads

$$S_{\text{eff}} [a_\mu, f_{\mu\nu}^m] = \frac{1}{4} \int d^4x (f_{\mu\nu} + f_{\mu\nu}^m)^2. \quad (2)$$

Here,  $a_\mu \equiv A_\mu^3$ ;  $f_{\mu\nu} = \partial_\mu a_\nu - \partial_\nu a_\mu$ ; and  $f_{\mu\nu}^m$  is the monopole field-strength tensor, which obeys Bianchi identities modified by monopoles,

$$\partial_\mu \tilde{f}_{\mu\nu}^m \equiv \frac{1}{2} \varepsilon_{\mu\nu\lambda\rho} \partial_\mu f_{\lambda\rho}^m = j_\nu^m.$$

The monopole currents  $j_\mu^m$  should eventually be averaged over in the sense which will be specified below.

To proceed with the investigation of the monopole ensemble, it is useful to dualize the theory under study. This yields the following expression for the partition function:

$$\mathcal{Z} = \left\langle \int \mathcal{D}B_\mu \exp \left[ - \int d^4x \left( \frac{1}{4} F_{\mu\nu}^2 - i B_\mu j_\mu^m \right) \right] \right\rangle_{j_\mu^m}, \quad (3)$$

where  $B_\mu$  is the magnetic vector-potential dual to the electric one,  $a_\mu$ , and  $F_{\mu\nu} = \partial_\mu B_\nu - \partial_\nu B_\mu$ . Since the  $j_\mu^m$  dependence of the action became explicit, it is now possible to set up the properties of the monopole ensemble. To describe the condensation of monopoles, it is first necessary to specify  $j_\mu^m$  as the collective current of  $N$  of those:

$$j_\mu^{m(N)}(x) = g_m \sum_{n=1}^N \oint dx_\mu^n(s) \delta(x - x^n(s)).$$

Here, the world line of the  $n$ th monopole is parametrized by the vector  $x_\mu^n(s)$ , and  $g_m$  is the magnetic coupling constant, which is related to the QCD coupling constant  $g$  via the quantization condition  $gg_m = 4\pi n$  with  $n$  being an integer. In what follows, we will for concreteness restrict ourselves to the monopoles possessing the minimal charge, i.e., set  $n = 1$ , although the generalization to an arbitrary  $n$  is straightforward. Further, it is necessary to set for the measure  $\langle \dots \rangle_{j_\mu^m}$  the following expression [15]:

$$\begin{aligned} \left\langle \exp \left( i \int d^4x B_\mu j_\mu^m \right) \right\rangle_{j_\mu^m} &= 1 + \sum_{N=1}^{\infty} \frac{1}{N!} \quad (4) \\ &\times \left[ \prod_{n=1}^N \int_0^\infty \frac{ds_n}{s_n} e^{2\lambda\eta^2 s_n} \int_{u(0)=u(s_n)} \mathcal{D}u(s'_n) \right] \\ &\times \exp \left\{ \sum_{l=1}^N \int_0^{s_l} ds'_l \left[ -\frac{1}{4} \dot{u}^2(s'_l) \right. \right. \\ &\quad \left. \left. + i g_m \dot{u}_\mu(s'_l) B_\mu(u(s'_l)) \right] \right\} \\ &- \lambda \sum_{l,k=1}^N \int_0^{s_l} ds'_l \int_0^{s_k} ds''_k \delta [u(s'_l) - u(s''_k)] \left. \right\}. \end{aligned}$$

Here, the vector  $u_\mu(s'_n)$  parametrizes the same contour as the vector  $x_\mu^n(s)$ . Clearly, the world-line action present in the exponent on the right-hand side of Eq. (4) contains, besides the usual free part, also the term responsible for the short-range repulsion (else called self-avoidance) of the trajectories of monopoles. Equation (4) can further be rewritten as an integral over the dual Higgs field as follows:

$$\left\langle \exp \left( i \int d^4x B_\mu j_\mu^m \right) \right\rangle_{j_\mu^m} = \int \mathcal{D}\Phi \mathcal{D}\Phi^* \quad (5)$$

$$\times \exp \left\{ - \int d^4x \left[ |D_\mu \Phi|^2 + \lambda (|\Phi|^2 - \eta^2)^2 \right] \right\},$$

where  $D_\mu = \partial_\mu - ig_m B_\mu$  is the covariant derivative. Finally, substituting Eq. (5) into Eq. (3), we arrive at the DAHM:

$$\mathcal{Z} = \int |\Phi| \mathcal{D}|\Phi| \mathcal{D}\theta \mathcal{D}B_\mu \exp \left\{ - \int d^4x \quad (6)\right.$$

$$\left. \times \left[ \frac{1}{4} F_{\mu\nu} + |D_\mu \Phi|^2 + \lambda (|\Phi|^2 - \eta^2)^2 \right] \right\},$$

where  $\Phi(x) = |\Phi(x)|e^{i\theta(x)}$ . The masses of the dual vector boson and of the dual Higgs field, derivable upon the substitution  $\Phi(x) = \eta + \varphi(x)/\sqrt{2}$ , read  $m_B \equiv m = \sqrt{2}g_m\eta$  and  $m_H = 2\eta\sqrt{\lambda}$ , respectively. Clearly, the two main assumptions made in the course of this derivation were the neglect of the off-diagonal degrees of freedom and the postulate that the monopole condensate can be modeled by the dual Higgs field.

### Bilocal Electric Field-Strength Correlator

In order to investigate the bilocal cumulant of electric field strengths in the model (6), it is necessary to extend this model by external electrically charged test particles [i.e., particles, charged with respect to the Cartan subgroup of the original  $SU(2)$  group]. It is therefore natural to call these particles simply “quarks.” Such an extension can be performed by adding to the action (2) the term  $i \int d^4x a_\mu j_\mu^e$  with

$$j_\mu^e(x) \equiv g \oint_C dx_\mu(s) \delta(x - x(s))$$

standing for the conserved electric current of a quark, which moves along a certain closed contour  $C$ . Then, performing the dualization of the so-extended action and summing up over monopole currents according to Eq. (4), we arrive at Eq. (6) with  $F_{\mu\nu}$  replaced by  $F_{\mu\nu} + F_{\mu\nu}^e$ . Here,  $F_{\mu\nu}^e$  stands for the field-strength tensor generated by quarks according to the equation

$\partial_\mu \tilde{F}_{\mu\nu}^e = j_\nu^e$ . A solution to this equation reads  $F_{\mu\nu}^e = -g \hat{\Sigma}_{\mu\nu}^e$ , where

$$\Sigma_{\mu\nu}^e(x) \equiv \int_{\Sigma^e} d\sigma_{\mu\nu}(\bar{x}(\xi)) \delta(x - \bar{x}(\xi))$$

is the so-called vorticity tensor current defined at an arbitrary surface  $\Sigma^e$  (which is just the world sheet of an open dual Nielsen–Olesen string), bounded by the contour  $C$ , and  $\xi$  is a 2D coordinate.

From now on, we will be interested in the London limit of DAHM,  $\lambda \rightarrow \infty$ , where it admits an exact string representation. In that limit, the partition function (6) with external quarks reads

$$\mathcal{Z} = \int \mathcal{D}B_\mu \mathcal{D}\theta \exp \left\{ - \int d^4x \quad (7)\right.$$

$$\left. \times \left[ \frac{1}{4} (F_{\mu\nu} + F_{\mu\nu}^e)^2 + \eta^2 (\partial_\mu \theta - g_m B_\mu)^2 \right] \right\}.$$

In Eq. (7), one next performs a decomposition of the phase of the dual Higgs field  $\theta = \theta^{\text{sing}} + \theta^{\text{reg}}$ , where the multivalued field  $\theta^{\text{sing}}(x)$  describes a certain configuration of dual strings and obeys the equation [16, 17]

$$\varepsilon_{\mu\nu\lambda\rho} \partial_\lambda \partial_\rho \theta^{\text{sing}}(x) = 2\pi \Sigma_{\mu\nu}(x), \quad (8)$$

and the integration measure becomes factorized,  $\mathcal{D}\theta = \mathcal{D}\theta^{\text{sing}} \mathcal{D}\theta^{\text{reg}}$ . Here,  $\Sigma_{\mu\nu}$  stands for the vorticity tensor current, defined at the world sheet  $\Sigma$  of a closed dual string, parametrized by the vector  $x_\mu(\xi)$ . On the other hand, the field  $\theta^{\text{reg}}(x)$  describes simply a single-valued fluctuation around the above-mentioned string configuration. Note that Eq. (8) is nothing but Stokes’ theorem for  $\partial_\mu \theta^{\text{sing}}$ , written in the local form.

The string representation of the theory (7) can be derived analogously to [16], where this has been done for a model with a global  $U(1)$  symmetry. One obtains

$$\mathcal{Z} = \int \mathcal{D}x_\mu(\xi) \mathcal{D}h_{\mu\nu} \exp \left\{ - \int d^4x \quad (9)\right.$$

$$\left. \times \left[ \frac{1}{24\eta^2} H_{\mu\nu\lambda}^2 + \frac{g_m^2}{4} h_{\mu\nu}^2 + i\pi h_{\mu\nu} \hat{\Sigma}_{\mu\nu} \right] \right\},$$

where  $\hat{\Sigma}_{\mu\nu} \equiv 2\Sigma_{\mu\nu}^e - \Sigma_{\mu\nu}$ , and  $H_{\mu\nu\lambda} \equiv \partial_\mu h_{\nu\lambda} + \partial_\lambda h_{\mu\nu} + \partial_\nu h_{\lambda\mu}$  is the field-strength tensor of a massive antisymmetric spin-1 tensor field  $h_{\mu\nu}$ . This field emerges as a solution of some constraints arising from the integration over  $\theta^{\text{reg}}$  and represents the massive dual vector boson. As far as the integration over the world sheets of closed strings,  $\int \mathcal{D}x_\mu(\xi)$ , is concerned, it appeared from the integration over  $\theta^{\text{sing}}$  by virtue of Eq. (8), which established a one-to-one

correspondence between  $\theta^{\text{sing}}$  and  $x_\mu(\xi)$ . Physically, this correspondence stems from the fact that the singularity of the phase of the dual Higgs field takes place just at closed-string world sheets. [Notice that, since in what follows we will be interested in effective actions, rather than the integration measures, the Jacobian emerging during the change of the integration variables  $\theta^{\text{sing}} \rightarrow x_\mu(\xi)$ , which has been evaluated in [18], will not be discussed below and is assumed to be included in the measure  $\mathcal{D}x_\mu(\xi)$ .]

Finally, the Gaussian integration over the field  $h_{\mu\nu}$  in Eq. (9) leads to the following expression for the partition function (7):

$$\mathcal{Z} = \exp \left[ -\frac{g^2}{2} \oint_C dx_\mu \oint_C dy_\nu D_m^{(4)}(x-y) \right] \quad (10)$$

$$\times \int \mathcal{D}x_\mu(\xi) \exp \left[ -2(\pi\eta)^2 \int d^4x \right.$$

$$\left. \times \int d^4y \hat{\Sigma}_{\mu\nu}^e(x) D_m^{(4)}(x-y) \hat{\Sigma}_{\mu\nu}^e(y) \right].$$

Here,  $D_m^{(4)}(x) \equiv mK_1(m|x|)/(4\pi^2|x|)$  is the propagator of the dual vector boson, and  $K_\nu$  henceforth stand for modified Bessel functions. Clearly, the first exponential factor on the right-hand side of Eq. (10) is the standard result, which can be obtained without accounting for dual Nielsen–Olesen strings. Contrary to that, the integral over string world sheets on the right-hand side of that equation stems just from the contribution of closed strings to the partition function and is the essence of the string representation. The respective string effective action describes both the interaction of closed world sheets  $\Sigma$  with the open world sheets  $\Sigma^e$  and self-interactions of these objects.

We are now in the position to discuss the bilocal correlator of electric field strengths in the model (7). Indeed, owing to Stokes’ theorem, such an extended partition function (which is actually nothing but the Wilson loop of a test quark) can be written as

$$\left\langle \exp \left( -\frac{ig}{2} \int d^4x \Sigma_{\mu\nu}^e f_{\mu\nu} \right) \right\rangle_{a_\mu, j_\mu^m},$$

where

$$\langle \dots \rangle_{a_\mu, j_\mu^m} \equiv \left\langle \int \mathcal{D}a_\mu \exp(-S_{\text{eff}}[a_\mu, f_{\mu\nu}]) (\dots) \right\rangle_{j_\mu^m},$$

with  $S_{\text{eff}}$  and  $\langle \dots \rangle_{j_\mu^m}$  given by Eqs. (2) and (4), respectively. Applying to this expression the cumulant expansion, we have in the bilocal approximation

$$\mathcal{Z} \simeq \exp \left[ -\frac{g^2}{8} \int d^4x \int d^4y \Sigma_{\mu\nu}^e(x) \Sigma_{\lambda\rho}^e(y) \right] \quad (11)$$

$$\times \langle \langle f_{\mu\nu}(x) f_{\lambda\rho}(y) \rangle \rangle_{a_\mu, j_\mu^m} \Big].$$

Following the SVM, let us parametrize the bilocal cumulant  $\langle \langle f_{\mu\nu}(x) f_{\lambda\rho}(0) \rangle \rangle$  similarly to the parametrization of Eq. (1), namely, set for this quantity the following ansatz:

$$(\delta_{\mu\lambda} \delta_{\nu\rho} - \delta_{\mu\rho} \delta_{\nu\lambda}) \mathcal{D}(x^2) \quad (12)$$

$$+ \frac{1}{2} [\partial_\mu(x_\lambda \delta_{\nu\rho} - x_\rho \delta_{\nu\lambda})$$

$$+ \partial_\nu(x_\rho \delta_{\mu\lambda} - x_\lambda \delta_{\mu\rho})] \mathcal{D}_1(x^2).$$

Owing to Stokes’ theorem, Eq. (12) yields

$$\mathcal{Z} \simeq \exp \left\{ -\frac{1}{8} \int d^4x \int d^4y \quad (13)$$

$$\times \left[ 2g^2 \Sigma_{\mu\nu}^e(x) \Sigma_{\mu\nu}^e(y) \mathcal{D}((x-y)^2) \right.$$

$$\left. + j_\mu^e(x) j_\mu^e(y) \int_{(x-y)^2}^\infty dt \mathcal{D}_1(t) \right] \Big\}.$$

On the other hand, Eq. (13) should coincide with Eq. (10) divided by  $\mathcal{Z} [\Sigma_{\mu\nu}^e = 0]$  (that is just the standard normalization condition, encoded in the integration measures); i.e., it reads

$$\mathcal{Z} = \exp \left\{ -\int d^4x \int d^4y D_m^{(4)}(x-y) \quad (14)$$

$$\times \left[ 8(\pi\eta)^2 \Sigma_{\mu\nu}^e(x) \Sigma_{\mu\nu}^e(y) + \frac{1}{2} j_\mu^e(x) j_\mu^e(y) \right] \right\}$$

$$\times \left\langle \exp \left[ 8(\pi\eta)^2 \int d^4x \right. \right.$$

$$\left. \times \int d^4y D_m^{(4)}(x-y) \Sigma_{\mu\nu}^e(x) \Sigma_{\mu\nu}^e(y) \right] \Big\rangle_{x_\mu(\xi)},$$

where the average  $\langle \dots \rangle_{x_\mu(\xi)}$  is defined with respect to the action

$$2(\pi\eta)^2 \int d^4x \int d^4y \Sigma_{\mu\nu}^e(x) D_m^{(4)}(x-y) \Sigma_{\mu\nu}^e(y).$$

As has already been discussed in the Introduction, in the semiclassical approximation, closed dual strings can be disregarded, since their typical areas  $|\Sigma|$  are much smaller than the area  $|\Sigma^e|$  of the world sheet of a long open string, which confines a test quark. Owing to this fact, the exponential factor, which should be averaged over closed strings on the right-hand side of Eq. (14), may be disregarded with respect to the first exponential factor in that equation as well. Then, the comparison of the latter one with Eq. (13) readily

yields for the functions  $\mathcal{D}$  and  $\mathcal{D}_1$  the following expressions:

$$\mathcal{D}(x^2) = \frac{m^3 K_1(m|x|)}{4\pi^2 |x|}, \tag{15}$$

$$\mathcal{D}_1(x^2) = \frac{m}{2\pi^2 x^2} \left[ \frac{K_1(m|x|)}{|x|} + \frac{m}{2} (K_0(m|x|) + K_2(m|x|)) \right]. \tag{16}$$

In the IR limit,  $|x| \gtrsim m^{-1}$ , the asymptotic behaviors of the coefficient functions (15) and (16) are given by

$$\mathcal{D} \longrightarrow \frac{m^4}{4\sqrt{2}\pi^{3/2}} \frac{e^{-m|x|}}{(m|x|)^{3/2}} \tag{17}$$

and

$$\mathcal{D}_1 \longrightarrow \frac{m^4}{2\sqrt{2}\pi^{3/2}} \frac{e^{-m|x|}}{(m|x|)^{5/2}}. \tag{18}$$

One can now see that, according to the lattice data [3, 4], the asymptotic behaviors (17) and (18) are very similar to the IR ones of the nonperturbative parts of the functions  $D$  and  $D_1$ , which parametrize the bilocal cumulant (1) in QCD. In particular, both functions decrease exponentially, and the function  $\mathcal{D}$  is much larger than the function  $\mathcal{D}_1$  due to the preexponential powerlike behavior. We also see that the role of the correlation length of the vacuum,  $T_g$ , i.e., the distance at which the functions  $D$  and  $D_1$  decrease, is played in the model (7) by the inverse mass of the dual vector boson,  $m^{-1}$ .

Hence, we see that, within the approximation when the contribution of closed strings to the partition function (14) is disregarded, the bilocal approximation to the SVM is an exact result in the theory (7), i.e., all the cumulants of the orders higher than the second one vanish. Higher cumulants naturally appear upon performing in Eq. (14) the average over closed strings. However, this average yields important modifications even on the level of the bilocal cumulant. Namely, as we will see in the next section, it modifies the semiclassical expressions (15) and (16).

### CORRECTIONS TO THE $\bar{Q}Q$ POTENTIAL PRODUCED BY CLOSED STRINGS AND A FINITE HIGGS MASS

To study the properties of closed strings, it is enough to consider the theory without external quarks. The field-strength correlators can be addressed afterwards, i.e., already after the summation over the grand canonical ensemble of closed strings. Thus, let us first consider the theory (7) with  $F_{\mu\nu}^e = 0$ .

Upon the derivation of the string representation of such a theory, we are then left with Eq. (9), where  $\Sigma_{\mu\nu}^e = 0$ . To study the grand canonical ensemble of closed strings, it is necessary to replace  $\Sigma_{\mu\nu}$  in Eq. (9) by the following expression:

$$\Sigma_{\mu\nu}^N(x) = \sum_{i=1}^N n_i \int d\sigma_{\mu\nu}(x_i(\xi)) \delta(x - x_i(\xi)).$$

Here,  $n_i$  stand for winding numbers. In what follows, we will restrict ourselves to closed strings possessing the minimal winding numbers,  $n_i = \pm 1$ . That is because, analogously to the 3D case [13, 19], the energy of a single closed string is known to be a quadratic function of its flux, owing to which the vacuum prefers to maintain two closed strings of a unit flux, rather than one string of the double flux.

Then, taking into account that the plasma of closed strings is dilute, one can perform the summation over the grand canonical ensemble of these objects, which yields [instead of Eq. (9)] the following expression for the partition function:

$$\mathcal{Z} = \int \mathcal{D}h_{\mu\nu} \exp \left\{ - \int d^4x \times \left[ \frac{1}{24\eta^2} H_{\mu\nu\lambda}^2 + \frac{g_m^2}{4} h_{\mu\nu}^2 - 2\zeta \cos \left( \frac{|h_{\mu\nu}|}{\Lambda^2} \right) \right] \right\}. \tag{19}$$

Here,  $|h_{\mu\nu}| \equiv \sqrt{h_{\mu\nu}^2}$ , and  $\Lambda \equiv \sqrt{L/a^3}$  is a UV momentum cutoff with  $L$  and  $a$  denoting the characteristic distances between closed strings and their typical sizes, respectively. Clearly, in the dilute-plasma approximation under study,  $a \ll L$  and  $\Lambda \gg a^{-1}$ . Also, in Eq. (19),  $\zeta \propto e^{-S_0}$  stands for the fugacity (Boltzmann factor) of a single string, which has the dimension (mass)<sup>4</sup>, with  $S_0$  denoting the action of a single string. The value of  $S_0$  parametrically equals  $\sigma a^2$ , where the area of the string world sheet is proportional to  $a^2$  and  $\sigma$  is the string tension;  $\sigma \simeq 2\pi\eta^2 \ln(\lambda/g_m^2)$  in the London limit  $\ln(\lambda/g_m^2) \gg 1$ .

The square of the full mass of the field  $h_{\mu\nu}$  following from Eq. (19) reads  $M^2 = m^2 + m_D^2 \equiv Q^2\eta^2$ . Here,  $m_D^2 = 8\zeta\eta^2/\Lambda^4$  is the additional contribution emerging due to the Debye screening of the dual vector boson in the plasma of closed strings, and  $Q^2 = 2(g_m^2 + 4\zeta/\Lambda^4)$  is the (squared) full magnetic charge of the dual vector boson.

To study the correlation functions of closed strings, it is convenient to represent the partition function (19) directly as an integral over the densities of these objects. This can be done by means of some kind

of Legendre transformation, and the resulting action reads

$$S = 2(\pi\eta)^2 \int d^4x \quad (20)$$

$$\times \int d^4y \Sigma_{\mu\nu}(x) D_m^{(4)}(x-y) \Sigma_{\mu\nu}(y) + V[\Sigma_{\mu\nu}],$$

where the effective potential of closed strings,  $V$ , is

$$V[\Sigma_{\mu\nu}] = \int d^4x \quad (21)$$

$$\times \left\{ \Lambda^2 |\Sigma_{\mu\nu}| \ln \left[ \frac{\Lambda^2}{2\zeta} |\Sigma_{\mu\nu}| + \sqrt{1 + \left( \frac{\Lambda^2}{2\zeta} |\Sigma_{\mu\nu}| \right)^2} \right] \right.$$

$$\left. - 2\zeta \sqrt{1 + \left( \frac{\Lambda^2}{2\zeta} |\Sigma_{\mu\nu}| \right)^2} \right\}.$$

It can be proven that the correlation functions of  $\Sigma_{\mu\nu}$ , evaluated by virtue of the representation (20), are nothing but the correlation functions of densities of closed strings in the plasma. These correlation functions can be calculated in the approximation when the plasma is sufficiently dilute, namely, its density obeys the inequality  $|\Sigma_{\mu\nu}| \ll \zeta/\Lambda^2$ , and the potential (21) becomes a simple quadratic functional of  $\Sigma_{\mu\nu}$ . In particular, the simplest nontrivial correlation function  $\langle \langle \Sigma_{\mu\nu}(y) \Sigma_{\lambda\rho}(y') \rangle \rangle_{x_\mu(\xi)}$  can be evaluated in this approximation. Inserting further the thus-obtained expression for this correlation function into the average on the right-hand side of Eq. (14) (evaluated by means of the cumulant expansion in the bilocal approximation), one obtains for the functions  $\mathcal{D}$  and  $\mathcal{D}_1$  [12]

$$\mathcal{D}^{\text{full}}(x^2) = \frac{m^2 M K_1(M|x|)}{4\pi^2 |x|}, \quad (22)$$

$$\mathcal{D}_1^{\text{full}}(x^2) = \frac{m_D^2}{\pi^2 M^2 |x|^4} + \frac{m^2}{2\pi^2 M x^2} \quad (23)$$

$$\times \left[ \frac{K_1(M|x|)}{|x|} + \frac{M}{2} (K_0(M|x|) + K_2(M|x|)) \right].$$

We see that, as it should be, the functions (22) and (23) go over to Eqs. (15) and (16), respectively, when  $m_D \rightarrow 0$ , i.e., when one neglects the effect of screening in the ensemble of closed strings. An obvious important consequence of Eqs. (22) and (23) is that the correlation length of the vacuum,  $T_g$ , becomes modified from  $m^{-1}$  [according to Eqs. (15) and (16)] to  $M^{-1}$ . (It is worth pointing out once again that this effect is due to the Debye screening of the dual vector boson in the ensemble of closed strings, which makes this particle heavier, namely, its mass becomes

increased from  $m$  to  $M$ .) Indeed, it is straightforward to see that, at  $|x| \gtrsim M^{-1}$ ,

$$\mathcal{D}^{\text{full}} \longrightarrow \frac{(mM)^2}{4\sqrt{2}\pi^{3/2}} \frac{e^{-M|x|}}{(M|x|)^{3/2}},$$

$$\mathcal{D}_1^{\text{full}} \longrightarrow \frac{m_D^2}{\pi^2 M^2 |x|^4} + \frac{(mM)^2}{2\sqrt{2}\pi^{3/2}} \frac{e^{-M|x|}}{(M|x|)^{5/2}}.$$

A remarkable fact is that the leading term of the IR asymptotics of the function  $\mathcal{D}_1^{\text{full}}$  is a pure powerlike one, rather than that of the function  $\mathcal{D}_1$ , given by Eq. (18). This term produces a nonperturbative ( $1/r$ ) contribution to the  $\bar{q}q$  potential,

$$\Delta V(r) = -\frac{(m_D/M)^2}{4\pi r},$$

which by its structure resembles the Lüscher term. Typically, modeling the Lüscher term within the SVM is rather problematic. Indeed, in the standard approach, in order to get the Lüscher term, one should consider string fluctuations, while the SVM is well defined only on the minimal-area surface (see, e.g., [2]). Now, we have found another mechanism that might generate a Lüscher-type term via a novel nonperturbative perimeter interaction.

It is also worth noting that, despite the modification of the  $\mathcal{D}$  function, the string tension of the open dual-string world sheet  $\Sigma^e$ ,

$$\sigma = 4T_g^2 \int d^2z \mathcal{D}(z^2)$$

(cf. [20]), becomes modified only by means of the logarithm of the Landau–Ginzburg parameter. Indeed, one obtains  $\sigma = 8\pi\eta^2 \ln(\lambda/Q^2) \propto \eta^2$ , and  $\eta$  is not affected by the Debye screening. The screening instead modifies more significantly the coupling constant of the next-to-leading term in the derivative expansion of the nonlocal string effective action (the so-called rigidity term). Indeed, by virtue of the results of [20], one can see that, for the same world sheet  $\Sigma^e$ , this coupling constant without taking screening into account reads  $-\pi/(2g_m^2)$ , whereas in the presence of screening it goes over to

$$-\frac{\pi}{2 \left( g_m^2 + \frac{4\zeta}{\Lambda^4} \right)} = -\frac{\pi}{Q^2}.$$

Another origin of corrections to the  $\bar{q}q$  potential (even without accounting for closed strings) is due to the deviation from the London limit [21]:

$$V(r) = -g^2 \frac{e^{-mr}}{4\pi r}$$

$$\times \left[ 1 - e^{-(\sqrt{m^2+m_H^2}-m)r} + e^{-(m_H-m)r} \right],$$

$$r > m_H^{-1}.$$

Clearly, this potential is neither Yukawa nor Coulombic, but it goes over to the Yukawa potential in the London limit  $m_H \rightarrow \infty$ .

STRING REPRESENTATION  
OF THE  $SU(N)$ -INSPIRED DAHM  
WITH THE  $\Theta$  TERM

In this section, we will present a string representation of the  $SU(N)$ -inspired analog of the model (6), extended, for completeness, by the  $\Theta$  term. Owing to this term, quarks acquire a nonvanishing magnetic charge (i.e., they become dyons) and scatter off closed dual strings. As one of the consequences of our result, we will get the critical values of  $\Theta$  at which the long-range topological interaction of dual strings with dyons disappears. These values, in particular, reproduce the respective  $SU(2)$  and  $SU(3)$  ones found in [22] and [23], respectively. The partition function of the effective  $[U(1)]^{N-1}$  gauge-invariant Abelian-projected theory that we are going to explore reads

$$\begin{aligned} \mathcal{Z}_\alpha = & \int \left( \prod_i |\Phi_i| \mathcal{D}|\Phi_i| \mathcal{D}\theta_i \right) \mathcal{D}\mathbf{B}_\mu \delta \left( \sum_i \theta_i \right) \quad (24) \\ & \times \exp \left\{ - \int d^4x \left[ \frac{1}{4} \left( \mathbf{F}_{\mu\nu} + \mathbf{F}_{\mu\nu}^{(\alpha)} \right)^2 \right. \right. \\ & + \sum_i \left[ |(\partial_\mu - ig_m \mathbf{q}_i \cdot \mathbf{B}_\mu) \Phi_i|^2 + \lambda (|\Phi_i|^2 - \eta^2)^2 \right] \\ & \left. \left. - \frac{i\Theta g_m^2}{16\pi^2} \left( \mathbf{F}_{\mu\nu} + \mathbf{F}_{\mu\nu}^{(\alpha)} \right) \cdot \left( \tilde{\mathbf{F}}_{\mu\nu} + \tilde{\mathbf{F}}_{\mu\nu}^{(\alpha)} \right) \right] \right\}. \end{aligned}$$

Here, the index  $i$  runs from 1 to the number of positive roots  $\mathbf{q}_i$  of the  $SU(N)$  group, which is  $N(N-1)/2$ . Note that the origin of root vectors in Eq. (24) is the fact that monopole charges are distributed along them. Further,  $\Phi_i = |\Phi_i|e^{i\theta_i}$  are the dual Higgs fields, which describe the condensates of monopoles, and  $\mathbf{F}_{\mu\nu} = \partial_\mu \mathbf{B}_\nu - \partial_\nu \mathbf{B}_\mu$  is the field-strength tensor of the  $(N-1)$ -component “magnetic” potential  $\mathbf{B}_\mu$ . The latter is dual to the “electric” potential, whose components are diagonal gluons. Since the  $SU(N)$  group is special, the phases  $\theta_i$  of the dual Higgs fields are related to each other by the constraint  $\sum_i \theta_i = 0$ , which is imposed by introducing the corresponding  $\delta$  function into the right-hand side of Eq. (24) {cf. [7] for the  $SU(3)$  case}. Next, the index  $\alpha$  runs from 1 to  $N$  and denotes a certain quark color. Finally,  $\mathbf{F}_{\mu\nu}^{(\alpha)}$  is the field-strength tensor of a test quark of the color  $\alpha$ , which moves along a certain contour  $C$ . This tensor obeys the equation  $\partial_\mu \tilde{\mathbf{F}}_{\mu\nu}^{(\alpha)} = g\mathbf{m}_\alpha j_\nu$ , where

$$j_\mu(x) = \oint_C dx_\mu(s) \delta(x - x(s)),$$

and  $\mathbf{m}_\alpha$  is a weight vector of the fundamental representation of the group  $SU(N)$ . One thus has  $\mathbf{F}_{\mu\nu}^{(\alpha)} = -g\mathbf{m}_\alpha \tilde{\Sigma}_{\mu\nu}^e$ . Note further that the  $\Theta$  term can be rewritten as

$$\begin{aligned} & - \frac{i\Theta g_m^2}{16\pi^2} \left( \mathbf{F}_{\mu\nu} + \mathbf{F}_{\mu\nu}^{(\alpha)} \right) \cdot \left( \tilde{\mathbf{F}}_{\mu\nu} + \tilde{\mathbf{F}}_{\mu\nu}^{(\alpha)} \right) \quad (25) \\ & = \frac{i\Theta g_m}{\pi} \mathbf{m}_\alpha \cdot \int d^4x \mathbf{B}_\mu j_\mu. \end{aligned}$$

This means that, by means of the  $\Theta$  term, quarks acquire a nonvanishing magnetic charge  $\Theta g_m/\pi$ , i.e., become dyons, that enables them to interact with the magnetic gauge field  $\mathbf{B}_\mu$  [24].

Expanding for a while  $|\Phi_i|$  around the Higgs VEV  $\eta$ , one gets the mass of the dual vector boson,  $m = \sqrt{N}g_m\eta$ , that generalizes the respective  $SU(2)$  expression. In what follows, we will again consider the London limit of the model (24), which admits a construction of the string representation. This is the limit when  $m$  is much smaller than the mass of any of the Higgs fields,  $m_H = 2\eta\sqrt{\lambda}$ . Since we would like our model to be consistent with QCD, we must have  $g = \sqrt{\lambda/N}$ , where  $\bar{\lambda}$  remains finite in the large- $N$  limit. Therefore, in the London limit, the Higgs coupling  $\lambda$  should grow with  $N$  faster than  $\mathcal{O}(N^2)$ ; namely, it should obey the inequality  $\lambda \gg (2\pi N)^2/\bar{\lambda}$ .

Then integrating  $|\Phi_i|$  out, we arrive at the following expression for the partition function (24) in the London limit:

$$\begin{aligned} \mathcal{Z}_\alpha = & \int \left( \prod_i \mathcal{D}\theta_i^{\text{sing}} \mathcal{D}\theta_i^{\text{reg}} \right) \mathcal{D}\mathbf{B}_\mu \mathcal{D}k \delta \left( \sum_i \theta_i^{\text{sing}} \right) \\ & \times \exp \left\{ - \int d^4x \left[ \frac{1}{4} \left( \mathbf{F}_{\mu\nu} + \mathbf{F}_{\mu\nu}^{(\alpha)} \right)^2 \right. \right. \\ & + \eta^2 \sum_i (\partial_\mu \theta_i - g_m \mathbf{q}_i \cdot \mathbf{B}_\mu)^2 - ik \sum_i \theta_i^{\text{reg}} \\ & \left. \left. - \frac{i\Theta g_m^2}{16\pi^2} \left( \mathbf{F}_{\mu\nu} + \mathbf{F}_{\mu\nu}^{(\alpha)} \right) \cdot \left( \tilde{\mathbf{F}}_{\mu\nu} + \tilde{\mathbf{F}}_{\mu\nu}^{(\alpha)} \right) \right] \right\}. \end{aligned}$$

The multivalued fields  $\theta_i^{\text{sing}}$  here are related to the world sheets of closed dual strings  $\Sigma_i$  by the same Eq. (8). The string representation of this partition function reads [25]

$$\begin{aligned} \mathcal{Z}_\alpha = & \exp \left\{ - \frac{N-1}{4N} \left[ g^2 + \left( \frac{\Theta g_m}{\pi} \right)^2 \right] \right\} \quad (26) \\ & \times \int d^4x \int d^4y j_\mu(x) D_m(x-y) j_\mu(y) \\ & \times \int \left( \prod_i \mathcal{D}x^{(i)}(\xi) \right) \delta \left( \sum_i \Sigma_{\mu\nu}^i \right) \end{aligned}$$

$$\begin{aligned} &\times \exp \left[ -2(\pi\eta)^2 \int d^4x \int d^4y \hat{\Sigma}_{\mu\nu}^i(x) D_m(x-y) \right. \\ &\times \hat{\Sigma}_{\mu\nu}^i(y) - 2i\Theta s_i^{(\alpha)} \hat{L}(\Sigma_i, C) + 2i\Theta \int d^4x \int d^4y \\ &\times \left( \frac{N-1}{N} \tilde{\Sigma}_{\mu\nu}^e(x) - s_i^{(\alpha)} \tilde{\Sigma}_{\mu\nu}^i(x) \right) j_\mu(y) \partial_\nu^x \\ &\left. \times D_m(x-y) \right]. \end{aligned}$$

Here,

$$\hat{L}(\Sigma_i, C) \equiv \int d^4x \int d^4y \tilde{\Sigma}_{\mu\nu}^i(x) j_\nu(y) \partial_\mu^x D_0(x-y)$$

is 4D Gauss' linking number of the surface  $\Sigma_i$  with the contour  $C$ ,  $D_0(x) \equiv 1/(4\pi^2 x^2)$ ,  $\tilde{\Sigma}_{\mu\nu}^i \equiv \Sigma_{\mu\nu}^i - N s_i^{(\alpha)} \Sigma_{\mu\nu}^e$ , and nonvanishing  $s_i^{(\alpha)}$  are equal to  $\pm N^{-1}$ . Note that, for every color  $\alpha$ , it is straightforward to integrate out one of the world sheets  $\Sigma_i$  by resolving the constraint imposed by the  $\delta$  function.

The first exponent on the right-hand side of Eq. (26) represents the short-ranged interaction of quarks via dual vector bosons. Noting that, for any  $\alpha$ ,  $\mathbf{m}_\alpha^2 = (N-1)/(2N)$ , one readily deduces from this term the total charge of the quark,  $\sqrt{g^2 + (\Theta g_m/\pi)^2}$ . The magnetic part of this charge coincides with the one stemming from Eq. (25). Further, the first term in the second exponent on the right-hand side of Eq. (26) is again the short-ranged (self)-interaction of closed world sheets  $\Sigma_i$  and an open one,  $\Sigma^e$ , responsible for confinement. The last term on the right-hand side of Eq. (26) describes the short-range interactions of dyons with both closed and open strings (obviously, the latter confine these very dyons themselves). Instead, the term  $-2i\Theta s_i^{(\alpha)} \hat{L}(\Sigma_i, C)$  in Eq. (26) describes the long-range interaction of dyons with closed world sheets, that is, the 4D analog of the Aharonov–Bohm effect [26]. Since nonvanishing values of  $s_i^{(\alpha)}$  are equal to  $\pm N^{-1}$ , at  $\Theta \neq N\pi \times \text{integer}$ , dyons (due to their magnetic charge) do interact by means of this term with closed dual strings. On the contrary, these critical values of  $\Theta$  correspond to such a relation between the magnetic charge of a dyon and an electric flux inside string when the scattering of dyons off strings is absent.

### SUMMARY

In the present article, we have first briefly reviewed the properties of electric field-strength correlators in the DAHM, which correspond to the gauge-invariant correlators in the real QCD. First, we have reviewed the semiclassical analysis of these correlators. Then,

the leading correction to this result, produced by the interaction of the open-string world sheet with closed dual strings, has been evaluated. This effect is essentially quantum, as well as the plasma of closed strings itself. In this way, it has been shown that the correlation length of the vacuum becomes modified from the inverse mass of the dual vector boson, which it acquires by means of the Higgs mechanism, to its inverse full mass, which also takes into account the effect of Debye screening. What is more important is that, in one of the two coefficient functions which parametrize the bilocal correlator of electric field strengths within the SVM, a nonperturbative powerlike IR part appears, which was absent on the semiclassical level. This novel term opens up the possibility of generating a Lüscher-type term within the SVM. We have further presented another type of modification of the  $\bar{q}q$  potential, which appears beyond the London limit. The novel potential is a certain combination of Yukawa potentials with various effective masses, but it goes over to the standard Yukawa potential in the London limit. Finally, we have discussed the string representation of the  $SU(N)$  counterpart of DAHM in the London limit, extended by the  $\Theta$  term. Owing to the latter, quarks have been shown to acquire a magnetic charge and scatter off closed dual strings, provided  $\Theta$  does not take its values from a certain discrete set.

In conclusion, the obtained results demonstrate similarities in the vacuum structures of DAHM and QCD by means of the SVM. They might also shed some light on the origin of the Lüscher term in QCD, as well as on the structure of the color flux tubes.

### ACKNOWLEDGMENTS

One of the authors (D.V.A.) is grateful to the Alexander von Humboldt Foundation for financial support. He would also like to thank the staff of the Institute of Physics of the Humboldt University of Berlin for the cordial hospitality.

### REFERENCES

1. H. G. Dosch, Phys. Lett. B **190**, 177 (1987); Yu. A. Simonov, Nucl. Phys. B **307**, 512 (1988); H. G. Dosch and Yu. A. Simonov, Phys. Lett. B **205**, 339 (1988).
2. H. G. Dosch, Prog. Part. Nucl. Phys. **33**, 121 (1994); Yu. A. Simonov, Usp. Fiz. Nauk **166**, 337 (1996) [Phys. Usp. **39**, 313 (1996)]; A. Di Giacomo, H. G. Dosch, V. I. Shevchenko, and Yu. A. Simonov, Phys. Rep. **372**, 319 (2002).
3. M. Campostrini, A. Di Giacomo, and G. Mussardo, Z. Phys. C **25**, 173 (1984); A. Di Giacomo and H. Panagopoulos, Phys. Lett. B **285**, 133 (1992).

4. For the latest developments see: A. Di Giacomo and E. Meggiolaro, Phys. Lett. B **537**, 173 (2002); for reviews see, e.g.: A. Di Giacomo, *Nonperturbative QCD*, in *Proceedings of the XVII Autumn School of Physics "QCD: Perturbative or Nonperturbative?"*, Lisbon, 1999, p. 1; hep-lat/9912016; E. Meggiolaro, Phys. Lett. B **451**, 414 (1999).
5. For a review see: S. Donnachie, H. G. Dosch, P. Landshoff, and O. Nachtmann, *Pomeron Physics and QCD* (Cambridge Univ. Press, Cambridge, 2002).
6. S. Mandelstam, Phys. Rep. **23C**, 245 (1976); G. 't Hooft, in *High Energy Physics*, Ed. by A. Zichichi (Editrice Compositori, Bologna, 1976), Vol. 2, p. 1225; Nucl. Phys. B **190**, 455 (1981).
7. S. Maedan and T. Suzuki, Prog. Theor. Phys. **81**, 229 (1989).
8. A. M. Polyakov, Nucl. Phys. B **120**, 429 (1977).
9. M. Baker, N. Brambilla, H. G. Dosch, and A. Vairo, Phys. Rev. D **58**, 034010 (1998); U. Ellwanger, Eur. Phys. J. C **7**, 673 (1999); D. Antonov and D. Ebert, Eur. Phys. J. C **8**, 343 (1999).
10. D. Antonov and D. Ebert, Phys. Lett. B **444**, 208 (1998); D. A. Komarov and M. N. Chernodub, Pis'ma Zh. Éksp. Teor. Fiz. **68**, 109 (1998) [JETP Lett. **68**, 117 (1998)].
11. D. Antonov and D. Ebert, Eur. Phys. J. C **12**, 349 (2000).
12. D. Antonov, J. High Energy Phys. **07**, 055 (2000).
13. V. N. Popov, *Functional Integrals in Quantum Field Theory and Statistical Physics* (Atomizdat, Moscow, 1976; Reidel, Dordrecht, 1983).
14. Z. F. Ezawa and A. Iwazaki, Phys. Rev. D **25**, 2681 (1982); **26**, 631 (1982).
15. K. Bardakci and S. Samuel, Phys. Rev. D **18**, 2849 (1978).
16. K. Lee, Phys. Rev. D **48**, 2493 (1993).
17. P. Orland, Nucl. Phys. B **428**, 221 (1994); M. Sato and S. Yahikozawa, Nucl. Phys. B **436**, 100 (1995); M. Kiometzis, H. Kleinert, and A. M. J. Schakel, Fortschr. Phys. **43**, 697 (1995).
18. E. T. Akhmedov, M. N. Chernodub, M. I. Polikarpov, and M. A. Zubkov, Phys. Rev. D **53**, 2087 (1996).
19. E. M. Lifshitz and L. P. Pitaevski, *Statistical Physics* (Pergamon, New York, 1987), Part 2.
20. D. V. Antonov, D. Ebert, and Yu. A. Simonov, Mod. Phys. Lett. A **11**, 1905 (1996).
21. Y. Koma, M. Koma, D. Ebert, and H. Toki, J. High Energy Phys. **08**, 047 (2002); Nucl. Phys. B **648**, 189 (2003).
22. E. T. Akhmedov, Pis'ma Zh. Éksp. Teor. Fiz. **64**, 76 (1996) [JETP Lett. **64**, 82 (1996)]; for related studies see: E. T. Akhmedov, M. N. Chernodub, and M. I. Polikarpov, Pis'ma Zh. Éksp. Teor. Fiz. **67**, 367 (1998) [JETP Lett. **67**, 389 (1998)].
23. D. Antonov, Phys. Lett. B **475**, 81 (2000).
24. E. Witten, Phys. Lett. B **86B**, 283 (1979).
25. D. Antonov, Phys. Lett. B **543**, 53 (2002).
26. M. G. Alford, J. March-Russel, and F. Wilczek, Nucl. Phys. B **337**, 695 (1990); J. Preskill and L. M. Krauss, Nucl. Phys. B **341**, 50 (1990).

# QCD Sum Rules and Radial Excitations of Light Pseudoscalar and Scalar Mesons\*

A. L. Kataev\*\*

*Institute for Nuclear Research, Russian Academy of Sciences,  
pr. Shestidesyatiletiya Oktyabrya 7a, Moscow, 117312 Russia*

Received May 13, 2004

**Abstract**—The calculations of masses and decay constants of the radial excitations of light pseudoscalar and scalar mesons within the QCD sum rules method are briefly reviewed. The predictions are based on the  $1/N_c$ -supported model spectra, which consist of an infinite number of infinitely narrow resonances, and on the assumption that the ground states of light scalar mesons may be considered as  $\bar{q}q$ -bound states. The results of the studies are compared with the existing experimental data and with the predictions of other theoretical approaches. © 2005 Pleiades Publishing, Inc.

*Dedicated to the 70th Birthday  
of Prof. Yu.A. Simonov*

## 1. INTRODUCTION

Despite the fact that QCD is an indisputable theory of strong interactions, there are still a number of important open areas where, using QCD methods, one can arrive at different conclusions which can serve as various alternative descriptions of the results of concrete experimental studies.

The status of QCD predictions for the properties of light hadronic bound states is among the open and intriguing problems of modern phenomenology. The main puzzle is that the long-awaited glueball states do not yet have well-identified candidates even in the most prominent scalar channel. Indeed, different phenomenological studies indicate that they can mix with low-lying scalar mesons with a mass of over 1 GeV (for a review, see, e.g., [1]). It is known that this sector is rich in different scalar resonances, like  $I = 0$   $\delta$  or  $f_0(600)$ ,  $f_0(980)$ ,  $f_0(1370)$ ,  $f_0(1500)$ ,  $I = 1/2$   $K^*(1430)$ ,  $I = 1$   $a_0(980)$  and  $a_0(1450)$  (see the most recent Particle Data Group report [2]). This list is minimal and does not include all actual resonances, which can manifest themselves, say, as the radial excitations of low-lying scalar hadronic states, systematized, e.g., in [3].

Moreover, there are different points of view on the nature of even low-lying scalar hadrons, such as the  $a_0(980)$  particle. Indeed, it is described by different authors either as the 4-quark state [4],  $\bar{q}q$ -quark

mixed structure [5], or the  $\bar{q}q$ -bound state. The latter point of view is supported by the studies [6, 7].

The important logical check of the assumption that scalar mesons may be considered as  $\bar{q}q$ -bound states is based on the investigations of the possibilities to predict masses and decay constants of their radial excitations and on the comparisons of the predictions of different methods. It is also interesting to study the results of applications of these methods in the pseudoscalar channel, where low-lying  $\bar{q}q$  states are well identified as  $\pi$  and  $K$  mesons.

Quite recently, several approaches were developed that have the aim to describe the properties of radial excitations of light mesons in various channels. Among others, we can mention the QCD-string-inspired methods of the studies [8, 9], the methods of effective chiral Lagrangians [10], and the large- $N_c$  expansion-motivated approaches (see, e.g., [9]).

Let us recall that, within pure  $1/N_c$  expansion, originally proposed in [11], all quark–antiquark mesons become infinitely narrow resonances. The spectrum of the theory in the large- $N_c$  limit consists of an infinite number of these resonances, which belong to flavor nonets [12]. Of course, in the real world, we have  $N_c = 3 \neq \infty$  and the families of resonances with nonzero widths. However, the  $1/N_c$ -motivated spectrum is often used in various concrete physical considerations in four-dimensional QCD. Indeed, the phenomenological spectra modeled by a comb of an infinite number of infinitely narrow resonances were used, e.g., in [9, 13] and in older studies [14–16], which attracted definite interest again only recently (see, e.g., the comparison of the results obtained in [14–16] with those from [9] and [10]).

\*This article was submitted by the author in English.

\*\* e-mail: [kataev@ms2.inr.ac.ru](mailto:kataev@ms2.inr.ac.ru)

These studies, like some other similar analyses, are based on the concept of duality, proposed within the context of QCD in [17, 18] some time ago, tested in two dimensions within the  $1/N_c$  expansion in [19], and studied in detail in the review of [20]. The method of QCD finite-energy sum rules (FESRs) [21], which are analogous to the dual sum rules in the theory of strong interactions [22], is another important technical tool applied to theoretical investigations of the properties of radial excitations of mesons performed in [14–16].

Since quite recently definite interest in the studies of the predictions for the spectra of radial excitations of light hadronic states was observed, which is motivated in part by the experimental programs of the collaboration COMPASS at CERN and CEBAF Jefferson Laboratory facility, we decided to recall some basic theoretical results, obtained at the beginning of the 1990s in the Theoretical Division of the Institute for Nuclear Research, concentrating on the considerations of the pseudoscalar and scalar sectors.

## 2. THE PSEUDOSCALAR AND SCALAR CHANNEL: PRELIMINARIES

Let us first introduce the (pseudo)scalar quark currents

$$\partial_\mu J_\mu^{(5)} = im_q^{(+)-} \bar{q}(\gamma_5)u, \quad (1)$$

which are proportional to the divergence of (axial)vector currents:

$$J_\mu^{(5)} = \bar{q}\gamma_\mu(\gamma_5)u, \quad (2)$$

where  $m_q^{(+)-} = m_q \pm m_u$  are the sum and difference of the current quark masses with  $q = d, s$ . The two-point functions of the (pseudo)scalar quark currents can be defined as

$$\begin{aligned} \Pi^{(P)S}(Q^2) &= i(8\pi^2) \quad (3) \\ &\times \int e^{iqx} \langle 0 | \partial_\mu J_\mu^{(5)}(x) \partial_\mu J_\mu^{(5)}(0) | \rangle d^4x, \end{aligned}$$

where  $Q^2 = -q^2$  is the Euclidean momentum transfer, and the indices  $P$  and  $S$  label the pseudoscalar and scalar quark channels. These two-point functions have the following imaginary part:

$$\begin{aligned} R_{\overline{MS}}^{(P)S}(s/\mu^2) &= 3(m_q^{(+)-}(\mu^2))^2 s \quad (4) \\ &\times \left[ 1 + \frac{\alpha_s(\mu^2)}{\pi} \left( \frac{17}{4}C_F - \frac{3}{2}C_F \ln(s/\mu^2) \right) + \dots \right], \end{aligned}$$

where  $s$  is the Minkowskian variable and  $\mu^2$  is the normalization point of the  $\overline{MS}$  scheme. Here,  $C_F = (N_c^2 - 1)/(2N_c)$  is one of the Casimir operators, and we retain the one-loop massless perturbative QCD correction only. The result for this correction can be

extracted from the original  $\overline{MS}$ -scheme calculation of [23]. The spectral density of Eq. (4) enters in the Euclidean function [24]

$$D^{(P)S}(Q^2) = Q^2 \int_0^\infty \frac{R_{\overline{MS}}^{(P)S}(s/\mu^2)}{(s+Q^2)^3} ds, \quad (5)$$

which obeys the renormalization group equation with anomalous mass dimension term, namely,

$$\begin{aligned} &\left( \frac{\partial}{\partial \ln \mu^2} + \beta(a_s) \frac{\partial}{\partial a_s} \right. \quad (6) \\ &\left. + 2\gamma_m(a_s) \frac{\partial}{\partial m_q^{(+)-}} \right) D^{(P)S}(Q^2/\mu^2) = 0. \end{aligned}$$

Here,  $a_s(\mu^2) = \alpha_s(\mu^2)/(4\pi)$  and  $m_q^{(+)-}(\mu^2)$  are related to the renormalized coupling constant and quark masses, which depend on the normalization point  $\mu^2$ . The QCD  $\beta$  function and the anomalous dimension  $\gamma_m$  of quark mass  $m_q$  are defined as

$$\beta(a_s) = \frac{da_s(\mu^2)}{d \ln \mu^2} = - \sum_{n \geq 0} \beta_n \left( \frac{\alpha_s}{4\pi} \right)^{n+2}, \quad (7)$$

$$\gamma_m(a_s) = \frac{d \ln m_q(\mu^2)}{d \ln \mu^2} = - \sum_{n \geq 0} \gamma_n \left( \frac{\alpha_s}{4\pi} \right)^{n+1}. \quad (8)$$

In the class of the  $\overline{MS}$  schemes, the analytical expressions for the first two coefficients of the QCD  $\beta$  function and the anomalous dimension function  $\gamma_m$  read

$$\beta_0 = \left( \frac{11}{3}C_A - \frac{2}{3}N_F \right), \quad (9)$$

$$\beta_1 = \left( \frac{34}{3}C_A^2 - 2C_F N_F - \frac{10}{3}C_A N_F \right), \quad (10)$$

$$\gamma_0 = 3C_F, \quad (11)$$

$$\gamma_1 = \left( \frac{3}{2}C_F^2 + \frac{97}{2}C_F C_A - 5C_F N_F \right), \quad (12)$$

where  $C_F$  was introduced previously and  $C_A = N_c$ . Within the class of gauge-independent schemes, the coefficient  $\gamma_1$  is scheme dependent, while the coefficients  $\beta_0$ ,  $\beta_1$ , and  $\gamma_0$  do not depend on the choice of the subtraction scheme. Note that the general analytical four-loop expressions for the QCD  $\beta$  function and the  $\gamma_m$  function were calculated in [25] and [26], respectively. The results from [26], expressed in terms of  $N_c$ , are in agreement with the outcomes of independent calculation of [27]. As to the perturbative corrections to the function of Eq. (5), we will limit ourselves to the consideration of the following one-loop expression:

$$D^{(P)S}(Q^2) = 3(m_q^{(+)-}(Q^2))^2 \quad (13)$$

$$\times \left[ 1 + \frac{11}{3} C_F \left( \frac{\alpha_s(Q^2)}{\pi} \right) + \dots \right],$$

where within the  $\overline{MS}$  scheme the running quark masses are related to the invariant quark masses  $\hat{m}_q^{(+)-}$  as

$$m_q^{(+)-}(Q^2) = \hat{m}_q^{(+)-} \exp \left[ \int_0^{\alpha_s(Q^2)} \frac{\gamma_m(x)}{\beta(x)} dx \right] \quad (14)$$

$$- \int_0^{2\beta_0} \frac{\gamma_0}{\beta_0 x} dx + 2 \frac{\gamma_0}{\beta_0} \ln(2\beta_0)$$

$$= \hat{m}_q^{(+)-} (\beta_0 \alpha_s(Q^2) / 2\pi)^{\gamma_0/\beta_0}$$

$$\times \left[ 1 + \left( \frac{\gamma_1}{\beta_1} - \frac{\gamma_0}{\beta_0} \right) \frac{\beta_1}{\beta_0} \left( \frac{\alpha_s}{4\pi} \right) + \dots \right],$$

and the two-loop expression for the QCD coupling constant in the  $\overline{MS}$  scheme, which corresponds to  $N_F = 3$  numbers of active flavors, reads

$$\alpha_s(Q^2) = \frac{4\pi}{\beta_0 \ln(Q^2/\Lambda^2)} \left[ 1 - \frac{\beta_1 \ln \ln(Q^2/\Lambda^2)}{\beta_0^2 \ln(Q^2/\Lambda^2)} \right], \quad (15)$$

$$\Lambda = \Lambda_{\overline{MS}}^{(N_F=3)}.$$

Note that the relation between the running and invariant quark masses was originally chosen in [23] in the way of Eq. (14) to fix the following scale dependence of the quark running mass:

$$m_q(\mu) = \hat{m}_q \left( \frac{1}{\ln(Q/\Lambda)} \right)^{\gamma_0/\beta_0}. \quad (16)$$

Notice that the application of the  $1/N_c$  expansion is used in QCD for the choice of model phenomenological spectral function only. Of course, one can be more consistent, expanding all Casimir operators  $C_F$  and  $C_A$  in powers of  $N_c$  and keeping the leading terms of this expansion. In this case, one may use the formula

$$\frac{m_q^{(+)-}(Q^2)}{m_q^{(+)-}(\mu^2)} = \left( \frac{\alpha_s(Q^2)}{\alpha_s(\mu^2)} \right)^{9/22}, \quad (17)$$

where

$$\frac{\alpha_s(Q^2)}{\pi} = \frac{12}{11 N_c \ln(Q^2/\Lambda^2)}. \quad (18)$$

However, we will avoid applications of these formulas in concrete considerations, which will be discussed below.

It should be stressed that the convention of choosing the renormalization scale of running quark masses at  $Q^2 = 1 \text{ GeV}^2$  moved in our times to

$2 \text{ GeV}^2$ . Moreover, since partly unknown QCD corrections of order  $(\alpha_s/\pi)^4$  to Eqs. (4) and (13) (the available results of the total calculations of this term, which are now continuing,<sup>1)</sup> see in [24] and [28]) may affect the precision of the determination of light quark masses from the scalar and pseudoscalar quark channels, we will not present here any concrete results for the running and invariant quark masses.

Before proceeding to the main part of this work, let us emphasize the essential role of the  $\langle m_q \bar{q} q \rangle$  and  $\langle (\beta(\alpha_s)/\alpha_s) G_{\mu\nu}^a G_{\mu\nu}^a \rangle$  condensates [29] in the description of the properties of the ground states of hadrons. Indeed, together with instanton effects (see, e.g., [30, 31]), these nonperturbative contributions should mostly be important for the calculations of the hadronic ground-states masses and decay width coupling constant using the operator-product expansion (OPE) technique and the Borel sum rules approach [29]. Note that the infrared renormalon calculus, rediscovered in QCD in [32], supports the importance of consideration of the condensates with dimension  $d \geq 4$ . Moreover, this approach favors the application of the dispersion relation of Eq. (5) in the scalar and pseudoscalar channels. Due to the theoretical arguments given in [24], the renormalon calculus indicates that the ill-defined dispersion relation

$$\bar{D}^{P(S)}(Q^2) = Q^2 \int_0^\infty \frac{R_{\overline{MS}}^{P(S)}(s)}{s(s+Q^2)^2} ds \quad (19)$$

contains a  $(\Lambda^2/Q^2)$  correction, which is not consistent with the general structure of the standard massless OPE technique. This fact indicates that, in the process of concrete phenomenological studies, it is more consistent to consider the  $D$  function of Eq. (5) [24] (in fact, it is proportional to the double-differentiated dispersion relation, originally defined and used in [23]). Indeed, as in the vector channel, the standard OPE expansion of Eq. (5) starts from the terms of order  $O(\Lambda^4/Q^4)$ . Thus, following the scalar-channel consideration of [24], we conclude that, in the  $\overline{MS}$  scheme, the infrared renormalon (IRR) calculus is a rather useful tool for the investigation of the general structure of the standard OPE formalism. Note, however, that the concept of IRR contributions is scheme dependent. In the schemes with the frozen coupling constant (see, e.g., [33–35]), the IRR contributions are absent. The question of the existence in this case of ultraviolet renormalon contributions seems to be open. Another problem on which we are going to concentrate in this presentation is related to the possibility of estimating the

<sup>1)</sup>Private communications by P.A. Baikov and K.G. Chetyrkin are gratefully acknowledged.

properties of radial excitations, namely, their masses and decay width coupling constants, using the QCD sum rules method and the duality approach. In the next sections, we will concentrate on the analysis of this problem in the pseudoscalar and scalar quark channels.

### 3. RADIAL EXCITATIONS OF LIGHT PSEUDOSCALAR MESONS

In [15, 16], the properties of radial excitations of light pseudoscalar mesons were studied with the help of the following FESR:

$$\begin{aligned} M_k^{\text{th}} &= \int_{s_{n-1}}^{s_n} R_{\text{th}}^P(s) s^k ds = M_k^{\text{ph}} \\ &= \int_{s_{n-1}}^{s_n} R_{\text{ph}}^P(s) s^k ds, \end{aligned} \quad (20)$$

where  $s_n$  are the duality intervals, which will be defined below; the theoretical (th) spectral density of FESR is calculated in four-dimensional QCD; and the phenomenological (ph) model for the spectral function of FESR is chosen in the form of a  $1/N_c$ -motivated model

$$R_{\text{ph}}^P(s) = \sum_{l=1}^{\infty} 2f_P^2(l) m_P^4(l) \delta(s - m_P^2(l)). \quad (21)$$

Index  $P$  labels the sets of masses  $m_P(l)$  and decay constants  $f_P(l)$  of the radial excitations of light pseudoscalar mesons, namely,  $\pi$  and  $K$  mesons, which are considered as massless particles.

Neglecting the slight  $\alpha_s$  dependence, which comes from the leading-order terms of Eq. (4), the authors of [15, 16] obtained the following sum rule:

$$\frac{M_0^{\text{th}}(s_n)}{M_{-1}^{\text{th}}(s_n)} = \frac{1}{2}(s_n + s_{n-1}) = \frac{M_0^{\text{ph}}(s_n)}{M_{-1}^{\text{ph}}(s_n)} = m_P^2(n). \quad (22)$$

As the next step, the bounds of integration in Eq. (20) were chosen as

$$s_n = \frac{1}{2}[m_P^2(n) + m_P^2(n+1)], \quad (23)$$

$$s_0 = \frac{m_P^2(1)}{2}, \quad (24)$$

where  $m_P(1)$  is the mass of the first radial excitations of  $\pi$  mesons, namely, the  $\pi'$  state. The choice of these duality intervals is supported by the studies of possibilities to combine the  $1/N_c$ -motivated spectrum with the duality approach in two and four dimensions [19].

As the results of iterative solution of the system of Eqs. (22)–(24), the following mass formula for

the radial excitations of the  $\pi$  meson was obtained [15, 16]:

$$m_{\pi}^2(l) = m_{\pi'}^2 l, \quad l \geq 1. \quad (25)$$

In [16], these considerations were generalized to the case of the  $K$ -meson radial excitations and the identical expression for the mass spectrum

$$m_K^2(l) = m_{K'}^2 l, \quad l \geq 1, \quad (26)$$

was derived.

It should be stressed that the  $\pi'$  meson was observed by several experimental collaborations (see [2]). In [16], the result  $m_{\pi'} = 1240$  MeV, obtained at the Protvino accelerator by the Dubna–Milan–Bologna Collaboration [36], was used. Substituting it into Eq. (25), it is easy to get the following predictions:  $m_{\pi}(2) = 1753$  MeV,  $m_{\pi}(3) = 2148$  MeV, and  $m_{\pi}(4) = 2480$  MeV [16]. These numbers are in good agreement with the linear trajectories obtained in [3] and with the results of the recent OPE-based analysis in [9]. Note also that the application of effective chiral Lagrangians gives  $m_{\pi}(2) = 1.98$  GeV [10], while the experimental number from [36] is  $m_{\pi}(2) = 1.77 \pm 0.03$  GeV. The inclusion of the  $\pi$ -meson radial excitations in the studies of the QCD sum rule model for the pion wave function gave the following prediction:  $m_{\pi}(2) = 2.05 \pm 0.15$  GeV [37]. It is consistent with the result of [10], but is slightly higher than the prediction from [16], which is in surprisingly good agreement with the experimental result of [36].

Fixing now the experimental value of  $m_{K'} = 1.46$  GeV [2] as the input parameter, it is possible to obtain predictions for the masses of higher radial excitations of the  $K$  meson [16], namely,  $m_K(2) = 2.06$  GeV and  $m_K(3) = 2.53$  GeV. The prediction for the mass of the second radial excitation is consistent with the result  $m_K(2) = 2.1$  GeV obtained in [10], which is slightly higher than the experimental result  $m_K(2) = 1.86$  GeV [2]. Comparisons of the results of [16] in the  $K$ -meson channel with the results of other theoretical studies are really welcome.

As the next step, the FESR model for the decay constants of the radial excitations of light pseudoscalar mesons was estimated [15, 16]. Recalling that the duality interval of the ground state for the pseudoscalar particles can be defined as  $s_0 = m_P^2(1)/2$ , taking the ratio of the FESRs

$$\frac{M_2^{\text{th}}(s_n)}{M_2^{\text{th}}(s_0)} = \frac{s_{n+1}^2 - s_n^2}{s_0^2} = \frac{f_P^2(n) m_P^4(n)}{f_P^2 m_P^4}, \quad (27)$$

and supplementing it with Eq. (23), it is possible to get the following “linear dual model” for the coupling constants of radial excitations of the light pseudoscalar mesons [15, 16]:

$$f_P(l) = 2\sqrt{2} \frac{m_P^2}{m_P(1) m_P(l)} f_P, \quad l \geq 1. \quad (28)$$

Taking into account the concrete values for  $m_\pi$  and  $m_K$ , the values of the decay constants  $f_\pi$  and  $f_K$ , and the expressions for the masses of radial excitations of the pseudoscalar mesons  $m_\pi(l)$  and  $m_K(l)$ , one can get the FESR-inspired estimates for the decay constants of radial excitations of  $\pi$  and  $K$  mesons. It will be interesting to study the possible numerical uncertainties of this model using other approaches.

To conclude this section, it is also worth mentioning that a similar “linear dual spectrum” in the vector channel [14] can also be obtained within the Veneziano model [38].

#### 4. RADIAL EXCITATIONS OF LIGHT SCALAR MESONS

We are now ready to discuss the most intriguing part of the study [16], which is devoted to the derivation of linear dual spectra in the light scalar meson channel, whose ground state representatives  $a_0(980)$  and  $K^*(1430)$  will be considered as massive  $\bar{q}q$ -bound states. The only difference with the discussions presented in Section 3 is related to the redefinition of the ground-state duality interval from  $(s_0)_P = m_P^2(1)/2$  to  $(s_0)_S = 3m_S^2/2$ , where  $m_S$  are the masses of the  $a_0(980)$  and  $K^*(1430)$  light scalar mesons. This definition of  $(s_0)_S$  comes from the following ratio of the FESRs:

$$\frac{M_1^{\text{th}}(s_0)}{M_0^{\text{th}}(s_0)} = \frac{2(s_0)_S}{3} = m_S^2. \quad (29)$$

Combining this new value of the duality interval with Eqs. (22) and (23), the authors of [16] obtained the following scalar analog of the “pseudoscalar linear dual model” derived in the previous section [16]:

$$m_S(n) = (n+1)m_S^2, \quad (30)$$

$$f_S^2(n) = \frac{1}{n+1}f_S^2. \quad (31)$$

Thus, assuming the  $\bar{q}q$  structure of  $a_0(980)$  meson, we expected that the masses of its radial excitations may be estimated as  $a_0(1) = 1380$  MeV,  $a_0(2) = 1697$  MeV, and  $a_0(3) = 1960$  MeV. Note that the study [16] was the first one where the possibility of the existence of an extra light scalar resonance near  $a_0(1) = 1.4$  GeV was predicted. It is known now that there is an  $a_0(1450)$  meson in nature [2]. So, it may be treated as a possible candidate for the first radial excitation of the  $a_0(980)$  meson. Another pleasant feature of the linear dual spectrum derived in [16] for the  $a_0$ -meson excitations is that it turns out to be in satisfactory agreement with the results from [9]. As to the strange light scalar particle, namely, the  $K_0^*(1430)$  meson, within the approach described above, its possible radial excitations should

have the following masses:  $m_{K_0^*}(1) = 2022$  MeV and  $m_{K_0^*}(2) = 2477$  MeV. Note that the experimental data indicate the existence of the  $K_0^*(1950)$  meson, which, following the classification discussed above, can be considered as a candidate for the first radial excitation of the  $K_0^*(1430)$  meson. This meson may be a good candidate for the nonet partner of the  $a_0(1450)$  meson. However, to get a better understanding of the structure of the scalar nonets and the nature of both the  $a_0(980)$  and  $a_0(1450)$  mesons, it is rather important to continue studies of the classification of hadrons in the light scalar sector using various approaches.

#### 5. CONCLUSION

In this work, the applications of the QCD FESR approach for the derivation of linear dual spectra of radial excitations in the pseudoscalar and scalar quark–antiquark channel were recalled. In the process of consideration, both nonperturbative and, probably more important in the investigation of this problem, perturbative QCD effects were neglected. It is worth emphasizing that higher order perturbative QCD corrections for the massless two-point function of pseudoscalar and scalar quark currents calculated in [39, 40] are more important than the ones for the two-point function of the vector channel calculated in [41, 42]. In view of this, it can be of interest to take these calculated corrections into account in the studies of the properties of radial excitations of light mesons based on the OPE approach.

#### ACKNOWLEDGMENTS

I would like to thank Prof. Yu.A. Simonov for stimulating me to recall the results of the studies [15, 16], made at the beginning of the 1990s.

The work on this minireview was done within the framework of the Russian Foundation for Basic Research, project nos. 02-01-00601, 03-02-17047, and 03-02-17177.

#### REFERENCES

1. F. E. Close and N. A. Tornqvist, *J. Phys. G* **28**, R249 (2002); hep-ph/0204205.
2. K. Hagiwara *et al.* (Particle Data Group), *Phys. Rev. D* **66**, 010001 (2002).
3. A. V. Anisovich, V. V. Anisovich, and A. V. Sarantsev, *Phys. Rev. D* **62**, 051502 (2000); hep-ph/0003113.
4. N. N. Achasov and V. V. Gubin, *Phys. Rev. D* **56**, 4084 (1997); hep-ph/9703367.
5. S. B. Gerasimov, in *Proceedings of the 12th International Conference on Selected Problems of Modern Physics (Blokhintsev 03)*, Dubna, Russia, 2003; hep-ph/0311080.

6. T. Umekawa, K. Naito, M. Oka, and M. Takizawa, hep-ph/0403032.
7. S. Narison, Nucl. Phys. B (Proc. Suppl.) **96**, 244 (2001); hep-ph/0012235.
8. A. M. Badalian, B. L. G. Bakker, and Yu. A. Simonov, Phys. Rev. D **66**, 034026 (2002); hep-ph/0204088.
9. S. S. Afonin, A. A. Andrianov, V. A. Andrianov, and D. Espriu, J. High Energy Phys. **0404**, 039 (2004); hep-ph/0403268.
10. S. M. Fedorov and Yu. A. Simonov, Pis'ma Zh. Éksp. Teor. Fiz. **78**, 67 (2003) [JETP Lett. **78**, 57 (2003)]; hep-ph/0306216.
11. G. 't Hooft, Nucl. Phys. B **72**, 461 (1974).
12. E. Witten, Nucl. Phys. B **160**, 57 (1979).
13. M. Golterman, S. Peris, B. Phily, and E. De Rafael, J. High Energy Phys. **0201**, 024 (2002); hep-ph/0112042.
14. N. V. Krasnikov and A. A. Pivovarov, Phys. Lett. B **112B**, 397 (1982).
15. A. L. Kataev, N. V. Krasnikov, and A. A. Pivovarov, Phys. Lett. B **123B**, 93 (1983).
16. S. G. Gorishny, A. L. Kataev, and S. A. Larin, Phys. Lett. B **135B**, 457 (1984).
17. A. Bramon, E. Etim, and M. Greco, Phys. Lett. B **41B**, 609 (1972).
18. J. J. Sakurai, Phys. Lett. B **46B**, 207 (1973).
19. A. Bradley, C. S. Langensiepen, and G. Shaw, Phys. Lett. B **102B**, 180 (1981).
20. M. A. Shifman, in *Boris Ioffe Festschrift "At the Frontier of Particle Physics. Handbook of QCD"* (World Sci., Singapore, 2001), Vol. 3, p. 1447; hep-ph/0009131.
21. K. G. Chetyrkin, N. V. Krasnikov, and A. N. Tavkhelidze, Phys. Lett. B **76B**, 83 (1978).
22. A. A. Logunov, L. D. Soloviev, and A. N. Tavkhelidze, Phys. Lett. B **24B**, 181 (1967).
23. C. Becchi, S. Narison, E. De Rafael, and F. J. Yndurain, Z. Phys. C **8**, 335 (1981).
24. D. J. Broadhurst, A. L. Kataev, and C. J. Maxwell, Nucl. Phys. B **592**, 247 (2001); hep-ph/0007152.
25. T. van Ritbergen, J. A. M. Vermaseren, and S. A. Larin, Phys. Lett. B **400**, 379 (1997); hep-ph/9701390.
26. J. A. M. Vermaseren, S. A. Larin, and T. van Ritbergen, Phys. Lett. B **405**, 327 (1997); hep-ph/9703284.
27. K. G. Chetyrkin, Phys. Lett. B **404**, 161 (1997); hep-ph/9703278.
28. P. A. Baikov, K. G. Chetyrkin, and J. H. Kuhn, Phys. Rev. Lett. **88**, 012001 (2002); hep-ph/0108197.
29. M. A. Shifman, A. I. Vainshtein, and V. I. Zakharov, Nucl. Phys. B **147**, 385 (1979).
30. V. A. Novikov, M. A. Shifman, A. I. Vainshtein, and V. I. Zakharov, Nucl. Phys. B **191**, 301 (1981).
31. P. Nason and M. Palassini, Nucl. Phys. B **444**, 310 (1995); hep-ph/9411246.
32. V. I. Zakharov, Nucl. Phys. B **385**, 452 (1992).
33. N. V. Krasnikov and A. A. Pivovarov, Mod. Phys. Lett. A **11**, 835 (1996); hep-ph/9602272.
34. D. V. Shirkov and I. L. Solovtsov, Phys. Rev. Lett. **79**, 1209 (1997); hep-ph/9704333.
35. Yu. A. Simonov, Yad. Fiz. **65**, 140 (2002) [Phys. At. Nucl. **65**, 135 (2002)]; hep-ph/0109081.
36. G. Bellini *et al.*, Phys. Rev. Lett. **48**, 1697 (1982).
37. A. V. Radyushkin, in *Continuous Advances of QCD, Minneapolis 1994* (World Sci., River Edge, 1994), p. 238; hep-ph/9406237.
38. G. Veneziano, Nuovo Cimento A **57**, 190 (1968).
39. S. G. Gorishny, A. L. Kataev, S. A. Larin, and L. R. Surguladze, Mod. Phys. Lett. A **5**, 2703 (1990); Phys. Rev. D **43**, 1633 (1991).
40. K. G. Chetyrkin, Phys. Lett. B **390**, 309 (1997); hep-ph/9608318.
41. K. G. Chetyrkin, A. L. Kataev, and F. V. Tkachov, Phys. Lett. B **85B**, 277 (1979); M. Dine and J. R. Sapirstein, Phys. Rev. Lett. **43**, 68 (1979); W. Celmaster and R. J. Gonsalves, Phys. Rev. Lett. **44**, 560 (1980).
42. S. G. Gorishny, A. L. Kataev, and S. A. Larin, Phys. Lett. B **259**, 144 (1991); L. R. Surguladze and M. A. Samuel, Phys. Rev. Lett. **66**, 560 (1991); **66**, 2416(E) (1991); K. G. Chetyrkin, Phys. Lett. B **391**, 402 (1997); hep-ph/9608480.

# Lower Dimension Vacuum Defects in Lattice Yang–Mills Theory\*

V. I. Zakharov<sup>1)</sup>

Received May 21, 2004

**Abstract**—We overview lattice data on  $d = 0, 1, 2, 3$  dimensional vacuum defects in lattice four-dimensional  $SU(2)$  ( $SU(3)$ ) gluodynamics. In all the cases, defects have a total volume which scales in physical units (with zero fractal dimension). In the case of  $d = 1, 2$ , the defects are distinguished by ultraviolet divergent non-Abelian action as well. This sensitivity to the ultraviolet scale allows us to derive strong constraints from the continuum theory on the properties of the defects, which turn out to be satisfied by the lattice data. We discuss a classification scheme of the defects which allows us to (at least) visualize the defect properties in a simple and unified way. A not-yet-checked relation of the defects to the spontaneous chiral symmetry breaking is suggested by the scheme. Finally, we present some arguments that the defects considered could become fundamental variables of a dual formulation of the theory. © 2005 Pleiades Publishing, Inc.

## 1. INTRODUCTION

Somehow, it went largely unnoticed that nonperturbative QCD has been changing fast. The change is mostly due to results of lattice simulations which ask sometimes for a reshuffle of the continuum-theory models (see, in particular, [1]). Moreover, in many cases, the lattice measurements use a specific language, not easy to translate into standard field theory. As a result, there arises a mismatch between richness of the lattice data and scarceness of their interpretation in the continuum theory. An important example of this type is models of confinement. Indeed, instantons still dominate thinking on nonperturbative physics on the continuum-theory side. On the other hand, it is known from lattice measurements that instantons are not confined [2]. Moreover, the vacuum fluctuations which are responsible for the confinement have also been identified and turn out to be monopoles and P vortices (for a review see, e.g., [3, 4]).

There is no understanding whatsoever of these confining fluctuations on the fundamental level. Moreover, if now someone decides to go into interpretation of the lattice data on confinement, there is no regular way to approach the problem. The point is that the monopoles and vortices are defined on the lattice rather algorithmically, then directly in terms of the gluonic fields. The central step is the use of projections which replace, say, the original non-Abelian fields by the closest Abelian-field configurations. The

projection is a highly nonlocal procedure and blocks out any direct interpretation of the data.

To circumvent this difficulty, we try to summarize here the lattice data on the confining vacuum fluctuations entirely in a gauge-invariant way. Hopefully, this could facilitate appreciation of the results in terms of the continuum theory.

What challenges the continuum theory the most is a relatively recent discovery that the monopoles (see [5] and references therein) and vortices (see [6]) are associated with ultraviolet divergent non-Abelian action. Since gluodynamics is well understood at short distances, this newly discovered sensitivity of the vacuum defects to the ultraviolet scale makes them subject to strong constraints from the continuum theory [7].

The presentation is as follows. In Section 2, we summarize lattice data on the confining fluctuations. In Section 3, constraints from the continuum theory are outlined. In Section 4, a possible relation to dual formulations of the Yang–Mills theories is discussed.

## 2. LATTICE PHENOMENOLOGY

### 2.1. Total Volume

Imagine that indeed there exist low-dimensional structures in the vacuum state of gluodynamics. Which  $SU(2)$  invariants could be associated with such defects?

First of all, we could expect that the total volume of the corresponding defects scales in physical units. What this means is easier to explain using particular examples.

\*This article was submitted by the author in English.

<sup>1)</sup>Max-Planck Institut für Physik Werner-Heisenberg Institut, Munich, Germany; e-mail: xxz@mppmu.mpg.de

**$d = 0$  defects.** In this case, we are discussing density of points in the  $d = 4$  space. And our expectation for the total number of the pointlike defects would be

$$N_{\text{tot}} = c_0 \Lambda_{\text{QCD}}^4 V_4, \quad (1)$$

where  $V_4$  is the volume of the lattice and  $\Lambda_{\text{QCD}}$  can be understood either as a position of the pole of the (perturbative) running coupling or, say, as  $\Lambda_{\text{QCD}} = \sqrt{\sigma_{SU(2)}}$ , where  $\sigma_{SU(2)}$  is the string tension. Appearance of  $\Lambda_{\text{QCD}}$  in (1) would signal possible relevance of the fluctuations to the confinement.

Equation (1) could be readily understood if we were discussing instantons. And, as far as dimensional considerations are concerned, the instanton example is valid. However, it might be worth mentioning from the very beginning that instantons actually do not belong to the sequence of vacuum fluctuations which we are going to consider. We will come back later to the physical meaning of the  $d = 0$  defects.

**$d = 1$  defects.** The  $d = 1$  defects are lines. For the total length, one can expect

$$L_{\text{tot}} = c_1 \Lambda_{\text{QCD}}^3 V_4. \quad (2)$$

Such defects can be identified with the percolating monopoles {for the latest data on (2), see [8, 9]}. Percolation<sup>2)</sup> means that there exists a large cluster of monopole trajectories stretching itself through the whole volume of the lattice. In the limit of infinite volume, the percolating cluster also becomes infinite. Note also that the monopole trajectories are closed by as reflection of the monopole charge conservation.

It is worth emphasizing that the scaling law (2) is highly nontrivial and, from the point of view of the lattice measurements, represents a spectacular phenomenon. Indeed, on the lattice, one changes arbitrarily the lattice spacing  $a$ , while the corresponding bare coupling,  $g(a)$ , is changed logarithmically, according to the renormgroup. The scaling law (2) implies that the probability  $\theta(a)$  for a given link (actually, on the dual lattice) to belong to the percolating cluster changes as a power of  $a$ :

$$\theta(a) \sim (\Lambda_{\text{QCD}} a)^3. \quad (3)$$

Thus, in this case, powers, not logs of the ultraviolet cutoff, are observed. In other words, there is no perturbative background to the defects which we are discussing and we are addressing directly nonperturbative physics. In a way, it looks like a miracle that such pure nonperturbative objects exist.

**$d = 2$  defects.** The defects are now two-dimensional surfaces, and for the total area, the scaling law would read

$$A_{\text{tot}} = c_2 \Lambda_{\text{QCD}}^2 V_4. \quad (4)$$

Such defects can be identified with percolating P vortices which are known to satisfy (4) (for the latest data, see [6]). As in all other cases discussed here, the evidence is purely numerical, though. Because of space considerations, we do not discuss here error bars, concentrating only on the general picture. Details can be found in the original papers.

**$d = 3$  defects.** For a percolating three-dimensional volume we could expect

$$V_3 = c_3 \Lambda_{\text{QCD}} V_4. \quad (5)$$

Defects obeying this scaling law were indeed discovered recently [11]. However, their observation is too recent and there is no commonly accepted name attached to these defects.

## 2.2. Non-Abelian Action Associated with the Defects

Defects can be distinguished by their non-Abelian action as well. Since we have not yet specified the defects, at first sight, we cannot say anything about their action. Surprisingly enough, there exist educated guesses concerning the non-Abelian action of the defects based on their dimension alone.

**$d = 1$  defects.** This case is singled out by the consideration that trajectories correspond to particles. Particles, on the other hand, belong to field theory and we may hope to get insight into the properties of the trajectories from field theory. And, indeed, the action

$$S = ML, \quad (6)$$

where  $L$  is the length of the trajectory and  $M$  is a mass parameter, coincides with the classical action for a free particle of mass  $M$ . One may hope, therefore, that, by evaluating propagation of a particle as a path integral with the action (6), one can reconstruct the quantum propagator of a free particle. And, indeed, this theoretical construction works. Moreover, it is well known as the polymer approach to the field theory (see, in particular, [12]). Note that the use of the Euclidean (rather than Minkowski) space is actually crucial to evaluate the corresponding path integral. Also, one needs to introduce a lattice to formulate the theory.

Although the use of the action (6) does allow one to recover the free-field propagator, the propagating mass turns out not to be the same  $M$  but is equal to

$$m_{\text{prop}}^2 = \frac{\text{const}}{a} \left( M(a) - \frac{\ln 7}{a} \right), \quad (7)$$

where the constants “const” and  $\ln 7$  are of pure geometrical origin and depend on the lattice used. In particular,  $\ln 7$  corresponds to the hypercubic lattice.

<sup>2)</sup>For theoretical background, see, e.g., [10].

Note that, in Eq. (7), we reserved now for the dependence of the mass parameter  $M(a)$  on the lattice spacing  $a$ . Indeed, tuning of  $M(a)$  to  $(\ln 7)/a$  is needed to consider a particle with mass independent of the lattice spacing  $a$ .

Thus, our prediction for the action associated with  $d = 1$  defects (which are nothing else but monopole trajectories) is that the action is close to

$$S_{\text{mon}} \approx \frac{\ln 7}{a} L. \tag{8}$$

Indeed, in this way, we can explain that the length of the trajectories does not depend on  $a$  [see Eq. (2)].

Prediction (8) does agree with the results of direct measurements of the non-Abelian action of the monopoles [5]. Let us emphasize that the prediction (8) does not use anything specific for monopoles and is rooted in the standard field theory. Indeed, the polymer approach to field theory is no better or no worse than other approaches.

**$d = 2$  defects.** There exists simple theoretical argumentation in favor of an ultraviolet divergent action of the two-dimensional defects (or vortices) as well. Consider the so-called gluon condensate

$$\langle (G_{\mu\nu}^a)^2 \rangle \approx \frac{N_c^2 - 1}{a^4} (1 + O(\alpha_s)), \tag{9}$$

where  $G_{\mu\nu}^a$  is the non-Abelian field strength tensor and  $a$  is the color index. Note that the condensate (9) on the lattice is in fact nothing else but the average plaquette action [13].

The vacuum expectation value (9) diverges as the fourth power of the ultraviolet cutoff. This divergence is in one-to-one correspondence with the divergence in the density of the vacuum energy, well known in the continuum theory. If one neglects interaction of the gluons, the gluon condensate (9) reduces to a sum over energies of the zero-point fluctuations. That is why the right-hand side of (9) in the zero approximation is proportional to the number of degrees of freedom, i.e., to the number of gluons. Accounting for the gluon interaction brings in perturbative corrections. For details and the most advanced calculations, see the last paper in [13].

Note now that the monopole trajectories with the properties (2) and (8) give the following contribution to the gluon condensate:

$$\langle (G_{\mu\nu}^a)^2 \rangle_{\text{mon}} \approx \frac{N_c^2 - 1}{a^4} \text{const}(\Lambda_{\text{QCD}} a)^3. \tag{10}$$

In other words, monopoles correspond to a powerlike correction to the perturbative value of the gluon condensate.

Now, the central point is that there exists a rather well developed theory of the power corrections (for a

review, see [14]). The leading powerlike correction is expected to be associated with the so-called ultraviolet renormalon. The corresponding contribution is of order

$$\langle (G_{\mu\nu}^a)^2 \rangle_{\text{uv. ren}} \approx \frac{N_c^2 - 1}{a^4} \text{const}(\Lambda_{\text{QCD}} a)^2. \tag{11}$$

Note that the power of  $(\Lambda_{\text{QCD}} a)$  here is different from what the monopoles give [see Eq. (10)].

From this point of view it would be unnatural if the monopoles exhausted the power corrections. Moreover, if the  $d = 2$  defects with the total area satisfying (4) had the action

$$S_{\text{vort}} = \text{const} \frac{A}{a^2}, \tag{12}$$

then their contribution would fit the ultraviolet renormalon (11). In this way, one could have predicted (12). The data on the non-Abelian action associated with the P vortices [6] do agree with (12):

$$S_{\text{vort}} \approx 0.54 \frac{A}{a^2}, \tag{13}$$

where  $A$  is the total area of the vortices.

**$d = 3$  defects.** Proceeding to the three-dimensional defects, we could predict that the story does not repeat itself and there is no ultraviolet action associated with the  $V_3$ . Indeed, if the action were of order  $V_3/a^3$ , the corresponding power correction to the gluon condensate would exceed the ultraviolet renormalon [see (11)] by  $(\Lambda_{\text{QCD}} a)^{-1}$  and contradict the theory.

The data [11] indeed do not indicate any excess of the action associated with the  $V_3$ . One could claim this to be a success of the theory. On the other hand, the three-dimensional defects so far are lacking identity in terms of gauge invariant characteristics. The only known characteristic of this type is the total volume [see (5)].

### 2.3. Entropy Associated with the Defects

The ultraviolet divergences in the action of the monopoles [see (8)] and of vortices [see (12)] suggest, at first sight, that these fluctuations are not physical and exist only on scale of the lattice spacing  $a$ . Indeed, the probability, say, to observe a monopole trajectory of length  $L$  is suppressed by the action as

$$W(L) \approx \exp(-S_{\text{mon}}) \text{Entropy} \tag{14} \\ \sim \exp(-(\ln 7)L/a) \text{Entropy},$$

and in the continuum limit of  $a \rightarrow 0$ , the suppression due to the action is infinitely strong. Since, on the other hand, the observed length of the monopole trajectories does not tend to zero in the limit  $a \rightarrow 0$ , the suppression by action is to be canceled by the

same strong enhancement due to the entropy. Let us discuss this issue in more detail in cases  $d = 1, 2$ .

**$d = 1$  defects.** In this case, the entropy factor is the number  $N(L)$  of different trajectories of same length  $L$ . It is quite obvious that, for  $L$  fixed and  $a \rightarrow 0$ ,  $N(L)$  grows exponentially with  $L$  [12]. Indeed, the trajectory on the lattice is a sequence of steps of length  $a$ . The number of steps is  $L/a$ , and at each step, one can arbitrarily choose the direction. The number of directions is determined by the geometry of the lattice. This is the origin of the factor  $(\ln 7)/a$  in Eq. (7) valid for the hypercubic lattice.

Therefore, the observation (8) is nothing else but the statement that, in the case of monopole trajectories, the entropy is fine-tuned to the action. Moreover, since there is actually no free parameter in the theory (the QCD coupling is running and cannot be tuned), we are dealing instead with self-tuning of the monopole trajectories. This should be a dynamical phenomenon. The author of the present review finds this observation of self-tuned objects on the lattice absolutely remarkable.

**$d = 2$  defects.** The suppression due to the action is again there [see (13)]. Moreover, the observation (4) implies that the entropy is again self-tuned to the action. However, the theory of this self-tuning, even on an algebraical (to say nothing, dynamical) level is actually missing. Namely, there is no theory which would fix the constant in front of  $A/a^2$  [see Eq. (13)] and which is an analog of  $\ln 7$  in the case of trajectories. Moreover, there is a solid argumentation showing that the action associated with the vortices cannot be the Nambu–Goto action (which is simply proportional to the area). Details of the proof can be found in textbooks on quantum geometry (see, e.g., [15]). Detailed investigations of the action of the percolating vortices on the lattice are summarized in [16].

In view of the lack of a theory of fine-tuned vortices, it is worth emphasizing that one can at least check directly on the lattice that the entropy does provide an exponential enhancement for the vortices. Indeed, the mutual orientation of the neighboring plaquettes constituting the vortex is close to random (see [16]). This observation suffices to prove an exponential enhancement with the total area  $A$  of the number of vortices with the same area  $A$ .

To summarize, the lattice phenomenology seems to have jumped ahead of the theory of crumpled manifolds of dimension  $d = 2$ . The very existence of such fine-tuned surfaces is a very important observation (qualified, as usual, for the fact that measurements refer to some finite, although small, lattice spacings  $a$ ) for the theory of surfaces.

## 2.4. Alignment of Geometry and Non-Abelian Fields

So far, we have considered geometry and non-Abelian fields associated with the defects separately. The total volume is a geometrical scalar and the total action is a scalar constructed on the fields. Of course, observation of invariant characteristics which mix up geometry and fields would be even more interesting.

**$d = 3$ .** Let us start with  $d = 3$  and assume existence of three-dimensional volumes to be granted. The volume percolates on the scale  $\Lambda_{\text{QCD}}^{-1}$ . However, if we let  $a \rightarrow 0$ , then we can think in terms of large (in lattice units)  $d = 3$  defects. What are the possible  $SU(2)$  invariants associated with these volumes?

In  $d = 3$ , the  $SU(2)$  gluodynamics is described by three vectors  $\mathbf{H}^a$  ( $a = 1, 2, 3$ ), where the “magnetic fields”  $\mathbf{H}^a$  are vectors in both the coordinate and color spaces. Generically, there are three independent vectors and the simplest invariant constructed on these fields is their determinant. However, the absolute value of the determinant varies from one point of the  $d = 3$  volume to another. The invariant which can be associated with the whole volume is, obviously, the sign of the determinant:<sup>3)</sup>

$$I_3 = \text{sgn}\{\epsilon^{ikl} \epsilon_{abc} H_i^a H_k^b H_l^c\}. \quad (15)$$

Unfortunately, there are no lattice data which could confirm or reject this prediction.

**$d = 2$  defects.** The invariant (15) is uniquely defined as far as all three magnetic fields are indeed independent. If there are only two independent vectors, the determinant has a zero of first order and geometrically we then have a closed  $d = 2$  surface which bounds the  $d = 3$  defects. It seems natural to speculate that these boundaries are the  $d = 2$  defects, or vortices.

Thus, we come to the prediction that the percolating  $d = 2$  surfaces and non-Abelian fields are aligned with each other. In other words, the non-Abelian fields associated with the vortices and resulting in the excess of the action (12) are predicted to spread over the surface, while the perpendicular component is to vanish. This prediction works [6] perfectly well.

**$d = 1$  defects.** The next step is a reiteration of the previous one. Namely, there could be zeros of the

<sup>3)</sup>The classification scheme of the defects we are proposing below, to our knowledge, has not been discussed in the literature. However, at least partially, it is close to or motivated by well-known papers (see, in particular, [17]). It is worth emphasizing that we are using the continuum-theory language, assuming fields to be continuous functions of the coordinates. Since on the lattice the measurements are performed on the scale of the lattice spacing  $a$ , the lattice fields fluctuate wildly on the same scale. Thus, the underlying assumption is that the continuum-theory language is still valid on average, so that the perturbative fluctuations do not interfere with the topology.

second order of the determinant in (15) and geometrically zeros of the second order are closed trajectories. Moreover, if these closed lines are monopole trajectories (which are indeed closed by definition), the non-Abelian field of the monopoles is to be aligned with their trajectories. This expectation is confirmed by the existing data [18].

It is amusing that the monopoles are expected to be locally Abelian. Indeed, there is only one independent color magnetic field associated with them. Moreover, they are singular [see (8)]. Thus, we are coming to an after-the-fact justification of the use of the Abelian projection to detect the monopoles. On the other hand, their field is absolutely not spherically symmetrical (which would be the case for the Dirac monopoles). And this spatial asymmetry is manifested in the measurements [18].

### 2.5. Spontaneous Breaking of Chiral Symmetry

Note that our classification scheme predicts that the  $d = 3$  defects are characterized by invariants which distinguish between left- and right-hand coordinates. Of course, on average, the regions with determinants (15) positive and negative occupy the same volume. {Moreover, in the continuum limit, the percolating  $d = 3$  volume [see Eq. (5)] occupies a vanishing part of the whole  $d = 4$  space.}

As mentioned above, there is no direct observational confirmation of the classification scheme for  $d = 3$  defects. However, it is known that removal of the P vortices restores chiral symmetry [19].

Moreover, there is an interesting suggestion that the winding number, i.e., the difference between left- and right-handed zero fermionic modes, is associated with self-intersections of the P vortices.<sup>4)</sup> Then the  $d = 0$  defects of our scheme could naturally be identified with the number of self-intersections of the P vortices.

## 3. THEORETICAL CONSTRAINTS

### 3.1. Consistency with the Asymptotic Freedom

It is worth emphasizing that there is no developed theory of the defects considered. So far, we have summarized lattice observations. Moreover, we have even been avoiding discussion on how the defects are defined and observed on the lattice (for reviews, see, e.g., [3, 4, 20]). Let us only mention that the guiding principle to define the defects was the search for effective infrared degrees of freedom responsible for the confinement.

However, what is most amusing from the theoretical point of view is that the defects have highly

nontrivial properties in the ultraviolet. The ultraviolet divergence in the action [see (8), (13)] is most remarkable.

Indeed, Yang–Mills theories are well understood at short distances. The only divergence which is allowed on the fundamental level is the one in the coupling  $\alpha_s$ . Thus, one could argue that all the ultraviolet divergences are calculable perturbatively in asymptotically free theories. Moreover, this statement seems rather trivial. What is actually not so trivial is that, on the lattice, one can also consider powerlike divergences [see, e.g., (10), (11)]. In the continuum theory, powerlike ultraviolet divergences usually are used, at best, for estimates. On the lattice, the ultraviolet cutoff is introduced explicitly and one can treat powerlike divergent observables in a fully quantitative way [see, e.g., (9)]. This extends in fact the predictive power of the theory.

It is, therefore, no surprise that, using the asymptotic freedom, one can derive strong constraints on the properties of the vortices [7].

### 3.2. Classical Condensate $\langle \phi_{\text{magn}} \rangle$

Let us consider first the vacuum condensate of the magnetically charged field  $\langle 0 | \phi_{\text{magn}} | 0 \rangle$ . Of course, in the Yang–Mills theory, there is no fundamental magnetically charged field. However, the monopole trajectories are observed on the lattice. Using the polymer approach to field theory, we can translate the lattice data on trajectories into a field-theoretic language (see [7, 21] and references therein). The only assumption is that there exists an effective field theory for the magnetically charged field.

In particular, the percolating cluster corresponds to the classical vacuum expectation value  $\langle \phi \rangle$ . One can derive [21]

$$\langle \phi_{\text{magn}} \rangle^2 \approx \frac{a}{8} \rho_{\text{perc}} \approx \text{const} \Lambda_{\text{QCD}}^2 (a \Lambda_{\text{QCD}}). \quad (16)$$

### 3.3. Vacuum Expectation Value $\langle |\phi_{\text{magn}}|^2 \rangle$

One can also expect that there exist quantum fluctuations. And indeed, apart from the percolating cluster, there are observed finite monopole clusters, which are naturally identified with quantum fluctuations. A basic characteristic for these clusters is again their total length. By definition,

$$L_{\text{tot}} \equiv L_{\text{perc}} + L_{\text{fin}} \equiv \rho_{\text{perc}} V_4 + \rho_{\text{fin}} V_4, \quad (17)$$

where  $\rho_{\text{perc}}$  and  $\rho_{\text{fin}}$  are called the densities of the percolating and finite monopole clusters, respectively.

Using the polymer approach to the field theory, one can express the vacuum expectation value of the

<sup>4)</sup>This remark is due to R. Alkofer, private communication.

magnetically charged field in terms of the monopole trajectories [21]:

$$\langle |\phi|^2 \rangle = \frac{a}{8} (\rho_{\text{perc}} + \rho_{\text{fin}}). \quad (18)$$

Instead of deriving this relation (which is also quite straightforward), let us explain why (18) is natural. Concentrate on the quantum fluctuations, i.e., on  $\rho_{\text{fin}}$ . Moreover, consider small clusters  $L \ll \Lambda_{\text{QCD}}^{-1}$ . Then there is no mass parameter at all, and on pure dimensional ground, one would expect

$$(\rho_{\text{fin}})_{\text{dim}} = \frac{\text{const}}{a^{D-1}} = \frac{\text{const}}{a^3}, \quad (19)$$

where  $D$  is the number of dimensions of space and we consider the  $D = 4$  case. If this dimensional estimate holds, then the vacuum expectation value will be quadratically divergent in the ultraviolet:

$$\langle |\phi|^2 \rangle_{\text{dim}} \sim a^{-2}. \quad (20)$$

And we rederive the standard quadratic divergence in the vacuum expectation value of a scalar field.

Now, the central point is that, although we call all these estimates “dimensional” or “natural,” we are not allowed to have (20). Indeed, Eq. (20) would hold for an elementary scalar field. However, we are not allowed to have new elementary particles at short distances. Because of the asymptotic freedom, there are only free gluons at short distances. And what are we allowed to have for the vacuum expectation value in point? Clearly,

$$\langle |\phi|^2 \rangle_{\text{allow}} \sim \Lambda_{\text{QCD}}^2. \quad (21)$$

In terms of the monopole trajectories (which are our observables) Eq. (21) reduces to

$$\rho_{\text{fin}} \sim \Lambda_{\text{QCD}}^2/a. \quad (22)$$

It is most remarkable that the data [8, 9] do comply with (22)!

### 3.4. Branes

It is of course very gratifying that the data comply with the constraint (21). On the other hand, the reader may feel that our summary of the phenomenology looks self-contradictory. Indeed, first we observed that the non-Abelian monopole action corresponds to a pointlike particle [see (8)]. But then we said that there should be no new particles, and the data agree with that constraint.

Still, there is no contradiction between these observations. Rather, taken together, they amount to observation of a new object, which can be called branes. Indeed, cancellation of  $(\ln 7)/a$  in the equation for the mass is needed to balance the entropy at very short distances of order  $a$ . Equation (21),

on the other hand, is a global constraint. The geometrical meaning of this constraint is actually transparent. Namely, it means that, on a large scale, the monopoles live not on the whole  $d = 4$  space but on its  $d = 2$  subspace.

Within the classification scheme of the defects which we discussed above, this association of the monopoles with surfaces is automatic. Algorithmically, however, the trajectories and surfaces are defined independently. And the fact that the monopole trajectories do belong to surfaces is highly nontrivial from the observational point of view.

Thus, what is observed on the lattice are  $d = 2$  surfaces populated with “particles” (better to say, with the tachyonic mode of the monopole field). When we call these objects branes, we emphasize that the affinity of the monopoles to the surfaces remains true even at the scale  $a$ . Traditional discussions of the P vortices and monopoles emphasize, on the other hand, physics in the infrared, and one talks about “thick vortices” (see, e.g., [4]).

### 3.5. Implications for Models

**Abelian Higgs model.** The lattice data on monopoles are usually interpreted in terms of an effective Abelian Higgs model (see, in particular, [22] and references therein). Our Eq. (16) implies, however,

$$\langle \phi_{\text{magn}} \rangle \sim (a\Lambda_{\text{QCD}})^{1/2} \Lambda_{\text{QCD}}. \quad (23)$$

It is most remarkable that the classical condensate vanishes in the continuum limit  $a \rightarrow 0$ . Nevertheless, the heavy quark potential at large distances generated by the monopoles remains the same since it is determined entirely by  $\rho_{\text{perc}}$ , which scales in the physical units!

To establish a relation to the standard fit to the Abelian Higgs model, one should use, most probably, matching of the two approaches at some  $a$ .<sup>5)</sup>

**Gauge-invariant condensate of dimension two.** Equations (21), (22) provide us with a value for a gauge-invariant condensate of dimension two:

$$\langle |\phi_{\text{magn}}|^2 \rangle \approx a\rho_{\text{fin}} \sim \Lambda_{\text{QCD}}^2. \quad (24)$$

In terms of the fundamental variables, a condensate of dimension two was introduced [23] as the minimum value along the gauge orbit of the gauge potential squared  $(A_\mu^a)^2_{\text{min}}$ . While the  $\langle (A_\mu^a)^2 \rangle_{\text{min}}$  is contaminated with perturbative divergences, the condensate (24) provides us, on the phenomenological level, directly with a nonperturbative condensate of dimension two. On the theoretical side, the nonperturbative part of the condensate of dimension two in

<sup>5)</sup>The author would like to acknowledge discussion of this point with M.N. Chernodub.

the Hamiltonian picture is related to the Gribov horizon [24]. Existence of a gauge-invariant condensate of dimension two is crucial for models of hadrons (see, in particular, [25]).

**Magnetic condensation.** It has been speculated for a long time that the perturbative vacuum is not stable against formation of a nonperturbative condensate of the magnetic field,  $\langle H^2 \rangle$  (for a recent analysis and references, see [26]). The lattice data reviewed above suggest that, indeed, there is condensation of the (locally) Abelian magnetic field, and the corresponding vacuum expectation value is of order

$$\langle (\mathbf{H}_{\text{Abel}})^2 \rangle \sim \Lambda_{\text{QCD}}^2 a^{-2}. \quad (25)$$

Note the ultraviolet divergence on the right-hand side.

**Singular fields.** Although we repeatedly emphasize that the branes are associated with singular fields, it should also be mentioned that the non-Abelian fields are, on the logarithmic scale, much smaller than the corresponding projected fields. In particular, the Dirac monopole would have a larger action:

$$S_{\text{Dir}} \sim \frac{1}{g^2} \frac{L}{a} \gg \ln 7 \frac{L}{a}, \quad (26)$$

where  $g^2$  is the gauge coupling and we consider the limit  $g^2 \rightarrow 0$ . Even at presently available  $g^2$ , the action calculated in terms of the projected Abelian fields (corresponding to the Dirac monopole) is a few times larger than the actual non-Abelian action, which determines the dynamics and which we have discussed so far. A similar inequality holds for the vortices.

This distinction—in terms of the action—between the Dirac and lattice monopoles is very important from the theoretical point of view. The observed monopoles are associated with singular non-Abelian fields, but these fields are no more singular than ordinary zero-point fluctuations, or perturbative fields. The Dirac monopoles, on the other hand, in the limit of  $g^2 \rightarrow 0$ , would be more singular than the perturbative fields. According to the standard ideas of the lattice theories, such fields could actually be removed without affecting the basic physical content of the theory. The lattice monopoles and vortices, on the other hand, cannot be removed without affecting perturbative fluctuations as well. In the next section, we will consider this issue in much more detail.

#### 4. TOWARDS DUALITY

It is well known that topological excitations of a “direct” formulation of a theory may become fundamental variables of a dual formulation of the same theory. Examples can be found, e.g., in the review [27]. Little, if anything, is known theoretically

on the dual formulation of the Yang–Mills theories without supersymmetry. Nevertheless, generically, one might think in terms of branes [28]. In case of supersymmetric extensions of Yang–Mills theories, the branes are classical solutions. One could speculate that the branes discussed in this review are “quantum branes.” Of course, it remains a pure speculation until something definite can be said on the properties of the quantum branes on the theoretical side. It is amusing, however, that there is a sign of duality between the branes discussed in the preceding section and high orders of perturbation theory [29].

### 5. LONG PERTURBATIVE SERIES

#### 5.1. Expectations

Let us start with recalling some basic facts about perturbative expansions (for detailed reviews, see, e.g., [14]). A generic perturbative expansion for a matrix element of a local operator has the form

$$\langle O \rangle = (\text{Parton model}) \cdot \left( 1 + \sum_{n=1}^{\infty} a_n \alpha_s^n \right), \quad (27)$$

where we normalized the anomalous dimension of the operator  $O$  to zero and  $\alpha_s$  is small,  $\alpha_s \ll 1$ .

In fact, expansions (27) are only formal since the coefficients  $a_n$  grow factorially at large  $n$ :

$$|a_n| \sim c_i^n n!, \quad (28)$$

where  $c_i$  are constants. Moreover, there are a few sources of the growth (28) and, respectively,  $c_i$  can take on various values. The factorial growth of  $a_n$  implies that the expansion (27) is asymptotic at best, which means, in turn, that (27) cannot approximate a physical quantity to an accuracy better than

$$\Delta \sim \exp(-1/c_i \alpha_s) \sim (\Lambda_{\text{QCD}}^2 a^2)^{b_0/c_i}, \quad (29)$$

where  $b_0$  is the first coefficient in the  $\beta$  function. To compensate for these intrinsic uncertainties, one modifies the original expansion (27) by adding the corresponding power corrections with unknown coefficients.

In the case of the gluon condensate, the theoretical expectations can be summarized as

$$\begin{aligned} \left\langle 0 \left| \frac{-\beta(\alpha_s)}{\alpha_s b_0} (G_{\mu\nu}^a)^2 \right| 0 \right\rangle &\approx \alpha_s \frac{N_c^2 - 1}{a^4} \\ &\times \left( 1 + \sum_{n=1}^{\sim N_{\text{ir}}} a_n \alpha_s^n + \text{const}(a^4 \Lambda_{\text{QCD}}^4) \right), \end{aligned} \quad (30)$$

where

$$N_{\text{ir}} \approx 2/(b_0 \alpha_s)$$

and terms proportional to  $\Lambda_{\text{QCD}}^4$  correspond to  $\langle 0|(G_{\mu\nu}^a)^2|0\rangle_{\text{soft}}$ , which enters the QCD sum rules (for review, see [30]).

A conspicuous feature of the prediction (30) is the absence of a quadratic correction [compare (11)].

Thus, we are seemingly coming close to a contradiction between the lattice branes and continuum-theory perturbation theory. Let us, however, have a closer look at the problem.

### 5.2. Numerical Results

Numerically, this problem was studied in greatest detail in the papers in [13] (especially in the latest one). The results can be summarized in the following way. Represent the plaquette action  $\langle P \rangle$  as

$$\langle P \rangle \approx P_{\text{pert}}^N + b_N a^2 \Lambda_{\text{QCD}}^2 + c_N a^4 \Lambda_{\text{QCD}}^4, \quad (31)$$

where the average plaquette action  $\langle P \rangle$  is measurable directly on the lattice and is known to high accuracy;  $P_{\text{pert}}^N$  is the perturbative contribution calculated up to order  $N$ ,

$$P_{\text{pert}}^N \equiv 1 - \sum_{n=1}^{n=N} p_n g^{2n}; \quad (32)$$

and, finally, coefficients  $b_N$  and  $c_N$  are fitting parameters whose value depends on the number of loops  $N$ . Moreover, the form of the fitting function (31) is suggested by the data rather than imposed because of theoretical considerations.

The conclusion is that, up to ten loops,  $N = 10$ , it is the quadratic correction which is seen on the plots, while  $c_N$  are consistent with zero. However, the value of  $b_N$  decreases monotonically with growing  $N$  [13]. The factorial divergence (28) is not yet seen and the perturbative series reproduces the measured plaquette action at the level of  $10^{-3}$ . Finally, at the level of  $10^{-4}$ , the  $\Lambda_{\text{QCD}}^4$  term seems to emerge [13].

### 5.3. Implications

Now, we see a fundamental difference between the instantons and branes. The instantons correspond to the “soft” gluon condensate and are hidden in the  $(\Lambda_{\text{QCD}} a)^4$  corrections which are not calculable perturbatively. In short, instantons are added to perturbation theory.

The branes, on the other hand, appear to be dual to long perturbative series. If one is able to calculate many orders of perturbation theory, there is no need to account for the branes as far as local quantities are concerned.

This might first sound disappointing for those who are beginning to believe in the important role of lattice branes. In fact, it is not disappointing at all. On the contrary, we have the first firm piece of evidence that the branes belong to a dual world. To reiterate, the instantons belong to the “direct” formulation and they are added to the perturbation theory of the direct formulation. Branes belong to the dual formulation. Adding them to the perturbation theory of the direct formulation would be mixing up two different (dual to each other) representations of the same theory.

Actually, the very existence of fine-tuned branes could not be understood within the direct formulation of the Yang–Mills theory. However, if there were an existence theorem for a dual formulation, the fine (or self) tuning would be implied by the theorem. Reversing the argument, we can say that observation of the fine tuning might indicate existence of a dual formulation.

### ACKNOWLEDGMENTS

This minireview is written on the occasion of the seventieth birthday of Yuri Antonovich Simonov. I am grateful to him for many years of sharing his ideas on QCD, discussions, and friendship.

This minireview is devoted to interpretation of the lattice data obtained mostly by the colleagues of Yu.A. Simonov from ITEP: P.Yu. Boyko, M.N. Chernodub, F.V. Gubarev, A.N. Kovalenko, M.I. Polikarpov, and S.N. Syritsyn. I am grateful to all of them for the common work used in these notes and numerous discussions. My special thanks go to M.I. Polikarpov, whose role in organizing this common work was most crucial. I am grateful to R. Alkofer, A. Di Giacomo, Ch. Gatttringer, J. Greensite, and L. Stodolsky for enlightening discussions.

The notes above were presented as a talk at the Workshop on Quantum Field Theory at Ringberg in February 2004. I am grateful to the organizers, W. Zimmermann, D. Maison, and E. Seiler, for the invitation and hospitality.

The text of the review was finalized while the author was visiting Pisa University. I am grateful to A. Di Giacomo for the hospitality.

This work was partially supported by the grant INTAS-00-00111 and by the DFG program “From Lattices to Phenomenology of Hadrons.”

### REFERENCES

1. Yu. A. Simonov, hep-ph/0211330; A. Di Giacomo, H. G. Dosch, V. I. Shevchenko, and Yu. A. Simonov, Phys. Rep. **372**, 319 (2002); hep-ph/0007223; V. I. Shevchenko and Yu. A. Simonov, Phys. Rev. Lett. **85**, 1811 (2000); hep-ph/0001299.

2. D. Chen, R. C. Brower, J. W. Negele, and E. V. Shuryak, Nucl. Phys. B (Proc. Suppl.) **73**, 512 (1999); hep-lat/9809091.
3. M. N. Chernodub, F. V. Gubarev, M. I. Polikarpov, and A. I. Veselov, Progr. Theor. Phys. Suppl. **131**, 309 (1998); A. Di Giacomo, Progr. Theor. Phys. Suppl. **131**, 161 (1998); hep-lat/9802008; H. Ichie and H. Suganuma, hep-lat/9906005; T. Suzuki, Progr. Theor. Phys. Suppl. **131**, 633 (1998).
4. J. Greensite, hep-lat/0301023; K. Langfeld *et al.*, hep-lat/0209040.
5. V. G. Bornyakov *et al.*, Phys. Lett. B **537**, 291 (2002).
6. F. V. Gubarev, A. V. Kovalenko, M. I. Polikarpov, *et al.*, hep-lat/0212003.
7. V. I. Zakharov, hep-ph/0204040; hep-lat/0309034; hep-ph/0306362.
8. V. Bornyakov and M. Müller-Preussker, Nucl. Phys. B (Proc. Suppl.) **106–107**, 646 (2002).
9. V. G. Bornyakov, P. Yu. Boyko, M. I. Polikarpov, and V. I. Zakharov, hep-lat/0305021; hep-lat/0309021.
10. G. Grimmelt, *Percolation*, in *A Series of Comprehensive Studies in Mathematics* (Springer, 1999), Vol. 321.
11. M. I. Polikarpov, S. N. Syritsyn, and V. I. Zakharov, hep-lat/0402018.
12. K. Symanzik, in *Local Quantum Theory, Varenna International School of Physics, 1969*, Course XLV, p. 152; A. M. Polyakov, *Gauge Fields and Strings* (Harwood Academic Publ., 1987), Chap. 9.
13. A. Di Giacomo and G. C. Rossi, Phys. Lett. B **100B**, 481 (1981); F. Di Renzo, E. Onofri, and G. Marchesini, Nucl. Phys. B **457**, 202 (1995); R. Horsley, P. E. L. Rakow, and G. Schierholz, Nucl. Phys. B (Proc. Suppl.) **106–107**, 870 (2002); hep-lat/0110210.
14. M. Beneke, Phys. Rep. **317**, 1 (1999); R. Akhoury and V. I. Zakharov, Nucl. Phys. B (Proc. Suppl.) **54A**, 217 (1997); hep-ph/9610492; A. H. Mueller, Phys. Lett. B **308**, 355 (1993); V. I. Zakharov, Nucl. Phys. B **385**, 452 (1992).
15. J. Ambjorn, hep-th/9411179.
16. A. V. Kovalenko, M. I. Polikarpov, S. N. Syritsyn, and V. I. Zakharov, hep-lat/0309032.
17. G. 't Hooft, Nucl. Phys. B **190**, 455 (1981); G. Mack, Nucl. Phys. B **205**, 145 (1982); P. de Forcrand and M. Pepe, Nucl. Phys. B **598**, 557 (2001); hep-lat/0008016.
18. J. Ambjorn, J. Giedt, and J. Greensite, J. High Energy Phys. **0002**, 033 (2000); hep-lat/9907021.
19. P. de Forcrand and M. D'Elia, Phys. Rev. Lett. **82**, 458 (1999); hep-lat/9901020.
20. V. I. Zakharov, hep-ph/0306361.
21. M. N. Chernodub and V. I. Zakharov, Nucl. Phys. B **669**, 233 (2003); hep-th/0211267.
22. M. N. Chernodub, S. Fujimoto, S. Kato, *et al.*, Phys. Rev. D **62**, 094506 (2000); hep-lat/0006025.
23. F. V. Gubarev, L. Stodolsky, and V. I. Zakharov, Phys. Rev. Lett. **86**, 2220 (2001); hep-ph/0010057; F. V. Gubarev and V. I. Zakharov, Phys. Lett. B **501**, 28 (2001); hep-ph/0010096; K.-I. Kondo, T. Murakami, T. Shinohara, and T. Imai, Phys. Rev. D **65**, 085034 (2002); hep-th/0111256; D. Dudal, H. Verschelde, R. E. Browne, and J. A. Dracey, Phys. Lett. B **562**, 87 (2003); hep-th/0302128.
24. L. Stodolsky, P. van Baal, and V. I. Zakharov, Phys. Lett. B **552**, 214 (2003); hep-th/0210204.
25. A. J. Niemi, hep-th/0403175.
26. K.-I. Kondo, hep-th/0404252.
27. R. Savit, Rev. Mod. Phys. **52**, 453 (1980).
28. J. M. Maldacena, Adv. Theor. Math. **2**, 231 (1998); hep-th/9711200; A. M. Polyakov, Int. J. Mod. Phys. A **14**, 645 (1999); hep-th/9809057.
29. V. I. Zakharov, hep-ph/0309301.
30. S. Narison, *QCD as a Theory of Hadrons: from Partons to Confinement*, Cambridge Monogr. Part. Phys. Nucl. Phys. Cosmol. **17** (1) (2002); hep-ph/0205006.

# The Static Force in Background Perturbation Theory\*

A. M. Badalian and A. I. Veselov\*\*

*Institute of Theoretical and Experimental Physics,  
Bol'shaya Cheredushinskaya ul. 25, Moscow, 117259 Russia*

Received May 21, 2004

**Abstract**—The static force  $F_B(r)$  and the strong coupling  $\alpha_F(r)$ , which defines the gluon-exchange part of  $F_B(r)$ , are studied in QCD background perturbation theory (BPT). In the region  $r \lesssim 0.6$  fm,  $\alpha_F(r)$  turns out to be substantially smaller than the coupling  $\alpha_B(r)$  in the static potential. For the dimensionless function  $\Phi_B(r) = r^2 F_B(r)$ , the characteristic values  $\Phi_B(r_1) = 1.0$  and  $\Phi_B(r_0) = 1.65$  are shown to be reached at the following  $Q\bar{Q}$  separations:  $r_1\sqrt{\sigma} = 0.77$  and  $r_0\sqrt{\sigma} = 1.09$  in the quenched approximation and  $r_1\sqrt{\sigma} = 0.72$  and  $r_0\sqrt{\sigma} = 1.04$  for  $n_f = 3$ . The numbers obtained appear to be only 8% smaller than those calculated in lattice QCD, while the values of the couplings  $\alpha_F(r_1)$  and  $\alpha_F(r_0)$  in BPT are  $\sim 30\%$  ( $n_f = 3$ ) and  $50\%$  ( $n_f = 0$ ) larger than the corresponding lattice couplings. With the use of BPT potential, a good description of the bottomonium spectrum is obtained. © 2005 Pleiades Publishing, Inc.

## 1. INTRODUCTION

The static  $Q\bar{Q}$  interaction plays a special role in hadron physics, and the modern understanding of the spin-independent part of the static potential  $V(r)$  comes from different approaches: QCD phenomenology [1–3], perturbative QCD (PQCD) [4, 5], analytical perturbation theory [6], background perturbation theory (BPT) [7, 8], and lattice QCD [9–11]. It has been established that, in the region  $r \gtrsim 0.2$  fm, this potential can be taken as a sum of a nonperturbative (NP) confining potential plus a gluon-exchange term:

$$V(r) = V_{\text{NP}}(r) + V_{\text{GE}}(r). \quad (1)$$

Such an additive form was introduced by the Cornell group as long as 30 years ago, just after discovery of charmonium [1], and later it was supported by numerous calculations in QCD phenomenology and also on the lattice, where for the lattice potential a parametrization like the Cornell potential is used [9, 10],

$$V_{\text{lat}}(r) = \sigma r - \frac{e_{\text{lat}}}{r} \quad (r \gtrsim 0.2 \text{ fm}) \quad (2)$$

with  $e_{\text{lat}} = \text{const}$  and  $\alpha_{\text{lat}} = 3e_{\text{lat}}/4$ . [For the lattice static potential, we use here the notation  $\alpha_{\text{lat}}$  ( $e_{\text{lat}}$ ) to distinguish it from the phenomenological case.]

In BPT, the additive form (1) can automatically be obtained in the lowest approximation when both NP and Coulomb terms satisfy the Casimir scaling law

with an accuracy of a few percent, in good agreement with the lattice data [12].

The explicit form of NP term is well known now:  $V_{\text{NP}}(r) = \sigma r$  at  $Q\bar{Q}$  separations  $r > T_g$ , where  $T_g$  is the gluonic correlation length,  $T_g \cong 0.2$  fm, measured on the lattice [13]. Such linear behavior is valid up to distances  $r \sim 1.0$  fm, while, at larger  $r$ , due to the  $q\bar{q}$ -pair creation, a flattening of the confining potential is expected to take place [14]. Here, in our paper, we restrict our consideration to the region  $r \lesssim 1.0$  fm.

Numerous calculations of the meson spectra have shown that the linear potential defines gross features of the spectra, in particular, the slope and the intercept of Regge trajectories for light mesons [15]. At the same time, the splittings between low-lying levels, the fine-structure splittings, and the wave function at the origin in heavy quarkonia are shown to be very sensitive to the gluon-exchange part of the static potential (1) [2, 16]:

$$V(r) = \sigma r + V_{\text{GE}}(r), \quad V_{\text{GE}}(r) \equiv -\frac{4}{3} \frac{\alpha_{\text{st}}(r)}{r}. \quad (3)$$

Unfortunately, our knowledge of this term (or the vector coupling  $\alpha_{\text{st}}(r)$ ) in the IR region remains insufficient and the choice of  $\alpha_{\text{st}}(r)$  essentially differs in different theoretical approaches. The only common feature of  $\alpha_{\text{st}}(r)$ , used in QCD phenomenology and BPT and supported by the lattice calculations, is that this coupling freezes at large distances,

$$\alpha_{\text{st}}(\text{large } r) = \text{const} = \alpha_{\text{crit}}, \quad (4)$$

but the true value of  $\alpha_{\text{crit}}$  has not been fixed up to now. For example, in the Cornell potential, used in

\*This article was submitted by the authors in English.

\*\*e-mail: veselov@itep.ru

the phenomenology, the typical values of the Coulomb constant in (2) lie in the range 0.39–0.45 [1–3, 16], while on the lattice in the same parametrization (2)  $\alpha_{\text{lat}}$  has values 50–30% smaller: in the quenched approximation ( $n_f = 0$ ),  $\alpha_{\text{lat}} \cong 0.20\text{--}0.23$  [9–11], and in (2 + 1) QCD,  $\alpha_{\text{lat}} \cong 0.30$  [11].

An even larger freezing value is obtained if the asymptotic freedom (AF) behavior of  $\alpha_{\text{st}}(r)$  (or  $\alpha_{\text{st}}(q)$  in momentum space) is taken into account. In BPT, large  $\alpha_{\text{crit}} = 0.58 \pm 0.02$  follows from the analysis of the splittings between low-lying levels in bottomonium [16, 17] and this number is in striking agreement with  $\alpha_{\text{crit}}$  introduced by Godfrey and Isgur in [3] in a phenomenological way. From the analysis of the hadronic decays of the  $\tau$  lepton, the number  $\alpha_s(1 \text{ GeV}) \cong 0.9 \pm 0.1$  was determined in [18], while a substantially smaller value,  $\alpha_s(1 \text{ GeV}) \cong 0.45$ , was obtained in PQCD with higher order corrections [19]. The Richardson potential, as well as “analytical perturbation theory,” gives an even larger  $\alpha_{\text{crit}}(n_f = 3) = 1.4$  [6]. Thus, at present, the true freezing value of the vector coupling, as well as  $\alpha_s(1 \text{ GeV})$ , remains unknown.

Besides the vector coupling  $\alpha_{\text{st}}(r)$  (in the static potential), the coupling  $\alpha_F(r)$ , associated with the static force, can be introduced,

$$F(r) = V'(r) = \sigma + V'_{\text{GE}}(r), \quad (5)$$

$$V'_{\text{GE}}(r) \equiv \frac{4}{3} \frac{\alpha_F(r)}{r^2}, \quad (6)$$

where by definition  $\alpha_F(r)$  is expressed through  $\alpha_{\text{st}}(r)$ ,

$$\alpha_F(r) = \alpha_{\text{st}}(r) - r\alpha'_{\text{st}}(r). \quad (7)$$

Then, important information about the derivative  $\alpha'_{\text{st}}(r)$  can be obtained from the study of the force  $F(r)$ . Note that the matrix elements over the static force define the squared wave function at the origin for the  $nS$  states in heavy quarkonia. In the lattice analysis, the vector coupling  $\alpha_{\text{lat}}$  in  $V_{\text{lat}}(r)$  (2) is supposed to be independent of the  $Q\bar{Q}$  separation  $r$  over the whole region 0.2–1.0 fm [10], i.e.,  $\alpha'_{\text{lat}} = 0$ , and therefore in this region  $\alpha_{\text{lat}} \cong \alpha_F = \text{const}$ . This statement is in accord with recent calculations of the lattice force in [11], where equal values  $\alpha_F^{\text{lat}}(r_1) = \alpha_F^{\text{lat}}(r_0)$  at the points  $r_1 \approx 0.34 \text{ fm}$  and  $r_0 = 0.5 \text{ fm}$  have been obtained.

A different picture takes place in BPT, where the vector coupling  $\alpha_B(r)$  at the points  $r_1 = 0.34 \text{ fm}$  and  $r_0 = 0.5 \text{ fm}$  changes by 20% (see Section 4), being close to the freezing value only at large distances,  $r \gtrsim 0.6 \text{ fm}$ . Also, due to the  $r$  dependence, an essential difference between  $\alpha_F(r)$  and  $\alpha_B(r)$  occurs just in the range  $0.2 \leq r \lesssim 0.6 \text{ fm}$ .

Therefore, several features of the vector coupling still need to be clarified.

First, why in lattice QCD and in QCD phenomenology does the Coulomb constant, used in the same Cornell potential, differ by 30% ( $n_f = 3$ )?

Second, does the  $r$  dependence of the vector coupling  $\alpha_{\text{st}}(r)$  (also of  $\alpha_F(r)$ ) really exist and why is it not observed on the lattice?

Third, what is the true freezing value?

To answer some of these questions, we shall use in our analysis here BPT, which gives a consistent analytical description of the vector coupling both in momentum and in coordinate spaces. To test the BPT conception about the vector-coupling behavior in the IR region, recently, the heavy-quarkonia spectra have been successfully described in this approach with the use of only fundamental quantities: the current (pole) quark mass,  $\Lambda_{\overline{MS}}(n_f)$ , and the string tension [16, 17]. It is important that, in BPT, the vector coupling  $\alpha_B(q)$  has a correct perturbative limit at large  $q^2$ , and therefore it is fully defined by the QCD constant  $\Lambda_{\overline{MS}}$  and also by the so-called background mass  $M_B$  which is proportional to  $\sqrt{\sigma}$ .

Additional information about  $Q\bar{Q}$  static interaction can be extracted from the study of the static force  $F_B(r)$  in BPT, with further comparison to recent lattice results from [11]. To this end, it is convenient to calculate the dimensionless function  $\Phi(r) = r^2 F(r)$  at two characteristic points,  $r_1\sqrt{\sigma}$  and  $r_0\sqrt{\sigma}$ , where

$$\Phi(r_1\sqrt{\sigma}) = 1.0, \quad \Phi(r_0\sqrt{\sigma}) = 1.65. \quad (8)$$

On the lattice, the values  $r_1^{\text{lat}}\sqrt{\sigma}$  and  $r_0^{\text{lat}}\sqrt{\sigma}$  are shown to be different in the quenched approximation and in (2 + 1) QCD. The same function  $\Phi_B(r)$ , calculated here in BPT, acquires the values (8) at points  $r_1\sqrt{\sigma}$  and  $r_0\sqrt{\sigma}$  which appear to be only 8% smaller than those on the lattice. However, the freezing value  $\alpha_{\text{crit}}$  in BPT is shown to be substantially larger than  $\alpha_{\text{lat}}$ . To compare the BPT and the lattice potentials, we calculate here the splittings between low-lying states in bottomonium and demonstrate that the lattice static potential cannot provide good agreement with experiment, while in BPT such an agreement takes place for the conventional values of the pole mass of the  $b$  quark, the string tension, and  $\Lambda_{\overline{MS}}(n_f = 5)$ . We also give an explanation why, between the freezing values in BPT and in the Cornell potential, used in the phenomenology, there is a difference of about 25%.

The paper is organized as follows. In Section 2, we briefly present the vector coupling in BPT and discuss the correct choice of the QCD constant  $\Lambda_V$  in the vector scheme. In Section 3, the characteristics of the lattice force are presented, while in Section 4 the

values  $r_1\sqrt{\sigma}$  and  $r_0\sqrt{\sigma}$  are calculated in BPT. The difference between the vector couplings in both approaches is also discussed. In Section 5, the splittings between low-lying states in bottomonium are used as a test to compare the static potentials from the lattice data, in the phenomenology and in BPT. We show that the lattice static potential cannot provide good agreement with experiment. In Section 6, we present our conclusions.

## 2. THE STRONG COUPLING IN BPT

In BPT, the gluon-exchange term  $V_{\text{GE}}^B(r)$  defines the vector (background) coupling  $\alpha_B(r)$  in the same way as “the exact coupling”  $\alpha_{\text{st}}(r)$  is defined in Eq. (3):

$$V_B(r) = \sigma r + V_{\text{GE}}^B(r), \quad V_{\text{GE}}^B(r) = -\frac{4\alpha_B(r)}{3r}. \quad (9)$$

With the use of the Fourier transform of the potential  $V_{\text{GE}}^B(q)$ , the background coupling in coordinate space can be expressed through the coupling  $\alpha_B(q)$  in momentum space [20]:

$$\alpha_B(r) = \frac{2}{\pi} \int_0^\infty \frac{dq}{q} \sin(qr) \alpha_B(q), \quad (10)$$

where the vector coupling in momentum space is defined at all momenta in Euclidean space and has no singularity for  $q^2 > 0$  [7]. In the two-loop approximation, the coupling

$$\alpha_B(q) = \frac{4\pi}{\beta_0 t_B} \left( 1 - \frac{\beta_1 \ln t_B}{\beta_0^2 t_B} \right), \quad (11)$$

$$t_B = \ln \frac{q^2 + M_B^2}{\Lambda_V^2}, \quad (12)$$

contains the background mass  $M_B$  which enters under logarithm as a moderator of the IR behavior of the perturbative coupling. In  $\alpha_B(q)$ , the Landau ghost pole disappears, while the short-distance perturbative behavior, as well as the Casimir scaling property of the static potential, stays intact [12].

The value of  $M_B$  is determined by the lowest excitation of a hybrid [21]; however, this mass cannot be considered as an additional (fitting) parameter in the theory, since in QCD string theory it can be calculated on the same grounds as mesons, being expressed through the only dimensional parameter  $\sqrt{\sigma}$ :

$$M_B = \xi \sqrt{\sigma}. \quad (13)$$

We suppose here that, in the static limit, the coefficient  $\xi$  does not depend (or weakly depends) on the number of flavors  $n_f$ . Direct calculation of  $M_B$

has not yet been done and, therefore, the number  $\xi$  has been extracted from two fits: from the comparison of the lattice static potential at small distances to that in BPT [20] and from the analysis of the spectra in charmonium and bottomonium [16, 17], with the following result:

$$M_B = 2.236(11)\sqrt{\sigma}. \quad (14)$$

In particular, the values  $M_B = 1.0$  and  $0.95$  GeV correspond to  $\sigma = 0.20$  and  $0.18$  GeV<sup>2</sup>.

Note that the logarithm (12) in  $\alpha_B(q)$  formally coincides with that suggested in [22] many years ago in the picture where the gluon acquires an effective mass  $m_g$  and, as a result, in (11), instead of  $M_B^2$ , the value  $(2m_g)^2$  enters. However, the physical gluon has no mass and in BPT the parameter  $M_B$  has been interpreted in correct way as a hybrid excitation of the  $Q\bar{Q}$  string, which is proportional to  $\sqrt{\sigma}$  [21].

The background coupling  $\alpha_B(q)$  has a correct PQCD limit at  $q^2 \gg M_B^2$  and, therefore, the constant  $\Lambda_V(n_f)$  (in the vector scheme) under the logarithm (12) can be expressed through the conventional QCD constant  $\Lambda_{\overline{MS}}(n_f)$  as in PQCD [23]:

$$\Lambda_V(n_f) = \Lambda_{\overline{MS}}(n_f) \exp\left(\frac{a_1}{2\beta_0}\right) \quad (15)$$

with

$$a_1 = \frac{31}{3} - \frac{10}{9}n_f, \quad \beta_0 = 11 - \frac{2}{3}n_f.$$

At present, the values of  $\Lambda_{\overline{MS}}(n_f)$  are well established in two cases—from high-energy processes for  $n_f = 5$  [24] and in the quenched approximation from lattice calculations [25],

$$\Lambda_{\overline{MS}}^{(5)}(2\text{-loop}) = 216 \pm 25 \text{ MeV}, \quad (16)$$

which corresponds to the “world average”  $\alpha_s(M_Z) = 0.117 \pm 0.002$ , and the value

$$\Lambda_{\overline{MS}}^{(0)}(2\text{-loop}) = \frac{0.602(48)}{r_0} = 237 \pm 19 \text{ MeV} \quad (17)$$

(with  $r_0 = 0.5$  fm =  $2.538$  GeV<sup>-1</sup>) was calculated on the lattice in [25].

Then, from (15), the corresponding values of  $\Lambda_V(n_f)$  in the vector scheme are the following:

$$\Lambda_V^{(5)} = 295 \pm 35 \text{ MeV}, \quad (18)$$

$$\Lambda_V^{(0)} = 379 \pm 30 \text{ MeV}. \quad (19)$$

It is worthwhile to note that the background coupling  $\alpha_B(r)$  (10) is a universal function of the ratio

$$\lambda(n_f) = \frac{\Lambda_V(n_f)}{M_B}, \quad (20)$$

and it actually depends on the dimensionless variable  $x = rM_B$  and  $\lambda$ :

$$\alpha_B(r, \Lambda_V, M_B) \equiv \alpha_B(rM_B; \lambda) \quad (21)$$

$$= \frac{2}{\pi} \int \frac{dx}{x} \sin(x, rM_B) \alpha_B(x, \lambda).$$

The same ratio  $\lambda$  also defines the freezing (critical) value of the coupling (which coincides in momentum and coordinate spaces), and it is given by the analytical expression

$$\alpha_{\text{crit}}(q \rightarrow 0) = \alpha_{\text{crit}}(r \rightarrow \infty) \quad (22)$$

$$= \frac{4\pi}{\beta_0 t_{\text{crit}}} \left\{ 1 - \frac{\beta_1 \ln t_{\text{crit}}}{\beta_0^2 t_{\text{crit}}} \right\},$$

$$t_{\text{crit}} = \ln \frac{M_B^2}{\Lambda_V^2} = \ln[\lambda^2(n_f)]. \quad (23)$$

Taking  $\Lambda_V$  from (18), (19) and  $M_B$  from (14), one obtains the following values for  $\alpha_{\text{crit}}$ : in the quenched approximation,

$$\alpha_{\text{crit}}(n_f = 0) = 0.419_{-0.038}^{+0.045}, \quad (24)$$

while for  $n_f = 5$  the freezing value is  $\sim 30\%$  larger,

$$\alpha_{\text{crit}}(n_f = 5) = 0.510_{-0.049}^{+0.055} \quad (M_B = 1.0 \text{ GeV}) \quad (25)$$

and

$$\alpha_{\text{crit}}(n_f = 5) = 0.533_{-0.053}^{+0.062} \quad (M_B = 0.95 \text{ GeV}). \quad (26)$$

Note that the freezing value (26) turns out to be very close to that phenomenologically introduced by Godfrey and Isgur in [3] to describe a lot of experimental data in the meson sector. As shown in [17], the choice of  $M_B = 0.95 \text{ GeV}$ ,  $\Lambda_V^{(5)} \cong 320 \text{ MeV}$ , and  $\alpha_{\text{crit}} = 0.58$  provides good agreement between experiment and BPT calculations of the splittings in bottomonium.<sup>1)</sup> Thus, in BPT, the large freezing value  $\alpha_{\text{crit}}(n_f = 5) \approx 0.58$  appears to be consistent with the conventional value of  $\Lambda_{\overline{MS}}^{(5)} \approx 230 \text{ MeV}$ ,  $\alpha_s(M_Z, 2\text{-loop}) = 0.119 \pm 0.001$ .

However, the large freezing value in BPT (and in QCD phenomenology) does not agree with the value used in the lattice parametrization (2) of the static potential. For example, in the quenched approximation,  $\alpha_{\text{lat}} \cong 0.23$  was obtained in [9, 10], while in BPT the minimal value  $\alpha_{\text{crit}}$  (which corresponds to the minimal value in (19),  $\Lambda_{\overline{MS}}^{(0)}(\text{min}) = 218 \text{ MeV}$ ) is

<sup>1)</sup>Recent experimental data give  $\alpha_s(M_Z) = 0.119 \pm 0.002$ , therefore, both  $\Lambda_{\overline{MS}}^{(5)}$  and  $\alpha_{\text{crit}}(n_f = 5)$  appear to be about 10% larger than the values in (16) and (26), in very good agreement with our analysis presented in Section 5.

**Table 1.** The strong coupling  $\alpha_{\text{st}}^P(2\text{-loop}, r)$  in PQCD and the background coupling  $\alpha_B(2\text{-loop}, r)$  in BPT in the quenched approximation with  $\Lambda_{\overline{MS}}^{(0)} = 237 \text{ MeV}$  ( $\Lambda_V^{(0)} = 379 \text{ MeV}$ ,  $\Lambda_R^{(0)} = 675 \text{ MeV}$ ,  $M_B = 1.0 \text{ GeV}$ )

$r, \text{ fm}$	$\alpha_{\text{st}}^P(r)$	$\alpha_B(r)$
0.01	0.128	0.138
0.02	0.156	0.166
0.04	0.202	0.204
0.06	0.248	0.232
0.08	0.301	0.254
0.10	0.368	0.272
0.12	0.457	0.288
0.14	0.588	0.301

equal to  $\alpha_{\text{crit}}^{\text{min}}(n_f = 0) = 0.38$ , i.e., 40% larger. Such a difference between the two numbers partly occurs due to the fact that, on the lattice, the  $r$  dependence of the vector coupling is not seen (or is neglected) at  $r > 0.2 \text{ fm}$ .

In Table 1, the background coupling  $\alpha_B(r)$  is compared to  $\alpha_{\text{st}}^P(r)$ , calculated in PQCD, where according to the perturbative prescription the QCD constant  $\Lambda_R(n_f)$  in coordinate space is defined as  $\Lambda_R(n_f) = e^\gamma \Lambda_V(n_f)$  ( $\gamma$  is the Euler constant). These couplings (both in the two-loop approximation) appear to be close to each other only at very small distances,  $r < 0.1 \text{ fm}$ , and have the characteristic feature that the difference  $\Delta\alpha = \alpha_B(r) - \alpha_{\text{st}}^P(r)$  is positive at  $r \leq 0.04 \text{ fm}$  and becomes negative at  $r > 0.04 \text{ fm}$ ; just such a change of the sign of  $\Delta\alpha$  has been observed in the lattice static potential [10].

### 3. THE STATIC FORCE ON THE LATTICE

The study of the static force is especially convenient through the dimensionless function  $\Phi_{\text{lat}}(r)$  since this function depends on a dimensionless variable like  $r/a$ , where  $a$  is a lattice spacing, or on  $r\sqrt{\sigma}$  (if the string tension is taken as the only mass scale). Recently,  $\Phi_{\text{lat}}(r)$  was measured by the MILC group both in the quenched case and in  $(2+1)$  lattice QCD [11] with the following results:

First, the function  $\Phi_{\text{lat}}(r) = r^2 F_{\text{lat}}(r) = (r\sqrt{\sigma})^2 F(r\sqrt{\sigma})$  acquires the value  $\Phi_{\text{lat}}(r_1^{\text{lat}}) = 1.0$  at the  $Q\bar{Q}$  separation  $r_1^{\text{lat}}$ :

$$r_1^{\text{lat}} \sqrt{\sigma} = 0.769 \pm 0.002 \quad (n_f = 3), \quad (27)$$

$$r_1^{\text{lat}} \sqrt{\sigma} = 0.833 \pm 0.002 \quad (n_f = 0). \quad (28)$$

**Table 2.** The background couplings  $\alpha_F(r) = \alpha_B(r) - r\alpha'_B(r)$  and  $\alpha_B(r)$  in the quenched approximation ( $\Lambda_V^{(0)} = 379$  MeV,  $M_B = 1.0$  GeV,  $\alpha_{\text{crit}} = 0.419$ )

$r$ , fm	$\alpha_F(r)$	$\alpha_B(r)$	$r$ , fm	$\alpha_F(r)$	$\alpha_B(r)$
0.099	0.188	0.272	0.355	0.312	0.379
0.118	0.201	0.289	0.394	0.324	0.386
0.138	0.213	0.301	0.433	0.335	0.391
0.158	0.225	0.313	0.473	0.345	0.396
0.197	0.246	0.333	0.493	0.350	0.398
0.236	0.265	0.348	0.512	0.354	0.400
0.296	0.290	0.365	0.532	0.358	0.401
0.335	0.305	0.375	0.552	0.366	0.404

Second, the function  $\Phi_{\text{lat}}$  has the value  $\Phi_{\text{lat}}(r_0\sqrt{\sigma}) = 1.65$  at the following separation  $r_0^{\text{lat}}$  (the Sommer scale):

$$r_0^{\text{lat}}\sqrt{\sigma} = 1.114 \pm 0.002 \quad (n_f = 3), \quad (29)$$

$$r_0^{\text{lat}}\sqrt{\sigma} = 1.160 \pm 0.002 \quad (n_f = 0). \quad (30)$$

Also, in [11], the ratio

$$r_0^{\text{lat}}/r_1^{\text{lat}} = 1.449(5) \quad (n_f = 3) \quad (31)$$

is defined with a precision accuracy. If in (27)–(31) one takes the string tension  $\sigma = 0.20$  GeV<sup>2</sup>, then the characteristic points are  $r_1^{\text{lat}} = 0.34$  fm and  $r_0^{\text{lat}} = 0.49$  fm for  $n_f = 3$  and are slightly larger,  $r_1^{\text{lat}} = 0.37$  fm and  $r_0^{\text{lat}} = 0.51$  fm, in the quenched case. The numbers obtained can be used to extract the vector coupling  $\alpha_F^{\text{lat}}(r)$ , associated with the force in lattice QCD:

$$F_{\text{lat}}(r) = \sigma + \frac{4}{3r^2}\alpha_F^{\text{lat}}(r), \quad (32)$$

$$\Phi_{\text{lat}}(r) = \sigma r^2 + \frac{4}{3}\alpha_F^{\text{lat}}(r). \quad (33)$$

From (27)–(31), it follows that the values of  $\alpha_F^{\text{lat}}(r)$  are equal at the points  $r_1^{\text{lat}}$  and  $r_0^{\text{lat}}$  with a good accuracy:

$$\alpha_F^{\text{lat}}(r_1^{\text{lat}}) = \alpha_F^{\text{lat}}(r_0^{\text{lat}}) = 0.307(4) \quad (n_f = 3), \quad (34)$$

$$\alpha_F^{\text{lat}}(r_1^{\text{lat}}) = \alpha_F^{\text{lat}}(r_0^{\text{lat}}) = 0.229(3) \quad (n_f = 0). \quad (35)$$

Note that, in the quenched case, the value (35) for  $\alpha_F^{\text{lat}}(r)$  numerically coincides with the lattice coupling  $\alpha_{\text{lat}} = 0.23$  in the static potential (where  $\alpha_{\text{lat}} = \text{const}$  is assumed over the whole region  $0.2 \leq r \lesssim 1.0$  fm).

**Table 3.** The background couplings  $\alpha_F(r) = \alpha_B(r) - r\alpha'_B(r)$  and  $\alpha_B(r)$  for  $n_f = 3$  ( $\Lambda_V^{(3)} = 370$  MeV,  $M_B = 1.0$  GeV,  $\alpha_{\text{crit}} = 0.510$ )

$r$ , fm	$\alpha_F(r)$	$\alpha_B(r)$	$r$ , fm	$\alpha_F(r)$	$\alpha_B(r)$
0.099	0.233	0.336	0.355	0.385	0.464
0.118	0.250	0.355	0.394	0.399	0.472
0.138	0.265	0.371	0.433	0.413	0.478
0.158	0.279	0.385	0.473	0.425	0.484
0.197	0.305	0.409	0.493	0.430	0.486
0.236	0.328	0.427	0.512	0.435	0.488
0.296	0.358	0.448	0.532	0.440	0.490
0.335	0.376	0.459	0.591	0.453	0.495

Thus, existing lattice data are consistent with the assumption that the derivative in this region is equal to zero,  $\alpha'_{\text{lat}}(r) = 0$ .

The lattice number (34) in full QCD appears to be substantially smaller than the coupling used in BPT and also in QCD phenomenology in the IR region. In order to draw a conclusion as to which value provides a better description of experimental data, in Section 5, as a test, we shall calculate the bottomonium spectrum with the lattice as well as with the BPT static potentials.

#### 4. THE STATIC FORCE IN BPT

In BPT, the static force can be represented as in (5),

$$F_B(r) = \sigma + \frac{4}{3r^2}\alpha_F(r), \quad (36)$$

where the coupling  $\alpha_F(r)$ , associated with the force  $F_B(r)$ , can be expressed through the known coupling  $\alpha_B(r)$  (10) and its derivative:

$$\alpha_F(r) = \alpha_B(r) - r\alpha'_B(r). \quad (37)$$

Correspondingly, the dimensionless function  $\Phi_B(r)$  is

$$\Phi_B(r) = r^2 F_B(r) = (\sqrt{\sigma}r)^2 + \frac{4}{3}\alpha_F(r). \quad (38)$$

The coupling  $\alpha_F(r)$  can easily be calculated from expression (10), and due to the negative contribution of the term with the derivative, it appears to be substantially smaller than  $\alpha_B(r)$  (in the region  $r \lesssim 0.6$  fm). The values of  $\alpha_F(r)$  for  $n_f = 0$  and  $n_f = 3$  are given in Tables 2 and 3 (see also figure), from which the  $r$  dependence of  $\alpha_F(r)$  is explicitly seen:

(i) At the distances  $r \approx 0.2, 0.35,$  and  $0.50$  fm, the coupling  $\alpha_F(r) (n_f = 3)$  is smaller than  $\alpha_B(r)$  (in the static potential) by 25, 18, and 12%, respectively.

(ii) The derivative  $\alpha'_B(r)$  is larger for larger  $n_f$ , being approximately proportional to  $\beta_0^{-1}$  ( $\beta_0 = 11 - 2n_f/3$ ).

(iii) At the distance  $r \approx 0.2$  fm, the coupling  $\alpha_F(r, n_f)$  in BPT coincides with  $\alpha_{\text{lat}}$  both for  $n_f = 3$  and for  $n_f = 0$ , but at larger  $r > 0.2$  fm, it manifests substantial growth: for  $n_f = 3$ ,  $\alpha_F(r = 0.335 \text{ fm}) = 0.376$  and  $\alpha_F(r_0 = 0.493 \text{ fm}) = 0.430$ , being  $\sim 20$  and  $\sim 40\%$  larger than  $\alpha_{\text{lat}} = 0.306$  from [11].

Knowing  $\alpha_F(r)$ , the function  $\Phi_B(r)$  from (38) can easily be calculated. Note that the coupling  $\alpha_F(r)$  (as well as  $\alpha_B(r)$ ) weakly depends on the string tension through the background mass  $M_B = 2.236\sqrt{\sigma}$  (14). We have obtained the following numbers for the separations  $r_1$  and  $r_0$ , where  $\Phi_B(r_1) = 1.0$  and  $\Phi_B(r_0) = 1.65$ :

$$r_1\sqrt{\sigma} = 0.769(5), \quad r_0\sqrt{\sigma} = 1.090(5); \quad (39)$$

$$(n_f = 0),$$

and the ratio  $r_0/r_1$  coincides with  $r_0^{\text{lat}}/r_1^{\text{lat}} (n_f = 0)$  on the lattice with 2% accuracy:

$$r_0/r_1 = 1.417(16) \quad (n_f = 0).$$

For  $n_f = 3$  in BPT, the characteristic separations are the following:

$$r_1\sqrt{\sigma} = 0.716(4), \quad r_0\sqrt{\sigma} = 1.044(5),$$

$$r_1/r_0 = 1.458(15), \quad (n_f = 3). \quad (40)$$

The comparison of the obtained numbers to those in lattice QCD shows that  $r_1\sqrt{\sigma} (r_0\sqrt{\sigma})$  in BPT is only 8% (6%) smaller than the lattice values (27)–(30), while the ratio  $r_1/r_0$  in (40) coincides with (31) with 1% accuracy.

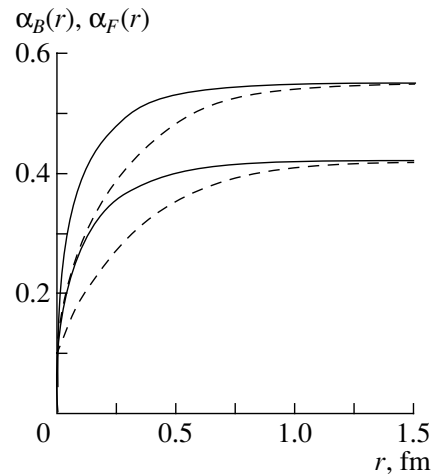
To have a full picture of how the separations  $r_1\sqrt{\sigma}$  and  $r_0\sqrt{\sigma}$  change with an increase in flavors, below we give their values also for  $n_f = 5$  (see Table 4):

$$r_1\sqrt{\sigma} = 0.673(4), \quad r_0\sqrt{\sigma} = 1.016(5), \quad (41)$$

with their ratio

$$r_0/r_1 = 1.510(16) \quad (n_f = 5).$$

Comparing (39)–(41), one can see the points  $r_1(n_f)$  and  $r_0(n_f)$  are smaller for larger  $n_f$  (for  $n_f = 5$ , they are 12% smaller than in the quenched case). Also, for  $n_f = 5$ , the coupling  $\alpha_F(r)$  approaches the freezing value at smaller distances; e.g., the value  $\alpha_F(r_0)/\alpha_{\text{crit}}$  is equal to 0.835 ( $n_f = 0$ ), 0.843 ( $n_f = 3$ ), and 0.874 ( $n_f = 5$ ).



The couplings  $\alpha_B(r)$  (solid curves) and  $\alpha_F(r)$  (dashed curves). The upper curves refer to case with  $n_f = 5$  and the lower curves refer to quenched case ( $n_f = 0$ ).

In contrast to lattice coupling  $\alpha_F^{\text{lat}}(r)$ , which is supposed to be  $r$  independent between  $r_1$  and  $r_0$ , Eqs. [(34), (35)], in BPT, the coupling  $\alpha_F(r)$  depends on  $r$  and the calculated values of  $\alpha_F(r_1)$  and  $\alpha_F(r_0)$  are given below,

$$\alpha_F(r_1^{(0)}\sqrt{\sigma}) = 0.306 \quad (n_f = 0),$$

$$\alpha_F(r_1^{(3)}\sqrt{\sigma}) = 0.366 \quad (n_f = 3), \quad (42)$$

$$\alpha_F(r_1^{(5)}\sqrt{\sigma}) = 0.412 \quad (n_f = 5),$$

and at the Sommer scale  $r_0\sqrt{\sigma}$ , their values are  $\sim 12\%$  larger,

$$\alpha_F(r_0^{(0)}\sqrt{\sigma}) = 0.346 \quad (n_f = 0),$$

$$\alpha_F(r_0^{(3)}\sqrt{\sigma}) = 0.42 \quad (n_f = 3), \quad (43)$$

$$\alpha_F(r_0^{(5)}\sqrt{\sigma}) = 0.46 \quad (n_f = 5).$$

From our analysis, one can conclude the following:

**Table 4.** The background couplings  $\alpha_B(r)$  and  $\alpha_F(r)$  for  $n_f = 5$  ( $\Lambda_V^{(5)} = 320$  MeV,  $M_B = 1.0$  GeV,  $\alpha_{\text{crit}} = 0.548$ )

$r, \text{ fm}$	$\alpha_F(r)$	$\alpha_B(r)$	$r, \text{ fm}$	$\alpha_F(r)$	$\alpha_B(r)$
0.099	0.274	0.381	0.355	0.435	0.508
0.118	0.292	0.401	0.394	0.450	0.515
0.138	0.309	0.417	0.433	0.463	0.521
0.158	0.324	0.432	0.473	0.474	0.526
0.197	0.352	0.455	0.493	0.479	0.528
0.236	0.377	0.473	0.512	0.484	0.530
0.296	0.409	0.494	0.532	0.488	0.532
0.335	0.427	0.504	0.591	0.501	0.536

**Table 5.** The splittings (in MeV) between spin-averaged masses in bottomonium for the Cornell potential with (A)  $\alpha_{\text{lat}} = 0.306$  and (B)  $\alpha_{\text{phen}} = 0.42$  and for the BPT potential (C) with  $\Lambda_V^{(5)} = 330$  MeV ( $M_B = 0.95$  GeV)

Splitting	(A) $\alpha_{\text{lat}} = 0.306$ , $\sigma = 0.20$ GeV <sup>2</sup> , $m = 4.85$ GeV	(B) $\alpha_{\text{phen}} = 0.42$ , $\sigma = 0.183$ GeV <sup>2</sup> , $m = 4.631$ GeV	(C) $\alpha_{\text{crit}} = 0.565$ , $\sigma = 0.178$ GeV <sup>2</sup> , $m = 4.828$ GeV	Experiment
$2S-1S$	527	615	557	563 <sup>a)</sup>
$2S-1P$	114	97	123	123 <sup>a)</sup>
$1P-1S$	413	517	434	440 <sup>a)</sup>
$1D-1P$	241	260	260	$261 \pm 2^{\text{b)}$
$2P-1P$	359	368	370	$360.1 \pm 1.2$

<sup>a)</sup> Since the mass of  $\eta_b(nS)$  is unknown and in any case  $\bar{M}(1S) < M(\Upsilon(1S))$ , we give here only the lower limit of the experimental splitting.

<sup>b)</sup> The experimental number for  $M(1D_2) = 10\,161.2 \pm 2.2$  MeV is obtained in [27].

(i) The characteristic quantities  $r_1\sqrt{\sigma}$  and  $r_0\sqrt{\sigma}$  in BPT are very close to the corresponding lattice values, being only 8% smaller.

(ii) At the same time, the coupling  $\alpha_F(r_0)$  in the “background force”  $F_B(r)$  is shown to be 30–40% larger than  $\alpha_F^{\text{lat}}$ .

## 5. THE $b\bar{b}$ SPECTRUM AS A TEST OF THE VECTOR COUPLING IN THE IR REGION

Recently, it was demonstrated that the bottomonium spectrum, especially the splittings between low-lying levels, appears to be very sensitive both to the freezing value and to the  $r$  dependence of the vector coupling [16, 17]. Therefore, just these splittings can be used for testing of  $\alpha_{\text{st}}(r)$  in the IR region. For illustration, we consider here three typical static potentials.

The first one imitates the lattice static potential (2) but has the form of the Cornell potential over the whole region  $r \geq 0$ . The coupling  $\alpha_{\text{lat}}(r) = \text{const} = 0.306$  is taken from lattice calculations with  $n_f = 3$  from [11], which is the largest Coulomb constant obtained in lattice measurements up to now. In this potential, the AF behavior of  $\alpha_{\text{lat}}(r)$  (which was observed on the lattice at small  $Q\bar{Q}$  separations,  $r \lesssim 0.2$  fm [9]) is neglected and, therefore, such a gluon-exchange potential with  $\alpha_{\text{lat}} = \text{const}$  over the whole region is stronger than the lattice potential and gives rise to larger values of the splittings between levels in bottomonium.

The second variant refers to the phenomenological Cornell potential with  $\alpha_{\text{st}}(r) = \text{const} = 0.42$  which is used in analysis of charmonium [1, 26].

The third potential is taken as in BPT for  $n_f = 5$ ,  $\Lambda_V^{(5)} = 330$  MeV (or  $\Lambda_{\overline{MS}}^{(5)}(2\text{-loop}) = 241$  MeV) and  $M_B = 0.95$  GeV. The calculations with the first two potentials are performed with nonrelativistic kinematics, while for the third potential the solutions to the relativistic Salpeter equation are used.

The splittings between the spin-averaged masses  $\bar{M}(nL)$  in bottomonium for these three potentials are given in Table 5.

From our calculations presented in Table 5, one can make important conclusions. First, the calculations with “the lattice” potential (A) with  $\alpha_{\text{lat}} = 0.306$  ( $n_f = 3$ ) define the upper bounds of the splittings between different states in bottomonium (since the AF behavior at  $r \leq 0.2$  fm is neglected). Nevertheless, even upper bounds of the  $2S-1S$ ,  $1P-1S$  splittings appear to be 40–30 MeV smaller than the experimental numbers (for which we know only the lower bounds since the  $\eta_b(nS)$  mesons are still unobserved,  $\bar{M}(nS) < M(\Upsilon(nS))$ ).

It is of special importance to compare the theoretical and experimental number for the  $1D-1P$  splitting, which is measured now with precision accuracy [27]:

$$\begin{aligned} \Delta_{\text{exp}} &= \bar{M}(1D) - \bar{M}(1P) \\ &= 261.1 \pm 2.2(\text{exp.}) \pm 1.0_{0.0}(\text{theor.}) \text{ MeV}, \end{aligned} \quad (44)$$

where  $\bar{M}(1P) = 9900.1 \pm 0.6$  MeV and  $\bar{M}(1D) = M_{\text{exp}}(1D_2) \pm 1.0_{0.0}(\text{theor.})$  MeV;  $M_{\text{exp}}(1D_2) = 10\,161.2 \pm 1.6(\text{exp.})$  MeV (see a discussion of the  $1D-1P$  splitting in [17]).

For the lattice potential (A), the upper limit  $\Delta_{\text{lat}}$  turns out to be 20 MeV smaller than  $\Delta_{\text{exp}}$  (the difference is about ten standard deviations).

On the contrary, the calculations with the phenomenological potential (B) (with  $\alpha_{\text{phen}} = 0.42$ ) and with the BPT potential (C) give precision agreement with  $\Delta_{\text{exp}}$ .

In BPT, the  $2S-1S$ ,  $1P-1S$  splittings are also close to the experimental numbers, being only  $\sim 10$  MeV smaller (note that the spin-averaged mass  $\bar{M}(1S) = 9460$  MeV is slightly larger than the expected experimental number). The same splittings for the Cornell potential ( $\alpha_{\text{phen}} = \text{const} = 0.42$ ) turn out to be too large (since  $\bar{M}(1S) \cong 9300$  MeV is small) because the Coulomb part of the static potential is overestimated if the AF behavior of the vector coupling is neglected. This AF effect is small for the  $1D-1P$  splitting for which agreement with experiment takes place.

Note that, in the BPT potential (C), the freezing value  $\alpha_{\text{crit}} = 0.565$  is substantially larger than  $\alpha_{\text{phen}} = 0.42$ , and to understand what kind of approximation corresponds to  $\alpha_{\text{st}}(r) = \text{const}$ , let us introduce an effective coupling in BPT according to the relation

$$\left\langle \frac{\alpha_B(r)}{r} \right\rangle_{nL} = \alpha_{\text{eff}}(nL) \left\langle \frac{1}{r} \right\rangle_{nL}. \quad (45)$$

Our calculations of the matrix elements demonstrate (see Table 6) the following:

- (i)  $\alpha_{\text{eff}}$  depends on the quantum numbers  $n, L$ .
- (ii) The values of  $\alpha_{\text{eff}}(nL)$  appear to be 30–15% smaller than the freezing value  $\alpha_{\text{crit}} = 0.565$  and those values for the  $1S, 2S$  states are close to  $\alpha_{\text{phen}}$  used in the phenomenology.
- (iii) For the orbital excitations, the effective coupling  $\alpha_{\text{eff}} \cong 0.50$  is  $\sim 20\%$  larger than for the  $1S, 2S$  states, and just this fact results in an increase in the splittings like  $2S-1P, 1D-1P$  which is observed in bottomonium.

To make a decisive conclusion about the behavior of  $\alpha_{\text{st}}(r)$  in the IR region, it would also be important to take into account a screening of the gluon-exchange potential at large distances. At present there is no theory of this phenomenon on the fundamental level, although in some cases the Coulomb screening is introduced in a phenomenological way [28].

## 6. CONCLUSION

Our study of the vector couplings  $\alpha_B(r)$  (in the static potential) and  $\alpha_F(r)$  in the static force  $F(r)$  is performed in the framework of BPT with the following results.

Due to the derivative term  $\alpha'_B(r)$ , an essential difference between  $\alpha_F(r)$  and  $\alpha_B(r)$  is observed at the  $Q\bar{Q}$  separations  $r \lesssim 0.6$  fm with  $\alpha_F(r)$  being 50,

**Table 6.** The effective vector coupling  $\alpha_{\text{eff}}(nL)$  for the BPT potential (C) ( $\Lambda_V^{(5)} = 330$  MeV,  $M_B = 0.95$  GeV,  $\sigma = 0.178$  GeV<sup>2</sup>,  $\alpha_{\text{crit}} = 0.565$ )

State	1S	2S	3S	1P	1P	1D	2D
$\alpha_{\text{eff}}(nL)$	0.405	0.439	0.448	0.495	0.501	0.528	0.528

30, and 15% smaller at the points about 0.2, 0.3, and 0.5 fm, respectively.

At the same time, the freezing values of both couplings coincide and are rather large:  $\alpha_{\text{crit}} \cong 0.41$  ( $n_f = 0$ ), 0.51 ( $n_f = 3$ ), and  $0.58 \pm 0.04$  ( $n_f = 5$ ). The last number turns out to be very close to that introduced by Godfrey and Isgur in their phenomenological analysis.

The dimensionless quantities  $r_1\sqrt{\sigma}$  and  $r_0\sqrt{\sigma}$ , where the function  $\Phi(r) = r^2F(r)$  has the values 1.0 and 1.65, are calculated in BPT and their values are 6–8% smaller than those calculated on the lattice in the quenched case and in (2 + 1) QCD.

In contrast to lattice observation, where  $\alpha_F^{\text{lat}}(r_1) = \alpha_F^{\text{lat}}(r_0) = \text{const}$  and this constant is small,  $\alpha_{\text{lat}} = 0.23$  ( $n_f = 0$ ) and 0.306 ( $n_f = 3$ ), in BPT,  $\alpha_F(r)$  at these points is found to be 40% larger for  $n_f = 0$  and 30% larger for  $n_f = 3$ . Because the Coulomb constant in the lattice static potential is small, this potential gives substantially smaller  $2S-1S, 1P-1S, 1D-1P$  splittings in bottomonium.

The meaning of the Coulomb constant  $\alpha_{\text{phen}}$ , used in the phenomenology as an effective coupling in BPT, is suggested. This interpretation explains why  $\alpha_{\text{phen}} \cong 0.42$  is 30% smaller than the freezing value  $\alpha_{\text{crit}} \cong 0.56$  for the potentials with the AF taken into account.

The knowledge of the static force in BPT is important to perform precision calculations of the wave functions at the origin, hadronic decays, and fine-structure splitting in bottomonium.

## ACKNOWLEDGMENTS

For many years, we have had remarkable opportunities to discuss a lot of problems in hadron physics with Prof. Yu.A. Simonov. His scope and attitude in physics had an enormous influence on us. We appreciate very much our collaboration with Prof. Simonov and his permanent support in our research activity.

## REFERENCES

1. E. Eichten *et al.*, Phys. Rev. Lett. **34**, 369 (1975); Phys. Rev. D **21**, 203 (1980); E. J. Eichten, K. Lane, and C. Quigg, Phys. Rev. Lett. **89**, 162002 (2002) (and references therein).
2. D. P. Stanley and D. Robson, Phys. Rev. D **21**, 3180 (1980); Phys. Rev. Lett. **45**, 325 (1980); W. Buchmuller and S. Tye, Phys. Rev. D **24**, 132 (1981); W. Kwong, J. L. Rosner, and C. Quigg, Annu. Rev. Nucl. Part. Sci. **37**, 325 (1987); D. Ebert, R. N. Faustov, and V. O. Galkin, Phys. Rev. D **62**, 034014 (2000).
3. S. Godfrey and N. Isgur, Phys. Rev. D **32**, 189 (1985); L. P. Fulcher, Phys. Rev. D **44**, 2079 (1991); S. Jacobs, M. G. Olsson, and C. Suchyta, Phys. Rev. D **33**, 3338 (1986); T. Y. Allen, M. G. Olsson, and S. Veseli, Phys. Rev. D **62**, 094021 (2000).
4. A. Pineda and F. J. Yndurain, Phys. Rev. D **58**, 094022 (1998) (and references therein).
5. Y. J. Ng, Y. Pantaleone, and S. H. H. Tye, Phys. Rev. D **33**, 777 (1986); S. Recksiegel and Y. Sumino, Phys. Rev. D **67**, 014004 (2003) (and references therein); A. S. Mattingly and P. M. Stevenson, Phys. Rev. D **49**, 437 (1994).
6. D. V. Shirkov and I. L. Solotsov, Phys. Rev. Lett. **79**, 1209 (1997); Phys. Lett. B **442**, 344 (1998).
7. Yu. A. Simonov, Yad. Fiz. **65**, 140 (2002) [Phys. At. Nucl. **65**, 135 (2002)]; **58**, 113 (1995) [**58**, 107 (1995)]; Pis'ma Zh. Éksp. Teor. Fiz. **57**, 513 (1993) [JETP Lett. **57**, 525 (1993)].
8. Yu. A. Simonov, in *Proceedings of the XVII International School on QCD: "Perturbative or Nonperturbative"*, Lisbon, 1999, Ed. by L. S. Ferreira *et al.* (World Sci., Singapore, 1999), p. 60.
9. S. P. Booth *et al.*, Phys. Lett. B **294**, 385 (1992); G. S. Bali and K. Schilling, Phys. Rev. D **47**, 661 (1993); G. S. Bali, Phys. Rep. **343**, 1 (2001) (and references therein).
10. G. S. Bali, Phys. Lett. B **460**, 170 (1999).
11. C. W. Bernard *et al.* (MILC Collab.), Phys. Rev. D **64**, 054506 (2001); **62**, 034503 (2000); A. S. Kronfeld, hep-lat/0310063.
12. G. S. Bali, Phys. Rev. D **62**, 114503 (2000); V. I. Shevchenko and Yu. A. Simonov, Phys. Rev. Lett. **85**, 1811 (2000); Int. J. Mod. Phys. A **18**, 127 (2003); Yu. A. Simonov, Pis'ma Zh. Éksp. Teor. Fiz. **71**, 187 (2000) [JETP Lett. **71**, 127 (2000)].
13. A. Di Giacomo, H. G. Dosch, V. I. Shevchenko, and Yu. A. Simonov, Phys. Rep. **372**, 319 (2002) (and references therein).
14. A. Duncan, E. Eichten, and H. Tacker, Phys. Rev. D **63**, 111501 (2001); B. Bolder *et al.*, Phys. Rev. D **63**, 074504 (2001); C. Bernard *et al.*, Phys. Rev. D **64**, 074509 (2001).
15. A. M. Badalian and B. L. G. Bakker, Phys. Rev. D **66**, 034025 (2002).
16. A. M. Badalian, A. I. Veselov, and B. L. G. Bakker, Yad. Fiz. **67**, 1392 (2004) [Phys. At. Nucl. **67**, 1367 (2004)]; hep-ph/0311010.
17. A. M. Badalian, B. L. G. Bakker, and A. I. Veselov, hep-ph/0311009; Phys. Rev. D **70**, 016007 (2004).
18. S. J. Brodsky *et al.*, Phys. Rev. D **67**, 055008 (2003).
19. A. A. Pivovarov, *Talk Given at 15th International Seminar "Quarks-2002", Novgorod, Russia, 2002*; hep-ph/0301074.
20. A. M. Badalian, Yad. Fiz. **63**, 2269 (2000) [Phys. At. Nucl. **63**, 2173 (2000)]; A. M. Badalian and D. S. Kuzmenko, Phys. Rev. D **65**, 016004 (2002).
21. A. M. Badalian and Yu. A. Simonov, Yad. Fiz. **60**, 714 (1997) [Phys. At. Nucl. **60**, 630 (1997)]; Yu. A. Simonov, Lect. Notes Phys. **479**, 139 (1997).
22. G. Parisi and R. Petronzio, Phys. Lett. B **94B**, 51 (1980); J. M. Cornwall, Phys. Rev. D **26**, 1453 (1982).
23. A. Billore, Phys. Lett. B **92B**, 343 (1980); M. Peter, Nucl. Phys. B **501**, 471 (1997); Y. Schröder, Phys. Lett. B **447**, 321 (1999).
24. Particle Data Group, Phys. Rev. D **66**, 89 (2002).
25. S. Capitani, M. Lüscher, R. Sommer, and H. Witting, Nucl. Phys. B **544**, 669 (1999).
26. A. M. Badalian and B. L. G. Bakker, Phys. Rev. D **67**, 071903 (2003); A. M. Badalian and V. L. Morgunov, Phys. Rev. D **60**, 116008 (1999).
27. G. Bonvicini *et al.* (CLEO Collab.), hep-ex/0404021; S. E. Csorna *et al.* (CLEO Collab.), hep-ex/0207060; T. Skwarnicki, Int. J. Mod. Phys. A **19**, 1030 (2004).
28. T. A. Lahde and D. O. Riska, Nucl. Phys. A **707**, 425 (2002); C. Semay and B. Silvester-Brac, Phys. Rev. D **52**, 6553 (1995); Y. Vijande, P. Gonzalez, H. Carcilaro, and A. Valcarce, Phys. Rev. D **69**, 074019 (2004).

# Effects of Perturbative Exchanges in a QCD String Model\*

J. Weda<sup>1)</sup> and J. A. Tjon<sup>2)</sup>

Received May 13, 2004; in final form, August 17, 2004

**Abstract**—The QCD string model for baryons derived by Yu.A. Simonov and used for the calculation of baryon magnetic moments in a previous paper is extended to include also perturbative gluon and meson exchanges. The mass spectrum of the baryon multiplet is studied. For the meson interaction, either pseudoscalar or pseudovector coupling is used. Predictions are compared with the experimental data. Besides these exchanges, the influence of excited quark orbitals on the baryon ground state are considered by performing a multichannel calculation. The nucleon– $\Delta$  splitting increases due to the mixing of higher quark states, while the baryon magnetic momenta decrease. The multichannel calculation with perturbative exchanges is shown to yield reasonable magnetic moments, while the mass spectrum is close to experiment.  
© 2005 Pleiades Publishing, Inc.

## 1. INTRODUCTION

As QCD is generally accepted as the theory of strong interactions,  $\bar{q}q$  and  $3q$  dynamics should be derived from QCD in a fully relativistically covariant way. This is a formidable task due to the large gluon–quark coupling constant in the low-energy regime and the non-Abelian character of QCD. In recent years, the formalism of field correlators was set up to deal with the two main characteristics of quark systems: confinement and chiral symmetry breaking. Using this field-correlator method (FCM), a nonlinear equation has been derived for a light quark in the field of a heavy antiquark [1, 2]. In the derivation, use has been made of the large- $N_c$  limit and the calculation has been restricted to include only the Gaussian (bilocal) field correlator, an approximation which has been shown to be correct within a few percent by lattice simulations, as was discussed in [3].

The developed method is quite general and can be extended to treat the light quark systems  $\bar{q}q$  and  $3q$  as was shown in [4, 5]. Using this formalism, the baryon magnetic moments and corrections on these from virtual mesonic excitations have been calculated. Reasonable agreement with experiment has been obtained without the need of introduction of constituent quark masses [4]. The outcome of the method is partially summarized in the next section.

In the present paper, we extend the model in the following way. Using the same formalism as in [4] to obtain the baryon wave functions, the baryon mass

spectrum of the lowest octet and decuplet representation of the  $SU(3)$  flavor group is obtained. In Section 3, perturbative corrections to this spectrum due to one-gluon and pseudoscalar-meson exchanges are calculated. For the coupling of the pseudoscalar mesons to the quark, both pseudoscalar and pseudovector couplings are exploited. Following [6–8], we consider the influence of excited states to the ground state. This is done by forming excited baryon states out of the orbital and radial excitations of the single-quark wave functions and using these as a basis to diagonalize the Hamiltonian. The results from the multichannel calculation are shown in Section 4. The consequences of the diagonalization of the Hamiltonian to the magnetic moments are calculated in Section 5. Section 6 is devoted to some discussions and the paper ends with several appendices showing details on the calculations.

## 2. FORMALISM

As was explained in [4, 5], the FCM can be used to obtain an effective quark Lagrangian  $L_{\text{eff}}$  from the QCD partition function. Integrating out the gluon fields by using the generalized Fock–Schwinger gauge with contour  $C$  [9–11], the QCD action can be rewritten as

$$Z = \int D\kappa(C) D\Psi D\Psi^\dagger \exp(L_0 + L_{\text{eff}}), \quad (1)$$

where  $L_0$  is the free-quark-field Lagrangian and the effective Lagrangian in lowest order in quark fields has the form of a nonlocal four-fermion interaction. Moreover, since  $Z$  is gauge invariant, we have introduced an additional integration over a set of contours  $C(k)$  with weight  $D\kappa(C)$  in the partition function. In the FCM, the Gaussian approximation is

\*This article was submitted by the authors in English.

<sup>1)</sup>Institute for Theoretical Physics, University of Utrecht, The Netherlands.

<sup>2)</sup>Jefferson Lab, Newport News, USA.

**Table 1.** Ground-state energy  $\epsilon_0$  (in MeV) of the single-particle orbitals (spo) for various values of  $\sigma$  for both the  $u, d$  quark and the  $s$  quark (for the current masses, the values  $m_u = m_d = 5$  MeV and  $m_s = 200$  MeV are adopted)

spo	$\sigma = 0.06$ GeV <sup>2</sup>		$\sigma = 0.09$ GeV <sup>2</sup>		$\sigma = 0.12$ GeV <sup>2</sup>	
	$\epsilon_0(u, d)$	$\epsilon_0(s)$	$\epsilon_0(u, d)$	$\epsilon_0(s)$	$\epsilon_0(u, d)$	$\epsilon_0(s)$
0(1/2) <sup>++</sup>	243	388	297	440	342	482
1(1/2) <sup>++</sup>	435	560	535	656	617	736
2(1/2) <sup>++</sup>	572	692	704	821	813	928
0(1/2) <sup>-+</sup>	375	497	460	579	531	646
0(3/2) <sup>++</sup>	339	479	415	553	478	614
1(3/2) <sup>++</sup>	501	626	616	739	711	832
0(3/2) <sup>-+</sup>	453	576	558	677	644	761
0(5/2) <sup>++</sup>	419	556	514	650	593	728

usually made, which has been discussed extensively in [3, 12]. Choosing the generalized Fock–Schwinger gauge [9–11] with contours going through a given point  $\mathbf{r}_0$ , an effective action is determined. In this way, a Hamiltonian equation has been derived for the baryon, depending on the parameter  $\mathbf{r}_0$ ,

$$(H_1 + H_2 + H_3 - E)\Psi(\mathbf{r}_1, \mathbf{r}_2, \mathbf{r}_3) = 0 \quad (2)$$

with

$$H_i = m_i \beta^{(i)} + \mathbf{p}_i \cdot \boldsymbol{\alpha}^{(i)} + \beta^{(i)} M_i(\mathbf{r}_i - \mathbf{r}_0). \quad (3)$$

The quark mass operator  $M_i$  produces both linear confinement and chiral symmetry breaking, as was shown in [1, 2, 13]. It is a nonlinear and nonlocal operator acting in the coordinate space of the  $i$ th quark. When only the dominant part of  $M_i$  leading to confinement is kept, the kernel can be characterized as

$$M(x, y) \approx \frac{1}{2T_g \sqrt{\pi} \sigma} \left| \frac{\mathbf{x} + \mathbf{y}}{2} \right| \times \exp\left(-\frac{(\mathbf{x} - \mathbf{y})^2}{4T_g^2}\right), \quad (4)$$

where  $T_g$  is the gluon correlation length corresponding to the length scale of correlations in the fluctuations of the gluon background field. From lattice gauge simulations, it has been found to be of the order of 1/4 fm. Following [13], we have adopted a value  $T_g = 0.24$  fm. For asymptotically large  $|x|$ , it has been shown that the kernel Eq. (4) leads for a fixed  $\mathbf{r}_0$  to a linear confining interaction  $\sigma|\mathbf{r}_i - \mathbf{r}_0|$  [13, 14]. Moreover, it is of a Lorentz scalar type. In this paper, we will also allow for a constant term in the confining interaction, corresponding to the next-leading-order corrections to the area law. The weight  $D\kappa(c)$

should be chosen as a stationary point of the effective action and such that the contours generate a string of minimal length. As a consequence, the parameter  $\mathbf{r}_0$  can in principle be found as the minimum of the interaction between the three quarks, yielding for  $\mathbf{r}_0$  the so-called Torricelli point. This would result in a single string  $Y$  junction which is of a genuine three-body nature. However, for practical reasons, we take as a first approximation  $\mathbf{r}_0$  as a constant parameter, as was done in [4]. Due to treating  $\mathbf{r}_0$  as a constant instead of adopting the Torricelli point  $\mathbf{r}_T$ , the distance  $\sum_{i=1}^3 |\mathbf{r}_i - \mathbf{r}_0|$  is about  $\sim 2.5$  times bigger than the minimal distance  $\sum_{i=1}^3 |\mathbf{r}_i - \mathbf{r}_T|$ . This means that the string tension  $\sigma$  has to be chosen  $\sim 2.5$  times smaller to yield about the same energy. Recent lattice simulations on static quarks obtain a value of about  $\sigma = 0.15$  GeV<sup>2</sup> for the three-quark  $Y$ -shaped interaction, which is close to the value for quark–antiquark interactions [15]. This result suggests that string tensions as low as  $\sigma = 0.06$  GeV<sup>2</sup> can be used in our calculations.

The solution to Eq. (2) is now of a factorizable form which enables us to represent the baryon wave function as the product of three single-particle solutions,

$$\Psi_{JM} = \Gamma_{JM}^{\alpha\beta\gamma}(f_1, f_2, f_3) e_{abc} \psi_{a\alpha}^{f_1}(\mathbf{r}_1 - \mathbf{r}_0) \times \psi_{b\beta}^{f_2}(\mathbf{r}_2 - \mathbf{r}_0) \psi_{c\gamma}^{f_3}(\mathbf{r}_3 - \mathbf{r}_0), \quad (5)$$

where  $a, b, c$  and  $f_i$  are the color and flavor indices, respectively. The orbital and radial excitations are indicated by  $\alpha, \beta$ , and  $\gamma$ . Because of the Pauli principle, the baryon wave function has to be a totally antisymmetric function of the three quark functions. As the baryon is a color white object (antisymmetric in color), the wave function Eq. (5) has to be totally symmetric in flavor, orbital, and radial excitations of the single-particle wave functions  $\psi_{a\alpha}^{f_i}$ . The totally antisymmetric tensor  $e_{abc}$  and the function  $\Gamma_{JM}^{\alpha\beta\gamma}$ , respectively, take care of this (anti)symmetrization. Explicit formulas for the lowest baryons are given in Appendix A.

Each single-particle solution satisfies a nonlinear Dirac-like Hamiltonian equation,

$$H_i \psi_{a_i \alpha_i}^{f_i} = \varepsilon_{n_i}^{(i)} \psi_{a_i \alpha_i}^{f_i}, \quad E = \sum_{i=1}^3 \varepsilon_{n_i}^{(i)}, \quad (6)$$

where  $H_i$  is given by Eq. (3). It has to be solved self-consistently, leading to confining solutions. Details can be found in [13]. In Table 1, some values of  $\varepsilon_n$ , for  $n = 0$ , are shown. The solutions are listed as

$$n(j)^{\text{sgn}(\kappa)\text{sgn}(\varepsilon_n)}, \quad \kappa = \pm \left(j + \frac{1}{2}\right). \quad (7)$$

From these single-quark orbitals, the baryon spectrum  $M_B = E$  and the corresponding baryon wave functions (5) can immediately be constructed.

Using these baryon wave functions, the magnetic moments  $\mu_z$  have been determined in [4]. Following [16], we have

$$\begin{aligned} \mu_z &= \frac{e}{2M_p} G_{\text{mag}}(Q=0) \\ &= -\frac{i}{2} [\nabla_Q \times \mathbf{M}]_z (Q=0), \end{aligned} \quad (8)$$

where  $e$ ,  $M_p$ , and  $G_{\text{mag}}$  are the charge, mass, and Sachs magnetic moment of the proton. The electromagnetic current matrix element  $M_\mu$  is given by

$$M_\mu = \langle \Psi | J_\mu(Q) | \Psi \rangle. \quad (9)$$

For the operator  $J_\mu$ , the single-quark current operator is taken as the first approximation. Higher order contributions come from two-body currents like one-pion-exchange currents and mesonic one-loop corrections which give rise to the anomalous magnetic moment of the quark. Reasonable values were obtained for the magnetic moments of the baryon octet and decuplet in the case of a string tension of  $\sigma = 0.1 \text{ GeV}^2$  without the need of introduction of constituent quark masses [4]. In the present paper, we extend this analysis to also include the one-gluon exchange (OGE) and study the effects of the use of different forms for the interaction in the one-pion exchange (OPE).

### 3. EXCHANGE POTENTIALS

Until now, the picture of quarks moving in the confining sea of gluons has been used. This leads to confinement and chiral symmetry breaking, but it lacks spin-dependent interactions. Typical spin-dependent structures in the baryon spectrum such as the splitting between the nucleon and the  $\Delta$  are therefore not present in such a simplified model. To remove this deficiency, a perturbative OGE interaction is now introduced. The Coulomb part is expected to lower the baryon masses and the color magnetic part is expected to give rise to a splitting between the  $J = 1/2$  and  $J = 3/2$  states. Besides this one-gluon interaction, we also introduce perturbative pseudoscalar-meson exchanges which can be considered as an effective interaction representing the exchange of correlated quark–antiquark pairs. The interactions are schematically shown in Fig. 1.

The Hamiltonian Eq. (2) is equivalent to a Bethe–Salpeter equation with an instantaneous interaction. Of all possible three-particle wave functions of the type (5), it couples only to  $(+++)$  and  $(---)$ , where  $\pm$  indicates the sign of  $\epsilon_n$  as in Eq. (7). All other

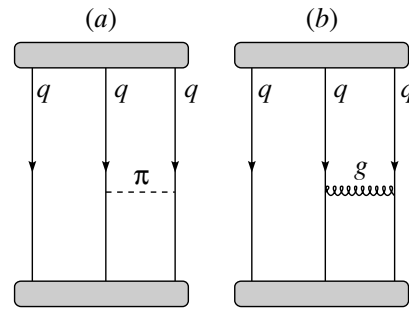


**Fig. 1.** A schematic view of the exchange of a pion (a) and a gluon (b) between two quarks in a baryon. The blobs at the beginning and the end of the diagram represent bound states of the quarks.

wave functions decouple. Within such an equal-time approximation, we now consider the effects of the perturbative exchanges. Following [17–19], where the instantaneous three-particle Bethe–Salpeter equation is considered, we assume that the perturbative gluon and meson exchanges only take place between these purely positive and negative energy components. As discussed in [17], we write for the interaction potential in the Hamiltonian

$$\begin{aligned} &H_{\text{int}}^{(23)} \Psi(P, \mathbf{p}_\rho, \mathbf{p}_\lambda) \\ &= \left( \Lambda^+(\mathbf{p}_1) \Lambda^+(\mathbf{p}_2) \Lambda^+(\mathbf{p}_3) \right. \\ &\quad \left. + \Lambda^-(\mathbf{p}_1) \Lambda^-(\mathbf{p}_2) \Lambda^-(\mathbf{p}_3) \right) \\ &\quad \times \int \frac{d^3 p'_\rho}{(2\pi)^3} \frac{d^3 p'_\lambda}{(2\pi)^3} \gamma^0(2) \gamma^0(3) \\ &\quad \times V_{\text{ex}}^{(23)}(\mathbf{p}_\rho, \mathbf{p}_\lambda, \mathbf{p}'_\rho, \mathbf{p}'_\lambda) \Psi(P, \mathbf{p}'_\rho, \mathbf{p}'_\lambda), \end{aligned} \quad (10)$$

with the energy projection operators defined as

$$\Lambda^\pm(\mathbf{p}) = \frac{\omega \pm H(\mathbf{p})}{2\omega}, \quad \omega = |\epsilon_n|. \quad (11)$$

The interactions between the other quark pairs,  $H_{\text{int}}^{(12)}$  and  $H_{\text{int}}^{(13)}$ , can very similarly be written down and easily be included. The Hamiltonian Eq. (2) becomes

$$\begin{aligned} &H \Psi(\mathbf{r}_1, \mathbf{r}_2, \mathbf{r}_3) \\ &= \left( H_1 + H_2 + H_3 + H_{\text{int}}^{(12)} + H_{\text{int}}^{(13)} + H_{\text{int}}^{(23)} \right) \\ &\quad \times \Psi(\mathbf{r}_1, \mathbf{r}_2, \mathbf{r}_3) = (E + \Delta E) \Psi(\mathbf{r}_1, \mathbf{r}_2, \mathbf{r}_3). \end{aligned} \quad (12)$$

The exchange interactions are treated perturbatively,

$$\Delta E = 3 \left\langle \Psi_{JM} \left| H_{\text{int}}^{(23)} \right| \Psi_{JM} \right\rangle, \quad (13)$$

where  $\Psi_{JM}$  represents the baryon wave function (5). Because of symmetry considerations, the interactions between the other quark pairs can simply be included by adding a factor of 3 shown in Eq. (13).

The exchange potential  $V_{\text{ex}}^{(23)}$  in Eq. (10) for the nonstrange baryons can be split into two contributions, the OGE and OPE. They are explicitly written as

$$V_{\text{OGE}}^{(23)}(\mathbf{k}) = -4\pi \frac{2}{3} \alpha_s \frac{\gamma_\mu(2)\gamma^\mu(3)}{\mathbf{k}^2}, \quad (14a)$$

$$V_{\text{OPE}}^{(23)}(\mathbf{k}) = 4\pi g_{qq\pi}^2 \boldsymbol{\tau}(2) \cdot \boldsymbol{\tau}(3) \gamma_5(2)\gamma_5(3) \quad (14b)$$

$$\times \frac{1}{\mathbf{k}^2 + m_\pi^2} \left( \frac{\Lambda^2}{\mathbf{k}^2 + \Lambda^2} \right)^2,$$

where a pseudoscalar (PS) coupling for the pion is assumed. The factor  $2/3$  in the OGE originates from the color content of the baryons and the term  $\boldsymbol{\tau}(2) \cdot \boldsymbol{\tau}(3)$  in the OPE takes care of the isospin. The exchange potentials can also be written in coordinate space by performing Fourier transformations:

$$V_{\text{OGE}}^{(23)}(\mathbf{r}_2 - \mathbf{r}_3) = -\frac{2}{3} \alpha_s \frac{\gamma_\mu(2)\gamma^\mu(3)}{|\mathbf{r}_2 - \mathbf{r}_3|}, \quad (15a)$$

$$V_{\text{OPE}}^{(23)}(\mathbf{r}_2 - \mathbf{r}_3) = g_{qq\pi}^2 \boldsymbol{\tau}(2) \cdot \boldsymbol{\tau}(3) \quad (15b)$$

$$\times \gamma_5(2)\gamma_5(3) \left( \frac{\Lambda^2}{\Lambda^2 - m_\pi^2} \right)^2$$

$$\times \left( -\frac{e^{-m_\pi|\mathbf{r}_2-\mathbf{r}_3|}}{|\mathbf{r}_2 - \mathbf{r}_3|} + \frac{e^{-\Lambda|\mathbf{r}_2-\mathbf{r}_3|}}{|\mathbf{r}_2 - \mathbf{r}_3|} \right.$$

$$\left. + \frac{\Lambda^2 - m_\pi^2}{\Lambda} \frac{e^{-\Lambda|\mathbf{r}_2-\mathbf{r}_3|}}{2} \right) \quad (\text{PS}).$$

Details on the calculation of the perturbative calculation of the matrices Eq. (13) can be found in Appendix B.

When a pseudovector (PV) pion–quark coupling is assumed, some modifications have to be made. In Eq. (14b), the PV coupling is obtained by the replacement

$$g_{\pi qq} \gamma_5 \boldsymbol{\tau}_a \rightarrow \frac{g_{\pi qq}}{2m_{\text{eff}}} \boldsymbol{\not{k}} \boldsymbol{\tau}^a, \quad (16)$$

where  $m_{\text{eff}}$  is a scaling mass of the order of the constituent quark mass, to be discussed later. By Fourier transformation, the momenta in Eq. (16) turn into derivatives in coordinate space. In this way, the matrices  $\boldsymbol{\not{k}}$  can be evaluated when they act upon the quark wave functions, resulting in some derivatives on the radial wave function and a changed angular dependence. Details are given in Appendix B.

The model can easily be extended to include the strange baryons. Apart from pion exchanges,

we now also have to add kaon and eta exchanges. These exchanges can be included by changing the  $SU(2)$  isospin matrices  $\boldsymbol{\tau}(2) \cdot \boldsymbol{\tau}(3)$  in Eq. (14b) into  $SU(3)$  flavor matrices  $\sum_{a=1}^8 \lambda_2^a \lambda_3^a$  and substituting the correct coupling constants and meson and cutoff masses.

For the coupling of the gluon to the quark, a running coupling constant is used which depends on the distance. Following [20], the coupling is parametrized as

$$\alpha^{(2)}(q) = \alpha^{(1)}(q) \left( 1 - \frac{\beta_1}{\beta_0^2} \frac{\ln t_B}{t_B} \right), \quad (17)$$

$$\alpha^{(1)}(q) = \frac{4\pi}{\beta_0 t_B}$$

with

$$t_B = \ln \frac{q^2 + m_B^2}{\Lambda_V^2} \quad (18)$$

and

$$\beta_0 = 11 - \frac{2}{3}n_f, \quad \beta_1 = 102 - \frac{38}{3}n_f. \quad (19)$$

As the calculation is performed in coordinate space, the coupling constant has to be Fourier-transformed, which can be done as

$$\tilde{\alpha}(r) = \frac{2}{\pi} \int_0^\infty dq \frac{\sin(qr)}{q} \alpha(q) \quad (20)$$

$$= \frac{2}{\pi} \int_0^\infty dx \frac{\sin x}{x} \alpha(x/r).$$

The constants are fixed at  $m_B = 1.0$  GeV,  $\Lambda_V = 385$  MeV, and  $n_f = 3$  as discussed in [20].

Following [21], we exploit the Goldberger–Treiman relation [22] for the pion–quark vertex to find the PV coupling constant to meson  $m$ ,

$$f_{mqq} = M_m \frac{g_A^q}{2f_m}, \quad (21)$$

where  $M_m$  is the meson mass,  $g_A^q$  is the quark axial coupling constant, and  $f_m$  is the decay constant. From [23, 24], we take the decay constants  $f_\pi = 93$  MeV,  $f_\kappa = 113$  MeV, and  $f_\eta = 112$  MeV.

The axial coupling constant of the quark is not well known. In the static quark model, it can be related to the nucleon axial coupling constant as  $g_A^q = \frac{3}{5}g_A^N$ , which would give  $g_A^q = 0.76$  for  $g_A^N = 1.26$ . In the large- $N_c$  limit, however, the coupling would be  $g_A^q = 1$ , as was derived in [25] and confirmed by Simonov [26] using the FCM. If  $1/N_c$  corrections are taken into account, the coupling decreases to  $g_A^q = 0.87$  [27].

**Table 2.** The parameters involved in the meson–quark interaction used for the calculation with the axial coupling constant  $g_A^q = 1$  [the decay constants  $f_m$  and all (cutoff) masses are in MeV, the coupling constants  $f_{mqq}$  and  $g_{mqq}$  are dimensionless]

$m$	$M_m$	$f_m$	$f_{mqq}^2/4\pi$	$\Lambda_m$	$\sigma = 0.06 \text{ GeV}^2$		$\sigma = 0.09 \text{ GeV}^2$		$\sigma = 0.12 \text{ GeV}^2$	
					$m_{\text{eff}}$	$g_{mqq}^2/4\pi$	$m_{\text{eff}}$	$g_{mqq}^2/4\pi$	$m_{\text{eff}}$	$g_{mqq}^2/4\pi$
$\pi$	139	93	0.0444	678	206	0.39	254	0.59	294	0.79
$\kappa$	494	113	0.380	966	266	0.44	312	0.61	351	0.76
$\eta$	547	112	0.475	1008	266	0.45	312	0.62	351	0.78

For consistency reasons, we try to keep close to the FCM and choose  $g_A^q = 1$ . The resulting values for  $f_{mqq}$  are determined from the Goldberger–Treiman relation and shown in Table 2. The parametrization of the cutoff mass is taken to be the same as in [21]:

$$\Lambda_m = \Lambda_0 + \kappa M_m \quad (22)$$

with the parameters  $\Lambda_0 = 565 \text{ MeV}$ ,  $\kappa = 0.81$ ; the results are given in Table 2.

The pseudoscalar coupling constant  $g_{mqq}$  is related to the PV coupling constant  $f_{mqq}$  as

$$\frac{g_{mqq}}{2m_{\text{eff}}} = \frac{f_{mqq}}{M_m}. \quad (23)$$

The  $m_{\text{eff}}$  can be looked at as the effective constituent mass of the quark. In the case of pion coupling,  $m_{\text{eff}}$  is the effective constituent mass of the  $u, d$  quark; in the case of kaon and eta coupling,  $m_{\text{eff}}$  is a mixture of  $u$ -,  $d$ -, and  $s$ -quark masses. The mass is chosen such that the one-pion and one-kaon exchanges using PS coupling give the same value as using the PV coupling in only positive energy channels. So we require for both one-pion ( $V_{\text{OPE}}$ ) and one-kaon ( $V_{\text{OKE}}$ ) exchange

$$V_I^{(23)}(\text{PS}) = V_I^{(23)}(\text{PV}) \quad (24)$$

$$\times \left( \frac{1 + \gamma_0}{2} \right)_{(2)} \left( \frac{1 + \gamma_0}{2} \right)_{(3)},$$

$I = \text{OPE, OKE.}$

The effective mass  $m_{\text{eff}}$  for the eta meson is set equal to the  $m_{\text{eff}}$  for the kaon. The parameters are summarized in Table 2. It can be seen that the coupling constants  $g_{mqq}$  are almost equal, as would be the case in a chiral symmetric world. In the case of  $\sigma = 0.09 \text{ GeV}^2$ , we find values which are somewhat smaller than  $g_{mqq}^2/4\pi = 0.67$ , as was used by Glozman *et al.* [21, 28]; in the case of  $\sigma = 0.12 \text{ GeV}^2$ , somewhat larger.

Using these coupling constants, the perturbative exchanges are calculated, where as a first approximation the baryon wave function Eq. (5) is used. Results

are shown in Tables 3, 4, and 5 for string tensions of  $\sigma = 0.06, 0.09$ , and  $0.12 \text{ GeV}^2$ , respectively.

As can be seen from Tables 3–5, an extra parameter  $C_0$  has been introduced which is of a Lorentz vector nature. This parameter is added to the confining potential as

$$M(\mathbf{r}^{(i)} - \mathbf{r}^{(0)}) \rightarrow M(\mathbf{r}^{(i)} - \mathbf{r}^{(0)}) + \beta^{(i)} C_0. \quad (25)$$

In the derivation of the confining potential in [5, 13], the large-distance behavior of the interaction was examined. The actual dependence at short distances,

**Table 3.** The mass is calculated for the baryon multiplet for the string tension  $\sigma = 0.06 \text{ GeV}^2$  ( $C_0$  is adjusted such as to yield the correct value for the nucleon; the contributions of the exchange potentials are also shown; all numbers are in MeV)

	$N$	$V_{\text{Coul}}$	$V_{\text{hf}}$	$V_\pi$	$V_\kappa$	$V_\eta$	$M_N$	$M_{\text{exp}}$	$C_0$	
PS	$p, n$	-130	-9	-175	0	4	939	939	174	
	$\Lambda$	-138	-9	-105	-25	4	1121	1116		
	$\Sigma$	-138	-7	-12	-42	-12	1184	1193		
	$\Xi$	-147	-8	0	-42	-15	1327	1318		
	$\Delta$	-130	9	-35	0	-4	1089	1232		
	$\Sigma^*$	-138	8	-12	-17	4	1240	1385		
	$\Xi^*$	-147	7	0	-17	0	1383	1516		
	$\Omega$	-158	7	0	0	-14	1518	1672		
	PV	$p, n$	-130	-9	-121	0	1	939	939	157
		$\Lambda$	-138	-9	-72	-19	1	1106	1116	
$\Sigma$		-138	-7	-8	-32	-7	1151	1193		
$\Xi$		-147	-8	0	-32	-13	1288	1318		
$\Delta$		-130	9	-24	0	-1	1052	1232		
$\Sigma^*$		-138	8	-8	-13	3	1195	1385		
$\Xi^*$		-147	7	0	-13	-3	1332	1516		
$\Omega$		-158	7	0	0	-20	1462	1672		

**Table 4.** The same as in Table 3, but for the string tension  $\sigma = 0.09 \text{ GeV}^2$ 

	$N$	$V_{\text{Coul}}$	$V_{\text{hf}}$	$V_{\pi}$	$V_{\kappa}$	$V_{\eta}$	$M_N$	$M_{\text{exp}}$	$C_0$
PS	$p, n$	-159	-11	-314	0	9	939	939	175
	$\Lambda$	-167	-11	-189	-52	9	1148	1116	
	$\Sigma$	-167	-9	-21	-86	-24	1250	1193	
	$\Xi$	-177	-10	0	-86	-31	1396	1318	
	$\Delta$	-159	11	-63	0	-9	1195	1232	
	$\Sigma^*$	-167	10	-21	-34	8	1353	1385	
	$\Xi^*$	-177	9	0	-34	1	1499	1516	
	$\Omega$	-187	8	0	0	-30	1634	1672	
	PV	$p, n$	-159	-11	-222	0	3	939	939
$\Lambda$		-167	-11	-133	-39	3	1123	1116	
$\Sigma$		-167	-9	-15	-65	-16	1199	1193	
$\Xi$		-177	-10	0	-65	-27	1335	1318	
$\Delta$		-159	11	-44	0	-3	1132	1232	
$\Sigma^*$		-167	10	-15	-26	6	1279	1385	
$\Xi^*$		-177	9	0	-26	-5	1415	1516	
$\Omega$		-187	8	0	0	-37	1539	1672	

however, is quite unknown. There can be contributions of the Lorentz vector or scalar type; even spin-spin interactions are possible. Our results seem to suggest that a constant  $C_0$  with a value of about 170–190 MeV has to be added in the case of PS coupling.

When the PV coupling is used, we find smaller values of the meson exchanges as compared to the PS coupling. Considering only positive energy components, both couplings give the same results by definition, Eq. (24). The inclusion of negative energy components decreases the effect of meson exchanges such that a smaller value of  $C_0$ , in the range of  $C_0 \approx 140$ –160 MeV, is needed in the case of PV coupling.

The hyperfine splitting and the OPE show some symmetry. The origin of the symmetry can be understood by performing a nonrelativistic reduction on the exchanges Eqs. (14a), (14b). The resulting Breit interaction yields the  $\boldsymbol{\sigma}_2 \cdot \boldsymbol{\sigma}_3$  structure which causes the well-known  $(-3) : 1$  splitting between the spin singlet and triplet state. From Appendix A, it can be seen that the  $\Delta$  consists solely of spin triplet ( $j_{23} = 1$ ) states and the nucleon is built up from a sum of spin singlet ( $j_{23} = 0$ ) and spin triplet ( $j_{23} = 1$ ) states. This results exactly in the  $(-1) : 1$  hyperfine splitting observed for the nucleon and the  $\Delta$  in Tables 3–5. The splitting  $(-5) : (-1)$  in the OPE can similarly

**Table 5.** The same as in Table 3, but for the string tension  $\sigma = 0.12 \text{ GeV}^2$ 

	$N$	$V_{\text{Coul}}$	$V_{\text{hf}}$	$V_{\pi}$	$V_{\kappa}$	$V_{\eta}$	$M_N$	$M_{\text{exp}}$	$C_0$
PS	$p, n$	-182	-13	-458	0	14	939	939	184
	$\Lambda$	-191	-13	-275	-82	14	1174	1116	
	$\Sigma$	-191	-11	-31	-136	-39	1312	1193	
	$\Xi$	-200	-12	0	-136	-51	1462	1318	
	$\Delta$	-182	13	-92	0	-14	1303	1232	
	$\Sigma^*$	-191	12	-31	-55	13	1468	1385	
	$\Xi^*$	-200	11	0	-55	1	1618	1516	
	$\Omega$	-210	10	0	0	-48	1753	1672	
	PV	$p, n$	-182	-13	-327	0	6	939	939
$\Lambda$		-191	-13	-196	-61	6	1142	1116	
$\Sigma$		-191	-11	-22	-101	-25	1247	1193	
$\Xi$		-200	-12	0	-101	-42	1383	1318	
$\Delta$		-182	13	-65	0	-6	1215	1232	
$\Sigma^*$		-191	12	-22	-40	10	1365	1385	
$\Xi^*$		-200	11	0	-40	-7	1501	1516	
$\Omega$		-210	10	0	0	-56	1622	1672	

be understood when it is realized that, in the non-relativistic reduction of Eq. (15b), the spin-isospin structure looks like  $(\boldsymbol{\sigma}_2 \cdot \boldsymbol{\sigma}_3)(\boldsymbol{\tau}_2 \cdot \boldsymbol{\tau}_3)$ .

When the string tension  $\sigma$  is increased, the single-particle orbitals tend to become more compact. Due to the  $1/r$  behavior of the exchange potentials, this results in larger values in the perturbative calculation Eq. (13).

The results for the baryon octet ( $J = 1/2$ ) are quite close to the experimental masses in the case of PS coupling for  $\sigma = 0.06 \text{ GeV}^2$  and in the case of PV coupling for  $\sigma = 0.09 \text{ GeV}^2$ . From Table 4, it can be seen that the PS coupling does somewhat better for the baryon decuplet ( $J = 3/2$ ), where the PV calculation misses about 100 MeV. For  $\sigma = 0.12 \text{ GeV}^2$  in Table 5, the PV coupling leads to a reasonable overall agreement, while the PS calculation produces values which are too large.

#### 4. MULTICHANNEL CALCULATION

Up to this point, the baryon wave functions contain only the ground state of the single-quark orbital. That is, the baryon wave function Eq. (5) can schematically be written as

$$\Psi_{JM} = \prod_{k=1}^3 \left( 0 \left( \frac{1}{2} \right)^{++} \right)_k, \quad (26)$$

where the notation from Eq. (7) has been used. Coefficients needed for symmetrization and coupling to the proper angular momentum are left out for simplicity. Quarks, however, can also be in excited orbitals, which means that, generally, baryon wave functions which are (partly) built up from excited single-particle solutions also contribute to the baryon. So contributions like

$$\begin{aligned}\Psi_{JM} &= \left(1 \left(\frac{1}{2}\right)^{++}\right)_1 \prod_{k=2}^3 \left(0 \left(\frac{1}{2}\right)^{++}\right)_k, \quad (27) \\ \Psi_{JM} &= \left(0 \left(\frac{1}{2}\right)^{++}\right)_1 \left(0 \left(\frac{1}{2}\right)^{-+}\right)_2 \left(1 \left(\frac{1}{2}\right)^{++}\right)_3, \\ \Psi_{JM} &= \left(0 \left(\frac{3}{2}\right)^{++}\right)_1 \left(0 \left(\frac{1}{2}\right)^{++}\right)_2 \left(0 \left(\frac{1}{2}\right)^{-+}\right)_3\end{aligned}$$

can mix into the baryon ground state and change the energy. Similarly as was done in [6, 7] for nonrelativistic quark models and in [8] for a relativized model, we take wave functions as Eq. (27) as a basis for diagonalizing the Hamiltonian Eq. (12).

As the color content of the baryon takes care of the antisymmetrization, the resulting three-particle wave function has to be totally symmetric with respect to particle interchanges when the color is disregarded. Spin, isospin, and orbital and radial excitations are taken into account in the symmetrization procedure. The three-quark state can be characterized in the following way. Let us consider the representation, where quark 1 plays a special role. Starting from the single-quark orbitals we may couple quarks 2 and 3 to a  $j_{23}$  and  $i_{23}$  state. These states can in general be made symmetric by adding the permutation  $2 \leftrightarrow 3$  to these states. An appropriate choice for the quantum numbers  $j_{23}$  and  $i_{23}$  has to be made, such that the wave function does not vanish. To form the three-quark state with total quantum numbers  $J$  and  $I$ , the single-quark orbital of quark 1 is added. Taking the proper linear combinations of the Faddeev components formed from the first term by the interchanges  $1 \leftrightarrow 2$  and  $1 \leftrightarrow 3$ , it is assured that the whole wave function is totally symmetric under the interchange of any two particles. Adopting for the moment the notation

$$|n_k j_k l_k m_{j_k}\rangle \otimes |i_k m_{i_k}\rangle \quad (28)$$

to represent the single-orbital solution, we have

$$\begin{aligned}\Psi_{J,I}(j_{23}, i_{23}) &= \sum \text{CG} \left\{ |1\rangle (|2\rangle |3\rangle \right. \\ &\quad \left. + |3\rangle |2\rangle) + (1 \leftrightarrow 2) + (1 \leftrightarrow 3) \right\} \\ &= \sum_{m_i, m_j} C(i_1, i_{23}, I; m_{i_1}, m_{i_{23}}, M_I) \\ &\quad \times C(j_1, j_{23}, J; m_{j_1}, m_{j_{23}}, M_J) \\ &\quad \times C(i_2, i_3, i_{23}; m_{i_2}, m_{i_3}, m_{i_{23}})\end{aligned} \quad (29)$$

$$\begin{aligned}&\times C(j_2, j_3, j_{23}, m_{j_2}, m_{j_3}, m_{j_{23}}) \\ &\quad \times \left\{ |n_1 j_1 l_1 m_{j_1}\rangle \otimes |i_1 m_{i_1}\rangle \right. \\ &\quad \times \left( |n_2 j_2 l_2 m_{j_2}\rangle |n_3 j_3 l_3 m_{j_3}\rangle \otimes |i_2 m_{i_2}\rangle |i_3 m_{i_3}\rangle \right. \\ &\quad \left. \left. + |n_3 j_3 l_3 m_{j_3}\rangle |n_2 j_2 l_2 m_{j_2}\rangle \otimes |i_3 m_{i_3}\rangle |i_2 m_{i_2}\rangle \right) \right. \\ &\quad \left. + (1 \leftrightarrow 2) + (1 \leftrightarrow 3) \right\},\end{aligned}$$

where the  $C$  are the Clebsch–Gordan coefficients in the Rose notation [29]. In the first line of Eq. (29), we have summarized the summation over the Clebsch–Gordan coefficients by  $\sum \text{CG} \{ \dots \}$ . An allowed choice of  $j_{23}$  and  $i_{23}$  does not always lead to unique three-particle wave functions. If one takes, for example, three identical single-particle orbitals with  $j_1 = j_2 = j_3 = 1/2$  and  $i_1 = i_2 = i_3 = 1/2$ , the wave function  $\Psi_{1/2,1/2}(0,0)$  equals  $\Psi_{1/2,1/2}(1,1)$ . Independence of these basis functions is tested by calculating the determinant of the matrix  $\langle \Psi_\alpha | \Psi_\beta \rangle$ , where  $\Psi_\alpha$  and  $\Psi_\beta$  are wave functions like Eq. (29). A simple example of this procedure is shown in Appendix A, where the totally symmetric nucleon and  $\Delta$  wave functions are constructed.

The wave functions  $\Psi_\alpha$  are taken as a basis to solve the full Hamiltonian, including OGE and OPE. So let us consider

$$\langle \Psi_\alpha | V_{\text{ex}} | \Psi_\beta \rangle + \langle \Psi_\alpha | [H_0 - E] | \Psi_\beta \rangle = 0 \quad (30)$$

with

$$H_0 | \Psi_\beta \rangle = E_\beta | \Psi_\beta \rangle = \left( \epsilon^{(1)} + \epsilon^{(2)} + \epsilon^{(3)} \right) | \Psi_\beta \rangle \quad (31)$$

and

$$V_{\alpha\beta} = \langle \Psi_\alpha | V_{\text{ex}} | \Psi_\beta \rangle, \quad A_{\alpha\beta} = \langle \Psi_\alpha | \Psi_\beta \rangle. \quad (32)$$

Using these expressions we define

$$[A_{\alpha\gamma}^{-1} V_{\gamma\beta} + E_\beta \delta_{\alpha\beta}] = H_{\alpha\beta}, \quad (33)$$

from which the eigenvalues  $E$  have to be found.

From the calculations performed, it is found that the single-quark orbitals  $1 \left(\frac{1}{2}\right)^{++}$ ,  $0 \left(\frac{3}{2}\right)^{++}$ , and, to a smaller extent,  $0 \left(\frac{1}{2}\right)^{-+}$  give the largest change in the spectrum in the case of PS coupling. These orbitals have been used in a multichannel calculation for both the  $u$ ,  $d$  quark and the  $s$  quark. That is, all possible combinations of  $0 \left(\frac{1}{2}\right)^{++}(u, d)$ ,  $1 \left(\frac{1}{2}\right)^{++}(u, d)$ ,  $0 \left(\frac{3}{2}\right)^{++}(u, d)$ ,  $0 \left(\frac{1}{2}\right)^{-+}(u, d)$ ,  $0 \left(\frac{1}{2}\right)^{++}(s)$ ,  $1 \left(\frac{1}{2}\right)^{++}(s)$ ,  $0 \left(\frac{3}{2}\right)^{++}(s)$ , and  $0 \left(\frac{1}{2}\right)^{-+}(s)$  which couple to some specific total angular momentum  $J$  and total isospin  $I$  are taken into account. When a PV coupling is exploited, the single-particle orbital  $0 \left(\frac{5}{2}\right)^{++}$  is taken

**Table 6.** The result on the mass (in MeV) and the magnetic moment (in units of the nuclear magneton) of the multichannel calculation, where the single-particle orbitals (spo's)  $0(\frac{1}{2})^{++}$ ,  $0(\frac{1}{2})^{-+}$ ,  $0(\frac{3}{2})^{++}$ , and either  $1(\frac{1}{2})^{++}$  (PS) or  $0(\frac{5}{2})^{++}$  (PV) are used as input (the string tension is fixed at  $\sigma = 0.06 \text{ GeV}^2$ ; the  $C_0$  is adjusted to yield the correct nucleon mass; in the case of PS coupling,  $C_0(1) = 174 \text{ MeV}$ ,  $C_0(4) = 204 \text{ MeV}$ , and in the case of PV coupling,  $C_0(1) = 157 \text{ MeV}$ ,  $C_0(4) = 182 \text{ MeV}$ )

N	PS coupling				PV coupling				Exp.	
	1 spo		4 spo's		1 spo		4 spo's			
	$m_N$	$\mu_N$	$m_N$	$\mu_N$	$m_N$	$\mu_N$	$m_N$	$\mu_N$	$m_N$	$\mu_N$
$p$	939	3.58	939	3.18	939	3.64	939	3.19	938	2.79
$n$	939	-2.44	939	-2.15	939	-2.50	939	-2.17	940	-1.91
$\Lambda$	1121	-0.78	1133	-0.75	1106	-0.78	1120	-0.77	1116	-0.61
$\Sigma^+$	1184	3.43	1221	3.15	1151	3.48	1193	3.26	1189	2.46
$\Sigma^0$	1184	1.02	1221	0.94	1151	1.02	1193	0.96	1193	
$\Sigma^-$	1184	-1.39	1221	-1.28	1151	-1.43	1193	-1.34	1197	-1.16
$\Xi^0$	1327	-1.83	1363	-1.68	1288	-1.84	1331	-1.78	1315	-1.25
$\Xi^-$	1327	-0.62	1363	-0.63	1288	-0.62	1331	-0.62	1321	-0.65
$\Delta^{++}$	1089	7.13	1157	6.50	1052	7.24	1112	6.72	1232	4.52
$\Delta^+$	1089	3.52	1157	3.21	1052	3.56	1112	3.31	1232	
$\Delta^0$	1089	-0.09	1157	-0.08	1052	-0.13	1112	-0.11	1232	
$\Delta^-$	1089	-3.70	1157	-3.37	1052	-3.81	1112	-3.53	1232	
$\Sigma^{+*}$	1240	3.98	1311	3.68	1195	4.05	1258	3.84	1383	
$\Sigma^{0*}$	1240	0.37	1311	0.31	1195	0.36	1258	0.33	1384	
$\Sigma^{-*}$	1240	-3.70	1311	-3.05	1195	-3.32	1258	-3.18	1387	
$\Xi^{0*}$	1383	0.83	1456	0.77	1332	0.85	1395	0.82	1532	
$\Xi^{-*}$	1383	-2.79	1456	-2.68	1332	-2.83	1395	-2.76	1535	
$\Omega^-$	1518	-2.33	1590	-2.18	1462	-2.34	1522	-2.20	1672	-2.02

instead of  $1(\frac{1}{2})^{++}$  as it was found to give a larger contribution in this case. The results are shown in Tables 6, 7, and 8 for string tensions of  $\sigma = 0.06, 0.09$ , and  $0.12 \text{ GeV}^2$ , respectively.

The inclusion of the excited quark orbitals changes the spectrum considerably. All ground-state masses lower through this calculation. This effect is stronger for the baryon octet, which causes the nucleon- $\Delta$  splitting to increase by about 100 MeV. In the case of  $\sigma = 0.09 \text{ GeV}^2$ , the situation for the baryon decuplet thus improves considerably, leading to a rather close prediction for the PV calculation, as can be seen in Table 7. The baryon octet, however, is quite well reproduced in Table 6 for a string tension of  $\sigma = 0.06 \text{ GeV}^2$  and a PV coupling. The PS calculation with the string tension of  $\sigma = 0.09 \text{ GeV}^2$  yields values

somewhat too large, while the results in Table 8 are much too high for the decuplet.

As a second consequence of the lower masses, larger  $C_0$  values have to be used. The mass splittings inside the baryon octet and decuplet also get larger. In most cases, this behavior deteriorates the predictions inside the baryon octet somewhat, already being too large by a small amount in the calculation from the previous section.

These results for the mass spectrum seem to point in the direction of a small string tension of about  $\sigma = 0.08 \text{ GeV}^2$  and a slight preference for a PV coupling when the overall agreement is considered.

## 5. MAGNETIC MOMENTS

Now the influence of the perturbative exchanges on the mass spectrum has been calculated and the

**Table 7.** The same as in Table 6, but for  $\sigma = 0.09 \text{ GeV}^2$  and in the case of PS coupling  $C_0(1) = 175 \text{ MeV}$ ,  $C_0(4) = 221 \text{ MeV}$  and in case of the PV coupling  $C_0(1) = 146 \text{ MeV}$ ,  $C_0(4) = 190 \text{ MeV}$ 

$N$	PS coupling				PV coupling				Exp.	
	1 spo		4 spo's		1 spo		4 spo's			
	$m_N$	$\mu_N$	$m_N$	$\mu_N$	$m_N$	$\mu_N$	$m_N$	$\mu_N$	$m_N$	$\mu_N$
$p$	939	2.99	939	2.65	939	3.07	939	2.61	938	2.79
$n$	939	-2.06	939	-1.80	939	-2.13	939	-1.80	940	-1.91
$\Lambda$	1148	-0.69	1160	-0.67	1123	-0.70	1146	-0.69	1116	-0.61
$\Sigma^+$	1250	2.88	1292	2.60	1199	2.94	1264	2.65	1189	2.46
$\Sigma^0$	1250	0.85	1292	0.77	1199	0.86	1264	0.78	1193	
$\Sigma^-$	1250	-1.17	1292	-1.06	1199	-1.22	1264	-1.10	1197	-1.16
$\Xi^0$	1396	-1.58	1435	-1.43	1335	-1.61	1402	-1.51	1315	-1.25
$\Xi^-$	1396	-0.57	1435	-0.57	1335	-0.57	1402	-0.57	1321	-0.65
$\Delta^{++}$	1195	5.95	1297	5.35	1132	6.08	1240	5.43	1232	4.52
$\Delta^+$	1195	2.92	1297	2.63	1132	2.96	1240	2.70	1232	
$\Delta^0$	1195	-0.11	1297	-0.10	1132	-0.15	1240	-0.13	1232	
$\Delta^-$	1195	-3.15	1297	-2.82	1132	-3.27	1240	-2.96	1232	
$\Sigma^{+*}$	1353	3.28	1460	2.98	1279	3.36	1391	3.13	1383	
$\Sigma^{0*}$	1353	0.24	1460	0.19	1279	0.24	1391	0.21	1384	
$\Sigma^{-*}$	1353	-2.79	1460	-2.59	1279	-2.88	1391	-2.71	1387	
$\Xi^{0*}$	1499	0.60	1609	0.54	1415	0.63	1527	0.60	1532	
$\Xi^{-*}$	1499	-2.43	1609	-2.32	1415	-2.49	1527	-2.41	1535	
$\Omega^-$	1634	-2.07	1743	-1.92	1539	-2.09	1649	-1.93	1672	-2.02

mixing of excited quark orbitals into the baryon ground state has been estimated, the question arises as to what the consequences might be for the baryon magnetic moments. To this objective, the expressions obtained for the baryon magnetic moments in [4] have to be generalized to arbitrary quark orbitals to be used within the multichannel calculation. For the coupling of the meson to the quark we consider two possible forms, the PS and PV coupling, as was also done in the calculation of the meson exchanges in the previous sections.

Following the same procedure as in [4] to calculate the major contribution to the baryon magnetic moment, we introduce an external electromagnetic field  $\mathbf{A}$  into the Hamiltonian Eq. (6) by minimal substitution,  $\mathbf{p}_i \rightarrow \mathbf{p}_i - e_q^{(i)} \mathbf{A}$ ,  $\mathbf{A} = \frac{1}{2}(\mathbf{H} \times \mathbf{r})$ , and calculate the energy shift perturbatively,

$$\Delta E = -\boldsymbol{\mu} \cdot \mathbf{H}, \quad \Delta H = -e_q^{(1)} \boldsymbol{\alpha}^{(1)} \cdot \mathbf{A}. \quad (34)$$

Thus, we find for the magnetic moment operator

$$\mu_z^{(1)} = -\frac{1}{2} e_q^{(1)} \int d^3 r_1 \left\{ \phi^*(\mathbf{r}_1) \left( \boldsymbol{\sigma}^{(1)} \times \mathbf{r}_1 \right)_z \right. \quad (35)$$

$$\left. \times \chi(\mathbf{r}_1) + \chi^*(\mathbf{r}_1) \left( \boldsymbol{\sigma}^{(1)} \times \mathbf{r}_1 \right)_z \phi(\mathbf{r}_1) \right\},$$

where the single-quark orbital is denoted as

$$\psi_{\alpha\alpha}^{f_1}(\mathbf{r}_1 - \mathbf{r}_0) = \begin{pmatrix} \phi(\mathbf{r}_1) \\ \chi(\mathbf{r}_1) \end{pmatrix}. \quad (36)$$

The magnetic moment operator Eq. (35) can be evaluated by rewriting it in terms of spherical harmonics

$$\frac{1}{2} (\boldsymbol{\sigma} \times \mathbf{r})_z = -\frac{1}{2i} \sqrt{\frac{2\pi}{3}} (\sigma_+ Y_{1-1} + \sigma_- Y_{11}) r, \quad (37)$$

after which the angular part can easily be calculated analytically using Eq. (A.15), which leaves us with a numerical radial integral over  $\mathbf{r}_1$  (the integrals over  $\mathbf{r}_2$  and  $\mathbf{r}_3$  factorize and drop out),

$$\mu_z = 3\mu_z^{(1)} = -3i \frac{1}{N} \int d^3 r_1 \int d^3 r_2 \int d^3 r_3 \quad (38)$$

$$\times \Psi_{JM}^\dagger(\mathbf{r}_1, \mathbf{r}_2, \mathbf{r}_3) e_q^{(1)} \sqrt{\frac{2\pi}{3}} \times \left( \sigma_+^{(1)} Y_{1-1} + \sigma_-^{(1)} Y_{11} \right) r_1 \Psi_{JM}(\mathbf{r}_1, \mathbf{r}_2, \mathbf{r}_3),$$

**Table 8.** The same as in Table 6, but for  $\sigma = 0.12 \text{ GeV}^2$  and in case of the PS coupling  $C_0(1) = 184 \text{ MeV}$ ,  $C_0(4) = 242 \text{ MeV}$  and in case of the PV coupling  $C_0(1) = 143 \text{ MeV}$ ,  $C_0(4) = 204 \text{ MeV}$

$N$	PS coupling				PV coupling				Exp.	
	1 spo		4 spo's		1 spo		4 spo's			
	$m_N$	$\mu_N$	$m_N$	$\mu_N$	$m_N$	$\mu_N$	$m_N$	$\mu_N$	$m_N$	$\mu_N$
$p$	939	2.66	939	2.35	939	2.74	939	2.27	938	2.79
$n$	939	-1.85	939	-1.62	939	-1.93	939	-1.58	940	-1.91
$\Lambda$	1174	-0.64	1184	-0.61	1142	-0.65	1169	-0.63	1116	-0.61
$\Sigma^+$	1312	2.56	1350	2.29	1247	2.63	1325	2.32	1189	2.46
$\Sigma^0$	1312	0.75	1350	0.67	1247	0.76	1325	0.67	1193	
$\Sigma^-$	1312	-1.05	1350	-0.94	1247	-1.11	1325	-0.97	1197	-1.16
$\Xi^0$	1462	-1.44	1495	-1.29	1382	-1.46	1463	-1.37	1315	-1.25
$\Xi^-$	1462	-0.53	1495	-0.53	1382	-0.53	1463	-0.53	1321	-0.65
$\Delta^{++}$	1303	5.28	1430	4.72	1214	5.43	1364	4.85	1232	4.52
$\Delta^+$	1303	2.57	1430	2.30	1214	2.63	1364	2.35	1232	
$\Delta^0$	1303	-0.13	1430	-0.11	1214	-0.18	1364	-0.15	1232	
$\Delta^-$	1303	-2.84	1430	-2.53	1214	-2.98	1364	-2.65	1232	
$\Sigma^{+*}$	1468	2.88	1601	2.60	1364	2.97	1520	2.73	1383	
$\Sigma^{0*}$	1468	0.18	1601	0.13	1364	0.17	1520	0.14	1384	
$\Sigma^{-*}$	1468	-2.53	1601	-2.34	1364	-2.63	1520	-2.45	1387	
$\Xi^{0*}$	1618	0.49	1754	0.43	1500	0.52	1657	0.48	1532	
$\Xi^{-*}$	1618	-2.22	1754	-2.10	1500	-2.28	1657	-2.20	1535	
$\Omega^-$	1753	-1.91	1887	-1.75	1621	-1.94	1774	-1.76	1672	-2.02

with normalization Eq. (A.14) and symmetrized baryon wave functions Eq. (5). Because of symmetry considerations, we can calculate the contribution of the first quark only and take the second and the third quark into account by multiplying by a factor of 3.

In the calculation of the baryon mass spectrum, we introduced meson exchanges as an effective interaction representing the exchange of two quarks. We now study the one-loop effects of the mesonic fluctuations which give rise to modifications of the single-quark current, in particular, to an anomalous magnetic moment of the quark. Near  $Q^2 = 0$ , the current can be written as

$$J_\mu^{\gamma qq} = e_q \gamma_\mu + \kappa_q \frac{ie}{2M_p} \sigma_{\mu\nu} Q^\nu, \quad (39)$$

where  $\kappa_q = \kappa_s + \kappa_v \tau_z$  for the  $u, d$  quark. From Eq. (8), the magnetic moment contribution is found to be

$$\delta\mu_z^{(1)} = - \int d^3 r_1 \left\{ \phi^*(\mathbf{r}_1) \kappa_q^{(1)} \sigma_z^{(1)} \phi(\mathbf{r}_1) \right. \quad (40)$$

$$\left. - \chi^*(\mathbf{r}_1) \kappa_q^{(1)} \sigma_z^{(1)} \chi(\mathbf{r}_1) \right\},$$

which results in

$$\delta\mu_z = 3\delta\mu_z^{(1)} = 3 \frac{1}{N} \int d^3 r_1 \int d^3 r_2 \int d^3 r_3 \quad (41)$$

$$\times \Psi_{JM}^\dagger(\mathbf{r}_1, \mathbf{r}_2, \mathbf{r}_3) \kappa_q^{(1)} \sigma_z^{(1)} \gamma_0^{(1)} \Psi_{JM}(\mathbf{r}_1, \mathbf{r}_2, \mathbf{r}_3).$$

Repeating the procedure followed in [4], we determine the  $\kappa$  coefficients in a simple model, assuming that the loop corrections are given by only the one-loop mesonic contributions to the electromagnetic vertex. We approximate the single-quark orbital by a free-quark propagation with a constituent mass given by the ground-state orbital energy,  $\epsilon_0$ , shown in Table 1. With the above simplifying assumptions, the calculation amounts to calculating the magnetic moment contributions of the diagrams shown in Fig. 2. The diagram with the contact interaction is only present when a PV coupling is considered. Assuming a monopole form factor  $F_{\pi qq}(k) =$

$\Lambda_\pi^2 / (\Lambda_\pi^2 - k^2)$  we can write

$$J_\mu^{(a)} = i \int \frac{d^4 k}{(2\pi)^4} \Gamma_{\pi qq}^a(k+Q) S_q(p-k) \quad (42a)$$

$$\times \Delta_\pi(k+Q) \Gamma_{\gamma\pi\pi,\mu}^{ab}(k, k+Q) \Delta_\pi(k) \Gamma_{\pi qq}^b(-k)$$

$$\times \left( 1 + \frac{i}{\Lambda_\pi^2} \frac{F_{\pi qq}((k+Q)^2)}{\Delta_\pi(k)} + \frac{i}{\Lambda_\pi^2} \frac{F_{\pi qq}(k^2)}{\Delta_\pi(k+Q)} \right),$$

$$J_\mu^{(b)} = i \int \frac{d^4 k}{(2\pi)^4} \Gamma_{\pi qq}^a(k) S_q(p+Q-k) \quad (42b)$$

$$\times \Gamma_{\gamma qq,\mu} S_q(p-k) \Delta_\pi(k) \Gamma_{\pi qq}^a(-k),$$

$$J_\mu^{(c)} = i \int \frac{d^4 k}{(2\pi)^4} \left( \Gamma_{\pi qq}^a(k) S_q(p+Q-k) \quad (42c)$$

$$\times \Gamma_{\gamma\pi qq,\mu}^a(-k) + \Gamma_{\gamma\pi qq,\mu}^a(k) \right.$$

$$\left. \times S_q(p-k) \Gamma_{\gamma\pi qq,\mu}^a(-k) \right) \Delta_\pi(k),$$

where we use for the propagators

$$S_q(p) = \frac{i(\not{p} + M_q)}{p^2 - M_q^2 + i\epsilon}, \quad (43)$$

$$\Delta_\pi(p) = \frac{i}{p^2 - m_\pi^2} \quad (44)$$

and for the vertices

$$\Gamma_{\gamma\pi\pi,\mu}^{ab}(k', k) = -e\epsilon^{ab3}(k_\mu + k'_\mu), \quad (45)$$

$$\Gamma_{\gamma qq,\mu} = -ie_q \gamma_\mu, \quad (46)$$

$$\Gamma_{\pi qq}^a(k) = g_{\pi qq} \gamma_5 \tau^a F_{\pi qq}(k) \quad (\text{PS}). \quad (47)$$

The PV-coupling vertex can be found from Eq. (47) by applying the replacement Eq. (16). In the case of a PV coupling of the meson, the minimal coupling of the electromagnetic field gives rise to the contact interaction

$$\Gamma_{\gamma\pi qq,\mu}^a(k) = ie \frac{g}{2m_{\text{eff}}} \gamma_5 \gamma_\mu \tau_b \epsilon_{ba3} F_{\pi qq}(k) \quad (\text{PV}). \quad (48)$$

In Eq. (42a), an extra term has been added to satisfy the Ward–Takahashi identity in the second order [30],

$$Q_\mu \Gamma_{\gamma qq}^{\mu,(2)} = e_q \left( S_q^{(2)-1}(p+Q) - S_q^{(2)-1}(p) \right), \quad (49)$$

where the three-point vertex  $\Gamma_{\gamma qq}^{\mu,(2)}$  is given by the sum of the currents Eqs. (42a)–(42c). The currents can now be simplified by shifting the  $\gamma_5$  through the expression and assuming that the incoming and outgoing quarks are on the mass shell. As a result, we find

$$J_\mu^{(a,c)} = -2ie\tau_z \left( \gamma^\nu C_{\mu\nu}^{(a,c)} + C_\mu^{(a,c)} \right) \quad (50a)$$

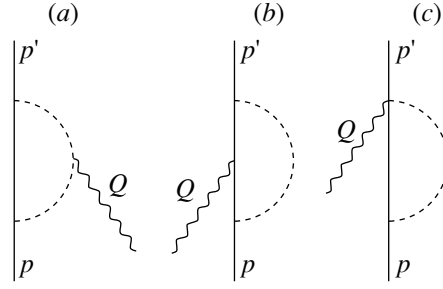


**Fig. 2.** The diagrams contributing to the anomalous magnetic moment of the single quark. Diagram *c* is only present when a PV coupling has been taken.

and

$$J_\mu^{(b)} = ie \frac{1 - \tau_z}{2} \left( \gamma^\nu C_{\mu\nu}^{(b)} + C_\mu^{(b)} \right). \quad (50b)$$

From these currents, the anomalous magnetic moment has to be extracted. To isolate this term, we first note that the tensors  $C^{\mu\nu}$  and the vectors  $C^\mu$  depend only on the initial and final momenta. Therefore, they can be written as

$$C_{\mu\nu}^{(i)} = A_1^{(i)} K_\mu K_\nu + A_2^{(i)} K_\mu Q_\nu \quad (51)$$

$$+ A_3^{(i)} Q_\mu K_\nu + A_4^{(i)} Q_\mu Q_\nu + A_5^{(i)} g_{\mu\nu},$$

$$C_\mu^{(i)} = B_1^{(i)} K_\mu + B_2^{(i)} Q_\mu, \quad (52)$$

where  $A_n^{(i)}$  and  $B_n^{(i)}$  are Lorentz invariants. By applying the Gordon decomposition to the current Eq. (39) near  $Q^2 = 0$ , it can be seen that the anomalous magnetic moment  $\kappa$  is the term proportional to  $-\frac{e}{2M} K_\mu$  with  $K_\mu = p_\mu + p'_\mu$ . So only the first terms,  $A_1^{(i)}$  and  $B_1^{(i)}$ , contribute to the anomalous magnetic moment. Substituting Eqs. (51) and (52) into Eq. (50) and taking the initial and final quark on the mass shell, we find for the anomalous magnetic moment corrections

$$\kappa^{(a,c)} = 4iM_p \tau_z \left[ 2m_q A_1^{(a,c)} + B_1^{(a,c)} \right], \quad (53)$$

$$\kappa^{(b)} = -2iM_p \frac{1 - \tau_z}{2} \left[ 2m_q A_1^{(b)} + B_1^{(b)} \right]. \quad (54)$$

Equation (53) corresponds to the coupling of the photon to the pion and Eq. (54) to the coupling of the photon to the quark. Formally, the contact term is also represented by Eq. (53) in the case of PV coupling; this term, however, vanishes and does not contribute to the quark anomalous magnetic moment.

The Lorentz-invariant expressions  $A_1^{(i)}$  and  $B_1^{(i)}$  can immediately be determined from the tensor  $C_{\mu\nu}^{(i)}$ . We get

$$A_1^{(i)} = \frac{1}{3K^4} (4K^\mu K^\nu - K^2 g^{\mu\nu}) C_{\mu\nu}^{(i)} \quad (55)$$

**Table 9.** The anomalous magnetic moment of the quark (in units of the nucleon magneton) for different string tensions  $\sigma$  (the parameters are taken from Table 2; the first set is the prediction for only the pion loops, while the second set is with both pion and kaon loops included, and the third set shows the results where pion, kaon, and eta loops are taken into account)

$\kappa_{f_i}$	$\sigma = 0.06 \text{ GeV}^2$		$\sigma = 0.09 \text{ GeV}^2$		$\sigma = 0.12 \text{ GeV}^2$	
	PS	PV	PS	PV	PS	PV
Pion loops						
$\kappa_u$	0.065	0.091	0.089	0.121	0.109	0.147
$\kappa_d$	-0.110	-0.153	-0.141	-0.193	-0.166	-0.224
$\kappa_s$	0.0	0.0	0.0	0.0	0.0	0.0
Pion and kaon loops						
$\kappa_u$	0.097	0.136	0.129	0.178	0.155	0.211
$\kappa_d$	-0.100	-0.138	-0.129	-0.176	-0.152	-0.206
$\kappa_s$	-0.028	-0.040	-0.039	-0.054	-0.048	-0.066
Pion, kaon, and eta loops						
$\kappa_u$	0.092	0.131	0.123	0.172	0.148	0.205
$\kappa_d$	-0.097	-0.136	-0.126	-0.173	-0.149	-0.202
$\kappa_s$	-0.021	-0.025	-0.031	-0.038	-0.038	-0.048

and

$$B_1^{(i)} = \frac{1}{K^2} K^\mu C_\mu^{(i)}. \quad (56)$$

Details on the calculation of the integrals and explicit expressions for  $A_1^{(i)}$  and  $B_1^{(i)}$  can be found in Appendix C.

The kaon and eta one-loop diagrams can be calculated in a similar way. The starting point is Eq. (42) again, where the mass of the pion is replaced by the mass of the kaon and the eta, respectively. In the case of the kaon loop, the isospin structure is changed as  $\tau_z \rightarrow (\tau_z + 3Y)/2$  and  $(1 - \tau_z)/2 \rightarrow -(\frac{2}{9} + \frac{4}{3}Y)$  in Eqs. (53) and (54), respectively, with  $Y$  being the hypercharge. Only the eta loop contributes to the diagram, where the photon couples to the quark, as the eta is a charge-neutral meson. Therefore, the isospin structure changes into  $\tau_z \rightarrow 0$  and  $(1 - \tau_z)/2 \rightarrow -\frac{1}{9} + \frac{1}{6}\tau_z + \frac{1}{2}Y$  in Eqs. (53) and (54), respectively. The coupling constants  $g_{Kqq}$ ,  $g_{\eta qq}$  and the cutoff masses  $\Lambda_\kappa$ ,  $\Lambda_\eta$  are taken as discussed in Section 3 and as shown in Table 2.

From the calculation, it is found that the results using a PV coupling can easily be related to the outcome using the PS coupling

$$A_1^{(a,b)}(\text{PV}) = \left( \frac{m_q + M_q}{2m_{\text{eff}}} \right)^2 A_1^{(a,b)}(\text{PS}), \quad (57a)$$

$$B_1^{(a,b)}(\text{PV}) = \left( \frac{m_q + M_q}{2m_{\text{eff}}} \right)^2 B_1^{(a,b)}(\text{PS}), \quad (57b)$$

where  $m_q$  is the constituent mass of the external quark and  $M_q$  is the constituent mass of the internal quark, both given by the respective ground-state orbital energy  $\epsilon_0$ . In the case of pionic loops, both internal and external quarks are  $u, d$  quarks,  $m_q = M_q$ . Kaons, however, change  $u, d$  quarks into  $s$  quarks and back, resulting in  $m_q \neq M_q$ . If the effective mass  $m_{\text{eff}}$  in the PV coupling is taken to be the same as the constituent quark mass  $m_q$ , both couplings give the same value. However, from Table 2, it can be seen that the effective mass differs from the ground-state orbital energy  $\epsilon_0$  shown in Table 1, resulting in different values when the PS or PV coupling is employed. The results are shown in Table 9. The analysis performed shows that the contact term does not contribute to the anomalous magnetic moment of the quark.

As the contribution from pion-exchange currents are predicted to be small [4], we leave them out in a first approximation.

The results on the baryon magnetic moments are shown in Tables 6, 7, and 8 for string tensions of  $\sigma = 0.06, 0.09$ , and  $0.12 \text{ GeV}^2$ , respectively. The inclusion of the excited quark orbitals decreases the baryon magnetic moment. This behavior results in overly low values in the case of  $\sigma = 0.09$  and  $0.12 \text{ GeV}^2$ , while  $\sigma = 0.06 \text{ GeV}^2$  yields values which are too large. The best overall agreement is obtained for a string tension in between,  $\sigma = 0.08 \text{ GeV}^2$ . When a PV coupling is exploited, the anomalous magnetic moment contributions are larger, which causes an increment of the resulting total magnetic moments of the baryons. Although the results obtained by using either PS or PV couplings are rather similar, the PS case seems to produce results slightly closer to experiment.

## 6. CONCLUSIONS

In the present paper, we have extended the work started in [4], where the field correlator method was applied to light baryons and magnetic moments were calculated for the baryon multiplet. The extension comes from the calculation of the influence of perturbative one-gluon and one-meson exchanges on the mass spectrum and magnetic moments of the baryon multiplet.

The described method should be looked at as a second approximation to calculate both the magnetic moments and the baryon mass spectrum in the QCD string model. The first approximation is described in [4], where no correlations between the quarks were taken into account. This means that the baryon wave function was described as a product of single-quark orbitals. In the present paper, this is partially repaired by considering one-gluon and meson exchanges and taking excited single-quark orbitals into account. However, effects from neglecting the actual position of  $\mathbf{r}_0$  at the Torricelli point and instead choosing a fixed value for the parameter  $\mathbf{r}_0$  are not considered and are left for further study.

From the results presented in this paper, it appears to be possible to obtain a reasonable agreement of the baryon magnetic moments in a region where the predicted masses are close to experiment. Although there is a small preference for a PS coupling when the magnetic moments are considered, the mass spectrum puts more weight in favor of a PV coupling. So the best overall agreement is obtained when a PV coupling is assumed and a string tension of  $\sigma = 0.08 \text{ GeV}^2$  is taken.

#### ACKNOWLEDGMENTS

The work of J.W. was supported in part by the Stichting voor Fundamenteel Onderzoek der Materie (FOM), which is sponsored by NWO, and of J.A.T. by the DOE, contract no. DE-AC05-84ER40150, under which SURA operates the Thomas Jefferson National Accelerator Facility.

We are very grateful to Yu.A. Simonov for numerous discussions concerning the topic of this paper.

#### APPENDIX A

##### SYMMETRIC BARYON WAVE FUNCTIONS

In this appendix, the explicit formulas of the baryon wave function are constructed for the nucleon and the  $\Delta$  revealing the (iso)spin structure. Assuming that all quarks are in their ground state, the spin-isospin wave function has to be symmetric under the exchange of any two quarks. The color which takes care of the total antisymmetrization is disregarded.

From three (iso)spin-1/2 particles, different combinations can be formed, which are denoted as [6–8]

$$\chi_{3/2}^S = \left| \frac{3}{2} \frac{3}{2} \right\rangle = \uparrow\uparrow\uparrow, \quad (\text{A.1a})$$

$$\chi_{1/2}^S = \left| \frac{3}{2} \frac{1}{2} \right\rangle = \sqrt{\frac{1}{3}} (\uparrow\uparrow\downarrow + \uparrow\downarrow\uparrow + \downarrow\uparrow\uparrow), \quad (\text{A.1b})$$

$$\chi_{1/2}^\rho = \left| \frac{1}{2} \frac{1}{2} \right\rangle_\rho = \sqrt{\frac{1}{2}} (\downarrow\uparrow\uparrow - \uparrow\downarrow\uparrow), \quad (\text{A.1c})$$

$$\chi_{1/2}^\lambda = \left| \frac{1}{2} \frac{1}{2} \right\rangle_\lambda = \sqrt{\frac{1}{6}} (\uparrow\downarrow\uparrow + \downarrow\uparrow\uparrow - 2 \uparrow\uparrow\downarrow). \quad (\text{A.1d})$$

Negative spin functions are obtained by flipping all spins. It can be seen that (A.1a), (A.1b), and (A.1d) are obtained by coupling a  $j_{12} = 1$  state with  $j_3 = \frac{1}{2}$ , whereas Eq. (A.1c) is formed from a  $j_{12} = 0$  state and a  $j_3 = \frac{1}{2}$  state. Isospin functions can similarly be written down, resulting in  $\eta_{m_i}^S$ ,  $\eta_{m_i}^\rho$ , and  $\eta_{m_i}^\lambda$ . Equations (A.1) contain all possible combinations and are orthonormal. The states  $S$  are totally symmetric, while  $\rho$  and  $\lambda$  are mixed-symmetric states. When the interchange of particle  $i$  and  $j$  is denoted by  $P_{ij}$ , they behave as

$$P_{12}\chi^S = \chi^S, \quad P_{13}\chi^S = \chi^S, \quad (\text{A.2})$$

$$P_{12}\chi^\rho = -\chi^\rho, \quad P_{13}\chi^\rho = -\frac{1}{2}\sqrt{3}\chi^\lambda + \frac{1}{2}\chi^\rho, \quad (\text{A.3})$$

$$P_{12}\chi^\lambda = \chi^\lambda, \quad P_{13}\chi^\lambda = -\frac{1}{2}\sqrt{3}\chi^\rho - \frac{1}{2}\chi^\lambda. \quad (\text{A.4})$$

The states  $\rho$  and  $\lambda$  are clearly not symmetric under the permutation of any two quarks. However, some specific combination of  $\chi^{\rho,\lambda}$  and  $\eta^{\rho,\lambda}$  is symmetric; actually, from the states Eqs. (A.1a)–(A.1d), only two totally symmetric states can be formed,

$$\Delta(m_s, m_i) = \chi_{m_s}^S \eta_{m_i}^S, \quad (\text{A.5})$$

$$J = 3/2, \quad I = 3/2,$$

$$N(m_s, m_i) = \frac{1}{\sqrt{2}} (\chi_{m_s}^\rho \eta_{m_i}^\rho + \chi_{m_s}^\lambda \eta_{m_i}^\lambda), \quad (\text{A.6})$$

$$J = 1/2, \quad I = 1/2.$$

Equations (A.5) and (A.6) represent the  $\Delta$  and the nucleon, respectively. The formalism can be extended to the total baryon octet and decuplet by including the  $s$  quark in writing down a complete orthonormal set.

#### APPENDIX B

##### CALCULATION OF THE EXCHANGE POTENTIALS

In the calculation of the matrix elements, Eqs. (13), (35), (40), use has been made of the partial wave decomposition of the single-quark orbitals and the expansion of the operator in spherical harmonics. This enables an easy analytic calculation of the angles.

The single-quark orbital is decomposed as [13]

$$\psi_{a\alpha}^f(\mathbf{r}) = |n_j l m_j\rangle \otimes |i m_i\rangle \quad (\text{A.7})$$

$$= \begin{pmatrix} g_n(r) \Omega_{j l m_j} \\ i f_n(r) \Omega_{j \tilde{l} m_j} \end{pmatrix} \otimes \eta_{m_i}, \quad \tilde{l} = 2j - l,$$

with

$$\Omega_{jlm_j} = \sum_{m_s} C(l\frac{1}{2}j; m_j - m_s, m_s, m_j) \quad (\text{A.8})$$

$$\times Y_{lm_j - m_s} \chi_{m_s},$$

where  $\chi_{m_s}$  ( $\eta_{m_i}$ ) is the (iso)spin function and  $C$  is the Clebsch–Gordan coefficient in the notation of Rose [29].

A totally symmetric baryon wave function can be composed from the single-quark orbitals as described in Section 4. This procedure is summarized as

$$\Psi_{JM}(\mathbf{r}_1, \mathbf{r}_2, \mathbf{r}_3) = \Gamma_{JM}^{\alpha\beta\gamma}(f_1, f_2, f_3) \quad (\text{A.9})$$

$$\times \psi_\alpha^{f_1}(\mathbf{r}_1) \psi_\beta^{f_2}(\mathbf{r}_2) \psi_\gamma^{f_3}(\mathbf{r}_3),$$

where the  $\Gamma$  takes care of the symmetrization;  $f_i$  are the flavor indices;  $\alpha$ ,  $\beta$ , and  $\gamma$  indicate the quark excitation; and the color indices are left out for simplicity. It is understood that the baryon wave function is in a color singlet state.

The energy shift can quite easily be calculated after some modifications of the exchange potential. Let us consider the equations written in coordinate space [Eqs. (15a), (15b)]. Then, expand the potentials in terms of spherical harmonics  $Y_{lm}$  as

$$V(\mathbf{r}_2, \mathbf{r}_3) = \sum_{l=0}^{\infty} V_l(r_2, r_3) \frac{2l+1}{4\pi} P_l(x) \quad (\text{A.10})$$

$$= \sum_{l=0}^{\infty} V_l(r_2, r_3) \sum_{m=-l}^l Y_{lm}^*(\Omega_2) Y_{lm}(\Omega_3)$$

with  $P_l$  the Legendre polynomials and  $x = \cos \gamma$ , the angle between the vectors  $\mathbf{r}_2$  and  $\mathbf{r}_3$ . The function  $V_l(r_2, r_3)$  can be found by using the orthonormality condition of the Legendre polynomials

$$V_l(r_2, r_3) = \frac{4\pi}{2} \int_{-1}^1 V(\mathbf{r}_2, \mathbf{r}_3) P_l(x) dx. \quad (\text{A.11})$$

In the special case of the Coulomb potential  $V(\mathbf{r}_2, \mathbf{r}_3) = 1/|\mathbf{r}_2 - \mathbf{r}_3|$ , the integral can be done analytically and the expansion looks like

$$V_l(r_2, r_3) = \frac{4\pi}{2l+1} \frac{r_{<}^l}{r_{>}^{l+1}}, \quad (\text{A.12})$$

with  $r_{<}$  ( $r_{>}$ ) the smaller (greater) of  $r_2$  and  $r_3$ . The advantage of this expansion is the easy analytic evaluation of the integrals over the angles appearing in the calculation of the matrix elements in Eq. (13).

The matrix element Eq. (13) can now be generalized as

$$\langle \Psi'_{JM} | H_{\text{int}}^{(23)} | \Psi_{JM} \rangle \quad (\text{A.13})$$

$$= \frac{1}{N} \int d^3r_1 \int d^3r_2 \int d^3r_3 \Psi_{JM}'^\dagger(\mathbf{r}_1, \mathbf{r}_2, \mathbf{r}_3)$$

$$\times (\Lambda^+(1)\Lambda^+(2)\Lambda^+(3) + \Lambda^-(1)\Lambda^-(2)\Lambda^-(3))$$

$$\times \gamma_0(2)\gamma_0(3) V(\mathbf{r}_2, \mathbf{r}_3) \Psi_{JM}(\mathbf{r}_1, \mathbf{r}_2, \mathbf{r}_3)$$

with the normalization

$$N = \int d^3r_1 \int d^3r_2 \int d^3r_3 \quad (\text{A.14})$$

$$\times \Psi_{JM}'^\dagger(\mathbf{r}_1, \mathbf{r}_2, \mathbf{r}_3) \Psi_{JM}(\mathbf{r}_1, \mathbf{r}_2, \mathbf{r}_3)$$

and the projection matrices  $\Lambda^\pm$  defined as Eq. (11).

The integral over the first quark factorizes and drops out. The remaining part contains two angular integrals,  $d\Omega_2$  and  $d\Omega_3$ , over three spherical harmonics each. The product of three spherical harmonics can analytically be evaluated as (see, for example, [29])

$$\int d\Omega Y_{l'm'}^* Y_{LM} Y_{lm} = \sqrt{\frac{(2l+1)(2L+1)}{4\pi(2l'+1)}} \quad (\text{A.15})$$

$$\times C(lLl'; mMm') C(lLl'; 000).$$

The remaining radial integral over  $r_2$  and  $r_3$  is done numerically.

In the case of PV coupling, extra matrices  $\not{k}$  in Eq. (16) are added to Eq. (A.13) and become derivatives in coordinate space. As the derivatives act on the wave functions, the actual potential  $V_{\text{OPE}}^{(23)}(\mathbf{r}_2 - \mathbf{r}_3)$  can still be expanded in terms of spherical harmonics in exactly the same way as is done for PS coupling, which results in

$$\langle \Psi'_{JM} | H_{\text{int}}^{(23)} | \Psi_{JM} \rangle \quad (\text{A.16})$$

$$= \frac{1}{N} \int d^3r_1 \int d^3r_2 \int d^3r_3 \Psi_{JM}'^\dagger(\mathbf{r}_1, \mathbf{r}_2, \mathbf{r}_3)$$

$$\times (\Lambda^+(1)\Lambda^+(2)\Lambda^+(3) + \Lambda^-(1)\Lambda^-(2)\Lambda^-(3))$$

$$\times \gamma_0(2)\gamma_0(3) \begin{pmatrix} i\boldsymbol{\sigma}^{(2)} \cdot \overleftarrow{\nabla}_2 & \varepsilon_{n_2}^{(2)} \\ \varepsilon_{n_2'}^{(2)} & i\boldsymbol{\sigma}^{(2)} \cdot \overleftarrow{\nabla}_2 \end{pmatrix}_{(2)}$$

$$\times \begin{pmatrix} -i\boldsymbol{\sigma}^{(3)} \cdot \overleftarrow{\nabla}_3 & -\varepsilon_{n_3}^{(3)} \\ -\varepsilon_{n_3'}^{(3)} & -i\boldsymbol{\sigma}^{(3)} \cdot \overleftarrow{\nabla}_3 \end{pmatrix}_{(3)}$$

$$\times V(\mathbf{r}_2, \mathbf{r}_3) \begin{pmatrix} i\boldsymbol{\sigma}^{(2)} \cdot \overrightarrow{\nabla}_2 & -\varepsilon_{n_2}^{(2)} \\ -\varepsilon_{n_2}^{(2)} & i\boldsymbol{\sigma}^{(2)} \cdot \overrightarrow{\nabla}_2 \end{pmatrix}_{(2)}$$

$$\times \begin{pmatrix} -i\boldsymbol{\sigma}^{(3)} \cdot \vec{\nabla}_3 & \varepsilon_{n_3}^{(3)} \\ \varepsilon_{n_3}^{(3)} & -i\boldsymbol{\sigma}^{(3)} \cdot \vec{\nabla}_3 \end{pmatrix} \quad (3)$$

$$\times \Psi_{JM}(\mathbf{r}_1, \mathbf{r}_2, \mathbf{r}_3).$$

The arrows point in the direction in which the derivatives operate. Again, the integral over  $\mathbf{r}_1$  factorizes and drops out. The derivative in the wave function has to be calculated, which can be done by using

$$\boldsymbol{\sigma} \cdot \nabla g(r) \Omega_{jlm} \quad (A.17)$$

$$= - \left( \frac{d}{dr} g(r) + \frac{1 + \kappa}{r} g(r) \right) \Omega_{j\tilde{l}m}$$

with  $\tilde{l} = 2j - l$ ,  $\Omega_{j\tilde{l}m} = -(\boldsymbol{\sigma} \cdot \hat{\mathbf{r}}) \cdot \Omega_{jlm}$ , and  $\kappa = \pm(j + \frac{1}{2})$  as  $j = l \pm \frac{1}{2}$ . The integral over the angles can again be evaluated using Eq. (A.15), while the integral over the radial wave functions, also containing derivatives in the radial wave functions, is done numerically.

### ANOMALOUS MAGNETIC MOMENT CONTRIBUTIONS FROM MESON LOOPS

In this appendix, explicit formulas on the contribution to the anomalous magnetic moment of one-loop diagrams are shown. In the first subsection, the PS coupling has been used [Eq. (47)]; in the second subsection, the PV coupling has been used. In the last subsection, some useful formulas on the calculation of the integrals are given.

#### *Pseudoscalar Coupling*

Our starting point is the electromagnetic currents, corresponding to the one-loop diagrams shown in Fig. 2, assuming a  $\gamma_5$  coupling of the pion to the quark,

$$J_\mu^{(a)} = -2ig_{\pi qq}^2 e\tau_z \int \frac{d^4k}{(2\pi)^4} \frac{\gamma_5 (\not{p} - \not{k} + M_q) \gamma_5 (2k_\mu + Q_\mu)}{[(p-k)^2 - M_q^2 + i\epsilon] [k^2 - m_\pi^2 + i\epsilon] [(k+Q)^2 - m_\pi^2 + i\epsilon]} \quad (A.18)$$

$$\times \frac{\Lambda_\pi^2}{k^2 - \Lambda_\pi^2} \frac{\Lambda_\pi^2}{(k+Q)^2 - \Lambda_\pi^2} \left( 1 + \frac{k^2 - m_\pi^2}{(k+Q)^2 - \Lambda_\pi^2} + \frac{(k+Q)^2 - m_\pi^2}{k^2 - \Lambda_\pi^2} \right) \equiv -2ie\tau_z \left( \gamma^\nu C_{\mu\nu}^{(a)} + C_\mu^{(a)} \right)$$

and

$$J_\mu^{(b)} = -ig_{\pi qq}^2 e \frac{1 - \tau_z}{2} \int \frac{d^4k}{(2\pi)^4} \frac{\gamma_5 (\not{p}' - \not{k} + M_q) \gamma_\mu (\not{p} - \not{k} + M_q) \gamma_5}{[(p'-k)^2 - M_q^2 + i\epsilon] [(p-k)^2 - M_q^2 + i\epsilon] [k^2 - m_\pi^2 + i\epsilon]} \quad (A.19)$$

$$\times \left( \frac{\Lambda_\pi^2}{k^2 - \Lambda_\pi^2} \right)^2 \equiv ie \frac{1 - \tau_z}{2} \left( \gamma^\nu C_{\mu\nu}^{(b)} + C_\mu^{(b)} \right).$$

In writing these equations, use has been made of explicit evaluation of the  $\gamma$ -matrix algebra and of the approximation that the initial and final quark are on the mass shell. To be able to discuss more general diagrams, the masses of the external quark  $m_q$  and the intermediate quark  $M_q$  are taken differently. In the case of pionic fluctuations of the  $u, d$  quark, the equations can be reduced using  $M_q = m_q$ . Since we have assumed a finite form factor at the  $\pi qq$  vertex, similar to the two-body current case, two additional

terms are needed in the last factor of Eq. (A.18) to satisfy the Ward–Takahashi identity [Eq. (49)]. From these currents, the anomalous magnetic moment has to be extracted. As was discussed in Section 5, this can be done by calculation of the Lorentz-invariant terms  $A_1^{(i)}$  and  $B_1^{(i)}$ , which are found as described in Eqs. (55) and (56). The expressions for  $A_1^{(a)}$  and  $B_1^{(a)}$  are

$$A_1^{(a)} = \frac{g_{\pi qq}^2}{6m_q^4} \int \frac{4(p \cdot k)^2 - p^2 k^2}{[k^2 - 2pk + m_q^2 - M_q^2 + i\epsilon] [k^2 - m_\pi^2 + i\epsilon]^2} \left( \frac{\Lambda_\pi^2}{\Lambda_\pi^2 - k^2} \right)^2 \left( 1 + 2 \frac{k^2 - m_\pi^2}{k^2 - \Lambda_\pi^2} \right) \quad (A.20)$$

$$\times \frac{d^4k}{(2\pi)^4} = \frac{-i}{32\pi^2} g_{\pi qq}^2 \int_0^1 d\alpha (1 - \alpha)^2 \left[ \left( \frac{1}{F_{m_\pi}} - \frac{1}{F_{\Lambda_\pi}} \right) \left( \frac{\Lambda_\pi^2}{\Lambda_\pi^2 - m_\pi^2} \right)^2 - \alpha \frac{\Lambda_\pi^2}{F_{\Lambda_\pi}^2} \frac{\Lambda_\pi^2}{\Lambda_\pi^2 - m_\pi^2} \right]$$

and 
$$B_1^{(a)} = \frac{g_{\pi qq}^2}{m_q^2} \int \frac{(M_q - m_q) p \cdot k}{[k^2 - 2pk + m_q^2 - M_q^2 + i\epsilon] [k^2 - m_\pi^2 + i\epsilon]^2} \left( \frac{\Lambda_\pi^2}{\Lambda_\pi^2 - k^2} \right)^2 \left( 1 + 2 \frac{k^2 - m_\pi^2}{k^2 - \Lambda_\pi^2} \right) \quad (A.21)$$

$$\times \frac{d^4 k}{(2\pi)^4} = \frac{-i}{16\pi^2} g_{\pi qq}^2 (M_q - m_q) \int_0^1 d\alpha (1 - \alpha) \left[ \left( \frac{1}{F_{m_\pi}} - \frac{1}{F_{\Lambda_\pi}} \right) \left( \frac{\Lambda_\pi^2}{\Lambda_\pi^2 - m_\pi^2} \right)^2 - \alpha \frac{\Lambda_\pi^2}{F_{\Lambda_\pi}^2} \frac{\Lambda_\pi^2}{\Lambda_\pi^2 - m_\pi^2} \right].$$

The expressions for  $A_1^{(b)}$  and  $B_1^{(b)}$  are

$$A_1^{(b)} = \frac{g_{\pi qq}^2}{6m_q^4} \int \frac{4(p \cdot k)^2 - p^2 k^2}{[k^2 - 2pk + m_q^2 - M_q^2 + i\epsilon]^2 [k^2 - m_\pi^2 + i\epsilon]} \left( \frac{\Lambda_\pi^2}{\Lambda_\pi^2 - k^2} \right)^2 \frac{d^4 k}{(2\pi)^4} \quad (A.22)$$

$$= \frac{-i}{32\pi^2} g_{\pi qq}^2 \int_0^1 d\alpha (1 - \alpha)^3 \left[ \left( \frac{1}{F_{m_\pi}} - \frac{1}{F_{\Lambda_\pi}} \right) \left( \frac{\Lambda_\pi^2}{\Lambda_\pi^2 - m_\pi^2} \right)^2 - \alpha \frac{\Lambda_\pi^2}{F_{\Lambda_\pi}^2} \frac{\Lambda_\pi^2}{\Lambda_\pi^2 - m_\pi^2} \right]$$

and

$$B_1^{(b)} = \frac{g_{\pi qq}^2}{m_q^2} \int \frac{(M_q - m_q) p \cdot k}{[k^2 - 2pk + m_q^2 - M_q^2 + i\epsilon]^2 [k^2 - m_\pi^2 + i\epsilon]} \left( \frac{\Lambda_\pi^2}{\Lambda_\pi^2 - k^2} \right)^2 \frac{d^4 k}{(2\pi)^4} \quad (A.23)$$

$$= \frac{-i}{16\pi^2} g_{\pi qq}^2 (M_q - m_q) \int_0^1 d\alpha (1 - \alpha)^2 \left[ \left( \frac{1}{F_{m_\pi}} - \frac{1}{F_{\Lambda_\pi}} \right) \left( \frac{\Lambda_\pi^2}{\Lambda_\pi^2 - m_\pi^2} \right)^2 - \alpha \frac{\Lambda_\pi^2}{F_{\Lambda_\pi}^2} \frac{\Lambda_\pi^2}{\Lambda_\pi^2 - m_\pi^2} \right].$$

In these formulas  $F_m$  is defined as

$$F_m = (1 - \alpha)^2 m_q^2 + (1 - \alpha) \times (M_q^2 - m_q^2) + \alpha m^2. \quad (A.24)$$

Frequent use has been made of the formulas listed below in the last subsection.

*Pseudovector Coupling*

In the case of PV coupling, the PS vertex has to be changed into the PV vertex by applying Eq. (16). The currents can be reduced to

$$J_\mu^{(a)} = -2i \frac{g_{\pi qq}^2}{4m_{\text{eff}}^2} e\tau_z \int \frac{d^4 k}{(2\pi)^4} \quad (A.25)$$

$$\times \left\{ \frac{2k_\mu \not{k} (k^2 - 2p \cdot k + 2m_q (m_q + M_q))}{[k^2 - 2pk + m_q^2 - M_q^2 + i\epsilon] [k^2 - m_\pi^2 + i\epsilon]^2} + \frac{2k_\mu (k^2 - 2p \cdot k) (M_q + m_q)}{[k^2 - 2pk + m_q^2 - M_q^2 + i\epsilon] [k^2 - m_\pi^2 + i\epsilon]^2} \right\}$$

$$\times \left( \frac{\Lambda_\pi^2}{\Lambda_\pi^2 - k^2} \right)^2 \left( 1 + 2 \frac{k^2 - m_\pi^2}{k^2 - \Lambda_\pi^2} \right)$$

$$\equiv -2ie\tau_z \left( \gamma^\nu C_{\mu\nu}^{(a)} + C_\mu^{(a)} \right),$$

$$J_\mu^{(b)} = ie \frac{1 - \tau_z}{2} \frac{g_{\pi qq}^2}{4m_{\text{eff}}^2} \quad (A.26)$$

$$\times \int \frac{d^4 k}{(2\pi)^4} \frac{\not{k} (m_q + M_q) + k^2 - 2p' \cdot k}{[k^2 - 2p' \cdot k + m_q^2 - M_q^2 + i\epsilon]} \gamma_\mu$$

$$\times \frac{\not{k} (m_q + M_q) + k^2 - 2p \cdot k}{[k^2 - 2p \cdot k + m_q^2 - M_q^2 + i\epsilon]} \frac{1}{[k^2 - m_\pi^2 + i\epsilon]}$$

$$\times \left( \frac{\Lambda_\pi^2}{\Lambda_\pi^2 - k^2} \right)^2 \equiv ie \frac{1 - \tau_z}{2} \left( \gamma^\nu C_{\mu\nu}^{(b)} + C_\mu^{(b)} \right),$$

and

$$J_\mu^{(c)} = 2i \frac{g_{\pi qq}^2}{4m_{\text{eff}}^2} e\tau_z \int \frac{d^4 k}{(2\pi)^4} \quad (A.27)$$

$$\times \left( \frac{(m_q + M_q) \not{k} + k^2 - 2p' \cdot k}{[k^2 - 2p' \cdot k + m_q^2 - M_q^2 + i\epsilon]} \gamma_\mu + \gamma_\mu \frac{(m_q + M_q) \not{k} + k^2 - 2p \cdot k}{[k^2 - 2p \cdot k + m_q^2 - M_q^2 + i\epsilon]} \right)$$

$$\times \frac{1}{[k^2 - m_\pi^2 + i\epsilon]} \left( \frac{\Lambda_\pi^2}{\Lambda_\pi^2 - k^2} \right)^2$$

$$\equiv -2ie\tau_z \left( \gamma^\nu C_{\mu\nu}^{(c)} + C_\mu^{(c)} \right).$$

Again, the Ward–Takahashi identity requires the extra term in Eq. (A.25). The expressions for  $A_1^{(a)}$  and

$B_1^{(a)}$  are

$$A_1^{(a)} = \frac{g_{\pi qq}^2}{24m_{\text{eff}}^2 m_q^4} \int \frac{(4(p \cdot k)^2 - p^2 k^2) (k^2 - 2p \cdot k + 2m_q(m_q + M_q))}{[k^2 - 2pk + m_q^2 - M_q^2 + i\epsilon] [k^2 - m_\pi^2 + i\epsilon]^2} \times \left( \frac{\Lambda_\pi^2}{\Lambda_\pi^2 - k^2} \right)^2 \left( 1 + 2 \frac{k^2 - m_\pi^2}{k^2 - \Lambda_\pi^2} \right) \frac{d^4 k}{(2\pi)^4} \quad (\text{A.28})$$

$$= \frac{-i}{32\pi^2} \frac{g_{\pi qq}^2}{4m_{\text{eff}}^2} (M_q + m_q)^2 \int_0^1 d\alpha (1 - \alpha)^2 \left[ \left( \frac{1}{F_{m_\pi}} - \frac{1}{F_{\Lambda_\pi}} \right) \left( \frac{\Lambda_\pi^2}{\Lambda_\pi^2 - m_\pi^2} \right)^2 - \alpha \frac{\Lambda_\pi^2}{F_{\Lambda_\pi}^2} \frac{\Lambda_\pi^2}{\Lambda_\pi^2 - m_\pi^2} \right]$$

and

$$B_1^{(a)} = \frac{g_{\pi qq}^2}{4m_{\text{eff}}^2 m_q^2} \int \frac{(M_q + m_q) (k^2 - 2p \cdot k) p \cdot k}{[k^2 - 2pk + m_q^2 - M_q^2 + i\epsilon] [k^2 - m_\pi^2 + i\epsilon]^2} \left( \frac{\Lambda_\pi^2}{\Lambda_\pi^2 - k^2} \right)^2 \times \left( 1 + 2 \frac{k^2 - m_\pi^2}{k^2 - \Lambda_\pi^2} \right) \frac{d^4 k}{(2\pi)^4} = \frac{-i}{16\pi^2} \frac{g_{\pi qq}^2}{4m_{\text{eff}}^2} (M_q - m_q) (m_q + M_q)^2 \times \int_0^1 d\alpha (1 - \alpha) \left[ \left( \frac{1}{F_{m_\pi}} - \frac{1}{F_{\Lambda_\pi}} \right) \left( \frac{\Lambda_\pi^2}{\Lambda_\pi^2 - m_\pi^2} \right)^2 - \alpha \frac{\Lambda_\pi^2}{F_{\Lambda_\pi}^2} \frac{\Lambda_\pi^2}{\Lambda_\pi^2 - m_\pi^2} \right]. \quad (\text{A.29})$$

The expressions for  $A_1^{(b)}$  and  $B_1^{(b)}$  are

$$A_1^{(b)} = \frac{g_{\pi qq}^2}{24m_{\text{eff}}^2 m_q^4} \int \frac{(4(p \cdot k)^2 - p^2 k^2) (m_q + M_q)^2}{[k^2 - 2pk + m_q^2 - M_q^2 + i\epsilon]^2 [k^2 - m_\pi^2 + i\epsilon]} \left( \frac{\Lambda_\pi^2}{\Lambda_\pi^2 - k^2} \right)^2 \frac{d^4 k}{(2\pi)^4} \quad (\text{A.30})$$

$$= \frac{-i}{32\pi^2} \frac{g_{\pi qq}^2}{4m_{\text{eff}}^2} (m_q + M_q)^2 \int_0^1 d\alpha (1 - \alpha)^3 \left[ \left( \frac{1}{F_{m_\pi}} - \frac{1}{F_{\Lambda_\pi}} \right) \left( \frac{\Lambda_\pi^2}{\Lambda_\pi^2 - m_\pi^2} \right)^2 - \alpha \frac{\Lambda_\pi^2}{F_{\Lambda_\pi}^2} \frac{\Lambda_\pi^2}{\Lambda_\pi^2 - m_\pi^2} \right]$$

and

$$B_1^{(b)} = \frac{g_{\pi qq}^2}{4m_{\text{eff}}^2 m_q^2} \int \frac{(M_q + m_q) p \cdot k (k^2 - 2p \cdot k)}{[k^2 - 2pk + m_q^2 - M_q^2 + i\epsilon]^2 [k^2 - m_\pi^2 + i\epsilon]} \left( \frac{\Lambda_\pi^2}{\Lambda_\pi^2 - k^2} \right)^2 \frac{d^4 k}{(2\pi)^4} \quad (\text{A.31})$$

$$= \frac{-i}{16\pi^2} \frac{g_{\pi qq}^2}{4m_{\text{eff}}^2} (M_q - m_q) (m_q + M_q)^2 \int_0^1 d\alpha (1 - \alpha)^2 \left[ \left( \frac{1}{F_{m_\pi}} - \frac{1}{F_{\Lambda_\pi}} \right) \left( \frac{\Lambda_\pi^2}{\Lambda_\pi^2 - m_\pi^2} \right)^2 - \alpha \frac{\Lambda_\pi^2}{F_{\Lambda_\pi}^2} \frac{\Lambda_\pi^2}{\Lambda_\pi^2 - m_\pi^2} \right].$$

The current resulting from the contact term does not contribute to the anomalous magnetic moment,  $A_1^{(c)} = 0$  and  $B_1^{(c)} = 0$ . In the formulas above,  $F_m$  is defined as before [Eq. (A.24)]. Although the expressions for the currents become much more involved using a PV coupling, the final expression can simply be written in terms of the result from the previous calculation as shown in Eqs. (57a), (57b).

### Useful Formulas

In the calculation of one-loop integrals, frequent use has been made of the Feynman parametrization

$$\frac{1}{ab} = \int_0^1 d\alpha \frac{1}{[\alpha a + (1 - \alpha)b]^2}. \quad (\text{A.32})$$

This formula can be generalized to

$$\frac{1}{a_1 a_2 \dots a_n} = (n - 1)! \int_0^1 d\alpha_1 \int_0^{1-\alpha_1} d\alpha_2 \dots \int_0^{1-\alpha_1-\alpha_2-\dots-\alpha_{n-2}} d\alpha_{n-1} \quad (\text{A.33})$$

$$\times \frac{1}{[\alpha_1 a_1 + \alpha_2 a_2 + \dots + \alpha_{n-1} a_{n-1} + (1 - \alpha_1 - \alpha_2 \dots - \alpha_{n-1}) a_n]^n}$$

for  $n > 2$ . This can be proven by induction. All loop integrals in the text can be reduced to one of the following forms [31]:

$$\int \frac{d^4 k}{(2\pi)^4} \quad (\text{A.34})$$

$$\times \left( \frac{1}{[(k-l)^2 - F_m]^2} - \frac{1}{[(k-l)^2 - F_{\Lambda\pi}]^2} \right)$$

$$\times \{1, k^\mu\} = \frac{-i}{16\pi^2} \ln \left( \frac{F_m}{F_{\Lambda\pi}} \right) \{1, l^\mu\}$$

or

$$\int \frac{d^4 k}{(2\pi)^4} \quad (\text{A.35})$$

$$\times \left( \frac{1}{[(k-l)^2 - F_m]^3} - \frac{1}{[(k-l)^2 - F_{\Lambda\pi}]^3} \right) k^\mu k^\nu$$

$$= \frac{-i}{32\pi^2} \left( -\frac{1}{2} \ln \left( \frac{F_m}{F_{\Lambda\pi}} \right) g^{\mu\nu} \right.$$

$$\left. + \left( \frac{1}{F_m} - \frac{1}{F_{\Lambda\pi}} \right) l^\mu l^\nu \right).$$

If the previous formulas do not apply, one can use ( $n \geq 3$ )

$$\int \frac{d^4 k}{(2\pi)^4} \frac{1}{[(k-l)^2 - F + i\eta]^n} \quad (\text{A.36})$$

$$\times \{1, k^\mu, k^\mu k^\nu\} = \frac{i(-1)^n}{(n-1)(n-2)16\pi^2}$$

$$\times \left\{ \frac{1}{F^{n-2}}, \frac{l^\mu}{F^{n-2}}, \frac{l^\mu l^\nu}{F^{n-2}} - \frac{g^{\mu\nu}}{2(n-3)F^{n-3}} \right\}.$$

## REFERENCES

1. Y. A. Simonov, *Yad. Fiz.* **60** (1997) [*Phys. At. Nucl.* **60**, 2069 (1997)]; hep-ph/9704301.
2. Y. A. Simonov, *Few-Body Syst.* **25**, 45 (1998); hep-ph/9712248.
3. V. I. Shevchenko and Y. A. Simonov, *Phys. Rev. Lett.* **85**, 1811 (2000); hep-ph/0001299.
4. Y. A. Simonov, J. A. Tjon, and J. Weda, *Phys. Rev. D* **65**, 094013 (2002); hep-ph/0111344.
5. Y. A. Simonov, *Yad. Fiz.* **62**, 2087 (1999) [*Phys. At. Nucl.* **62**, 1932 (1999)]; hep-ph/9912383.
6. N. Isgur and G. Karl, *Phys. Rev. D* **18**, 4187 (1978).
7. N. Isgur and G. Karl, *Phys. Rev. D* **19**, 2653 (1979).
8. S. Capstick and N. Isgur, *Phys. Rev. D* **34**, 2809 (1986).
9. V. I. Shevchenko and Y. A. Simonov, *Phys. Lett. B* **437**, 146 (1998); hep-th/9807157.
10. S. V. Ivanov and G. P. Korchemsky, *Phys. Lett. B* **154B**, 197 (1985).
11. S. V. Ivanov, G. P. Korchemsky, and A. V. Radyushkin, *Yad. Fiz.* **44**, 230 (1986) [*Sov. J. Nucl. Phys.* **44**, 145 (1986)].
12. Y. A. Simonov, *Pis'ma Zh. Éksp. Teor. Fiz.* **71**, 187 (2000) [*JETP Lett.* **71**, 127 (2000)]; hep-ph/0001244.
13. Y. A. Simonov and J. A. Tjon, *Phys. Rev. D* **62**, 014501 (2000); hep-ph/0001075.
14. Y. A. Simonov and J. A. Tjon, *Phys. Rev. D* **62**, 094511 (2000); hep-ph/0006237.
15. T. T. Takahashi, H. Matsufuru, Y. Nemoto, and H. Suganuma, *Phys. Rev. Lett.* **86**, 18 (2001); hep-lat/0006005.
16. W. M. Kloet and J. A. Tjon, *Nucl. Phys. A* **176**, 481 (1971).
17. U. Loring, K. Kretzschmar, B. C. Metsch, and H. R. Petry, *Eur. Phys. J. A* **10**, 309 (2001); hep-ph/0103287.
18. B. Metsch, hep-ph/9712246.
19. B. Metsch and U. Loring, *PiN Newslett.* **16**, 225 (2002); hep-ph/0110415.
20. A. M. Badalian and D. S. Kuzmenko, *Phys. Rev. D* **65**, 016004 (2002); hep-ph/0104097.
21. L. Y. Glozman, Z. Papp, W. Plessas, *et al.*, *Phys. Rev. C* **57**, 3406 (1998); nucl-th/9705011.
22. M. L. Goldberger and S. B. Treiman, *Phys. Rev.* **110**, 1178 (1958).
23. T. A. Lahde and D. O. Riska, *Nucl. Phys. A* **710**, 99 (2002); hep-ph/0204230.
24. K. Hagiwara, K. Hikasa, K. Nakamura, *et al.*, *Phys. Rev. D* **66**, 010001 (2002); URL <http://pdh.lbl.gov>
25. S. Weinberg, *Phys. Rev. Lett.* **65**, 1181 (1990).
26. Y. A. Simonov, *Phys. Rev. D* **65**, 094018 (2002); hep-ph/0201170.
27. S. Weinberg, *Phys. Rev. Lett.* **67**, 3473 (1991).
28. L. Y. Glozman and D. O. Riska, *Phys. Rep.* **268**, 263 (1996); hep-ph/9505422.
29. M. E. Rose, *Elementary Theory of Angular Momentum* (John Wiley and Sons, 1957).
30. P. C. Tiemeijer and J. A. Tjon, *Phys. Rev. C* **42**, 599 (1990).
31. J. A. Tjon and S. J. Wallace, *Phys. Rev. C* **62**, 065202 (2000); nucl-th/0002051.

# Nonperturbative QCD near the Light Cone\*

H. J. Pirner\*\*

*Institut für Theoretische Physik, Universität Heidelberg, Germany*

Received May 13, 2004

**Abstract**—We give an overview of current theoretical approaches to nonperturbative QCD. We especially discuss QCD near the light cone. © 2005 Pleiades Publishing, Inc.

## 1. INTRODUCTION

Commonly, the existence of high-energy divergences in field theories which cannot be controlled by standard renormalization schemes of quantum field theories signals that the theory is valid only up to a certain energy scale. Beyond that scale, there is new physics that requires a different description. For example, diverging high-energy weak cross sections calculated in Fermi theory predicted the existence of heavy vector bosons. In strong interaction physics, we have the reverse. We cannot calculate quantitatively the properties of hadrons which are the composite QCD degrees of freedom outside of the Standard Model. The phenomenon that composite systems are more difficult to describe than elementary systems is not unusual. Composite systems have features which go beyond the sum of their constituents. This phenomenon of new qualities emerging in the process of assembling the system out of simple parts is common in condensed matter physics and in biology; e.g., in the theory of the fractional Hall effect, the Hall observables give fractional charges originating from integer-charged electrons moving in a magnetic field. Laughlin [1] remarks in his Nobel lecture about the Hall effect, “I myself have come to suspect that most of the important problems in physics are emergent in nature,” and continues, “even the standard model of elementary particles itself.”

Hadronic physics is well researched up to a mass scale of 1.5 GeV. Its spectroscopy still lacks a clear identification of glueballs and hybrid states. Yukawa models, like the sigma model, are natural to describe hadron physics up to an energy scale of about 1 GeV. The running Yukawa coupling diverges at about 1 GeV. This divergence signals the unsatisfactory high-energy behavior of hadronic theory above the 1-GeV scale, when the compositeness of hadronic

objects and multiple production of pions become important.

Quarks and gluons are the ultimate building blocks of hadrons. They carry color charges which increase dynamically at low resolution. Hopes have only partially materialized that the growth of the strong coupling constant for low energies in quantum chromodynamics explains the confinement of quarks and gluons. QCD forms new structures as dominant collective units like quark/antiquark and gluon condensates. In fact, there is a very successful extension of QCD based on nonpolynomial link operators as new collective operators. Lattice compactification [2, 3], i.e., the rewriting of the continuum QCD Lagrangian with the help of compact gauge link operators, matches nicely with the underlying continuum QCD at short distances and smoothly continues the infinitesimal phase factors  $ig \int A_\mu dx^\mu$  into the region of growing coupling. This extension of QCD is not unique; other attempts to solve QCD in the infrared have been made:

chiral perturbation theory [4], meson quark models [5, 6];

QCD as a dual superconductor [7], color dielectric medium [8, 9];

Gaussian distributed field strength correlators [10];

Hamiltonian light cone QCD [11];

QCD as a string theory [12].

Together with nuclear physics, the low-energy domain of QCD has been researched over six decades. If one asks whether the work on QCD is complete, the question must be answered whether additional theoretical or experimental work can improve the situation decisively. The relevance of yet another resonance or yet another model calculation is debatable. New theoretical work has to be seen in its relation to lattice QCD, where progress has been slow but systematic. In the following, I will emphasize questions in QCD where the lattice has not been able to guide our intuition and, even on the contrary, where we need

\*This article was submitted by the author in English.

\*\* e-mail: [pir@tphys.uni-heidelberg.de](mailto:pir@tphys.uni-heidelberg.de); <http://wwwnp.tphys.uni-heidelberg.de>

analytical work to understand lattice results. Any theory based on the low-energy degrees of freedom will never be as economical and esthetic as QCD. The possibility, however, can be discussed whether an inclusion of a finite number of composite fields, perhaps hadronic fields, at low energies can provide a smooth transition from the quark–gluon-dominated regime into the hadronic regime. Since one expects that low-energy QCD is the physics of bound states made up of QCD quarks and gluons, these new operators must be composite operators expressible in terms of quark and gluon fields. If you add the folklore that QCD becomes a nonlocal theory in the infrared, you are almost at the stochastic vacuum model invented by Dosch and Simonov [10]. It contains the vacuum condensate as a composite operator and a string connecting the locations of the two field strengths as a nonlocal feature.

The very successful chiral perturbation theory [4] alone cannot connect low-energy hadron physics to QCD in the ultraviolet. Chiral perturbation theory needs phenomenological input. With increasing order, the number of coupling constants becomes very large. It is an asymptotic expansion which typically fails when the resolution scale is of the order of half the  $\rho$  mass. Models [6] which contain meson degrees of freedom and quarks extend to larger scales, where they develop the characteristic behavior of increasing mesonic and Yukawa couplings of scalar theories. The connection to QCD must be sought on the level of the four-fermion interaction as in the Nambu–Jona-Lasinio (NJL) model. This four-fermion interaction for one-loop irreducible graphs is driven by two-gluon exchange leading to a smooth transition to the strongly coupled mesonic theory. Wetterich and Berges [5], Schaefer and Wambach [13], and our group [14] have investigated these renormalization group flow equations also for finite temperature and finite density. At finite temperature, the  $O(4)$  transition for two massless flavors is quite well reproduced because of the careful treatment of long-range fluctuations. For finite density, the model is more complicated, both numerically and conceptionally. The Darmstadt group [13] has recently shown a phase diagram with interesting structure at high densities and low temperatures which does not coincide with the simple NJL model. In Heidelberg [14], we have extended the model with high-energy gluons at high temperatures, which are very important if one wants an adequate equation of state. For nuclei, a theory which contains free quarks and bound quarks in nucleons seems to be the most efficient way to describe the transition from purely nucleonic matter to quark matter at high baryon density [15]. Most models mixing QCD and hadronic degrees of freedom lack a field-theoretic mechanism to avoid the appearance

of free quarks as asymptotic states. Major progress is achieved if one can rewrite the smooth infrared limit of lattice QCD in a field-theoretic continuum picture. Yu. Simonov with his work on the stochastic vacuum model has made important contributions to show such a possibility (see [16]).

Very early, G. 't Hooft proposed that the QCD vacuum is nontrivial (see a recent talk to learn his view [17]). The vacuum is the key to understand hadrons as its excitations. In QCD, gluon monopole configurations are supposed to lead to a vacuum which confines electric flux. This concept is dual to the picture of superconductivity in solid-state physics, where paired electrons make up the medium which expels magnetic flux. Monopoles have received some support from lattice gauge simulations using Abelian gauge fixing. In color dielectric models [9], the condensation of magnetic monopoles translates into a dielectric constant which fluctuates around zero. It allows one to describe QCD in the infrared in strong coupling approximation with the advantage that the connection to the continuum theory is not obstructed by a roughening transition. The integration over the dielectric fields smoothes out the transition from strong coupling to weak coupling. Finite-size domains with condensed gluons are behind the ansatz of Gaussian field strength correlators underlying the stochastic vacuum model invented by Dosch and Simonov [10]. The size of these domains with aligned gluonic fields in color and spin defines a correlation length of about 0.3 fm. Simonov and his collaborators at ITEP, H.G. Dosch and A. Di Giacomo, have worked on this stochastic vacuum model to describe many features of low-energy QCD and/or analyze lattice QCD simulations. The full scope of this work can only be seen in recent reviews [16, 18]. In Heidelberg, we have benefited very much from the stochastic vacuum model and applied it to all kinds of high-energy scattering processes, e.g., [19], where most other approaches to QCD fail. This intrinsically Minkowskian problem is outside of lattice QCD; only a bona fide light-cone approach can help to solve the scattering problem.

## 2. LIGHT-CONE QCD

A simple extension of the quantum mechanics of bound states to a relativistic field theory of massless quanta bound into hadrons is not possible. The light-cone Hamiltonian approach attacks this problem from a quite different point of view. Take a cube of length 2 fm filled with quarks and gluons and boost it in the 3-direction with a Lorentz factor of  $\gamma = 1000$ . This gedanken experiment is well suited to imagine a proton moving with fast speed in the laboratory. The box will contract on one side, valence quark momenta

will be high, and valence states will have very high energies. By some suitable kinematic choices of coordinates, one can construct invariants. Commonly, the light-cone energy  $P^- = (E - P_z)/\sqrt{2}$  and the light-cone momentum  $P^+ = (E + P_z)/\sqrt{2}$  are chosen and  $M^2 = 2P_+P_- - P_\perp^2$  is invariant. With these variables, all light-cone energies are positive and increase as  $P^- = (P_\perp^2 + m^2)/(\sqrt{2}P^+)$  for small light-cone momenta. Only fluctuations with small  $P^+$  momenta may pose a problem. Their light-cone energies are very high. In light-cone physics, the ultraviolet problem gets mixed up with the infrared problem. Formally, the problem reappears in the context of constraint equations for  $x^-$ -independent fields [20]. These constraint equations arise in the light-cone Hamiltonian framework, since the Lagrangian contains the velocities in linear form  $L = \partial_- \phi \partial_+ \phi$ . The momenta related to these velocities obey constraint equations including  $\partial_- \phi$ . Therefore, integrals of the equations of motion over the spatial light-cone distance  $x^-$  become operator equations of reduced dimensionality (two transverse spatial dimensions and one time dimension). These equations are called zero-mode equations. For example, in equal-time theory, zero-mode equations determine the condensate of a scalar field. The  $x^-$ -independent zero-mode field couples to the transverse fluctuations of all other fields; consequently, these equations depend on the cutoff and are involved in the whole renormalization procedure. This feature is often overlooked in naive pictures assuming either superrenormalizable models or models with a simple cutoff. In NJL models, one has been able to solve [21, 22] these zero-mode equations, e.g., in the large- $N_c$  approximation, giving a view of chiral symmetry breaking on the light cone, which is quite special. These zero-mode equations have not been solved in QCD.

A common argument goes as follows: Zero modes decouple from the rest of the theory, because their energies lie beyond the cutoff. Naively, the light-cone momentum  $P^+ = 0$  means that the light-cone energy  $P^- = \infty$ . If, however, the mass  $m$  of the zero mode is zero, the mode does not disappear into infinity for very small transverse momenta. How is the situation in QCD? Can we just ignore this problem, buy a big computer, use some suitable Fock truncation, put all transverse gluon modes into a Hamiltonian matrix, and diagonalize it? Pauli and Brodsky [23] and many others have solved successfully  $(1+1)$ -dimensional theories. QCD on the light cone is a tremendously seductive field theory, since the Euler–Lagrange equation for a timelike light-cone potential can be solved directly in a gauge where the potential along the spatial light-cone direction vanishes. The resulting

Hamiltonian contains the light-cone Coulomb energy plus the kinetic energies of the transverse gluons and nothing else. The light-cone Coulomb energy is already in a form which linearly confines sources separated along the spatial light-cone directions. This is a simple consequence of the massless gluon propagator in one spatial dimension.

The massless gluon interaction also has to be implemented correctly for colored line sources smeared over the spatial light-cone direction. Otherwise, we violate the equal treatment of all spatial directions. This necessity can be demonstrated rather easily in perturbation theory, where the rotational invariance of the gluon exchange is reconstituted via the exchange of one transverse gluon. I think, one can be easily misled by the experience that QCD will always favor a finite correlation mass for color sources moving along timelike directions. At finite energies, one sees this phenomenon in the hadronic cross sections which are given by the geometrical sizes of the hadrons; the low-light-cone-momentum partons do not matter at finite (small) energies. There is a natural transverse scale of the moving proton. The energy dependence of the high- $Q^2$  structure functions indicates, however, an abnormal increase in “size” in the transverse direction. The proton first gets blacker, but then its transverse radius has to increase. Purely theoretical arguments point towards conformal invariance at high energies, a conjecture which supports the view that partons with small light-cone momenta sampling large spatial light-cone distances correlate over large transverse distances compared to normal hadronic scales.

We have analyzed QCD approaching the light cone with a tilted near-light-cone coordinate reference system [24, 25] containing a parameter  $\eta \neq 0$  giving the distance away from the light cone. The constraint equations appear in the near-light-cone Hamiltonian as terms proportional to  $1/\eta^2$ . We then multiply the light-cone energy by  $\eta$ , considering  $\tilde{P}^- = \eta T^{+-}$ , and divide the light-cone momentum by  $\eta$ , defining  $\tilde{P}^+ = T^{++}/\eta$ . The invariant masses remain unchanged up to terms of higher order in  $\eta$ . For simplicity, I will refer to a completely discretized treatment of transverse and lightlike spatial directions. By the trick with near-lightlike coordinates, we can derive a full quantum Hamiltonian for the zero modes which now depends on the QCD coupling  $g$ , the extension  $L_{||}$  of the spatial light-cone distance compared to some lattice size  $a$  (or ultraviolet cutoff  $\Lambda = 1/a$ ), and the parameter  $\eta$  which gives the nearness to the light cone. Having fixed the QCD coupling  $g$  which determines the lattice size  $a$ , we would like to study in this Hamiltonian the physics at large longitudinal distances  $L_{||}/a \rightarrow \infty$  close to the

light cone  $\eta \rightarrow 0$ . Because of dimensional reduction, the product

$$s = \frac{\eta L_{\parallel}}{a} \quad (1)$$

appears as a coupling in the Hamiltonian. Its limit is not defined. The order of the limiting process is important, as one knows from simple superrenormalizable models. One first has to let  $L_{\parallel}/a \rightarrow \infty$  and then  $\eta \rightarrow 0$  in order not to lose the nonperturbative properties of the vacuum. For QCD, an analytical limiting process is impossible. Therefore, the only way out is to start for large  $s$ , corresponding to fixed  $\eta$  and large  $L_{\parallel}$ , and then approach smaller values of  $s$ .

This procedure ends when we have found a fixed point  $s^* = \eta L_{\parallel}/a$  where the mass gap of the zero-mode theory vanishes. Approaching this fixed point from the correct side which corresponds to a large longitudinal extension of the lattice, we include the nonperturbative dynamics of the zero modes. The trivial, wrong other side, where  $s$  is arbitrarily small, would be disconnected from the large  $L_{\parallel}$  limit. When the  $(2+1)$ -dimensional system has an infinite correlation length, both the infrared limit of large longitudinal distances and of nearness to the light cone are realized. For a simplified zero-mode theory in  $SU(2)$ , we have demonstrated such a possibility on the lattice. In principle, the full  $(3+1)$ -dimensional theory can be solved for any  $\eta$  as long  $g, L_{\parallel}/a$  are chosen in such a way that we have asymptotic scaling. But in order to synchronize the infrared behavior encoded in the zero-mode system correctly with the ultraviolet behavior of small lattice size, the choice of  $\eta$  is no longer free for a given length of the longitudinal direction; one must choose  $\eta$  in agreement with the fixed point found in the zero-mode calculation; i.e., in the  $(3+1)$ -dimensional calculation, the number of slices  $L_{\parallel}/a$  in the spatial light-cone direction determines  $\eta$ :

$$\eta = \frac{s^*}{L_{\parallel}/a}. \quad (2)$$

It has to be demonstrated numerically that, with decreasing QCD coupling  $g$ , the value  $s^*$  becomes smaller in such a way that we approach the light cone  $\eta \rightarrow 0$  having a reasonable number of slices  $L_{\parallel}/a$  in the spatial light-cone direction. The reduced calculation in  $SU(2)$  [24] was done without the inclusion of transverse gluons, so we still have to prove that this procedure works. Phenomenologically [26], we have conjectured that the increase in the high-energy electron–proton cross section is due to this critical point  $s^*$ . When this point, which corresponds to infinite energies, is approached, the correlation length of near-lightlike Wilson lines of the partons

increases with a critical index from  $Z(3)$  symmetry. The photon density remains power behaved beyond the short-distance scale given by the resolution of the photon. According to our conjecture, this critical opalescence phenomenon is the cause of the increase in the virtual-photon cross section with high energies. We are now in the process [27] of extending the lattice work by including more transverse gluon modes in the simulation of the zero-mode theory. It seems that the light-cone solution of QCD is not simple, but in approaching this solution, we learn a lot about high-energy scattering.

### 3. A VALENCE-QUARK LIGHT-CONE HAMILTONIAN

In this section, I would like to present a derivation where the near-light-cone method and the field strength correlators work nicely together. This example demonstrates their practicality as a calculational and heuristic tool. Firstly, one can analytically do the calculation in the stochastic vacuum model and, secondly, the result is so close to reality that one can see the model-independent result. In our application of the stochastic vacuum model to high-energy scattering, we always use Wilson loops which are on the light cone. The expectation value of a Wilson loop along the light cone is unity, because the area of a lightlike Wilson loop is zero. I was always disturbed by this fact, because I thought that a color dipole moving with the speed of light should feel confining forces. The wave-function renormalization due to single loops cancels out in the  $S$  matrix, but the puzzle remained with me. So, recently, Nurpeissov and I [28] have looked into this problem again using a tilted Wilson loop corresponding to a fast moving dipole in Euclidean and in Minkowski space; i.e., we applied the near-light-cone trick.

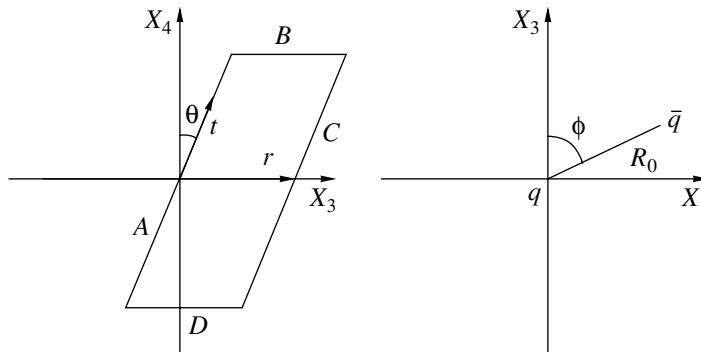
In Euclidean space, the Wegner–Wilson loop can be represented with the help of the Casimir operator in the fundamental representation  $C_2(3) = t^2 = 4/3$ :

$$\langle W[C] \rangle_G = \exp \left[ -\frac{C_2(3)}{2} \chi_{ss} \right]. \quad (3)$$

We calculate  $\chi_{ss}$  as the double area integral of the correlation function over the surface of the loop. Let us consider the  $\chi_{ss}$  function for large separations  $R_0$  of the quark and antiquark, where the confinement term plays the main role. For the nonperturbative (NP) confining (c) component  $\chi_{ss}^{\text{NP c}}$ , we get the following expression for large distances  $R_0 \alpha \gg 2a$ :

$$\chi_{ss}^{\text{NP c}} = \lim_{T \rightarrow \infty} \left[ \frac{2\pi^3 a^2 G_2 \kappa T}{3(N_c^2 - 1)} R_0 \alpha \right]. \quad (4)$$

Here,  $G_2$  denotes the gluon condensate,  $\kappa$  is the weight of the confining correlator compared to the



Configuration of the Wegner–Wilson loop in Euclidean space–time.

nonconfining correlator,  $a$  gives the correlation length, and  $T$  is the extension of the loop in Euclidean time. The orientation of the loop is shown in the figure.

The geometry of the arrangement enters into the factor

$$\alpha = \sqrt{1 - \cos^2 \phi \sin^2 \theta}. \tag{5}$$

One recognizes that the confining interaction leads to a VEV of the tilted Wilson loop which is consistent with the area law for large distances  $R_0$ :

$$\langle W[C] \rangle = e^{-\sigma R_0 \alpha T}, \tag{6}$$

$$\sigma = \frac{\pi^3 G_2 a^2 \kappa}{18}, \tag{7}$$

where  $\sigma$  is the string tension [19] and the area is obtained from

$$\text{Area} = TR_0 \int_{-1/2}^{1/2} du \int_0^1 dv \tag{8}$$

$$\times \sqrt{\left(\frac{dX_\mu}{du}\right)^2 \left(\frac{dX_\mu}{dv}\right)^2 - \left(\frac{dX_\mu}{du} \frac{dX_\mu}{dv}\right)^2} = TR_0 \alpha.$$

For the Wegner–Wilson loop in Minkowski space–time, we define  $\chi_{ss}$  in the same way as in [19]:

$$\langle W[C] \rangle_G = \exp \left[ -i \frac{C_2(3)}{2} \chi_{ss} \right]. \tag{9}$$

Minkowskian geometry enters via the factor

$$\alpha_M = \sqrt{1 + \cos^2 \phi \sinh^2 \psi}, \tag{10}$$

which is consistent with the analytical continuation of the Euclidean expression  $\alpha = 1 - \cos^2 \phi \sin^2 \theta$  into Minkowski space by transforming the angle  $\theta \rightarrow i\psi$ . This analytical continuation is similar to the analytical continuation used in high-energy scattering [29–31], where the angle between two Wilson loops transforms in the same way.

The confining contribution to  $\chi_{ss}$  reads in Minkowski space

$$\chi_{ss}^{\text{NP c}} = \lim_{T \rightarrow \infty} \left[ \frac{2\pi^3 a^2 G_2 \kappa T}{3(N_c^2 - 1)} R_0 \alpha_M \right]. \tag{11}$$

In order to interpret this result, one must define the four velocities of the particles described by the tilted loop

$$u_\mu = (\gamma, 0_\perp, \gamma\beta). \tag{12}$$

The exponent giving the expectation value of the Wilson loop acquires a new meaning now, since  $-ig \int d\tau A^\mu u_\mu = -ig \int d\tau (\gamma A^0 - \gamma\beta A^3)$ , which leads in the VEV to a value for  $\beta \approx 1$

$$\langle W_r[C] \rangle = e^{-i\gamma(P^0 - P^3)T}. \tag{13}$$

The light-cone energy arising from the confining part of the correlation function has the form

$$P^- = \frac{1}{\sqrt{2}} \left( \sigma R_0 \sqrt{\cos^2 \phi + \sin^2 \phi / \gamma^2} \right). \tag{14}$$

One sees that the Wilson loop for boosts with large  $\gamma$  indicates that the light-cone energy does not depend on the transverse distance  $R_0 \sin \phi$  between the quarks. We introduce the relative plus momentum  $k^+$  and transverse momentum  $k_\perp$  for the quarks with mass  $\mu$ . By adding the above “potential” term to the kinetic term of relative motion of the two particles, we complete the Hamiltonian  $P^-$ :

$$P^- = \frac{(\mu^2 + k_\perp^2)P}{2(1/4P^2 - k^+)} + \frac{1}{\sqrt{2}} \sigma \sqrt{x_3^2 + x_\perp^2 / \gamma^2}. \tag{15}$$

Next, we multiply  $P^-$  with the plus component of the momentum  $P^+$  and use the fact that  $P^+/M = \sqrt{2}\gamma M$  to eliminate the boost variable from the Hamiltonian. Further, we introduce the fraction  $\xi = k^+/P^+$  with  $|\xi| < 1/2$  and its conjugate, the scaled longitudinal space coordinate  $\sqrt{2}\rho = P^+ x_3$ , as dynamical variables. For our configuration, the

relative time of the quark and antiquark is zero. Then we get the light-cone Hamiltonian in a Lorentz-invariant manner, because the variables  $\xi$ ,  $\rho$ ,  $k_\perp$ , and  $x_\perp$  are invariant under boosts

$$M^2 = 2P^+P^- = \frac{\mu^2 + k_\perp^2}{1/4 - \xi^2} + 2\sigma\sqrt{\rho^2 + M^2x_\perp^2}. \quad (16)$$

To solve the  $M^2$  operator, one has to replace the square-root operator by introducing an auxiliary parameter  $s$  of dimension mass squared and minimize  $M^2$  with respect to variations of  $s$ . Final self-consistency must be reached with a guessed mass eigenvalue  $M_0$ :

$$M^2 = \frac{\mu^2 + k_\perp^2}{1/4 - \xi^2} + \frac{1}{2}\left(4\sigma^2\frac{\rho^2 + M_0^2x_\perp^2}{s} + s\right). \quad (17)$$

In addition, one has to set the self-energy correction calculated by Simonov [32], which is  $\Delta\mu^2 = -4\sigma f(m_q)/\pi$ , and get

$$M^2 = \frac{\mu^2 - 4\sigma f/\pi + k_\perp^2}{1/4 - \xi^2} + \frac{1}{2}\left(4\sigma^2\frac{\rho^2 + M_0^2x_\perp^2}{s} + s\right). \quad (18)$$

For light quarks, the function  $f(m_q)$  is close to unity. We have used the above equation with a simple trial function

$$\psi(\xi, x_\perp) = N \cos(\xi\pi)e^{-x_\perp^2/(2x_0^2)}. \quad (19)$$

We obtain two solutions [33] with positive masses due to the  $s$  minimization. One solution is very low in mass and the other rather high. By tuning  $f(mq) = 0.8615$  away from unity, the lower solution is pion-like with a really low mass, whereas the other solution lies at a typical hadronic scale

$$M_{\text{low}} = 0.138 \text{ GeV}, \quad (20)$$

$$M_{\text{high}} = 1.1 \text{ GeV}. \quad (21)$$

Since on the light cone, the mechanism of chiral symmetry breaking is of particular interest, we would like to understand this result better. In the approach given here, confinement plays an important role in contrast to NJL effective models, which give an adequate description of spontaneous chiral symmetry breaking but do not include confinement.

The confining interaction in the light Hamiltonian was derived in the specific model of the stochastic vacuum. But it also can be inferred from the simple Lorentz transformation properties of the phase in the Wilson loop and a lattice determination of the tilted Wilson expectation values. In this respect, the final Hamiltonian is model independent.

The inclusion of confining forces in the initial- and final-state wave functions can put all scattering cross sections calculated with the stochastic vacuum model on a much safer base, when wave functions and cross sections are derived consistently. For low- $Q^2$  photon wave functions, the long-distance part of the wave function matters strongly and confinement is important (cf. [34]). Especially the diffractive cross section has a large contribution from large-dipole sizes and a correct behavior can only be expected when the problem of the large-dipole wave function is treated adequately. Another extension of the above calculation is the coupling of the initial  $q\bar{q}$  state to higher Fock states  $q\bar{q}g$  with gluons which can be calculated with Wilson loops near the light cone in Minkowski space.

#### 4. DISCUSSION AND CONCLUSIONS

I have tried to give some impression how QCD appears near the light cone. I think we have now a calculational framework to approach the light cone in a systematic way. It does not look much easier than equal-time lattice gauge theory. One may hope that some simplifications arise in the process of studying it. The work on a Wilson loop near the light cone looked very complicated and intransparent at the beginning, but it reduced to some simple form. I like this example because it shows how the stochastic vacuum model can really solve complicated problems. Simonov has shown in many applications how it gets us to the heart of the problem and helps us to find some approximate solution.

#### ACKNOWLEDGMENTS

I would like to thank J. Bluemlein and the Zeuthen theoretical physics group for the hospitality with which they received me during my sabbatical stay. M. Ilgenfritz and E. Prokhorov have been very patient to discuss parts of this article with me.

This work is supported by the EU Program Computational Hadron Physics.

#### REFERENCES

1. R. B. Laughlin, Rev. Mod. Phys. **71**, 863 (1999).
2. K. G. Wilson, Phys. Rev. D **10**, 2445 (1974).
3. M. Creutz, Phys. Rev. Lett. **43**, 553 (1979).
4. H. Leutwyler, hep-ph/0212325.
5. J. Berges, N. Tetradis, and C. Wetterich, Phys. Rep. **363**, 223 (2002).
6. H. J. Pirner, hep-ph/0209221.
7. S. Mandelstam, Phys. Rev. D **19**, 2391 (1979).
8. G. Mack, Nucl. Phys. B **235**, 197 (1984).
9. H. J. Pirner, Prog. Part. Nucl. Phys. **29**, 33 (1992).

10. H. G. Dosch and Yu. Simonov, *Phys. Lett. B* **205**, 339 (1988).
11. S. J. Brodsky, H. C. Pauli, and S. S. Pinsky, *Phys. Rep.* **301**, 299 (1998).
12. J. M. Maldacena, *Adv. Theor. Math. Phys.* **2**, 231 (1998)[*Int. J. Theor. Phys.* **38**, 1113 (1999)].
13. B. J. Schaefer and J. Wambach, *nucl-th/0403039*.
14. J. Braun, K. Schwenzer, and H. J. Pirner, *hep-ph/0312277*.
15. J. Meyer, K. Schwenzer, and H. J. Pirner, *Phys. Lett. B* **473**, 25 (2000).
16. D. S. Kuzmenko, V. I. Shevchenko, and Yu. A. Simonov, *hep-ph/0310190*.
17. G. 't Hooft, *Nucl. Phys. A* **721**, 3 (2003).
18. A. Di Giacomo, H. G. Dosch, V. I. Shevchenko, and Yu. A. Simonov, *Phys. Rep.* **372**, 319 (2002).
19. A. I. Shoshi, F. D. Steffen, H. G. Dosch, and H. J. Pirner, *Phys. Rev. D* **68**, 074004 (2003).
20. V. A. Franke, Yu. V. Novozhilov, S. A. Paston, and E. V. Prokhorov, *hep-th/0404031*.
21. K. Itakura and S. Maedan, *Prog. Theor. Phys.* **105**, 537 (2001).
22. F. Lenz, K. Ohta, M. Thies, and K. Yazaki, *hep-th/0403186*.
23. K. Hornbostel, S. J. Brodsky, and H. C. Pauli, *Phys. Rev. D* **41**, 3814 (1990).
24. E. M. Ilgenfritz, Yu. P. Ivanov, and H. J. Pirner, *Phys. Rev. D* **62**, 054006 (2000).
25. H. W. L. Naus, H. J. Pirner, T. J. Fields, and J. P. Vary, *Phys. Rev. D* **56**, 8062 (1997).
26. H. J. Pirner and F. Yuan, *Phys. Rev. D* **66**, 034020 (2002).
27. M. Ilgenfritz, H. J. Pirner, and E. Prokhorov, work in progress.
28. H. J. Pirner and N. Nurpeisov, *hep-ph/0404179*.
29. E. Meggiolaro, *Z. Phys. C* **76**, 523 (1997).
30. E. Meggiolaro, *Nucl. Phys. B* **625**, 312 (2002).
31. A. Hebecker, E. Meggiolaro, and O. Nachtmann, *Nucl. Phys. B* **571**, 26 (2000).
32. Yu. A. Simonov, *Phys. Lett. B* **515**, 137 (2001).
33. O. Schlaudt and H. J. Pirner, work in progress.
34. H. G. Dosch, T. Gousset, and H. J. Pirner, *Phys. Rev. D* **57**, 1666 (1998).

## Structure of the Gauge Fields inside Baryon\*

A. G. Bornyakov<sup>1)\*\*</sup>, M. N. Chernodub<sup>2)\*\*\*</sup>, H. Ichie<sup>3)</sup>, Y. Mori<sup>3)</sup>,  
M. I. Polikarpov<sup>2)\*\*\*\*</sup>, G. Schierholz<sup>4)</sup>, and T. Suzuki<sup>3)</sup>

Received May 13, 2004; in final form, November 3, 2004

**Abstract**—We present the results of lattice calculations of the distributions of the gauge fields inside a baryon constructed from three heavy quarks. It turns out that the chromoelectric flux tube has a  $Y$  shape. At nonzero temperature, we observe the breaking of the confining string below the deconfining temperature and the disappearance of the string above the critical temperature. © 2005 Pleiades Publishing, Inc.

### 1. INTRODUCTION

It is important to learn about the forces and the distribution of color electric flux in the  $3Q$  system. A particularly interesting question is whether a three-body force exists and the confining flux tube is of  $Y$  shape, or whether the long-range potential is simply the sum of two-body potentials, resulting in a flux tube of  $\Delta$  shape. Several lattice studies give evidence for a  $\Delta$ -type long-range potential [1, 2], while others show the existence of a  $Y$ -type potential [3, 4]. The latter result is also supported by the field correlators method [5]. The difference between a  $\Delta$  and  $Y$ -shape potential is rather small and it is difficult to detect it numerically. Below, we present the results of the study of the static potential and the flux tube of the  $3Q$  system in quenched lattice QCD and in QCD with two flavors of nonperturbatively improved Wilson fermions (“full” QCD). The long-distance physics appears to be predominantly Abelian and we use Abelian variables (after fixing the maximally Abelian gauge), which leads to a substantial reduction of the statistical noise. We observe that, above the critical temperature (at  $T > T_c$ ), the string in the  $3Q$  system disappears as in full QCD as in quenched QCD. At  $T < T_c$ , for sufficiently large separation of the heavy quarks, the string disappears only in the case of full QCD, which corresponds to the creation

of a quark–antiquark pair from the vacuum. Some results of these investigations have been reported in [6]. The numbers of the gauge field configurations and parameters of the lattice Lagrangian are also given in [6].

### 2. SIMULATION DETAILS AND OBSERVABLES

To study QCD with dynamical quarks, we consider  $N_f = 2$  flavors of degenerate quarks, using the Wilson gauge field action and nonperturbatively  $\mathcal{O}(a)$  improved Wilson fermions [7]. The calculations in full QCD at zero temperature are performed on the  $L^3 \cdot L_t = 24^3 \cdot 48$  lattice at  $\beta = 5.29$  and  $\kappa = 0.1355$ , which corresponds to a pion mass of  $m_\pi/m_\rho \approx 0.7$  and a lattice spacing of  $a/r_0 = 0.18$  (i.e.,  $a = 0.09$  fm for the force parameter  $r_0 = 0.5$  fm). Here,  $L$  is the spatial extension of the lattice and  $L_t$  is the temporal extension. For comparison, we also did quenched simulations at zero temperature on the  $16^3 \cdot 32$  lattice at  $\beta = 6.0$ . Configurations for finite temperature are generated on  $16^3 \cdot 8$  lattice at  $\beta = 5.2$  and  $0.1330 \leq \kappa \leq 0.1360$ , corresponding to temperatures near the transition temperature  $T_c = 213(10)$  MeV ( $\kappa_t = 0.1344$ ), and at  $\beta = 5.25$ , corresponding to temperatures near the transition temperature. Details of the simulations can be found in [6]. We perform the maximally Abelian gauge fixing on generated configurations employing the simulated annealing algorithm [8]. The Abelian projection procedure [9] defines the diagonal  $SU(3)$  link matrices:

$$u_\mu(s) = \text{diag}\{u_\mu^1(s), u_\mu^2(s), u_\mu^3(s)\}, \quad (1)$$

$$u_\mu^a(s) = e^{i\theta_\mu^a(s)}, \quad (2)$$

where  $\theta_\mu^a(s)$  can in turn be decomposed into monopole (singular) and photon (regular) parts [10, 11]:

$$\theta_\mu^a(s) = \theta_\mu^{\text{mon},a}(s) + \theta_\mu^{\text{ph},a}(s). \quad (3)$$

\*This article was submitted by the authors in English.

<sup>1)</sup>Institute for High Energy Physics, Protvino, Moscow oblast, 142284 Russia.

<sup>2)</sup>Institute of Theoretical and Experimental Physics, Bol'shaya Cheremushkinskaya ul. 25, Moscow, 117259 Russia.

<sup>3)</sup>Institute for Theoretical Physics, Kanazawa University, Kanazawa, Japan.

<sup>4)</sup>NIC/DESY Zeuthen, Germany.

\*\* e-mail: bornvit@sirius.ihep.su

\*\*\* e-mail: Maxim.Chernodub@itep.ru

\*\*\*\* e-mail: polykarp@itep.ru

Monopole and photon parts are defined by the following expressions:

$$\theta_\mu^{\text{mon},a}(s) = -2\pi \sum_{s'} D(s-s') \partial'_\nu n_{\nu\mu}^a(s), \quad (4)$$

$$\theta_\mu^{\text{ph},a}(s) = - \sum_{s'} D(s-s') \partial'_\nu \bar{\theta}_{\nu\mu}^a(s), \quad (5)$$

where

$$\bar{\theta}_{\mu\nu}^a(s) = \partial_\mu \theta_\nu^a(s) - \partial_\nu \theta_\mu^a(s) - 2\pi n_{\mu\nu}^a(s), \quad (6)$$

$$\bar{\theta}_{\mu\nu}^a(s) \in (-\pi, \pi], \quad n_{\mu\nu}^a(s) = 0, \pm 1, \pm 2,$$

$\partial'_\nu$  and  $\partial_\nu$  are backward and forward lattice derivatives, and  $D(s)$  denotes the lattice Coulomb propagator.

We study the Abelian action density

$$\rho_{\text{Ab}}(s) = \frac{\beta}{3} \sum_{\mu>\nu} \sum_a \cos(\bar{\theta}_{\mu\nu}^a(s)), \quad (7)$$

the Abelian color electric field

$$E_j^a(s) = i\bar{\theta}_{j4}^a(s), \quad (8)$$

and the monopole current

$$k_\mu^a(s) = -\frac{i}{4\pi} \epsilon_{\mu\nu\rho\sigma} \partial_\nu \bar{\theta}_{\rho\sigma}^a(s + \hat{\mu}). \quad (9)$$

At finite temperature, we consider three types of Polyakov loops to create static sources:

Abelian

$$L_{\text{Ab}}^a(\mathbf{s}) = \exp \left\{ i \sum_{t=1}^{L_t} \theta_4^a(\mathbf{s}, t) \right\}, \quad (10)$$

$$L_{\text{Ab}}(\mathbf{s}) = \frac{1}{3} \sum_{a=1}^3 L_{\text{Ab}}^a(\mathbf{s});$$

monopole

$$L_{\text{mon}}^a(\mathbf{s}) = \exp \left\{ i \sum_{t=1}^{L_t} \theta_4^{\text{mon},a}(\mathbf{s}, t) \right\}, \quad (11)$$

$$L_{\text{mon}}(\mathbf{s}) = \frac{1}{3} \sum_{a=1}^3 L_{\text{mon}}^a(\mathbf{s});$$

photon

$$L_{\text{ph}}^a(\mathbf{s}) = \exp \left\{ i \sum_{t=1}^{L_t} \theta_4^{\text{ph},a}(\mathbf{s}, t) \right\}, \quad (12)$$

$$L_{\text{ph}}(\mathbf{s}) = \frac{1}{3} \sum_{a=1}^3 L_{\text{ph}}^a(\mathbf{s}).$$

The vacuum averages of our observables are defined by

$$\langle \rho_{\text{Ab}}(s) \rangle_{3Q} = \frac{\langle \rho_{\text{Ab}}(s) \mathcal{P}_{3Q}(L_Y) \rangle}{\langle \mathcal{P}_{3Q}(L_Y) \rangle} - \langle \rho_{\text{Ab}}(s) \rangle, \quad (13)$$

$$\langle E_j(s) \rangle_{3Q} \quad (14)$$

$$= \frac{\langle \frac{1}{3!} \sum_{a,b,c} |\varepsilon_{abc}| E_j^a(s) L^a(\mathbf{s}_1) L^b(\mathbf{s}_2) L^c(\mathbf{s}_3) \rangle}{\langle \mathcal{P}_{3Q}(L_Y) \rangle},$$

$$\langle k_j(s) \rangle_{3Q} \quad (15)$$

$$= \frac{\langle \frac{1}{3!} \sum_{a,b,c} |\varepsilon_{abc}| k_j^a(s) L^a(\mathbf{s}_1) L^b(\mathbf{s}_2) L^c(\mathbf{s}_3) \rangle}{\langle \mathcal{P}_{3Q}(L_Y) \rangle},$$

where

$$\mathcal{P}_{3Q}(L_Y) = \frac{1}{3!} \sum_{a,b,c} |\varepsilon_{abc}| L^a(\mathbf{s}_1) L^b(\mathbf{s}_2) L^c(\mathbf{s}_3); \quad (16)$$

$\mathbf{s}_i$  denotes the position of the  $i$ th quark;  $L_Y$  is the minimal  $Y$ -type distance between the three quarks, i.e., the sum of the distances from the three quarks to the Fermat point,

$$L_Y^2 = \frac{1}{2} \sum_{i>j} r_{ij}^2 + 2\sqrt{3}S_\Delta; \quad (17)$$

$r_{ij} = |\mathbf{s}_i - \mathbf{s}_j|$ ; and  $S_\Delta$  is the area of the corresponding triangle. Equation (17) defines  $L_Y$  when all angles in the three-quark triangle are less than  $2\pi/3$ . If one of the angles is equal to or larger than  $2\pi/3$ , then  $L_Y = \sum_{i>j} r_{ij} - \max r_{ij}$ .  $L^a(\mathbf{s})$  stands for one of the three types of Polyakov loops introduced above [Eqs. (10)–(12)].

To create a baryon made from three infinitely heavy quarks at zero temperature instead of the product of three Polyakov lines, we use the baryonic Wilson loop:

$$W_{3Q} = \frac{1}{3!} \varepsilon_{ijk} \varepsilon_{i'j'k'} U^{ii'}(\mathcal{C}_1) U^{jj'}(\mathcal{C}_2) U^{kk'}(\mathcal{C}_3), \quad (18)$$

where

$$U(\mathcal{C}) = \prod_{s,\mu \in \mathcal{C}} U_\mu(s) \quad (19)$$

is the ordered product of link matrices,  $U \in SU(3)$ , along the paths  $\Gamma_{\mathcal{C}_1}$ ,  $\Gamma_{\mathcal{C}_2}$ , and  $\Gamma_{\mathcal{C}_3}$ , as shown in Fig. 1. The potential energy of this system is given by

$$V_{3Q} = -\frac{1}{L_t} \lim_{L_t \rightarrow \infty} \log \langle W_{3Q} \rangle, \quad (20)$$

$L_t$  being the temporal extent of the loop. The Abelian baryonic Wilson loop is given by

$$W_{3Q}^{\text{Ab}} = \frac{1}{3!} |\varepsilon_{ijk}| u^i(\mathcal{C}_1) u^j(\mathcal{C}_2) u^k(\mathcal{C}_3), \quad (21)$$

where  $u(\mathcal{C})$  is the Abelian counterpart of (19).

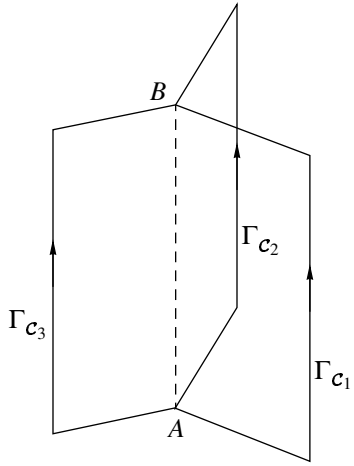


**Fig. 1.** Three-quark Wilson loop. The heavy quarks are moving along the contours  $\Gamma_{c_1}$ ,  $\Gamma_{c_2}$ , and  $\Gamma_{c_3}$ .

### 3. STATIC POTENTIAL AND BARYONIC FLUX AT ZERO TEMPERATURE

In Fig. 2, we compare the Abelian potential in full and quenched QCD as a function of minimal  $Y$ -type distance between the quarks,  $L_Y$ . We see that the Abelian string tension in full QCD is slightly larger than the quenched value.

In Fig. 3, we show the distribution of the color electric field  $\mathbf{E}^{3Q}$ , and its surrounding monopole currents  $k^{3Q}$ , on the  $24^3 \cdot 48$  lattice in full QCD. The time direction of the Wilson loop has been taken in one of the spatial directions of the lattice. Points on the hyperplane orthogonal to the time direction of the Wilson loop are marked by  $(x, y, z)$ . The static quarks are placed at  $(x, y, z) = (20, 10, 8)$ ,  $(25, 18, 8)$ , and  $(30, 10, 8)$ , respectively; i.e., they lie in the  $(x, y)$  plane. The color index of the electric field operator is identified with the color index of the quark in the bottom-right corner (in the center bottom figure). Note that the sum of the electric field over the three color indices vanishes at any point. As expected, the flux emanates from the quark in the bottom-right corner and near the center of the  $3Q$  system splits into two parts. A similar picture holds for the top and the bottom-left quark and their respective fluxes. In the adjacent figures, we show the monopole current in the planes perpendicular to the electric flux lines, i.e., the  $(x, z)$  and  $(y, z)$  planes. They form a solenoidal current in agreement with the dual superconductor picture of confinement.

If the confining flux is of  $Y$  shape, we would expect the long-distance part of the potential to be a universal function of  $L_Y$ . In Fig. 4, we plot the Abelian potential as a function of  $L_Y$  and as a function of the

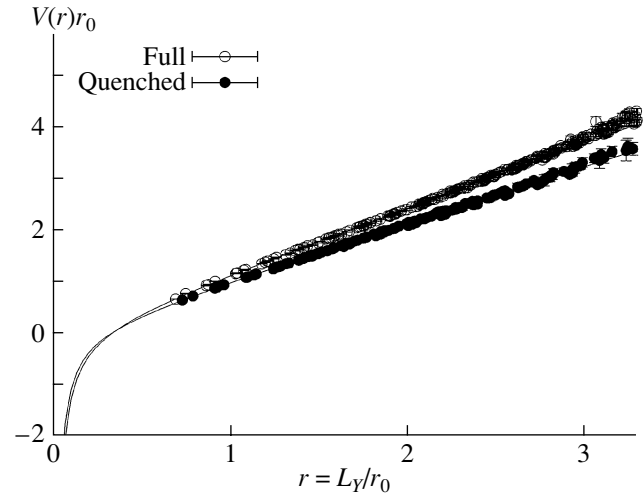


**Fig. 2.** The Abelian baryon potential in full and quenched QCD is shown in units of the so-called force parameter  $r_0$ . We used the value  $r_0 = 0.5$  fm.

perimeter of the triangle formed by the quarks

$$L_{\Delta} = \sum_{i < j} |\mathbf{r}_i - \mathbf{r}_j|. \quad (22)$$

The data show a universal behavior when plotted against  $L_Y$ . This is to a lesser extent the case when plotted against  $L_{\Delta}$ , which supports a genuine three-body force of  $Y$  type. In Fig. 4, we see that the monopole part is largely responsible for the linear behavior of the potential, as was already found in the case of the  $Q\bar{Q}$  potential [12]. The ratio of monopole to Abelian string tension turns out to be 0.81(3).

### 4. STATIC POTENTIAL OF THE BARYONIC SYSTEM AT FINITE TEMPERATURE

Now we discuss the baryonic system constructed from three static quarks at finite temperature. As is seen from Fig. 5, the static three-quark potential has a tendency to flatten at large  $L_Y$ . The reason is that, at finite temperature, not only the lowest energy state (baryon) but also other states may contribute to the baryonic potential. The breaking of the baryonic string may go via three different processes:

(i) Process  $QQQ + q\bar{q} \rightarrow QQq + Q\bar{q}$ .

The most energetically favorable string breaking corresponds to the creation of one virtual meson,  $q\bar{q}$ , from the vacuum. The light quark from this pair and two heavy quarks form a baryon system,  $QQq$ . The chromoelectric string inside the  $QQq$  baryon is spanned between the two heavy quarks. The light antiquark and the third heavy quark form a heavy-light,  $Q\bar{q}$ , meson state. There are three possible ways to break the  $Y$  string by one light meson.

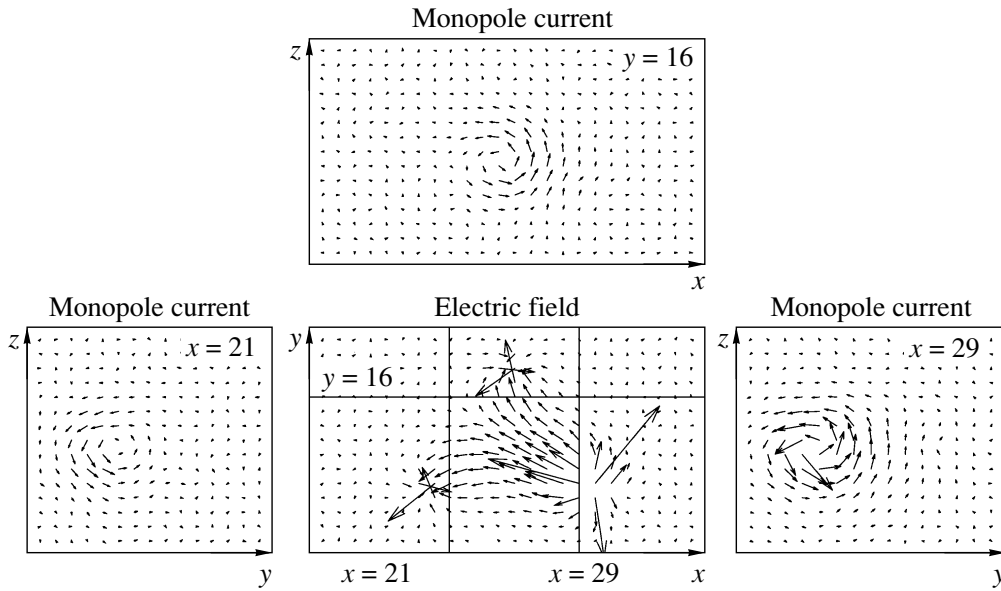


**Fig. 3.** Distribution of the color electric field  $\mathbf{E}^{3Q}$  in the  $(x, y)$  plane on the  $24^3 \cdot 48$  lattice (center-bottom figure), together with the monopole currents  $k^{3Q}$  in the  $(x, z)$  and  $(y, z)$  planes (adjacent figures), respectively, at the position marked by the respective solid lines. The magnitude of  $E^{3Q}$  and  $k^{3Q}$  is indicated by the length of the arrows.

(ii) Process  $QQQ + 2q\bar{q} \rightarrow Qqq + 2Q\bar{q}$ .

Another possibility is a creation of two light meson states,  $2(q\bar{q})$ , from the vacuum. As a result, two heavy–light mesons  $2(Q\bar{q})$  and one baryon made from the heavy quark and two light quarks ( $Qqq$ ) are produced.

(iii) Process  $QQQ + 3q\bar{q} \rightarrow qqq + 3Q\bar{q}$ .

Finally, three light mesons can be created from the vacuum producing three heavy–light mesons  $3(Q\bar{q})$  and one  $qqq$  baryon made from the light quarks.

All these states must be taken into account in the correlator of the three static quarks. Thus, we have the six-exponential ansatz

$$\begin{aligned}
 e^{-L_t V_{3Q}} &= \left\langle \sum \frac{1}{3!} |\varepsilon_{abc}| L^a(\mathbf{s}_1) L^b(\mathbf{s}_2) L^c(\mathbf{s}_3) \right\rangle \quad (23) \\
 &= e^{-V_0/T} \left\{ e^{-\sigma_{QQQ} L_Y/T} + e^{-m_{Q\bar{q}}/T - m_{QQq}/T} \right. \\
 &\times \left[ e^{-\sigma_{QQq} r_{12}/T} + e^{-\sigma_{QQq} r_{23}/T} + e^{-\sigma_{QQq} r_{31}/T} \right] \\
 &\left. + 3e^{-2(m_{Q\bar{q}} + m_{QQq})/T} + e^{-3(m_{Q\bar{q}} + m_{qqq})/T} \right\},
 \end{aligned}$$

where  $V_0$  is the self-energy of the heavy quark.

This simplified formula takes into account only the linear potentials between the heavy quarks as well as the broken string states, disregarding other possible interactions between the quarks. It is known [8, 12, 13] that, in quenched and unquenched QCD, the monopole part of the mesonic potential is linear at large and at small distances. Thus, we expect that

the correlator of the monopole Polyakov loops can be described by Eq. (23).

In Eq. (23), we explicitly use two different string tensions, one for the tension of the Y-shaped unbroken string state [the first term on the right-hand side of (23)] and the other for the string tension of the  $QQQ$  baryon. On the classical level, there is no difference between strings inside  $QQQ$  and  $QQq$  states. The only difference is in the shape of strings: the  $QQQ$  state has a Y-shaped string, while in the  $QQq$  state the string between heavy quarks is a straight flux tube. In the  $QQq$  state, the quark  $q$  is located somewhere inside the string. On the quantum level, the string tension may be renormalized due to interaction of the quark  $q$  with the string.

The correlator (23) and, thus, the potential  $V_{3Q}$  depend not only on  $L_Y$  but also on  $r_{ij}$ , and this is the reason of the broad distribution of points in Fig. 5. Note that two states,  $Qqq + 2Q\bar{q}$  and  $qqq + 3Q\bar{q}$ , provide distance-independent contributions to the potential (23), since we neglect the interaction between the mesons and the baryons.

We have analyzed the data for the three-quark correlation function with the ansatz (23), which takes into account the breaking of the string. The results for all string tensions ( $\sigma_{QQq}$ ,  $\sigma_{QQQ}$ ,  $\sigma_{Q\bar{q}}$ ) are presented in Fig. 6. We show for comparison the string tension for the mesonic case for  $N_f = 2$  QCD and the corresponding quenched value [15]. One can see that string tensions are almost independent of the temperature in the region close to the phase transition.

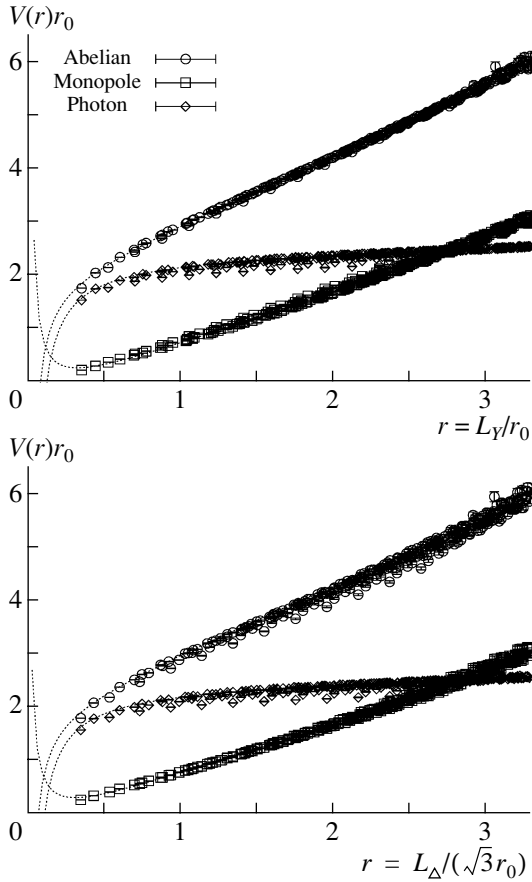


**Fig. 4.** The Abelian baryon potential in full QCD, together with its monopole and photon part, as a function of  $L_Y$  (top) and  $L_\Delta$  (bottom), respectively.

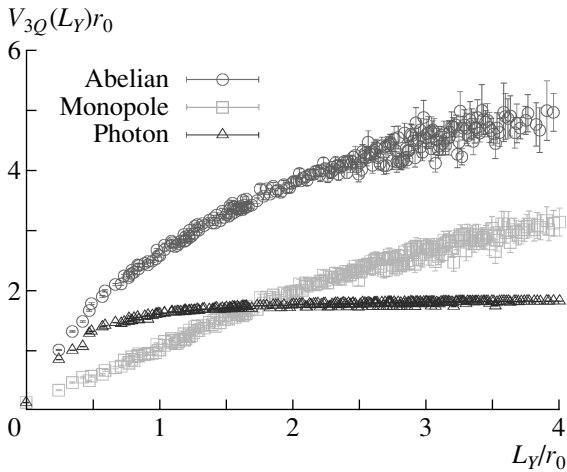


**Fig. 5.** The static three-quark potential at  $T/T_c = 0.94$ .

Moreover, the string tension of the  $QQQ$  system is slightly higher than the string tension of the  $QQq$  state. Thus, we conclude that the quark  $q$  lowers the energy of the string. Another interesting result seen

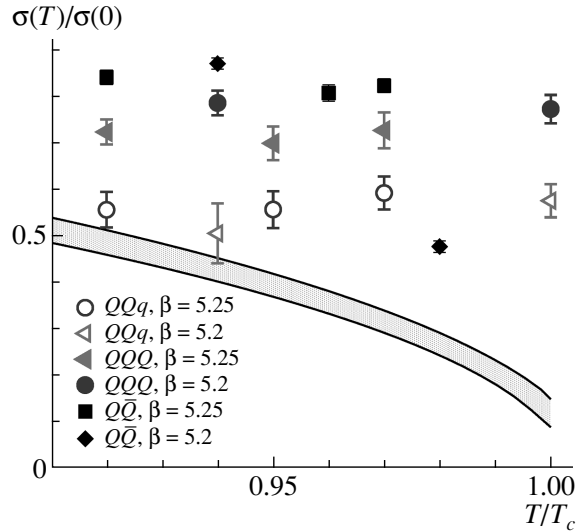


**Fig. 6.** The monopole contribution to string tensions for  $QQQ$  and  $QQq$  states at  $\beta = 5.2$  and  $\beta = 5.25$ . We show for comparison the tension of the string obtained in the meson state ( $Q\bar{Q}$ ) [14], and the shaded area shows the quenched value of the  $Q\bar{Q}$  string tension [15].  $\sigma(0)$  is the zero-temperature string tension for the quenched case.

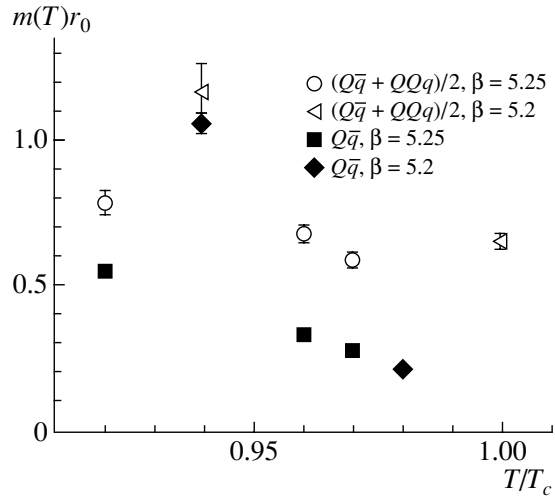


**Fig. 7.** The same as in Fig. 6 but for the average of the effective quark masses in the  $Q\bar{q}$  meson and the  $QQQ$  baryon,  $(m_{Q\bar{q}} + m_{QQQ})/2$ . We also show the effective quark mass of the  $Q\bar{q}$  meson obtained from two-point Polyakov-loop correlators in [14].

in Fig. 6 is that the tension of the unbroken string in the baryon,  $\sigma_{QQQ}$ , is slightly lower than the tension of the string in meson,  $\sigma_{Q\bar{Q}}$  (except for one point which may be an artifact of the fitting procedure).

Using the fitting function (23), we obtain the sum of the constituent masses of the light quarks in the  $Q\bar{q}$  and  $QQq$  states. As one can see from the form of the fitting function (23), we cannot get the values

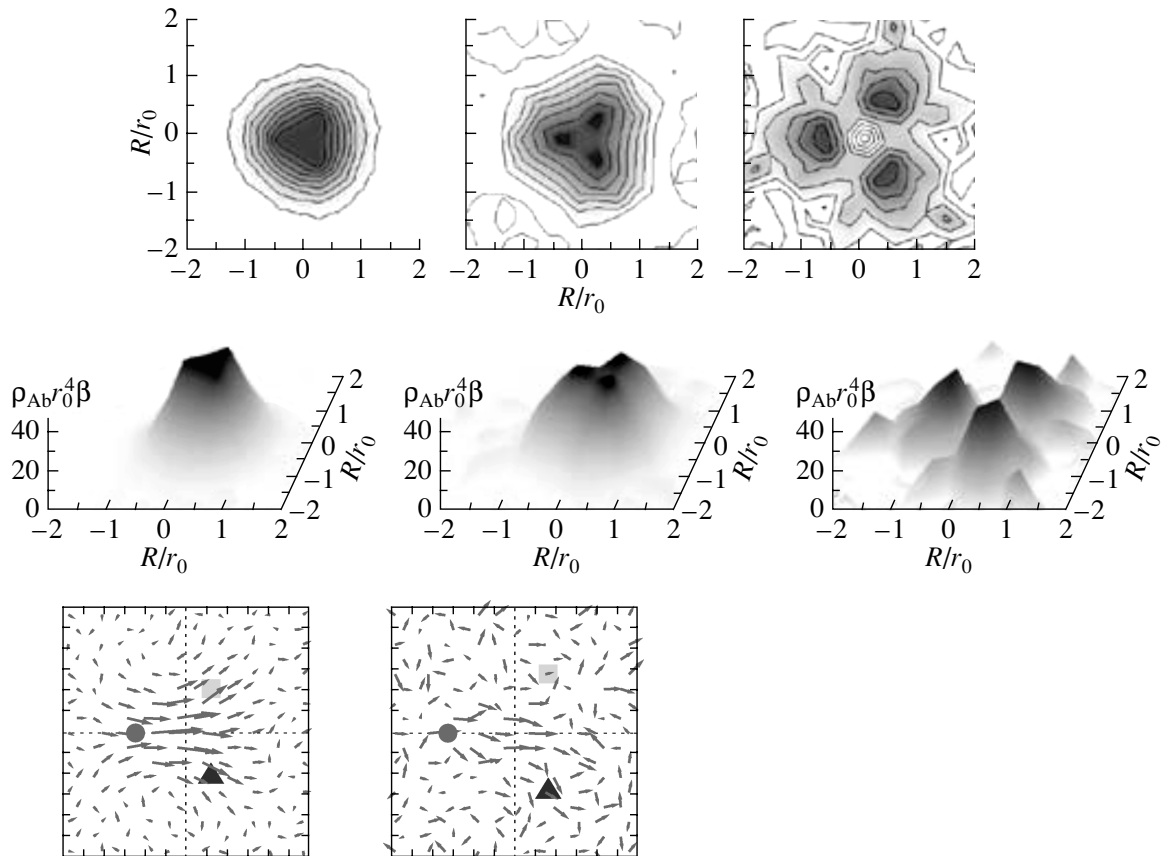


**Fig. 8.** The action density shown as a contour plot (top) and as the three-dimensional plot (middle), and the color electric field (bottom) of the baryonic system. The sources are made of the monopole part of Polyakov loops. The distances are  $L_Y/r_0 = 2.08$  (left),  $2.77$  (center), and  $3.46$  (right), and the temperature is fixed at  $T/T_c = 0.82$  ( $\kappa = 0.1330$ ). The electric field for  $L_Y/r_0 = 3.46$  is not shown since data are too noisy. In all figures the  $x$  and  $y$  axes show coordinates in the plane which is perpendicular to the string. The  $z$  axis shows the energy density in units of the force parameter  $r_0$ .

of these masses separately. In Fig. 7, we present the averaged constituent quark mass,  $(m_{Q\bar{q}} + m_{QQq})/2$ , which shows a tendency to decrease with increasing temperature. We also depict in this figure the constituent quark mass in the  $Q\bar{q}$  meson which has been obtained from two-point Polyakov loop correlators. Our data show that the constituent quark mass in the  $QQq$  baryon is higher than the mass in the heavy-light meson,  $Q\bar{q}$ .

## 5. PROFILES OF THE BARYONIC SYSTEM AT FINITE TEMPERATURE

In Fig. 8, we show profiles of the action density and the color electric field in the baryonic system. For the static quark sources, we use the monopole Polyakov loops. For  $L_Y/r_0 = 2.08, 2.77$ , the monopole potential is linear (see Fig. 5) and the profile of the action density has a  $Y$  shape. The electric field is also squeezed into a  $Y$  shape. However, the noise is much greater than that for the  $T = 0$  case.

We are using the correlator of three Polyakov loops to describe the baryonic system at finite temperature. Thus, there is no information about a  $Y$ -shape junction in the operator itself, contrary to the zero-temperature case, where the three-quark Wilson loop is used. Nevertheless, we see that the flux distribution has a  $Y$ -shape geometry with a junction, similar to the zero-temperature case.

For large enough  $L_Y$ , string breaking is expected. We see this effect in the action density in Fig. 8 at  $L_Y/r_0 = 3.46$ . The color electric field is too noisy to observe any structure.

In Fig. 9, we plot the profile of the baryonic system at various temperatures for  $L_Y/r_0 \sim 2.0$ ; the static quarks are represented by monopole Polyakov loops. When the temperature increases, the density of the action and the electric field decreases and almost disappears in the deconfinement region.

## 6. CONCLUSIONS

We have studied the three-quark system in the maximally Abelian gauge in full and quenched QCD

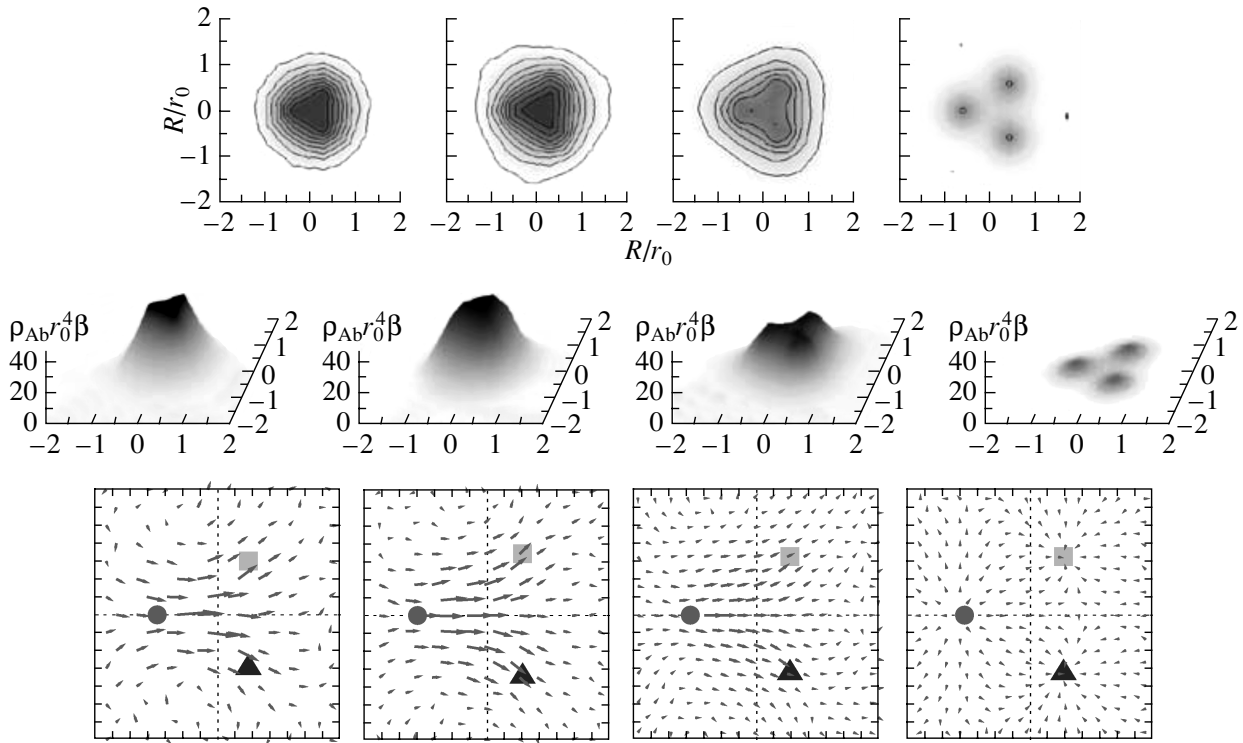


**Fig. 9.** The same as in Fig. 8, but for physical distance  $L_Y/r_0 \sim 2.0$  and different temperatures  $T/T_c = 0.82, 0.94, 1.00,$  and  $1.28$ .

at zero and at finite temperature. In the confined phase at small  $L_Y$ , we observed that the color flux flows from one quark to the other quarks and for each flux there appears the solenoidal monopole current. The profile of the action density definitely supports the Y shape and the potential is linearly dependent on  $L_Y$ . It is interesting that we could observe the Y-shape profile without introducing any junction in the baryon creation operator at finite temperature. The flattening of the baryonic potential is observed for large  $L_Y$ . In the deconfinement phase, the squeezed flux disappears and the color electric flux is similar to the sum of the Coulomb-like fields. Our results are in qualitative agreement with the theoretical predictions of the field correlators method [5] and of the dual Ginzburg–Landau model of the vacuum [16].

#### ACKNOWLEDGMENTS

Twenty-five years ago, one of the authors (M.I.P.) defended his PhD thesis under the guidance of Yu.A. Simonov. M.I.P. will ever remember the time when he learned how to work in theoretical physics, and he is greatly obliged to Simonov for creative discussions and invaluable assistance in research work.

This work is supported by the SR8000 Supercomputer Project of the High Energy Accelerator Re-

search Organization (KEK). A portion of the numerical measurements have been done using the NEC SX-5 at RCNP of Osaka University and the MVS 1000M at Moscow. T.S. is partially supported by JSPS Grant-in-Aid for Scientific Research on Priority Areas nos. 13135210 and 15340073. The Moscow group is grateful to the staff of the Moscow Joint Supercomputer Center, especially to A.V. Zabrodin, for their help in calculations on the MVS 1000M. The Moscow group is partially supported by the Russian Foundation for Basic Research, project nos. 02-02-17308 and 01-02-17456; grants DFG-RFBR RUS 113 1739/0, RFBR-DFG 03-02-04016, INTAS-00-00111, and MK-4019.2004.2; and CRDF awards RPI-2364-MO-02 and MO-011-0.

#### REFERENCES

1. G. S. Bali, Phys. Rep. **343**, 1 (2001).
2. C. Alexandrou, Ph. de Forcrand, and A. Tsapalis, Phys. Rev. D **65**, 054503 (2002).
3. T. T. Takahashi, H. Suganuma, Y. Nemoto, and H. Matsufuru, Phys. Rev. D **65**, 114509 (2002); T. T. Takahashi, H. Matsufuru, Y. Nemoto, and H. Suganuma, Phys. Rev. Lett. **86**, 18 (2001).
4. C. Alexandrou, Ph. de Forcrand, and O. Jahn, Nucl. Phys. B (Proc. Suppl.) **119**, 667 (2003).
5. D. S. Kuzmenko and Yu. A. Simonov, Phys. Lett. B **494**, 81 (2000); hep-ph/0302071.

6. H. Ichie, V. Bornyakov, T. Streuer, and G. Schierholz, Nucl. Phys. B (Proc. Suppl.) **119**, 751 (2003); H. Ichie, V. Bornyakov, T. Streuer, and G. Schierholz, Nucl. Phys. A **721**, 899 (2003); V. G. Bornyakov *et al.* (DIK Collab.), hep-lat/0401026; hep-lat/0401027.
7. S. Booth *et al.* (QCDSF–UKQCD Collab.), Phys. Lett. B **519**, 229 (2001).
8. G. S. Bali, V. G. Bornyakov, M. Müller-Preussker, and K. Schilling, Phys. Rev. D **54**, 2863 (1996).
9. A. S. Kronfeld, M. L. Laursen, G. Schierholz, and U. J. Wiese, Phys. Lett. B **198**, 516 (1987).
10. J. Smit and A. van der Sijs, Nucl. Phys. B **355**, 603 (1991).
11. T. Suzuki, S. Ilyar, Y. Matsubara, *et al.*, Phys. Lett. B **347**, 375 (1995); **351**, 603(E) (1995).
12. DIK Collab. (V. G. Bornyakov *et al.*), Phys. Rev. D **70**, 074511 (2004).
13. H. Shiba and T. Suzuki, Phys. Lett. B **333**, 461 (1994); J. D. Stack, S. D. Neiman, and R. J. Wensley, Phys. Rev. D **50**, 3399 (1994).
14. V. G. Bornyakov *et al.* (DIK Collab.), hep-lat/0310011; hep-lat/0401014.
15. O. Kaczmarek, F. Karsch, E. Laermann, and M. Lutgemeier, Phys. Rev. D **62**, 034021 (2000).
16. Y. Koma, E.-M. Ilgenfritz, T. Suzuki, and H. Toki, Phys. Rev. D **64**, 014015 (2001); M. N. Chernodub and D. A. Komarov, Pis'ma Zh. Éksp. Teor. Fiz. **68**, 109 (1998) [JETP Lett. **68**, 117 (1998)].

# $1/N_c$ Countings in Baryons\*

J. L. Goity

*Department of Physics, Hampton University, Hampton, USA;  
Thomas Jefferson National Accelerator Facility, Newport News, USA*

Received June 2, 2004; in final form, September 7, 2004

**Abstract**—The  $1/N_c$ -power countings for baryon decays and configuration mixings are determined by means of a nonrelativistic quark picture. Such countings are expected to be robust under changes in the quark masses and, therefore, valid as these become light. It is shown that excited baryons have natural widths of  $\mathcal{O}(N_c^0)$ . These dominant widths are due to the decays that proceed directly to the ground-state baryons, with cascade decays being suppressed to  $\mathcal{O}(1/N_c)$ . Configuration mixings, defined as mixings between states belonging to different  $O(3) \times SU(2N_f)$  multiplets, are shown to be subleading in an expansion in  $1/\sqrt{N_c}$  when they involve the ground-state baryons, while the mixings between excited states can be  $\mathcal{O}(N_c^0)$ . © 2005 Pleiades Publishing, Inc.

## 1. INTRODUCTION

In this contribution to the proceedings honoring Prof. Yuri Simonov on his 70th birthday, I address some of the still open issues concerning the  $1/N_c$ -power counting for baryons. In particular, the power counting for the decay widths of excited baryons as well as for configuration mixings is analyzed. Several new conclusions result from this analysis. The  $1/N_c$  expansion is one of the methods to which Prof. Yu. Simonov has made important contributions in his extensive work in QCD.

The  $1/N_c$  expansion was introduced by 't Hooft in a notable paper [1] thirty years ago. Although it has not led to the ultimate goal of “solving” QCD in its nonperturbative domain through analytic tools, it has proven to be powerful at the level of effective theory. The ability of implementing an ordering in powers of  $1/N_c$  at the hadronic level has led to the understanding of numerous phenomenological facts. The large- $N_c$  properties of mesons and their interactions can be established with little difficulty from the topological picture provided in 't Hooft's original paper [1]. The implementation of the expansion in combination with chiral perturbation theory (ChPT) in the light pseudoscalar sector [2] is one example of how it can be made to work at an effective theory level. In the other qualitatively different sector, namely, the baryons, the implementation of the  $1/N_c$  expansion is substantially more involved. The pioneering work by Witten [3] provided the guiding ideas for that implementation, and subsequent works by Gervais and Sakita [4] and by Dashen and Manohar [5] established the framework for the study of ground-state

baryons. In this framework, a key role is played by the emergent spin-flavor symmetry in the large- $N_c$  limit. This provides the basis for the so-called operator analysis that has been applied extensively to the ground-state baryons [6, 7]. The derivation of the spin-flavor structure can also be carried out in a less formal fashion than in [4, 5] by means of a nonrelativistic quark picture [8, 9]. At the effective theory level, based on the results of the operator analysis, it has been possible to bring the strictures of the  $1/N_c$  expansion into baryon ChPT [10]. Here, and because the baryon flavor multiplet contents depend on  $N_c$ , the formulation of the effective theory is somewhat complicated. The operator analysis has been further extended to the sector of excited baryons [11–13], where by now many results have been obtained [14–18]. These results, in particular, show that the  $1/N_c$  expansion can play an important and useful role in sorting out the apparently complicated dynamics that determine the properties of baryonic resonances.

Although the operator analysis for excited baryons is fairly well established, there have been a few open questions regarding the  $1/N_c$  power counting for the decay widths, and the issue of configuration mixings, where states belong to different spin-flavor and/or orbital multiplets, has been little studied. In this paper, both aspects are addressed by means of a nonrelativistic quark picture. This picture is expected to reliably determine these  $1/N_c$  power countings.

## 2. BARYONS IN THE LARGE- $N_c$ LIMIT

The first step towards implementing an analysis of baryons in the framework of the  $1/N_c$  expansion

\*This article was submitted by the author in English.

is to establish the counting rules associated with the different operators that are needed in an effective theory. To proceed with this, it is convenient to work in the limit where the quark masses are large enough for a nonrelativistic picture to be reliable. In this way, the problem of determining the  $1/N_c$  counting is significantly simplified. Because the  $1/N_c$  counting should be largely unaffected by the quark masses, the counting established in that limit should hold also for the situation where current quark masses are small. In the following, therefore, the discussion is based on such a nonrelativistic quark picture of baryons.

Using that approach, Witten [3] showed that, obviously, baryon masses are proportional to  $N_c$ , while the baryon size is only affected by corrections  $\mathcal{O}(1/N_c)$ . In consequence, baryons are compact systems in large- $N_c$ , allowing for the rigorous usage of the effective potential approach à la Hartree. A baryon state can be expressed as follows:

$$|\Psi\rangle = \frac{1}{N_c!} \int \prod_{j=1}^{N_c} d^3x_j \Psi_{\xi_1, \dots, \xi_{N_c}}(x_1, \dots, x_{N_c}) \quad (1)$$

$$\times \epsilon_{\alpha_1, \dots, \alpha_{N_c}} |x_1, \xi_1, \alpha_1; \dots; x_{N_c}, \xi_{N_c}, \alpha_{N_c}\rangle,$$

where  $x_i$  are spatial positions,  $\xi_i$  are spin-flavor indices, and  $\alpha_i$  are color indices. The states defined in terms of the nonrelativistic quark creation operators with the standard anti-commutation relations are given by

$$|x_1, \xi_1, \alpha_1; \dots; x_{N_c}, \xi_{N_c}, \alpha_{N_c}\rangle \quad (2)$$

$$= \int \prod_{j=1}^{N_c} \frac{d^3k_j}{(2\pi)^3} e^{ik_j x_j} q_{\xi_1 \alpha_1}^\dagger(k_1) \dots q_{\xi_{N_c} \alpha_{N_c}}^\dagger(k_{N_c}) |0\rangle.$$

The wave functions  $\Psi_{\xi_1, \dots, \xi_{N_c}}(x_1, \dots, x_{N_c})$  are totally symmetric under simultaneous permutations of positions and spin-flavor labels, and they satisfy the normalization

$$\int \prod_{j=1}^{N_c} d^3x_j \Psi_{\xi_1, \dots, \xi_{N_c}}^*(x_1, \dots, x_{N_c}) \quad (3)$$

$$\times \Psi_{\xi_1, \dots, \xi_{N_c}}(x_1, \dots, x_{N_c}) = 1.$$

A convenient basis of wave functions is furnished by functions factorized into a spatial and a spin-flavor part added over permutations, namely,

$$\sum_{\sigma} \chi_{\xi_{\sigma_1}, \dots, \xi_{\sigma_{N_c}}} \psi(x_{\sigma_1}, \dots, x_{\sigma_{N_c}}). \quad (4)$$

In particular, it is convenient to take the spin-flavor wave functions  $\chi$  to belong to an irreducible representation of the spin-flavor group  $SU(2N_f)$  if one is considering the case of  $N_f$  flavors with degenerate or nearly degenerate masses. This means that such

wave functions also belong to an irreducible representation of the permutation group of the  $N_c$  indices. The crucial role played by the spin-flavor group in the large- $N_c$  limit makes this choice of basis natural. In a Hartree picture, the spatial wave function  $\psi$  will have the form of a product of  $N_c$  one-quark wave functions. Ground-state baryons in the large- $N_c$  limit will therefore have wave functions of the form

$$\Psi_{\xi_1, \dots, \xi_{N_c}}^{\text{g.s.}}(x_1, \dots, x_{N_c}) = \chi_{\xi_1, \dots, \xi_{N_c}}^S \prod_{i=1}^{N_c} \phi(x_i), \quad (5)$$

where the one-quark spatial wave function  $\phi$  is an  $S$  wave. Later on, the admixture in the ground state of other spatial wave functions will be addressed (e.g.,  $D$ -wave components) and shown to be a subleading effect. The spin-flavor wave function here must be totally symmetric, this being indicated by the upper label “ $S$ .”

Excited baryons result from exciting one or more quarks, leaving a core of quarks in the ground state. A quark in the core has, up to corrections proportional to  $1/N_c$ , the same wave function as a quark in the ground-state baryons. Although only excited states with one excited quark are going to be discussed in detail, the generalization to two or more excited quarks can be carried out quite easily. The wave functions with one excited quark come in two types, namely, symmetric ( $S$ ) and mixed-symmetric ( $MS$ ) in spin-flavor. They are, respectively, given by

$$\Psi_{\xi_1, \dots, \xi_{N_c}}^S(x_1, \dots, x_{N_c}) \quad (6)$$

$$= \frac{1}{\sqrt{N_c}} \chi_{\xi_1, \dots, \xi_{N_c}}^S \sum_{i=1}^{N_c} \phi(x_1) \dots \phi'(x_i) \dots \phi(x_{N_c}),$$

$$\Psi_{\xi_1, \dots, \xi_{N_c}}^{\text{MS}}(x_1, \dots, x_{N_c}) = \frac{1}{\sqrt{N_c(N_c - 1)!}}$$

$$\times \sum_{\sigma} \chi_{\xi_{\sigma_1}, \dots, \xi_{\sigma_{N_c}}}^{\text{MS}} \phi(x_{\sigma_1}) \dots \phi(x_{\sigma_{N_c-1}}) \phi'(x_{\sigma_{N_c}}),$$

where  $\phi'$  is the excited quark wave function which is taken to be orthonormal to the ground-state wave function  $\phi$ . The  $MS$  spin-flavor wave function  $\chi^{\text{MS}}$  belongs to the representation with a Young tableaux having  $N_c - 1$  boxes in the first row and one box in the second row. In this case, the last index in the spin-flavor wave function is the one associated with the excited quark. The normalization of the spin-flavor wave functions is conveniently chosen to be unity so that the one-quark spatial wave functions have the same normalization.

There is one point that needs mention. This is the center-of-mass degree of freedom that the wave functions used here do not treat properly. The effects introduced by this deficiency are in general subleading

in  $1/N_c$  and should not, therefore, affect the power countings addressed here. However, there is the possibility that countings, which are suppressed only on orthogonality grounds of one-quark wave functions used here, will be modified when the center-of-mass motion is properly treated.

Since the contents of this paper have to do with the  $1/N_c$  counting of operator matrix elements, it is convenient at this point to define operators in the current framework. The nonrelativistic quark field operator from which the various composite operators can be built reads

$$q_{\xi\alpha}(x) = \int \frac{d^3k}{(2\pi)^3} \sum_{\lambda} q_{\lambda}(k) u_{\xi\alpha}^{\lambda}(k) e^{ikx}, \quad (7)$$

where  $\lambda$  represents the polarization in color and spin-flavor. A natural choice for it is just in terms of the color and spin-flavor projections that make the Pauli spinor become delta functions,

$$u_{\xi\alpha}^{\lambda=\xi'\alpha'}(k) = \delta_{\xi\xi'} \delta_{\alpha\alpha'}. \quad (8)$$

Note that, throughout the analysis that follows, all operators have the same time argument, and therefore only the position vectors  $x$  are displayed.

A color singlet one-body local operator has the general form

$$\Gamma_1(x) = q_{\xi\alpha}^{\dagger}(x) \Gamma_{\xi\xi'}(x) q_{\xi'\alpha}(x), \quad (9)$$

where  $\Gamma_{\xi\xi'}(x)$  is some functional operator acting on the quark fields. Note here that no generality for the application in this paper is gained by considering nonlocal operators. An explicit evaluation of the matrix elements of one-body operators between generic baryonic states leads to

$$\begin{aligned} \langle \Psi' | \Gamma_1(x) | \Psi \rangle &= \int \prod_{j=1}^{N_c-1} d^3x_j dx'_{N_c} dx_{N_c} \quad (10) \\ &\times \Psi_{\xi_1, \dots, \xi_{N_c-1}, \xi'_{N_c}}^{I^*}(x_1, \dots, x_{N_c-1}, x'_{N_c}) \Gamma_{\xi'\xi}(x) \\ &\times \Psi_{\xi_1, \dots, \xi_{N_c-1}, \xi_{N_c}}(x_1, \dots, x_{N_c-1}, x_{N_c}) \\ &\times \int \frac{d^3k d^3k'}{(2\pi)^6} e^{ik(x_{N_c}-x)} e^{-ik'(x'_{N_c}-x)} \\ &\times \delta_{\lambda(\xi_{N_c}, \alpha)} \delta_{\lambda'(\xi'_{N_c}, \alpha')} u_{\xi'\alpha'}^{\lambda'\dagger}(k') u_{\xi\alpha}^{\lambda}(k). \end{aligned}$$

The sum over polarizations boils down to a factor  $N_c$  from the sum over color indices times a spin-flavor factor  $\delta_{\xi\xi_{N_c}} \delta_{\xi'\xi'_{N_c}}$ . This can be easily seen using the natural basis of Pauli spinors and performing the momentum integrations. As expected, the final form is

$$\langle \Psi' | \Gamma_1(x) | \Psi \rangle = N_c \int \prod_{j=1}^{N_c-1} d^3x_j \quad (11)$$

$$\begin{aligned} &\times \Psi_{\xi_1, \dots, \xi_{N_c-1}, \xi'}^{I^*}(x_1, \dots, x_{N_c-1}, x) \Gamma_{\xi'\xi}(x) \\ &\times \Psi_{\xi_1, \dots, \xi_{N_c-1}, \xi}(x_1, \dots, x_{N_c-1}, x). \end{aligned}$$

As an illustration, consider the important case of the axial-vector current operator

$$A_{ia}(x) \equiv \frac{1}{4} q_{\alpha}^{\dagger}(x) \sigma_i t_a q_{\alpha}(x) = q_{\alpha}^{\dagger}(x) g_{ia} q_{\alpha}(x), \quad (12)$$

where  $t_a$  are flavor generators. For the sake of simplicity, consider here the case of two flavors and the matrix elements between ground-state baryons. Applying Eq. (11), the matrix elements are given by

$$\begin{aligned} \langle \Psi'_{g.s} | A_{ia}(x) | \Psi_{g.s} \rangle &= N_c \chi_{\xi_1, \dots, \xi_{N_c-1}, \xi'_{N_c}}^{I^* S \dagger} \quad (13) \\ &\times (g_{ia})_{\xi'_{N_c} \xi_{N_c}} \chi_{\xi_1, \dots, \xi_{N_c-1}, \xi_{N_c}}^S \phi^*(x) \phi(x). \end{aligned}$$

The matrix elements of the spin-flavor generator  $g_{ia}$  taken as shown in this equation are order  $N_c^0$  when the spin-flavor wave functions have spin  $\mathcal{O}(N_c^0)$  (for two flavors, the symmetric spin-flavor states have all  $I = S$ ). Thus, the result is that the axial current matrix elements are order  $N_c$ . As a check, it is easy to verify that the matrix elements of the spin and isospin operators are, as they should be,  $\mathcal{O}(N_c^0)$ . Operators that, like the axial currents, receive the  $N_c$  factor enhancement are called coherent operators.

The above example leads to important implications. Since pions couple to baryons through the axial-vector current, the pion couplings are proportional to  $N_c/F_{\pi} = \mathcal{O}(\sqrt{N_c})$  ( $F_{\pi}$  scales as  $\sqrt{N_c}$ ). As is briefly discussed in the next section, this large- $N_c$  behavior of the  $\pi$ -baryon couplings demands the existence of a spin-flavor dynamical symmetry. Such a symmetry is the main reason why, in the large- $N_c$  limit, there is a simplified picture of baryons.

Continuing with the issue of operators, consider now two-body operators. A generic color singlet operator has the general form

$$\Gamma_2(x, y) = q^{\dagger}(x) \otimes q(x) q^{\dagger}(y) \otimes q(y) \Gamma(x, y), \quad (14)$$

where color and flavor indices are contracted through the tensor operator  $\Gamma(x, y)$ . A lengthier but equally straightforward evaluation as in the case of the one-body operators gives the following expression for two-body operator matrix elements:

$$\begin{aligned} \langle \Psi' | \Gamma_2(x, y) | \Psi \rangle &= \frac{N_c - 1}{N_c} \quad (15) \\ &\times \int \prod_{j=1}^{N_c-2} d^3x_j dx_{N_c-1} dx_{N_c} dx'_{N_c-1} dx'_{N_c} \\ &\times \Psi_{\xi_1, \dots, \xi_{N_c-2}, \xi'_{N_c-1}, \xi'_{N_c}}^{I^*}(x_1, \dots, x_{N_c-2}, x'_{N_c-1}, x'_{N_c}) \\ &\quad \times \Gamma(x, y) \\ &\times \Psi_{\xi_1, \dots, \xi_{N_c-2}, \xi_{N_c-1}, \xi_{N_c}}(x_1, \dots, x_{N_c-2}, x_{N_c-1}, x_{N_c}) \end{aligned}$$

$$\begin{aligned}
 & \times \int \frac{d^3 k_1 d^3 k_2 d^3 k'_1 d^3 k'_2}{(2\pi)^{12}} \times \int d^3 x d^3 y \phi^*(x) \phi^*(y) \phi(x) \phi(y) \\
 & \times e^{i(k_1(x_{N_c} - x) - k'_1(x'_{N_c} - x))} \times \left( -\frac{1}{4|x-y|} + \frac{1}{4m_q^2} \right) \\
 & \times e^{i(k_2(x_{N_c-1} - y) - k'_2(x'_{N_c-1} - y))} \times \left( \left( -\pi\delta^3(x-y) + \frac{1}{4|x-y|^3} \right) \delta_{ij} \right. \\
 & \quad \times \left. \left( -\frac{3(x-y)_i(x-y)_j}{4|x-y|^5} \right) \right) \\
 & \quad \times \chi_{\xi_1, \dots, \xi'_{N_c-1}, \xi'_{N_c}}^{S*} s_{\xi'_{N_c-1} \xi_{N_c-1}}^i s_{\xi'_{N_c} \xi_{N_c}}^j \chi_{\xi_1, \dots, \xi_{N_c-1}, \xi_{N_c}}^S \\
 & \quad \times u^{\dagger \lambda'_1}(k'_1) \otimes u^{\lambda_1}(k_1) \\
 & \quad \times u^{\dagger \lambda'_2}(k'_2) \otimes u^{\lambda_2}(k_2) \delta_{\lambda_1, (\xi_{N_c} \alpha_{N_c})} \\
 & \quad \times \delta_{\lambda_2, (\xi_{N_c-1} \alpha_{N_c-1})} (\delta \lambda'_1, (\xi'_{N_c} \alpha_{N_c-1})) \\
 & \quad \times \delta \lambda'_2, (\xi'_{N_c-1} \alpha_{N_c}) \\
 & \quad - \delta \lambda'_1, (\xi'_{N_c} \alpha_{N_c}) \delta \lambda'_2, (\xi'_{N_c-1} \alpha_{N_c-1}).
 \end{aligned}$$

This can be further evaluated, leading to

$$\begin{aligned}
 \langle \Psi' | \Gamma_2(x, y) | \Psi \rangle &= \frac{N_c - 1}{N_c} \int \prod_{j=1}^{N_c-2} d^3 x_j \quad (16) \\
 & \times \Psi_{\xi_1, \dots, \xi_{N_c-2}, \xi'_{N_c-1}, \xi'_{N_c}}^* (x_1, \dots, x_{N_c-2}, x, y) \\
 & \quad \times \left( \Gamma_{\xi_{N_c} \alpha_{N_c}, \xi'_{N_c-1} \alpha_{N_c}}^{\xi'_{N_c} \alpha_{N_c-1}, \xi'_{N_c-1} \alpha_{N_c}}(x, y) \right. \\
 & \quad \left. - \Gamma_{\xi_{N_c} \alpha_{N_c}, \xi'_{N_c-1} \alpha_{N_c-1}}^{\xi'_{N_c} \alpha_{N_c}, \xi'_{N_c-1} \alpha_{N_c-1}}(x, y) \right) \\
 & \times \Psi_{\xi_1, \dots, \xi_{N_c-2}, \xi_{N_c-1}, \xi_{N_c}} (x_1, \dots, x_{N_c-2}, x, y).
 \end{aligned}$$

An illustrative application of relevance for baryon masses is the one-gluon-exchange interaction. The two-body operator associated with it is given by (disregarding spin-independent pieces that are order  $1/m_q^2$  and other momentum-dependent terms which do not affect the point of the discussion)

$$\begin{aligned}
 \mathcal{H}_{\text{OGE}}(x-y) &\sim g^2 \quad (17) \\
 & \times \left( -\frac{1}{|x-y|} q^\dagger(x) \frac{\lambda^A}{2} q(x) q^\dagger(y) \frac{\lambda^A}{2} q(y) \right. \\
 & + \frac{1}{4m_q^2} \left( \left( -4\pi\delta^3(x-y) + \frac{1}{|x-y|^3} \right) \delta_{ij} \right. \\
 & \quad \left. \left. - 3\frac{(x-y)_i(x-y)_j}{|x-y|^5} \right) \right. \\
 & \quad \left. \times q^\dagger(x) \sigma_i \frac{\lambda^A}{2} q(x) q^\dagger(y) \sigma_j \frac{\lambda^A}{2} q(y) \right),
 \end{aligned}$$

where  $\lambda^A$  are the  $SU(N_c)$  generators in the fundamental representation. The first term on the right-hand side is the color Coulomb interaction and the second term is the hyperfine interaction. When this is applied to the ground-state baryons, the mass shift due to one-gluon exchange has the structure

$$\langle \Psi_{g.s.} | H_{\text{OGE}} | \Psi_{g.s.} \rangle \sim g^2 \frac{N_c - 1}{N_c} \frac{N_c^2 - 1}{2} \quad (18)$$

The factor  $(N_c^2 - 1)$  stems from the trace over color indices. Taking into account that  $g^2 = \mathcal{O}(1/N_c)$ , the Coulomb interaction gives a contribution  $\mathcal{O}(N_c)$  that is independent of the spin-flavor of the state. The spin matrix elements in the hyperfine term only contribute for  $s_i s_j$  coupled to zero angular momentum. Thus, for states with spin  $\mathcal{O}(N_c^0)$ , the spin-flavor matrix elements in Eq. (18) satisfy

$$\langle \chi^S | s^i s^i | \chi^S \rangle = \mathcal{O}\left(\frac{1}{N_c}\right) \mathbf{1} + \mathcal{O}\left(\frac{1}{N_c^2}\right); \quad (19)$$

i.e., they have a spin-flavor-independent piece  $\mathcal{O}(1/N_c)$  and a spin-flavor-dependent piece  $\mathcal{O}(1/N_c^2)$ . This implies that the hyperfine interaction gives a spin-flavor-independent mass shift of  $\mathcal{O}(N_c^0)$  and a breaking of spin-flavor symmetry of  $\mathcal{O}(1/N_c)$ . This important result establishes that the spin-flavor tower of ground-state baryons has splittings that are suppressed by  $1/N_c$  for states with spins  $\mathcal{O}(N_c^0)$ .

Recently [19], a bosonic operator method has been introduced that should equally serve to carry out the derivations made in this section.

### 3. GROUND-STATE BARYONS

The previous section gave the tools for determining the counting in the  $1/N_c$  expansion associated with various matrix elements. In all cases, the counting is in the end determined by a few characteristics of the operator being considered, namely, their  $n$ -bodiness and spin-flavor structure, and, as shown later, by the spin-flavor representation to which the states belong and the degree of excitation of the states (number of excited quarks). This permits the implementation of the counting at the effective theory level. This section briefly outlines how this has been carried out for the ground-state baryons.

The result at the end of the previous section can be put in a more general framework in which the

constraints of unitarity in pion–baryon scattering demand a dynamical spin–flavor symmetry [4, 5]. This symmetry is of course satisfied by the nonrelativistic quark picture. Thanks to the spin–flavor symmetry, ground-state baryons can be chosen to fill an  $SU(2N_f)$  multiplet, namely, the totally symmetric irreducible representation with  $N_c$  spin–flavor indices. Any color singlet operator in QCD will then be represented at the level of the effective theory by a series of composite effective operators ordered in powers of  $1/N_c$ . These composite operators, when acting on a specific spin–flavor representation, can be further represented via the Wigner–Eckart theorem by appropriate products of generators of the spin–flavor group [5, 6]. For instance, the matrix elements of the QCD Hamiltonian between ground-state baryons give the masses of these states. The most general mass operators that one could write down are proportional to  $\mathbf{1}$ ,  $S^2$ ,  $G^2$ ,  $T^2$ , etc. Here,  $S_i$ ,  $T_a$ , and  $G_{ia}$  are the generators of  $SU(2N_f)$ , which in the nonrelativistic quark picture are given by

$$\begin{aligned} S_i &= \frac{1}{2} \int q^\dagger(x) \sigma_i q(x) d^3x, \\ T_a &= \frac{1}{2} \int q^\dagger(x) t_a q(x) d^3x, \\ G_{ia} &= \frac{1}{4} \int q^\dagger(x) \sigma_i t_a q(x) d^3x. \end{aligned} \quad (20)$$

The  $1/N_c$  counting associated with an  $n$ -body effective operator is given by the general formula

$$\nu = N_c^{(1-n)} N_c^\kappa, \quad (21)$$

where  $\nu$  is the order in  $1/N_c$  of the matrix elements of the operator. The first factor on the right-hand side results from the fact that, in order to generate an effective  $n$ -body operator starting from a one-body operator at the QCD level,  $n - 1$  gluon exchanges are necessary (this factor is usually included in the definition of the effective operator as shown below), and the second factor results from the number  $\kappa$  of coherent factors (the generator  $G$  above is a coherent factor as the result in the previous section about the axial current matrix elements shows). As an illustration, consider the mass operator for the ground-state baryons (for the sake of simplicity, take two degenerate flavors, where  $S = I$ ). The most general mass operator that one can write down is therefore

$$\begin{aligned} H_{\text{g.s. mass}} &= N_c m_0 \cdot \mathbf{1} \\ &+ m_1 \frac{1}{N_c} S^2 + m'_1 \frac{1}{N_c} G^2 + \text{3-body} + \dots \end{aligned} \quad (22)$$

The first term gives the overall spin–flavor singlet  $\mathcal{O}(N_c)$  mass, and the second term gives the  $\mathcal{O}(1/N_c)$  mass splittings. On the other hand, the third term,

which according to the counting rule given above is  $\mathcal{O}(N_c)$ , turns out to be linearly dependent up to  $\mathcal{O}(1/N_c)$  with the first two terms, and therefore to that order it can be eliminated (a series of such reduction rules have been established [6]). Thus, up to and including  $\mathcal{O}(1/N_c)$  effects, the ground-state baryon masses can be represented by the first two terms on the right-hand side of Eq. (22). Ground-state matrix elements associated with other operators (axial currents, magnetic moments, etc.) have been extensively analyzed elsewhere [7].

#### 4. EXCITED BARYONS

The existence of a spin–flavor symmetry at the level of ground-state baryons suggests that such a symmetry ought to play an important role in excited baryons. An approach that has been proposed [9, 12, 13], which is the natural one in the nonrelativistic quark picture, is to describe the excited baryons using a basis of states filling multiplets of the  $O(3) \times SU(2N_f)$  group. The  $O(3)$  group has as generators the orbital angular momentum operators. While in the ground-state baryons the spin–flavor symmetry is broken at  $\mathcal{O}(1/N_c)$ , in the excited baryons the extended  $O(3) \times SU(2N_f)$  symmetry can be broken at zeroth order [12]. The reason for this zeroth-order breaking is the possibility of spin–orbit couplings. In the quark picture, this can be easily demonstrated. The induced Thomas precession term, which is represented by a one-body operator of  $\mathcal{O}(N_c^0)$ , reads

$$H_{\text{SO}} = w \mathbf{l} \cdot \mathbf{s}, \quad (23)$$

where the parameter  $w$  contains the details about the binding of the excited quark in the baryon and  $\mathbf{s}$  is the spin operator acting on the excited quark. Upon calculating its matrix elements for excited states with the generic wave functions

$$\begin{aligned} \Psi'_{\xi_1, \dots, \xi_{N_c}}(x_1, \dots, x_{N_c}) &= \frac{1}{\sqrt{N_c(N_c - 1)!}} \\ &\times \sum_{\sigma} \chi'_{\xi_{\sigma_1}, \dots, \xi_{\sigma_{N_c}}} \phi(x_{\sigma_1}) \dots \phi(x_{\sigma_{N_c-1}}) \phi'(x_{\sigma_{N_c}}), \end{aligned} \quad (24)$$

the spin–orbit mass shift has the form

$$\langle \Psi' | H_{\text{SO}} | \Psi' \rangle = w \mathbf{l}_i \langle \chi | s_i | \chi \rangle, \quad (25)$$

where in the spin–flavor matrix element the spin operator  $s_i$  acts only on the spin of the excited quark (i.e., the last index of the spin–flavor wave function). If  $\chi$  belongs to the symmetric spin–flavor representation,  $\langle \chi | s_i | \chi \rangle$  is  $\mathcal{O}(1/N_c)$ , while, if it belongs to the MS representation, the result is  $\mathcal{O}(N_c^0)$ . Thus, the spin–orbit coupling affects states in the MS representation at order  $N_c^0$ . Among other effects, this leads

to a breaking of spin–flavor symmetry at the same order [12]. This would seem to have bad consequences for the spin–flavor symmetry in MS states, but it turns out not to be so. First, the spin–orbit breaking leaves a remnant symmetry associated with states of the core of  $N_c - 1$  quarks as shown in [20, 21]. This remnant symmetry is broken at subleading order by hyperfine effects. Second, as various detailed analyses have shown [12, 14, 15], the spin–orbit effects in the  $SU(6)$  70-plet of negative parity baryons are unnaturally small for not as yet fully understood dynamical reasons (substantially smaller than the subleading hyperfine effects). From a practical point of view, this implies that the basis of states in terms of multiplets of  $O(3) \times SU(2N_f)$  is very useful. Other operators that couple the orbital angular momentum do contribute to zeroth-order spin–flavor breaking. The complete analysis of the negative-parity baryon masses [12, 14, 15] shows in general that the zeroth-order breaking is unnaturally small.

The operator analysis in the case of excited baryons proceeds in analogy with that for the ground-state baryons, except that now one has an extended set of generators that includes the orbital angular momentum generators. The details of the procedure have been given elsewhere [12, 14, 15] and will not be repeated here.

The main point of this paper is to establish a few results of general validity and importance for excited baryons. These have to do with the  $1/N_c$  counting for the various decays of excited baryons and with the possible mixings of  $O(3) \times SU(2N_f)$  multiplets (configuration mixings).

#### 4.1. Decays

The original work of Witten [3] indicated, correctly as shown below, that excited baryons have width order  $N_c^0$ . This is in sharp contrast with mesons, which become stable in the large- $N_c$  limit, their widths being  $\mathcal{O}(1/N_c)$  or higher. More recently, some questions have been raised about the general validity of that zeroth-order result. An appraisal of the situation can be found in [22].

Since the determination of the  $1/N_c$  counting for the widths will not depend on fine details, a model for the decay process through one-pion emission can be used. The emission of an  $\eta$  meson such as in the decay  $N^*(1535) \rightarrow N\eta$  will be briefly mentioned as well. The model for the discussion is the chiral quark model [23] in which the pion couples to the constituent quark according to

$$H_{\text{ChQM}} = -\frac{g_A^q}{4F_\pi} \int d^3x \partial_i \pi_a(x) q^\dagger(x) \sigma_i \tau_a q(x), \quad (26)$$

where  $g_A^q$  is the constituent quark axial-vector coupling of order  $N_c^0$ . Using the one-body Eq. (11), the amplitudes for the various possible transitions are readily calculated. The first type of transitions are the ones that occur within a multiplet. The dominant amplitude for these transitions is easy to obtain using the result already derived in Section 2 for the matrix elements of the axial-vector currents to which the pion couples as shown by the above Hamiltonian. For ground-state as well as excited baryons, these amplitudes are in general proportional to  $\sqrt{N_c}$ . The ground-state widths in this case are suppressed by phase space as the baryon states for which the amplitude is order  $\sqrt{N_c}$  have mass differences that are order  $1/N_c$ . Because these transitions are  $P$ -wave, the end result is that the partial widths are  $\mathcal{O}(1/N_c^2)$ . One such transition is the  $\Delta \rightarrow \pi N$  transition. Note that, for states at the top of the ground-state tower, the amplitude is proportional to  $1/\sqrt{N_c}$ , and since the splittings are zeroth order, the widths are  $\mathcal{O}(1/N_c)$ . In the real world,  $\Delta$  is the second and top state of the tower, and its width should therefore be between the two limits. The transitions within an excited multiplet containing zeroth-order mass splittings can be shown to have amplitudes  $\sim \sqrt{N_c}$  only between states whose relative mass splittings are  $\mathcal{O}(1/N_c)$ . The reason is that these amplitudes only change the core’s state, and such a change can only affect the energy level through a two-body mass operator. Since the core piece of matrix elements of the two-body operator can only be affected at  $\mathcal{O}(N_c^0)$  by that change of the core state, the effect on the energy level must be at most  $\mathcal{O}(1/N_c)$ .

The second kind of transitions are from excited baryons to ground-state baryons. The decay amplitudes in this case have the form

$$\begin{aligned} \langle \Psi_{\text{g.s.}} + \pi | \Psi' \rangle &= \frac{g_A^q}{F_\pi} \sqrt{N_c} k_{\pi_i} \quad (27) \\ &\times \int d^3x e^{ik_\pi x} \phi^*(x) \phi'(x) \langle \chi^S | g_{ia} | \chi' \rangle, \end{aligned}$$

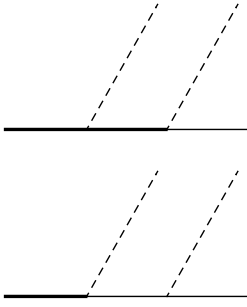
where

$$\langle \chi^S | g_{ia} | \chi' \rangle = \chi_{\xi_1, \dots, \xi'_{N_c}}^{S*} (g_{ia})_{\xi'_{N_c} \xi_{N_c}} \chi'_{\xi_1, \dots, \xi_{N_c}}. \quad (28)$$

These spin–flavor matrix elements are order  $N_c^0$  for both symmetric and MS  $\chi'$ . Thus, irrespective of the spin–flavor character of the excited state, the decay rate to the ground state via one-pion emission is of zeroth order in the  $1/N_c$  expansion.

The third type of transitions are those between different excited baryon multiplets, where now the amplitude becomes

$$\langle \Psi'' + \pi | \Psi' \rangle = \frac{g_A^q}{F_\pi} k_{\pi_i} \quad (29)$$



The thick solid line represents excited baryons belonging to a single multiplet, the thin one represents a ground-state baryon, and the dashed lines represent pions. The vertices connecting an excited and ground-state baryon are proportional to  $1/\sqrt{N_c}$  for two-quark excited baryons, while the other vertices are proportional to  $\sqrt{N_c}$ .

$$\times \int d^3x e^{ik_\pi x} \phi^{**}(x) \phi'(x) \langle \chi'' | g_{ia} | \chi' \rangle.$$

This amplitude is similar to that for the transition to the ground state except for the absence of the factor  $\sqrt{N_c}$ . Thus, the transition amplitudes between excited states are generically suppressed by a factor  $1/\sqrt{N_c}$  with respect to the ones to the ground state. This has an important implication; namely, in the large- $N_c$  limit, the dominant channel of decay for excited baryons is the direct decay to the ground state. If  $\eta$  emission is considered, the analysis is similar except that  $g_{ia}$  is replaced by  $s_i$ . The result in this case is that the corresponding spin-flavor matrix elements are  $\mathcal{O}(N_c^0)$  if  $\chi'$  is in the MS representation and  $\mathcal{O}(1/N_c)$  if it is in the symmetric representation. These countings have been used to implement the operator analysis for the decays of the negative-parity baryons [11, 24] as well as the Roper multiplet [16].

The discussion above is valid for excited states where only one quark is excited. If more than one quark is excited, further suppressions occur, namely, a factor  $1/\sqrt{N_c}$  per excited quark. In these cases, it is necessary to consider two- or higher body decay operators. With omission of the details, for two excited quarks, the decay amplitude with emission of a single-pion is order  $1/\sqrt{N_c}$  for decay to the ground state and order  $1/N_c$  for decay to other excited states. This implies that the decay rate via single-pion emission is order  $1/N_c$ . The total width is, however, expected to be of zeroth order. The answer to this riddle seems to be that the two-pion emission is order  $N_c^0$ . One way to see this is shown by the diagrams in the figure, where the suppression factor in one amplitude, the one connecting excited and ground states, is compensated by the enhancement

factor of the amplitude connecting states in the same multiplet. This implies that these excited states decay predominantly by emitting two pions. There is a subtlety to be dealt with here. It has to do with the application of the same mechanism to the baryons with only one excited quark. Naively, for these states, the dominant contribution for two-pion emission would then be order  $\sqrt{N_c}$ , which cannot be right. Such an unacceptable contribution must be canceled through the interference of the various baryonic intermediate states. This results from consistency relations similar to those that eliminate the order- $N_c$  terms in  $\pi$ -baryon scattering [5, 13]. This issue of consistency relations involving excited baryons in general has not been extensively analyzed, and it certainly deserves further consideration.

The discussions of the decays have been carried out in a limited framework. This, however, should fully clarify the picture: for excited baryons, the decay amplitudes are of zeroth order, so that, when building an effective theory such as in [11, 16, 24], it is necessary to carefully trace the power counting; namely, for one-pion decays, there is a factor  $1/F_\pi$ , whose origin is rather obvious, and there is the less obvious factor of  $\sqrt{N_c}$  that is shown in Eq. (27), whose origin is very clear in the model considered here.

#### 4.2. Configuration Mixing

All large- $N_c$  analyses carried out in the literature disregard the mixing of different spin-flavor as well as orbital states. As the following discussion shows, this is in most cases the correct thing to do. The only relevant mixings that are of any significance are mixings between states belonging to different representations of  $O(3) \times SU(2N_f)$ , for instance, the admixture of  $\ell = 2$  states in the ground-state baryons and/or the admixture of states belonging to the symmetric and MS spin-flavor representations. In this subsection, the  $1/N_c$  countings for the various mixings are obtained.

The Hamiltonian that drives the mixings is rotationally invariant, which means that, under  $O(3) \times SU_{\text{spin}}(2)$ , it must transform, in obvious notation, as  $(\ell, s = \ell)$ . It is also taken to be flavor symmetric.

There is only one one-body operator that can produce configuration mixing, namely, the spin-orbit operator [22]. This operator can only give  $\Delta\ell = 0$  mixings of symmetric and MS spin-flavor representations. The mixing amplitudes are given by a formula similar to (25):

$$\langle \Psi'' | H_{\text{SO}}^{\text{mix}} | \Psi' \rangle = c \ell_i \langle \chi^{\text{MS}} | s_i | \chi^{\text{S}} \rangle, \quad (30)$$

where  $c$  is of zeroth order and the spin-flavor matrix element is  $\mathcal{O}(N_c^0)$ . Thus, at the one-body level, there

is zeroth-order  $\Delta\ell = 0$  mixing between states with  $\ell > 0$ .

At the level of two-body operators, other mixing possibilities exist, in particular, mixings involving the ground-state baryons. A generic two-body Hamiltonian that contributes to mixing is

$$H_{\text{mix}} = \frac{1}{N_c} \int d^3x d^3y L_{ij}(x, y) \mathcal{S}_{ij}, \quad (31)$$

where  $L_{ij}$  is a tensor operator of up to rank 2, and  $\mathcal{S}_{ij}$  is a spin-flavor operator that is a flavor singlet.

The mixing amplitude for two generic states is readily determined by applying Eq. (16). Up to sub-leading terms in  $1/N_c$ , the result is

$$\begin{aligned} \langle \Psi' | H_{\text{mix}} | \Psi \rangle &= -N_c \quad (32) \\ &\times \int \prod_{j=1}^{N_c} d^3x_j \Psi_{\xi_1, \dots, \xi'_{N_c-1}, \xi'_{N_c}}^{*/} (x_1, \dots, x_{N_c-1}, x_{N_c}) \\ &\quad \times L_{ij}(x_{N_c-1}, x_{N_c}) \\ &\quad \times \Psi_{\xi_1, \dots, \xi_{N_c-1}, \xi_{N_c}} (x_1, \dots, x_{N_c-1}, x_{N_c}) \\ &\quad \times (\mathcal{S}_{ij})_{\xi_{N_c-1}, \xi_{N_c}}^{\xi'_{N_c-1}, \xi'_{N_c}}. \end{aligned}$$

There are several cases to be considered. The first case is configuration mixings involving the ground-state baryons. The mixing amplitude with excited states having wave functions of the form given by Eq. (24) becomes

$$\begin{aligned} \langle \Psi' | H_{\text{mix}} | \Psi_{\text{g.s.}} \rangle &= -\sqrt{N_c} \quad (33) \\ &\times \int d^3x d^3y (\phi^*(x) \phi'^*(y) + x \leftrightarrow y) \\ &\quad \times L_{ij}(x, y) \phi(x) \phi(y) \langle \chi' | \mathcal{S}_{ij} | \chi \rangle, \end{aligned}$$

where the two-body spin-flavor matrix element is defined by

$$\begin{aligned} \langle \chi' | \mathcal{S}_{ij} | \chi \rangle &= \chi_{\xi_1, \dots, \xi'_{N_c-1}, \xi'_{N_c}}^{*/} \quad (34) \\ &\times (\mathcal{S}_{ij})_{\xi_{N_c-1}, \xi_{N_c}}^{\xi'_{N_c-1}, \xi'_{N_c}} \chi_{\xi_1, \dots, \xi_{N_c-1}, \xi_{N_c}}. \end{aligned}$$

The order in  $1/N_c$  of the amplitude is determined by this latter matrix element. There are a couple of cases to be considered. One case is when  $\chi'$  is in the symmetric representation, implying that the excited state must have  $\ell \neq 0$  for an observable configuration mixing to take place. Since the two-body spin-flavor operator can be at most of rank 2, parity conservation implies that  $\ell = 2$ . The second case is when  $\chi'$  is in the MS representation, where now both possibilities exist, namely,  $\ell = 0$  and 2. The most general forms of  $\mathcal{S}_{ij}$  are  $\mathcal{S}_{ij} = s_i \otimes s_j$  and  $\mathcal{S}_{ij} = g_{ia} \otimes g_{ja}$  coupled to  $\ell = 0$  and 2. The countings in  $1/N_c$  of the various relevant matrix elements of these operators can be obtained by explicit evaluation and are shown in

List of spin-flavor matrix elements relevant to configuration mixings and their counting in  $1/N_c$  (here,  $\mathbf{1}$  denotes the singlet spin-flavor operator; \* indicates entries that produce irrelevant configuration mixings)

Matrix elements	$\ell = 0$	$\ell = 2$
$\langle S   s_i \otimes s_j   S \rangle$	* $\mathcal{O}(1/N_c) \cdot \mathbf{1}$	$\mathcal{O}(1/N_c^2)$
$\langle S   g_{ia} \otimes g_{ja}   S \rangle$	* $\mathcal{O}(N_c^0) \cdot \mathbf{1} + \mathcal{O}(1/N_c^2)$	$\mathcal{O}(1/N_c^2)$
$\langle \text{MS}   s_i \otimes s_j   S \rangle$	$\mathcal{O}(1/N_c)$	$\mathcal{O}(1/N_c)$
$\langle \text{MS}   g_{ia} \otimes g_{ja}   S \rangle$	$\mathcal{O}(1/N_c^2)$	$\mathcal{O}(1/N_c)$
$\langle \text{MS}   s_i \otimes s_j   \text{MS} \rangle$	* $\mathcal{O}(1/N_c)$	$\mathcal{O}(1/N_c)$
$\langle \text{MS}   g_{ia} \otimes g_{ja}   \text{MS} \rangle$	* $\mathcal{O}(N_c^0) \cdot \mathbf{1} + \mathcal{O}(1/N_c^2)$	$\mathcal{O}(N_c^0)$

the table. These countings imply that the mixings in the ground-state baryons are as follows: mixings with states in the symmetric spin-flavor representation (which, as mentioned earlier, require the spin-flavor operator to be  $\ell = 2$ ) are order  $1/N_c^{3/2}$ , while mixings with an MS representation are, in general, order  $1/\sqrt{N_c}$ . Thus, the mixing effects affect ground-state baryons primarily at the level of their spin-flavor representation content. Notice that these mixings can only affect the mass splittings at  $\mathcal{O}(1/N_c)$ , as should be the case.

Finally, the configuration mixings between excited states are given by generic matrix elements

$$\begin{aligned} \langle \Psi'' | H_{\text{mix}} | \Psi' \rangle &\quad (35) \\ &= - \int d^3x d^3y (\phi^*(x) \phi''^*(y) + x \leftrightarrow y) \\ &\quad \times L_{ij}(x, y) \phi(x) \phi'(y) \langle \chi'' | \mathcal{S}_{ij} | \chi' \rangle. \end{aligned}$$

Using the countings of the table, if  $\chi'$  and  $\chi''$  are both symmetric, the configuration mixing is order  $1/N_c^2$ , and it is order  $1/N_c$  if only one of them is symmetric. Note here that the effective operator  $1/N_c : \ell^{(2)} g G^c$ , unlike the one-body spin-orbit operator, gives sub-leading mixings. If both states are in the MS representation, observable configuration mixing only occurs for  $\ell = 2$ , and as the last entry in the table shows, this is order  $N_c^0$ . Thus, with the exception of the latter case, configuration mixings of excited states induced by two-body operators are suppressed by  $1/N_c$ .

From the discussion above, the zeroth-order mixings affecting excited states come in two types:  $\Delta\ell = 0$  mixings that require states with  $\ell > 0$  and which

mix symmetric and  $MS$  representations, and  $\Delta\ell = 2$  mixings involving only  $MS$  states. The strength of zeroth-order mixings depends on the dynamics. Because this type of mixing requires spin and orbital couplings, the observed weakness of the spin-orbit coupling that consistently results from analyses of the baryon spectrum hints that the mixing effect is, for little understood reasons, dynamically suppressed. An example of zeroth-order configuration mixing would be  $\ell = 3$  components in the negative parity  $SU(6)$  70-plet wave functions or the mixing between an  $\ell = 1$  56-plet with the  $\ell = 1$  70-plet as noted in [22]. Finally, it is not difficult to extend the discussion to configuration mixings involving states with more than one excited quark. Such mixings are suppressed by extra factors of  $1/\sqrt{N_c}$ .

## 5. CONCLUSIONS

The  $1/N_c$  counting in baryons discussed in this paper from the point of view of a nonrelativistic quark picture gives a good perspective about what the physics of baryons would be like in a world with a large number of colors. It is expected that the countings obtained here will hold also as the quark masses become small.

The results show that excited baryons have finite widths in that world. This also means that a picture in which excited baryons are resonances of pions and ground-state baryons is perfectly viable [18, 25]. The other observation is that the dominant decay channel is always the one that leads most directly to the ground state; cascading through other excited states belonging to different multiplets is a subleading effect.

Configuration mixing is an issue that will need further understanding because it can occur in some cases at zeroth order in  $1/N_c$ . This possesses some difficulties of principle for the study of the excited baryon sector. The mixings affecting the ground-state baryons are suppressed at least by one factor  $1/\sqrt{N_c}$ . The dominant configuration mixing in this case involves spin-flavor mixing. On the other hand, the mixings of excited multiplets can be  $\mathcal{O}(N_c^0)$ . Because these zeroth-order mixings are driven by the couplings of the orbital angular momentum, and orbital couplings are phenomenologically known to be small, it is very plausible that the mixings are dynamically suppressed. This is an open issue, however, which deserves further scrutiny.

It is not quite clear how well or how poorly the general structures implied by the countings just discussed survive in the real world with  $N_c = 3$ . This is a difficult issue involving the convergence of the expansion that is far from being established. Further phenomenological analyses such as those carried out

for masses, decays, and scattering and the applications of the expansion to lattice QCD simulations of excited baryons will eventually clarify the issue.

## ACKNOWLEDGMENTS

I would like to thank Prof. Yurii Simonov for enlightening discussions about the  $1/N_c$  expansion during his visit to Jefferson Lab. I would also like to thank Winston Roberts for pointing out the importance of the two-pion decay channels, Carlos Schat and Norberto Scoccola for very useful discussions on the problems addressed in this paper, and Richard Lebed for a discussion that served to expose a mistake in the first version of this paper.

This work was partially supported by the National Science Foundation through grants PHY-9733343 and PHY-0300185, and by Department of Energy contract DOE-AC05-84ER40150.

## REFERENCES

1. G. 't Hooft, Nucl. Phys. B **72**, 461 (1974).
2. P. Herrera-Siklody, J. I. Latorre, P. Pascual, and J. Taron, Nucl. Phys. B **497**, 345 (1997); R. Kaiser and H. Leutwyler, Eur. Phys. J. C **17**, 623 (2000); hep-ph/9806336.
3. E. Witten, Nucl. Phys. B **160**, 57 (1979).
4. J. L. Gervais and B. Sakita, Phys. Rev. Lett. **52**, 87 (1984); Phys. Rev. D **30**, 1795 (1984).
5. R. Dashen and A. V. Manohar, Phys. Lett. B **315**, 425, 438 (1993).
6. R. Dashen, E. Jenkins, and A. V. Manohar, Phys. Rev. D **49**, 4713 (1994); **51**, 3697 (1995).
7. E. Jenkins, Phys. Lett. B **315**, 441 (1993); E. Jenkins and R. F. Lebed, Phys. Rev. D **52**, 282 (1995); J. Dai, R. Dashen, E. Jenkins, and A. V. Manohar, Phys. Rev. D **53**, 273 (1996); A. Buchmann and R. F. Lebed, Phys. Rev. D **62**, 096005 (2000); A. Buchmann, J. A. Hester, and R. F. Lebed, Phys. Rev. D **66**, 056002 (2002); T. D. Cohen, Phys. Lett. B **554**, 28 (2003).
8. M. A. Luty and J. March-Russell, Nucl. Phys. B **426**, 71 (1994); M. A. Luty, J. March-Russell, and M. White, Phys. Rev. D **51**, 2332 (1995).
9. C. D. Carone, H. Georgi, and S. Osofsky, Phys. Lett. B **322**, 227 (1994).
10. R. Flores-Mendieta, Ch. P. Hofmann, E. Jenkins, and A. V. Manohar, Phys. Rev. D **62**, 034001 (2000).
11. C. D. Carone, H. Georgi, L. Kaplan, and D. Morin, Phys. Rev. D **50**, 5793 (1994).
12. J. L. Goity, Phys. Lett. B **414**, 140 (1997).
13. J. L. Pirjol and T. M. Yan, Phys. Rev. D **57**, 1449, 5434 (1998).
14. C. E. Carlson, C. D. Carone, J. L. Goity, and R. F. Lebed, Phys. Lett. B **438**, 327 (1998); Phys. Rev. D **59**, 114008 (1999).
15. C. L. Schat, J. L. Goity, and N. N. Scoccola, Phys. Rev. Lett. **88**, 102002 (2002); J. L. Goity, C. L. Schat, and N. N. Scoccola, Phys. Rev. D **66**, 114014 (2002).

16. C. E. Carlson and C. D. Carone, Phys. Lett. B **484**, 260 (2000).
17. J. L. Goity, C. L. Schat, and N. N. Scoccola, Phys. Lett. B **564**, 83 (2003).
18. T. D. Cohen and R. F. Lebed, Phys. Rev. D **67**, 096008 (2003); **68**, 056003 (2003).
19. A. V. Manohar, hep-ph/0404122.
20. D. Pirjol and C. L. Schat, Phys. Rev. D **67**, 096009 (2003).
21. T. D. Cohen and R. F. Lebed, Phys. Rev. Lett. **91**, 012001 (2003).
22. T. D. Cohen, D. C. Dakin, A. Nellore, and R. F. Lebed, Phys. Rev. D **69**, 056001 (2004).
23. A. Manohar and H. Georgi, Nucl. Phys. B **234**, 189 (1984).
24. J. L. Goity, C. L. Schat, and N. N. Scoccola, in preparation.
25. M. Lutz and E. Kolomeitsev, Nucl. Phys. A **700**, 193 (2002).

# Monopoles in Gluodynamics and Blocking from Continuum to Lattice\*

M. N. Chernodub<sup>1)</sup>, K. Ishiguro<sup>2)\*\*</sup>, and T. Suzuki<sup>2)\*\*\*</sup>

Received May 21, 2004; in final form, October 29, 2004

**Abstract**—We review the method of blocking of topological defects from continuum to lattice as a nonperturbative tool to construct effective actions for these defects. The actions are formulated in the continuum limit, while the couplings of these actions can be derived from simple observables calculated numerically on lattices with a finite lattice spacing. We demonstrate the success of the method in deriving the effective actions for Abelian monopoles in the pure  $SU(2)$  gauge models in an Abelian gauge. In particular, we discuss the gluodynamics in three and four spacetime dimensions at zero and nonzero temperatures. Besides the action, the quantities of our interest are the monopole density, the magnetic Debye mass, and the monopole condensate. © 2005 Pleiades Publishing, Inc.

## 1. INTRODUCTION

The blocking from continuum (BFC) is a well-known tool to construct the “perfect actions” for lattice field theories [1]. By definition, a perfect lattice action does not depend on the cutoff parameter, which is usually associated with the finite lattice spacing. The cutoff dependence provides a systematic error in the lattice observables that is of the order of the lattice spacing for the standard Wilson action. The various improvement schemes [2] are used to decrease the cutoff influence on the lattice results, and the BFC method [1] is one of the practically useful tools used in lattice simulations nowadays.

Although the main idea of introducing the BFC is to reduce the systematic errors in the numerical simulations, a philosophically similar method can be applied to various topological defects. As a result, one can derive effective actions for the defects in the continuum limit using results of lattice simulations obtained on lattices with finite lattice spacings. This short review is devoted to a demonstration of success of the method applied to the Abelian monopoles in lattice gluodynamics in three dimensions (where the monopoles are instanton-like objects) and in four dimensions (where the monopoles are particle-like defects) following [3–5]. One should stress from the very beginning that the method is quite general and is not limited to the lattice monopoles only.

First, let us recall the basics of the BFC method for field degrees of freedom. A simplest way to associate, say, a continuum free fermion field  $\psi(x)$  with a lattice fermion field  $\Psi_s$  is [1]

$$\Psi_s = \int_{C_s} d^4x \psi(x), \quad \bar{\Psi}_s = \int_{C_s} d^4x \bar{\psi}(x), \quad (1)$$

where the integration is carried out over the lattice hypercube,  $C_s$ , centered at the lattice point  $s$  (we will come to the precise definition of  $C_s$  later). Equations (1) can then be inserted into the partition function as the  $\delta$ -function constraint. To complete the procedure of blocking, the continuum fields  $\psi(x)$  should be integrated out, leaving us with the partition function depending solely on the lattice fields  $\Psi_s$ . Similar relations can also be written for the gauge fields, etc. We refer a reader interested in the blocking of fields to the original articles, switching at this point to the blocking of the topological defects.

Suppose that we have a (gauge) model which describes topological defects, say, for definiteness, monopoles. In four spacetime dimensions (4D), the monopole is a particle-like object (i.e., its trajectory is linelike), and the monopole charge is quantized and conserved (i.e., the monopole trajectories are closed loops). Obviously, the basic requirements to the topological BFC procedure should be the following: (i) the procedure should provide us with the configuration of the lattice monopole currents for a given configuration of the continuum monopole currents; (ii) the lattice monopole currents must be closed; (iii) the lattice magnetic charge for such monopoles must be quantized. We show below that one may write a blocking relation similar (but, in general, not identical) to Eq. (1), which associates the lattice and the continuum monopole charges and preserves their

\*This article was submitted by the authors in English.

<sup>1)</sup>Institute of Theoretical and Experimental Physics, Bol'shaya Cheremushkinskaya ul. 25, Moscow, 117259 Russia; E-mail: Maxim.Chernodub@itep.ru

<sup>2)</sup>Institute for Theoretical Physics, Kanazawa University, Kanazawa, Japan.

\*\*E-mail: ishiguro@hep.s.kanazawa-u.ac.jp

\*\*\*E-mail: suzuki@hep.s.kanazawa-u.ac.jp

basic properties. We insert this relation into the partition function in a form of the  $\delta$ -function constraint, integrate out the continuum degrees of freedom, and get a lattice model which contains only the lattice monopole currents. Using the BFC method, one can also get analytical formulas for various lattice observables expressed through the parameters of the continuum model. A comparison of the numerical data for such observables with the corresponding analytical expressions provides us with the parameters of the monopole action in the continuum. Note that the blocking of the topological defects from the continuum to the lattice is similar to ideas of [6, 7], which discussed theoretically the blocking of the monopoles from fine lattices to coarse lattices.

Below, we describe how the method works for the Abelian monopoles in  $SU(2)$  gluodynamics. Many monopole observables have been calculated numerically [8]. Even an almost perfect monopole action on the lattice has been determined (in a truncated form) using an inverse Monte Carlo method [9]. However, the correctness of the truncation or, in other words, the correct form of the perfect lattice action is not known. The BFC method allows us to find couplings of the (truncated) perfect monopole action in the continuum, estimate the error of the truncation, and obtain certain nonperturbative quantities. Our interest in the physics of the Abelian monopoles in the non-Abelian pure gauge theories is stimulated by the relation of the monopole dynamics to one of the most important problems of QCD, the confinement of color. One popular approach to this problem is the so-called dual superconductor mechanism [10] (for a review of another interesting approach, the vacuum correlator method, see [11]). The key role in the dual superconductor mechanism is played by Abelian monopoles, which are identified with the help of the Abelian projection method [12]. The basic idea behind the Abelian projections is to fix partially the non-Abelian gauge symmetry up to an Abelian subgroup. For  $SU(N)$  gauge theories, the residual Abelian symmetry group is compact, since the original non-Abelian group is compact as well. The Abelian monopoles arise naturally due to the compactness of the residual gauge subgroup.

The Abelian monopoles are not present in QCD from the beginning: they are not solutions to the classical equation of motion of this theory. However, the monopoles may be considered as effective degrees of freedom, which are responsible for confinement of quarks. According to the numerical results [13], the monopoles are condensed in the low-temperature (confinement) phase. The condensation of the monopoles leads to formation of the chromoelectric string due to the dual Meissner effect. As a result, the fundamental sources of chromoelectric

field, quarks, are confined by the string. The importance of the Abelian monopoles is also stressed by the existence [14] of the Abelian dominance phenomena which were first observed in the lattice  $SU(2)$  gluodynamics: the monopoles in the so-called maximal Abelian projection [15] make a dominant contribution to the zero-temperature string tension.

In the deconfinement phase (high temperatures), the monopoles are not condensed and the quarks are liberated. This does not mean, however, that monopoles do not play a role in nonperturbative physics. It is known that, in the deconfinement phase, the vacuum is dominated by static monopoles (which run along the “temperature” direction in the Euclidean theory), while monopoles running in spatial directions are suppressed. The static monopoles should contribute to the “spatial string tension”—a coefficient in front of the area term of large spatial Wilson loops. And, according to numerical simulations in the deconfinement phase [16], the monopoles make a dominant contribution to the spatial string tension. Thus, the monopoles may play an important role not only at low temperatures but also in the high-temperature phase.

We refer the reader to [8] for a review on the Abelian projections and the dual superconductor models in non-Abelian gauge theories.

The structure of the paper is as follows. In Section 2, we describe the BFC method in the simplest three-dimensional (3D) case. Assuming that, in the continuum, the monopole action is of the Coulomb form, we derive the lattice monopole action and the lattice density of the (squared) monopole charges. In Section 3, we apply the BFC procedure to the Abelian monopoles in the four-dimensional  $SU(2)$  gauge theory. Assuming that the monopoles are described by the dual Ginzburg–Landau model, one can get an analytical form for the quadratic monopole action on the lattice.

Then, in Section 4, we compare the analytical formulas with the corresponding numerical data obtained in the three-dimensional  $SU(2)$  gauge model. As a result, we get the density of the monopoles and the monopole contribution to the magnetic screening length in the continuum limit of this model. We show that the results obtained with the help of the BFC method are in agreement with the results of other (independent) calculations. In Section 5, we apply the 3D BFC method to the temporal components of the monopole currents in the  $SU(2)$  gauge model in four spacetime dimensions at high temperature. This gives us a numerical value of the product of the Abelian magnetic screening mass and the monopole density in the continuum model. The self-consistency check shows that the dynamics of the static monopole

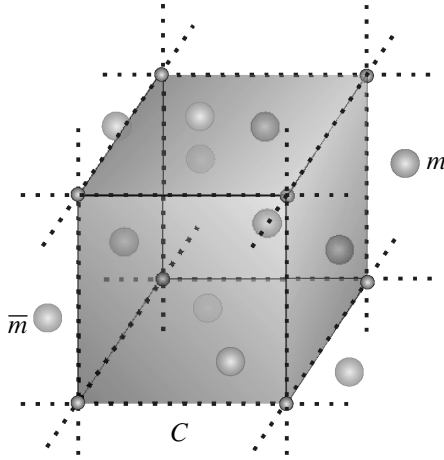


**Fig. 1.** Blocking of the continuum monopoles to the lattice in three dimensions. The charge of the lattice monopole in the cube  $C$  is given by the total magnetic charge of the continuum monopoles inside this cube.

currents can be described by the Coulomb gas model starting from the temperatures  $T \gtrsim 2.5T_c$ .

Finally, in Section 6, we get the value of the monopole condensate in the continuum using the 4D BFC method. This value is in agreement with the results obtained with the help of other methods. Our conclusion is presented in the last section.

## 2. BLOCKING IN THREE DIMENSIONS

It is instructive to start the description of the BFC method from the simplest three-dimensional case. In three dimensions, the Abelian monopoles are point-like objects characterized by a position  $x$  and magnetic charge  $q$  (measured in units of a fundamental magnetic charge,  $g_M$ ). The simplest model possessing the monopoles is the 3D compact quantum electrodynamics (cQED<sub>3</sub>) in which the monopole action is given by the 3D Coulomb gas model [17]:

$$\mathcal{Z} = \sum_{N=0}^{\infty} \frac{\zeta^N}{N!} \left[ \prod_{a=1}^N \int d^3x^{(a)} \sum_{q_a=\pm 1} \right] \quad (2)$$

$$\times \exp \left\{ -\frac{g_M^2}{2} \sum_{\substack{b,c=1 \\ b \neq c}}^N q_b q_c D(x^{(b)} - x^{(c)}) \right\}.$$

The Coulomb interaction in Eq. (2) is represented by the inverse Laplacian  $D$

$$-\partial_i^2 D(x) = \delta^{(3)}(x),$$

and the latin indices  $a, b$  label different monopoles. To get analytical expressions, below we make a standard assumption that the density of the monopoles is low. The monopole charges therefore are restricted by the

condition  $|q_a| \leq 1$ , which means that the monopoles do not overlap. The average monopole density  $\rho$  is controlled by the fugacity parameter  $\zeta$ , giving  $\rho = 2\zeta$  in the leading order of the dilute gas approximation [17].

The magnetic charges in the Coulomb gas (2) are screened: at large distances the two-point charge correlation function is exponentially suppressed,

$$\langle \rho(x)\rho(y) \rangle \sim \exp\{-|x-y|/\lambda_D\}.$$

Here,  $\lambda_D$  is the Debye screening length [17],

$$\lambda_D = \frac{1}{g_M \sqrt{\rho}}. \quad (3)$$

The three-dimensional Debye screening length corresponds to a *magnetic* screening in four dimensions. Below, we choose the vacuum expectation value of the continuum monopole density  $\rho$  and the Debye screening length  $\lambda_D$  as suitable parameters of the continuum model (instead of  $g_M$  and  $\zeta$ ).

Next, let us consider a lattice with a finite lattice spacing  $b$  which is embedded in the continuum space-time. The cells of the lattice are defined as follows:

$$C_s = \left\{ b \left( s_i - \frac{1}{2} \right) \leq x_i \leq b \left( s_i + \frac{1}{2} \right), \quad (4) \right.$$

$$\left. i = 1, 2, 3 \right\},$$

where  $s_i$  is the lattice dimensionless coordinate and  $x_i$  corresponds to the continuum coordinate.

The basic idea of the BFC method is to treat each lattice 3D cell as a “detector” of the magnetic charges of the continuum monopoles. The relation between the lattice magnetic charge  $k_s$  and the density of the continuum monopoles  $\rho(x)$  is<sup>3)</sup>

$$k_s = \int_{C_s} d^3x \rho(x), \quad \rho(x) = \sum_a q_a \delta^{(a)}(x - x^{(a)}) \quad (5)$$

(see an illustration in Fig. 1).

The fluctuations of the monopole charges of the lattice cells must depend on the properties of the continuum monopoles. As a result, the lattice observables—such as the vacuum expectation value of the lattice monopole density—must carry information about dynamics of the continuum monopoles. The observables should depend not only on the size of the lattice cell,  $b$ , but also on the features of the continuum model which describes the monopole dynamics.

<sup>3)</sup>This relation is similar to the blocking of the continuum fields (1). In four dimensions, this similarity disappears.

It is worth stressing the difference between the continuum and lattice monopoles: the continuum monopoles are fundamental pointlike objects,<sup>4)</sup> while the lattice monopoles are associated with the finite-sized lattice cells with nonvanishing total magnetic charge.

According to definitions (5), the lattice monopole charge shares similar properties with the continuum monopole charge. The monopole charge  $k_s$  is quantized,  $k_s \in \mathbb{Z}$ , and it is conserved in the three-dimensional sense,

$$\sum_{s \in \Lambda} k_s \equiv \int_V d^3x \rho(x) = 0, \quad (6)$$

if the continuum charge is conserved. Here,  $\Lambda$  and  $V$  denote the lattice and the continuum volume occupied by the lattice, respectively. In other words, the total magnetic charge of the lattice monopole configuration is zero on a finite lattice with periodic boundary conditions.

In the next two subsections, we follow [3] in presenting, in the BFC approach, the simplest quantities characterizing the lattice monopoles: the monopole action  $S_{\text{mon}}(k)$  and the vacuum expectation value of the squared magnetic charge  $\langle k_s^2 \rangle$ .

### 2.1. Monopole Action in 3D

To derive the lattice monopole action, we substitute the unity

$$1 = \sum_{k(\Lambda) \in \mathbb{Z}} \prod_{s \in \Lambda} \delta_\Lambda \left( k_s - \int_{C_s} d^3x \rho(x) \right) \quad (7)$$

into Eq. (2). Here,  $\sum_{k(\Lambda) \in \mathbb{Z}} \equiv \prod_{s \in \Lambda} \sum_{k_s \in \mathbb{Z}}$  is the sum over the integer-valued form,  $k_s \in \mathbb{Z}$ , ascribed to all sites of the lattice;  $\delta_\Lambda$  stands for the Kronecker symbol (i.e., lattice  $\delta$  function). We get

$$\begin{aligned} \mathcal{Z} = & \sum_{k(\Lambda) \in \mathbb{Z}} \sum_{N=0}^{\infty} \frac{\zeta^N}{N!} \left[ \prod_{a=1}^N \int d^3x^{(a)} \sum_{q_a = \pm 1} \right] \quad (8) \\ & \times \int_{-\pi}^{\pi} \mathcal{D}_\Lambda h \int \mathcal{D}\chi \exp \left\{ - \int d^3x \left[ \frac{1}{2g_M^2} (\partial_i \chi(x))^2 \right. \right. \\ & \left. \left. + i\rho(x) \left( \chi(x) - \sum_{s' \in \Lambda} \theta_{s'}(x) h_{s'} \right) + i \sum_{s' \in \Lambda} k_{s'} h_{s'} \right] \right\}, \end{aligned}$$

where we have introduced two additional integrations over the continuum field  $\chi$  and the compact lattice

field  $h$  to represent the inverse Laplacian in Eq. (2) and the Kronecker symbol in Eq. (7), respectively. The subscript  $\Lambda$  in  $\mathcal{D}_\Lambda h$  indicates that the integration goes over the lattice fields  $h$ . The representative function of the  $s$ th lattice cell is denoted as  $\theta_s$ :

$$\theta_s(x) = \begin{cases} 1, & x \in C_s, \\ 0, & \text{otherwise.} \end{cases} \quad (9)$$

Summing over the monopole position according to [17], expanding the cosine function over the small fluctuations in the fields  $\chi$  and  $h$ , and integrating over these fields, we get the monopole action

$$S_{\text{mon}}^{\text{tree}}(k) = \frac{1}{4\zeta b^3} \sum_{s,s'} k_s \mathcal{F}_{s,s'} k_{s'}, \quad (10)$$

where

$$\mathcal{F}_{s,s'}^{-1} = \delta_{s,s'} - m_D^2 b^2 \mathcal{G}_{s,s'}, \quad (11)$$

$$\mathcal{G}_{s,s'} = \frac{1}{b^5} \int d^3x \int d^3y \theta_s(x) D_{m_D}(x-y) \theta_{s'}(y), \quad (12)$$

and  $D_{m_D}$  is the scalar propagator for a massive particle,  $(-\partial_i^2 + m^2)D_m(x) = \delta^{(3)}(x)$ , with the Debye mass  $m = m_D \equiv \lambda_D^{-1}$ . Note that the lattice operators  $\mathcal{F}$  and  $\mathcal{G}$  are dimensionless quantities.

In the infinite lattice case, Eq. (11) can be rewritten as follows:

$$\begin{aligned} \mathcal{F}_{s,s'} = & \int_{-\pi}^{\pi} \frac{d^3u}{(2\pi)^3} \left[ \sum_{r(\Lambda) \in \mathbb{Z}} \sum_{i=1}^3 \frac{4 \sin^2(u_i/2)}{(\mathbf{u} + 2\pi\mathbf{r})^2 + \mu^2} \right. \\ & \left. \times \prod_{\substack{j=1 \\ j \neq i}}^3 \left( \frac{2 \sin(u_j/2)}{u_j + 2\pi r_j} \right)^2 \right]^{-1} e^{i(s-s',u)}, \end{aligned} \quad (13)$$

where  $\sum_{r(\Lambda)}$  is a sum over the integer-valued scalar form  $r$  [similar to  $k(\Lambda)$  from Eq. (7)] and

$$\mu = b/\lambda_D. \quad (14)$$

The finite-volume expression for the monopole action can be obtained from Eq. (13) by the standard substitution:

$$\begin{aligned} u_i \rightarrow & \frac{2\pi k_i}{L_i}, \quad k = 0, 1, \dots, L_i - 1, \quad (15) \\ & \int_{-\pi}^{\pi} \frac{du_i}{2\pi} \rightarrow \frac{1}{L_i} \sum_{k_i=0}^{L_i-1}, \end{aligned}$$

where  $L_i$  is the lattice size in the  $i$ th direction.

In the infinite-volume case, the lattice operator  $\mathcal{F}_{s,s'}$  depends only on the dimensionless quantity

<sup>4)</sup>In fact, the Abelian  $SU(2)$  monopoles have a finite core [18] of the order of 0.06 fm, which is neglected in our approach.

$\mu$  (14), which is the ratio of the monopole size  $b$  and the Debye screening length, Eq. (3). The form of the operator  $\mathcal{F}$  is qualitatively different in the limits of small and large  $\mu$ . Namely, the leading contribution to the monopole action is given by the mass (Coulomb) terms for small (large) lattice monopoles [3]:

$$S_{\text{mon}}(k) = \begin{cases} \frac{1}{4\rho} \frac{1}{b^3} \sum_s k_s^2 + \dots, & b \ll \lambda_D; \\ \frac{1}{\rho\lambda_D} \frac{1}{b^2} \sum_{s,s'} k_s D_{s,s'} k_{s'} + \dots, & b \gg \lambda_D, \end{cases} \quad (16)$$

where  $D_{s,s'}$  is the inverse Laplacian on the lattice. Thus, the Debye length  $\lambda_D$  sets a scale for the lattice monopole size (or, better to say, for the size of the lattice cell) which characterizes different behavior of the monopole action.

## 2.2. Squared Monopole Density in 3D

The simplest quantity characterizing the lattice monopoles is the monopole density  $\rho_{\text{latt}}(b)$  measured in the *lattice* units

$$\rho_{\text{latt}}(b) = \frac{1}{L^3} \left\langle \sum_{s \in \Lambda} |k_s| \right\rangle, \quad (17)$$

where  $L$  is the lattice size in units of  $b$ . However, analytically, it is easier to calculate the density of the squared monopole charges,

$$\langle k^2(b) \rangle = \frac{1}{L^3} \left\langle \sum_{s \in \Lambda} k^2(s) \right\rangle, \quad (18)$$

which has a similar physical meaning to the monopole density.

Having used Eq. (5), we write the lattice density (18) in the continuum theory as follows:

$$\langle k^2(b) \rangle = \int_{C_s} d^3x \int_{C_s} d^3y \langle \rho(x) \rho(y) \rangle, \quad (19)$$

where the lattice site  $s$  is fixed and the average is taken in the Coulomb gas of the magnetic monopoles described by the partition function  $\mathcal{Z}$  presented in (2).

The correlator of the monopole densities,  $\langle \rho(x) \rho(y) \rangle$ , is well known from [17]. Having introduced the source for the magnetic monopole density,  $J$ , we rewrite (19) as follows:

$$\langle k^2 \rangle = - \int_{C_s} d^3x \int_{C_s} d^3y \frac{\delta^2}{\delta J(x) \delta J(y)} \quad (20)$$

$$\times \left\langle \exp \left\{ i \int d^3z \rho(z) J(z) \right\} \right\rangle \Big|_{J=0}.$$

Then we repeat the transformations in the previous subsection which led us to Eqs. (10) and (13). Integrating over quadratic fluctuations of the field  $\chi$ , we get in the leading order

$$\langle \rho(x) \rho(y) \rangle = \rho \left[ \delta^{(3)}(x-y) - m_D^2 D_{m_D}(x-y) \right]. \quad (21)$$

Substituting Eq. (21) into Eq. (19) and taking the integrals over the cell  $C_s$ , we get

$$\langle k^2 \rangle = \rho b^3 \mathcal{F}_{0,0}^{-1}(\mu), \quad (22)$$

where the inverse matrix  $\mathcal{F}_{s,s'}$  is given by Eq. (11). Equation (22) establishes a direct relation between the density of the squared monopole charges and the monopole action (10) in a leading approximation of the dilute gas.

The squared monopole charge satisfies the following:

$$\langle k^2 \rangle = \begin{cases} C_1 \rho \lambda_D b^2 \left[ 1 + O\left((\lambda_D/b)^2\right) \right], & b \gg \lambda_D, \\ \rho b^3 \left[ 1 + C_2 \rho (b/\lambda_D)^2 + O\left((b/\lambda_D)^4\right) \right], & b \ll \lambda_D, \end{cases} \quad (23)$$

where  $C_1 \approx 2.94$  and  $C_2 \approx 0.148$  in the infinite lattice case.

Equation (23) can qualitatively be understood as follows. In the small- $b$  region, the density of the squared lattice monopole charges is equal to the density of the continuum monopoles times the volume

of the cell. This is natural, since the smaller the volume of the lattice cell ( $\text{Vol} = b^3$ ), the smaller the chance for two monopoles to be located in the same cell. Therefore, each cell predominantly contains not more than one monopole, which leads to the relation  $k_s^2 = |k_s| = 0, 1$ . As a result, we get  $\langle k^2 \rangle \rightarrow$

$\rho_{\text{latt}}(b) \rightarrow \rho b^3$  in the limit  $b \rightarrow 0$ . In the large- $b$  region, correlations between monopoles start to play a role. The monopoles separated from the boundary of the cell by a distance larger than  $\lambda_D$  do not contribute to  $\langle k^2 \rangle$ . Consequently, the  $b^3$  proportionality for the random gas turns into  $\lambda_D b^2$  in the Coulomb gas and we get  $\langle k^2 \rangle \sim \rho \lambda_D b^2$ .

Finally, let us mention interesting relations between the density of the small- and large-sized monopoles and the coefficients in front of, respectively, the Coulomb terms and the mass terms of the monopole action, Eqs. (16) and (23):

$$C(b) = \frac{C_1}{\langle k^2(b) \rangle}, \quad b \gg \lambda_D, \quad \text{and} \quad (24)$$

$$M(b) = \frac{1}{4\langle k^2(b) \rangle}, \quad b \ll \lambda_D.$$

### 3. BLOCKING IN FOUR DIMENSIONS

In four spacetime dimensions, the monopole trajectories are closed loops. Let us superimpose a cubic lattice with the lattice spacing  $b$  on a particular configuration of the monopoles. Each of the (oriented) lattice 3D cells can be characterized by an integer magnetic charge that it contains. Thus, we can relate the continuum configuration of the monopoles to the lattice configuration. The three-dimensional cubes are defined as follows:

$$C_{s,\mu} = \left\{ b \left( s_\nu - \frac{1}{2} \right) \leq x_\nu \leq b \left( s_\nu + \frac{1}{2} \right) \right. \quad (25)$$

$$\left. \text{for } \nu \neq \mu; \text{ and } x_\mu = b s_\mu \right\},$$

where  $s_\nu$  is the dimensionless lattice coordinate of the lattice cube  $C_{s,\mu}$  and  $x_\nu$  is the continuum coordinate. The direction of the 3D cube in the 4D space is defined by the Lorentz index  $\mu$ .

The monopole charge  $K_C$  inside the lattice cube  $C_{s,\mu}$  is equal to the total charge of the continuum monopoles,  $k$ , which pass through this cube. Geometrically, the total monopole corresponds to the linking number between the cube  $C$  and the monopole trajectories,  $k$  (an illustration is presented in Fig. 2). The mutual orientation of the cube and the monopole trajectory is obviously important. The corresponding mathematical expression for the monopole charge  $K_C$  inside the cube  $C$  is a generalization of the Gauss linking number  $\mathbb{L}$  to four-dimensional spacetime [5]:

$$K_C(k) \equiv \mathbb{L}(\partial C, k) = \frac{1}{2} \int d^4x \quad (26)$$

$$\times \int d^4y \epsilon_{\mu\nu\alpha\beta} \Sigma_{\mu\nu}^{\partial C}(x) k_\alpha(y) \partial_\beta \mathcal{D}^{(4)}(x-y)$$

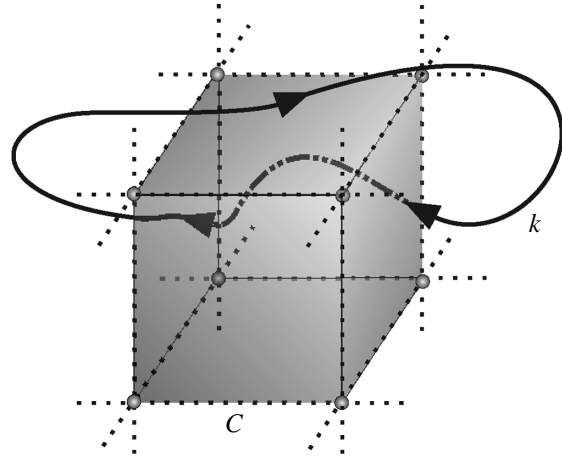


**Fig. 2.** Blocking of the continuum monopoles to the lattice in four dimensions. The lattice monopole charge is equal to the linking number of the monopole trajectory,  $k$ , with the surface of the three-dimensional cube  $C$ .

$$= \frac{1}{4\pi^2} \int d^4x \int d^4y \epsilon_{\mu\nu\alpha\beta} \Sigma_{\mu\nu}^{\partial C}(x) k_\alpha(y) \frac{(x-y)_\beta}{|x-y|^4}.$$

Here, the function  $\Sigma_{\mu\nu}^{\partial C}(x)$  is the two-dimensional  $\delta$  function representing the boundary  $\partial C$  of the cube  $C$ . In a general form, it can be written as follows:

$$\Sigma_{\alpha\beta}(x) = \int_{\Sigma} d\tau_1 d\tau_2 \quad (27)$$

$$\times \left( \frac{x_\alpha(\tau) x_\beta(\tau)}{\partial\tau_1 \partial\tau_2} - \frac{x_\beta(\tau) x_\alpha(\tau)}{\partial\tau_1 \partial\tau_2} \right) \delta^{(4)}[x - \tilde{x}(\tau)],$$

where the four-dimensional vector  $\tilde{x}(\tau)$ ,  $\tau = (\tau_1, \tau_2)$ , parametrizes the position of the two-dimensional surface  $\Sigma$ . The function  $\mathcal{D}^{(4)}$  in Eq. (26) is the inverse Laplacian in four dimensions,  $\partial_\mu^2 \mathcal{D}^{(4)}(x) = \delta^{(4)}(x)$ . It is obvious that the lattice currents  $K_{s,\mu}$  are closed,

$$\partial' K = 0, \quad (28)$$

due to the conservation of the continuum monopole charge,  $\partial_\mu k_\mu = 0$ . In Eq. (28), the symbol  $\partial'$  denotes the backward derivative on the lattice.

Following [5], we derive the lattice monopole action starting from a particular model for the monopole currents. We consider the model dual superconductor, the partition function of which can be written as a sum over the monopole trajectories:

$$\mathcal{Z}_{\text{mon}} = \int \mathcal{D}k \int \mathcal{D}B \exp \left\{ - \int d^4x \quad (29)$$

$$\times \left[ \frac{1}{4g^2} F_{\mu\nu}^2 + i k_\mu(x) B_\mu(x) \right] - S_{\text{int}}(k) \right\},$$

where  $F_{\mu\nu} = \partial_\mu B_\nu - \partial_\nu B_\mu$  is the field stress tensor of the dual gauge field  $B_\mu$ , and  $S_{\text{int}}(k)$  is the action of the

closed monopole currents  $k$ ,

$$k_\mu(x) = \oint d\tau \frac{\partial \tilde{x}_\mu(\tau)}{\partial \tau} \delta^{(4)}[x - \tilde{x}(\tau)]. \quad (30)$$

Here, the 4D vector function  $\tilde{x}_\mu(\tau)$  defines the trajectory of the monopole current. In Eq. (29), the integration is carried out over the dual gauge fields and over all possible monopole trajectories (the sum over disconnected parts of the monopole trajectories is also implicitly assumed).

The action in Eq. (29) contains three parts: the kinetic term for the dual gauge field, the interaction of the dual gauge field with the monopole current, and the self-interaction of the monopole currents. The integration over the monopole trajectories gives the Lagrangian of the dual Abelian Higgs model (DAHM) [19]:

$$\mathcal{Z}_{\text{mon}} \propto \mathcal{Z}_{\text{DAHM}} = \int \mathcal{D}\Phi \int \mathcal{D}B \exp \left\{ - \int d^4x \left[ \frac{1}{4g^2} F_{\mu\nu}^2 + \frac{1}{2} |(\partial_\mu + iB_\mu)\Phi|^2 + V(\Phi) \right] \right\}, \quad (31)$$

where  $\Phi$  is a complex monopole field. The self-interactions of the monopole trajectories described by the action  $S_{\text{int}}$  in Eq. (29) lead to the self-interaction of the monopole field  $\Phi$  described by the potential term  $V(\Phi)$  in Eq. (31). This model is nothing but the usual Ginzburg–Landau model written for the dual fields  $\Phi$  and  $B_\mu$ .

Similarly to the three-dimensional case, let us rewrite the dual superconductor model (31) in terms of the lattice currents  $K_C$ , Eq. (26). To this end, we insert the unity

$$1 = \sum_{K_C \in \mathbb{Z}} \prod_C \delta(K_C - \mathbb{L}(\partial C, k)) \quad (32)$$

into the partition function (29) (here, in this particular case,  $\delta$  represents the Kronecker symbol,  $\delta(x) \equiv \delta_{x,0}$ ). Then we integrate the continuum degrees of freedom,  $k_\mu$  and  $B_\mu$ , getting the partition function in terms of the lattice charges  $K_C$ . The simplest way to do so is to represent the product of the Kronecker symbols in Eq. (32) in terms of the integrals

$$1 = \sum_{K_C \in \mathbb{Z}} \left[ \prod_C \int_{-\infty}^{\infty} d\theta_C \right] \quad (33)$$

$$\times \exp \left\{ i \sum_{C'} \theta_{C'} K_{C'} - i \int d^4x k_\mu(x) \tilde{B}_\mu(\theta; x) \right\},$$

where

$$\tilde{B}_\mu(\theta; x) = \frac{1}{2} \int d^4y \epsilon_{\mu\nu\alpha\beta} \partial_\nu \mathcal{D}^{(4)}(x - y) \quad (34)$$

$$\times \sum_C \theta_C \Sigma_{\alpha\beta}^{\partial C}(y).$$

To derive Eqs. (33) and (34) from Eq. (32), we have used relation (26).

Substituting Eq. (33) into Eq. (29), we get

$$\mathcal{Z}_{\text{mon}} = \int \mathcal{D}k \int \mathcal{D}B \sum_{K_C \in \mathbb{Z}} \left[ \prod_C \int_{-\infty}^{\infty} d\theta_C \right] \quad (35)$$

$$\times \exp \left\{ i \sum_{C'} \theta_{C'} K_{C'} - \int d^4x \left[ \frac{1}{4g^2} F_{\mu\nu}^2 + i k_\mu(x) \left( B_\mu(x) + \tilde{B}_\mu(\theta; x) \right) \right] - S_{\text{int}}(k) \right\}.$$

One can see that the substitution of the unity (33) effectively shifts the gauge field in the interaction term with the monopole current,  $B_\mu \rightarrow B_\mu + \tilde{B}_\mu$ . Therefore, the integration over the monopole trajectories,  $k_\mu$ , in Eq. (35) is very similar to the integration which relates Eq. (29) and Eq. (31). Thus, we get

$$\mathcal{Z}_{\text{mon}} \propto \mathcal{Z}_{\text{DAHM}} \quad (36)$$

$$= \int \mathcal{D}\Phi \int \mathcal{D}B \sum_{K_C \in \mathbb{Z}} \left[ \prod_C \int_{-\infty}^{\infty} d\theta_C \right]$$

$$\times \exp \left\{ i \sum_{C'} \theta_{C'} K_{C'} - \int d^4x \left[ \frac{1}{4g^2} F_{\mu\nu}^2 + \frac{1}{2} \left| \left[ \partial_\mu + i \left( B_\mu(x) + \tilde{B}_\mu(\theta; x) \right) \right] \Phi \right|^2 + V(\Phi) \right] \right\}.$$

Next, we rewrite the continuum dual superconductor model in terms of the lattice monopole currents,  $K$ :

$$\mathcal{Z}_{\text{DAHM}} = \sum_{K \in \mathbb{Z}} e^{-S_{\text{mon}}(K)}, \quad (37)$$

where the monopole action is defined via the lattice Fourier transformation:

$$e^{-S_{\text{mon}}(K)} = \int_{-\infty}^{\infty} \mathcal{D}\theta \exp \left\{ -\tilde{S}(\theta) + i \sum_C \theta_C K_C \right\}. \quad (38)$$

Here, the action  $\tilde{S}(\theta)$  of the compact lattice fields  $\theta$  is expressed in terms of the dual Abelian Higgs model in the continuum:

$$e^{-\tilde{S}(\theta)} = \int \mathcal{D}\Phi \int \mathcal{D}B \exp \left\{ - \int d^4x \left[ \frac{1}{4g^2} F_{\mu\nu}^2 \right. \right. \quad (39)$$

$$+ \frac{1}{2} \left[ \left| \partial_\mu + i \left( B_\mu + \tilde{B}_\mu(\theta) \right) \Phi \right|^2 + V(\Phi) \right] \Bigg\}.$$

An exact integration over the monopole,  $\Phi$ , and dual gauge gluon,  $B_\mu$ , fields in Eq. (39) is impossible in a general case. Let us, however, consider the quadratic part of the monopole action. Neglecting the quantum fluctuations of the monopole field, we work in a mean-field approximation with respect to this field,  $\Phi \rightarrow \langle \Phi \rangle$ :

$$e^{-\tilde{S}(\theta)} = \int \mathcal{D}B \exp \left\{ - \int d^4x \left[ \frac{1}{4g^2} F_{\mu\nu}^2 \right. \right. \quad (40)$$

$$\left. \left. + \frac{\eta^2}{2} \left( B_\mu + \tilde{B}_\mu(\theta) \right)^2 \right] \right\},$$

where  $\eta = |\langle \Phi \rangle|$  is the monopole condensate.

The Gaussian integration over the dual gauge field can be done explicitly. In momentum space, the effective action (up to an irrelevant additive constant) reads as follows:

$$\tilde{S}(\theta) = \frac{\eta^2}{2} \int \frac{d^4p}{(2\pi)^4} \tilde{B}_\mu(\theta, p) \frac{p^2 \delta_{\mu\nu} - p_\mu p_\nu}{p^2 + M_B^2} \tilde{B}_\nu(\theta, -p), \quad (41)$$

where  $M_B = g\eta$  is the mass of the dual gauge boson  $B$ , and  $\tilde{B}_\mu(\theta, p)$  is related to the field  $\tilde{B}_\mu(\theta, x)$ , given in Eq. (34), by a continuum Fourier transformation:

$$\tilde{B}_\mu(\theta, p) \quad (42)$$

$$= \frac{b^3}{p^2} \sum_{s,\alpha} [p^2 \delta_{\mu\alpha} Q_\alpha(pb) - p_\mu p_\alpha Q_\alpha(pb)] e^{-ib(p,s)} \theta_{s,\alpha},$$

with

$$Q_\mu(x) = \prod_{\nu \neq \mu} \frac{\sin(x_\nu/2)}{x_\nu/2}. \quad (43)$$

To get Eq. (42) from Eq. (34), we notice that

$$\frac{1}{2} \epsilon_{\mu\nu\alpha\beta} \Sigma_{\alpha\beta}^{\partial C}(x) = \partial_\mu V_\nu^C(x) - \partial_\nu V_\mu^C(x), \quad (44)$$

where  $V_\mu^C$  is the characteristic function of the lattice cell  $C_{s,\mu}$ . Namely, the characteristic function of the 3D cube with the lattice coordinate  $s_\mu$  and the direction  $\alpha$  is

$$V_\mu(C_{s,\alpha}, x) = \delta_{\mu,\alpha} \delta(x_\alpha - bs_\alpha) \quad (45)$$

$$\times \prod_{\gamma \neq \alpha} \Theta(b(s_\gamma + 1/2) - x_\gamma) \Theta(x_\gamma - b(s_\gamma - 1/2)),$$

where  $\Theta(x)$  is the Heaviside function. The Fourier transform of the function (45) is

$$V_\mu(C_{x,\alpha}, p) = \delta_{\mu,\alpha} b^3 Q_\alpha(pb) e^{-ib(p,s)}. \quad (46)$$

Integrating all variables but the lattice monopole field  $K_{s,\mu}$ , we get the quadratic monopole action

$$S_{\text{mon}}(K) = \sum_{s,s'} \sum_{\alpha,\alpha'} K_{s,\alpha} \mathcal{S}_{ss',\alpha\alpha'} K_{s',\alpha'}, \quad (47)$$

$$\mathcal{S}_{ss',\alpha\alpha'} = \frac{1}{2\eta^2 b^2} \mathcal{F}_{ss',\alpha\alpha'},$$

where

$$\mathcal{F}_{ss',\alpha\alpha'}^{-1} \quad (48)$$

$$= \int \frac{d^4q}{(2\pi)^4} \frac{q^2 \delta_{\alpha\alpha'} - q_\alpha q_{\alpha'}}{q^2 + \mu^2} Q_\alpha(q) Q_{\alpha'}(q) e^{iq(s'-s)}$$

and

$$\mu = M_B b. \quad (49)$$

In the  $\mu \rightarrow \infty$  limit, the leading contribution to the operator  $\mathcal{F}$  can be found explicitly:

$$\mathcal{S}_{ss',\alpha\alpha'} = \frac{2\pi}{\eta^2 b^2 \Gamma} \delta_{\alpha\alpha'} \delta_{s_\alpha, s'_\alpha} \sum_{\substack{\text{cyclic} \\ i,j,k \neq \alpha}} \Delta_{s_i} \delta_{s_j} \delta_{s_k}, \quad (50)$$

where  $\delta_s$  is the Kronecker symbol;  $\Delta_s \equiv \mathcal{D}^{(1)}(s)$  is the one-dimensional Laplacian operator (double derivative); and  $\Gamma \equiv \Gamma(0, t_{\text{UV}} M_B^2 b^2)$ ,  $\Gamma(a, x)$  being the incomplete gamma function and  $t_{\text{UV}}$  being an ultraviolet (UV) cutoff.

#### 4. MONOPOLE DENSITY AND (MAGNETIC) DEBYE MASS IN 3D GLUODYNAMICS

##### 4.1. Technical Details of Numerical Simulations

In the next three sections, we discuss numerical results for the Abelian monopoles in the  $SU(2)$  gauge model. These monopoles obviously possess much more nontrivial dynamics than the monopoles in the simplest case of the cQED. Nevertheless, we show below that, in a certain limit, the dynamics of the Abelian monopoles in the 3D  $SU(2)$  gauge model can be described by the Coulomb gas as in the cQED<sub>3</sub> case. As for the 4D  $SU(2)$  model, the Abelian monopoles in this case can be described by the dual superconductor model.

We simulate numerically the pure  $SU(2)$  gauge model in three dimensions on a  $48^3$  lattice with the standard Wilson action  $S = (-1/2) \sum_P \text{Tr} U_P$ , where  $U_P$  is the plaquette matrix constructed from the gauge link fields  $U_l$ . To study the Abelian monopole dynamics, we perform Abelian projection in the maximally Abelian (MA) gauge [15], which is defined by a maximization condition of the quantity  $R[U] = \text{Tr} \sum_{s,\mu} [U_\mu(s) \sigma_3 U_\mu^\dagger(s + \hat{\mu}) \sigma_3]$ ,

$$\max_{\Omega} R[U^{(\Omega)}], \quad (51)$$

with respect to  $SU(2)$  gauge transformations,  $U \rightarrow U^{(\Omega)} = \Omega^\dagger U \Omega$ . The gauge-fixing condition (51) is invariant under an Abelian subgroup of the  $SU(2)$  group. Thus, the condition (51) corresponds to the partial gauge fixing,  $SU(2) \rightarrow U(1)$ .

After the MA gauge fixing, the Abelian  $\{u_\mu(s)\}$  and non-Abelian  $\{\tilde{U}_\mu(s)\}$  link fields are separated:  $\tilde{U}_\mu(s) = C_\mu(s)u_\mu(s)$ , where

$$C_\mu(s) = \begin{pmatrix} \sqrt{1 - |c_\mu(s)|^2} & -c_\mu^*(s) \\ c_\mu(s) & \sqrt{1 - |c_\mu(s)|^2} \end{pmatrix}, \quad (52)$$

$$u_\mu(s) = \begin{pmatrix} e^{i\theta_\mu(s)} & 0 \\ 0 & e^{-i\theta_\mu(s)} \end{pmatrix}.$$

The vector fields  $C_\mu(s)$  and  $u_\mu(s)$  transform, respectively, like a charged matter and a gauge field under the residual  $U(1)$  symmetry. Next, we define a lattice monopole current (DeGrand–Toussaint monopole) [20]. Abelian plaquette variables  $\theta_{\mu\nu}(s)$  are written as

$$\begin{aligned} \theta_{\mu\nu}(s) &= \theta_\mu(s) \\ &+ \theta_\nu(s + \hat{\mu}) - \theta_\mu(s + \hat{\nu}) - \theta_\nu(s) \\ &(-4\pi < \theta_{\mu\nu}(s) \leq 4\pi). \end{aligned} \quad (53)$$

They are decomposed into two terms,

$$\begin{aligned} \theta_{\mu\nu}(s) &\equiv \bar{\theta}_{\mu\nu}(s) + 2\pi n_{\mu\nu}(s) \\ &(-\pi < \bar{\theta}_{\mu\nu}(s) \leq \pi), \end{aligned} \quad (54)$$

where  $\bar{\theta}_{\mu\nu}(s)$  is interpreted as an electromagnetic flux through the plaquette and  $n_{\mu\nu}(s)$  corresponds to the number of the Dirac strings piercing the plaquette. The lattice monopole current is defined as

$$k(s) = \frac{1}{2} \epsilon_{\nu\rho\sigma} \partial_\nu n_{\rho\sigma}(s + \hat{\mu}). \quad (55)$$

In order to get the lattice density for monopoles of various sizes  $b$ , we perform numerically the blockspin transformations for the lattice monopole charges. The original model is defined on the fine lattice with the lattice spacing  $a$ , and after the blockspin transformation, the renormalized lattice spacing becomes  $b = na$ , where  $n$  is the number of steps of the blockspin transformations. The continuum limit is taken as the limit  $a \rightarrow 0$  and  $n \rightarrow \infty$  for a fixed physical scale  $b$ .

The monopoles on the renormalized lattices (“extended monopoles” [7]) have the physical size  $b^3$ . The charge of the  $n$ -blocked monopole is equal to the sum of the charges of the elementary lattice monopoles inside the  $n^3$  lattice cell:

$$k^{(n)}(s) = \sum_{i,j,l=0}^{n-1} k(ns + i\hat{\mu} + j\hat{\nu} + l\hat{\rho}).$$

For the sake of simplicity, we omit below the superscript ( $n$ ) while referring to the blocked currents. We perform the lattice blocking with the factors  $n = 1, \dots, 12$ . All dimensional quantities below are measured in units of the string tension  $\sigma$ . The values of the string tension are taken from [21, 22].

In order to get rid of the UV artifacts, we have removed the tightly bound dipole pairs from all configurations using a simple numerical algorithm. Namely, we remove a magnetic dipole if it is made of a monopole and an antimonopole which are touching each other (i.e., this means that the centers of the corresponding cubes are located at a distance smaller than or equal to  $\sqrt{3}a$ ). Note that we first apply this procedure to the elementary  $a^3$  monopoles, and only then do we perform the blockspin transformations. Below, we discuss the results obtained for the monopole ensembles with the artificial UV dipoles removed.

#### 4.2. Parameters of the Monopole Gas

In Fig. 3a we show the density of the squared monopole charges (without the UV dipoles and normalized by the factor  $b^2$ ) as a function of the scale  $b$  for various blocking factors  $n$ . One can see that the  $b$ -scaling violations are very small. As the blocking size  $b$  increases, the slope of the ratio  $\langle k_s^2 \rangle / b^2$  decreases in qualitative agreement with the prediction from the Coulomb gas model (23).

According to the prediction coming from the Coulomb gas model (23), the ratio  $\langle k_s^2 \rangle / b^3$  should tend to a constant as  $b$  becomes smaller. This behavior can indeed be seen from Fig. 3b. Note that, at small values of  $b$ , the  $b$  scaling of the monopole density is violated. This scaling violation is not unexpected due to the presence of lattice artifacts at the scale  $b \sim a$ . In order to get artifact-free results, we will use below large- $b$  monopoles.

The values of the parameters of the Coulomb gas model in the continuum limit [Eq. (2)] can be obtained by fitting the numerical results for  $\langle k_s^2 \rangle$  by the theoretical prediction (15). Technically, for each value of the blocking step  $n$ , we have a set of data corresponding to different values of the lattice coupling  $\beta$  and, consequently, to different values of  $b = na(\beta)$ . Note that, by fixing  $n$ , we simultaneously fix the extension of the coarse lattice,  $L/n$ , in units of  $b$ . The size of the coarse lattice enters in Eq. (15). We fit the set of data for the fixed blocking step  $n$ . The best-fit curves are shown in Figs. 3a and 3b by lines. The quality of the fit is very good,  $\chi^2/\text{d.o.f.} \sim 1$ .

The fits of the density provide us with the values of the continuum monopole density  $\rho^{(n)}$  and the Debye

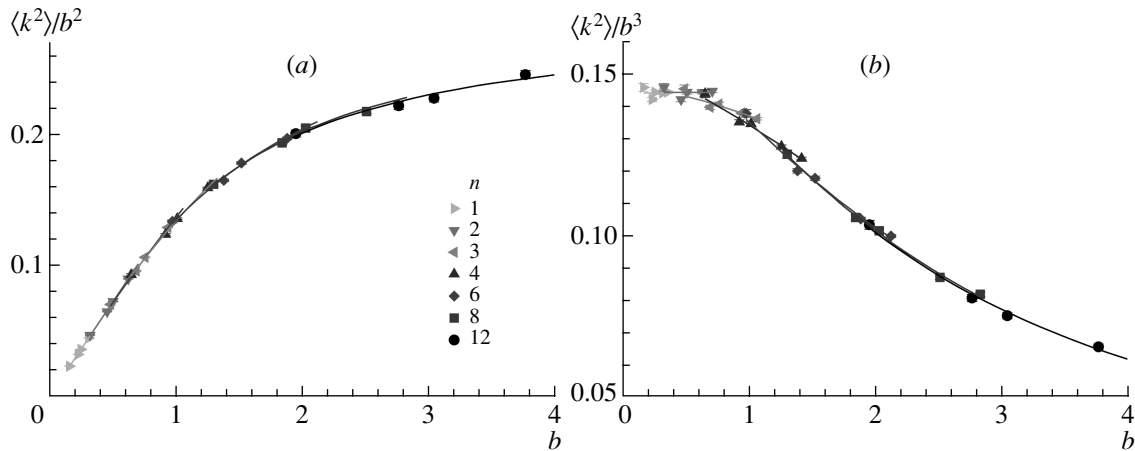


**Fig. 3.** The density of the squared monopole charges  $\langle k^2 \rangle$  with the UV dipoles removed. The density is normalized (a) by  $b^2$  and (b) by  $b^3$ . The fits by the function (18)—shown by lines—were done independently for each value of the blocking step  $n$ .

mass  $M_D^{(n)}$  obtained for the fixed blocking  $n$ . These results are shown (in units of the string tension) in Figs. 4a and 4b, respectively.

We expect to get the artifact-free results in the limit of large  $b$  or, in our case, in the limit of large  $n$ . Thus, one may naturally expect that, in the limit  $n \rightarrow \infty$ , the values of  $\rho^{(n)}$  and  $M_D^{(n)}$  converge to the physical values:  $\lim_{n \rightarrow \infty} \mathcal{O}^{(n)} = \mathcal{O}^{\text{ph}}$ , where  $\mathcal{O}$  stands for either  $\rho$  or  $M_D$ . We found that the dependence of both  $\rho$  and  $M_D$  on the blocking size  $n$  can be approximated by the dependence

$$\mathcal{O}^{(n)} = \mathcal{O}^{\text{ph}} + \text{const} \cdot n^{-2} \quad (56)$$

at  $n > 2$  according to Fig. 4. Using the extrapolation (56), we get the physical values for the monopole density  $\rho$  and the Debye screening mass  $M_D$  coming from the Coulomb gas model (here and below, we omit the superscript “ph” for the extrapolated values):

$$\rho/\sigma^{3/2} = 0.174(2), \quad M_D/\sigma^{1/2} = 1.77(4). \quad (57)$$

The value of  $M_D$  may be treated as the “monopole contribution to the Debye screening mass.”

In order to check whether the monopole dynamics can be described by the Coulomb gas model (2), we construct the dimensionless quantity [3]

$$C = \frac{M_D \sigma}{\rho}, \quad (58)$$

which is known to be equal to eight ( $C^{\text{CG}} = 8$ ) in the low-density limit of the Coulomb gas model [17]. In Fig. 5, we plot our numerical result for  $C$  as a function of  $n$ .

Using the large- $n$  extrapolation (56), we get

$$C = 10.1(1), \quad \text{i.e.,} \quad C/C^{\text{CG}} = 1.26(3). \quad (59)$$

The quantity  $C$  is about 25% larger than that predicted by the Coulomb gas model in the low-monopole density approximation,  $C^{\text{CG}} = 8$ . This discrepancy is most likely explained by the invalidity of the assumption that the monopole density is low. Indeed, the low-density approach requires the monopole density to be much lower than a natural scale for the density,  $g^6$  (remember that the coupling  $g$  has the dimensionality of mass to the one-half power). The requirement  $\rho \ll g^6$  can equivalently be reformulated as  $\rho/M_D^3 \gg 1$ , which means that the number of the monopoles in a unit Debye volume,  $\text{Vol}_D = \lambda_D^3 \equiv M_D^{-3}$ , must be high. Taking the numerical values for  $\rho$  and  $M_D$  from Eq. (57), we get  $\rho/M_D^3 \approx 0.03 \ll 1$ . Thus, the low-density assumption is not valid in the 3D  $SU(2)$  gluodynamics. However, the discrepancy of 25% observed in the quantity  $C$  (59) is a good signal that the Coulomb gas model may still provide us with predictions valid up to the specified accuracy.

One can compare our result for the monopole density, Eq. (57), with the result obtained by Bornyakov and Grigorev [23]:  $\rho^{\text{BG}} = 2^{-7}(1 \pm 0.02)g^6$ . Using the result of [21],  $\sqrt{\sigma} = 0.3353(18)g^2$ , we get the value  $\rho^{\text{BG}}/\sigma^{3/2} = 0.207(5)$ , which is close to our independent estimate in the continuum limit (57):  $\rho/\rho^{\text{BG}} = 0.83(4)$ . The result of [23] is about 20% higher than our estimate for the monopole density. Thus, although the condition of the low-monopole density approximation is strongly violated, the BFC method (based on the dilute gas approximation) gives a value of the monopole density that is consistent with other measurements.

It is interesting to compare the result for the screening mass (57) with the lightest glueball mass measured in [21, 22],  $M_{O^{++}} = 4.72(4)\sqrt{\sigma}$ . In the

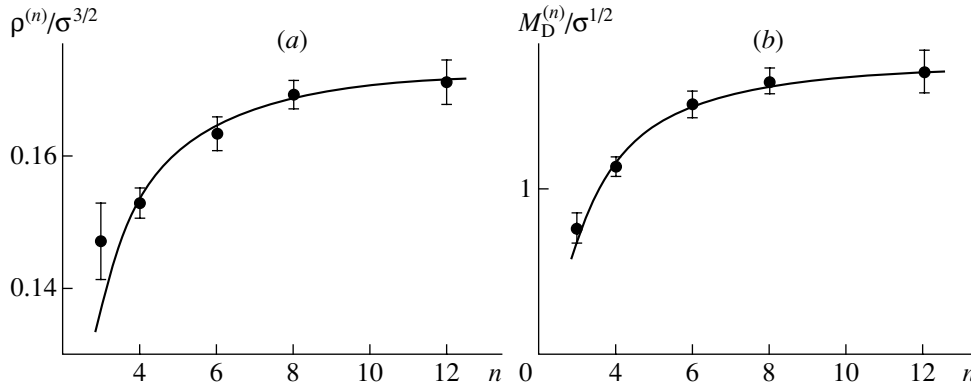


**Fig. 4.** (a) The density  $\rho$  of the continuum monopoles and (b) the Debye screening mass  $M_D$  obtained with the help of the fits of the  $n$ -blocked squared monopole density by function (18). The large- $n$  extrapolation (56) is shown by curves.

Abelian picture, the mass of the ground-state glueball obtained with the help of the correlator

$$\langle F_{\mu\nu}^2(0)F_{\alpha\beta}^2(R) \rangle = \text{const} \cdot e^{-M_{O^{++}}R} + \dots$$

must be twice the Debye screening mass:  $2M_D/M_{O^{++}} = 1$ , where the Debye mass is given by the correlator

$$\langle F_{\mu\nu}(0)F_{\mu\nu}(R) \rangle = \text{const} \cdot e^{-M_D R} + \dots$$

The comparison of our result (57) with the result of [21, 22] gives  $2M_D/M_{O^{++}} = 0.75(4)$ . The deviation is of the order of 25%, similar to the case of the quantity  $C$ .

Finally, let us compare our result for the monopole contribution to the Debye screening mass in Eq. (57) with the direct measurement of the Debye mass in the 3D  $SU(2)$  gauge model made in [24],  $m_D^{SU(2)}/\sqrt{\sigma} = 1.39(9)$ . The values agree with each other within 25%:  $M_D/m_D^{SU(2)} = 1.27(11)$ . Approximately the same accuracy is observed in the four-dimensional  $SU(2)$  gauge theory for the monopole contribution to the fundamental string tension [14].

#### 4.3. Short Summary

The results of Section 4 indicate that the dynamics of the Abelian monopoles in the three-dimensional  $SU(2)$  gauge model can be described by the Coulomb gas model. Using a novel method called the blocking of the monopoles from the continuum, we have calculated the monopole density and the Debye screening mass in the continuum using the numerical results for the (squared) monopole charge density. We have concluded that the Abelian monopole gas in the 3D  $SU(2)$  gluodynamics is not dilute. A self-consistency check of our results shows that the predictions of the Coulomb gas model for the monopole density and the Debye screening mass are consistent with the known data within an accuracy of 25%.

## 5. STATIC MONOPOLES IN HIGH-TEMPERATURE 4D GLUODYNAMICS

### 5.1. Details of Simulations

A finite-temperature system possesses a periodic boundary condition for time direction and the physical length in the time direction is limited to less than  $1/T$ . In this case, it is useful to introduce anisotropic lattices. In the space direction, we perform the blockspin transformation and the continuum limit is taken as  $a_s \rightarrow 0$  and  $n_s \rightarrow \infty$  for a fixed physical scale  $b = n_s a_s$ . Here,  $a_s$  is the lattice spacing in the space directions and  $n_s$  is the blockspin factor. In the time direction, the continuum limit is taken as  $a_t \rightarrow 0$  and  $N_t \rightarrow \infty$  for a fixed temperature  $T = 1/(N_t a_t)$ . Here,  $a_t$  is the lattice spacing in the time direction and  $N_t$  is the number of lattice sites for the time direction. In general,  $a_t \neq a_s$  (anisotropic lattice). After taking the continuum limit, we finally get the effective monopole action, which depends on the physical scale  $b$  and the temperature  $T$ .

The anisotropic Wilson action for pure four-dimensional  $SU(2)$  QCD is written as

$$S = \beta \left\{ \frac{1}{\gamma} \sum_s \sum_{\substack{i>j \\ i,j \neq 4}} P_{ij}(s) + \gamma \sum_s \sum_{i \neq 4} P_{i4}(s) \right\}, \quad (60)$$

$$P_{\mu\nu}(s) \equiv \frac{1}{4} \text{Tr} [\mathbb{1} - U_\mu(s)U_\nu(s + \hat{\mu}) \times U_\mu^\dagger(s + \hat{\nu})U_\nu^\dagger(s)] + \text{h.c.} \quad (61)$$

The procedure to determine the relation between the lattice spacings  $a_s$ ,  $a_t$  and the parameters  $\beta$ ,  $\gamma$  is described in [25].

The monopole current is defined similarly to the three-dimensional case:

$$k_\mu(s) = \frac{1}{2} \epsilon_{\mu\nu\rho\sigma} \partial_\nu n_{\rho\sigma}(s + \hat{\mu}). \quad (62)$$

The monopole current satisfies the conservation law:  $\partial'_\mu k_\mu(s) = 0$ .

At a finite temperature, the blockspin transformation of the spatial and temporal currents should be done separately [25]:

$$K_{\mu \neq 4}(s_s, s_4) = \sum_{i,j=0}^{n_s-1} \sum_{l=0}^{n_t-1} k_{\mu \neq 4}(n_s s_s + (n_s - 1)\hat{\mu} + i\hat{\nu} + j\hat{\rho}, n_t s_4 + l), \quad (63)$$

$$K_4(s_s, s_4) = \sum_{i,j,l=0}^{n_s-1} k_4(n_s s_s + i\hat{\mu} + j\hat{\nu} + l\hat{\rho}, n_t s_4 + (n_t - 1)), \quad (64)$$

where  $n_s$  ( $n_t$ ) is the number of blocking steps in the space (time) direction.

We consider only the  $n_t = 1$  case, since we are interested in high temperatures, for which the monopoles are almost static. The lattice blocking is performed only in the spatial directions,  $n_s = 1, \dots, 8$ , and we study only the static components  $K_4$  among the 4D monopole currents  $K_\mu$  (below, we denote  $K_4$  as  $k$ ). At high temperature, we disregard the spatial currents  $K_i$  since they are not interesting from the point of view of long-range nonperturbative spatial physics. The size of the lattice monopoles is measured in terms of the zero-temperature string tension  $\sigma_{T=0}$ .

### 5.2. Monopole Action

First, let us discuss the action for the static monopole currents. This action at high temperatures was found numerically in [25] with the help of an inverse Monte Carlo procedure. It turns out that the self-interaction of the temporal currents can be successfully described by the quadratic monopole action:

$$S_{\text{mon}}(k) = \sum_i f_i S_i(k), \quad (65)$$

where  $S_i$  are two-point operators of the monopole currents corresponding to different separations between the currents. The term  $S_1$  corresponds to the zero distance between the monopoles,  $S_2$  corresponds to the unit distance, etc. (see [25] for further details). The two-point coupling constants  $f_i$  of the monopole action are shown in Fig. 6 as a function of the distance between the lattice points. The numerical data correspond to the lowest,  $T = 1.6T_c$ , and highest,  $T =$

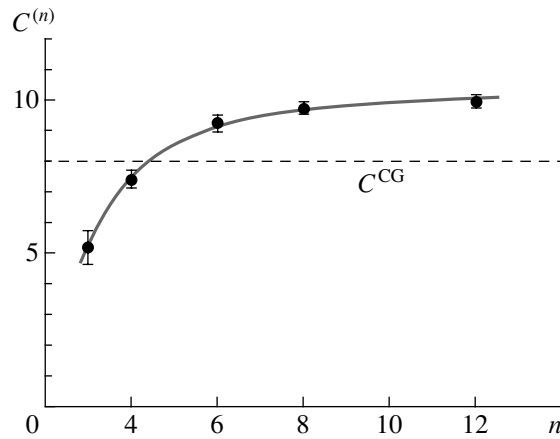


Fig. 5. The ratio  $C = M_D \sigma / \rho$  (see Fig. 4). The dashed line corresponds to the low-density limit of Coulomb gas model [17],  $C^{\text{CG}} = 8$ .

$4.8T_c$ , available temperatures. The spatial spacings of the fine lattice range from  $a_s = 0.16\sigma^{-1/2}$  to  $a_s = 0.25\sigma^{-1/2}$ .

According to Eq. (16) the leading term in the monopole action for large lattice monopoles ( $b \gg \lambda_D$ ) must be proportional to the Coulomb interaction,

$$S_{\text{mon}}(k) = C_C \sum_{s,s'} k_s D_{s,s'} k_{s'}. \quad (66)$$

To check this prediction, we fit the coupling constants  $f_i$  by the Coulomb interaction (66) treating  $C_C$  as a fitting parameter. The fits are visualized by the dashed curves in Fig. 6. As one can see from the figures, this *one-parametric* fit works almost perfectly.

By fitting the action, we obtain values of  $C_C$  for a range of lattice monopole sizes  $b\sqrt{\sigma} = 0.96-1.5$  and temperatures  $T = (1.6-4.8)T_c$ . According to Eq. (16), the pre-Coulomb coefficient  $C_C(b, T)$  at sufficiently large monopole size  $b \gg \lambda_D$  must depend on the lattice monopole size  $b$  as follows:

$$C_C(b, T) = \frac{1}{R(T)b^2}, \quad (67)$$

where  $R$  is the product of the screening length and the monopole density

$$R(T) = \lambda_D(T)\rho(T). \quad (68)$$

We present the data for the pre-Coulomb coefficient,  $C_C(b, T)$ , and the corresponding *one-parametric* fits (67) in Fig. 7a. The fit is one-parametric with  $R$  being the fitting parameter. Again, we observe that the agreement between the data for  $C_C$  and the fits is very good. We show the quantity  $R$  vs. temperature in Fig. 7b.

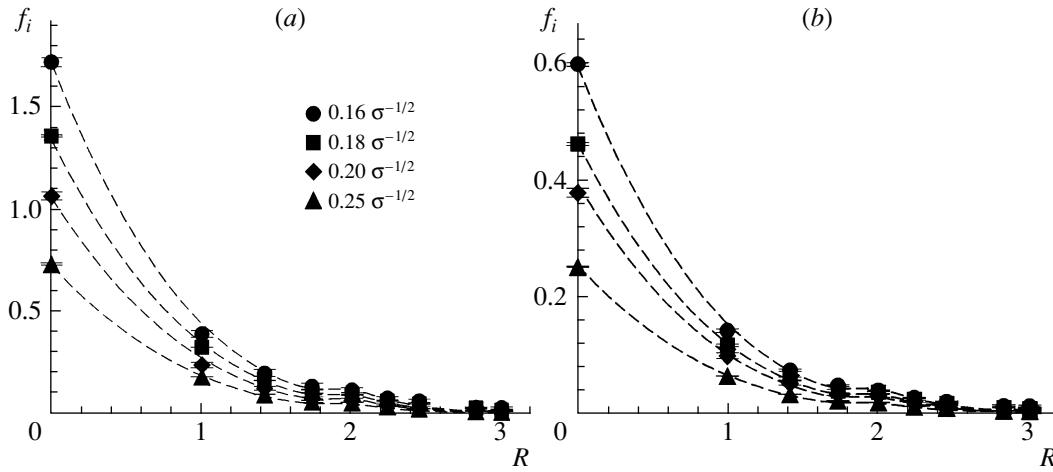


**Fig. 6.** Two-point coupling constants  $f_i$  of the monopole action vs. the distance between the lattice points  $R$  (in lattice units) for  $n_s = 6$  and various spatial spacings  $a_s = (0.16\text{--}0.25\sigma)^{-1/2}$  of the fine lattice. The temperature is (a)  $T = 1.6T_c$  and (b)  $T = 4.8T_c$ . The fits by the Coulomb interaction (66) are visualized by the dashed curves.

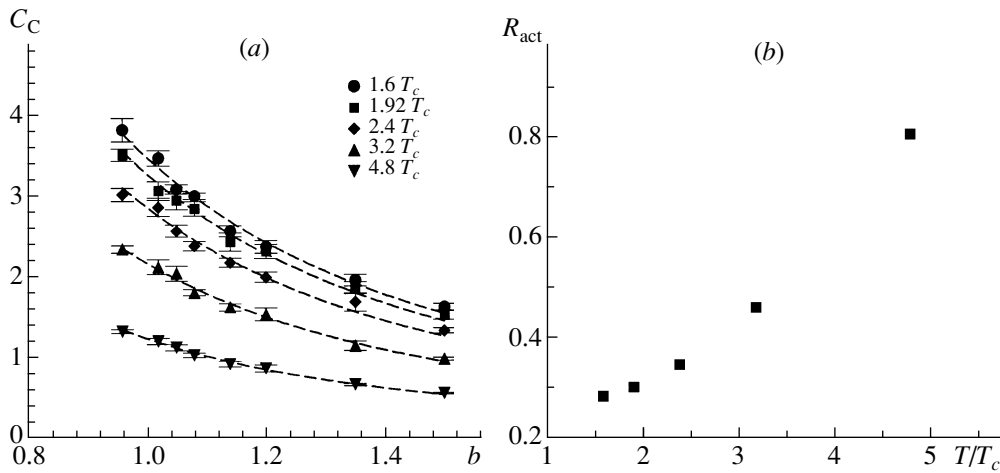


**Fig. 7.** (a) The pre-Coulomb coupling  $C_C$  and the fits of  $C_C$  by Eq. (67) for various temperatures  $T = (1.6\text{--}4.8)T_c$ . (b) The product of the screening length and the monopole density,  $R_{\text{act}}$  (68), calculated from the monopole action, in units of the string tension.

### 5.3. Monopole Density

Independent information about the monopole dynamics can be obtained from the behavior of the lattice monopole density at various lattice monopole sizes. According to Eq. (23), the large- $b$  asymptotics of the quantity  $\langle k^2(b) \rangle / b^2$  can be used to extract the product of the screening length and the continuum monopole density  $R$  (68). We plot in Figs. 8a and 8b the quantity  $\langle k^2(b) \rangle / b^2$  vs. the lattice monopole size  $b$  for the lowest and highest available temperatures.

Our theoretical expectations (23) indicate that the function  $\langle k^2(b) \rangle / b^2$  must vanish at small monopole sizes and tend to a constant at large  $b$ . This behavior can be observed in our numerical data (Fig. 8). The

large- $b$  asymptotics of  $\langle k^2(b) \rangle / b^2$  allows us to get the quantity [4]  $R$  in Eq. (68).

### 5.4. Check of Coulomb Gas Picture

Let us denote by  $R_{\text{act}}$  ( $R_\rho$ ) the quantity  $R$  obtained from the behavior of the monopole action (density). From a numerical point of view, these quantities are independent. Theoretically, we expect that these quantities are equal. To check the self-consistency of our approach, we plot the ratio of these quantities in Fig. 9a. It is clearly seen that the ratio is independent of the temperature and very close (with 10–15% deviations) to unity, as expected.

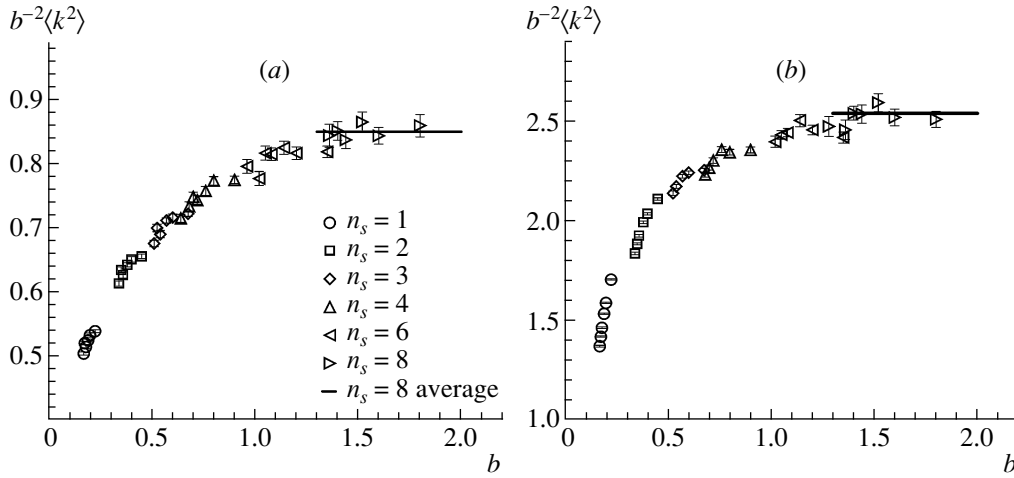


Fig. 8. The ratio  $\langle k^2(b) \rangle / b^2$  vs. the lattice monopole size  $b$  at (a)  $T = 1.6T_c$  and (b)  $T = 4.8T_c$ .

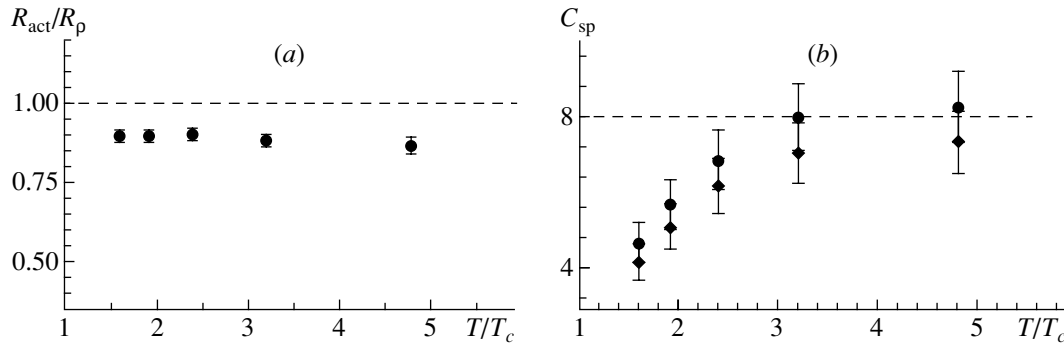


Fig. 9. (a) Check of self-consistency: the ratio of the quantities  $R$  (68), obtained from the lattice monopole action,  $R_{act}$ , and density,  $R_\rho$ ; (b) check of the dilute Coulomb gas picture: quantities  $C_{sp}$ , Eq. (69), calculated from the action ( $\bullet$ ) and density ( $\blacklozenge$ ).

A check of the validity of the Coulomb gas picture can be obtained with the help of the quantity

$$C_{sp}(T) = \frac{\sigma_{sp}(T)}{\lambda_D(T)\rho(T)} \equiv \frac{\sigma_{sp}(T)}{R(T)}, \quad (69)$$

where  $\sigma_{sp}$  is the spatial string tension. This quantity is similar to the one discussed in Eq. (58) in Section 4. In the Abelian projection approach, the spatial string tension should be saturated by the contributions from the static monopoles. In the dilute Coulomb gas of monopoles, the string tension is [17]  $\sigma = 8\sqrt{\rho}/g_M$ , while the screening length is given by (3). These relations imply that, in the dilute Coulomb gas of monopoles, we should get  $C_{sp} = 8$ .

We use the results for the spatial string tension of [26] in the high-temperature  $SU(2)$  gluodynamics. It was found that, for temperatures higher than  $T \approx 2T_c$ , the spatial string tension can be well described by the formula  $\sigma_{sp}(T) = 0.136(11)g_{4D}^4(T)T^2$ , where  $g_{4D}(T)$  is the four-dimensional  $SU(2)$  two-loop run-

ning coupling constant:

$$g_{4D}^{-2}(T) = \frac{11}{12\pi^2} \log\left(\frac{T}{\Lambda_T}\right) + \frac{17}{44\pi^2} \log\left[2 \log\left(\frac{T}{\Lambda_T}\right)\right]$$

with the scale parameter  $\Lambda_T = 0.076(13)T_c$ . Taking also into account the relation between the critical temperature and the zero-temperature string tension [27],  $T_c = 0.69(2)\sqrt{\sigma}$ , we calculate the quantity  $C_{sp}$  and plot it in Fig. 9b as a function of the temperature  $T$ . If the Coulomb picture works, then  $C_{sp}$  should be close to 8. From Fig. 9b, we conclude that this is, indeed, the case at sufficiently high temperatures,  $T/T_c \gtrsim 2.5$ .

### 5.5. Short Summary

The main result of Section 5 is that temporal currents of the Abelian monopoles in the  $SU(2)$  gluodynamics at high temperatures can be described

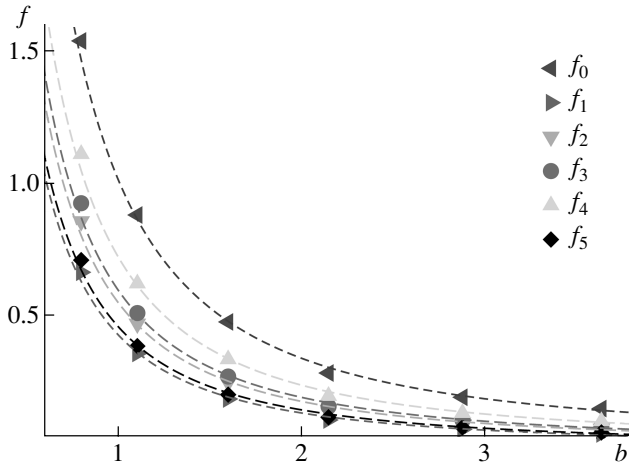


**Fig. 10.** The fits of the transverse  $n = 6$  monopole couplings by function (50).

by the three-dimensional Coulomb model with good accuracy. This result indicates that the nonzero value of the three-dimensional (spatial) string tension at high temperatures is due to the temporal Abelian monopoles.

## 6. MONOPOLE CONDENSATE IN 4D GLUODYNAMICS

Finally, let us consider the  $SU(2)$  gluodynamics at zero temperature. The value of the monopole condensate  $\eta$  was previously estimated from the chromoelectric string analysis of [28] to be  $\eta = 194(19)$  MeV. Below, we determine the value of the monopole condensate from the effective monopole action. We skip a description of the numerical simulations, since it is quite similar to the one discussed in the previous sections (we use the isotropic Wilson action for the gauge fields and fix the MA gauge). We mention only the explicit construction of the extended  $n^3$  monopoles:

$$k_{\mu}^{(n)}(s) = \sum_{i,j,l=0}^{n-1} k_{\mu}(ns + (n-1)\hat{\mu} + i\hat{\nu} + j\hat{\rho} + l\hat{\sigma}). \quad (70)$$

We get the quadratic monopole action using inverse Monte Carlo simulations. The definition of the couplings  $f_i$  of the monopole action is quite similar to the three-dimensional case discussed in the previous sections. The couplings are described in detail in [5]. We illustrate the success of the method by showing the fitting of the couplings by the theoretical prediction (50) in Fig. 10. The best-fit parameters obtained from the fits of different couplings  $f_i$  are very close to each other. This fact provides a nice self-consistency test of our approach. The numerical

value of the monopole condensate turns out to be  $\eta = 243(42)$  MeV. This value is very close to the value  $\eta = 194(19)$  MeV obtained in [28] using a completely different method.

## 7. CONCLUSIONS

The BFC method together with numerical simulations turns out to be a useful tool to obtain nonperturbative information about the topological defects in the continuum limit. The application of this method to the Abelian monopoles in the  $SU(2)$  gauge model gives rise to the following results:

(i) In the three-dimensional  $SU(2)$  gluodynamics, the Abelian monopoles can be described by the Coulomb gas model. The monopoles do not seem to be in the dilute gas regime. Nevertheless, the continuum values of the monopole density ( $\rho = 0.175(3)\sigma^{3/2}$ ) and the Debye screening mass ( $M_D = 1.75(10)\sigma^{1/2}$ )—obtained with the help of the dilute monopole gas model—are consistent within an accuracy of 25% with the known data obtained from independent measurements.

(ii) In the four-dimensional  $SU(2)$  gluodynamics, the static Abelian monopoles can also be described by the Coulomb gas model at sufficiently high temperatures,  $T \gtrsim 2.5T_c$ . The monopoles form the dilute gas. The spatial string tension—obtained in independent measurements—is consistent with the prediction of the monopole Coulomb gas model. In other words, in the continuum, the spatial string tension is dominated by contributions from the static monopoles.

(iii) In the four-dimensional zero-temperature  $SU(2)$  gluodynamics, the value of the monopole condensate,  $\eta = 243(42)$  MeV, was obtained in the framework of the dual superconductor picture. This result is consistent with the result obtained previously by an independent analysis.

## ACKNOWLEDGMENTS

This work is supported by JSPS Grant-in-Aid for Scientific Research on Priority Areas 13135210 and 15340073; JSPS grant S04045; and grants RFBR 01-02-17456, DFG 436 RUS 113/73910, RFBR-DFG 03-02-04016, and MK-4019.2004.2.

## REFERENCES

1. W. Bietenholz and U. J. Wiese, Nucl. Phys. B **464**, 319 (1996); Phys. Lett. B **378**, 222 (1996); W. Bietenholz, Int. J. Mod. Phys. A **15**, 3341 (2000).
2. K. Symanzik, Nucl. Phys. B **226**, 187, 205 (1983); B. Sheikholeslami and R. Wohlert, Nucl. Phys. B **259**, 572 (1985); G. P. Lepage and P. B. Mackenzie, Phys. Rev. D **48**, 2250 (1993).

3. M. N. Chernodub, K. Ishiguro, and T. Suzuki, *Prog. Theor. Phys.* (in press); hep-lat/0407040.
4. M. N. Chernodub, K. Ishiguro, and T. Suzuki, *J. High Energy Phys.* **0309**, 027 (2003).
5. M. N. Chernodub, K. Ishiguro, and T. Suzuki, *Phys. Rev. D* **69**, 094508 (2004).
6. S. Fujimoto, S. Kato, and T. Suzuki, *Phys. Lett. B* **476**, 437 (2000).
7. T. L. Ivanenko, A. V. Pochinsky, and M. I. Polikarpov, *Phys. Lett. B* **252**, 631 (1990).
8. T. Suzuki, *Nucl. Phys. B (Proc. Suppl.)* **30**, 176 (1993); M. N. Chernodub and M. I. Polikarpov, in *Confinement, Duality, and Nonperturbative Aspects of QCD*, Ed. by P. van Baal (Plenum Press, New York, 1998), p. 387; hep-th/9710205; R. W. Haymaker, *Phys. Rep.* **315**, 153 (1999).
9. H. Shiba and T. Suzuki, *Phys. Lett. B* **351**, 519 (1995); N. Arasaki, S. Ejiri, S. I. Kitahara, *et al.*, *Phys. Lett. B* **395**, 275 (1997); M. N. Chernodub, S. Fujimoto, S. Kato, *et al.*, *Phys. Rev. D* **62**, 094506 (2000); K. Yamagishi, T. Suzuki, and S. I. Kitahara, *J. High Energy Phys.* **0002**, 012 (2000).
10. G. 't Hooft, in *High-Energy Physics, EPS International Conference, Palermo, 1975*, Ed. by A. Zichichi, p. 1225; S. Mandelstam, *Phys. Rep.* **23**, 245 (1976).
11. Y. A. Simonov, *Usp. Fiz. Nauk* **166**, 337 (1996) [*Phys. Usp.* **39**, 313 (1996)]; hep-ph/0211330; D. S. Kuzmenko, V. I. Shevchenko, and Yu. A. Simonov, hep-ph/0310190.
12. G. 't Hooft, *Nucl. Phys. B* **190**, 455 (1981).
13. M. N. Chernodub, M. I. Polikarpov, and A. I. Veselov, *Phys. Lett. B* **399**, 267 (1997); *Nucl. Phys. B (Proc. Suppl.)* **49**, 307 (1996); A. Di Giacomo and G. Paffuti, *Phys. Rev. D* **56**, 6816 (1997).
14. T. Suzuki and I. Yotsuyanagi, *Phys. Rev. D* **42**, 4257 (1990); G. S. Bali, V. Bornyakov, M. Müller-Preussker, and K. Schilling, *Phys. Rev. D* **54**, 2863 (1996).
15. A. S. Kronfeld, M. L. Laursen, G. Schierholz, and U. J. Wiese, *Phys. Lett. B* **198**, 516 (1987); A. S. Kronfeld, G. Schierholz, and U. J. Wiese, *Nucl. Phys. B* **293**, 461 (1987).
16. S. Ejiri, S. I. Kitahara, Y. Matsubara, and T. Suzuki, *Phys. Lett. B* **343**, 304 (1995); S. Ejiri, *Phys. Lett. B* **376**, 163 (1996).
17. A. M. Polyakov, *Nucl. Phys. B* **120**, 429 (1977).
18. V. G. Bornyakov, M. N. Chernodub, F. V. Gubarev, *et al.*, *Phys. Lett. B* **537**, 291 (2002).
19. S. Maedan and T. Suzuki, *Prog. Theor. Phys.* **81**, 229 (1989); T. Suzuki, *Prog. Theor. Phys.* **81**, 752 (1989).
20. T. A. DeGrand and D. Toussaint, *Phys. Rev. D* **22**, 2478 (1980).
21. M. Teper, *Phys. Lett. B* **311**, 223 (1993).
22. M. J. Teper, *Phys. Rev. D* **59**, 014512 (1999); *Phys. Lett. B* **397**, 223 (1997).
23. V. Bornyakov and R. Grigorev, *Nucl. Phys. B (Proc. Suppl.)* **30**, 576 (1993).
24. F. Karsch, M. Oevers, and P. Petreczky, *Phys. Lett. B* **442**, 291 (1998).
25. K. Ishiguro, T. Suzuki, and T. Yazawa, *J. High Energy Phys.* **0201**, 038 (2002).
26. G. S. Bali *et al.*, *Phys. Rev. Lett.* **71**, 3059 (1993).
27. J. Fingberg, U. Heller, and F. Karsch, *Nucl. Phys. B* **392**, 493 (1993).
28. F. V. Gubarev, E. M. Ilgenfritz, M. I. Polikarpov, and T. Suzuki, *Phys. Lett. B* **468**, 134 (1999).

# Spectrum of Heavy–Light Mesons in the QCD String Picture\*

Yu. S. Kalashnikova and A. V. Nefediev

*Institute of Theoretical and Experimental Physics,  
Bol'shaya Cheremushkinskaya ul. 25, Moscow, 117259 Russia*

Received May 13, 2004

**Abstract**—We describe in detail predictions of the QCD string approach for the masses of the heavy–light  $D$ ,  $D_s$ ,  $B$ , and  $B_s$  mesons, including orbitally and radially excited states. We discuss the role of the proper dynamics of the QCD string in the formation of the spectrum of the heavy–light mesons, with quark self-energy corrections calculated self-consistently in the same picture. We give our predictions in terms of the current quark masses; the string tension—the only dimensional parameter describing the interquark interaction; and the strong coupling constant, which differs for the fine and the hyperfine interactions. The results are compared with the predictions of other models and with the experimental and lattice results.  
© 2005 Pleiades Publishing, Inc.

## 1. INTRODUCTION

In the last few years, properties of heavy–light  $D$ ,  $D_s$ ,  $B$ , and  $B_s$  mesons attracted the attention of many experimental and lattice collaborations as well as of theorists working in the field of quark models. Indeed, from the viewpoint of a theorist, a heavy–light quark–antiquark state is an example of a relativistic system, due to the light component, but on the other hand, the presence of the heavy particle simplifies the problem considerably since it suppresses the backward-in-time motion of the light particle; allows various expansions, like the heavy-quark effective theory (HQET) expansion [1]; and, in the extreme static limit for the heavy quark, makes the problem a one-particle problem, which is very convenient for studies of the form and the structure of the interquark interaction in QCD [2]. In the meantime, recent experimental studies of the  $D$  and  $B$  mesons have brought a number of problems which puzzle theorists and, in some respects, seem to contradict the standard quark-model-inspired picture of hadrons. Among those, one should mention, first of all, new narrow  $D_J$  [3] and  $D_{s,J}$  [4] mesons. Finally, most of the theoretical approaches involve many model-dependent parameters which diminish the predictive power of such models.

The aim of this paper is to describe the spectrum of all heavy–light  $D$  and  $B$  mesons using, as the minimalistic set of parameters, only the current quark masses; the string tension, which remains the only dimensional parameter for the interaction; and the strong coupling constant. For the latter, we use

two different values: a larger one for the fine interaction and a smaller one for the hyperfine interaction. We give up the idea of using the quark self-energy correction as a fitting parameter and, following the approach suggested in [5], calculate such corrections self-consistently in the framework of the same QCD string picture.

The paper is organized as follows. In the second section, we briefly describe the einbein field method used in our approach in order to arrive naturally at the notion of effective quark masses. In the third section, the reader will find necessary details of the QCD string approach to quarkonia, including the discussion of the QCD string with spinless quarks at the ends, the proper dynamics of the QCD string, the self-energy correction to the quark masses, and the derivation of the spin-dependent terms. We present our results, as well as a comparison with other approaches and experimental and lattice calculations, in the fourth section. The last, fifth, section contains our conclusions and a discussion of possible developments of the method.

## 2. EINBEIN FIELD FORMALISM

In this section, we give a short introduction to the einbein field method, which plays a crucial role in the QCD string approach. As compared to the nonrelativistic dynamics, the relativistic case brings an extra complication due to the square roots in the kinetic energies of relativistic particles. Even the procedure of the center-of-mass motion separation for the system of two free particles appears to be very technically

\*This article was submitted by the authors in English.

involved (see, for example, the textbook [6]). Switching on the interaction between particles makes the problem much more complex. In the meantime, one can get rid of the “square-root” dynamics by resorting to a nonrelativistic-like form, but at the expense of introduction of extra degrees of freedom—the einbein fields [7]; and, at the same time, in order to preserve the number of physical degrees of freedom, one has to introduce constraints. Let us demonstrate how the method works using the example of one free particle. The Lagrangian of the system is changed according to

$$L = -m\sqrt{\dot{x}^2} \rightarrow -\frac{m^2}{2\mu} - \frac{\mu\dot{x}^2}{2}, \quad (1)$$

with  $\mu$  being the aforementioned einbein field. In the path integral formalism, this transformation is based on the following relation:

$$\int D\mu(\tau) \exp\left(-\int d\tau \left(\frac{a\mu}{2} + \frac{b}{2\mu}\right)\right) \sim \exp\left(-\int d\tau \sqrt{ab}\right). \quad (2)$$

The Lagrangian (1) with the einbein field preserves all the symmetries of the original Lagrangian. Namely, the reparametrization invariance with respect to the proper time rescaling,

$$\tau \rightarrow f(\tau), \quad \frac{df}{d\tau} > 0, \quad f(\tau_i) = \tau_i, \quad f(\tau_f) = \tau_f, \quad (3)$$

remains the invariance of the new Lagrangian, provided the einbein  $\mu(\tau)$  transforms as  $\mu \rightarrow \mu/f$ . The invariance (3) is a specific feature of relativistic systems which leads to the mass-shell condition,

$$p^2 - m^2 = 0. \quad (4)$$

Meanwhile, the presence of the extra degree of freedom  $\mu$  leads to an extra constraint,  $\pi = 0$ ,  $\pi$  being the momentum canonically conjugated to  $\mu$ . Indeed, since the Lagrangian (1) does not contain derivatives with respect to the einbein, the corresponding canonical momentum vanishes. Consequently, the Euler–Lagrange equation of motion for the einbein amounts to the extremum condition in  $\mu$  and thus the original form of the Lagrangian can be restored.

The advantage of the modified form of the Lagrangian (1) is obvious since now the kinetic term has a nonrelativistic form, although the dynamics described by this Lagrangian is essentially relativistic. Therefore, for example, one may perform the standard nonrelativistic change of variables in order to separate the motion of the center of mass in the system of several particles. Notice, however, that einbein fields also

depend on time, so that the corresponding expressions for velocities turn out to be more complex than in the nonrelativistic case with constant masses. As a result, the algebra of constraints becomes nontrivial and the Dirac bracket for canonically conjugated variables (the generalization of the Poisson bracket for the case of constrained systems [8]) appears distorted and must be brought to the canonical form before quantization. The interested reader can find examples of such calculations in [9].

The mass-shell condition (4) is an example of the first-class constraint (see [8] for details) which indicates the presence of a gaugelike degree of freedom. Physically, this degree of freedom is related to quantization of the classical system on various hypersurfaces. For example, quantization in the laboratory frame can be fixed by associating the time  $\tau$  with the laboratory time  $x_0$ ,  $\tau = x_0$ . Quantization on the light cone can be achieved by setting  $\tau = x_+$ . Also, more sophisticated gauge conditions can be used, like the proper-time gauge which corresponds to quantization in the comoving frame [10]. The standard way of gauge fixing consists in imposing extra constraints on the system variables and building the full set of canonical brackets. Then the number of variables is to be reduced by the number of second-class constraints [8], so that the remaining variables are physical and they provide the proper basis for canonical quantization. For example, if the laboratory gauge,  $\tau = x_0$ , is fixed in the Lagrangian (1), the latter takes the form

$$L = -\frac{m^2}{2\mu} - \frac{\mu}{2} + \frac{\mu\dot{\mathbf{x}}^2}{2}, \quad (5)$$

so that the corresponding Hamiltonian is readily built using the standard rules and reads

$$H = \frac{\mathbf{p}^2 + m^2}{2\mu} + \frac{\mu}{2}. \quad (6)$$

Now, getting rid of the einbein by taking the extremum in  $\mu$ , one arrives at the familiar expression for the Hamiltonian of the free relativistic particle,

$$H = \sqrt{\mathbf{p}^2 + m^2}. \quad (7)$$

Strictly speaking, one has to eliminate einbeins before quantization—by means of second-class constraints. In practice, however, this could be difficult even at the classical level, due to complicated nonlinear constraint equations, and, during quantization, one meets severe operator ordering problems.

An approximate approach to einbeins is to treat them as variational parameters [11]. According to this method, einbeins are changed for variational parameters and the resulting spectrum is minimized with respect to them.

For example, for a relativistic particle in an external potential,

$$H = \sqrt{\mathbf{p}^2 + m^2} + V(r), \quad H\psi_n = E_n\psi_n, \quad (8)$$

the einbein form of kinetic energy can be used,

$$H = \frac{\mathbf{p}^2 + m^2}{2\mu} + \frac{\mu}{2} + V(r), \quad (9)$$

$$H\psi_n = \tilde{E}_n(\mu)\psi_n,$$

and the variational eigenvalues of the Hamiltonian (8) can be found as

$$E_n \approx \tilde{E}_n(\mu_n^{(0)}), \quad \left. \frac{\partial \tilde{E}_n(\mu)}{\partial \mu} \right|_{\mu=\mu_n^{(0)}} = 0. \quad (10)$$

Notice that, although the Lagrangian approach is abandoned for massless particles, the einbein method remains usable even in this case, so that one can easily set  $m = 0$  in the Hamiltonian (9). This nice property of the method can be used to describe massless particles, like chiral quarks or gluons, and an effective mass of such particles appears, in the form of a non-vanishing extremal value of the einbein, due to the interaction. This approach was successfully used to describe hybrids [12], glueballs [13], and gluelumps [14].

The accuracy of such a variational method can be estimated using an exactly solvable eigenvalue problem. For instance, a Salpeter equation for two relativistic particles connected by a linearly rising potential (only radial motion is considered for the sake of simplicity),

$$H_1 = 2\sqrt{p_r^2 + m^2} + \sigma r, \quad H_1\psi_n = M_n\psi_n, \quad (11)$$

can be rewritten using the einbein  $\mu$ ,

$$H_2 = \frac{p_r^2 + m^2}{\mu} + \mu + \sigma r, \quad H_2\psi_n = M_n\psi_n, \quad (12)$$

and the eigenvalue problem is solved using the quasi-classical quantization method. For the massless case,  $m = 0$ , we compare the WKB spectra of the problems (11) and (12), after the einbein is excluded, as discussed before—see Eq. (10). The results read

$$M_n^2(H_1) = 4\pi\sigma \left( n + \frac{3}{4} \right), \quad (13)$$

$$M_n^2(H_2) = \frac{8\pi}{\sqrt{3}}\sigma \left( n + \frac{3}{4} \right)$$

with the accuracy

$$\delta = \frac{M_n(H_2) - M_n(H_1)}{M_n(H_2)} = 1 - \sqrt{\frac{\sqrt{3}}{2}} \approx 0.07. \quad (14)$$

Therefore, we conclude that the expected systematic error of the variational einbein method does not exceed 7%. We shall assume such an accuracy in what follows.

### 3. QCD STRING APPROACH TO QUARKONIA

#### 3.1. QCD String with Spinless Quarks at the Ends

QCD at large distances is believed to be a string theory with an effective extended object, the QCD string, formed by nonperturbative background gluonic fields, developed between colored sources. An elegant way to describe the QCD string in hadrons, starting from the fundamental QCD Lagrangian, was suggested in [15, 16]. Here, we give a brief insight into the method.

The starting point of the method is the Green's function of the meson,

$$G_{q\bar{q}} = \langle \Psi_{q\bar{q}}^{(f)}(\bar{x}, \bar{y}|A) + \Psi_{q\bar{q}}^{(i)}(x, y|A) \rangle_{q\bar{q}A}, \quad (15)$$

where the initial and the final mesonic wave functions,

$$\Psi_{q\bar{q}}^{(i,f)}(x, y|A) = \bar{\Psi}_{\bar{q}}(x)\Phi(x, y)\Gamma^{(i,f)}\Psi_q(y), \quad (16)$$

are gauge invariant due to the standard path-ordered parallel transporter,

$$\Phi(x, y) = P \exp \left( ig \int_y^x dz_\mu A_\mu \right), \quad (17)$$

$\Gamma^{(i,f)}$  denoting the matrices which stand for the initial and final meson—quark—antiquark vertices.

The gluonic field can be integrated now, using the area-law asymptote for the isolated Wilson loop, so that the resulting mesonic Green's function reads [15]

$$\begin{aligned} G_{q\bar{q}} = & \int D\mu_1(t_1)D\mu_2(t_2)D\mathbf{x}_1D\mathbf{x}_2 e^{-K_1-K_2} \quad (18) \\ & \times \text{Tr} \left[ \Gamma^{(f)}(m_1 - \hat{D})\Gamma^{(i)}(m_2 - \hat{D}) \right. \\ & \times P_\sigma \exp \left[ \int_0^T \frac{dt_1}{2\mu_1(t_1)} \sigma_{\mu\nu}^{(1)} \frac{\delta}{i\delta s_{\mu\nu}(x_1(t_1))} \right] \\ & \times \exp \left[ - \int_0^T \frac{dt_2}{2\mu_2(t_2)} \sigma_{\mu\nu}^{(2)} \frac{\delta}{i\delta s_{\mu\nu}(x_2(t_2))} \right] \\ & \left. \times \exp(-\sigma S_{\min}) \right], \end{aligned}$$

where  $K_i$  are the kinetic energies of the quarks,

$$K_i = \int_0^T dt_i \left( \frac{m_i^2}{2\mu_i} + \frac{\mu_i}{2} + \frac{\mu_i \dot{\mathbf{x}}_i^2}{2} \right), \quad i = 1, 2; \quad (19)$$

$\sigma_{\mu\nu} = \frac{1}{4i}(\gamma_\mu\gamma_\nu - \gamma_\nu\gamma_\mu)$ ; and  $\delta/\delta s_{\mu\nu}$  denotes the derivative with respect to the element of the area  $S$ .

In expression (18), a change of variables was used to proceed from the integration in the time components of the quark four-coordinates to the integration in the einbeins  $\mu_{1,2}$ . Such a change of variables is equivalent to the procedure of the reparametrization invariance fixing in the laboratory reference frame described in Eq. (5). From the Green's function (18), one can extract the Lagrangian of the spinless quarks connected by the straight-line—a reasonable approximation for the minimal surface—Nambu-Goto string in the laboratory frame:

$$L(t) = -\frac{m_1^2}{2\mu_1} - \frac{m_2^2}{2\mu_2} - \frac{\mu_1 + \mu_2}{2} + \frac{\mu_1 \dot{\mathbf{x}}_1^2}{2} + \frac{\mu_2 \dot{\mathbf{x}}_2^2}{2} - \sigma r \int_0^1 d\beta \sqrt{1 - [\mathbf{n} \times (\beta \dot{\mathbf{x}}_1 + (1 - \beta) \dot{\mathbf{x}}_2)]^2}, \quad (20)$$

where  $\mathbf{r} = \mathbf{x}_1 - \mathbf{x}_2$  and  $\mathbf{n} = \mathbf{r}/r$ . The derivative pre-exponential terms in Eq. (18) produce nonperturbative spin-dependent corrections in the effective interaction [17]. We give these terms later.

As discussed above, we have introduced the einbein fields  $\mu_{1,2}$  to get rid of the square roots in the kinetic energies of the quarks. In the same manner, we also simplify the string actions by introducing a continuous einbein  $\nu(\beta)$  for the string term [16]. Then one can proceed to the Hamiltonian of the system,

$$H = \sum_{i=1}^2 \left[ \frac{p_r^2 + m_i^2}{2\mu_i} + \frac{\mu_i}{2} \right] + \int_0^1 d\beta \left[ \frac{\sigma^2 r^2}{2\nu} + \frac{\nu}{2} \right] + \frac{\hat{L}^2}{2r^2[\mu_1(1 - \zeta)^2 + \mu_2\zeta^2 + \int_0^1 d\beta \nu(\beta - \zeta)^2]}, \quad (21)$$

$$\zeta = \frac{\mu_1 + \int_0^1 d\beta \nu \beta}{\mu_1 + \mu_2 + \int_0^1 d\beta \nu}.$$

Notice an important feature of the Hamiltonian (21): effective mass terms are complemented by the contributions of the string—in the form of various integrals of the string energy density  $\nu(\beta)$ . This should not come as a surprise since the rotating string possesses its own inertia and, therefore, must contribute to the total inertia of the system.

### 3.2. Proper Dynamics of the String and the String Correction

As discussed before, the contribution of the proper string dynamics can be easily identified in the Hamiltonian of the quark-antiquark meson (21); namely, the last summand in the denominator of the angular-momentum-dependent term in Eq. (21) describes the proper inertia of the rotating string. The influence of this extra contribution over the mesonic spectra was studied in detail in [16, 18–21], and it was demonstrated that it brings the Regge trajectory (inverse) slope to the correct value of  $2\pi\sigma$  for the light-light system and  $\pi\sigma$  for the heavy-light system [16, 18–20].

Expansion of the Hamiltonian (21) for  $\sqrt{\sigma} \ll m_{1,2}$  gives

$$H \approx m_1 + m_2 + \frac{p^2}{2m} + \sigma r - \frac{\sigma \hat{L}^2}{6m^2 r} + \dots, \quad (22)$$

$$m = \frac{m_1 m_2}{m_1 + m_2}.$$

The last term in expression (22), called the string correction, lowers the energy of orbitally excited states. A more accurate expansion of the Hamiltonian (21) for  $\sqrt{\sigma} \ll \mu_{1,2}$  gives for this correction

$$V_{\text{string}} \approx -\frac{\sigma(\mu_1^2 + \mu_2^2 - \mu_1\mu_2)}{6\mu_1^2\mu_2^2} \frac{\hat{L}^2}{r}, \quad (23)$$

which we use below.

### 3.3. Self-energy Corrections for Quarks

In this subsection, for the sake of future references, we give the result of calculations of the nonperturbative correction to the quark self-energy [5]. Making a more accurate expansion in the meson Green's function (15) with respect to the spin-dependent terms, one finds

$$\text{Tr}\langle W \rangle + \text{Tr}\langle P_F W(g\sigma F(u))(g\sigma F(v)) \rangle + \dots, \quad (24)$$

$$\text{Tr}\langle W \rangle = \exp(-\sigma S_{\text{min}}),$$

where averaging over nonperturbative gluonic background is understood,  $W$  being the Wilson loop formed by the quark trajectories;  $\sigma_{\mu\nu} = \frac{1}{4i}(\gamma_\mu\gamma_\nu - \gamma_\nu\gamma_\mu)$ . The operator  $P_F$  ensures the correct ordering of the  $(g\sigma F)$  insertions. Making the corresponding calculations, one can find that the combination

$$\Delta m^2 \equiv \int d^4(u - v) g^2 \times \langle \sigma F(u)\Phi(u, v)\sigma F(v)\Phi(v, u) \rangle G(u, v) \quad (25)$$

plays the role of the nonperturbative quark self-

**Table 1.** Parameters of quarks used in calculations

	$u/d$	$s$	$c$	$b$
$m$ [GeV]	$7 \times 10^{-3}$	0.175	1.44	4.8
$\eta$	0.9	0.59	0.25	0.05
$\Delta m^2$ [GeV <sup>2</sup> ]	-0.195	-0.112	-0.055	-0.011

energy. In the last expression,

$$G(u, v) = \int_0^\infty ds (Dz)_{uv} e^{-K} \Phi(u, v), \quad (26)$$

$\Phi$  and  $K$  being the parallel transporter along the quark trajectory (17) and the quark kinetic energy (19), respectively. Using, as an approximation, the free Green's function for  $G(u, v)$  and the exponential form of the field correlators, one arrives at the following approximate formula for the self-energy correction:

$$\Delta m^2 = -\frac{4\sigma}{\pi}\eta, \quad (27)$$

$\sigma$  being the string tension and the correcting factor  $\eta$  varying from 0.9 for the light quarks to very small values, of order 0.05, for the  $b$  quark [5]. In Table 1, we give the masses, the values of the parameter  $\eta$ , and  $\Delta m^2$  for all quarks relevant for the  $D$  and  $B$  mesons considered in this paper. The formulas used to estimate the values of  $\eta$  can be found in [5]. Notice that one needs to know only the product  $mT_g$ ,  $T_g$  being the gluonic correlation length [17, 22] of order 0.2–0.3 fm [23], to find this coefficient. We use the value  $T_g = 0.2$  fm to calculate  $\eta$  listed in Table 1.

It was found in [21], where the quark self-energy was used as a fitting parameter, that the latter was a constant for the given flavor of quarks and did not depend on the details of the interaction. In particular, it was observed that the negative constants, to be added to the masses of heavy–light mesons, almost coincided for  $D$  and  $B$  mesons, as well as for  $D_s$  and  $B_s$  mesons, respectively. The formalism suggested in [5] provides an explanation of this result.

From Eq. (27), one can see that, for  $\eta \sim 1$ , the self-energy correction has the natural value of order of the interaction scale  $\sqrt{|\Delta m^2|} \sim \sqrt{\sigma}$ , in agreement with any reasonable qualitative estimate. An important difference between this work and the papers [21] is that the self-energy constant is not a fitting parameter anymore—on the contrary, it is calculated self-consistently in the framework of the QCD string picture.

### 3.4. Spin-Dependent Corrections to the Spinless Hamiltonian

To complete building of the Hamiltonian of a heavy–light meson, we add perturbative interaction and restore the spin-dependent terms, both perturbative and nonperturbative. To this end, the pure confining interaction should be supplied by the perturbative Coulomb interaction,

$$V_{\text{Coul}} = -\frac{\kappa}{r}, \quad \kappa = \frac{4}{3}\alpha_s, \quad (28)$$

together with the spin-dependent correction generated by the latter,

$$V_{\text{sd}} = \frac{8\pi\kappa'}{3\mu_1\mu_2} (\mathbf{S}_1 \cdot \mathbf{S}_2) |\psi(0)|^2 \quad (29)$$

$$+ \frac{\kappa}{r^3} \left( \frac{1}{2\mu_1} + \frac{1}{\mu_2} \right) \frac{\mathbf{S}_1 \cdot \mathbf{L}}{\mu_1}$$

$$+ \frac{\kappa}{r^3} \left( \frac{1}{2\mu_2} + \frac{1}{\mu_1} \right) \frac{\mathbf{S}_2 \cdot \mathbf{L}}{\mu_2}$$

$$+ \frac{\kappa}{\mu_1\mu_2 r^3} (3(\mathbf{S}_1 \cdot \mathbf{n})(\mathbf{S}_2 \cdot \mathbf{n}) - (\mathbf{S}_1 \cdot \mathbf{S}_2)),$$

and also by the nonperturbative spin–orbit term,

$$V_{\text{so}}^{\text{np}} = -\frac{\sigma}{2r} \left( \frac{\mathbf{S}_1 \cdot \mathbf{L}}{\mu_1^2} + \frac{\mathbf{S}_2 \cdot \mathbf{L}}{\mu_2^2} \right), \quad (30)$$

following from derivatives applied to the averaged Wilson loop formed by the quark and the antiquark trajectories [17]. Notice that we use a different value of the strong coupling constant,  $\kappa' = \frac{4}{3}\alpha'_s$ , in the hyperfine interaction in Eq. (29). This conjecture is based on the analysis of the distances at which the corresponding interaction is localized. Indeed, if the strong coupling constant is running with the logarithm regularized by the nonperturbative scale,  $\alpha_s(q^2) \propto \ln \left( \frac{q^2 + \Lambda_{\text{np}}^2}{\Lambda_{\text{QCD}}^2} \right)$ , then, in the coordinate space, the hyperfine interaction appears rather short range—localized at the nonperturbative scale  $(\Lambda_{\text{np}})^{-1}$  of order  $(1 \text{ GeV})^{-1}$ . As a result, the corresponding strong coupling constant  $\alpha'_s$  appears smaller than the one used in the remaining interaction [24]. We shall take this fact into account introducing two different values of the strong coupling constant,  $\alpha'_s < \alpha_s$ .

Notice also an important difference between the spin-dependent interaction given in Eqs. (29), (30) as compared to the expressions used in many works on hadronic spectroscopy—see, for example, [25]. Although, formally, our interaction has the form compliant with the general Eichten–Feinberg–Gromes results [26], it is given in terms of effective quark masses  $\mu$ , which, even for the lightest quarks, appear to be

of order of the interaction scale  $\mu \sim \sqrt{\sigma} \sim 400$  MeV, that is, much larger than the current quark masses. Therefore, in order to use expansions like (29), (30), there is no need to introduce the constituent quark masses by hand—on the contrary, as input parameters, we use only the current quark masses and arrive at the large effective masses self-consistently, as a result of the nonperturbative interaction between quarks.

### 3.5. Eigenvalue Problem for the Heavy-Light System Hamiltonian

Following the method suggested in [27, 28], we formulate the eigenvalue problem for the spinless Hamiltonian using for this purpose the complete set of terms  $\{n^{2S+1}L_J\}$ ,

$$H_0 = \sum_{i=1}^2 \left( \frac{\mathbf{p}^2 + m_i^2 + \Delta m_i^2}{2\mu_i} + \frac{\mu_i}{2} \right) + \sigma r - \frac{4}{3} \frac{\alpha_s}{r}, \quad (31)$$

$$H_0 |n^{2S+1}L_J\rangle = M_0 |n^{2S+1}L_J\rangle.$$

Notice that the self-energy correction is already included in this zeroth-order Hamiltonian. Now we use the lowest approximation for the self-energy—namely, we extract it in the form of the negative subtractive constant in the Hamiltonian (31),

$$H_0 \approx H_0^{(0)} - C_0, \quad (32)$$

$$C_0 = - \sum_{i=1}^2 \frac{\Delta m_i^2}{2\mu_i^{(0)}} = \sum_{i=1}^2 \frac{2\sigma\eta_i}{\pi\mu_i^{(0)}},$$

$\mu_{1,2}^{(0)}$  being the extremal values of the einbeins calculated without the self-energy terms. From Eq. (32), one can see that, as discussed before, the self-energy correction is suppressed for heavy quarks by the large  $\mu^{(0)}$  as well as due to the small correcting factor  $\eta$  (see Table 1). As a result, for any two heavy-light mesons containing the same light quark, the total self-energy constants  $C_0$  will almost coincide, the difference coming from the slightly different values of the effective light-quark mass.

In order to build the spectrum of the Hamiltonian (31), it is necessary to solve the following dimensionless Schrödinger equation:

$$\left( -\frac{d^2}{d\mathbf{x}^2} + |\mathbf{x}| - \frac{\lambda}{|\mathbf{x}|} \right) \chi_\lambda = a(\lambda)\chi_\lambda, \quad (33)$$

where

$$\lambda = \kappa \left( \frac{2\mu}{\sqrt{\sigma}} \right)^{2/3}, \quad \kappa = \frac{4}{3}\alpha_s, \quad \mu = \frac{\mu_1\mu_2}{\mu_1 + \mu_2}.$$

Solutions to the eigenvalue problem (33) depend only on the reduced strength of the Coulomb potential  $\lambda$ . The extrema in the einbeins  $\mu_{1,2}$  can easily be taken explicitly, giving the effective quark masses,

$$\mu_1(\lambda) = \sqrt{m_1^2 + \Delta^2(\lambda)}, \quad (34)$$

$$\mu_2(\lambda) = \sqrt{m_2^2 + \Delta^2(\lambda)},$$

$$\mu(\lambda) = \frac{1}{2}\sqrt{\sigma} \left( \frac{\lambda}{\kappa} \right)^{3/2}$$

with  $\Delta(\lambda)$  given by

$$\Delta^2(\lambda) = \frac{\sigma\lambda}{3\kappa} \left( a + 2\lambda \left| \frac{\partial a}{\partial \lambda} \right| \right).$$

Relations (34) are very physically transparent and demonstrate how the effective quark mass appears in this approach. Indeed,  $\mu_{1,2}$  contain the current quark masses as well as the dynamical contribution of the interquark interaction in the form of  $\Delta(\lambda)$ . The actual value of  $\lambda$  is defined by the algebraic equation coming from relations (34) and the definition of the reduced einbein field  $\mu$  [21],

$$\mu(\lambda) = \frac{\mu_1(\lambda)\mu_2(\lambda)}{\mu_1(\lambda) + \mu_2(\lambda)}. \quad (35)$$

Equation (35), together with relations (34), constitutes a problem which we readily solve numerically, arriving at the extremal values of the einbein fields to be used in further calculations, as well as at the mesonic wave function at the origin,

$$|\psi(0)|^2 = \frac{2\mu\sigma}{4\pi} (1 + \lambda\langle x^{-2} \rangle), \quad (36)$$

which enters the perturbative hyperfine interaction. All averaged values, like the one in Eq. (36), can be defined through the integrals from the dimensionless wave function  $\chi_\lambda(x)$ ,

$$\begin{aligned} \langle r^N \rangle &= (2\mu\sigma)^{-N/3} \langle x^N \rangle = (2\mu\sigma)^{-N/3} \\ &\times \int_0^\infty x^{N+2} |\chi_\lambda(x)|^2 dx, \quad N > -3 - 2l. \end{aligned} \quad (37)$$

In Table 2, we give the solutions for the eigenvalue problem (31) for several sets of quantum numbers which we shall need for future references. For all parameters, we use their standard values. Notice, however, that we get better fits for rather large values of the strong coupling constant  $\alpha_s$ , which is in agreement with the conclusions of the recent paper [29], where the same idea was advocated after studying the heavy-quarkonia spectrum.

**Table 2.** Solutions to Eqs. (33)–(35) for standard values of the string tension  $\sigma$ , the strong coupling constant  $\alpha_s$ , and the current masses of the quarks ( $E_0$  is the bare mass of the corresponding state; all parameters are given in GeV to the appropriate powers)

$n$	$l$	Meson	$m_1$	$m_2$	$\sigma$	$\alpha_s$	$\lambda$	$\mu_1$	$\mu_2$	$\mu$	$E_0$	$ \psi(0) $	$C_0$
0	0	$D$	1.44	0.007	0.168	0.5	1.07	1.550	0.573	0.419	2.158	0.189	0.185
		$D_s$	1.44	0.175	0.168	0.5	1.11	1.555	0.614	0.440	2.184	0.197	0.108
		$B$	4.8	0.007	0.168	0.47	1.27	4.847	0.676	0.593	5.455	0.249	0.143
		$B_s$	4.8	0.175	0.168	0.47	1.19	4.850	0.717	0.624	5.477	0.261	0.079
0	1	$D$	1.44	0.007	0.168	0.5	1.11	1.565	0.612	0.440	2.629	0	0.174
		$D_s$	1.44	0.175	0.168	0.5	1.14	1.568	0.646	0.457	2.654	0	0.104
		$B$	4.8	0.007	0.168	0.47	1.29	4.850	0.691	0.605	5.906	0	0.140
		$B_s$	4.8	0.175	0.168	0.47	1.33	4.851	0.724	0.630	5.928	0	0.078
0	2	$D$	1.44	0.007	0.168	0.5	1.17	1.594	0.684	0.479	2.957	0	0.158
		$D_s$	1.44	0.175	0.168	0.5	1.20	1.597	0.713	0.493	2.979	0	0.095
		$B$	4.8	0.007	0.168	0.47	1.37	4.861	0.771	0.665	6.209	0	0.126
		$B_s$	4.8	0.175	0.168	0.47	1.40	4.863	0.799	0.686	6.229	0	0.071
1	0	$D$	1.44	0.007	0.168	0.5	1.19	1.601	0.699	0.487	2.828	0.178	0.154
		$D_s$	1.44	0.175	0.168	0.5	1.21	1.604	0.729	0.501	2.849	0.182	0.093
		$B$	4.8	0.007	0.168	0.47	1.40	4.866	0.798	0.685	6.079	0.227	0.122
		$B_s$	4.8	0.175	0.168	0.47	1.43	4.867	0.826	0.706	6.098	0.232	0.069

As the next step, we restore the spin-dependent terms in the Hamiltonian of the quark–antiquark system, Eqs. (29), (30), as well as the string correction (23), which now reads

$$\delta M_l \approx -\frac{\sigma(\mu_1^2 + \mu_2^2 - \mu_1\mu_2)}{6\mu_1^2\mu_2^2}l(l+1)\langle r^{-1} \rangle, \quad (38)$$

and find the corresponding contributions to the masses of the heavy–light mesons. Notice, however, that the full quark–antiquark Hamiltonian does not commute with the operators of the angular momentum and of the total spin, so that the basis  $\{^{2S+1}L_J\}$  does not diagonalize the Hamiltonian. Indeed, together with diagonal matrix elements,

$$\begin{aligned} &^{2S+1}P_J \\ \langle ^1P_1|\mathbf{S}_1 \cdot \mathbf{L}|^1P_1 \rangle &= 0, \quad \langle ^1P_1|\mathbf{S}_2 \cdot \mathbf{L}|^1P_1 \rangle = 0, \quad (39) \\ \langle ^1P_1|(\mathbf{S}_1 \cdot \mathbf{n})(\mathbf{S}_2 \cdot \mathbf{n})|^1P_1 \rangle &= -\frac{1}{4}, \\ \langle ^3P_0|\mathbf{S}_1 \cdot \mathbf{L}|^3P_0 \rangle &= -1, \quad \langle ^3P_0|\mathbf{S}_2 \cdot \mathbf{L}|^3P_0 \rangle = -1, \\ \langle ^3P_0|(\mathbf{S}_1 \cdot \mathbf{n})(\mathbf{S}_2 \cdot \mathbf{n})|^3P_0 \rangle &= -\frac{1}{4}, \\ \langle ^3P_1|\mathbf{S}_1 \cdot \mathbf{L}|^3P_1 \rangle &= -\frac{1}{2}, \quad \langle ^3P_1|\mathbf{S}_2 \cdot \mathbf{L}|^3P_1 \rangle = -\frac{1}{2}, \end{aligned}$$

$$\begin{aligned} \langle ^3P_1|(\mathbf{S}_1 \cdot \mathbf{n})(\mathbf{S}_2 \cdot \mathbf{n})|^3P_1 \rangle &= \frac{1}{4}, \\ \langle ^3P_2|\mathbf{S}_1 \cdot \mathbf{L}|^3P_2 \rangle &= \frac{1}{2}, \quad \langle ^3P_2|\mathbf{S}_2 \cdot \mathbf{L}|^3P_2 \rangle = \frac{1}{2}, \\ \langle ^3P_2|(\mathbf{S}_1 \cdot \mathbf{n})(\mathbf{S}_2 \cdot \mathbf{n})|^3P_2 \rangle &= \frac{1}{20}; \\ &^{2S+1}D_J \\ \langle ^1D_2|\mathbf{S}_1 \cdot \mathbf{L}|^1D_2 \rangle &= 0, \quad \langle ^1D_2|\mathbf{S}_2 \cdot \mathbf{L}|^1D_2 \rangle = 0, \quad (40) \\ \langle ^1D_2|(\mathbf{S}_1 \cdot \mathbf{n})(\mathbf{S}_2 \cdot \mathbf{n})|^1D_2 \rangle &= -\frac{1}{4}, \\ \langle ^3D_1|\mathbf{S}_1 \cdot \mathbf{L}|^3D_1 \rangle &= -\frac{3}{2}, \quad \langle ^3D_1|\mathbf{S}_2 \cdot \mathbf{L}|^3D_1 \rangle = -\frac{3}{2}, \\ \langle ^3D_1|(\mathbf{S}_1 \cdot \mathbf{n})(\mathbf{S}_2 \cdot \mathbf{n})|^3D_1 \rangle &= -\frac{1}{12}, \\ \langle ^3D_2|\mathbf{S}_1 \cdot \mathbf{L}|^3D_2 \rangle &= -\frac{1}{2}, \quad \langle ^3D_2|\mathbf{S}_2 \cdot \mathbf{L}|^3D_2 \rangle = -\frac{1}{2}, \\ \langle ^3D_2|(\mathbf{S}_1 \cdot \mathbf{n})(\mathbf{S}_2 \cdot \mathbf{n})|^3D_2 \rangle &= \frac{1}{4}, \\ \langle ^3D_3|\mathbf{S}_1 \cdot \mathbf{L}|^3D_3 \rangle &= 1, \quad \langle ^3D_3|\mathbf{S}_2 \cdot \mathbf{L}|^3D_3 \rangle = 1, \\ \langle ^3D_3|(\mathbf{S}_1 \cdot \mathbf{n})(\mathbf{S}_2 \cdot \mathbf{n})|^3D_3 \rangle &= \frac{1}{28}, \end{aligned}$$

**Table 3.** Spectrum of mass of the  $D$  mesons, in MeV

	$n^{2S+1}L_J$	$J^P$	$M_{\text{exp}}$	$M_{\text{th}}$	$M_{\text{th}}$ [30]	$M_{\text{th}}$ [31]	$M_{\text{th}}$ [32]	$M_{\text{th}}$ [33]	$M_{\text{lat}}$ [34]	$M_{\text{lat}}$ [35]
$D$	$1^1S_0$	$0^-$	1869	1869	1880	1875	1874	1868	1884	1857
$D^*$	$1^3S_1$	$1^-$	2010	2008	2040	2009	2006	2005	1994	1974
$D_1$	$1^X P_1$	$1^+$	2400	2405	2440	2414	2389	2417		2405
$D_1$	$1^X P_1$	$1^+$	2420	2430	2490	2501	2407	2490		2414
$D_0$	$1^3P_0$	$0^+$		2333	2400	2438	2341	2377		2444
$D_2$	$1^3P_2$	$2^+$	2460	2442	2500	2459	2477	2460		2445
	$1^X D_2$	$2^-$		2754			2689	2775		
	$1^X D_2$	$2^-$		2774			2727	2833		
	$1^3D_3$	$3^-$		2724	2830		2688	2799		
	$2^3S_1$	$0^-$		2698	2640	2629	2601	2692		

several off-diagonal ones also exist,

$$\begin{aligned} \langle {}^1P_1 | \mathbf{S}_1 \cdot \mathbf{L} | {}^3P_1 \rangle &= \frac{1}{\sqrt{2}}, & (41) \\ \langle {}^1P_1 | \mathbf{S}_2 \cdot \mathbf{L} | {}^3P_1 \rangle &= -\frac{1}{\sqrt{2}}, \\ \langle {}^1D_2 | \mathbf{S}_1 \cdot \mathbf{L} | {}^3D_2 \rangle &= \sqrt{\frac{3}{2}}, \\ \langle {}^1D_2 | \mathbf{S}_2 \cdot \mathbf{L} | {}^3D_2 \rangle &= -\sqrt{\frac{3}{2}}. \end{aligned}$$

Therefore, in order to determine the masses of the states with  $J = L = 1, 2, \dots$ , we solve the eigenvalue problem,

$$\begin{vmatrix} E_1 - E & V_{12} \\ V_{12}^* & E_2 - E \end{vmatrix} = 0 \quad (42)$$

with  $V_{12}$  being proportional to the transition matrix elements (41).

The only parameter which is not yet specified is the strong coupling constant  $\alpha'_s$  used in the hyperfine perturbative interaction in (29). We extract the value of the latter from the splittings between  ${}^3S_1$  and  ${}^1S_0$  states and find

$$\begin{aligned} \alpha'_s(D) &= \alpha'_s(D_s) = 0.31, & (43) \\ \alpha'_s(B) &= \alpha'_s(B_s) = 0.23. \end{aligned}$$

As discussed before, these values appear to be smaller than the strong coupling constants used in the fine interaction.

This completes the overview of the method and we come to next section, which is devoted to the physics of the heavy-light  $D$ ,  $D_s$ ,  $B$ , and  $B_s$  mesons.

#### 4. HEAVY-LIGHT MESONS

In this section, in Tables 3–6, we give the results of our numerical calculations based on the approach of the QCD string described in the previous section. For the  $P_1$  and  $D_2$  states, we do not distinguish between  ${}^{1/2}P_1$  and  ${}^{3/2}P_1$ , and  ${}^{1/2}D_2$  and  ${}^{3/2}D_2$  partners (in the notation of the HQET). We always list the state with the lower mass first.

We compare our results with the predictions of other approaches as well as with the lattice data and find a good agreement with the latter. The experimental numbers in Tables 3 and 4 include the well-established narrow  $D_1(2420)$  and  $D_{s1}(2536)$  states [36], as well as new states  $D_{sJ}(2317)$  and  $D_{sJ}(2457)$  [4], assuming the former to be a  $0^+$  state, and the latter to be a  $1^+$  state, and  $D_J(2308)$  and  $D_J(2400)$  [3], also assuming them to be  $0^+$  and  $1^+$  states, respectively.

In our approach, one can naturally arrive at rather light orbitally excited states as a consequence of the proper string dynamics. Our result for the  ${}^3P_0$  state in the spectrum of  $D_s$  mesons is one of the lowest predictions in various quark models. Nevertheless, the predicted mass is still higher than the observed one of 2317 MeV. Lattice calculations also fail to reproduce the small  $0^+ - 0^-$  splitting of 338 MeV and give a larger value of  $468 \pm 67$  MeV [37].

If the nearby hadronic threshold ( $DK$  with mass of 2463 MeV) is taken into account, then the mass of the  $D_{s0}$  state may appear in the vicinity of the observed value of 2317 MeV [38]. Note that such a correction does not affect much the mass of the nonstrange  $D_0$  state, as the corresponding threshold  $D\pi$  is far away. Similarly, the inclusion of coupling to  $D^*K$  could explain the observed splitting between  $1^+$  strange

**Table 4.** Spectrum of mass of the  $D_s$  mesons, in MeV

	$n^{2S+1}L_J$	$J^P$	$M_{\text{exp}}$	$M_{\text{th}}$	$M_{\text{th}}$ [30]	$M_{\text{th}}$ [31]	$M_{\text{th}}$ [32]	$M_{\text{th}}$ [33]	$M_{\text{lat}}$ [34]	$M_{\text{lat}}$ [35]
$D_s$	$1^1S_0$	$0^-$	1968	1970	1980	1981	1975	1965	1984	Input
$D_s^*$	$1^3S_1$	$1^-$	2112	2111	2130	2111	2108	2113	2087	2072
$D_{1s}$	$1^X P_1$	$1^+$	2462	2504	2530	2515	2502	2535		2500
$D_{1s}$	$1^X P_1$	$1^+$	2536	2526	2570	2569	2522	2605	2494	2511
$D_{0s}$	$1^3P_0$	$0^+$	2317	2429	2480	2508	2455	2487		2499
$D_{2s}$	$1^3P_2$	$2^+$	2573	2542	2590	2560	2586	2581	2411	2554

**Table 5.** Spectrum of mass of the  $B$  mesons, in MeV

	$n^{2S+1}L_J$	$J^P$	$M_{\text{exp}}$	$M_{\text{th}}$	$M_{\text{th}}$ [30]	$M_{\text{th}}$ [31]	$M_{\text{th}}$ [32]	$M_{\text{th}}$ [33]	$M_{\text{lat}}$ [34]	$M_{\text{lat}}$ [35]
$B$	$1^1S_0$	$0^-$	5279	5275	5310	5285	5277	5279	5293	5277
$B^*$	$1^3S_1$	$1^-$	5325	5324	5370	5324	5325	5324	5322	5302
$B_1$	$1^X P_1$	$1^+$		5724		5719	5686	5700		5684
$B_1$	$1^X P_1$	$1^+$	5732	5736		5757	5699	5742		5730
$B_0$	$1^3P_0$	$0^+$	5639	5697	5760	5738	5678	5706		5754
$B_2$	$1^3P_2$	$2^+$	5732	5740	5800	5733	5704	5714		5770
	$1^X B_2$	$2^-$	5860	5998			5920	5985		
	$1^X B_2$	$2^-$		6043			5955	6037		
	$1^3 B_3$	$3^-$		6005	6110		5871	5993		
	$2^3 S_1$	$0^-$		5966	5700	5930	5848	5920	5898	5890

**Table 6.** Spectrum of mass of the  $B_s$  mesons, in MeV

	$n^{2S+1}L_J$	$J^P$	$M_{\text{exp}}$	$M_{\text{th}}$	$M_{\text{th}}$ [30]	$M_{\text{th}}$ [31]	$M_{\text{th}}$ [32]	$M_{\text{th}}$ [33]	$M_{\text{lat}}$ [34]	$M_{\text{lat}}$ [35]
$B_s$	$1^1S_0$	$0^-$	5369	5360	5390	5375	5366	5373	5383	Input
$B_s^*$	$1^3S_1$	$1^-$	5416	5411	5450	5412	5417	5421	5401	5395
$B_{1s}$	$1^X P_1$	$1^+$		5811		5831	5795	5805	5783	5794
$B_{1s}$	$1^X P_1$	$1^+$	5853	5821	5860	5859	5805	5842		5818
$B_{0s}$	$1^3P_0$	$0^+$		5781	5830	5841	5781	5804		5820
$B_{2s}$	$1^3P_2$	$2^+$		5825	5880	5844	5815	5820	5848	5847

states [38]. Again, as the relevant threshold  $D^*\pi$  in the nonstrange sector is far away, the nonstrange  $1^+$  states remain unsplit and do not suffer much from coupling to this channel.

## 5. CONCLUSIONS

In this paper, we present the results of calculations of the spectrum of mass of the heavy–light  $D$ ,  $D_s$ ,

$B$ , and  $B_s$  mesons. We use the approach of the QCD string with quarks at the ends supplied by the einbein field method. Let us enumerate the main advantages of this approach: (i) the Hamiltonian of the quark–antiquark system is derived starting from the fundamental QCD Lagrangian; (ii) the proper dynamics of the QCD string is naturally taken into account; (iii) a large effective mass of light quarks appears dynamically in this approach, as a result of interaction

between quarks; (iv) the self-energy correction to the quark mass can be calculated self-consistently in the framework of the same approach; (v) the number of parameters in the model is minimal, the latter being only the quark current masses, the strong coupling constant, and the tension of the QCD string (the string tension is the only dimensional parameter defining the interaction); (vi) the approach is physically very transparent and does not lead to complex algebra; (vii) the accuracy of the approach appears to be quite good—better than 10% even for the lowest states.

In conclusion, let us give some arguments why one should trust the results of this quantum mechanical approach for heavy-light quarkonia. A naive argument against the method would be to mention the presence of a light particle in the system, for which effects of retardation are very important. To beat this argument, notice that, as stated above, the dynamics of the system remains entirely relativistic, although, formally, many intermediate formulas resemble non-relativistic calculations. On the other hand, lattice calculations give a rather small value of the gluonic correlation length  $T_g$ , also playing the role of the QCD string radius. As a result, in the strict string limit of QCD, which corresponds to  $T_g = 0$ , the interquark interaction provided by the QCD string is close to instantaneous interaction in some proper string time. For such interactions, it is known that the motions of the quark and the antiquark in a meson are strongly correlated, so that they move backward in time simultaneously. Therefore, in a heavy-light quarkonium, the heavy component suppresses retardations for the whole system.

All these arguments taken together give evidence that the quantum mechanical approach of the QCD string with quarks at the ends appears to be a very powerful method for studies of hadronic properties. In the meantime, further developments of the method are needed; for example, a more accurate account of the time dependence of einbeins would improve the accuracy of the method. Such a version of the approach should be able to provide good predictions of the decay constants of heavy-light mesons [39].

#### ACKNOWLEDGMENTS

We are grateful to A.M. Badalian and Yu.A. Simonov for many stimulating discussions and permanent interest in this work.

The financial support from the grant NS-1774.2003.2 as well as from the Federal Program of the Russian Ministry of Industry, Science, and Technology, grant no. 40.052.1.1.1112, is acknowledged.

#### REFERENCES

1. N. Isgur and M. Wise, *Phys. Lett. B* **232**, 113 (1989); **237**, 527 (1990); T. Mannel, in *Lecture Notes in Physics* (Springer, New York, 1996), Vol. 479, p. 387.
2. Yu. A. Simonov, *Yad. Fiz.* **60**, 2252 (1997) [*Phys. At. Nucl.* **60**, 2069 (1997)]; Yu. S. Kalashnikova and A. V. Nefediev, *Phys. Lett. B* **414**, 149 (1997).
3. Belle Collab. (K. Abe *et al.*), hep-ex/0307021.
4. BaBar Collab. (B. Aubert *et al.*), *Phys. Rev. Lett.* **90**, 242001 (2003); CLEO Collab. (D. Besson *et al.*), hep-ex/0305017; Belle Collab. (Y. Mikami *et al.*), *Phys. Rev. Lett.* **92**, 012002 (2004).
5. Yu. A. Simonov, *Phys. Lett. B* **515**, 137 (2001).
6. Yu. V. Novozhilov, *Introduction to Elementary Particle Theory* (Nauka, Moscow, 1972; Pergamon Press, Oxford, 1975).
7. L. Brink, P. Di Vecchia, and P. Howe, *Nucl. Phys. B* **118**, 76 (1977); Yu. S. Kalashnikova and A. V. Nefediev, *Yad. Fiz.* **60**, 1529 (1997) [*Phys. At. Nucl.* **60**, 1389 (1997)].
8. P. A. M. Dirac, *Lectures on Quantum Mechanics* (Yeshiva University, New York, 1964; Mir, Moscow, 1968).
9. M. H. L. Pryce, *Proc. R. Soc. London, Ser. A* **150**, 166 (1935); G. V. Grygoryan and R. P. Grigoryan, *Yad. Fiz.* **53**, 1737 (1991) [*Sov. J. Nucl. Phys.* **53**, 1062 (1991)]; Yu. S. Kalashnikova and A. V. Nefediev, *Yad. Fiz.* **62**, 359 (1999) [*Phys. At. Nucl.* **62**, 323 (1999)].
10. F. Rohrlich, *Ann. Phys. (N.Y.)* **117**, 292 (1979); M. J. King and F. Rohrlich, *Ann. Phys. (N.Y.)* **130**, 350 (1980).
11. Yu. A. Simonov, *Phys. Lett. B* **226**, 151 (1989).
12. Yu. A. Simonov, in *Proceedings of Hadron'93, Como*, Ed. by T. Bressani, A. Felicielo, G. Preparata, and P. G. Ratcliffe; *Nuovo Cimento A* **107**, 2629 (1994); Yu. S. Kalashnikova and Yu. B. Yufryakov, *Phys. Lett. B* **359**, 175 (1995); *Yad. Fiz.* **60**, 374 (1997) [*Phys. At. Nucl.* **60**, 307 (1997)].
13. Yu. A. Simonov and A. B. Kaidalov, *Phys. Lett. B* **477**, 163 (2000); *Yad. Fiz.* **63**, 1507 (2000) [*Phys. At. Nucl.* **63**, 1428 (2000)].
14. Yu. A. Simonov, *Nucl. Phys. B* **592**, 350 (2000).
15. Yu. A. Simonov, *Nucl. Phys. B* **307**, 512 (1988); Yu. A. Simonov and J. A. Tjon, *Ann. Phys. (N.Y.)* **228**, 1 (1993).
16. A. Yu. Dubin, A. B. Kaidalov, and Yu. A. Simonov, *Phys. Lett. B* **323**, 41 (1994); **343**, 310 (1995).
17. Yu. A. Simonov, *Nucl. Phys. B* **324**, 67 (1989).
18. M. G. Olsson, *Phys. Rev. D* **55**, 5479 (1997).
19. C. Olson, M. G. Olsson, and D. La Course, *Phys. Rev. D* **49**, 4675 (1994).
20. V. L. Morgunov, A. V. Nefediev, and Yu. A. Simonov, *Phys. Lett. B* **459**, 653 (1999).
21. Yu. S. Kalashnikova and A. V. Nefediev, *Phys. Lett. B* **492**, 91 (2000); **530**, 117 (2002); Yu. S. Kalashnikova, A. V. Nefediev, and Yu. A. Simonov, *Phys. Rev. D* **64**, 014037 (2001).
22. H. G. Dosch, *Phys. Lett. B* **190**, 177 (1987); H. G. Dosch and Yu. A. Simonov, *Phys. Lett. B* **205**, 339 (1988).

23. M. Campostrini, A. Di Giacomo, and G. Mussardo, *Z. Phys. C* **25**, 173 (1984); A. Di Giacomo and H. Panagopoulos, *Phys. Lett. B* **285**, 133 (1992); G. Bali, N. Brambilla, and A. Vairo, *Phys. Lett. B* **421**, 265 (1998).
24. Yu. A. Simonov, private communications.
25. D. R. Stanley and D. Robson, *Phys. Lett.* **45**, 235 (1980); P. Cea, G. Nardulli, and G. Preparata, *Z. Phys. C* **16**, 135 (1982); C. Cea, P. Colangelo, G. Nardulli, and G. Preparata, *Phys. Lett. B* **115B**, 310 (1982); J. Carlson *et al.*, *Phys. Rev. D* **27**, 233 (1983).
26. E. Eichten and F. L. Feinberg, *Phys. Rev. D* **23**, 2724 (1981); D. Gromes, *Z. Phys. C* **26**, 401 (1984).
27. Yu. A. Simonov, *Z. Phys. C* **53**, 419 (1992).
28. Yu. A. Simonov, in *Proceedings of the XVII International School of Physics "QCD: Perturbative or Nonperturbative"*, Lisbon, 1999, Ed. by L. S. Ferreira, P. Nogueira, and J. I. Silva-Marcos (World Sci., Singapore, 2000), p. 60.
29. A. M. Badalian, A. I. Veselov, and B. L. G. Bakker, hep-ph/0311009.
30. S. Godfrey and N. Isgur, *Phys. Rev. D* **32**, 189 (1985); S. Godfrey and R. Kokoski, *Phys. Rev. D* **43**, 1679 (1991).
31. D. Ebert, V. O. Galkin, and R. N. Faustov, *Phys. Rev. D* **57**, 5663 (1998).
32. T. A. Lähde, C. J. Nyfält, and D. O. Riska, *Nucl. Phys. A* **674**, 141 (2000).
33. M. Di Pierro and E. Eichten, *Phys. Rev. D* **64**, 114004 (2001).
34. J. Hein *et al.*, *Phys. Rev. D* **62**, 074503 (2000).
35. R. Lewis and R. M. Woloshyn, *Phys. Rev. D* **62**, 114507 (2000).
36. K. Hagiwara *et al.* (Particle Data Group), *Phys. Rev. D* **66**, 010001 (2002).
37. G. S. Bali, *Phys. Rev. D* **68**, 071501 (2003).
38. E. van Beveren and G. Rupp, *Phys. Rev. Lett.* **91**, 012003 (2003); *Eur. Phys. J. C* **32**, 493 (2004).
39. Yu. A. Simonov, work in progress.

# Why Breakup of Photons and Pions into Forward Dijets Is So Different: Predictions from Nonlinear Nuclear $k_{\perp}$ Factorization\*

N. N. Nikolaev<sup>1),2)</sup>, W. Schäfer<sup>1)\*\*</sup>, B. G. Zakharov<sup>2)</sup>, and V. R. Zoller<sup>3)</sup>

Received June 8, 2004

**Abstract**—Based on an approach to non-Abelian propagation of color dipoles in a nuclear medium, we formulate a nonlinear  $k_{\perp}$  factorization for the breakup of photons and pions into forward hard dijets in terms of the collective Weizsäcker–Williams glue of nuclei. We find quite distinct practical consequences of nonlinear nuclear  $k_{\perp}$  factorization for interactions of pointlike photons and nonpointlike pions. In the former case, the large transverse momentum  $p_{\perp}$  of jets comes from the intrinsic momentum of quarks and antiquarks in the photon, and nuclear effects manifest themselves as an azimuthal decorrelation with an acoplanarity momentum of the order of the nuclear saturation momentum  $Q_A$ . In the breakup of pions off free nucleons to the leading order in pQCD, the spectator parton has a small transverse momentum and the hard dijet cross section is suppressed. In the breakup of pions off heavy nuclei, the forward hard jets are predicted to be entirely decorrelated. We comment on the sensitivity of the pionic dijet cross section to the pion distribution amplitude. The predicted distinction between the breakup of photons and pions can be tested by the sphericity and thrust analysis of the forward hadronic system in the COMPASS experiment at CERN. © 2005 Pleiades Publishing, Inc.

## INTRODUCTION

The trademark of the conventional perturbative QCD (pQCD) factorization theorems for hard interactions of leptons and hadrons is that the hard scattering observables are linear functionals of the appropriate parton densities in the projectile and target [1]. In contrast to that, from the parton model point of view, the opacity of heavy nuclei to high-energy projectiles entails a highly nonlinear relationship between the parton densities of free nucleons and nuclei. In deep inelastic scattering (DIS) off nuclei, there emerges a new large scale—the nuclear saturation scale  $Q_A$ —which separates the opaque nucleus, i.e., nonlinear, and weak attenuation, i.e., linear, regimes [2–5]. A priori, it is not obvious that, in the nonlinear regime with a large saturation scale, one can define nuclear parton densities such that they enter different observables in a universal manner, i.e., if useful factorization theorems can be formulated for hard phenomena in ultrarelativistic heavy-ion collisions. In our previous work [6, 7], we presented a partial solution to this problem—a nonlinear nuclear

$k_{\perp}$  factorization for the production of forward hard dijets in DIS off nuclei.

The salient feature of hard dijets in DIS and real photoabsorption is that the large transverse momentum  $p_{\perp}$  of forward jets comes from the intrinsic momentum of quarks and antiquarks in the (virtual) photon. In the  $k_{\perp}$ -factorization description of the underlying photon–gluon fusion parton subprocess  $\gamma^*g \rightarrow q\bar{q}$ , valid at small  $x$ , the disparity of the quark and antiquark transverse momenta and departure from the exact back-to-back configuration—the acoplanarity momentum—is caused by the transverse momentum  $\kappa$  of gluons. It can be quantified in terms of the unintegrated gluon density of the target (see [8, 9] and references therein). Our nonlinear  $k_{\perp}$  factorization for breakup of photons into dijets on nuclei gives a coherent description of the nuclear mass number dependence of the dijet inclusive cross section in terms of the collective Weizsäcker–Williams (WW) unintegrated nuclear glue. This WW nuclear glue has the form of an expansion over the collective gluon structure function of spatially overlapping nucleons [10] of the Lorentz-contracted ultrarelativistic nucleus [5, 11]. Apart from the case of minijets with  $p_{\perp}$  comparable to or below the saturation scale  $Q_A$ , the primary nuclear effect is a broadening of the acoplanarity momentum distribution, and in [6] we showed how this broadening can be calculated through the collective WW nuclear unintegrated gluon density.

The breakup of pions into forward dijets in inelastic  $\pi A$  collisions is an excitation of the quark–antiquark

\*This article was submitted by the authors in English.

<sup>1)</sup>IKP, Forschungszentrum Jülich, Germany.

<sup>2)</sup>Landau Institute for Theoretical Physics, Russian Academy of Sciences, Chernogolovka, Russia.

<sup>3)</sup>Institute for Theoretical and Experimental Physics, Bol'shaya Cheredushinskaya ul. 25, Moscow, 117259 Russia.

\*\*E-mail: wo.schaefer@fz.-juelich.de

Fock states of the pion. The intrinsic momentum of quarks in the nonpointlike pion is limited. To the leading order in pQCD, the breakup of the pion goes via the pQCD analog of the electrodisintegration of the deuteron (for a review, see [12]), i.e., the subprocess  $\pi g \rightarrow q\bar{q}$  in which the struck parton carries the transverse momentum of the absorbed gluon and the spectator parton emerges in the final state with the small transverse momentum it had in the pion (see Fig. 1 below). On the other hand, multiple gluon exchange in collisions with opaque nuclei can give a large transverse kick to both partons. In this communication, we report the nonlinear nuclear  $k_{\perp}$ -factorization formulas for the breakup of pions into forward hard dijets off nuclei. One of our central results is the prediction of a complete azimuthal decorrelation of forward hard dijets.

At the parton level, the produced forward jets retain the fraction  $z_{\pm}$  of the light-cone momentum of the pion that they carried in the incident pion. One may wonder whether the jet longitudinal momentum distributions would give a handle on the so-called pion distribution amplitude ( $\pi$ DA) introduced in [13] (for reviews and recent analyses, see, e.g., [14]), which with some reservations about large higher twist and next-to-leading order pQCD corrections was indeed the case in the coherent diffractive breakup of pions into dijets off nuclei [11, 15, 16]. Our analysis of nonlinear nuclear  $k_{\perp}$ -factorization formulas shows that these expectations are indeed met by the contribution to the dijet inclusive cross section from the in-volume absorption of pions, which comes from the perturbatively small  $q\bar{q}$  dipole states of the pion. However, this contribution is overwhelmed by a large contribution from soft absorption of large  $q\bar{q}$  dipole states of the pion on the front face of a nucleus. In this case, there emerges some infrared-sensitive modulation of the  $z$  dependence of the  $\pi$ DA which brings a model dependence into tests of the pion wave function (WF).

The further presentation is organized as follows. The major thrust is on the distinction between breakup of pointlike photons and nonpointlike pions. To make the discussion self-contained, we present the basic formalism in sufficient detail. In Section 1, we set up the formalism with a brief discussion of the decorrelation of jets in DIS and  $\pi N$  scattering off free nucleons. In Section 2, we present the color-dipole  $S$ -matrix formalism for the breakup into dijets on nuclear targets. In Section 3, we formulate a nonlinear nuclear  $k_{\perp}$  factorization for the inclusive dijet cross section in terms of the collective WW unintegrated gluon density of the nucleus and comment on the salient features of dijet production in DIS off nuclei. The subject of Section 4 is the breakup of nonpointlike pions into dijets. In contrast to the breakup of pointlike photons in DIS, excitation of two hard jets

from pions is only possible on heavy nuclei. The most striking difference from DIS and real photoproduction is that the two pionic forward hard jets produced off a nucleus are completely azimuthally decorrelated. This leading contribution to the breakup cross section comes from soft absorption of pions on the front face of a nucleus. The hard contribution from the in-volume breakup gives rise to back-to-back dijets as in DIS and has the form of a higher twist correction. Its isolation is a challenging but not impossible task and would allow the determination of the  $\pi$ DA. In the Summary and Conclusions, we summarize our main findings and comment on possible experimental tests of our predictions. The predicted distinction between breakup of photons and pions can be tested by the sphericity and thrust analysis of the forward hadronic system in the COMPASS experiment at CERN [17].

## 1. FORWARD DIJETS OFF FREE NUCLEONS AND UNINTEGRATED GLUE OF THE NUCLEON

We set up the formalism using an example of breakup into dijets off free nucleons. Production of high-mass forward hard dijets selects excitation of the  $q\bar{q}$  Fock states of the projectile photon and meson. The relevant pQCD diagrams are shown in Figs. 1a–1d. In the color dipole approach [18–25], the fundamental quantity is the total cross section for interaction of the color dipole  $\mathbf{r}$  with the target nucleon

$$\begin{aligned} \sigma(x, \mathbf{r}) &= \alpha_s(r) \sigma_0(x) \quad (1) \\ &\times \int d^2\boldsymbol{\kappa} f(\boldsymbol{\kappa}) [1 - \exp(i\boldsymbol{\kappa} \cdot \mathbf{r})] = \frac{1}{2} \alpha_s(r) \sigma_0(x) \\ &\times \int d^2\boldsymbol{\kappa} f(\boldsymbol{\kappa}) [1 - \exp(i\boldsymbol{\kappa} \cdot \mathbf{r})] [1 - \exp(-i\boldsymbol{\kappa} \cdot \mathbf{r})], \end{aligned}$$

where  $f(\boldsymbol{\kappa})$  is normalized as  $\int d^2\boldsymbol{\kappa} f(\boldsymbol{\kappa}) = 1$  and is related to the so-called Fadin–Kuraev–Lipatov unintegrated gluon density ([26]; for a recent review and phenomenology, see [27, 28]) of the target nucleon  $\mathcal{F}(x, \kappa^2) = \partial G(x, \kappa^2) / \partial \log \kappa^2$  by

$$f(\boldsymbol{\kappa}) = \frac{4\pi}{N_c \sigma_0(x)} \frac{1}{\kappa^4} \mathcal{F}(x, \kappa^2). \quad (2)$$

Here,  $\sigma_0(x)$  is an auxiliary soft parameter which drops out from major nuclear observables.

First, we consider DIS, where the perturbative small size of dipoles is set by the large virtuality  $Q^2$  of the photon and, then, comment on how the results extend to breakup of real photons and pions into hard dijets. The total photoabsorption cross section equals

$$\sigma_N(Q^2, x) = \int d^2\mathbf{r} dz |\Psi(Q^2, z, \mathbf{r})|^2 \sigma(\mathbf{r}), \quad (3)$$

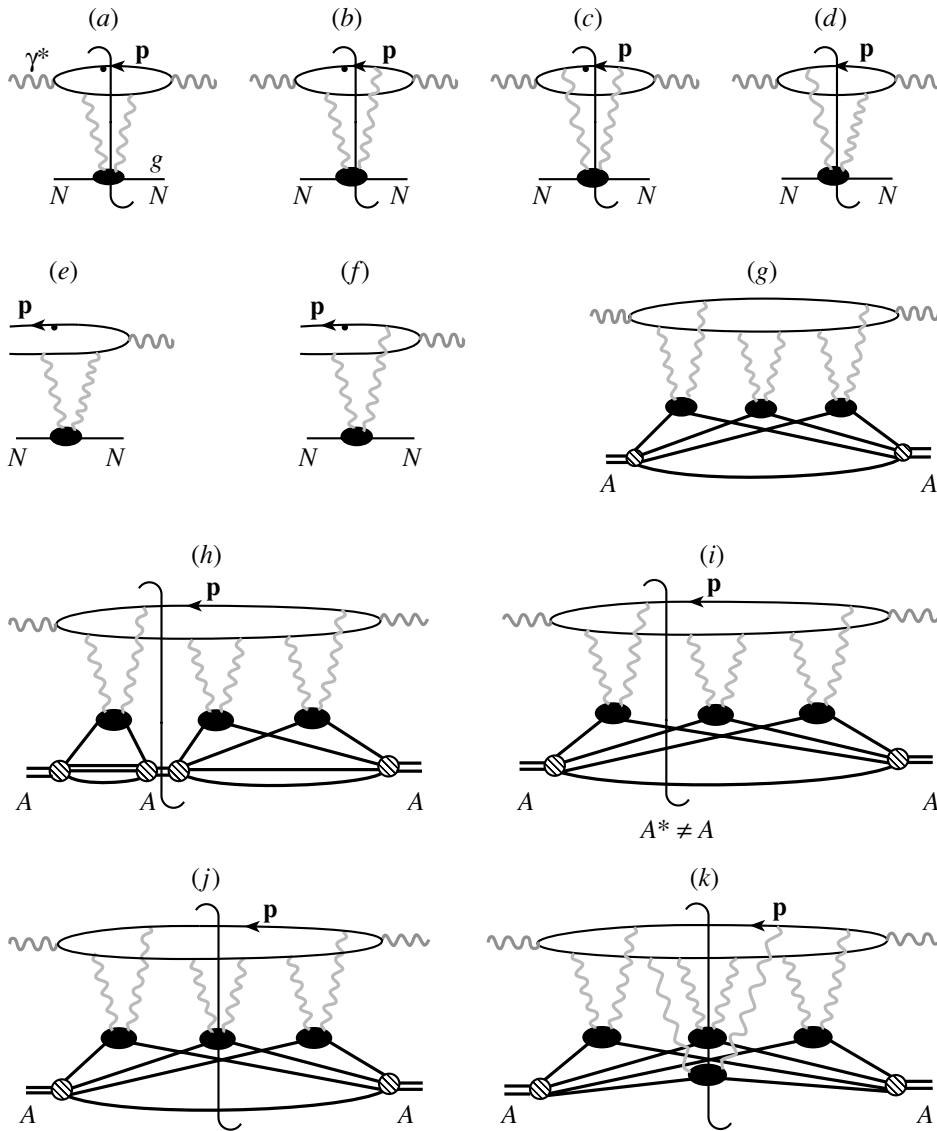


**Fig. 1.** The pQCD diagrams for inclusive (a–d) and diffractive (e, f) DIS off protons and nuclei (g–k). Diagrams (a–d) show the unitarity cuts with color excitation of the target nucleon, (g) is a generic multiple scattering diagram for Compton scattering off nucleus, (h) is the unitarity cut for a coherent diffractive DIS, (i) is the unitarity cut for quasielastic diffractive DIS with excitation of the nucleus  $A^*$ , (j, k) are the unitarity cuts for truly inelastic DIS with single and multiple color excitation of nucleons of the nucleus.

where  $\Psi(Q^2, z, \mathbf{r}) = \langle z, \mathbf{r} | \gamma^* \rangle$  is the WF of the  $q\bar{q}$  Fock state of the photon; here and below, we suppress the argument  $Q^2$  in  $\Psi(Q^2, z, \mathbf{r})$ . Upon the relevant Fourier transformations, one finds the momentum spectrum of the final-state quark prior to the hadronization

$$\frac{d\sigma_N}{d^2\mathbf{p}_+ dz} = \frac{\sigma_0(x)}{2} \frac{\alpha_s(\mathbf{p}_+^2)}{(2\pi)^2} \quad (4)$$

$$\times \int d^2\boldsymbol{\kappa} f(\boldsymbol{\kappa}) |\langle \gamma^* | z, \mathbf{p}_+ \rangle - \langle \gamma^* | z, \mathbf{p}_+ - \boldsymbol{\kappa} \rangle|^2,$$

where  $\mathbf{p}_+$  is the transverse momentum of the quark jet,  $\mathbf{p}_- = -\mathbf{p}_+ + \boldsymbol{\kappa}$  is the transverse momentum of

the antiquark jet, and  $z_+ = z$  and  $z_- = 1 - z$  are the fractions of the photon's light-cone momentum carried by the quark and antiquark jets, respectively. For our formalism to apply, we require that the variables  $z_{\pm}$  for the observed jets add up to unity,  $x_{\gamma} = z_+ + z_- = 1$ , and the rapidity separation of jets be small,  $z_+ \sim z_- \sim 1/2$ , which in the realm of DIS is often referred to as the unresolved or direct photon interaction ([29] and references therein).

Now notice that the transverse momentum of the gluon is precisely the decorrelation momentum  $\boldsymbol{\Delta} =$

$\mathbf{p}_+ + \mathbf{p}_-$ , so that, in the still further differential form,

$$\begin{aligned} \frac{d\sigma_N}{dzd^2\mathbf{p}_+d^2\mathbf{\Delta}} &= \frac{\sigma_0(x)\alpha_s(\mathbf{p}_+^2)}{2(2\pi)^2} f(\mathbf{\Delta}) \quad (5) \\ &\times |\langle\gamma^*|z, \mathbf{p}_+\rangle - \langle\gamma^*|z, \mathbf{p}_+ - \mathbf{\Delta}\rangle|^2 = \frac{\alpha_s(\mathbf{p}_+^2)}{2\pi N_c} \\ &\times \frac{\mathcal{F}(x, \mathbf{\Delta}^2)}{\Delta^4} |\langle\gamma^*|z, \mathbf{p}_+\rangle - \langle\gamma^*|z, \mathbf{p}_+ - \mathbf{\Delta}\rangle|^2. \end{aligned}$$

This is the leading-order result from  $k_\perp$  factorization; for the applications to DIS off free nucleons, see [8, 9] and references therein. Upon summing over the helicities  $\lambda, \bar{\lambda}$  of the FS quark and antiquark, for transverse photons and flavor  $f$ , one has

$$\begin{aligned} &|\langle\gamma^*|z, \mathbf{p}\rangle - \langle\gamma^*|z, \mathbf{p} - \boldsymbol{\kappa}\rangle|_{\lambda\gamma=\pm 1}^2 \quad (6) \\ &= 2N_c e_f^2 \alpha_{\text{em}} \left\{ [z^2 + (1-z)^2] \right. \\ &\times \left( \frac{\mathbf{p}}{\mathbf{p}^2 + \varepsilon^2} - \frac{\mathbf{p} - \boldsymbol{\kappa}}{(\mathbf{p} - \boldsymbol{\kappa})^2 + \varepsilon^2} \right)_{\lambda+\bar{\lambda}=0}^2 \\ &\left. + m_f^2 \left( \frac{1}{\mathbf{p}^2 + \varepsilon^2} - \frac{1}{(\mathbf{p} - \boldsymbol{\kappa})^2 + \varepsilon^2} \right)_{\lambda+\bar{\lambda}=\lambda_\gamma}^2 \right\} \end{aligned}$$

and, for longitudinal photons,

$$\begin{aligned} &|\langle\gamma^*|z, \mathbf{p}\rangle - \langle\gamma^*|z, \mathbf{p} - \boldsymbol{\kappa}\rangle|_{\lambda_\gamma=0}^2 \quad (7) \\ &= 8N_c e_f^2 \alpha_{\text{em}} Q^2 z^2 (1-z)^2 \\ &\times \left( \frac{1}{\mathbf{p}^2 + \varepsilon^2} - \frac{1}{(\mathbf{p} - \boldsymbol{\kappa})^2 + \varepsilon^2} \right)_{\lambda+\bar{\lambda}=\lambda_\gamma}^2, \end{aligned}$$

where

$$\varepsilon^2 = z(1-z)Q^2 + m_f^2. \quad (8)$$

The leading  $\log Q^2$  contribution to the dijet cross section comes from  $\mathbf{\Delta}^2 \lesssim \mathbf{p}_+^2 + \varepsilon^2$ . A useful small- $\mathbf{\Delta}$  expansion for excitation of hard,  $\mathbf{p}_+^2 \gg \varepsilon^2 = z(1-z)Q^2$ , light flavor dijets from transverse photons is

$$\begin{aligned} \frac{d\sigma_N}{dzd^2\mathbf{p}_+d^2\mathbf{\Delta}} &\approx \frac{1}{\pi} e_f^2 \alpha_{\text{em}} \alpha_s(\mathbf{p}_+^2) [z^2 + (1-z)^2] \\ &\times \frac{1}{\Delta^4} \frac{\partial G(x, \mathbf{\Delta}^2)}{\partial \log \mathbf{\Delta}^2} \frac{\mathbf{\Delta}^2}{(\varepsilon^2 + \mathbf{p}_+^2)^2}. \quad (9) \end{aligned}$$

Then the single-jet cross section is proportional to the logarithmic integral

$$\frac{1}{\pi} \int_0^\pi d\phi \int \frac{d\mathbf{\Delta}^2}{\mathbf{\Delta}^2} \frac{\partial G(x, \mathbf{\Delta}^2)}{\partial \log \mathbf{\Delta}^2} = G(x, \mathbf{p}_+^2) \quad (10)$$

familiar from the conventional collinear approximation [1].

The small- $x$  result (9) shows that for a pointlike projectile of which the photon is just a representative, the dijets acquire their large transverse momentum from the intrinsic momentum of the quark and antiquark in the WF of the projectile; hence, dubbing this process a breakup of the photon into hard dijets is appropriate. The perturbative hard scale  $Q_h^2$  for our process is set by  $Q_h^2 \simeq (4\mathbf{p}_+^2 + Q^2)$  and unintegrated gluon density of the proton enters (8) at the Bjorken variable  $x = (4\mathbf{p}_+^2 + Q^2)/W^2$ , where  $W$  is the  $\gamma^*p$  center-of-mass energy. One of the major findings of [6] is that the azimuthal decorrelation of dijets exhibits only a marginal dependence on  $Q^2$ , and the above-presented formalism is fully applicable to real photons.

Similar formulas apply as well to nonpointlike pions. Indeed, as argued in [11], the FS interaction between the FS quark and antiquark can be neglected and the  $q\bar{q}$  plane-wave approximation becomes applicable as soon as the invariant mass of the forward hard jets exceeds a typical mass scale of prominent meson resonances. As shown in [11], in the coherent diffractive breakup of pions into hard dijets at small  $x$ , the diffractive amplitude is dominated by the Pomeron-splitting mechanism of Fig. 1*f*, when the quark and antiquark with small intrinsic transverse momentum in the pion simultaneously acquire large back-to-back transverse momentum from exchanged gluons [30] (for confirmation of the dominance of the Pomeron-splitting mechanism to higher orders in pQCD, see [15, 16]). The transverse momentum distribution in truly inelastic  $\pi N$  collisions is different. In contrast to pointlike photons, for pions, the  $q\bar{q}$  WF  $\langle\pi|\pi\rangle$  is a soft function which decreases steeply at  $\mathbf{p}^2 > 1/R_\pi^2$  (here,  $R_\pi$  is the pion radius; for a review of the dominance of the soft WF and references, see [31, 32]). We are interested in jets with a transverse momentum much larger than the intrinsic transverse momentum of (anti)quarks in a pion. The unitarity cuts of diagrams of Figs. 1*a*–*d* show that, to the leading order in pQCD, only one parton of the pion—let it be the quark—can pick up the large transverse momentum from the exchanged gluon and give rise to a hard jet in the pion fragmentation region of  $\pi N$  interactions; the spectator jet retains the soft intrinsic transverse momentum that the antiquark had inside the pion. Specifically, if the quark jet has a large transverse momentum  $\mathbf{p}_+$ , then  $\langle\pi|z, \mathbf{p}_+\rangle$  can be neglected,  $\mathbf{\Delta} \approx \mathbf{p}_+$ , and the pion breakup cross section takes the form

$$\frac{d\sigma_{\pi N}}{dzd^2\mathbf{p}_+d^2\mathbf{p}_-} = \frac{\alpha_s(\mathbf{p}_+^2)}{2\pi} \frac{\mathcal{F}(x, \mathbf{p}_+^2)}{p_+^4} |\langle\pi|z, \mathbf{p}_-\rangle|^2. \quad (11)$$

It shows clearly how the spectator antiquark retains the small intrinsic transverse momentum that it had in the incident pion (as an analogy, cf. the electrodisintegration of the deuteron [12]). Evidently, excitation of two forward hard jets in  $\pi N$  collisions is only possible to higher orders in pQCD. In hard inelastic  $\pi A$  collisions, the higher order pQCD contributions from multiple scatterings are enhanced by the size of the extended nuclear target, and the purpose of this communication is a description of the breakup of pions into hard dijets in inelastic collisions off heavy nuclei within our nonlinear nuclear  $k_{\perp}$ -factorization formalism [6].

The minor technical difference from DIS is the change from the pointlike  $\gamma^* q\bar{q}$  vertex  $eA_{\mu}\bar{\Psi}\gamma_{\mu}\Psi$  to the nonpointlike  $\pi q\bar{q}$  vertex  $i\Gamma_{\pi}(M^2)\bar{\Psi}\gamma_5\Psi$ . In terms of the quark and antiquark helicities  $\lambda$  and  $\bar{\lambda}$ , the  $\pi q(\mathbf{k})\bar{q}(-\mathbf{k})$  vertex has the form [11, 33]

$$\begin{aligned} & \bar{\Psi}_{\lambda}(\mathbf{k})\gamma_5\Psi_{\bar{\lambda}}(-\mathbf{k}) \\ &= \frac{\lambda}{\sqrt{z(1-z)}}[m_f\delta_{\lambda-\bar{\lambda}} - \sqrt{2}\mathbf{k}\cdot\mathbf{e}_{-\lambda}\delta_{\lambda\bar{\lambda}}], \end{aligned} \quad (12)$$

where  $m_f$  is the quark mass and  $\mathbf{e}_{\lambda} = \frac{1}{\sqrt{2}}(\lambda\mathbf{e}_x + i\mathbf{e}_y)$  is the familiar polarization vector for the state of helicity  $\lambda$ . In transitions of spin-zero pions into  $q\bar{q}$  states with the sum of helicities  $\lambda + \bar{\lambda} = \pm 1$ , the latter is compensated by the orbital momentum of quark and antiquark. In what follows, we shall only need the leading twist term,  $\propto\delta_{\lambda-\bar{\lambda}}$ , in (12) (cf. with the coherent diffractive breakup [11]). The corresponding radial WF  $\Psi_{\pi}(z, \mathbf{r})$  is related to the  $\pi \rightarrow \mu\nu$  decay constant  $F_{\pi}$  and the so-called  $\pi$ DA  $\varphi_{\pi}(z)$  by

$$\Psi_{\pi}(z, \mathbf{r} = 0) = \int \frac{d^2\mathbf{p}}{(2\pi)^2} \langle z, \mathbf{p} | \pi \rangle = \sqrt{\frac{\pi}{2N_c}} F_{\pi} \varphi_{\pi}(z). \quad (13)$$

For the purposes of our discussion, a convenient normalization is  $\int_0^1 dz \varphi_{\pi}(z) = 1$ . We follow the Particle Data Group convention  $F_{\pi} = 131$  MeV [34]. The  $\pi$ DA depends [13] on the hard scale not shown in (13); we shall comment on the relevant scale whenever appropriate.

## 2. THE COLOR-DIPOLE $S$ -MATRIX TREATMENT OF THE BREAKUP INTO DIJETS ON NUCLEAR TARGETS

We focus on the breakup into dijets at small  $x$ ,  $x \ll x_A = 1/R_A m_N \ll 1$  ( $R_A$  is the radius of the nucleus, and  $m_N$  is the mass of a nucleon), when the propagation of the  $q\bar{q}$  pair inside the nucleus can be treated in the straight-path approximation. First, we review

the simpler case of DIS [6]. We work in the conventional approximation of two  $t$ -channel gluons for DIS off free nucleons. The relevant unitarity cuts of the forward Compton scattering amplitude are shown in Figs. 1a–1d and describe the transition from the color-neutral  $q\bar{q}$  dipole to the color-octet  $q\bar{q}$  pair.<sup>4)</sup> The unitarity cuts of the nuclear Compton scattering amplitude which correspond to the genuine inelastic DIS with color excitation of the nucleus are shown in Figs. 1j and 1k. The diagram 1k describes multiple color excitations of a nucleus when the propagating color-octet  $q\bar{q}$  pair rotates in the color space.

Let  $\mathbf{b}_+$  and  $\mathbf{b}_-$  be the impact parameters of the quark and antiquark, respectively, and  $S_A(\{\mathbf{b}_j\}, \mathbf{b}_+, \mathbf{b}_-)$  be the  $S$  matrix for interaction of the  $q\bar{q}$  pair with the nucleus, where  $\{\mathbf{b}_j\}$  stands for the positions of nucleons. The initial state  $|A; 1\rangle$  is a color-singlet nucleus made of color-singlet nucleons and a color-singlet  $q\bar{q}$  dipole; in the final state, we sum over all excitations of the target nucleus when one or several nucleons have been color excited. A convenient way to sum such cross sections is offered by the closure relation [35]. Regarding the color states  $c_{km}$  of the  $q_k\bar{q}_m$  pair, we sum over all octet and singlet states. Then, the two-body inclusive spectrum is calculated in terms of the two-body density matrix as

$$\begin{aligned} & \frac{d\sigma_{\text{inel}}}{dzd^2\mathbf{p}_+d^2\mathbf{p}_-} = \frac{1}{(2\pi)^4} \\ & \times \int d^2\mathbf{b}'_+d^2\mathbf{b}'_-d^2\mathbf{b}_+d^2\mathbf{b}_- \exp[-i\mathbf{p}_+(\mathbf{b}_+ - \mathbf{b}'_+) \\ & - i\mathbf{p}_-(\mathbf{b}_- - \mathbf{b}'_-)] \Psi^*(z, \mathbf{b}'_+ - \mathbf{b}'_-) \Psi(z, \mathbf{b}_+ - \mathbf{b}_-) \\ & \times \Omega^{\text{inel}}(\mathbf{b}'_+, \mathbf{b}'_-, \mathbf{b}_+, \mathbf{b}_-), \end{aligned} \quad (14)$$

where the superscript “inel” refers to the truly inelastic cross section, with the contribution from diffractive processes subtracted. The projectile WF  $\Psi$  in general carries a dependence on helicities, flavor, and, for the photon, virtuality  $Q^2$ , which have not been put into evidence here. The generalized cross section operator  $\Omega^{\text{inel}}(\mathbf{b}'_+, \mathbf{b}'_-, \mathbf{b}_+, \mathbf{b}_-)$  is expressed through the  $q\bar{q}$ -nucleus  $S$  matrix as

$$\begin{aligned} & \Omega^{\text{inel}}(\mathbf{b}'_+, \mathbf{b}'_-, \mathbf{b}_+, \mathbf{b}_-) \\ &= \sum_{A^*} \sum_{km} \langle 1; A | S_A^*(\{\mathbf{b}_j\}, \mathbf{b}'_+, \mathbf{b}'_-) | A^*; c_{km} \rangle \\ & \times \langle c_{km}; A^* | S_A(\{\mathbf{b}_j\}, \mathbf{b}_+, \mathbf{b}_-) | A; 1 \rangle \\ & - \langle 1; A | S_A^*(\{\mathbf{b}_j\}, \mathbf{b}'_+, \mathbf{b}'_-) | A; 1 \rangle \\ & \times \langle 1; A | S_A(\{\mathbf{b}_j\}, \mathbf{b}_+, \mathbf{b}_-) | A; 1 \rangle. \end{aligned} \quad (15)$$

<sup>4)</sup>To be more precise, for arbitrary  $N_c$ , the color-excited  $q\bar{q}$  pair is in the adjoint representation and quarks in fundamental representation of  $SU(N_c)$ ; our reference to the color octet and triplet must not cause any confusion.

Upon the application of closure in the sum over nuclear states, the first term in Eq. (15) becomes

$$\begin{aligned} & \sum_{A^*} \sum_{km} \langle A | \{ \langle 1 | S_A^* (\{ \mathbf{b}_j \}, \mathbf{b}'_+, \mathbf{b}'_-) | c_{km} \rangle \} | A^* \rangle \quad (16) \\ & \times \langle A^* | \{ \langle c_{km} | S_A (\{ \mathbf{b}_j \}, \mathbf{b}_+, \mathbf{b}_-) | 1 \rangle \} | A \rangle \\ & = \left\langle A \left| \left\{ \sum_{km} \langle 1 | S_A^* (\{ \mathbf{b}_j \}, \mathbf{b}'_+, \mathbf{b}'_-) | c_{km} \rangle \right. \right. \right. \\ & \quad \left. \left. \times \langle c_{km} | S_A (\{ \mathbf{b}_j \}, \mathbf{b}_+, \mathbf{b}_-) | 1 \rangle \right\} \right| A \rangle \end{aligned}$$

and can be considered as an intranuclear evolution operator for the two-body density matrix.

The further analysis of (16) is a non-Abelian generalization of the formalism developed by one of the authors (B.G.Z.) for the in-medium evolution of ultrarelativistic positronium [36]. Let the QCD eikonal for the quark–nucleon and antiquark–nucleon one-gluon exchange interaction be  $T_+^a \Delta(\mathbf{b})$  and  $T_-^a \Delta(\mathbf{b})$ , where  $T_+^a$  and  $T_-^a$  are the  $SU(N_c)$  generators for the quark and antiquarks states, respectively. The vertex  $V_a$  for excitation of the nucleon  $g^a N \rightarrow N_a^*$  into a color-octet state is so normalized that, after application of closure, the vertex  $g^a g^b NN$  in the diagrams of Figs. 1a–1d is  $\delta_{ab}$ . Then, to the two-gluon exchange approximation, the  $S$  matrix of the  $q\bar{q}$ -nucleon interaction equals

$$\begin{aligned} S_N(\mathbf{b}_+, \mathbf{b}_-) &= 1 + i[T_+^a \Delta(\mathbf{b}_+) \quad (17) \\ &+ T_-^a \Delta(\mathbf{b}_-)] V_a - \frac{1}{2} [T_+^a \Delta(\mathbf{b}_+) + T_-^a \Delta(\mathbf{b}_-)]^2. \end{aligned}$$

The profile function for interaction of the  $q\bar{q}$  dipole with a nucleon is  $\Gamma(\mathbf{b}_+, \mathbf{b}_-) = 1 - S_N(\mathbf{b}_+, \mathbf{b}_-)$  and the dipole cross section for the color-singlet  $q\bar{q}$  dipole equals

$$\begin{aligned} \sigma(\mathbf{b}_+ - \mathbf{b}_-) &= 2 \int d^2 \mathbf{b}_+ \langle N | \Gamma(\mathbf{b}_+, \mathbf{b}_-) | N \rangle \quad (18) \\ &= \frac{N_c^2 - 1}{2N_c} \int d^2 \mathbf{b}_+ [\Delta(\mathbf{b}_+) - \Delta(\mathbf{b}_-)]^2. \end{aligned}$$

The nuclear  $S$  matrix of the straight-path approximation for the dilute-gas nucleus is given by [35]

$$S_A(\{ \mathbf{b}_j \}, \mathbf{b}_+, \mathbf{b}_-) = \prod_{j=1}^A S_N(\mathbf{b}_+ - \mathbf{b}_j, \mathbf{b}_- - \mathbf{b}_j), \quad (19)$$

where the ordering along the longitudinal path is understood. To the two-gluon exchange approximation, only the terms quadratic in  $\Delta(\mathbf{b}_j)$  must be kept in the evaluation of the single-nucleon matrix elements

$$\langle N_j | S_N^*(\mathbf{b}'_+ - \mathbf{b}_j, \mathbf{b}'_- - \mathbf{b}_j)$$

$$\times S_N(\mathbf{b}_+ - \mathbf{b}_j, \mathbf{b}_- - \mathbf{b}_j) | N_j \rangle$$

which enter the calculation of  $S_A^* S_A$ . The evolution operator for the two-body density matrix (16) equals the  $S$  matrix  $S_{4A}(\mathbf{b}_+, \mathbf{b}_-, \mathbf{b}'_+, \mathbf{b}'_-)$  for scattering of a fictitious four-parton state composed of two  $q\bar{q}$  pairs in an overall color-singlet state [36–38]. Namely, because  $(T_+^a)^* = -T_-^a$ , within the two-gluon exchange approximation, the quarks entering the complex-conjugate  $S_A^*$  in (16) can be viewed as antiquarks, so that

$$\begin{aligned} & \sum_{km} \langle 1 | S_A^* (\{ \mathbf{b}_j \}, \mathbf{b}'_+, \mathbf{b}'_-) | c_{km} \rangle \quad (20) \\ & \times \langle c_{km} | S_A (\{ \mathbf{b}_j \}, \mathbf{b}_+, \mathbf{b}_-) | 1 \rangle \\ & = \sum_{kmjl} \delta_{kl} \delta_{mj} \langle c_{km} c_{jl} | S_{4A}(\mathbf{b}'_+, \mathbf{b}'_-, \mathbf{b}_+, \mathbf{b}_-) | 11 \rangle. \end{aligned}$$

While the first  $q\bar{q}$  pair is formed by the initial quark  $q$  and antiquark  $\bar{q}$  at impact parameters  $\mathbf{b}_+$  and  $\mathbf{b}_-$ , respectively, in the second pair  $q'\bar{q}'$ , the quark  $q'$  propagates at an impact parameter  $\mathbf{b}'_-$  and the antiquark  $\bar{q}'$  at an impact parameter  $\mathbf{b}'_+$ . In the initial state, both the  $q\bar{q}$  and  $q'\bar{q}'$  pairs are in color-singlet states:  $|in\rangle = |11\rangle$ . The sum over color states of the produced  $q\bar{q}$  pair can be represented as

$$\begin{aligned} & \sum_{km} \langle c_{km} c_{km} | S_{4A}(\mathbf{b}'_+, \mathbf{b}'_-, \mathbf{b}_+, \mathbf{b}_-) | 11 \rangle \quad (21) \\ & = \langle 11 | S_{4A}(\mathbf{b}'_+, \mathbf{b}'_-, \mathbf{b}_+, \mathbf{b}_-) | 11 \rangle \\ & + \sqrt{N_c^2 - 1} \langle 88 | S_{4A}(\mathbf{b}'_+, \mathbf{b}'_-, \mathbf{b}_+, \mathbf{b}_-) | 11 \rangle. \end{aligned}$$

Let  $\sigma_4(\mathbf{b}'_+, \mathbf{b}'_-, \mathbf{b}_+, \mathbf{b}_-)$  be the color-dipole cross-section operator for the four-body state. It is convenient to introduce the average impact parameter

$$\mathbf{b} = \frac{1}{4} (\mathbf{b}_+ + \mathbf{b}'_+ + \mathbf{b}_- + \mathbf{b}'_-) \quad (22)$$

and

$$\mathbf{s} = \mathbf{b}_+ - \mathbf{b}'_+ \quad (23)$$

for the variable conjugate to the decorrelation momentum, in terms of which

$$\begin{aligned} \mathbf{b}_+ - \mathbf{b}'_- &= \mathbf{s} + \mathbf{r}', & \mathbf{b}_- - \mathbf{b}'_+ &= \mathbf{s} - \mathbf{r}, \\ \mathbf{b}_- - \mathbf{b}'_- &= \mathbf{s} - \mathbf{r} + \mathbf{r}'. \end{aligned} \quad (24)$$

Then the standard evaluation of the nuclear expectation value for a dilute gas nucleus neglecting the size of color dipoles compared to the radius of a heavy nucleus gives [35]

$$S_{4A}(\mathbf{b}'_+, \mathbf{b}'_-, \mathbf{b}_+, \mathbf{b}_-) = \exp \left[ -\frac{1}{2} \sigma_4(\mathbf{s}, \mathbf{r}, \mathbf{r}') T(\mathbf{b}) \right], \quad (25)$$

where

$$T(\mathbf{b}) = \int db_z n_A(b_z, \mathbf{b}) \quad (26)$$

is the optical thickness of a nucleus at an impact parameter  $\mathbf{b}$ , and the nuclear matter density  $n_A(b_z, \mathbf{b})$  is so normalized that  $\int db_z d^2\mathbf{b} n_A(z, \mathbf{b}) = A$ . The single-nucleon  $S$  matrix (17) contains transitions from the color-singlet to the both color-singlet and color-octet  $q\bar{q}$  pairs. However, only the color-singlet operators contribute to  $\langle N_j | S_N^*(\mathbf{b}'_+ - \mathbf{b}_j, \mathbf{b}'_- - \mathbf{b}_j) S_N(\mathbf{b}_+ - \mathbf{b}_j, \mathbf{b}_- - \mathbf{b}_j) | N_j \rangle$ , and the matrix  $\sigma_4(\mathbf{s}, \mathbf{r}, \mathbf{r}')$  only includes transitions between the  $|11\rangle$  and  $|88\rangle$  color-singlet four-parton states.

The calculation of  $\sigma_4(\mathbf{s}, \mathbf{r}, \mathbf{r}')$  is found in [6]; here, we only cite the results:

$$\sigma_{11} = \langle 11 | \sigma_4 | 11 \rangle = \sigma(\mathbf{r}) + \sigma(\mathbf{r}'), \quad (27)$$

$$\sigma_{88} = \langle 88 | \sigma_4 | 88 \rangle \quad (28)$$

$$\begin{aligned} &= \frac{N_c^2 - 2}{N_c^2 - 1} [\sigma(\mathbf{s}) + \sigma(\mathbf{s} - \mathbf{r} + \mathbf{r}')] \\ &+ \frac{2}{N_c^2 - 1} [\sigma(\mathbf{s} + \mathbf{r}') + \sigma(\mathbf{s} - \mathbf{r})] \\ &- \frac{1}{N_c^2 - 1} [\sigma(\mathbf{r}) + \sigma(\mathbf{r}')], \end{aligned}$$

$$\sigma_{18} = \sigma_{81} = \langle 11 | \sigma_4 | 88 \rangle = \frac{1}{\sqrt{N_c^2 - 1}} \quad (29)$$

$$\begin{aligned} &\times [\sigma(\mathbf{s}) - \sigma(\mathbf{s} + \mathbf{r}') - \sigma(\mathbf{s} - \mathbf{r}) + \sigma(\mathbf{s} - \mathbf{r} + \mathbf{r}')] \\ &\equiv -\frac{\Sigma_{18}(\mathbf{s}, \mathbf{r}, \mathbf{r}')}{\sqrt{N_c^2 - 1}}. \end{aligned}$$

The term in (14) which subtracts the contribution from processes without color excitation of the target nucleus equals

$$\begin{aligned} &\langle 1; A | S_A^*(\mathbf{b}'_+, \mathbf{b}'_-) | A; 1 \rangle \langle 1; A | S_A(\mathbf{b}_+, \mathbf{b}_-) | A; 1 \rangle \\ &= \exp \left\{ -\frac{1}{2} [\sigma(\mathbf{r}) + \sigma(\mathbf{r}')] T(\mathbf{b}) \right\} \\ &= \exp \left[ -\frac{1}{2} \sigma_{11} T(\mathbf{b}) \right]. \end{aligned} \quad (30)$$

It is convenient to use the Sylvester expansion

$$\begin{aligned} \exp \left[ -\frac{1}{2} \sigma_4 T(\mathbf{b}) \right] &= \exp \left[ -\frac{1}{2} \Sigma_1 T(\mathbf{b}) \right] \\ &\times \frac{\sigma_4 - \Sigma_2}{\Sigma_1 - \Sigma_2} + \exp \left[ -\frac{1}{2} \Sigma_2 T(\mathbf{b}) \right] \frac{\sigma_4 - \Sigma_1}{\Sigma_2 - \Sigma_1}, \end{aligned} \quad (31)$$

where  $\Sigma_{1,2}$  are the two eigenvalues of the operator  $\sigma_4$ ,

$$\Sigma_{1,2} = \frac{1}{2}(\sigma_{11} + \sigma_{88}) \mp \frac{1}{2}(\sigma_{11} - \sigma_{88}) \quad (32)$$

$$\times \sqrt{1 + \frac{4\sigma_{18}^2}{(\sigma_{11} - \sigma_{88})^2}}.$$

An application to (21) of the Sylvester expansion gives for the function  $\Omega^{\text{inel}}$  in the integrand of (14)

$$\begin{aligned} &\Omega^{\text{inel}}(\mathbf{b}'_+, \mathbf{b}'_-, \mathbf{b}_+, \mathbf{b}_-) \quad (33) \\ &= (\langle 11 | + \sqrt{N_c^2 - 1} \langle 88 |) \exp \left[ -\frac{1}{2} \sigma_4 T(\mathbf{b}) \right] | 11 \rangle \\ &- \exp \left[ -\frac{1}{2} \sigma_{11} T(\mathbf{b}) \right] = \exp \left[ -\frac{1}{2} \Sigma_2 T(\mathbf{b}) \right] \\ &- \exp \left[ -\frac{1}{2} \sigma_{11} T(\mathbf{b}) \right] + \frac{\sigma_{11} - \Sigma_2}{\Sigma_1 - \Sigma_2} \\ &\times \left\{ \exp \left[ -\frac{1}{2} \Sigma_1 T(\mathbf{b}) \right] - \exp \left[ -\frac{1}{2} \Sigma_2 T(\mathbf{b}) \right] \right\} \\ &+ \frac{\sqrt{N_c^2 - 1} \sigma_{18}}{\Sigma_1 - \Sigma_2} \left\{ \exp \left[ -\frac{1}{2} \Sigma_1 T(\mathbf{b}) \right] \right. \\ &\left. - \exp \left[ -\frac{1}{2} \Sigma_2 T(\mathbf{b}) \right] \right\}. \end{aligned}$$

Notice that the difference between  $\Sigma_2$  and  $\sigma_{11} = \sigma(\mathbf{r}) + \sigma(\mathbf{r}')$  is quadratic or of higher order in the off-diagonal  $\sigma_{18}$  [see Eq. (32)]. Consequently, the Sylvester expansion (33) starts with terms  $\propto \sigma_{18}^2$ , with the exception of the pieces in the last two lines of (33), which start with terms  $\propto \sigma_{18}$ . Then it is convenient to represent (33) as an impulse approximation (IA) term times a nuclear distortion factor  $D_A(\mathbf{s}, \mathbf{r}, \mathbf{r}', \mathbf{b})$ ,

$$\Omega^{\text{inel}}(\mathbf{b}'_+, \mathbf{b}'_-, \mathbf{b}_+, \mathbf{b}_-) \equiv \Sigma_{18}(\mathbf{s}, \mathbf{r}, \mathbf{r}') D_A(\mathbf{s}, \mathbf{r}, \mathbf{r}', \mathbf{b}), \quad (34)$$

so that

$$\begin{aligned} \frac{d\sigma^{\text{inel}}}{d^2\mathbf{b} dz d^2\mathbf{p}_+ d^2\mathbf{p}_-} &= \frac{1}{2(2\pi)^4} \int d^2\mathbf{s} d^2\mathbf{r} d^2\mathbf{r}' \quad (35) \\ &\times \exp[-i(\mathbf{p}_+ + \mathbf{p}_-) \cdot \mathbf{s} + i\mathbf{p}_- \cdot (\mathbf{r}' - \mathbf{r})] \\ &\times \Psi^*(z, \mathbf{r}') \Psi(z, \mathbf{r}) T(\mathbf{b}) D_A(\mathbf{s}, \mathbf{r}, \mathbf{r}', \mathbf{b}) \Sigma_{18}(\mathbf{s}, \mathbf{r}, \mathbf{r}'). \end{aligned}$$

What we need is a Fourier representation for each and every factor in (35).

### 3. NONLINEAR $k_\perp$ FACTORIZATION FOR BREAKUP INTO DIJETS AND COLLECTIVE WW GLUE OF NUCLEI

Upon the application of (1), the IA factor in (34) admits the simple Fourier representation

$$\Sigma_{18}(\mathbf{s}, \mathbf{r}, \mathbf{r}') = \sigma(\mathbf{s} + \mathbf{r}') + \sigma(\mathbf{s} - \mathbf{r}) - \sigma(\mathbf{s}) \quad (36)$$

$$- \sigma(\mathbf{s} - \mathbf{r} + \mathbf{r}') = \alpha_s \sigma_0(x) \int d^2\boldsymbol{\kappa} f(\boldsymbol{\kappa})$$

$$\times \exp[i\boldsymbol{\kappa} \cdot \mathbf{s}] \{1 - \exp[i\boldsymbol{\kappa} \cdot \mathbf{r}']\} \{1 - \exp[-i\boldsymbol{\kappa} \cdot \mathbf{r}]\}.$$

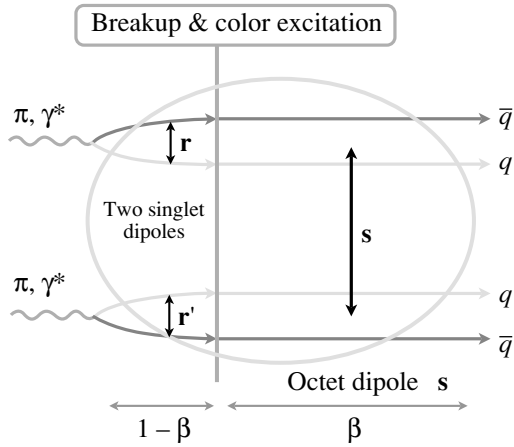


**Fig. 2.** To the leading order the dijet system is excited into the color-octet state on one nucleon after having travelled a fraction  $1 - \beta$  of the nucleus. After that an almost point-like octet  $q\bar{q}$  system travels the remaining fraction  $\beta$ .

The Fourier representation of the nuclear distortion factor in terms of the collective nuclear WW gluon distribution as defined in [5, 11] is not a trivial task, though appealing analytic results are derived in the large- $N_c$  approximation.

The crucial point is that, in the large- $N_c$  approximation,  $\Sigma_1 = \sigma(\mathbf{s}) + \sigma(\mathbf{s} + \mathbf{r}' - \mathbf{r})$  and  $\Sigma_2 = \Sigma_{22} = \sigma(\mathbf{r}) + \sigma(\mathbf{r}')$ , so that only the last term in the Sylvester expansion (33) contributes to the jet–jet inclusive cross section. At large  $N_c$ , the initial color-singlet dipole excites to the color-octet state and further intranuclear color exchanges only rotate the dipole between different color-octet states. This is indicated schematically in Fig. 2. Then the nuclear distortion factor takes on a simple form

$$D_A(\mathbf{s}, \mathbf{r}, \mathbf{r}', \mathbf{b}) = \frac{2}{(\Sigma_2 - \Sigma_1)T(\mathbf{b})} \quad (37)$$

$$\times \left\{ \exp \left[ -\frac{1}{2}\Sigma_1 T(\mathbf{b}) \right] - \exp \left[ -\frac{1}{2}\Sigma_2 T(\mathbf{b}) \right] \right\}.$$

The denominator  $(\Sigma_2 - \Sigma_1)$  is problematic from the point of view of the Fourier transform, but it can be eliminated by the integral representation

$$D_A(\mathbf{s}, \mathbf{r}, \mathbf{r}', \mathbf{b}) \quad (38)$$

$$\begin{aligned} &= \int_0^1 d\beta \exp \left\{ -\frac{1}{2}[\beta\Sigma_1 + (1-\beta)\Sigma_2]T(\mathbf{b}) \right\} \\ &= \int_0^1 d\beta \exp \left\{ -\frac{1}{2}(1-\beta)[\sigma(\mathbf{r}) + \sigma(\mathbf{r}')]T(\mathbf{b}) \right\} \\ &\times \exp \left\{ -\frac{1}{2}\beta[\sigma(\mathbf{s}) + \sigma(\mathbf{s} + \mathbf{r}' - \mathbf{r})]T(\mathbf{b}) \right\}. \end{aligned}$$

Here, the former two exponential factors describe the initial-state intranuclear distortion of the incoming color-singlet  $q\bar{q}$  dipole state, whereas the last two factors describe the final-state distortion of the outgoing color-octet states.

Next we apply to the exponential factors in (38) the NSS representation in terms of the collective WW unintegrated gluon density of the nucleus [5, 11]:

$$\begin{aligned} &\exp \left[ -\frac{1}{2}\sigma(\mathbf{s})T(\mathbf{b}) \right] \quad (39) \\ &= \int d^2\boldsymbol{\kappa} \Phi(\nu_A(\mathbf{b}), \boldsymbol{\kappa}) \exp(i\boldsymbol{\kappa} \cdot \mathbf{s}), \end{aligned}$$

where

$$\begin{aligned} \Phi(\nu_A(\mathbf{b}), \boldsymbol{\kappa}) &= \sum_{j \geq 0} w_j(\nu_A(\mathbf{b})) f^{(j)}(\boldsymbol{\kappa}) \quad (40) \\ &= \exp(-\nu_A(\mathbf{b})) f^{(0)}(\boldsymbol{\kappa}) + \phi_{\text{WW}}(\nu_A(\mathbf{b}), \boldsymbol{\kappa}). \end{aligned}$$

Here,  $\phi_{\text{WW}}(\nu_A(\mathbf{b}), \boldsymbol{\kappa})$  is the unintegrated collective nuclear WW glue per unit area in the impact parameter plane,

$$w_j(\nu_A(\mathbf{b})) = \frac{\nu_A^j(\mathbf{b})}{j!} \exp[-\nu_A(\mathbf{b})] \quad (41)$$

is the probability of finding  $j$  spatially overlapping nucleons at an impact parameter  $\mathbf{b}$  in a Lorentz-contracted nucleus,

$$\nu_A(\mathbf{b}) = \frac{1}{2}\alpha_s(r)\sigma_0(x)T(\mathbf{b}), \quad (42)$$

and

$$\begin{aligned} f^{(j)}(\boldsymbol{\kappa}) &= \int \prod_{i=1}^j d^2\boldsymbol{\kappa}_i f(\boldsymbol{\kappa}_i) \delta \left( \boldsymbol{\kappa} - \sum_{i=1}^j \boldsymbol{\kappa}_i \right), \quad (43) \\ f^{(0)}(\boldsymbol{\kappa}) &= \delta(\boldsymbol{\kappa}), \end{aligned}$$

is a collective gluon field of  $j$  overlapping nucleons. As shown in [5, 11], the collective nuclear unintegrated gluon density  $\phi_{\text{WW}}(\nu_A(\mathbf{b}), \boldsymbol{\kappa})$  enters the calculation of the nuclear sea quark density in precisely the same way as  $f(\boldsymbol{\kappa})$  in (5) for the free-nucleon target.

We cite two important features of  $\phi_{\text{WW}}(\nu_A(\mathbf{b}), \boldsymbol{\kappa})$ . First, the hard tail of the unintegrated nuclear glue per bound nucleon is calculated parameter free [11],

$$\begin{aligned} f_{\text{WW}}(\nu_A(\mathbf{b}), \boldsymbol{\kappa}) &= \frac{\phi_{\text{WW}}(\nu_A(\mathbf{b}), \boldsymbol{\kappa})}{\nu_A(\mathbf{b})} \quad (44) \\ &= f(\boldsymbol{\kappa}) \left[ 1 + \frac{2C_A\pi^2\gamma^2\alpha_s(r)T(\mathbf{b})}{C_F N_c \boldsymbol{\kappa}^2} G(\boldsymbol{\kappa}^2) \right], \end{aligned}$$

and does not depend on the infrared parameter  $\sigma_0(x)$ . In the hard regime, the differential nuclear glue is not shadowed; furthermore, because of the manifestly positive-valued and model-independent nuclear

higher twist correction, it exhibits a nuclear antishadowing property [11]. Second, for interactions with nuclei of  $q\bar{q}$  dipoles with  $|\mathbf{r}| \gtrsim 1/Q_A$ , the strong coupling enters (42) as  $\alpha_s(Q_A^2)$ , and in the saturation region of  $\kappa^2 \lesssim Q_A^2$ , we have [5, 6]

$$\Phi(\nu_A(\mathbf{b}), \boldsymbol{\kappa}) \approx \phi_{\text{WW}}(\nu_A(\mathbf{b}), \boldsymbol{\kappa}) \approx \frac{1}{\pi} \frac{Q_A^2}{(\boldsymbol{\kappa}^2 + Q_A^2)^2}, \quad (45)$$

where the width of the plateau  $Q_A$  which is the nuclear saturation scale equals

$$Q_A^2 \approx \frac{4\pi^2}{N_c} \alpha_s(Q_A^2) G(Q_A^2) T(\mathbf{b}) \quad (46)$$

and exhibits only a weak dependence on the infrared parameters through the  $Q_A^2$  dependence of the running strong coupling and scaling violations in the unintegrated gluon density of the nucleon. For instance, at  $x = 10^{-2}$ , the numerical results [27] for  $G(Q^2)$  correspond to a nearly  $Q^2$ -independent  $\alpha_s(Q^2)G(Q^2) \approx 1$ . For average DIS on a heavy nucleus,  $A^{1/3} = 6$ , we found  $\langle Q_A^2(\mathbf{b}) \rangle \approx 0.9 \text{ GeV}^2$ .

Now we are in the position to represent the nuclear distortion factor (38) as

$$D_A(\mathbf{s}, \mathbf{r}, \mathbf{r}', \mathbf{b}) = \int_0^1 d\beta \quad (47)$$

$$\times \int d^2\boldsymbol{\kappa}_1 \Phi((1-\beta)\nu_A(\mathbf{b}), \boldsymbol{\kappa}_1) \exp(-i\boldsymbol{\kappa}_1 \cdot \mathbf{r})$$

$$\times \int d^2\boldsymbol{\kappa}_2 \Phi((1-\beta)\nu_A(\mathbf{b}), \boldsymbol{\kappa}_2) \exp(i\boldsymbol{\kappa}_2 \cdot \mathbf{r}')$$

$$\times \int d^2\boldsymbol{\kappa}_3 \Phi(\beta\nu_A(\mathbf{b}), \boldsymbol{\kappa}_3) \exp[i\boldsymbol{\kappa}_3 \cdot (\mathbf{s} + \mathbf{r}' - \mathbf{r})]$$

$$\times \int d^2\boldsymbol{\kappa}_4 \Phi(\beta\nu_A(\mathbf{b}), \boldsymbol{\kappa}_4) \exp(i\boldsymbol{\kappa}_4 \cdot \mathbf{s}),$$

so that the jet–jet inclusive inelastic cross section takes the form

$$\frac{d\sigma_{\text{inel}}}{d^2\mathbf{b}dzd^2\mathbf{p}_-d^2\boldsymbol{\Delta}} = \frac{1}{2(2\pi)^2} \alpha_s \sigma_0(x) T(\mathbf{b}) \quad (48)$$

$$\times \int_0^1 d\beta \int d^2\boldsymbol{\kappa}_3 d^2\boldsymbol{\kappa} f(\boldsymbol{\kappa}) \Phi(\beta\nu_A(\mathbf{b}), \boldsymbol{\Delta} - \boldsymbol{\kappa}_3 - \boldsymbol{\kappa})$$

$$\times \Phi(\beta\nu_A(\mathbf{b}), \boldsymbol{\kappa}_3) \left| \int d^2\boldsymbol{\kappa}_1 \Phi((1-\beta)\nu_A(\mathbf{b}), \boldsymbol{\kappa}_1) \right.$$

$$\times \left. \left\{ \langle \gamma^* | z, \mathbf{p}_- + \boldsymbol{\kappa}_1 + \boldsymbol{\kappa}_3 \rangle \right. \right.$$

$$\left. \left. - \langle \gamma^* | z, \mathbf{p}_- + \boldsymbol{\kappa}_1 + \boldsymbol{\kappa}_3 + \boldsymbol{\kappa} \rangle \right\} \right|^2.$$

The transverse momentum distribution of dijets is uniquely calculable in terms of the collective WW glue of a nucleus and as such (48) can be regarded as a nonlinear nuclear  $k_\perp$  factorization for the inclusive inelastic dijet cross section. Notice that the convolution in the last line of Eq. (48) describes the initial-state distortion of the color-singlet  $q\bar{q}$  state in the projectile.

There are two important limiting cases. We start with hard dijets,  $|\mathbf{p}_\pm| \gtrsim Q_A$ . A crucial point is that the WF of the pointlike photon is a slowly decreasing function of the transverse momentum, in contrast to  $\Phi(\nu_A(\mathbf{b}), \boldsymbol{\kappa})$ , which is a steeply decreasing function [compare Eqs. (6), (7) to Eq. (45)]. Then, since  $\kappa_i^2 \lesssim Q_A^2$ , for hard dijets, one can neglect  $\boldsymbol{\kappa}_1, \boldsymbol{\kappa}_3$  compared to  $\mathbf{p}_\pm$  and approximate

$$\int d^2\boldsymbol{\kappa}_1 \Phi((1-\beta)\nu_A(\mathbf{b}), \boldsymbol{\kappa}_1) \quad (49)$$

$$\times \left\{ \langle \gamma^* | z, \mathbf{p}_- + \boldsymbol{\kappa}_1 + \boldsymbol{\kappa}_3 \rangle \right.$$

$$\left. - \langle \gamma^* | z, \mathbf{p}_- + \boldsymbol{\kappa}_1 + \boldsymbol{\kappa}_3 + \boldsymbol{\kappa} \rangle \right\}$$

$$\approx \langle \gamma^* | z, \mathbf{p}_- \rangle - \langle \gamma^* | z, \mathbf{p}_- + \boldsymbol{\kappa} \rangle,$$

which amounts to negligible initial-state distortion of small color-singlet dipoles with  $|\mathbf{r}|, |\mathbf{r}'| \sim 1/|\mathbf{p}_\pm| \lesssim 1/Q_A$ . Next we notice that

$$\int d^2\boldsymbol{\kappa}_3 \Phi(\beta\nu_A(\mathbf{b}), \boldsymbol{\Delta} - \boldsymbol{\kappa}_3 - \boldsymbol{\kappa}) \quad (50)$$

$$\times \Phi(\beta\nu_A(\mathbf{b}), \boldsymbol{\kappa}_3) = \Phi(2\beta\nu_A(\mathbf{b}), \boldsymbol{\Delta} - \boldsymbol{\kappa}),$$

so that the hard jet–jet inclusive cross section takes the form

$$\frac{d\sigma_{\text{inel}}}{d^2\mathbf{b}dzd^2\mathbf{p}_-d^2\boldsymbol{\Delta}} = T(\mathbf{b}) \int_0^1 d\beta \quad (51)$$

$$\times \int d^2\boldsymbol{\kappa} \Phi(2\beta\nu_A(\mathbf{b}), \boldsymbol{\Delta} - \boldsymbol{\kappa}) \frac{d\sigma_N}{dzd^2\mathbf{p}_-d^2\boldsymbol{\kappa}},$$

which is a close counterpart of, but still different from, the conventional  $k_\perp$  factorization (3) for the free-nucleon target. As a matter of fact, for hard dijets, one does not need to invoke the large- $N_c$  approximation: here,  $|\mathbf{r}|, |\mathbf{r}'| \ll |\mathbf{s}|$ , so that  $\Sigma_1 \sim 0$ ,  $\Sigma_2 \sim 2\lambda_c \sigma(\mathbf{s})$ , where  $\lambda_c = N_c^2/(N_c^2 - 1)$ , and one can replace  $\Phi(2\beta\nu_A(\mathbf{b}), \boldsymbol{\Delta} - \boldsymbol{\kappa})$  by  $\Phi(2\lambda_c \beta\nu_A(\mathbf{b}), \boldsymbol{\Delta} - \boldsymbol{\kappa})$  (see discussion in [6]). All the dependence on transverse momentum  $p_-$  of the hard jet is in the free-nucleon cross section  $d\sigma_N$ ; i.e., the pQCD treatment breakup into hard dijets is applicable to DIS on the free nucleon and nuclear targets on the same footing. The effect of the collective nuclear glue  $\Phi(2\beta\nu_A(\mathbf{b}), \boldsymbol{\kappa})$  is a smearing/broadening as well as decorrelation of the dijets. Numerical estimates for the azimuthal decorrelation of jets and a discussion

concerning the relevance to the RHIC–STAR finding [39] of the disappearance of the away jet in central AuAu collisions can be found in [6]. In this hard dijet limit, it is tempting to assign to  $\Phi(2\beta\nu_A(\mathbf{b}), \boldsymbol{\kappa})$  a probabilistic interpretation as an intrinsic transverse momentum distribution of collective nuclear gluons, but this collectivization only applies to the fraction  $\beta$  of the nuclear thickness which the  $q\bar{q}$  pair propagates in the color-octet state.

The second limiting case is that of minijets  $|\mathbf{p}_-|, |\boldsymbol{\Delta}| \lesssim Q_A$ . Since  $|\boldsymbol{\kappa}_i| \sim Q_A$ , one can neglect  $\mathbf{p}_-$  in the photon's WF,

$$\begin{aligned} & \int d^2\boldsymbol{\kappa}_1 \Phi((1-\beta)\nu_A(\mathbf{b}), \boldsymbol{\kappa}_1) \\ & \times \{ \langle \gamma^* | z, \mathbf{p}_- + \boldsymbol{\kappa}_1 + \boldsymbol{\kappa}_3 \rangle \\ & - \langle \gamma^* | z, \mathbf{p}_- + \boldsymbol{\kappa}_1 + \boldsymbol{\kappa}_3 + \boldsymbol{\kappa} \rangle \} \\ & \approx | \langle \gamma^* | z, \boldsymbol{\kappa}_3 \rangle - \langle \gamma^* | z, \boldsymbol{\kappa}_3 + \boldsymbol{\kappa} \rangle |^2. \end{aligned} \quad (52)$$

The main point is that the minijet–minijet inclusive cross section would depend neither on the minijet momentum nor on the decorrelation momentum. This proves a complete disappearance of the azimuthal correlation of minijets with a transverse momentum below the saturation scale.

#### 4. NONLINEAR $k_\perp$ FACTORIZATION FOR THE BREAKUP OF PIONS INTO FORWARD DIJETS ON NUCLEI

##### 4.1. From Pointlike Photons to Nonpointlike Pions

By requiring the production of forward dijets which satisfy the  $x_\gamma = 1$  criterion, we select the breakup of the  $q\bar{q}$  Fock state of the projectile. Above, we concentrated on the breakup of a pointlike projectile, in which case the back-to-back dijets stem from “lifting onto the mass-shell” of  $q\bar{q}$  states with a large intrinsic transverse momentum  $\mathbf{p}_\perp$ . In this section, we go to another extreme case—a nonpointlike projectile, a pion, with a soft  $q\bar{q}$  WF such that the intrinsic transverse momentum of the quark and antiquark is limited.

An important point is the role that unitarity plays in the isolation of truly inelastic collisions which is effected by a subtraction of the coherent diffractive components in (38). As is well known, in collisions of strongly interacting hadrons (pions) with opaque nuclei, unitarity entails that coherent elastic scattering off a nucleus,  $\pi A \rightarrow \pi A$ , makes up 50% of the total hadron–nucleus cross section. On the other hand, for weakly interacting pointlike projectiles (photons), it is coherent diffractive excitation of the continuum  $q\bar{q}$  states,  $\gamma^* A \rightarrow (q\bar{q})A$ , which makes up 50% of the total DIS cross section [23]. In our formalism as exposed in Section 2, we explicitly associate the subtracted coherent diffractive component in (14) with

the continuum  $q\bar{q}$  dijets. Strictly speaking, in the case of incident pions, the subtraction of coherent diffractive processes must include a sum over elastic pions, diffractively excited meson resonances, and, finally, the continuum diffractive states. Although the  $q\bar{q}$  interaction in the  $q\bar{q}$  Fock states of elastic pions and diffractive meson resonances is important for the formation of pions and its excitations, the contribution to their WF from large invariant mass,  $M_{q\bar{q}}$ , Fock states vanishes rapidly at very large  $M_{q\bar{q}}$ . Then, as argued in [11], the final-state interaction between the final-state quark and antiquark can be neglected and the  $q\bar{q}$  plane-wave approximation becomes applicable as soon as the invariant mass of the forward dijet system exceeds a typical mass scale of prominent meson resonances. Consequently, the technique of Section 2 and the derivation of a nonlinear nuclear  $k_\perp$  factorization in Section 3 are fully applicable to breakup of pions into high-mass hard dijets.

##### 4.2. In-Volume Breakup Is Hard pQCD Tractable, Probes the Pion Distribution Amplitude, but Is Subleading at Large $\mathbf{p}_\pm$

Whether the breakup of nonpointlike pions into hard dijets,  $\mathbf{p}_\pm^2 \gtrsim Q_A^2$ , is under full control of perturbative QCD or not needs further scrutiny. In the case of DIS, it was important that the WF of the photon was a slow function compared to the nuclear WW glue [see the discussion preceding the derivation of Eq. (51) in Section 3]. Here, we notice that, for extended heavy nuclei, the saturation scale  $Q_A$  is much larger than the ( $z$ -dependent) intrinsic transverse momentum of quarks,  $Q_\pi$ , in the pion, so that the pion WF would be the steepest function of transverse momentum in the problem. A closer inspection of the nonlinear  $k_\perp$ -factorization formula (48) shows that one must compare the momentum dependence of the pion WF  $\langle \pi | \boldsymbol{\kappa} \rangle$  with that of  $\Phi((1-\beta)\nu_A(\mathbf{b}), \boldsymbol{\kappa})$  and/or  $\Phi(\beta\nu_A(\mathbf{b}), \boldsymbol{\kappa})$ , i.e.,  $Q_\pi^2$  must be compared to the  $\beta$ -dependent saturation scale  $Q_\beta^2 = \beta Q_A^2$  or  $(1-\beta)Q_A^2$ .

We shall consider first the contribution to the dijet cross section from  $Q_\beta^2 \gtrsim Q_\pi^2$ , i.e.,  $\beta_{\min} = Q_\pi/Q_A^2 \lesssim \beta \lesssim \beta_{\max} = 1 - \beta_{\min}$ . It describes the in-volume breakup of pions [see the interpretation of Eq. (37)]. Here, the pion WF is the steepest one compared to other factors in (48) and can be approximated by a  $\delta$  function in transverse momentum space

$$\begin{aligned} \langle z, \mathbf{p} | \pi \rangle &= (2\pi)^2 \delta(\mathbf{p}) \int \frac{d^2\mathbf{k}}{(2\pi)^2} \langle z, \mathbf{k} | \pi \rangle \\ &= (2\pi)^2 \delta(\mathbf{p}) \sqrt{\frac{\pi}{2N_c}} F_\pi \varphi_\pi(Q_\beta^2, z), \end{aligned} \quad (53)$$

which gives

$$\begin{aligned} & \frac{1}{(2\pi)^2} \int d^2\boldsymbol{\kappa}_1 \Phi((1-\beta)\nu_A(\mathbf{b}), \boldsymbol{\kappa}_1) \\ & \quad \times \{ \langle z, \mathbf{p}_- + \boldsymbol{\kappa}_1 + \boldsymbol{\kappa}_3 | \pi \rangle \\ & \quad - \langle z, \mathbf{p}_- + \boldsymbol{\kappa}_1 + \boldsymbol{\kappa}_3 + \boldsymbol{\kappa} | \pi \rangle \} \\ & \approx \sqrt{\frac{\pi}{2N_c}} F_\pi \varphi_\pi(Q_\beta^2, z) [\Phi((1-\beta)\nu_A(\mathbf{b}), \mathbf{p}_- + \boldsymbol{\kappa}_3) \\ & \quad - \Phi((1-\beta)\nu_A(\mathbf{b}), \mathbf{p}_- + \boldsymbol{\kappa}_3 + \boldsymbol{\kappa})], \end{aligned} \quad (54)$$

where we indicated explicitly the factorization scale  $Q_\beta^2$  in the  $\pi$ DA  $\varphi_\pi(Q_\beta^2, z)$ . Of the two possible helicity structures in (13), only one,  $\propto \delta_{\lambda-\bar{\lambda}}$ , related to the pion decay constant, contributes in this hard regime (see also the related discussion of diffractive dijets in [11]). Then this contribution to the breakup of pions into high-mass dijets can be presented in two equivalent forms, which only differ by a reshuffling of the large jet momentum  $\mathbf{p}_-$  between different factors in the integrand:

$$\begin{aligned} \frac{d\sigma_\pi}{d^2\mathbf{b}dzd^2\mathbf{p}_-d^2\boldsymbol{\Delta}} &= \frac{\pi^3}{N_c} \alpha_s \sigma_0(x) T(\mathbf{b}) F_\pi^2 \\ & \quad \times \int_{\beta_{\min}}^{\beta_{\max}} d\beta \varphi_\pi^2(Q_\beta^2, z) \int d^2\boldsymbol{\kappa}_3 d^2\boldsymbol{\kappa} f(\boldsymbol{\kappa}) \\ & \quad \times \Phi(\beta\nu_A(\mathbf{b}), \boldsymbol{\Delta} - \boldsymbol{\kappa}_3 - \boldsymbol{\kappa}) \Phi(\beta\nu_A(\mathbf{b}), \boldsymbol{\kappa}_3) \\ & \quad \times [\Phi((1-\beta)\nu_A(\mathbf{b}), \mathbf{p}_- + \boldsymbol{\kappa}_3) \\ & \quad - \Phi((1-\beta)\nu_A(\mathbf{b}), \mathbf{p}_- + \boldsymbol{\kappa}_3 + \boldsymbol{\kappa})]^2 \\ &= \frac{\pi^3}{N_c} \alpha_s \sigma_0(x) T(\mathbf{b}) F_\pi^2 \int_{\beta_{\min}}^{\beta_{\max}} d\beta \varphi_\pi^2(Q_\beta^2, z) \\ & \quad \times \int d^2\mathbf{q} d^2\boldsymbol{\kappa} f(\boldsymbol{\kappa}) \\ & \quad \times \Phi(\beta\nu_A(\mathbf{b}), \mathbf{p}_+ - \mathbf{q} - \boldsymbol{\kappa}) \Phi(\beta\nu_A(\mathbf{b}), \mathbf{p}_- + \mathbf{q}) \\ & \quad \times [\Phi((1-\beta)\nu_A(\mathbf{b}), \mathbf{q}) - \Phi((1-\beta)\nu_A(\mathbf{b}), \mathbf{q} + \boldsymbol{\kappa})]^2. \end{aligned} \quad (55)$$

Alternatively, one could neglect the  $\mathbf{r}$  dependence of the pion WF, i.e., set the radial WF  $\Psi_\pi(z, \mathbf{r}) \approx \Psi_\pi(z, 0)$  and proceed with the calculations which lead to (48).

At first sight, in close similarity to the breakup into coherent diffractive dijets [11], the inclusive dijet cross section is proportional to the  $\pi$ DA squared. One must be careful with the isolation of the leading large- $\mathbf{p}_\pm$  behavior of the pion breakup, though.

Consider first the former representation of (55). According to [11, 27], in the hard region,  $f(\boldsymbol{\kappa}) \sim 1/(\boldsymbol{\kappa}^2)^\delta$  with the exponent  $\delta \sim 2$  and  $\Phi(\nu_A(\mathbf{b}), \boldsymbol{\kappa}) \approx \nu_A(\mathbf{b}) f(\boldsymbol{\kappa})$  [see Eq. (44)], so that it is tempting to

focus on  $\boldsymbol{\kappa}_3^2 \lesssim \beta Q_A^2$  and neglect  $\boldsymbol{\kappa}_3$  compared to  $\mathbf{p}_-$  in (54):

$$\begin{aligned} & [\Phi((1-\beta)\nu_A(\mathbf{b}), \mathbf{p}_- - \boldsymbol{\kappa}_3) \\ & - \Phi((1-\beta)\nu_A(\mathbf{b}), \mathbf{p}_- - \boldsymbol{\kappa}_3 - \boldsymbol{\kappa})]^2 \\ & \approx [\Phi((1-\beta)\nu_A(\mathbf{b}), \mathbf{p}_-) \\ & - \Phi((1-\beta)\nu_A(\mathbf{b}), \mathbf{p}_- - \boldsymbol{\kappa})]^2. \end{aligned} \quad (56)$$

Upon taking the convolution (50), this contribution to the dijet cross section can be cast into a form reminiscent of (51):

$$\begin{aligned} \frac{d\sigma_\pi}{d^2\mathbf{b}dzd^2\mathbf{p}_-d^2\boldsymbol{\Delta}} &= T(\mathbf{b}) \int_0^{\beta_{\max}} d\beta \\ & \quad \times \int d^2\boldsymbol{\kappa} \Phi(2\beta\nu_A(\mathbf{b}), \boldsymbol{\Delta} - \boldsymbol{\kappa}) \frac{d\sigma_{\text{eff}}}{dzd^2\mathbf{p}_-d^2\boldsymbol{\kappa}}, \end{aligned} \quad (57)$$

where

$$\begin{aligned} \frac{d\sigma_{\text{eff}}}{dzd^2\mathbf{p}_-d^2\boldsymbol{\kappa}} &= \frac{1}{2(2\pi)^2} \frac{\pi}{2N_c} \alpha_s \sigma_0(x) \\ & \quad \times F_\pi^2 \varphi_\pi^2(Q_\beta^2, z) f(\boldsymbol{\kappa}) [\Phi((1-\beta)\nu_A(\mathbf{b}), \mathbf{p}_-) \\ & \quad - \Phi((1-\beta)\nu_A(\mathbf{b}), \mathbf{p}_- - \boldsymbol{\kappa})]^2 \end{aligned} \quad (58)$$

plays the role of the free-nucleon cross section for DIS [Eq. (5)] and  $\Phi((1-\beta)\nu_A(\mathbf{b}), \mathbf{p})$  emerges as the counterpart of the WF  $\langle \mathbf{p} | \gamma^* \rangle$  in (5), (51). Now we notice that this consideration is fully applicable to  $\beta < \beta_{\min}$ , for which reason we already have set  $\beta = 0$  for the lower limit of the  $\beta$  integration in (57).

The nuclear WW gluon distribution  $\Phi(2\beta\nu_A(\mathbf{b}), \boldsymbol{\Delta} - \boldsymbol{\kappa})$  in (57) provides a cutoff of the  $\boldsymbol{\kappa}$  integration,  $\boldsymbol{\kappa}^2 \lesssim \beta Q_A^2 + \boldsymbol{\Delta}^2$ , which justifies the small- $\boldsymbol{\kappa}$  approximation

$$\begin{aligned} & [\Phi((1-\beta)\nu_A(\mathbf{b}), \mathbf{p}_-) \\ & - \Phi((1-\beta)\nu_A(\mathbf{b}), \mathbf{p}_- - \boldsymbol{\kappa})]^2 \approx 2 \left( \frac{f(\mathbf{p}_-)}{\mathbf{p}_-^2} \right)^2 \\ & \quad \times \delta^2(1-\beta)^2 \nu_A^2(\mathbf{b}) \mathbf{p}_-^2 \boldsymbol{\kappa}^2, \end{aligned} \quad (59)$$

where azimuthal averaging has been performed. Then the  $\boldsymbol{\kappa}$  integration subject to  $\boldsymbol{\kappa}^2 \lesssim \beta Q_A^2 + \boldsymbol{\Delta}^2$  yields

$$\int d^2\boldsymbol{\kappa} f(\boldsymbol{\kappa}) \boldsymbol{\kappa}^2 \approx \frac{4\pi^2}{\sigma_0(x) N_c} G(\boldsymbol{\Delta}^2 + \beta Q_A^2) \quad (60)$$

and the final results for this contribution to the dijet cross section reads

$$\begin{aligned} \frac{d\sigma_{\pi A}^{(\text{volume})}}{d^2\mathbf{b}dzd^2\mathbf{p}_-d^2\boldsymbol{\Delta}} \Big|_{\text{hard}} &\approx \frac{32\pi^6 F_\pi^2 T^3(\mathbf{b})}{N_c^4} \\ & \quad \times \frac{\delta^2 \alpha_s^3(\mathbf{p}_-^2) \mathcal{F}^2(x, \mathbf{p}_-^2)}{(\mathbf{p}_-^2)^5} \int_0^1 d\beta (1-\beta)^2 \varphi_\pi^2(Q_\beta^2, z) \end{aligned} \quad (61)$$

$$\times \Phi(2\beta\nu_A(\mathbf{b}), \mathbf{\Delta})G(\mathbf{\Delta}^2 + \beta Q_A^2).$$

Here, the  $\beta$  integration is dominated by the mid- $\beta$  contribution; hence, the  $\beta$  integration can safely be extended from 0 to 1. The dominance of the mid- $\beta$  contribution means that the incident pion breaks in the volume of a nucleus; i.e., it selects weakly attenuating small color-dipole configurations in the incident pion. For this reason, it is uniquely calculable in terms of hard quantities and collective nuclear WW glue, and the auxiliary soft parameter  $\sigma_0(x)$  does not enter (61), hence the subscript “hard” on the left-hand side of (61). All the approximations which have led to the proportionality of the pion breakup cross section to the  $\pi$ DA squared were indeed well justified. Unfortunately, as far as the  $p_+$  dependence is concerned, the in-volume hard absorption gives the subleading, higher twist contribution.

### 4.3. The Leading Asymptotics at Large $\mathbf{p}_\pm$

*Is Dominated by Soft Absorption on the Front Face of a Nucleus*

The leading asymptotics at large  $\mathbf{p}_\pm$  can be isolated starting with the latter representation of Eq. (55). It comes from  $|\mathbf{q}| = |\mathbf{p}_- - \boldsymbol{\kappa}_3| \ll Q_A$ ; furthermore, as we shall see a posteriori, the dominant contribution comes from a still narrower soft domain  $|\mathbf{q}| \lesssim Q_\pi$ . We start with the in-volume contribution from  $\beta_{\min} < \beta < 1 - \beta_{\min}$ . According to (44), for such hard jets, we can approximate

$$\Phi(\beta\nu_A(\mathbf{b}), \mathbf{p}_+ - \mathbf{q} - \boldsymbol{\kappa})\Phi(\beta\nu_A(\mathbf{b}), \mathbf{p}_- + \mathbf{q}) \quad (62)$$

$$\approx \beta^2\nu_A^2(\mathbf{b})f(\mathbf{p}_+)f(\mathbf{p}_-).$$

Now, using the convolution identity Eq. (50), we may simplify

$$\int d^2\mathbf{q}d^2\boldsymbol{\kappa}f(\boldsymbol{\kappa})[\Phi((1-\beta)\nu_A(\mathbf{b}), \mathbf{q}) \quad (63)$$

$$- \Phi((1-\beta)\nu_A(\mathbf{b}), \mathbf{q} + \boldsymbol{\kappa})]^2$$

$$= 2 \int d^2\boldsymbol{\kappa}f(\boldsymbol{\kappa})[\Phi(2(1-\beta)\nu_A(\mathbf{b}), \mathbf{0})$$

$$- \Phi(2(1-\beta)\nu_A(\mathbf{b}), \boldsymbol{\kappa})] = -2 \int d^2\boldsymbol{\kappa}f(\boldsymbol{\kappa})$$

$$\times \frac{\partial\Phi(2(1-\beta)\nu_A(\mathbf{b}), \boldsymbol{\kappa}^2)}{\partial\boldsymbol{\kappa}^2} \Big|_{\boldsymbol{\kappa}^2=0} \boldsymbol{\kappa}^2 \simeq \frac{4\pi}{(1-\beta)^2}$$

$$\times \frac{1}{Q_A^4} \frac{1}{\sigma_0(x)N_c} G(Q_\beta^2),$$

where  $Q_\beta^2 = (1-\beta)Q_A^2$  and we made explicit use of the parametrization (45). The singular behavior at  $\beta \rightarrow 1$  shows that the inclusive cross section will be

dominated by the soft end-point contribution from  $Q_\beta^2 \sim Q_\pi^2$ ,

$$\int_{\beta_{\min}}^{\beta_{\max}} \frac{d\beta G(Q_\beta^2)\beta^2\varphi_\pi^2(Q_\beta^2, z)}{(1-\beta)^2} \quad (64)$$

$$\sim \frac{G(Q_\pi^2)\varphi_\pi^2(Q_\pi^2, z)}{1-\beta_{\max}} = \frac{Q_A^2}{Q_\pi^2} G(Q_\pi^2)\varphi_\pi^2(Q_\pi^2, z),$$

i.e., the in-volume contribution is squeezed to the breakup of pions close to the front face of the nucleus. Finally, making use of (46) and neglecting the difference between  $G(Q_\pi^2)$  and  $G(Q_A^2)$ , we obtain an estimate

$$\frac{d\sigma_{\pi A}^{(\text{soft})}}{d^2\mathbf{b}dzd^2\mathbf{p}_-d^2\mathbf{p}_+} = \frac{4\pi^4 T^2(\mathbf{b})\alpha_s^2(\mathbf{p}_\pm^2)F_\pi^2}{N_c^3} \quad (65)$$

$$\times \phi_\pi^2(Q_\pi^2, z) \frac{1}{Q_\pi^2} \frac{\mathcal{F}(x, \mathbf{p}_+^2)}{(\mathbf{p}_+^2)^2} \frac{\mathcal{F}(x, \mathbf{p}_-^2)}{(\mathbf{p}_-^2)^2}.$$

The striking feature of this result is a complete decorrelation of the two jets. For an explanation of the superscript “soft,” see below.

In the evaluation of the contribution from  $\beta_{\max} \lesssim \beta \lesssim 1$ , i.e., from breakup of pions on the front face of the nucleus, we can take  $\Phi((1-\beta)\nu_A(\mathbf{b}), \boldsymbol{\kappa}_1) = \delta(\boldsymbol{\kappa}_1)$  [see Eq. (40)], so that, for hard dijets,

$$\int d^2\boldsymbol{\kappa}_1\Phi((1-\beta)\nu_A(\mathbf{b}), \boldsymbol{\kappa}_1) \quad (66)$$

$$\times \{\langle\pi|z, \mathbf{p}_- + \boldsymbol{\kappa}_1 + \boldsymbol{\kappa}_3\rangle$$

$$- \langle\pi|z, \mathbf{p}_- + \boldsymbol{\kappa}_1 + \boldsymbol{\kappa}_3 + \boldsymbol{\kappa}\rangle\}$$

$$\approx \langle\pi|z, \mathbf{p}_- + \boldsymbol{\kappa}_3\rangle - \langle\pi|z, \mathbf{p}_- + \boldsymbol{\kappa}_3 + \boldsymbol{\kappa}\rangle.$$

Setting  $\beta = 1$  in the rest of the integrand of (48), approximating  $\int_{\beta_{\max}}^1 d\beta \sim Q_\pi^2/Q_A^2$ , and reshuffling  $\mathbf{p}_-$  as in (55), we obtain

$$\frac{d\sigma_\pi^{(\text{surface})}}{d^2\mathbf{b}dzd^2\mathbf{p}_-d^2\mathbf{\Delta}} \approx \frac{1}{2(2\pi)^2 Q_A^2} \alpha_s \sigma_0(x) \quad (67)$$

$$\times T(\mathbf{b})\Phi(\nu_A(\mathbf{b}), \mathbf{p}_+)\Phi(\nu_A(\mathbf{b}), \mathbf{p}_-)Q_\pi^2$$

$$\times \int d^2\mathbf{q}d^2\boldsymbol{\kappa}f(\boldsymbol{\kappa})|\langle\pi|z, \mathbf{q}\rangle - \langle\pi|z, \mathbf{q} + \boldsymbol{\kappa}\rangle|^2.$$

Although  $f(\boldsymbol{\kappa})$  and the pion WF are distributions of comparable width, for estimation purposes, we can expand

$$|\langle\pi|z, \mathbf{q}\rangle - \langle\pi|z, \mathbf{q} + \boldsymbol{\kappa}\rangle|^2 \quad (68)$$

$$\sim \frac{|\langle\pi|z, \mathbf{q}\rangle|^2}{(Q_\pi^2 + \mathbf{q}^2)^2} \cdot 2\mathbf{q}^2\boldsymbol{\kappa}^2.$$

The  $\kappa$  integration will yield  $G(Q_\pi^2 + \mathbf{q}^2) \sim G(Q_\pi^2)$  [see Eq. (60)], whereas

$$2Q_\pi^2 \int d^2\mathbf{q} \frac{|\langle \pi | z, \mathbf{q} \rangle|^2 \mathbf{q}^2}{(Q_\pi^2 + \mathbf{q}^2)^2} \sim \frac{1}{\pi Q_\pi^2} \quad (69)$$

$$\times \left| \int d^2\mathbf{q} \langle \pi | z, \mathbf{q} \rangle \right|^2 \sim \frac{(2\pi)^4}{Q_\pi^2} \frac{1}{2N_c} F_\pi^2 \varphi_\pi^2(Q_\pi^2, z).$$

Notice that both helicity components of the pion WF would contribute in this soft regime. Then, our result for (67) is identical to (65), so that the final estimate for the soft cross section is (65) times a factor of  $\sim 2$ .

Several comments on our result (65), (67) are in order. First, the representation (38) for the distortion factor entails that the dominance by the contribution from  $\beta \rightarrow 1$  corresponds to an absorption of the pion in the state with normal hadronic size on the front surface of the nucleus, i.e., it is a soft-absorption-driven contribution to excitation of hard dijets, hence the superscript “soft” on the left-hand side of (65). Second, the same point about absorbed pions being in the state with large hadronic size is manifest from the emergence of the soft factor  $1/Q_\pi^2$  in the dijet cross section. Third, the back-to-back correlated hard contribution (61) is suppressed compared to the soft contribution (65), (67) by a factor  $1/\mathbf{p}_\pm^2$ ; i.e., it has the form of a higher twist correction. Fourth, as far as the dependence on transverse momentum is concerned, the dijet cross section from the soft absorption mechanism has the form of a product of two single-jet cross sections (12). This property indicates that hard jets acquire their large transverse momenta from hard scattering on different nucleons, which explains why the transverse momenta of the quark and antiquark are fully decorrelated both azimuthally and longitudinally, i.e., in the magnitude of the momenta  $|\mathbf{p}_+|$  and  $|\mathbf{p}_-|$  (in the scattering plane). This must be contrasted to the breakup of photons when the large momentum of jets comes from the intrinsic momentum in the photon WF and jets are produced predominantly back-to-back with the scale for both the azimuthal (out-of-plane) and longitudinal (in-plane) decorrelations being set by  $Q_A$ . Consequently, the out-of-plane decorrelation momentum in the breakup of pions into forward dijets is predicted to be much larger than in the breakup of photons in photoproduction or DIS.

#### 4.4. Transverse Energy Associated with Dijets in the Photon and Pion Breakup

There is still another interesting difference between the breakup of pointlike photons and non-pointlike pions. It is the surplus transverse energy of secondary particles associated with the forward hard jets.

What counterbalances the large transverse momenta  $\mathbf{p}_\pm$  of the two uncorrelated hard jets? According to [6, 11], the hard tail (44) of the collective nuclear WW glue which enters (62) is dominated by a single hard gluon. Then, in the pQCD Born approximation, the forward  $q, \bar{q}$  hard jets would recoil against the valence quarks of nucleons of the target nucleus. With allowance for the QCD evolution effects, the recoil is against the midrapidity gluons and quarks, which are separated from the forward hard dijets by at least several units of rapidity. Although the partons which counterbalance the forward dijets are not localized in rapidity, their overall contribution to the transverse energy production in an event (with the transverse energy from forward dijets excluded) will be an amount  $\Delta E_T \sim |\mathbf{p}_+| + |\mathbf{p}_-|$  in excess of the average transverse energy in a minimal bias event without hard forward jets. This surplus transverse energy production  $\Delta E_T$  would not depend on the azimuthal angle between the two jets.

In the breakup of photons, the surplus transverse energy  $\Delta E_T$  will be much smaller. Indeed, the large transverse momenta of jets come from the large intrinsic transverse momentum of the quark and antiquark in the photon. The dijet recoils against other secondary particles with a transverse momentum which is precisely equal to the acoplanarity momentum  $|\Delta|$ . The strong decorrelation,  $\Delta^2 \gtrsim Q_A^2$ , is driven by exchange of one hard gluon [see the discussion of (44)], and we expect a surplus transverse energy  $\Delta E_T \approx |\Delta|$ . In the back-to-back configuration,  $\Delta^2 \lesssim Q_A^2$ , the nuclear glue  $\Phi(\nu_A(\mathbf{b}), \Delta)$  is a result of the fusion of  $\propto A^{1/3}$  soft gluons, and we expect the surplus transverse energy  $\Delta E_T \approx Q_A$ .

#### 4.5. Is the Pion Distribution Amplitude Measurable in the Pion Breakup into Dijets?

The emergence of the  $z$ -dependent soft factor  $1/Q_\pi^2$  in (65), which depends on the model for the soft WF of the pion [see also the analysis (67)–(69)], is an unfortunate circumstance. It makes the relationship between the  $z$  dependence of the dijet cross section and the  $\pi$ DA squared a model-dependent one. Still, the experimental isolation of the hard component (61) and thereby the measurement of the  $\pi$ DA are not an entirely impossible task.

The point is that the hard component (61) from the in-volume breakup gives rise to back-to-back jets within a small angular cone limited by the decorrelation momentum  $\Delta^2 \lesssim Q_A^2$ . In the  $\Delta$  plane, it is a well-defined peak. Consequently, although the  $z$  dependence of  $Q_\pi^2$  is not under good theoretical control, it can be determined experimentally by measuring the dijet cross section beyond the back-to-back cone.

Then the soft contribution can reliably be extrapolated into the back-to-back cone and the observed excess signal can be identified with the hard contribution. Approximating the hard cross section at  $\Delta \sim 0$  by the integrand of (61) at  $\beta \sim 1/2$  and comparing it to the soft cross section (65) times the above estimated factor of 3 to 4, we find

$$\frac{d\sigma^{(\text{hard})}}{d\sigma^{(\text{soft})}} \sim \delta^2 \frac{Q_\pi^2}{\pi \mathbf{p}_\perp^2}. \quad (70)$$

As an example of the model estimate [11] for the pion WF which reproduces the pion electromagnetic form factor, the  $\pi^0 \rightarrow 2\gamma$  decay width, and the form factor of  $\gamma^*\gamma\pi$  transition, we cite  $Q_\pi^2 \sim 0.17 \text{ GeV}^2$ . The extraction of the small hard signal is facilitated by its specific dependence on  $\Delta$ .

#### 4.6. Dijets for the Power-Law Wave Function of the Pion

Above, we saw how substantially the dijet cross section changes from the pointlike photon to the nonpointlike pion with the limited intrinsic transverse momentum of the quark and antiquark in the pion. It is interesting to see how our main conclusions for the pion breakup will change—if at all—for a power-law WF of the form

$$\langle z, \mathbf{p} | \pi \rangle \propto (2\pi)^2 F_\pi \varphi(z) \sqrt{\frac{\pi}{2N_c}} \frac{1}{\pi} \frac{Q_\pi^2}{(\mathbf{p}^2 + Q_\pi^2)^2}. \quad (71)$$

A detailed discussion of properties of the pion for such a dipole, Coulomb-like, WF and its applications to the pion form factor and forward and nonforward parton distributions in the pion is found in [40], and an early discussion of some of these issues for the power-law WF of the proton is found in [25]. A simple choice [25, 41, 42] suggested by the relativization of Coulomb-like wave functions is  $Q_\pi^2 = z(1-z)\Lambda_\pi^2 + m_f^2$  {cf. Eq. (8) for the photon; for a slightly different parametrization, see [40]}. The dipole WF can be regarded as a minimal nonpointlike departure from the pointlike pion which would correspond to a monopole wave function [cf. Eq. (7)].

For the purposes of our discussion, the dipole WF has the same asymptotics at large transverse momenta as the unintegrated nuclear glue (45). Consequently, following the discussion in [6, 7], the convolution (54) can be evaluated as

$$\begin{aligned} & \frac{1}{(2\pi)^2} \int d^2\kappa_1 \Phi((1-\beta)\nu_A(\mathbf{b}), \kappa_1) \quad (72) \\ & \times \{ \langle \pi | z, \mathbf{p}_- + \kappa_1 + \kappa_3 \rangle \\ & - \langle \pi | z, \mathbf{p}_- + \kappa_1 + \kappa_3 + \kappa \rangle \} \approx \sqrt{\frac{\pi}{2N_c}} \end{aligned}$$

$$\begin{aligned} & \times F_\pi \varphi_\pi(Q_\beta^2, z) [\tilde{\Phi}(Q_\beta^2(\mathbf{b}) + Q_\pi^2, \mathbf{p}_- + \kappa_3) \\ & - \tilde{\Phi}(Q_\beta^2(\mathbf{b}) + Q_\pi^2, \mathbf{p}_- + \kappa_3 + \kappa)], \end{aligned}$$

where  $\tilde{\Phi}(Q_\beta^2(\mathbf{b}) + Q_\pi^2, \kappa)$  is described by the parametrization (45) subject to the substitution

$$Q_A^2 \rightarrow Q_\beta^2(\mathbf{b}) + Q_\pi^2. \quad (73)$$

The separation of the leading large- $\mathbf{p}_\pm$  asymptotics and isolation of the hard contribution for the dipole ansatz fully corroborates the main conclusions of Sections 4.2 and 4.3 on the dominance of the in-volume contribution to the back-to-back correlated hard dijets and the surface breakup contribution into uncorrelated dijets. The model dependence enters through  $Q_\pi^2$  in (73) and can be neglected at large  $\beta$ , i.e., for the in-volume breakup of pions. However, the model-dependent  $Q_\pi^2$  would dominate (73) for breakup on the front surface of the nucleus.

## SUMMARY AND CONCLUSIONS

We presented a comparison of consequences of the nuclear  $k_\perp$  factorization for the breakup of nonpointlike pions and pointlike photons into forward dijets. In striking contrast to the pQCD tractable hard breakup of photons, the dominant contribution to the breakup of pions starts from the soft breakup of pions into quark and antiquark at the front face of the target nucleus followed by hard intranuclear rescattering of the quark and antiquark. The most striking prediction is a complete azimuthal decorrelation of hard jets in the breakup of pions. An obvious implication is that the out-of-plane dijet decorrelation momentum squared  $\langle \Delta_T^2 \rangle_{\pi A}$  in the breakup of pions must be much larger than  $\langle \Delta_T^2 \rangle_{\gamma A}$  in the breakup of photons.

A direct comparison of the  $A$  dependence of photo- and pion-produced dijets at  $\sqrt{s} = 21 \text{ GeV}$  has been performed in the E683 Fermilab experiment [43] and gives solid evidence for  $\langle \Delta_T^2 \rangle_{\pi A} > \langle \Delta_T^2 \rangle_{\gamma A}$ . Unfortunately, these data are on midrapidity jets at relatively large values of  $x \gtrsim x_A$ , beyond the applicability of the concept of fusion of partons. Coherent diffractive forward dijets have been observed at Fermilab by the E791 Collaboration [44]. The experimental identification of diffractive dijets in the E791 experiment has been facilitated by their exact back-to-back property,  $\Delta^2 \lesssim 1/R_A^2$ . A similar identification of forward dijets from the breakup of pions in inelastic  $\pi A$  collisions might be problematic, but our main prediction of  $\langle \Delta_T^2 \rangle_{\pi A} > \langle \Delta_T^2 \rangle_{\gamma A}$  can be tested even under the most liberal event-selection criteria.

Specifically, one only needs to study the azimuthal distribution properties of the hadronic subsystem in

the first several units of the forward rapidity. For instance, one can define on an event-by-event basis the two-dimensional analogs of the familiar thrust and sphericity variables (for a review, see [45]). Then we predict that the forward system in  $\pi A$  interactions will be more spherical than in  $\gamma A$  interactions, and the 2D thrust for  $\gamma A$  will be larger than for  $\pi A$ . Such an analysis can be performed also in the COMPASS experiment at CERN in which the forward systems produced by photons and pions can be studied in the same apparatus [17]. Still another observable which differentiates between the breakup of pointlike photons and nonpointlike pions is a surplus transverse energy of secondary particles associated with forward hard jets—for the same transverse momenta of jets, it is larger in  $\pi A$  than in  $\gamma A$  collisions.

The experimental isolation of the higher twist back-to-back correlated hard contribution from the in-volume breakup is feasible and would allow the determination of the pion distribution amplitude. This challenging task can be accomplished because the background from decorrelated dijets can be determined experimentally and the back-to-back contribution has a specific dependence on the decorrelation momentum which broadens with the target mass number.

The breakup of pions into hard dijets involves the stage of soft absorption at the front face of the target nucleus and the cross section is sensitive to models of the pion wave function. Nonetheless, the predicted transverse momentum dependence of pionic dijets does not change from soft models with a strong bound on the intrinsic momentum of quarks in the pion to modern semihard, power-law (dipole) wave functions.

#### ACKNOWLEDGMENTS

We are glad to contribute to the Yu.A. Simonov Festschrift. One of us (N.N.N.) recalls vividly from his student years, the late 1960's, how much I.S. Shapiro, then the leader of the Nuclear Theory Group, praised Simonov's work on the hyperspherical approach to many-body systems, the subject of Yurii Antonovich's habilitation thesis. Ever since then, Yurii Antonovich has remained at the forefront of hadron physics and nonperturbative QCD and we take this occasion to wish Yurii Antonovich continued vigor and creativity.

This work has been partly supported by the INTAS grant no. 00-00366 and the DFG grant no. 436RUS17/72/03.

#### REFERENCES

1. E. Leader and E. Predazzi, *Introduction to Gauge Theories and Modern Particle Physics* (Cambridge Univ. Press, Cambridge, 1996), Vol. 1; G. Sterman, *An Introduction to Quantum Field Theory* (Cambridge Univ. Press, Cambridge, 1993).
2. A. H. Mueller, Nucl. Phys. B **335**, 115 (1990).
3. A. H. Mueller, Nucl. Phys. B **558**, 285 (1999); in *QCD Perspectives on Hot and Dense Matter: Proceedings*, Ed. by J.-P. Blaizot and E. Iancu (Kluwer, Dordrecht, The Netherlands, 2002), NATO Science Series, II, Mathematics, Physics, and Chemistry, Vol. 87, p. 45; hep-ph/0111244.
4. L. McLerran and R. Venugopalan, Phys. Rev. D **49**, 2233 (1994); J. Jalilian-Marian, A. Kovner, L. D. McLerran, and H. Weigert, Phys. Rev. D **55**, 5414 (1997); E. Iancu, A. Leonidov, and L. McLerran, in *QCD Perspectives on Hot and Dense Matter: Proceedings*, Ed. by J.-P. Blaizot and E. Iancu (Kluwer, Dordrecht, The Netherlands, 2002), NATO Science Series, II, Mathematics, Physics, and Chemistry, Vol. 87, p. 73; hep-ph/0202270.
5. N. N. Nikolaev, W. Schäfer, B. G. Zakharov, and V. R. Zoller, Pis'ma Zh. Éksp. Teor. Fiz. **76**, 231 (2002) [JETP Lett. **76**, 195 (2002)].
6. N. N. Nikolaev, W. Schäfer, B. G. Zakharov, and V. R. Zoller, Zh. Éksp. Teor. Fiz. **124**, 491 (2003) [JETP **97**, 441 (2003)].
7. I. P. Ivanov, N. N. Nikolaev, W. Schäfer, *et al.*, *Lectures on Diffraction and Saturation of Nuclear Partons in DIS off Heavy Nuclei*, in *Proceedings of 36th Annual Winter School on Nuclear and Particle Physics and 8th St. Petersburg School on Theoretical Physics, St. Petersburg, Russia, 2002*; hep-ph/0212161; *High Density QCD, Saturation and Diffractive DIS, Invited Talk at the NATO Advanced Research Workshop on Diffraction 2002, Alushta, Ukraine, 2002*; hep-ph/0212176; in *Proceedings of the Workshop on Exclusive Processes at High Momentum Transfer, Jefferson Lab, 2002*, Ed. by A. Radyushkin and P. Stoler (World Sc., River Edge, 2002), p. 205; hep-ph/0207045; *High Density QCD and Saturation of Nuclear Partons*, in *Proceedings of the Conference on Quark Nuclear Physics (QNP 2002), Jülich, Germany, 2002*, Ed. by C. Elster, J. Speth, and Th. Walcher (Springer-Verlag, New York, 2003); Eur. Phys. J. A **18**, 437 (2003); hep-ph/0209298; in *Multiparticle Dynamics: ISMD 2002: Proceedings*, Ed. by A. Sissakian, G. Kozlov, and E. Kolganova (World Sc., River Edge, N.J., 2003), p. 209; hep-ph/0212176.
8. A. Szczurek, N.N. Nikolaev, W. Schäfer, and J. Speth, Phys. Lett. B **500**, 254 (2001).
9. J. R. Forshaw and R. G. Roberts, Phys. Lett. B **335**, 494 (1994); A. J. Askew, D. Graudenz, J. Kwiecinski, and A. D. Martin, Phys. Lett. B **338**, 92 (1994); J. Kwiecinski, A. D. Martin, and A. M. Stasto, Phys. Lett. B **459**, 644 (1999).

10. V. I. Zakharov and N. N. Nikolaev, *Yad. Fiz.* **21**, 434 (1975) [*Sov. J. Nucl. Phys.* **21**, 227 (1975)]; N. N. Nikolaev and V. I. Zakharov, *Phys. Lett. B* **55B**, 397 (1975).
11. N. N. Nikolaev, W. Schäfer, and G. Schwiete, *Pis'ma Zh. Éksp. Teor. Fiz.* **72**, 583 (2000) [*JETP Lett.* **72**, 405 (2000)]; *Phys. Rev. D* **63**, 014020 (2001).
12. S. Frullani and J. Mougey, *Adv. Nucl. Phys.* **14**, 3 (1984).
13. A. V. Efremov and A. V. Radyushkin, *Theor. Math. Phys.* **42**, 97 (1980); *Phys. Lett. B* **94B**, 245 (1980); A. V. Radyushkin, JINR-P2-10717 (Dubna, 1977); hep-ph/0410276; G. P. Lepage and S. J. Brodsky, *Phys. Lett. B* **87B**, 359 (1979); *Phys. Rev. D* **22**, 2157 (1980).
14. V. L. Chernyak and A. R. Zhitnitsky, *Phys. Rep.* **112**, 173 (1984); S. J. Brodsky, H.-C. Pauli, and S. S. Pinsky, *Phys. Rep.* **301**, 299 (1998); R. Jakob and P. Kroll, *Phys. Lett. B* **315**, 463 (1993); **319**, 545(E) (1993); A. P. Bakulev, S. V. Mikhailov, and N. G. Stefanis, *Phys. Lett. B* **578**, 91 (2004).
15. V. M. Braun, D. Yu. Ivanov, A. Schäfer, and L. Szymanowski, *Phys. Lett. B* **509**, 43 (2001); *Nucl. Phys. B* **638**, 111 (2002).
16. V. L. Chernyak, *Phys. Lett. B* **516**, 116 (2001); V. L. Chernyak and A. G. Grozin, *Phys. Lett. B* **517**, 119 (2001).
17. COMPASS. A Proposal for a Common Muon and Proton Apparatus for Structure and Spectroscopy, CERN/SPSLC 96-14, SPSLC/P297 (Mar 1, 1996).
18. N. N. Nikolaev and B. G. Zakharov, *Z. Phys. C* **49**, 607 (1991).
19. N. N. Nikolaev and B. G. Zakharov, *Z. Phys. C* **53**, 331 (1992).
20. N. N. Nikolaev and B. G. Zakharov, *Zh. Éksp. Teor. Fiz.* **105**, 1498 (1994) [*JETP* **78**, 806 (1994)]; *Z. Phys. C* **64**, 631 (1994).
21. N. N. Nikolaev, B. G. Zakharov, and V. R. Zoller, *Pis'ma Zh. Éksp. Teor. Fiz.* **59**, 8 (1994) [*JETP Lett.* **59**, 6 (1994)].
22. N. N. Nikolaev and B. G. Zakharov, *Phys. Lett. B* **332**, 184 (1994).
23. N. N. Nikolaev, B. G. Zakharov, and V. R. Zoller, *Z. Phys. A* **351**, 435 (1995).
24. V. Barone, M. Genovese, N. N. Nikolaev, *et al.*, *Phys. Lett. B* **326**, 161 (1994).
25. V. Barone, M. Genovese, N. N. Nikolaev, *et al.*, *Z. Phys. C* **58**, 541 (1993).
26. L. N. Lipatov, *Yad. Fiz.* **23**, 642 (1976) [*Sov. J. Nucl. Phys.* **23**, 338 (1976)]; E. A. Kuraev, L. N. Lipatov, and V. S. Fadin, *Zh. Éksp. Teor. Fiz.* **71**, 840 (1976) [*Sov. Phys. JETP* **44**, 443 (1976)]; **72**, 377 (1977) [**45**, 199 (1977)]; Ya. Ya. Balitsky and L. N. Lipatov, *Yad. Fiz.* **28**, 1597 (1978) [*Sov. J. Nucl. Phys.* **28**, 822 (1978)].
27. I. P. Ivanov and N. N. Nikolaev, *Yad. Fiz.* **64**, 813 (2001) [*Phys. At. Nucl.* **64**, 753 (2001)]; *Phys. Rev. D* **65**, 054004 (2002).
28. B. Andersson *et al.* (Small x Collab.), *Eur. Phys. J. C* **25**, 77 (2002).
29. T. Ahmed *et al.* (H1 Collab.), *Nucl. Phys. B* **445**, 195 (1995) (and references therein).
30. N. N. Nikolaev and B. G. Zakharov, *Phys. Lett. B* **332**, 177 (1994).
31. A. V. Radyushkin, *Phys. Rev. D* **58**, 114008 (1998).
32. M. Diehl, T. Feldmann, R. Jakob, and P. Kroll, *Eur. Phys. J. C* **8**, 409 (1999).
33. W. Jaus, *Phys. Rev. D* **44**, 2851 (1991).
34. Review of Particle Physics, *Eur. Phys. J. C* **3**, 1 (1998).
35. R. J. Glauber, in *Lectures in Theoretical Physics*, Ed. by W. E. Brittin *et al.* (Intersci. Publ., New York, 1959), Vol. 1, p. 315.
36. B. G. Zakharov, *Yad. Fiz.* **46**, 148 (1987) [*Sov. J. Nucl. Phys.* **46**, 92 (1987)].
37. N. N. Nikolaev, G. Piller, and B. G. Zakharov, *Zh. Éksp. Teor. Fiz.* **108**, 1554 (1995) [*JETP* **81**, 851 (1995)]; *Z. Phys. A* **354**, 99 (1996).
38. B. G. Zakharov, *Pis'ma Zh. Éksp. Teor. Fiz.* **63**, 906 (1996) [*JETP Lett.* **63**, 952 (1996)]; **65**, 585 (1997) [**65**, 615 (1997)]; *Yad. Fiz.* **61**, 924 (1998) [*Phys. At. Nucl.* **61**, 838 (1998)].
39. C. Adler *et al.* (STAR Collab.), *Phys. Rev. Lett.* **90**, 082302 (2003).
40. A. Mukherjee, I. V. Musatov, H. C. Pauli, and A. V. Radyushkin, *Phys. Rev. D* **67**, 073014 (2003).
41. M. V. Terentiev, *Yad. Fiz.* **24**, 207 (1976) [*Sov. J. Nucl. Phys.* **24**, 106 (1976)].
42. J. Nemchik, N. N. Nikolaev, and B. G. Zakharov, *Phys. Lett. B* **341**, 228 (1994); J. Nemchik, N. N. Nikolaev, E. Predazzi, and B. G. Zakharov, *Phys. Lett. B* **374**, 199 (1996); *Z. Phys. C* **75**, 71 (1997).
43. D. Naples *et al.* (E683 Collab.), *Phys. Rev. Lett.* **72**, 2341 (1994).
44. E. M. Aitala *et al.* (E791 Collab.), *Phys. Rev. Lett.* **86**, 4768 (2001).
45. S. L. Wu, *Phys. Rep.* **107**, 59 (1984).

# Summation of Divergent Series and Zeldovich's Regularization Method

V. D. Mur, S. G. Pozdnyakov, S. V. Popruzhenko\*, and V. S. Popov<sup>1)</sup>

Moscow Engineering Physics Institute (State University), Kashirskoe sh. 31, Moscow, 115409 Russia

Received April 12, 2004; in final form, June 17, 2004

**Abstract**—A method for summing divergent series, including perturbation-theory series, is considered. This method is an analog of Zeldovich's regularization method in the theory of quasistationary states. It is shown that the method in question is more powerful than the well-known Abel and Borel methods, but that it is compatible with them (that is, it leads to the same value for the sum of a series). The constraints on the parameter domain that arise upon the removal of the regularization of divergent integrals by this method are discussed. The dynamical Stark shifts and widths of loosely bound  $s$  states in the field of a circularly polarized electromagnetic wave are calculated at various values of the Keldysh adiabaticity parameter and the multi-quantum parameter. © 2005 Pleiades Publishing, Inc.

*Dedicated to Yuriĭ Antonovich Simonov  
on the occasion of his 70th birthday*

## 1. INTRODUCTION

Perturbation theory is a universal method for performing calculations in quantum mechanics, field theory, and other realms of theoretical physics. The possibility of applying it in a large number of nontrivial physics problems is based on the presence of a small expansion parameter (coupling constant),  $g \ll 1$ , in such problems. Of course, it is also of interest to explore the possibility of employing perturbation theory beyond the weak-coupling region. As was noted long ago, however, perturbation-theory series diverge (Dyson's phenomenon [1]);<sup>2)</sup> therefore, it is impossible, without applying methods for summing (or regularizing) divergent series, to extract information about the behavior of the sought function (energy  $E_n(g)$  of a level, Gell-Mann–Low function  $\beta(g)$ , etc.) for  $g \geq 1$ .

Such methods have been studied in mathematics since the time of Euler and Poincaré (see, for example, the monograph of Hardy [2] and the first part of the treatise of Whittaker and Watson [3], which covers numerous summation methods and establishes detailed relationships between them—that is, their compatibility or incompatibility). In theoretical physics, use is most frequently made of the Abel

(A) and the Borel (B) method, which are the simplest and most convenient in computations. A survey of both of these summation methods, along with their application to specific problems, is given, for example, in [4, 5].

In the present article, we will discuss yet another summation method, that which arises from investigations into the theory of quasistationary states. As is well known [6], a quasistationary state is described by a Gamow wave function that satisfies the Sommerfeld radiation condition  $\chi_k(r) \sim \exp(ikr)$  for  $r \rightarrow \infty$ , where  $k = \sqrt{2E} = k_1 - ik_2$ , with  $k_1, k_2 > 0$ , and  $E = E_r - i\Gamma/2$  is the complex energy of this state, with  $E_r = (k_1^2 - k_2^2)/2$  and  $\Gamma = 2k_1k_2$  being the resonance position and width, respectively.

In view of an exponential growth of the wave function  $\chi_k(r)$  at infinity, there arise serious difficulties in solving specific problems since even the normalization integral  $\int_0^\infty |\chi_k(r)|^2 dr$  diverges. A possible way to overcome this difficulty was indicated by Zeldovich [7], who proposed treating a divergent integral as that which is regularized. In particular, the normalization integral for the radial wave function in the spherically symmetric case is defined in this approach as the limit

$$\lim_{\alpha \rightarrow +0} \int_0^\infty \chi_k^2(r) e^{-\alpha r^2} dr \equiv \int_0^\infty \chi_k^2(r) dr. \quad (1)$$

This makes it possible to construct perturbation theory for quasistationary states [6, 7] and to trace the analogy between them and ordinary stationary states of the discrete spectrum.

The regularization method specified by Eq. (1) was proposed by Zeldovich as far back as 1960 [7]. Al-

<sup>1)</sup>Institute of Theoretical and Experimental Physics, Bol'shaya Cheremushkinskaya ul. 25, Moscow, 117218 Russia.

<sup>2)</sup>This is not so only for a small number of extremely simple model problems where a perturbation-theory series reduces to the first few terms (as in the case of a harmonic oscillator in a uniform external field).

\*e-mail: poprz@theor.mephi.ru

though, in quantum mechanics and in atomic and nuclear physics, there had appeared, even at that time, a broad range of problems that called for developing a mathematical formalism for the theory of quasi-stationary states,<sup>3)</sup> there were no attempts, as far as we know, at applying Zeldovich's method to specific physics problems for a rather long period of time. In all probability, the reason was that the implementation of this procedure for regularizing integrals of the type in Eq. (1), which diverge exponentially at infinity, required computational capacities not available at that time. To date, the situation has changed radically: an ordinary PC is quite sufficient for obtaining the numerical results presented in this article.

In [9–11], the problem of the applicability of the regularization in (1) beyond perturbation theory was analyzed by considering an atomic level bound by short-range forces that undergoes ionization under the effect of intense monochromatic laser radiation having a circular polarization. It was shown that, in this way, the energy  $E_r$  and the width  $\Gamma$  of a quasistationary state can be calculated over a broad interval of external parameters (wave-field amplitude  $\mathcal{E}_0$  and wave frequency  $\omega$ ) and a broad interval of the energy of the initial bound state. In [11], the regularization specified by Eq. (1) was used to calculate the rate of negative-ion ( $H^-$ ,  $Na^-$ , etc.) photodecay. An alternative approach to exactly solved problems of photoionization—that which is based on a regularization of a form that is more special than that in Eq. (1)—was recently developed in [12].

The ensuing exposition is organized as follows. In Section 2, we describe a method for summing divergent series that is a natural generalization of that in (1) and which will be referred to as Zeldovich's method (Z). Several examples of its application in specific problems are considered. It is shown that method Z is compatible with methods A and B if all three of them are applicable to a given series. In Section 3, we consider an example of applying Zeldovich's method to regularizing a divergent integral. Section 4 is devoted to applications of Zeldovich's regularization method in the theory of photoionization.

## 2. SUMMATION OF DIVERGENT SERIES BY ZELDOVICH'S METHOD

The idea of imparting some specific meaning to the sum of a divergent series was quite clearly formulated back in the studies of Euler [2, 3] (although his methods and statements are naturally not in line

with the modern requirements of mathematical rigor). The subsequent development of Euler's ideas was formidable, and there are presently numerous methods for summing divergent series [2], but only some of them are used in theoretical physics. The methods due to Abel and Borel proved to be especially convenient for applications. We will now recall relevant definitions. For the sum  $S = \sum_n a_n$ , the limit

$$S = \lim_{\alpha \rightarrow +0} \sum_n a_n \exp(-\alpha n) \quad (A)$$

is referred to as its generalized sum (or merely the sum) according to Abel. If the series converges,  $S$  coincides with its ordinary sum. The method of summation according to Borel is specified (in its simplest version) by the formula

$$S = \int_0^\infty dx e^{-x} B(x), \quad B(x) = \sum_n a_n \frac{x^n}{n!}. \quad (B)$$

Method A is applicable to series whose coefficients show a power-law growth,  $|a_n| \sim n^\sigma$ , while method B is also applicable in the case where  $|a_n| \sim n!$  for  $n \rightarrow \infty$ , which usually occurs in quantum mechanics and field theory [1, 4]. Obviously, method B is more powerful than method A, this being rigorously established by relevant theorems [2]. It is of importance that these methods are compatible—that is, they lead to the same value of the generalized sum  $S$ .

Use is also made of the modified Borel method specified by the formula ( $B_{\mu\nu}$ )

$$S = \int_0^\infty dx \exp(-x^{1/\mu}) x^{\frac{\nu}{\mu}-1} B_{\mu\nu}(x),$$

$$B_{\mu\nu}(x) = \sum_n a_n \frac{x^n}{\Gamma(\mu n + \nu)}, \quad \mu > 0.$$

Method B is the particular case of this method at  $\mu = \nu = 1$ . The modified Borel method makes it possible to sum series whose coefficients grow in proportion to  $(\mu n)!$ , which occurs in a number of problems.<sup>4)</sup>

Apart from the aforementioned summation methods, which are well-known in the literature, we would like to indicate yet another method, that which will be referred to here as Zeldovich's method and which is specified by the definition

$$S = \lim_{\alpha \rightarrow +0} \sum_n a_n \exp(-\alpha n^2). \quad (Z)$$

<sup>4)</sup>By way of example, we indicate that  $\mu = N - 1$  for a quantum oscillator involving an anharmonicity of the  $gx^{2N}$  type [13] and that  $\mu = 1/2$  in the case of QED [14].

<sup>3)</sup>In this connection, see, for example, [8].

Since  $(\mu n)! \sim \exp(\mu n \ln n)$  for  $n \rightarrow \infty$ , we can expect that method Z is more powerful than method  $(B_{\mu\nu})$  for arbitrary parameters  $\mu$  and  $\nu$ ; however, there arises the question of whether method Z is compatible with the other summation methods. Without pursuing the goal of giving a rigorous mathematical solution to this problem, we will merely consider a few characteristic examples that will illustrate the application of the Z method and which will make it possible to set guidelines in this issue.

(i) We begin by considering the extremely simple divergent series [2]

$$S_0 = \sum_{n=0}^{\infty} (-1)^n = 1 - 1 + 1 - 1 + \dots \quad (2)$$

According to the Abel and Borel methods, we have

$$\begin{aligned} \text{(A): } S_0 &= \lim_{\alpha \rightarrow +0} \sum_{n=0}^{\infty} (-1)^n \exp(-\alpha n) \quad (2a) \\ &= \lim_{\alpha \rightarrow +0} \frac{1}{1 + e^{-\alpha}} = \frac{1}{2}, \end{aligned}$$

$$\begin{aligned} \text{(B): } B(x) &= \sum_{n=0}^{\infty} \frac{(-x)^n}{n!} = e^{-x}, \quad (2b) \\ S_0 &= \int_0^{\infty} dx e^{-2x} = \frac{1}{2}. \end{aligned}$$

The application of Zeldovich's method requires a more sophisticated knowledge of mathematics. The result is

$$\begin{aligned} S_0 &= \lim_{\alpha \rightarrow +0} \sum_{n=0}^{\infty} (-1)^n \exp(-\alpha n^2) \quad (3) \\ &= \frac{1}{2} [1 + \vartheta_4(0, e^{-\alpha})], \quad \alpha \rightarrow +0, \end{aligned}$$

where  $\vartheta_4(u, q)$  is one of the theta functions [3, 15]; it follows that

$$\text{(Z): } S_0 = 1/2 \quad (3a)$$

since

$$\vartheta_4(0, q) = \prod_{k=1}^{\infty} (1 - q^{2k-1})^2 (1 - q^{2k}) \quad (4)$$

(see [15, 8.181.1]) and  $\vartheta_4(0, 1) = 0$ .

Thus, all of the three summation methods lead to the same value of 1/2 for the series in (2).

(ii) We now consider the series

$$S_{\mu} = 1 - 2^{\mu} + 3^{\mu} - 4^{\mu} + \dots, \quad (5)$$

which is a generalization of the series in (2) and which converges for  $\mu \geq 0$ . At integral values of  $\mu = m = 0, 1, 2, \dots$ , the Abel method yields

$$S_m = \left( x \frac{d}{dx} \right)^m \frac{x}{1+x} \Big|_{x=1},$$

whence we successively obtain

$$\begin{aligned} S_0 &= 1/2, \quad S_1 = 1/4, \quad S_3 = -1/8, \quad (5a) \\ S_5 &= 1/4, \quad S_7 = -17/16, \quad S_9 = 31/4, \\ S_{11} &= -691/8, \dots, \\ S_{13} &= 5461/4, \quad S_{15} = -929\,569/32 \end{aligned}$$

and  $S_2 = S_4 = S_6 = \dots = 0$ . However, it is difficult to consider the case of an arbitrary value of the exponent  $\mu$  in this way. In order to do this, we notice that, at arbitrary  $\mu$ ,

$$S_{\mu} = \lim_{x \rightarrow 1} \sum_{n=1}^{\infty} n^{\mu} (-x)^{n-1} = \lim_{x \rightarrow 1} \Phi(-x, -\mu, 1), \quad (6)$$

where  $\Phi(z, s, v)$  is a special function [16] that has the cut  $1 < z < \infty$ . This function is analytic at  $z = -1$ ; therefore, we have (see [16, 1.12.2])

$$\begin{aligned} S_{\mu} &= (1 - 2^{\mu+1}) \zeta(-\mu) \quad (7) \\ &\equiv \frac{2 - 2^{-\mu}}{\pi^{\mu+1}} \sin \frac{\pi \mu}{2} \Gamma(\mu + 1) \zeta(\mu + 1), \end{aligned}$$

where  $\zeta(z)$  is a Riemann zeta function. In particular,  $\zeta(0) = -1/2$  and  $\zeta(1 - 2k) = -B_{2k}/2k$ , whence it follows that  $S_{-1} = \ln 2$  and  $S_0 = 1/2$ ; at integer  $m \geq 1$ , method A yields

$$\begin{aligned} S_m &= [1 + (-1)^{m+1}] \left( \frac{2^{m+1} - 1}{2m + 2} \right) B_{m+1}, \quad (8) \\ m &= 1, 2, 3, \dots, \end{aligned}$$

where  $B_k$  are Bernoulli numbers. The same result is obtained by means of an analytic continuation in the parameter  $\mu$ . The above values in (5a) readily follow from (8).

Let us now proceed to apply Zeldovich's method. We have

$$S_{\mu} = \lim_{\alpha \rightarrow +0} \sum_{n=0}^{\infty} (-1)^n n^{\mu} \exp(-\alpha n^2). \quad (9)$$

At even values of  $\mu = 2m = 0, 2, 4, \dots$ , method Z yields

$$S_{2m} = \frac{1}{2} \left( q \frac{d}{dq} \right)^m \vartheta_4(0, q) \Big|_{q=1} = 0.$$

Indeed, it follows from (4) that the point  $q = 1$  is an infinite-order zero of the function  $\vartheta_4(0, q)$ ; therefore, all finite-order derivatives vanish at  $q = 1$ . For

**Table 1.** Results of summation of the series in (5) by Zeldovich’s method [given here are the numerical values of partial sums of the series in (9)]

$\alpha$	$S_\mu$ at $\mu = 1$	$N_\alpha$	$S_\mu$ at $\mu = 1.5$	$N_\alpha$	$S_\mu$ at $\mu = 2$	$N_\alpha$	$S_\mu$ at $\mu = 2.5$	$N_\alpha$
0.5	0.3679	6	0.2788	6	0	7	0.0360	7
0.1	0.2640	14	0.1297	15	2.6(−8)	20	−0.1047	16
0.02	0.2526	31	0.1207	33	−2.1(−15)	53	−0.0907	36
0.01	0.2513	44	0.1197	47	−7.4(−16)	76	−0.0892	52
0.001	0.250125	142	0.11878	154	—	—	−0.08798	171
2.0(−4)	0.250025	324	0.11870	352	—	—	−0.087868	395
1.0(−4)	0.250012	462	0.118691	503	—	—	−0.087855	567
5.0(−5)	0.250006	659	0.118686	719	—	—	−0.087848	813
1.0(−5)	0.250001	1501	0.118681	1645	—	—	−0.087843	1874
1.0(−6)	0.250000	4868	0.118681	5370	—	—	−0.087841...	6170
Exact value	1/4		0.1186808...		0		−0.0878411...	

$\alpha$	$S_\mu$ at $\mu = 3$	$N_\alpha$	$S_\mu$ at $\mu = 5$	$N_\alpha$	$S_\mu$ at $\mu = 7$	$N_\alpha$	$S_\mu$ at $\mu = 10$	$N_\alpha$
0.1	−0.1571	16	0.4200	17	−2.801	19	3.17	21
0.02	−0.1302	37	0.2729	42	−1.236	45	−5.5(−7)	56
0.01	−0.1276	53	0.2610	60	−1.145	66	−3.2(−7)	86
0.001	−0.1253	178	0.25107	205	−1.070	228	—	—
5.0(−4)	−0.1251	256	0.25053	296	−1.067	330	—	—
2.0(−4)	−0.125050	413	0.25021	480	−1.066	538	—	—
1.0(−4)	−0.125025	592	0.25011	693	−1.076	777	—	—
5.0(−5)	−0.125012	851	0.25004	998	−1.542	1119	—	—
Exact value	−1/8		1/4		−1.0625		0	

Note: Here,  $N_\alpha$  is the number of terms of the series that are taken into account at given  $\alpha$ . The exact values of  $S_\mu$  were calculated by formula (7). The following notation is used:  $a(b) \equiv a \times 10^b$ . Dashes appear in the cases where the partial sums  $S_\mu$  were not calculated.

arbitrary  $\mu$ , the sum in (9) cannot be calculated analytically. The results of a numerical calculation are given in Table 1. They show that, at  $\alpha \sim 10^{-4}$ , the calculation of the sum  $S_\mu$  produces four to six reliable decimal places. It should be noted here that the terms of the series in (9) first increase, reaching a maximum at  $n \simeq n_0 = \sqrt{\mu/2\alpha}$ , and then begin to decrease. The order of the leading terms of the series is the following:

$$\begin{aligned} \langle n^\mu \rangle_{\max} &= \exp(-\alpha n_0^2) n_0^\mu & (10) \\ &= \left( \frac{\mu}{2e\alpha} \right)^{\mu/2} \sim \alpha^{-\mu/2}, \\ e &= 2.718\dots, \quad \alpha \rightarrow +0. \end{aligned}$$

By way of example, we indicate that, at  $\mu = 10$  and  $\alpha = 0.01$ , the results are  $n_0 \approx 22$ ,  $n_0^\mu \simeq 3 \times 10^{13}$ ,

$\langle n^\mu \rangle_{\max} \simeq 2 \times 10^{11}$ , and  $N_\alpha/n_0 \approx 4$ , where  $N_\alpha$  is the number of terms in the series that are taken into account at a given value of  $\alpha$ . Thus, the sum  $S_\mu$  (which is on the order of unity) is obtained upon the cancellation of very large terms, this imposing rather stringent requirements on the accuracy of relevant numerical calculations. Nevertheless, method Z works quite successfully (in obtaining data presented in Table 1, it was sufficient to perform calculations with a doubled precision). Table 1 also indicates the values of  $N_\alpha$ , which are determined by a preset precision (of about  $10^{-6}$ ) in the calculation of the sum. As a rule,  $N_\alpha$  exceeds  $n_0$  by a factor of 4 to 8. With increasing exponent  $\mu$ , the accuracy in calculating  $S_\mu$  becomes poorer, which is quite natural in view of (10). By way of example, we indicate that, at  $\mu = 0$ —that is, for the series in (2)— $S_\mu(\alpha) = 1/2$  to a precision of

**Table 2.** Results of summation of the series in (11) by Zeldovich’s method

$\alpha$	$S_\lambda$ at $\lambda = 0$	$N_\alpha$	$S_\lambda$ at $\lambda = 1$	$N_\alpha$	$S_\lambda$ at $\lambda = 2.5$	$N_\alpha$	$S_\lambda$ at $\lambda = 5$	$N_\alpha$
1.0	0.01819	5	0.02560	5	7.1705(−3)	5	−2.7336(−3)	5
0.1	0.40484	14	0.20309	14	2.7491(−2)	15	−4.7666(−2)	16
0.01	0.049005	43	0.22365	45	1.1960(−2)	47	−3.8739(−2)	51
1.0(−3)	0.49900	136	0.22558	142	1.0426(−2)	150	−3.7601(−2)	163
1.0(−5)	0.49990	1358	0.2257892	1429	1.02577(−2)	1530	−3.74742(−2)	1678
1.0(−8)	0.50000	42 920	0.2257914	45 600	1.02560(−2)	49 368	−3.74729(−2)	55 112
Exact value	1/2		0.22579135 ...					

Note: The notation is identical to that in Table 1.

$\delta \simeq 10^{-7}$  for all values of  $\alpha$  from 0.1 to 0.01, whereas, at  $\mu = 7$ , the error in the calculation of  $S_\mu$  is  $\delta \simeq 0.3\%$ . It is interesting to note the following: it can be seen from Table 1 that, at even values of the exponent, in which case  $S_{2m} = 0$ , the convergence of  $S_\mu(\alpha)$  to the limit for  $\alpha \rightarrow 0$  is much faster than in all other cases.

It should be emphasized that the correct value of the sum  $S_\mu$  of a series can be obtained only if a large number of terms ( $N_\alpha \gg 1$ ) is taken into account in (9). In this respect, the situation here is similar to that where one has to sum perturbation-theory series in quantum field theory.<sup>5)</sup> If we know only the first few orders of perturbation theory, no summation procedure can guarantee, for a function specified by a divergent perturbation-theory series, a reliable calculation far beyond the boundaries of the weak-coupling region (in this connection, see [4, 19–22]).

(iii) It is well known that, in renormalized quantum field theory (for example, in QED), divergences have a logarithmic character. In this connection, it is interesting to sum the series

$$S_\lambda = \sum_{k=1}^{\infty} (-1)^k (\ln k)^\lambda, \quad (11)$$

<sup>5)</sup>In quantum field theory, it is extremely difficult to calculate higher orders of perturbation theory because of a factorial growth of the number of Feynman diagrams, the presence of ultraviolet divergences, and the absence of efficient methods for calculating complex diagrams. Over more than 50 years since the calculation of the Schwinger correction  $\alpha/2\pi$  to the electron magnetic moment [17], only terms of order up to  $(\alpha/\pi)^4$  have been taken into account thus far [18], and we can hardly expect here considerable advances in the near future. Also, the calculation of each successive order of perturbation theory in  $\varphi_{(4)}^4$  scalar field theory and in Yang–Mills theory, where, at the present time, we know the first four to five perturbation-theory coefficients  $\beta_n$  in the Gell-Mann–Low function  $\beta(g)$ , required about ten years.

which is divergent at  $\lambda \geq 0$ . The results of the summation of this series by Zeldovich’s method are given in Table 2. The choice of the parameter value of  $\alpha = 10^{-5}$  provides five correct decimal places in  $S_\lambda$  for  $0 \leq \lambda \leq 5$ .

We note that, at integral values of  $\lambda = 1, 2, 3, \dots$ , the generalized sum of the series in (11) can be expressed in a finite form by successively differentiating expression (7) with respect to  $\mu$  and by setting  $\mu = 0$  after that. In particular, we have

$$S_1 = 2 \ln 2 \cdot \zeta(0) - \zeta'(0) = \frac{1}{2} \ln \frac{\pi}{2}. \quad (12)$$

From Table 2, it can be seen that, to a high precision, a numerical calculation within Zeldovich’s method leads to the same result.

(iv) Finally, we consider the Euler series [2]

$$S(g) = \sum_{n=0}^{\infty} n! (-g)^n = 1 - g + 2g^2 - 6g^3 + \dots \quad (13)$$

Obviously, method A is not applicable here, while method B leads to  $B(x) = (1 + gx)^{-1}$ ,

$$S(g) = \int_0^{\infty} \frac{e^{-x}}{1 + gx} dx = -g^{-1} e^{1/g} \text{Ei}(-g^{-1}) \quad (14)$$

$$\approx g^{-1} (\ln g - C) + O(g^{-2} \ln g), \quad g \rightarrow \infty,$$

where  $C = 0.5772 \dots$  and  $\text{Ei}(z)$  is an integral exponential [15].

The exact values of the function  $S(g)$ , which were calculated by formula (14), are given in Table 3, along with the results of the summation of the series in (13) by method Z, its precision being 0.015 to 0.04% (depending on the value of  $g$ ). In order to attain this

**Table 3.** Results of summation of the Euler series by Zeldovich’s method

$g$	Exact value	(Z)	$N$
0.1	0.915633	0.9155	41
0.3	0.801186	0.8011	80
0.5	0.722657	0.7225	71
0.7	0.663510	0.6633	61
0.8	0.638791	0.6386	65
0.9	0.616538	0.6163	54
1.0	0.596347	0.5961	56

Note: The exact values of  $S(g)$  were calculated by formula (14); the results of summation by Zeldovich’s method are given in column (Z); and  $N$  is the number of terms of the series in (13) that are taken into account in summation.

accuracy, the values of the sums

$$S(g, \alpha) = \sum_{n=0}^{\infty} n!(-g)^n \exp(-\alpha n^2) \quad (15)$$

calculated at  $\alpha = 0.01-0.2$  are extrapolated to the limit  $\alpha \rightarrow +0$ .<sup>6)</sup>

### 3. REGULARIZATION OF INTEGRALS BY ZELDOVICH’S METHOD

In the preceding section, we have considered a discrete analog of Zeldovich’s method. We will now discuss the conditions of applicability of this method in regularizing exponentially divergent integrals that appear in the theory of quasistationary states. The simplest generalization of the normalization integral in (1) for the Gamow wave function  $\chi_k(r)$  is the one-parameter set of integrals

$$J(\varepsilon, s) = \int_0^{\infty} dt t^{s-1} \exp\{-i\varepsilon t\} \quad (16)$$

$$= \Gamma(s)(i\varepsilon)^{-s}, \quad s > 0,$$

which are convergent in the lower half-plane of the complex variable  $\varepsilon = \varepsilon_1 + i\varepsilon_2$  and which can be analytically continued to the upper half-plane  $\text{Im}\varepsilon > 0$ .

Introducing the regularization according to Zeldovich’s recipe, we obtain

$$J_{\alpha}(\varepsilon, s) = \int_0^{\infty} dt t^{s-1} \exp\{-i\varepsilon t - \alpha t^2\} \quad (17)$$

<sup>6)</sup>In extrapolating these sums to  $\alpha = 0$ , we used the least squares approximation of the values of  $S(g, \alpha)$  by a second-degree polynomial (see Appendix 1 in [10]).

$$= \Gamma(s)(2\alpha)^{-s/2} \exp(-\varepsilon^2/8\alpha) D_{-s}(i\varepsilon/\sqrt{2\alpha}),$$

$\alpha > 0$

(see 3.462 in [15]). Taking into account the asymptotic behavior of the parabolic-cylinder functions  $D_{-s}(z)$  (Weber functions) for  $\alpha \rightarrow 0$ , we arrive at

$$J_{\alpha}(\varepsilon, s) = \Gamma(s)(i\varepsilon)^{-s} \left[ 1 + \frac{s(s+1)}{\varepsilon^2} \alpha + \dots \right] \quad (18)$$

under the condition  $-5\pi/4 < \arg \varepsilon < \pi/4$ ;

$$J_{\alpha}(\varepsilon, s) = \Gamma(s)(i\varepsilon)^{-s} \left[ 1 + \frac{s(s+1)}{\varepsilon^2} \alpha + \dots \right] \quad (19)$$

$$- \frac{2\sqrt{\pi\alpha}}{(2\alpha)^s} e^{-i\pi s} (i\varepsilon)^{s-1} \exp\left\{-\frac{\varepsilon^2}{4\alpha}\right\}$$

$$\times \left[ 1 - \frac{(s-1)(s-2)}{\varepsilon^2} \alpha + \dots \right]$$

under the condition  $-\pi/4 < \arg \varepsilon < 3\pi/4$ ; and

$$J_{\alpha}(\varepsilon, s) = \Gamma(s)(i\varepsilon)^{-s} \quad (20)$$

$$\times \left[ 1 + \frac{s(s+1)}{\varepsilon^2} \alpha + \dots \right]$$

$$- \frac{2\sqrt{\pi\alpha}}{(2\alpha)^s} e^{i\pi s} (i\varepsilon)^{s-1}$$

$$\times \exp\left\{-\frac{\varepsilon^2}{4\alpha}\right\} \left[ 1 - \frac{(s-1)(s-2)}{\varepsilon^2} \alpha + \dots \right]$$

for  $-7\pi/4 < \arg \varepsilon < -3\pi/4$ . The regions of admissible values of the argument  $\varepsilon$  are shown in Fig. 1. If  $\varepsilon_1^2 - \varepsilon_2^2 > 0$ , then the value of the integral in (16) in the limit  $\alpha \rightarrow 0$  follows from the expansions in (18)–(20). If, however,  $\varepsilon_1^2 - \varepsilon_2^2 < 0$ , the second term in (19) and the second term in (20) grow exponentially, so that the integral  $J_{\alpha}$  is unbounded. This circumstance is associated with the Stokes phenomenon, which is well known in the theory of asymptotic expansions. The data in Table 4 for  $s = 1$ , in which case

$$J_{\alpha}(\varepsilon, 1) = \frac{1}{2} \sqrt{\frac{\pi}{\alpha}} e^{-\varepsilon^2/4\alpha} \left[ 1 - \Phi\left(\frac{i\varepsilon}{2\alpha}\right) \right], \quad (21)$$

where  $\Phi$  is the error function [15], illustrate the convergence of Zeldovich’s method at various values of  $\arg \varepsilon$ , including those on the Stokes line  $\varepsilon_1^2 - \varepsilon_2^2 = 0$ . One can see the rate of convergence of the method for  $\alpha \rightarrow +0$  in the region  $\psi < \pi/4$  and a complete absence of convergence in the region  $\psi \geq \pi/4$ , including the Stokes line  $\psi = \pi/4$ .

Thus, Zeldovich’s method can be applied to regularize the integral in (16) in the upper half-plane of the complex variable  $\varepsilon$  only under the condition

$$\varepsilon_1^2 - \varepsilon_2^2 > 0. \quad (22)$$

**Table 4.** Regularization of the integral in (16) by Zeldovich’s method at  $s = 1$

$\alpha$	$\psi = 0$	$\psi = \pi/16$	$\psi = \pi/8$	$\psi = \pi/4$	$\psi = 5\pi/16$
$\text{Re}J_\alpha(\varepsilon, 1) \cdot a, \quad a = 10(-3)$					
1.00(-7)	0.2300	-0.1302	-0.7858	-5.2462	-1.0644(1)
3.16(-8)	1.8272(-3)	-0.2522	-0.4234	-1.2538	1.0717(2)
1.00(-8)	9.9999(-6)	-0.2070	-0.4026	1.6502(1)	-1.1598(5)
3.16(-9)	1.0001(-5)	-0.1984	-0.3889	5.0640(3)	–
1.00(-9)	1.0000(-5)	-0.1959	-0.3844	–	–
Exact value	0	-0.1947	-0.3830	-0.7071	-0.8316
$\text{Im}J_\alpha(\varepsilon, 1) \cdot a, \quad a = 10(-3)$					
1.00(-7)	-1.2815	-1.5237	-1.8195	-3.9012	-1.1209(1)
3.16(-8)	-1.0829	-1.0397	-0.9149	-1.0549(1)	-1.7603(2)
1.00(-8)	-1.0213	-0.9982	-0.9308	1.6073	2.2844(4)
3.16(-9)	-1.0064	-0.9862	-0.9263	1.6660(3)	–
1.00(-9)	-1.0020	-0.9825	-0.9245	–	–
Exact value	-1	-0.9809	-0.9238	-0.7071	-0.5554

Note: The real and imaginary parts of the integral in (16) that are multiplied by  $a$  are presented in the table for various values of the argument  $\varepsilon = a \exp(i\psi)$  that lie in the first quadrant ( $\pi/2 > \psi \geq 0$ ) of the upper half-plane of the complex variable  $\varepsilon$ . Given in the last row are the values of  $\sin \psi$  and  $-\cos \psi$ , which are equal to, respectively, the real and the imaginary parts of the integral in (16). Dashes stand for values that exceed  $10^6$ . The rest of the notation is identical to that in Table 1.

In the particular case of quasistationary states, the limit in (1) exists if

$$k_1 > k_2, \tag{23}$$

that is, if the pole of the scattering amplitude lies in that part of the fourth quadrant divided by its bisecting line which is adjacent to the real axis of the complex plane of the wave vector  $k$ .

Condition (23), which was not highlighted in [6, 7], is usually satisfied; for well-resolved resonances, it is satisfied even with a wide margin. However, this is not so for virtual states, so that Zeldovich’s method does not work for them. A similar situation can arise in calculating the shifts and widths of the  $s$  levels of negative ions in a variable external electric field. In the next section, we illustrate the application of Zeldovich’s method to such a problem.

#### 4. IONIZATION OF NEGATIVE IONS BY AN INTENSE LASER WAVE

As an example of the application of Zeldovich’s method to a specific physics problem, we consider an atomic  $s$  level bound by short-range forces that is ionized under the effect of the field of a circularly polarized monochromatic electromagnetic wave. The complex-valued quasienergy  $E = E_r - i\Gamma/2$  of a

quasistationary state is determined, in this case, from the equation that was first derived by Berson [23] and by Manakov and Rapoport [24]. This equation can be written in the form [10]

$$J(\varepsilon; \gamma, K_0) = \sqrt{\varepsilon} - 1, \tag{24}$$

where

$$\varepsilon = \varepsilon + \gamma^{-2}, \tag{25}$$

$$\varepsilon = E/E_0 = 1 + \delta + i\eta, \quad E_0 = -\kappa_0^2/2,$$

$$E_r = E_0(1 + \delta), \quad \Gamma = \kappa_0^2\eta,$$

$$\gamma = \omega\kappa_0/\mathcal{E} = 1/(2K_0F),$$

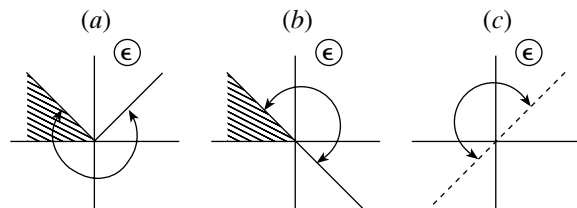


**Fig. 1.** Regions of admissible values of the argument  $\varepsilon$  in the asymptotic formulas (a) (18), (b) (19), and (c) (20). The shaded region corresponds to quasistationary states:  $\varepsilon_1 + i\varepsilon_2 = -k_1 + ik_2, k_1 > 0, k_2 > 0$ . The dashed line in Fig. 1c indicates that the relevant angles are reckoned in the clockwise direction.

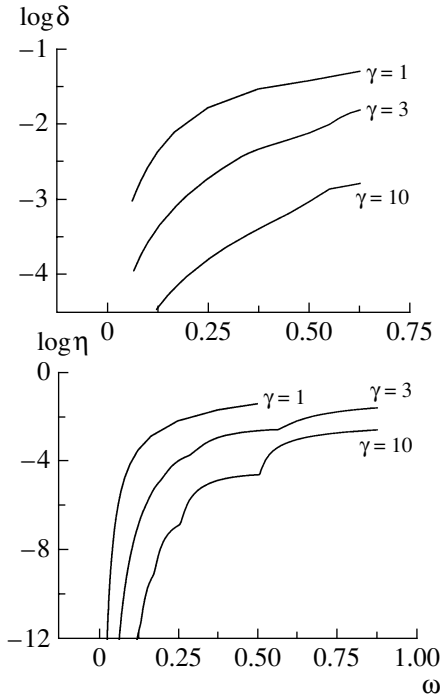


**Fig. 2.** Reduced shift  $\delta$  and width  $\eta$  of a level versus frequency at  $\kappa_0 = 1$  according to the numerical calculation based on Eq. (24) and on the regularization of the integral in (26) by Zeldovich's method. The values of the Keldysh parameter  $\gamma$  are indicated on the curves; the scale along the ordinate is logarithmic.

with  $\kappa_0 = \sqrt{2I_0}$ ,  $I_0$  being the ion ionization potential, and where use is made of the system of atomic units, in which  $\hbar = m = e = 1$ . Here,  $\varepsilon$  is the reduced quasienergy of the system;  $\gamma$  is the adiabaticity parameter introduced by Keldysh [25];  $F = \mathcal{E}/\kappa_0^3$  is the reduced electric field of the wave whose amplitude and frequency are denoted by  $\mathcal{E}$  and  $\omega$ , respectively; and  $K_0 = I_0/\omega$  is a parameter associated with the multiquantum character of the process.

The left-hand side of Eq. (24) is obtained by analytically continuing, to the upper half-plane ( $\text{Im}\varepsilon > 0$ ), the function specified in the lower half-plane of  $\varepsilon$  by the integral

$$J = \frac{1}{(8\pi i K_0)^{1/2}} \int_0^\infty \frac{du}{u^{3/2}} \quad (26)$$

$$\times \left\{ \exp\left(i \frac{2K_0 \sin^2 u}{\gamma^2} \frac{u}{u}\right) - 1 \right\} \exp(-2iK_0 \varepsilon u).$$

Following Zeldovich, we will take, for solutions to Eq. (24), functions that are derived by going over to the limit  $\alpha \rightarrow +0$  in solutions to the equation

$$J_\alpha(\varepsilon; \gamma, K_0) = \sqrt{\varepsilon} - 1, \quad (27)$$

where the function  $J_\alpha(\varepsilon; \gamma, K_0)$  is obtained from (26) by introducing the regulator  $\exp(-\alpha u^2)$  in the integrand—that is, by means of the substitution

$$\exp(-2iK_0 \varepsilon u) \rightarrow \exp(-2iK_0 \varepsilon u - \alpha u^2). \quad (28)$$

The convergence of Zeldovich's method over a broad interval of widths  $\Gamma$  is illustrated in Tables 1 and 2 from [10]. In order to compute  $\Gamma$  with a relative error of  $10^{-4}$ , it is necessary, as a rule, to reach parameter values of  $\alpha \leq 10^{-6} - 10^{-7}$ .

The reduced shift  $\delta$  and the reduced width  $\eta$  of the level in the zero-range potential are displayed in Fig. 2 according to the calculations based on numerically solving Eq. (24) with the aid of regularization by Zeldovich's method. Irregularities in the behavior of the quasienergy near the ionization thresholds become sizable as the Keldysh parameter grows. Moreover, the regularization in the form (28) does not work in the narrow threshold region. It turns out that Zeldovich's recipe is applicable in the case of quasienergy quasistationary states only if

$$\Gamma < |\text{Re}E + n\omega|, \quad (29)$$

that is, if the width of the level in question is smaller than the spacing between this level and the threshold of  $n$ -photon ionization. The constraint in (29) generalizes and refines condition (22), which appeared in the model problem of the regularization of the integral in (16).

## ACKNOWLEDGMENTS

This work was supported in part by the Russian Foundation for Basic Research (project nos. 03-02-17112, and 03-02-17348, and 04-02-17157).

## REFERENCES

1. F. J. Dyson, *Phys. Rev.* **85**, 631 (1952).
2. G. H. Hardy, *Divergent Series* (Oxford Univ. Press, Oxford, 1967; Inostrannaya Literatura, Moscow, 1951).
3. E. T. Whittaker and G. N. Watson, *A Course of Modern Analysis* (Cambridge Univ. Press, Cambridge, 1927; Fizmatlit, Moscow, 1963).
4. D. I. Kazakov and D. V. Shirkov, *Fortschr. Phys.* **28**, 465 (1980).
5. J. Zinn-Justin, *Quantum Field Theory and Critical Phenomena* (Clarendon Press, Oxford, 1989).
6. A. I. Baz', Ya. B. Zel'dovich, and A. M. Perelomov, *Scattering, Reactions and Decays in Nonrelativistic Quantum Mechanics* (Nauka, Moscow, 1971; Israel Program for Scientific Translations, Jerusalem, 1966).
7. Ya. B. Zel'dovich, *Zh. Éksp. Teor. Fiz.* **39**, 776 (1960) [*Sov. Phys. JETP* **12**, 542 (1960)].

8. A. I. Baz', *Some Problems in the Theory of Quasistationary States*, Appendix IX in E. C. Titchmarsh, *Eigenfunction Expansions Associated with Second-Order Differential Equations* (Clarendon, Oxford, 1961; Inostrannaya Literatura, Moscow, 1961), Vol. 2.
9. V. D. Mur, S. G. Pozdnyakov, V. S. Popov, and S. V. Popruzhenko, *Pis'ma Zh. Éksp. Teor. Fiz.* **75**, 294 (2002)[JETP Lett. **75**, 249 (2002)].
10. V. D. Mur, S. G. Pozdnyakov, S. V. Popruzhenko, and V. S. Popov, *Yad. Fiz.* **66**, 2014 (2003)[*Phys. At. Nucl.* **66**, 1964 (2003)].
11. V. D. Mur, S. V. Popruzhenko, S. G. Pozdnyakov, and V. S. Popov, *Phys. Lett. A* **316**, 226 (2003).
12. N. L. Manakov, M. V. Frolov, A. F. Starace, and I. I. Fabricant, *J. Phys. B* **33**, R141 (2000); M. V. Frolov, N. L. Manakov, B. Borca, and A. F. Starace, *J. Phys. B* **34**, L579 (2001); B. Borca, M. V. Frolov, N. L. Manakov, and A. F. Starace, *Phys. Rev. Lett.* **87**, 133001 (2001).
13. C. M. Bender and T. T. Wu, *Phys. Rev. Lett.* **27**, 461 (1971).
14. E. B. Bogomolny and V. A. Fateyev, *Phys. Lett. B* **76B**, 210 (1978).
15. I. S. Gradshteyn and I. M. Ryzhik, *Table of Integrals, Series, and Products* (Fizmatgiz, Moscow, 1962; Academic, New York, 1980).
16. G. Bateman and A. Erdelyi, *Higher Transcendental Functions* (McGraw-Hill, New York, 1955; Nauka, Moscow, 1973), Vol. 1.
17. J. Schwinger, *Phys. Rev.* **73**, 416 (1948).
18. V. W. Hughes and T. Kinoshita, *Rev. Mod. Phys.* **71**, S133 (1999).
19. V. S. Popov, V. L. Eletsy, and A. V. Turbiner, *Phys. Lett. B* **72B**, 99 (1977); *Zh. Éksp. Teor. Fiz.* **74**, 445 (1978)[*Sov. Phys. JETP* **47**, 232 (1978)].
20. D. I. Kazakov, O. V. Tarasov, and D. V. Shirkov, *Teor. Mat. Fiz.* **38**, 15 (1979).
21. Yu. A. Kubyshkin, *Teor. Mat. Fiz.* **58**, 137 (1984).
22. D. I. Kazakov and V. S. Popov, *Zh. Éksp. Teor. Fiz.* **122**, 675 (2002) [JETP **95**, 581 (2002)]; *Pis'ma Zh. Éksp. Teor. Fiz.* **77**, 547 (2003) [JETP Lett. **77**, 453 (2003)].
23. I. J. Berson, *J. Phys. B* **8**, 3078 (1975).
24. N. L. Manakov and L. P. Rapoport, *Zh. Éksp. Teor. Fiz.* **69**, 842 (1975)[*Sov. Phys. JETP* **42**, 430 (1975)].
25. L. V. Keldysh, *Zh. Éksp. Teor. Fiz.* **47**, 1945 (1964) [Sov. Phys. JETP **20**, 1307 (1964)].

*Translated by A. Isaakyan*

# Imaginary-Time Method in Quantum Mechanics and Field Theory

V. S. Popov

*Institute of Theoretical and Experimental Physics,  
Bol'shaya Cheremushkinskaya ul. 25, Moscow, 117218 Russia*

Received April 23, 2004

**Abstract**—An imaginary-time method was developed for calculating the probability of particle transmission through smooth barriers variable with time. Within the imaginary-time method, the tunneling process is described by using classical equations of motion written in terms of an imaginary time ( $t \rightarrow it$ ), while the probability of tunneling is determined by the imaginary part of the action functional, this imaginary part being calculated along the subbarrier particle trajectory. The fundamentals of the imaginary-time method are surveyed, and its applications in the theory of atomic-state ionization under the effect of constant electric and magnetic fields that have various configurations, in the field of intense monochromatic laser radiation and of an ultrashort electromagnetic pulse, in the process of Lorentz ionization of atoms and ions during their motion in a strong magnetic field, etc., are outlined. The applications of the imaginary-time method in relativistic cases—for example, in the theory of ionization of levels of multiply charged ions whose binding energy is commensurate with the electron rest energy—and in quantum field theory (Schwinger effect, which consists in the production of electron–positron pairs from a vacuum by a superstrong external field) are briefly described. Particular attention is given to methodological issues and details of the imaginary-time method that are of importance in solving specific physics problems, but which are usually skipped in original publications. © 2005 Pleiades Publishing, Inc.

## 1. INTRODUCTION

The imaginary-time method frequently appears to be of use in considering the process of particle tunneling through vibrating barriers (in general, barriers varying with time). It is a generalization of the well-known method of complex classical trajectories due to Landau,<sup>1)</sup> who developed it for calculating semiclassical matrix elements between quickly oscillating wave functions. Within this approach, the coordinate  $x$  goes to the complex plane, with the result that the matrix element  $f_{12} = \int_{-\infty}^{\infty} \psi_1 \hat{f} \psi_2 dx$  (which is exponentially small) is determined by the vicinity of the point  $x_0$  of intersection of the respective terms, which lies in the complex plane. If, however, the potential  $U = U(x, t)$  depends explicitly on time, then it would

be illegitimate to employ the expression

$$p(x, t) = \sqrt{2(E - U(x, t))} \quad (1.1)$$

since the energy  $E$  is not conserved (this is not so only if the potential parameters change slowly, in which case the Landau–Dykhne adiabatic approximation [1, 4–6] is applicable). In those cases where the potential barrier is rather broad and smooth, the semiclassical approximation is valid. Within this approximation, the probability of tunneling is determined by the action functional calculated along the subbarrier particle trajectory. Such a trajectory formally satisfies classical equations of motion and corresponding boundary conditions. Of course, a trajectory belonging to this class does not exist within classical mechanics, but it can be found if the time  $t$  is allowed to assume imaginary (in general, complex) values. Evaluating the imaginary part of the action functional along the trajectory found in this way and following Feynman's prescription [7, 8], we determine the subbarrier-transition amplitude  $A$  for an arbitrary relationship between the characteristic frequency  $\omega$  of variations in the potential and the particle-tunneling frequency  $\omega_t$ . Under the condition  $\omega \ll \omega_t$ , the result of such a calculation reduces to that within adiabatic theory [1, 5].

In the semiclassical limit, the main contribution to

<sup>1)</sup>See the original publications in [1, 2], the review article in [3], and § 51–53 in the textbook [4], which are devoted to considering the case of static fields, where the introduction of an imaginary “time” ( $t \rightarrow it$ ) is not necessary since energy is conserved, so that  $t$  can be eliminated from the expression for the semiclassical momentum,  $p = \sqrt{2(E - U(x))}$ . In [4], one can find applications of the Landau method to specific problems, including the problem of deuteron breakup in the Coulomb field of a heavy nucleus and the problems of calculating semiclassical matrix elements and the coefficient of above-barrier reflection.

the tunneling-transition probability<sup>2)</sup>

$$w = \oint \mathbf{j} \cdot d\boldsymbol{\sigma} \propto |A|^2 \quad (1.2)$$

comes from the so-called extremal [9, 10] trajectory that minimizes the action functional and which determines the most probable path of particle tunneling. In order to calculate the momentum spectrum of a particle going out from under the barrier, it is necessary to consider a narrow bundle of “classical” trajectories (for imaginary  $t$ ) close to the extremal trajectory and to find the second-order correction to the action functional in momenta. This is an outline of the imaginary-time method, which was first proposed in [9] and which was further developed in [10–26].

In the present article, an exposition of the fundamentals of the imaginary-time method is supplemented with a detailed description of some specific points in the respective computational procedure that are usually skipped in original publications for the sake of brevity. I hope that this will help readers—especially young physicists making their first steps in individual research—to master the method and to become able to apply it to concrete physics problems.<sup>3)</sup>

Part of the calculations given below come from sources that are not readily accessible [36, 37]. In the following, use is made of the system of atomic units, where  $\hbar = m = e = 1$ ,  $m$  being the electron mass. There, the Bohr radius  $a_B = \hbar^2/me^2$  and  $e^2/a_B = me^4/\hbar^2 = 27.2$  eV are taken for units of length and energy, respectively; the speed of light is  $c = \alpha^{-1} = 137$ ; and the strengths of electric and magnetic fields are measured in  $\mathcal{E}_a = e/a_B^2 = m^2e^5/\hbar^4 = 5.14 \times 10^9$  V/cm and  $\mathcal{H}_a = m^2e^3c/\hbar^3 = 2.35 \times 10^9$  G, respectively, the ratio of these units being  $\mathcal{E}_a/\mathcal{H}_a = \alpha$ .

## 2. FUNDAMENTALS OF THE IMAGINARY-TIME METHOD

The penetrability of a barrier that varies with time can in principle be found by solving the time-dependent Schrödinger equation

$$i\dot{\psi} = \left\{ -\frac{1}{2}\Delta + U(r) + \boldsymbol{\mathcal{E}}(t) \cdot \mathbf{r} \right\} \psi, \quad (2.1)$$

<sup>2)</sup>Here,  $\mathbf{j}$  is the flux of particles (electrons) going to infinity and  $d\boldsymbol{\sigma}$  is an element of a surface that surrounds the atom in question at large distances.

<sup>3)</sup>It should be noted that the imaginary-time method is a special version of the semiclassical approximation. The latter is extensively used in quantum mechanics and other realms of theoretical physics and was considered from different points of view in numerous textbooks and articles [4, 27–35]; however, a brief account of the imaginary-time method is given only in [30] (p. 224 and further). Naturally, many issues considered over the past 30 years were not reflected there.

$$\hbar = m = 1,$$

with the boundary condition (at  $t = t_1$ )

$$\begin{aligned} \psi(\mathbf{r}, t_1) &= \varphi_0(r)e^{-iE_0t_1}, \\ E_0 &= -I = -\kappa^2/2. \end{aligned} \quad (2.2)$$

Here,  $\hat{H}_0 = -\Delta/2 + U$ ,  $\hat{H}_0\varphi_0 = E_0\varphi_0$ ,  $U(r)$  is the atomic potential,  $\kappa = \sqrt{2I}$  is a characteristic bound-state momentum,  $I$  is the ionization potential for the  $s$  level, and  $\boldsymbol{\mathcal{E}}(t)$  is an external electric field (in the non-relativistic case,  $a_B \ll \lambda = 2\pi c/\omega$ , so that the field  $\boldsymbol{\mathcal{E}}(t)$  can be treated as a uniform field, while the effect of the magnetic field of the wave on the electron being considered can be disregarded since  $v/c \sim \alpha \ll 1$ ).

The potential of present-day computers is insufficient for obtaining an ab initio numerical solution to Eq. (2.1) in the three-dimensional case. Moreover, such a solution would describe the situation only for a specific atom and for specific values of the field strength and the laser frequency  $\omega$ . Without questioning the value of numerical calculations, it should yet be noted that an analytic (albeit approximate) solution to the problem at hand is always a useful supplement to them. Therefore, we invoke the semiclassical approximation. Representing Eq. (2.1) in the integral form

$$\begin{aligned} \psi(\mathbf{p}, t) &= -i \int_{-\infty}^t dt_1 e^{-iE_0t_1} \\ &\times \int d^3r_1 G(\mathbf{p}, t; \mathbf{r}_1, t_1) U(r_1) \varphi_0(r_1), \end{aligned} \quad (2.3)$$

where  $\mathbf{p}$  is the momentum of the emitted electron in the final state (that is, the momentum of the electron going out from under the barrier), we will evaluate the integral in Eq. (2.3) by the saddle-point method. According to Feynman [7, 8], the Green’s function can be represented as

$$\begin{aligned} G(\mathbf{r}, t; \mathbf{r}_1, t_1) \\ \approx \frac{\theta(t - t_1)}{[2\pi i(t - t_1)]^{3/2}} \exp\{iS(\mathbf{r}, t; \mathbf{r}_1, t_1)\}, \end{aligned} \quad (2.4)$$

where  $S$  is the classical action functional. Performing a Fourier transformation, we find that, in the mixed representation, the Green’s function has the form

$$\begin{aligned} G(\mathbf{p}, t; \mathbf{r}_1, t_1) &\approx (2\pi)^{-3/2} \\ &\times \exp\{i[S(\mathbf{p}, t; \mathbf{r}_1, t_1) - \mathbf{p} \cdot \mathbf{r}]\}. \end{aligned} \quad (2.5)$$

Here, the action functional  $S$  is calculated along the subbarrier “classical” trajectory, which is specified by the boundary conditions  $\mathbf{r}(t_1) = \mathbf{r}_1$  and  $\mathbf{p}(t) = \mathbf{p}$ , the quantities  $\mathbf{r} = \mathbf{r}(t)$  and  $\mathbf{p}_1 = \mathbf{p}(t_1)$  not being independent variables.

Substituting (2.5) into (2.3), we arrive at an integral that involves a quickly oscillating exponential function; that is,

$$\psi(\mathbf{p}, t) = \frac{\exp(-iE_0 t)}{(2\pi i)^{3/2}} \int_{-\infty}^t dt_1 \int d^3 r_1 \quad (2.6)$$

$$\times \exp\{iW(\mathbf{p}, t; \mathbf{r}_1, t_1)\} U(r_1) \varphi_0(r_1),$$

where

$$W(\mathbf{p}, t; \mathbf{r}_1, t_1) = \int_{t_1}^t [\mathcal{L}(t') + E_0] dt' - \mathbf{p} \cdot \mathbf{r}, \quad (2.7)$$

with  $\mathcal{L} = \dot{\mathbf{r}}^2/2 + \mathcal{E}(t) \cdot \mathbf{r}$  being the Lagrangian for an electron in a uniform external field.<sup>4)</sup>

The main contribution to the integral in (2.6) comes from the saddle point. We will now find the saddle point in terms of the variables  $t_1$  and  $\mathbf{r}_1$ . For the total derivative, we find from (2.7) that

$$\frac{dW}{dt_1} = -\mathcal{L}(t_1) - E_0;$$

on the other hand, we have

$$\frac{dW}{dt_1} = \frac{\partial W}{\partial t_1} + \frac{\partial W}{\partial \mathbf{r}_1} \dot{\mathbf{r}}_1 = \frac{\partial W}{\partial t_1} - \mathbf{p}_1 \cdot \dot{\mathbf{r}}_1,$$

where use is made of the relation  $\mathbf{p}_1 = -\partial W/\partial \mathbf{r}_1$ , which follows from (2.7) with allowance for the fact that  $\delta S = \mathbf{p} \cdot \delta \mathbf{r} - \mathbf{p}_1 \cdot \delta \mathbf{r}_1$  and  $\delta W = -\mathbf{r} \cdot \delta \mathbf{p} - \mathbf{p}_1 \cdot \delta \mathbf{r}_1$  at fixed  $t$  and  $t_1$  [39, 39]. As a result, we arrive at

$$\frac{\partial W}{\partial t_1} = \mathbf{p}_1 \cdot \dot{\mathbf{r}}_1 - \mathcal{L}(t_1) - E_0 = H(t_1) - E_0, \quad (2.8)$$

where  $H(t)$  is a Hamiltonian. For the sake of simplicity, we assume that the atom in question is situated at the origin of coordinates. The conditions specifying the initial instant  $t_1 \equiv t_0$  of subbarrier motion then have the form [9]

$$\mathbf{p}^2(t_0) = -\kappa^2, \quad \mathbf{r}(t_0) = 0 \quad (2.9)$$

in the case of a short-range potential; for potentials  $U(r)$  involving a Coulomb tail, the initial condition has a somewhat different form [10, 36]. Calculating the variation of the function  $W$  in the vicinity of the extremal trajectory, one can show that the boundary condition at the exit from under the barrier has the form

$$\text{Im } \mathbf{r}(0) = \text{Im } \dot{\mathbf{r}}(0) = 0 \quad (2.10)$$

<sup>4)</sup>Here, it is assumed that the atomic potential  $U(r)$  is a short-range potential (for example, a delta-function potential). The inclusion of the Coulomb interaction between the outgoing electron and the atomic core calls for a dedicated consideration, which is given in Section 4 below.

(for the instant at which the particle goes out from under the barrier, it is convenient to take  $t = 0$ ). The boundary conditions in (2.9) and (2.10), together with the classical equations of motion, determine the extremal subbarrier trajectory.

We also note that the integrand in (2.7) can be recast into the form

$$\frac{1}{2} \dot{\mathbf{r}}^2 + \ddot{\mathbf{r}} \cdot \mathbf{r} + E_0 = \frac{d}{dt} (\mathbf{r} \cdot \dot{\mathbf{r}}) - \frac{1}{2} (\dot{\mathbf{r}}^2 + \kappa^2),$$

whence it follows, with allowance for (2.9) and (2.10), that

$$W(0, t_0) = \frac{1}{2} \int_0^{t_0} (\kappa^2 + \dot{\mathbf{r}}^2) dt. \quad (2.11)$$

This simple but useful formula gives an imaginary part (recall that, here, the time  $t$  is a pure imaginary quantity) that the action functional develops during the subbarrier motion of the particle and determines, with an exponential accuracy,<sup>5)</sup> the tunneling probability:

$$w \propto \exp \left\{ -\frac{2}{\hbar} \text{Im } W \right\}. \quad (2.12)$$

This can be proven by calculating [9, 10], with the aid of (2.6), the flux of particles going to infinity—that is, the probability of initial-state decay per unit time (in laser physics, it is common practice to call it the rate of atomic-level ionization). If the potential is independent of time, then

$$W(t_2, t_1) = 2 \int_{t_1}^{t_2} \mathbf{p} \cdot d\mathbf{r} - \mathbf{p}_2 \cdot \mathbf{r}_2. \quad (2.13)$$

At  $\mathbf{p}_2 = 0$  (in the case where  $t_2$  is a turning point), this quantity is referred to in mechanics as a reduced action functional [38]. We will employ this term in the general case inclusive.

In the following, we assume fulfillment of the conditions

$$F = \mathcal{E}/\kappa^3 \mathcal{E}_a \ll 1, \quad \omega \ll I/\hbar, \quad (2.14)$$

owing to which the inequality  $\text{Im } W \gg \hbar$  holds, so that the imaginary-time method is applicable.

In accordance with Newton's statement that, in studying sciences, problems are more useful than rules, we will now proceed to consider specific examples of the application of the imaginary-time method.

<sup>5)</sup>The tunnel-ionization rate  $w$  (that is, the transition probability per unit time) depends very sharply on the electric-field strength; therefore, the calculation of the exponential factor in  $w$  alone is sufficient for describing the tunneling process qualitatively and even sometimes quantitatively. Also, this calculation is the most straightforward. In some cases, the preexponential factor in (2.12) can also be found by means of the imaginary-time method (see Appendix A).

3. SIMPLEST EXAMPLES

3.1. Constant Electric Field  $\mathcal{E}$

The subbarrier trajectory is given by

$$x(t) = \frac{1}{2}\mathcal{E}(t^2 - t_0^2) + p_{\parallel}(t - t_0), \quad (3.1)$$

$$\mathbf{r}_{\perp} = \mathbf{p}_{\perp}(t - t_0),$$

with  $\dot{x} = \mathcal{E}t + p_{\parallel}$ ,  $\dot{\mathbf{r}}_{\perp} = \mathbf{p}_{\perp}$  being an integral of the motion. The condition in (2.9) determines the initial instant  $t_0$  of subbarrier motion,  $(\mathcal{E}t_0 + p_{\parallel})^2 + p_{\perp}^2 = -\kappa^2$ , whence it follows that

$$t_0(\mathbf{p}) = \frac{i}{\mathcal{E}} \left( \sqrt{\kappa^2 + \mathbf{p}_{\perp}^2} + ip_{\parallel} \right) \quad (3.2)$$

$$= \frac{i\kappa}{\mathcal{E}} \left( \sqrt{1 + q_{\perp}^2} + iq_{\parallel} \right),$$

where  $\mathbf{q} = \mathbf{p}/\kappa$  and  $\kappa$  is a characteristic momentum corresponding to the bound state being considered. We will now see that effective momentum values satisfy the condition  $p_{\text{eff}} \ll \kappa$ ; that is,  $q \ll 1$ .

Substituting (3.1) into (2.11), we obtain

$$W = \frac{1}{2} \int_0^{t_0} [\kappa^2 + p_{\perp}^2 + (\mathcal{E}t + p_{\parallel})^2] dt \quad (3.3)$$

$$= \frac{1}{2\mathcal{E}} \int_{p_{\parallel}}^{i\sqrt{\kappa^2 + p_{\perp}^2}} (\kappa^2 + p_{\perp}^2 + \xi^2) d\xi$$

$$= \frac{i\kappa^3}{3\mathcal{E}} (1 + q_{\perp}^2)^{3/2} - \frac{\kappa^2 p_{\parallel}}{3\mathcal{E}} \left( 1 + \frac{1}{3}q_{\parallel}^2 + q_{\perp}^2 \right),$$

where  $\xi = \mathcal{E}t + p_{\parallel}$ . Since the last term in (3.3) is pure real, it does not contribute to  $\text{Im} W$ ; therefore, the tunneling probability has the form

$$w(\mathbf{p}_{\perp}) \propto \exp \left\{ -\frac{2\kappa^3}{3\mathcal{E}} (1 + q_{\perp}^2)^{3/2} \right\} \quad (3.4)$$

$$= \exp \left\{ -\left( \frac{2\kappa^3}{3\mathcal{E}} + \frac{\kappa}{\mathcal{E}} p_{\perp}^2 + \dots \right) \right\}.$$

Thus, the electron-momentum component transverse with respect to the field is  $p_{\perp} \sim \sqrt{\mathcal{E}/\kappa}$  or  $q_{\perp} \sim \sqrt{F} \ll 1$ , where we have introduced the reduced field  $F = \mathcal{E}/\kappa^3 \mathcal{E}_a$ . In the following, it is always assumed that  $F \ll 1$ , in which case the barrier width  $b$  is always much larger than the bound-state radius,

$$b = x(0) \approx \kappa^2/2\mathcal{E} \gg 1/\kappa, \quad \kappa b = 1/2F \gg 1; \quad (3.5)$$

in view of this, the barrier penetrability is exponentially small, with the result that the semiclassical

approximation, or the imaginary-time method, is applicable.

By using this example, we will now demonstrate how the condition in (2.10), which selects the extremal trajectory, operates. At the exit from under the barrier ( $t = 0$ ), we have

$$\mathbf{r}(0) = \left\{ -t_0(p_{\parallel} + \frac{1}{2}\mathcal{E}t_0), -\mathbf{p}_{\perp}t_0 \right\}.$$

Employing (3.2), we obtain

$$\text{Im } \mathbf{r}(0) = \left\{ 0, -\mathcal{E}^{-1} \sqrt{\kappa^2 + p_{\perp}^2} \mathbf{p}_{\perp} \right\} = 0, \quad (3.6)$$

$$\text{Im } \dot{\mathbf{r}}(0) = \text{Im} \{ p_{\parallel}, \mathbf{p}_{\perp} \} \equiv 0,$$

whence it follows that  $\mathbf{p}_{\perp} = 0$ . In the case being considered, the extremal subbarrier trajectory is one-dimensional and is aligned with the electric field, this also following immediately from (3.4) and being consistent with physical intuition.

If an atomic level has an orbital angular momentum  $l$ , its wave function has the form

$$\psi_{lm}(\mathbf{r}) = R_l(r) Y_{lm}(\mathbf{n}) \sim (\sin \theta)^{|m|},$$

$$\theta \sim p_{\perp}/p \ll 1,$$

and we have the following estimate for the probability of ionization of the  $|lm\rangle$  state:

$$w_{lm} \sim \int d^2 p_{\perp} p_{\perp}^{2|m|} \quad (3.7)$$

$$\times \exp \left\{ -\frac{2}{3\mathcal{E}} (\kappa^2 + p_{\perp}^2)^{3/2} \right\}$$

$$\propto F^{|m|+1} e^{-2/3F} [1 + O(F)].$$

This result was also obtained from a more rigorous calculation [9, 40]. As the magnetic quantum number  $|m|$  increases, the probability  $w_{lm}$  shows a power-law decrease.

3.2. Low-Frequency Laser Radiation ( $\gamma \ll 1$ )

The theory of tunneling in fields varying with time is based on the study of Keldysh [41]. The character of the tunneling process is determined by the adiabaticity (Keldysh) parameter

$$\gamma = \omega T_t = \omega \kappa / \mathcal{E}, \quad (3.8)$$

where  $\omega$  is the frequency of barrier vibrations (laser-light frequency in the present case) and  $T_t$  is the characteristic time of tunneling in the electric field  $\mathcal{E}$ ,

$$T_t = \int_0^b \frac{dx}{|p(x)|} = \int_0^{\kappa^2/2\mathcal{E}} \frac{dx}{\sqrt{\kappa^2 - 2\mathcal{E}x}} = \frac{\kappa}{\mathcal{E}}.$$

In the case of  $\gamma \ll 1$ , the ionization of an atom occurs predominantly at instants of time that correspond to electric-field strengths close to the maximum value. Setting

$$\mathcal{E}(t) = \mathcal{E} \left[ 1 - \frac{1}{2}(\omega t)^2 + \dots \right], \quad t \approx 0, \quad (3.9)$$

we find that, to terms of order  $\omega^2$  inclusive, the sub-barrier trajectory is given by

$$\dot{x}(t) = p_{\parallel} + \mathcal{E}t - \frac{1}{6}\mathcal{E}\omega^2 t^2, \quad \dot{\mathbf{r}}_{\perp} = \mathbf{p}_{\perp}.$$

With the aid of (2.9), we obtain

$$t_0 = \frac{i\kappa}{\mathcal{E}} \left[ 1 - \frac{1}{6}\gamma^2 + \frac{1}{2}q_{\perp}^2 + \frac{1}{6}\gamma^2 q_{\parallel}^2 + iq_{\parallel} + \dots \right].$$

The substitution into (2.11) yields the following expansion for the action functional:

$$\begin{aligned} W &= \frac{1}{2} \left\{ (\kappa^2 + \mathbf{p}^2)t_0 + \frac{1}{3}\mathcal{E}^2 t_0^3 \right. \\ &\quad \left. - \frac{1}{15}\mathcal{E}^2 \omega^2 t_0^5 + p_{\parallel} \mathcal{E} t_0^2 - \frac{1}{12} p_{\parallel} \mathcal{E} \omega^2 t_0^4 + \dots \right\} \\ &= i \frac{\kappa^3}{\mathcal{E}} \left\{ \frac{2}{3} - \frac{1}{15}\gamma^2 + \left[ \frac{1}{3}\gamma^2 q_{\parallel}^2 + \left( 1 - \frac{1}{6}\gamma^2 \right) q_{\perp}^2 \right] \right\}. \end{aligned} \quad (3.10)$$

Thus, the probability of ionization in the field given by (3.9) is of order

$$\exp \left\{ -\frac{2\kappa^3}{3\mathcal{E}} \left( 1 - \frac{1}{10}\gamma^2 \right) \right\}.$$

The adiabatic correction  $\gamma^2/10$  was first calculated (by a different method) by Keldysh [41], who also considered arbitrary values of the parameter  $\gamma$ . Although  $\gamma \ll 1$  in the present case, this correction appears in the exponent with the large coefficient  $1/F \gg 1$ . Therefore, it must be retained. With increasing  $\gamma$  (that is, with increasing light frequency  $\omega$ ), the ionization probability grows. The coefficient  $1/10$  corresponds to the linear polarization of radiation; in the case of a circular polarization, it is replaced by  $1/15$  [9, 40]. For elliptically polarized light, we have [9]

$$w \sim \exp \left\{ -\frac{2}{3F} \left[ 1 - \frac{1}{10} \left( 1 - \frac{\xi^2}{3} \right) \gamma^2 \right] \right\}, \quad (3.11)$$

where  $\xi$  is the ellipticity of light,  $-1 \leq \xi \leq 1$ ,  $\xi = 0$  ( $\xi = \pm 1$ ) corresponding to elliptic (circular) polarization [see Eq. (5.1) below].

The terms that are proportional to  $q^2$  in Eq. (3.10) determine the momentum spectrum of emitted photoelectrons. As in the case of a constant field,  $p_{\perp} \sim \kappa\sqrt{F} \ll \kappa$ , but, for the longitudinal momentum, we have  $p_{\parallel} \sim \gamma^{-1}\sqrt{\mathcal{E}/\kappa} \gg p_{\perp}$ , which is explained by the

possibility of electron acceleration along the slowly varying electric field.

Over the past 10 to 15 years, investigations in the low-frequency region  $\gamma \ll 1$  have gained momentum in connection with the advent of powerful lasers in the infrared range such that  $\omega \ll I$  for them (for example, a CO<sub>2</sub> laser of  $\hbar\omega = 0.117$  eV). There appeared numerous studies devoted to exploring this case (see, for example, [42–46] and references therein). However, the evaluation of the early studies reported in [9–11, 40], which have not lost their importance to date, was biased radically in some articles, including the reviews quoted in [45, 47]. The point is that those early studies resulted in deriving formulas that describe the ionization probability, the momentum and angular spectra of photoelectrons, and some other observables not only in the low-frequency region but also for all values of the parameter  $\gamma$  (for details on this issue, see the comment in [48] on the so-called ADK theory [43–47]).

### 3.3. Monochromatic Laser Field, $\mathcal{E}(t) = \mathcal{E}_0 \cos \omega t$

The extremal trajectory is given by

$$\begin{aligned} x(t) &= \frac{\mathcal{E}_0}{\omega^2} (\cosh \tau_0 - \cosh \tau), \\ \mathbf{r}_{\perp} &= 0, \quad \tau = -i\omega t \end{aligned} \quad (3.12)$$

in the case of linear polarization. The initial condition  $\dot{x}(t_0) = i\kappa$  leads to<sup>6)</sup>

$$\begin{aligned} \tau_0 &= \operatorname{arcsinh} \gamma \equiv \ln(\gamma + \sqrt{1 + \gamma^2}), \\ t_0 &= i\omega^{-1}\tau_0. \end{aligned} \quad (3.13)$$

We will now calculate the reduced action functional

$$\begin{aligned} W &= \int_{t_0}^0 \left( \frac{1}{2}\dot{x}^2 + \mathcal{E}x \cos \omega t - \frac{\kappa^2}{2} \right) dt \\ &= iK_0 \int_0^{\tau_0} \left[ 1 + \frac{1}{2\gamma^2} (1 + 3\cosh 2\tau \right. \\ &\quad \left. - 4\cosh \tau_0 \cosh \tau) \right] d\tau = iK_0 f(\gamma), \end{aligned}$$

<sup>6)</sup>A general solution is  $\omega t_0 = i \operatorname{arcsinh} \gamma + 2\pi n$ ,  $n = 0, \pm 1, \pm 2, \dots$ . All of these saddle points correspond to the same value of  $\operatorname{Im}W$  (since the external field is periodic) and contribute to the transition amplitude. This leads to the appearance of a delta function that expresses the energy-conservation law for the case of  $n$ -photon absorption, the tunneling-transition probability becoming proportional to the time  $T$  over which the field is operative (owing to this, one can introduce the concept of the ionization rate—that is, the probability of ionization per unit time).

where  $f(\gamma)$  is the Keldysh function [4, 41],

$$f(\gamma) = \left(1 + \frac{1}{2\gamma^2}\right) \tau_0 - \frac{\sinh 2\tau_0}{4\gamma^2} \tag{3.14}$$

$$= \left(1 + \frac{1}{2\gamma^2}\right) \operatorname{arcsinh} \gamma - \frac{\sqrt{1+\gamma^2}}{2\gamma},$$

and  $K_0$  is the multiquantum parameter of the process,

$$K_0 = I/\hbar\omega = \kappa^2/2\omega. \tag{3.15}$$

This is the number of photons that is required for ionizing the level being considered. The same result readily follows from (2.11):

$$\dot{x} = i\mathcal{E}_0\omega^{-1} \sinh \tau = i\kappa\gamma^{-1} \sinh \tau,$$

$$W = i\frac{\kappa^2}{2\omega} \int_0^{\tau_0} \left(1 - \frac{1}{\gamma^2} \sinh^2 \tau\right) d\tau = iK_0 f(\gamma).$$

A comparison of this easy calculation with that in [4] (§77) demonstrates how the application of the imaginary-time method simplifies the relevant analysis.

In order to find the momentum spectrum  $w(\mathbf{p})$  of photoelectrons at the exit from under the barrier, it is necessary to consider a bundle of “classical” trajectories (those that correspond to imaginary time!) close to the extremal one and to determine the quadratic correction to the action functional. Since this procedure has already been implemented above for the case of a low-frequency field, only the final result is presented here [9],

$$w(\mathbf{p}) = P(\gamma) \tag{3.16}$$

$$\times \exp \left\{ -2K_0 f(\gamma) - \frac{1}{\omega} \left[ c_1(\gamma) p_{\parallel}^2 + c_2(\gamma) p_{\perp}^2 \right] \right\},$$

$$c_1 = \operatorname{arcsinh} \gamma - \gamma(1 + \gamma^2)^{-1/2}, \quad c_2 = \operatorname{arcsinh} \gamma,$$

where  $p_{\parallel}$  and  $\mathbf{p}_{\perp}$  are the components of the electron momentum along the wave field  $\mathcal{E}(t)$  and in the direction orthogonal to it.

For a wave of elliptic polarization (general case of monochromatic laser radiation), the extremal sub-barrier trajectory is no longer one-dimensional, with the result that the application of the imaginary-time method is somewhat complicated. Nevertheless, it is much easier to apply this method than to solve the Schrödinger equation straightforwardly. This case will be considered in Section 5.

It should also be noted that formula (3.16) is convenient for  $\gamma \gtrsim 1$  (quickly varying fields), but, in the region  $\gamma \ll 1$  and in going over to the limiting case of a constant field ( $\omega \rightarrow 0, K_0 \rightarrow \infty$ ), it is reasonable

to recast it in a somewhat different (but equivalent) form,

$$w(\mathbf{p}) = P(\gamma) \tag{3.17}$$

$$\times \exp \left\{ -\frac{\kappa^3}{\mathcal{E}_0} \left[ \frac{2}{3} g(\gamma) + b_1(\gamma) \frac{p_{\parallel}^2}{\kappa^2} + b_2(\gamma) \frac{p_{\perp}^2}{\kappa^2} \right] \right\},$$

where

$$g(\gamma) = 3f(\gamma)/2\gamma, \quad b_{1,2}(\gamma) = c_{1,2}(\gamma)/\gamma. \tag{3.17a}$$

Here,  $g(0) = b_2(0) = 1$ ; therefore, (3.17) reduces to (3.4) for  $\omega \rightarrow 0$ . Since  $b_1(\gamma) = \gamma^2/3 + \dots$ , the electron longitudinal momentum  $p_{\parallel} \sim \gamma^{-1} p_{\perp}$  can exceed  $\kappa$  considerably. For  $\gamma \ll 1$ , we have the expansion

$$g(\gamma) = 1 - \frac{1}{10} \gamma^2 + \frac{9}{280} \gamma^4 - \frac{5}{336} \gamma^6 + \dots \tag{3.18}$$

In the opposite case of  $\gamma \gg 1$  (quickly varying field,  $\omega \gg \omega_t$ ), we have

$$g(\gamma) = \frac{3}{2\gamma} \tag{3.18a}$$

$$\times \left\{ \ln 2\gamma - 1/2 - \frac{\ln 2}{2\gamma^2} + O(\gamma^{-4}) \right\},$$

with  $p_{\parallel} \sim p_{\perp} \sim \sqrt{\omega/\ln 2\gamma} \ll \kappa$ , so that the kinetic energy of the photoelectron is estimated as  $p^2/2 \sim \omega/\ln 2\gamma < \omega$ .

The imaginary-time method makes it possible to determine the effective barrier width  $b$  in a laser field. From (3.12), we obtain

$$b \equiv x(0) = \frac{\mathcal{E}_0}{\omega^2} (\cosh \tau_0 - 1) = \frac{\kappa^2}{\mathcal{E}_0(1 + \sqrt{1 + \gamma^2})}, \tag{3.19}$$

or

$$b(\mathcal{E}_0, \omega) = \kappa^{-1} \begin{cases} \frac{1}{2F} \left(1 - \frac{1}{4}\gamma^2\right), & \gamma \ll 1, \\ 2K_0, & \gamma \gg 1. \end{cases} \tag{3.19a}$$

In Keldysh theory [41], it is assumed that  $F \ll 1$  and  $K_0 \gg 1$ , in which case the barrier width considerably exceeds the bound-state radius, this ensuring the applicability of the imaginary-time method. Since  $b(\mathcal{E}_0, \omega)$  decreases in proportion to  $\gamma^{-1}$  in the region  $\gamma \gtrsim 1$ , this qualitatively explains a fast growth of the ionization rate in going over from the adiabatic region to the region  $\gamma \gg 1$  (at a fixed value of the wave amplitude).

3.4. Field of the Form  $\mathcal{E}(t) = \mathcal{E}_0 \cos \omega t + \mathcal{E}_f$

Such a field corresponds to a plane wave supplemented with a constant electric field whose directions coincide. Equation (2.9) yields

$$(1 + \beta) \sinh \tau_0 + (1 - \beta) \tau_0 = 2\gamma, \quad (3.20)$$

$$\beta = (\varepsilon_0 - \varepsilon_1) / (\varepsilon_0 + \varepsilon_1).$$

As to  $g(\gamma)$ , it can be found from (2.11). The adiabatic expansion for this case has the form

$$g(\gamma) = 1 - \frac{1}{20}(1 + \beta)\gamma^2 \quad (3.21)$$

$$+ \frac{1}{560}(4 + 9\beta + 5\beta^2)\gamma^4 + \dots,$$

which reduces to (3.18) at  $\beta = 1$  and leads to  $g(\gamma) \equiv 1$  at  $\beta = -1$  (the case of a constant field).

4. COULOMB CORRECTION

The above formulas describe the ionization of a system that is bound by short-range forces (negative ions such as  $H^-$ ,  $Li^-$ , and  $Na^-$ ). In the case of a neutral atom, the motion of the valence electron is substantially distorted because of the long-range character of the respective Coulomb potential at distances larger than the atomic radius  $r_0$ , this changing the preexponential factor in the formula for  $w$ .

The effect of Coulomb interaction can be taken here into account by semiclassical perturbation theory [11]. Setting  $U \rightarrow U + \delta U$ , where  $\delta U \approx -Z/r$  for  $r > r_0$ , we find from (2.7) that

$$\delta W = - \int_{t_0}^0 \delta U(r_m(t)) dt,$$

where integration is performed along the unperturbed extremal trajectory  $\mathbf{r}_m(t)$  (that is, the trajectory calculated without allowing for  $\delta U$ ) and where it is assumed that the perturbation  $\delta U$  is small along the whole subbarrier trajectory. In our case, this is not so, however: the potential  $\delta U(r) = -Z/r$  is not bounded for  $r \rightarrow 0$  and cannot be treated as a small correction at the beginning of the trajectory since  $r_m(t_0) \rightarrow 0$ . In view of this, we will make use of the matching procedure [4, 11]: we introduce  $r_1$  such that  $1/\kappa \ll r_1 \ll b$ . At  $r \sim r_1$ , the intra-atomic potential is small, while the external field can still be disregarded. In the region around  $r \sim r_1$ , the wave function  $\chi(r)$  coincides with the asymptotic expression for the free-atom wave function:

$$\chi(r) \sim \exp\{-\text{Im } S(r)\}, \quad (4.1)$$

$$S(r) = \kappa r - \frac{Z}{\kappa} \ln \kappa r + O(1).$$

As a result, the Coulomb correction to the action functional is given by

$$\delta S_C = -i \frac{Z}{\kappa} \ln \kappa r_1 + Z \int_{t_1}^0 \frac{dt}{[r_m(t)]^{1/2}}, \quad (4.2)$$

$$r_1 = r_m(t_1).$$

It should be noted that, in atomic physics, the quantity  $n^* = Z/\kappa$  is usually referred to as the effective principal quantum number of a level (for a hydrogen-like atom,  $E_n = -Z^2/2n^2$  and  $n^* = n = 1, 2, \dots$ ).

We will now illustrate formula (4.2) by considering the example of a constant electric field  $\mathcal{E}$ . According to (3.1) and (3.6), the extremal trajectory is

$$x_m(t) = \frac{1}{2} \mathcal{E}(t^2 - t_0^2), \quad t_0 = i\kappa/\mathcal{E},$$

whence it follows that

$$\delta S_C = -i \frac{Z}{\kappa} \ln \kappa x_1 + \frac{2Z}{\mathcal{E}} \int_{t_1}^0 \frac{dt}{t^2 - t_0^2} \quad (4.3)$$

$$= -i \frac{Z}{\kappa} \ln \left[ \frac{(t_0 + t_1)\kappa x_1}{t_0 - t_1} \right].$$

Considering that  $x_m(t) = i\kappa(t - t_0) + \dots$  for  $t \rightarrow t_0$ , we obtain

$$\delta S_C = -in^* \ln(-2i\kappa^2 t_0) = -in^* \ln(2\kappa^3/\mathcal{E}).$$

Thus, the matching point  $x_1$  falls out of the result, and we find for the Coulomb factor  $Q$  in the ionization probability that

$$Q = \exp(-2\text{Im } \delta S_C) = (2\kappa^3/\mathcal{E})^{2n^*}. \quad (4.4)$$

By way of example, we will consider a three-dimensional delta-function potential, in which case  $Z = n^* = 0$ . For an  $s$  level of binding energy  $I = \kappa^2/2$ , the ionization probability is then given by [4, 49]

$$w_\delta = \frac{1}{2} \kappa^2 F \exp(-2/3F), \quad F = \mathcal{E}/\kappa^3 \ll 1. \quad (4.5)$$

For the ground state of the hydrogen atom, we have  $\kappa = 1$ ,  $F \equiv \mathcal{E}$ , and  $n^* = 1$ ; from (4.4) and (3.4), it then follows that {this well-known formula can be found in [4] (see § 77)}

$$w_H = 4\mathcal{E}^{-1} \exp(-2/3\mathcal{E}). \quad (4.6)$$

For the  $s$  level of an arbitrary atom, the rate of ionization induced by low-frequency laser radiation is

$$w = \kappa^2 C_\kappa^2 \sqrt{\frac{3F}{\pi}} \cdot 2^{2n^*} F^{1-2n^*} \quad (4.7)$$

$$\times \exp \left\{ -\frac{2}{3F} \left( 1 - \frac{1}{10} \gamma^2 \right) \right\}, \quad \gamma \ll 1.$$

For an arbitrary  $|lm\rangle$  state, the corresponding estimate can be found in [9, 10]. Here,  $C_\kappa$  is the asymptotic coefficient of the atomic wave function at large distances,

$$\chi_0(r) = rR(r) \approx 2\sqrt{\kappa}C_\kappa e^{-\kappa r}(\kappa r)^{n^*} + \dots, \quad (4.8)$$

$\kappa r \gg 1.$

The coefficients  $C_\kappa$  (at  $l = 0$ ) for some atoms and ions are given in [17, 23, 26]. For valence  $s$  electrons in neutral atoms, the numerical values of  $C_\kappa$  are close (within 10 to 15%) to unity; therefore, formulas of the type in (4.7) are nearly model-independent.

Formula (4.7) was obtained for the case of a linear polarization of the radiation and, like formulas (4.5) and (4.6), is asymptotically exact in the limit of a weak field,  $F \rightarrow 0$ . Its generalization to states of arbitrary orbital angular momentum  $l$  was given in [9]. In the case of a circular polarization, it is necessary to omit in (4.7) the factor  $\sqrt{3F/\pi}$ , which stems from the averaging of the static ionization probability over the period of the laser field, and to replace, in the exponential function, the coefficient  $1/10$  of  $\gamma^2$  by  $1/15$  [9, 40].

In the case of constant crossed ( $\mathcal{E} = \mathcal{H}$ ,  $\mathcal{E} \perp \mathcal{H}$ ) fields, the calculation of the Coulomb factor  $Q$  is quite involved technically, but it was performed in [23], where  $Q$  was found analytically.

In order to calculate the Coulomb correction at all values of  $\gamma$ , it is necessary to solve the equation of motion  $\ddot{x} = -Zx^{-2} + \mathcal{E}_0 \cos \omega t$  in the complex plane. Going over to the dimensionless variables  $\xi = \omega x/\kappa$  and  $\tau = -i\omega t$ , we obtain

$$\frac{d^2\xi}{d\tau^2} = \gamma^{-1} \left( \frac{\sigma}{\xi^2} - \cosh \tau \right), \quad (4.9)$$

$$\sigma = \frac{Z\omega^2}{\kappa^2 \mathcal{E}_0} = \frac{n^*}{4K_0^2 F} = \left( \frac{\gamma}{\gamma_*} \right)^2.$$

In the adiabatic region,  $K_0 \gg 1$  and  $\sigma \rightarrow 0$ ; therefore, Eq. (4.9) can be solved by considering  $\sigma/\xi^2$  as a small perturbation, this being equivalent to employing formulas (4.2) and (4.4). One can introduce a frequency-dependent correction in  $Q$ , terms of order  $\gamma^2$  being canceled completely; it follows that, for  $\gamma \lesssim 1$ , the Coulomb correction can be taken in the same form as in a constant field.

For  $\gamma \gtrsim \gamma_* = 2/\sqrt{n^*F}$ , however, the Coulomb force at the end of the subbarrier trajectory is no longer small in relation to the external field  $\mathcal{E}_0$ , and it is necessary to solve Eq. (4.9) exactly. There arise here difficulties that are associated with the nonlinearity of this equation (two classical solutions collide and go out to the complex plane [11]); therefore, the problem of taking into account Coulomb interaction within

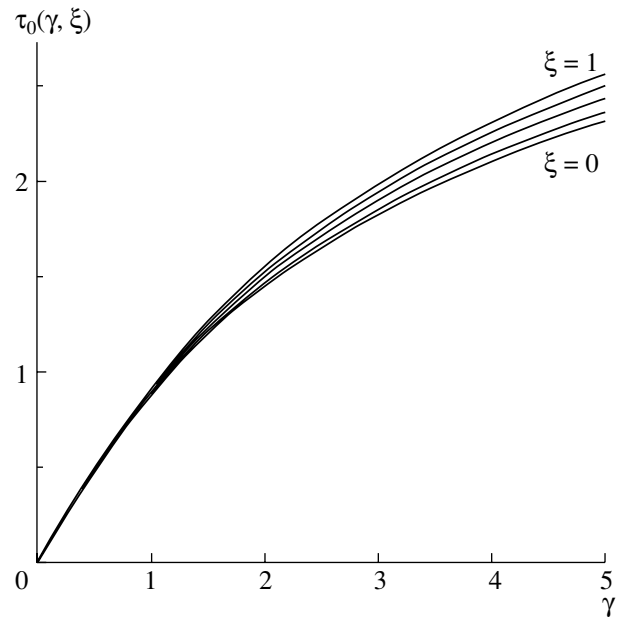


**Fig. 1.** Dimensionless time  $\tau_0(\gamma, \xi)$  of subbarrier motion in the case of elliptic polarization. The curves (from bottom to top) correspond to the values of  $\xi = 0, 0.5, 0.75, 0.9$ , and  $1$ .

the imaginary-time method at large values of  $\gamma > \gamma_*$  remains open. Yet,  $\gamma_* \gg 1$ , whence it follows that, in the region  $\gamma \lesssim 1$ , which is of greatest interest from the experimental point of view, formula (4.2), which was somewhat refined in [23], is applicable.

### 5. FURTHER APPLICATIONS OF THE IMAGINARY-TIME METHOD

Let us briefly consider the applications of the imaginary-time method to more complicated problems.

#### 5.1. Elliptic Polarization of Radiation

The extremal subbarrier trajectory in the field

$$\mathcal{E}(t) = \{\mathcal{E}_0 \cos \omega t, \xi \mathcal{E}_0 \sin \omega t, 0\}, \quad (5.1)$$

$-1 \leq \xi \leq 1,$

has the form<sup>7)</sup>

$$x(t) = \frac{\mathcal{E}_0}{\omega^2} (\cosh \tau_0 - \cosh \tau), \quad (5.2)$$

$$y(t) = -i\xi \frac{\epsilon_0}{\omega^2} \left( \sinh \tau - \frac{\sinh \tau_0}{\tau_0} \tau \right), \quad z(t) = 0,$$

where  $\tau = -i\omega t$  changes from  $\tau_0$  (initial instant of subbarrier motion) to  $\tau = 0$  (instant at which the

<sup>7)</sup>It can easily be verified that these expressions satisfy the equation of motion  $\ddot{\mathbf{r}} = \mathcal{E}(t)$  and the boundary conditions (2.9) and (2.10).

electron being considered goes out from under the barrier). It follows that

$$p_x(0) = p_z(0) = 0, \tag{5.3}$$

$$p_y(0) = -i\omega \frac{dy}{d\tau} = \pm \frac{\xi \mathcal{E}_0}{\omega} \left( \frac{\sinh \tau_0}{\tau_0} - 1 \right).$$

The initial condition (2.9) leads to the equation

$$\sinh^2 \tau_0 [1 - \xi^2 (\coth \tau_0 - 1/\tau_0)^2] = \gamma^2, \tag{5.4}$$

which determines the dependence  $\tau_0 = \tau_0(\gamma, \xi)$  (see Fig. 1). The exponential factor in the ionization probability and the coefficients in the momentum spectrum of photoelectrons are given by [9, 50]

$$dw(\mathbf{p}) \propto \exp \left\{ - \left[ 2K_0 f(\gamma, \xi) + \frac{1}{\omega} (c_1 p_x^2 + c_3 p_z^2) \right] \right\} \times \left\{ \exp \left[ - \frac{c_2}{\omega} (p_y - p_{\max})^2 \right] + \exp \left[ - \frac{c_2}{\omega} (p_y + p_{\max})^2 \right] \right\} d^3 p, \tag{5.5}$$

where

$$f(\gamma, \xi) = \left( 1 + \frac{1 + \xi^2}{2\gamma^2} \right) \tau_0 - \xi^2 \frac{\sinh^2 \tau_0}{\gamma^2 \tau_0} - (1 - \xi^2) \frac{\sinh 2\tau_0}{4\gamma^2}, \tag{5.6}$$

$$c_1 = \tau_0 - \operatorname{stanh} \tau_0, \tag{5.7}$$

$$c_2 = \tau_0 + \xi^2 s \frac{(\tau_0 - \tanh \tau_0)^2}{\tau_0^2 \tanh \tau_0}, \quad c_3 = \tau_0,$$

and  $s = [1 - \xi^2(1 - \tanh \tau_0/\tau_0)]^{-1}$ . For the calculation of the preexponential factor, the interested reader is referred to Appendix A. It should be noted that all quantities of interest are expressed rather simply in terms of  $\tau_0$ , which is the total imaginary time of subbarrier motion; the expressions that were obtained previously in [9] are equivalent to those that are given above, but they are more cumbersome. Formulas (5.4)–(5.7) specify all quantities analytically. We will now present their expansions in the low-frequency region to terms of order  $\gamma^3$  inclusive. We have

$$\tau_0 = \gamma - \frac{1}{18}(3 - \xi^2)\gamma^3 + \dots, \tag{5.7a}$$

$$c_1 = \frac{1}{3}(1 - \xi^2)\gamma^3, \quad c_2 = \gamma - \frac{1}{18}(1 - \xi^2)\gamma^3,$$

$$c_3 = \gamma - \frac{1}{18}(3 - \xi^2)\gamma^3,$$

$$P = 1 - \frac{1}{18}(9 - 5\xi^2)\gamma^2 + \dots$$

[for the function  $g(\gamma, \xi)$  appearing in the exponential, see (3.11)]. The momentum distribution of photoelectrons has the form of two Gaussian peaks [9] everywhere, with the exception of a comparatively narrow region  $1 - \xi^2 \lesssim F$ , where it begins spreading in the azimuthal angle (see Fig. 4 in [50]). For a circular polarization ( $\xi^2 = 1$ ), the distribution in question becomes isotropic in the  $xy$  plane (we assume that the wave propagates along the  $z$  axis).

Formulas (5.3) determine the most probable value of the electron momentum at the instant of exit from under the barrier. After that, the electron moves along the real trajectory, so that, for  $0 < t < \infty$ , we have

$$p_x(t) = p_x(0) + \mathcal{E}_0 \int_0^t \cos \omega t' dt',$$

$$p_y(t) = p_y(0) + \xi \mathcal{E}_0 \int_0^t \sin \omega t' dt'.$$

These integrals have an unambiguous meaning if one considers that the external field is switched off adiabatically for  $t \rightarrow +\infty$ :

$$J_1 = \lim_{\alpha \rightarrow +0} \int_0^\infty e^{-\alpha t} \cos \omega t dt = \frac{\alpha}{\omega^2 + \alpha^2} \rightarrow 0,$$

$$J_1 = \lim_{\alpha \rightarrow +0} \int_0^\infty e^{-\alpha t} \sin \omega t dt = \frac{\omega}{\omega^2 + \alpha^2} \rightarrow \frac{1}{\omega}$$

(the results of the integration here are independent of the specific form of the law according to which the external field vanishes—one must only require that this vanishing be rather slow,  $\alpha \ll \omega$ ). As a result, we find for  $t \rightarrow +\infty$  that

$$p_x(\infty) = p_z(\infty) = 0, \tag{5.8}$$

$$p_y(\infty) = p_y(0) + \frac{\xi \mathcal{E}_0}{\omega} = \frac{\xi \mathcal{E}_0}{\omega} \frac{\sinh \tau_0}{\tau_0} \equiv p_{\max},$$

which coincides with the value obtained (by a different method) in [9, 10]. From (5.2), it can be seen that, in subbarrier motion, the coordinate  $x(t)$  is real, while  $y(t)$  is pure imaginary. Accordingly, the velocity component  $v_x(t) = dx/dt$  is pure imaginary, while  $v_y(t)$  is real. Since the motion is classically allowed for  $t > 0$ , the electron momentum at the exit from under the barrier can be directed only along the  $y$  axis—that is, along the minor axis of the field ellipse in (5.1) (this is not so only in the cases of  $\xi \approx 0$  and  $|\xi| \rightarrow 1$ ). The above statements are also valid in the case of ionization induced by constant electric and

magnetic fields of arbitrary strength and direction [12, 17], in which case the subbarrier trajectory is not one-dimensional because of the effect of the Lorentz force. These examples demonstrate that, in multidimensional quantum-mechanical problems, the turning point (more precisely, the point of exit from under the barrier) is no longer, in general, the point at which the particle stops.

For  $\gamma \ll 1$ , the adiabatic expansion (3.11) follows from (5.6). From this expansion, one can see that, as the ellipticity of light grows, the function  $g(\gamma, \xi)$  increases, while the ionization probability  $w$  begins decreasing.<sup>8)</sup> These changes are even more pronounced in going over from the adiabatic region ( $\gamma \ll 1$ ) to the region of quickly varying fields ( $\gamma \gg 1$ ) (see Fig. 2).

For the case of a low-frequency laser field, the polarization dependences of the momentum, angular, and energy distributions of photoelectrons were calculated analytically and numerically in [50, 51] at all values of the ellipticity parameter  $\xi$ . It should be noted that, in recent years, considerable advances have been made in experimentally studying ionization induced by elliptically polarized light.

For reasons of space, other applications of the imaginary-time method will be considered only briefly. For details, the interested reader is referred to the articles referenced below.

5.2. Ionization in Constant Electric and Magnetic Fields [12, 17, 22]

The extremal trajectory is given by

$$x = i \frac{\mathcal{E}}{\omega_c^2} \left( \tau - \frac{\tau_0}{\sinh \tau_0} \sinh \tau \right) \sin \theta, \quad (5.9)$$

$$y = \frac{\mathcal{E}}{\omega_c^2} \frac{\tau_0}{\sinh \tau_0} (\cosh \tau_0 - \cosh \tau) \sin \theta,$$

$$z = \frac{\mathcal{E}}{2\omega_c^2} (\tau_0^2 - \tau^2) \cos \theta,$$

where  $\tau = -i\omega_c t$  and

$$\tau_0^2 - \sin^2 \theta (\tau_0 \coth \tau_0 - 1)^2 = \gamma_c^2, \quad (5.10)$$

$$\gamma_c = \frac{\omega_c}{\omega_t} = \frac{\kappa \mathcal{H}}{c\mathcal{E}}.$$

Here,  $\omega_c = e\mathcal{H}/mc$  is the cyclotron frequency,  $\omega_t = e\mathcal{E}/m\kappa$  is the frequency of electron tunneling in the field  $\mathcal{E}$ , and  $\kappa = \sqrt{2I}$ . Expressions (5.9) are obtained from known formulas for the trajectory of a nonrelativistic charged particle by constructing the analytic

<sup>8)</sup>The field amplitude  $\mathcal{E}$  is assumed to be fixed. Concurrently, the radiation intensity  $J = (1 + \xi^2)c\mathcal{E}^2/8\pi$  also increases, but not more than by a factor of 2.

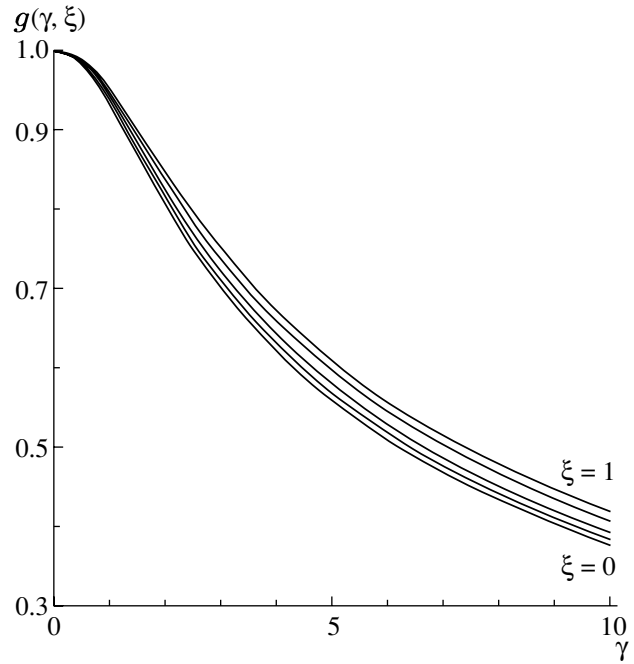


Fig. 2. Function  $g(\gamma, \xi)$  from (3.17) versus the Keldysh parameter  $\gamma$  ( $\xi$  is the ellipticity of laser radiation; the values of  $\xi$  are identical to those in Fig. 1).

continuation  $t \rightarrow it$  with allowance for the boundary conditions in (2.9) and (2.10). For an  $s$  level, the ionization probability is (here  $Z = 0$ —that is, for a short-range potential)

$$w(\mathcal{E}, \mathcal{H}) = \kappa^2 C_\kappa^2 P(\gamma_c, \theta) \times \exp \left\{ -\frac{2\kappa^3}{3\mathcal{E}} g(\gamma_c, \theta) \right\}, \quad (5.11)$$

where

$$g(\gamma_c, \theta) = \frac{3\tau_0}{2\gamma_c} \times \left[ 1 - \frac{1}{\gamma_c^2} \left( \sqrt{\tau_0^2 - \gamma_c^2} \sin \theta - \frac{1}{3} \tau_0^2 \cos^2 \theta \right) \right] = (\gamma_c \ll 1) 1 + \frac{1}{30} \gamma_c^2 \sin^2 \theta + O(\gamma_c^4),$$

$$P(\gamma_c, \theta) = 1 - \frac{1}{6} \gamma_c^2 + \dots$$

Here, it is assumed that the magnetic field is directed along the  $z$  axis and that the  $x$  axis is orthogonal to the fields  $\mathcal{E}$  and  $\mathcal{H}$ ,  $\theta$  being the angle between these two vectors;  $\gamma_c$  is the ratio of two characteristic frequencies,  $\omega_c$  and  $\omega_t$ , and is an analog of the Keldysh parameter (3.8) in the problem being considered.

It should be noted that the function  $g(\gamma_c, \theta)$  was first calculated in [12], where a formula that is equivalent to (5.12), but which was written in a more complicated form, was obtained. The Coulomb correction

and the preexponential factor  $P(\gamma, \theta)$  were calculated in [17, 26]. From (5.9), it can be seen that, at the exit from under the barrier, the electron momentum  $\mathbf{p}(0)$  is directed along the vector  $[\mathcal{E} \times \mathcal{H}]$ ; in contrast to what we have in the one-dimensional semiclassical approximation [4], it does not vanish.

The question of why we disregarded the effect of the magnetic field in the above consideration but take it into account in the case of constant fields may arise. The point is that, in the light wave,  $\mathcal{E} = \mathcal{H}$ , in which case the Lorentz force is  $\frac{e}{c}[\mathbf{v} \times \mathbf{H}] \sim \alpha\mathcal{E}$ , this yielding a smallness of order  $\alpha^2 \ll 1$  in the transition probability. In constant fields, the quantities  $\mathcal{E}$  and  $\mathcal{H}$  are not related to each other in general, so that values of  $\mathcal{E} \sim \mathcal{E}_a$  and  $\mathcal{H} \sim \mathcal{H}_a$  are possible, in which case  $\mathcal{H}_a/\mathcal{E}_a = c\hbar/e^2 = \alpha^{-1} \gg 1$ . Values in the region  $\mathcal{H} \gtrsim \mathcal{H}_a$  can be achieved in magnetic white dwarfs, to say nothing of neutron stars.

### 5.3. Lorentz Ionization

Lorentz ionization occurs as a particle moves in a strong magnetic field, in which case the electric field  $\mathcal{E} \perp \mathcal{H}$  arises in the rest frame of the atom owing to the respective Lorentz transformation. The relevant formulas are obtained by setting  $\theta = \pi/2$  in their counterparts given above; that is,

$$g(\gamma) = \frac{3\tau_0}{2\gamma^3} \left[ \gamma^2 - \sqrt{\tau_0^2 - \gamma^2} \right] \quad (5.13)$$

$$= \begin{cases} 1 + \frac{1}{30}\gamma^2 + \dots, & \gamma \rightarrow 0, \\ \frac{3}{8}\gamma + O(\gamma^{-1}), & \gamma \gg 1, \end{cases}$$

etc. If the atom being considered moves at a velocity  $v$  in the direction forming an angle  $\varphi$  with the direction of the magnetic field  $\mathcal{H}$ , then

$$\gamma = \frac{\kappa\mathcal{H}_0}{c\mathcal{E}_0} = \frac{\kappa}{v} \left[ 1 + \left( 1 - \frac{v^2}{c^2} \right) \cot^2 \varphi \right]^{1/2}, \quad (5.14)$$

where  $\mathcal{H}_0$  and  $\mathcal{E}_0$  are the field strengths in the rest frame of the atom. The magnetic field suppresses the decay of the bound state, stabilizing the atomic level (therefore, it would be incorrect to calculate the probability of Lorentz ionization,  $w_i$ , with allowance for the electric field  $\mathcal{E}_0$  alone). The exponential, the preexponential factor, the Coulomb correction, and the stabilization factor  $S$  (it determines the magnetic-field-induced suppression of the probability for the decay of a level) were calculated in [17, 26].

If  $\mathcal{H} < 1$  MG, the atom is nearly stable since the field  $\mathcal{E}_0$  is overly small. For  $\mathcal{H} \gtrsim 10$  MG, Lorentz ionization can be observed if the speed  $v$  is not very

small. For example, the results for the hydrogen atom (ground state) at  $\mathcal{H} = 25$  MG are  $w_L \approx 10^{-9}$ ,  $7 \times 10^{-4}$ ,  $1.5 \times 10^5$ ,  $10^{13}$ , and  $3 \times 10^{15} \text{ s}^{-1}$  for, respectively,  $v = 1, 1.25, 2, 5,$  and  $10$  a.u. ( $e^2/\hbar = 2.19 \times 10^8 \text{ cm/s}$ ). The application of the theory to Sakharov's experiments [52, 53], which were devoted to studying magnetic cumulation (generation of ultrastrong magnetic fields with the aid of an explosive compression of an axial magnetic field surrounded by a highly conducting shell—a value of  $\mathcal{H}_{\text{max}} \approx 25$  MG was obtained in this way), as well as its application in astrophysics (magnetic white dwarfs, for which  $\mathcal{H} \sim 10^5\text{--}10^6$  G), was considered in [26]. Lorentz ionization can occur when such a star traverses, in the course of its motion, an interstellar-gas cloud (neutral hydrogen). Further details can be found in [17, 26].

### 5.4. Ionization in the Field of an Ultrashort Laser Pulse [54, 55]

The generation of the most intense electromagnetic fields is associated with the shortening of a laser pulse. Its duration now becomes commensurate with an optical period, while the spectrum contains many high harmonics [56]. For an analysis of experimental data, it is therefore necessary to establish the pulse-shape dependence of the ionization probability and of the spectrum of photoelectrons.

In this connection, we will consider the problem of atomic-level ionization in a one-dimensional and linearly polarized electric field,

$$\mathcal{E}(t') = \mathcal{E}_0\varphi(t), \quad t = \omega t', \quad (5.15)$$

that involves an arbitrary dependence on the time  $t'$ . Here,  $\mathcal{E}_0$  is the amplitude of the field;  $\omega$  is its characteristic frequency; and  $t$  is the dimensionless time,  $t = 0$  being the time instant at which the field reaches a maximum and at which the electron goes out from under the barrier:

$$|\varphi(t)| \leq \varphi(0) = 1, \quad \varphi(-t) = \varphi(t), \quad (5.16)$$

$$-\infty < t < \infty.$$

It is clear that, here, the extremal trajectory is one-dimensional and is directed along the field. For it, we therefore have

$$\dot{x} = \frac{\mathcal{E}_0}{\omega} \int_0^{\omega t'} \varphi(t) dt \equiv \frac{i\kappa}{\gamma} h(\tau), \quad \tau = -i\omega t',$$

where  $h(\tau) = \int_0^\tau \varphi(it) dt$  is a real-valued function. The condition  $\dot{x} = i\kappa$  specifies the initial instant of subbarrier motion,  $t'_0 = i\omega^{-1}\tau_0$ :

$$\tau_0 = \tau(\gamma) \equiv h^{-1}(\gamma). \quad (5.17)$$

Here,  $h^{-1}(u)$  stands for the function inverse to  $h(u)$ . Further, we have

$$W = \frac{1}{2} \int_0^{t_0} (\dot{x}^2 + \kappa^2) dt \tag{5.18}$$

$$= \frac{i\kappa^3}{\mathcal{E}_0} \int_0^1 \chi(\gamma u)(1 - u^2) du,$$

$$\chi(u) \equiv \tau'(u).$$

In order to calculate the momentum spectrum of photoelectrons, it is necessary to consider the bundle of classical subbarrier trajectories that are close to the extremal one and which are specified by the momentum  $\mathbf{p} = (p_{\parallel}, \mathbf{p}_{\perp})$  at the exit from under the barrier and to calculate the function  $W(p_{\parallel}, \mathbf{p}_{\perp})$  to second-order terms in  $\mathbf{p}$  inclusive. As a result, we arrive at

$$w(\mathbf{p}) \propto \exp \left\{ -\frac{2\kappa^3}{3\mathcal{E}_0} g(\gamma) - \frac{\kappa}{\mathcal{E}_0} [b_1(\gamma)(p_{\parallel} - p_{\max})^2 + b_2(\gamma)p_{\perp}^2] \right\}, \tag{5.19}$$

$$g(\gamma) = \frac{3}{2} \int_0^1 \chi(\gamma u)(1 - u^2) du, \tag{5.20}$$

$$b_1(\gamma) = -\gamma b_2'(\gamma),$$

$$b_2(\gamma) = \int_0^1 \chi(\gamma u) du = \gamma^{-1} \tau(\gamma), \tag{5.21}$$

$$p_{\max} = \frac{\mathcal{E}_0}{\omega} \int_0^{\infty} \varphi(t) dt,$$

where  $p_{\parallel}$  and  $\mathbf{p}_{\perp}$  are, respectively, the longitudinal (with respect to the field) and the transverse momentum of the electron, while  $p_{\max}$  is its most probable momentum (at infinity).

These equations make it possible to calculate, for an arbitrary shape of the laser pulse  $\varphi(t)$  and at an arbitrary value of the parameter  $\gamma$ , all of the quantities that appear in the semiclassical formula for the ionization probability. Quite frequently, the function  $\chi(u)$  and the functions  $g$ ,  $b_1$ , and  $b_2$  from (5.19) can be found analytically (see Tables 1, 2). In any case, a numerical calculation by the above formulas does not present considerable difficulties.

With increasing adiabaticity parameter  $\gamma$ ,  $g(\gamma)$  decreases (see Figs. 1, 2), with the result that the ionization probability increases sharply if  $\gamma \gtrsim 1$ . The results obtained by calculating  $g(\gamma)$  and the coefficients

$b_{1,2}(\gamma)$  in the momentum spectrum for various pulsed fields can be found in [55]. The case of the modulated light pulse  $\varphi(t) = \exp(-t^2/2\sigma^2) \cos t$ , which is close to that in actual experiments, was also considered in that study.

### 5.5. Imaginary-Time Method and Asymptotic Behavior of Higher Orders of Perturbation Theory and 1/N Expansion in Quantum Mechanics

As a rule, perturbation-theory series in quantum mechanics and field theory diverge because of a factorial growth of higher orders in perturbation theory. Over the past 10–15 years, the method of 1/N expansion, or dimensional scaling, has been extensively used in quantum mechanics and atomic physics. In [18–21], the imaginary-time method was used to establish the asymptotic behavior of higher orders in perturbation theory and 1/N expansion for a number of problems.

In [20, 21], the structure of the perturbation-theory series (in powers of  $\mathcal{E}$  and  $\mathcal{H}$ ) was studied for the hydrogen atom in fields that are constant in time. It was shown that Eq. (5.10) has, apart from the ordinary real-valued solution  $\tau_0(\gamma, \theta)$ , which was considered above, a complex solution  $\tau_c$ . For  $\gamma \rightarrow \infty$ , we have

$$\tau_0 = \gamma \sec \theta - \tan^2 \theta + O(\gamma^{-1}), \tag{5.22}$$

$$\tau_c = i\pi[1 - i\gamma^{-1} \sin \theta + O(\gamma^{-3})],$$

the inequality  $|g_c(\gamma, \theta)| < g(\gamma, \theta)$  being valid for  $\gamma > \gamma_*(\theta)$ . In this case, the asymptotic behavior of higher orders of perturbation theory is determined by the second solution (that is, by  $\tau_c$  and  $\tau_c^*$ ) rather than by the saddle point  $\tau_0$ . As a result, the perturbation-theory series, which is a series of constant-sign terms for  $\gamma < \gamma_*$  (as in the case of the Stark effect for the ground state of the hydrogen atom), becomes a sign-alternating series for  $\gamma > \gamma_*$ , as that for the Zeeman effect. In the simplest case of parallel fields ( $\theta = 0$ ), we have

$$g(\gamma, 0) \equiv 1, \quad g_c(\gamma, 0) = i\frac{3\pi}{2\gamma}(1 + \pi^2/3\gamma^2),$$

whence it follows that

$$\gamma_*(0) = \pi q/(q^2 - 1) = 5.270\dots, \tag{5.23}$$

$$q = (1 + \sqrt{2})^{1/3}.$$

The numerical calculation performed in [21] revealed that the asymptotic behavior of higher orders in the perturbation-theory series for the ground-state energy,  $E_k$  for  $k \gg 1$ , does indeed change character at  $\gamma \approx 5$ .

In [18–20], the imaginary-time method was used to find the asymptotic behavior of higher orders in

**Table 1.** Models of a laser pulse

No.	$\varphi(t)$	$\tau_0(\gamma)$	$\chi(u)$
1	1	$\gamma$	1
2	$\cos t$	$\operatorname{arcsinh} \gamma$	$(1 + u^2)^{-1/2}$
3	$1/\cosh^2 t$	$\arctan \gamma$	$(1 + u^2)^{-1}$
4	$1/\cosh t$	$\arctan(\sinh \gamma)$	$1/\cosh u$
5	$(1 + \delta)/(\cosh t + \delta), \quad -1 < \delta \leq 1$	—	$(1 - \delta)/(\cosh \rho u - \delta), \quad \rho = \sqrt{(1 - \delta)/(1 + \delta)}$
6	$(\cosh^2 t + \beta^2 \sinh^2 t)^{-1}$	—	$\left( \cosh^2 u + \frac{\sinh^2 \beta u}{\beta^2} \right)^{-1}$
7	$(1 + t^2)^{-1}$	$\tanh \gamma$	$1/\cosh^2 u$
8	$(1 + t^2)^{-3/2}$	$\gamma/\sqrt{1 + \gamma^2}$	$(1 + u^2)^{-3/2}$
9	$\operatorname{cn}(t, q)$	—	$[1 + \sinh^2 qu/q^2]^{-1/2}$

Note: Here,  $\varphi(t)$  specifies the shape of a laser field;  $\tau_0$  is the initial instant (in dimensionless units) of subbarrier motion; and  $\operatorname{cn}$  is the elliptic cosine.

the  $1/N$  expansion in multidimensional quantum-mechanical problems, including that for the molecular hydrogen ion  $\text{H}_2^+$ . Within this approach, the energy is expanded in a series in powers of the small parameter  $1/N$ ; that is,

$$E = E^{(0)} + \frac{E^{(1)}}{N} + \dots + \frac{E^{(k)}}{N^k} + \dots, \quad (5.24)$$

**Table 2.** Analytic solutions

$\varphi(t)$	$f(\gamma) = \frac{2}{3}\gamma g(\gamma)$	$\gamma \gg 1$
$\cos t$	$[1 + (2\gamma^2)^{-1}]A - \frac{1}{2}\sqrt{1 + \gamma^{-2}}$	$\ln 2\gamma - 1/2$
$1/\cosh^2 t$	$(1 + \gamma^{-2}) \arctan \gamma - \gamma^{-1}$	$\pi/2 - 2\gamma^{-1}$
$(1 + t^2)^{-3/2}$	$\sqrt{1 + \gamma^{-2}} - A\gamma^{-2}$	$1 - \ln \gamma/\gamma^2$
$\varphi(t)$	$\tilde{g}(\gamma)$	$\gamma \gg 1$
$\cos t$	$4\pi^{-1}(1 + \gamma^2)^{-1/2}\mathbf{D}(q)$	$4 \ln \gamma/\pi\gamma$
$1/\cosh^2 t$	$2/(1 + \sqrt{1 + \gamma^2})$	$2\gamma^{-1}$
$(1 + t^2)^{-3/2}$	$4\pi^{-1}(1 + \gamma^2)^{-1/2}(\mathbf{K} - \mathbf{D})$	$4/\pi\gamma$

Note: The functions  $f$  and  $\tilde{g}$  determine, with an exponential accuracy, the probabilities of atom ionization [see Eq. (3.16)] and pair production [see Eq. (7.4)] induced by an electric field of the form (5.15). The following notation is used here:  $q = \gamma/\sqrt{1 + \gamma^2}$ ;  $A \equiv \operatorname{arcsinh} \gamma = \operatorname{arctanh} q$ ; and  $\mathbf{K}$  and  $\mathbf{D}$  are the total elliptic integrals of the first and the third kind, their modulus being denoted by  $q$ .

$$E^{(k)} \approx k! a^k k^\beta \left( c_0 + \frac{c_1}{k} + \frac{c_2}{k^2} + \dots \right),$$

where, for example,  $N = n$  is the principal quantum number of the level being considered. This series is asymptotic (that is, it diverges), the asymptotic parameter  $a$  being given by

$$a = \frac{1}{2\operatorname{Im} S}, \quad S = \int_{\mathbf{r}_0}^{\mathbf{r}_1} \mathbf{p} \cdot d\mathbf{r} = \int_0^\infty \dot{\mathbf{r}}^2 dt, \quad (5.25)$$

where  $\mathbf{r}_0$  is the point of a minimum of the effective potential  $U(\mathbf{r})$  and  $\mathbf{r}_1$  is a turning point that lies on the energy isosurface  $U(\mathbf{r}_1) = U(\mathbf{r}_0)$ . The action function  $S$  is calculated along the classical subbarrier trajectory, on which  $\dot{\mathbf{r}} = \nabla U$ ,  $t \rightarrow it$ , and  $\dot{\mathbf{r}}_0 = \dot{\mathbf{r}}_1 = 0$ .

In the two-center problem, where  $U(\mathbf{r}) = -(Z_1 r_1^{-1} + Z_2 r_2^{-1})$ , the variables are separated upon going over to the elliptical coordinates  $\xi, \eta = (r_1 \pm r_2)/R$  [4]. For the molecular hydrogen ion ( $Z_1 = Z_2 = 1$ ), the potential  $U(\eta)$  has a two-well shape if  $R > R_* = 1.299038 \dots$ , and the divergence of the series in (5.24) is due to the possibility of electron tunneling from one well to the other ( $\eta = \pm\eta_0$ ),

$$a^{-1} = 2\operatorname{Im} S = 2 \int_{-\eta_0}^{\eta_0} (-p_\eta^2)^{1/2} d\eta, \quad (5.26)$$

$$R > R_*.$$

This integral can be calculated analytically. As a result, the dependence of  $a$  on the internuclear distance

$R$  is determined in a parametric form [18–20]:

$$a = \frac{1}{4} \left( \frac{\eta_0}{1 - \eta_0^2} - \operatorname{arctanh} \eta_0 \right)^{-1}, \quad (5.27)$$

$$\eta_0 = \sqrt{\frac{3\tau - 1}{3\tau - \tau^2}},$$

$$R = 8\tau^{3/2}/(1 - \tau)(1 + \tau)^2,$$

$$1/3 < \tau < 1.$$

At  $\tau = 1/3$ , we have  $R = R_* = 3\sqrt{3}/4$  and there occurs a collision of two classical orbits, whereupon the turning points  $\pm\eta_0$  go to the complex plane. For  $R < R_*$ , it is possible to derive analytic formulas for  $a(R)$  that are similar to those in (5.27) and which are in excellent agreement with the results of the numerical calculation from [57]. In addition,  $a(R) < 0$  if  $R < R_*$  and  $a(R) > 0$  if  $R > R_*$ ; by virtue of this, the  $1/n$  expansion is a sign-alternating series in the former case and a sign-constant series in the latter case. For  $R \rightarrow R_*$ , the asymptotic parameter  $a(R)$  changes in proportion to a power-law function,  $(R - R_*)^{-3/2}$ .

For the hydrogen atom in constant external fields  $\mathcal{E}$  and  $\mathcal{H}$ , the variables in the Schrödinger equation are not separated; therefore, the subbarrier trajectory was determined by numerically integrating the equations of motion (in terms of the imaginary time). As a result, the dependence of the asymptotic parameter  $a$  on the reduced fields  $F = n^4\mathcal{E}$  and  $B = n^3\mathcal{H}$  was found in [19–21] for Rydberg states ( $n \gg 1$ ).

Thus, the imaginary-time method makes it possible to study the structure of higher orders of perturbation theory and the  $1/n$  expansion. We restrict ourselves to the comments made above since these issues do not belong to the main topic of the present article.

### 6. RELATIVISTIC THEORY OF TUNNELING [24]

Rapid advances in laser physics and technologies made it possible to reach record intensities of  $J \sim 10^{21}$  W/cm<sup>2</sup>. In the near future, it is planned to increase them by one to two orders of magnitude [56]. In such fields, there can arise atomic ions of charge  $Z \gtrsim 40$ –60, for which the binding energy of electron levels becomes commensurate with the rest energy  $m_e c^2$ . In this case, the subbarrier motion of an electron cannot be considered as a nonrelativistic motion, so that it is required to generalize Keldysh’s ionization theory.

A linearly polarized plane electromagnetic wave can be specified by the potentials

$$\mathbf{A} = \left( 0, -\frac{\mathcal{E}_0}{\omega} a(\eta), 0 \right), \quad \varphi \equiv 0, \quad (6.1)$$

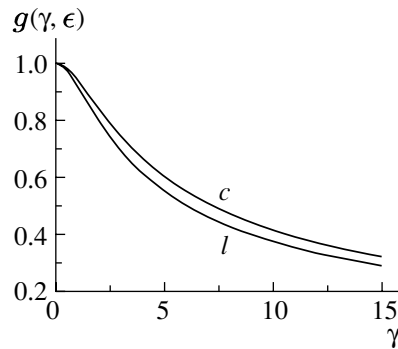


**Fig. 3.** Function  $g(\gamma, \epsilon)$  from (6.7) in the case of a linear ( $l$ ) and a circular ( $c$ ) polarization [here,  $\epsilon = \sqrt{1 - (Z\alpha)^2}$ , which corresponds to the  $1s_{1/2}$  ground state of a hydrogen-like atom, and  $Z = 60$ ].

where  $\mathcal{E} = \mathcal{H} = \mathcal{E}_0 a'(\eta)$ ,  $\eta = \omega(t - x)$ , the  $x$  axis is chosen along the wave-propagation direction, the electric field is directed along the  $y$  axis, and the magnetic field is directed along the  $z$  axis. The function  $a(\eta)$  specifies the pulse shape:  $a(\eta) = \sin \eta$  corresponds to laser light,  $a(\eta) = \eta$  corresponds to a constant crossed field, and  $a(\eta) = \tanh \eta$  corresponds to a soliton-like pulse, etc. The equations of motion for the electron 4-momentum have the form

$$\dot{p}_x = e\mathcal{E}v_y, \quad \dot{p}_y = e\mathcal{E}(1 - v_x), \quad (6.2)$$

$$\dot{p}_z = 0, \quad \dot{E} = e(\mathcal{E} \cdot \mathbf{v}) = e\mathcal{E}v_y,$$

where an overdot means a derivative with respect to the laboratory time  $t$ . For any dependence  $\mathcal{E}(\eta)$ , there exists the integral of the motion [40, 58, 59]

$$J = E - p_x = (1 - v_x)/\sqrt{1 - v^2} = \eta/\omega\tau,$$

where  $\tau = \int^t \sqrt{1 - v^2} dt$  is the proper time of the particle. The second equation in (6.2) yields

$$\frac{dp_y}{d\eta} = \frac{e\mathcal{E}_0}{\omega} a'(\eta), \quad p_y(\eta) = \frac{e\mathcal{E}_0}{\omega} a(\eta) = -eA_y(\eta).$$

(In choosing the integration constant, it has been considered that, upon going over to the imaginary time, the light-front variable  $\eta$  and the momentum  $p_y$  become pure imaginary quantities.) Further, we obtain

$$\frac{dy}{d\eta} = \frac{1}{J\omega} \frac{dy}{d\tau} = \frac{p_y(\eta)}{J\omega}, \quad y(\eta) = \frac{e\mathcal{E}_0}{J\omega^2} \int_{\eta_0}^{\eta} a(\eta') d\eta'.$$

The quantities  $p_x(\eta)$  and  $x(\eta)$  can be found in a similar way. The solution can be obtained for any dependence of the wave field on  $\eta$ .

We will now present explicitly the subbarrier trajectory for the case of monochromatic laser radiation.

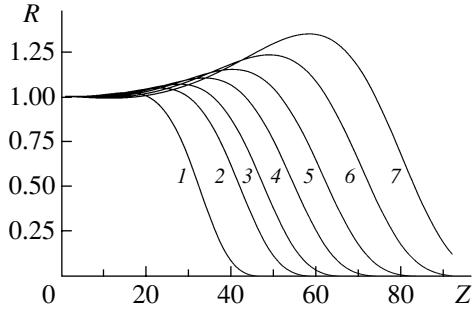


**Fig. 4.** Accuracy of nonrelativistic Keldysh's theory in the case of heavy atoms. Presented in the figure are the values of  $R = w_{NR}/w_R$  for the ionization of the  $1s_{1/2}$  level versus  $Z$  at the intensities of  $J = (1) 10^{20}$ ,  $(2) 10^{21}$ ,  $(3) 3 \times 10^{21}$ ,  $(4) 10^{22}$ ,  $(5) 3 \times 10^{22}$ ,  $(6) 10^{23}$ , and  $(7) 3 \times 10^{23}$  W/cm<sup>2</sup>.

We have

$$p_x(\eta) = \frac{1}{4\beta^2 J} \left( \frac{\sinh 2\eta_0}{2\eta_0} - \cosh 2\eta \right),$$

$$p_y(\eta) = i\beta^{-1} \sinh \eta,$$

$$x = \frac{i\eta}{4\omega\beta^2 J^2} \left( \frac{\sinh 2\eta_0}{2\eta_0} - \frac{\sinh 2\eta}{2\eta} \right), \quad (6.3)$$

$$y = \frac{1}{\omega\beta J} (\cosh \eta_0 - \cosh \eta), \quad z \equiv 0,$$

where  $\beta = \omega/e\mathcal{E}_0$  and where we have made the substitution  $\eta \rightarrow i\eta$  corresponding to the imaginary-time method; here,  $\eta_0 = -i\omega t_0 > 0$ . The quantities  $\eta_0$  and  $J$  are determined from the initial conditions,

$$E(\eta_0) = \sqrt{p_x^2(\eta_0) + p_y^2(\eta_0) + 1} = \epsilon, \quad (6.4)$$

$$p_x(\eta_0) = \epsilon - J$$

(here,  $\epsilon = E_0/m_e c^2$ ,  $0 < \epsilon < 1$ , and  $E_0$  is the initial energy of the level with allowance for the electron rest energy), whence it follows

$$\sinh^2 \eta_0 = \gamma^2 \frac{1 - 2\epsilon J + J^2}{1 - \epsilon^2}, \quad (6.5)$$

$$\frac{\sinh 2\eta_0}{2\eta_0} = 1 + 2\gamma^2 \frac{1 - J^2}{1 - \epsilon^2},$$

where  $\gamma$  is the adiabaticity parameter, which is the relativistic generalization of the Keldysh parameter (3.8):

$$\gamma = \omega T_t = \frac{\omega}{e\mathcal{E}_0} \sqrt{1 - \epsilon^2}. \quad (6.6)$$

Calculating the reduced action functional along the

subbarrier trajectory,

$$W = \int_{t_0}^0 \left\{ -\sqrt{1 - v^2} + e(\mathbf{A} \cdot \mathbf{v}) + \epsilon \right\} dt,$$

we find the rate of ionization of a relativistic bound state in the form

$$w_R \propto \exp(-2\hbar^{-1} \text{Im} W) = \exp \left\{ -\frac{2}{3F} g(\gamma, \epsilon) \right\},$$

$$g(\gamma, \epsilon) = \left( \sqrt{(1 + \xi^2) \left( 1 - \frac{1}{3}\xi^2 \right)} / \xi^2 \gamma \right) \times \eta_0(J - \epsilon), \quad (6.7)$$

where  $F = \mathcal{E}_0/\mathcal{E}_{ch}$  and where we have introduced a characteristic field that is determined by the initial energy of the level,<sup>9)</sup>

$$\mathcal{E}_{ch} = \frac{(\sqrt{3}\xi)^3}{1 + \xi^2} \mathcal{E}_{cr}, \quad (6.8)$$

$$\xi = \left[ 1 - \frac{1}{2}\epsilon \left( \sqrt{\epsilon^2 + 8} - \epsilon \right) \right]^{1/2},$$

$\mathcal{E}_{cr} = m_e^2 c^3 / e\hbar = 1.32 \times 10^{16}$  V/cm being the critical (Schwinger) field in QED [60, 61]. The value of  $\mathcal{E}_{ch}$  increases monotonically as the level being considered becomes deeper. In the nonrelativistic limit,  $\mathcal{E}_{ch} = (2I)^{3/2} \mathcal{E}_a$ , where  $\mathcal{E}_a = \alpha^3 \mathcal{E}_{cr}$ ,  $\alpha = 1/137$ , and  $I$  is the ionization potential (in a.u.). Concurrently, expression (6.7) reduces to the Keldysh formula (3.17). Equations (6.5)–(6.7) provide the generalization of this formula to the case of deep levels. These equations can readily be solved numerically with a computer (see Fig. 3).

The rate of level ionization induced by an elliptically polarized wave can be calculated in a similar way [24]. The growth of the ellipticity of light leads to a decrease in the ionization probability  $w_R$ ; on the contrary, a decrease in  $\epsilon$  (that is, the deepening of the bound-state level) increases this probability (at a fixed value of the reduced field  $F$ , which depends on  $\epsilon$ ).

In the course of subbarrier motion, the action functional also develops a spin-dependent correction, this leading to the dependence of the tunneling probability on the projection of the spin onto the magnetic-field direction. For information about this correction and for further details, the interested reader is referred to [24]. Here, we only present the results of the calculation of the ratio  $R = w_{NR}/w_R$ , where  $w_{NR}$  and  $w_R$  are the rates of ionization of the  $1s_{1/2}$  ground state

<sup>9)</sup>The notation  $\xi$  here is in accord with that in [22–24] (not to be confused with the ellipticity of radiation).

of the hydrogen-like atom whose nuclear charge is  $Z$  (Fig. 4),  $w_{NR}$  and  $w_R$  corresponding to the nonrelativistic (Keldysh) and the relativistic theory of ionization, respectively. As can be seen from Fig. 4, the deviations from Keldysh's theory become significant at  $J \sim 10^{21}$  W/cm<sup>2</sup> for  $Z = 40$ , at  $J \sim 10^{22}$  W/cm<sup>2</sup> for  $Z = 60$ , etc. At the present time, such intensities of laser radiation are becoming achievable in experiments [56].

It should be noted that the relativistic theory of tunneling was also considered in [62] but the "main results" of those studies were taken from [22, 23], use being made there of the same notation, including the transition from the energy  $\epsilon$  of a level to the auxiliary variable  $\xi$ , which was introduced in [22] and which is natural within the imaginary-time method. A comment on this situation, which is more than strange and which is absolutely unacceptable, is given in [24, 25]. For convenience of the reader, the text of this comment is reproduced in Appendix B.

### 7. IMAGINARY-TIME METHOD IN THE THEORY OF THE SCHWINGER EFFECT

The production of electron–positron pairs from a vacuum in a superstrong electric field is predicted within QED. This nonlinear and essentially nonperturbative effect was first considered for a constant field [60, 61] and was then studied for variable fields of the form

$$\mathcal{E}(t') = \{\mathcal{E}\varphi(t), 0, 0\}, \quad \mathbf{B}(t') \equiv 0 \quad (7.1)$$

in the case of the harmonically oscillating field  $\varphi(t) = \cos t$  [13, 14, 63–66] and some pulsed fields [67]. We impose, on the function  $\varphi(t)$ , which determines the field-pulse shape, the same conditions as in (5.16). In terms of the imaginary-time method, the production of an  $e^+e^-$  pair is described as the tunneling of an electron from the lower continuum (Dirac sea) to the upper continuum through the gap  $2mc^2$  between them (see Fig. 5). Under the condition  $\mathcal{E} \ll \mathcal{E}_{cr}$ , the barrier width is  $b = 2mc^2/e\mathcal{E} = 2\lambda_C(\mathcal{E}/\mathcal{E}_{cr})^{-1} \gg \lambda_C$ . In the case of a constant field, the equations of motion yield (here,  $\lambda_C = \hbar/mc$ ; in the following, we use the system of units where  $\hbar = c = 1$ )

$$p = e\mathcal{E}t, \quad \dot{x} = \frac{p}{\sqrt{p^2 + m^2}} = \frac{e\mathcal{E}t}{\sqrt{m^2 + (e\mathcal{E}t)^2}},$$

$$x(t) = \frac{1}{e\mathcal{E}}\sqrt{p^2 + m^2} + \text{const},$$

whence it follows that

$$S = \int_0^t (-m\sqrt{1 - v^2} + e\mathcal{E}x) dt \quad (7.2)$$

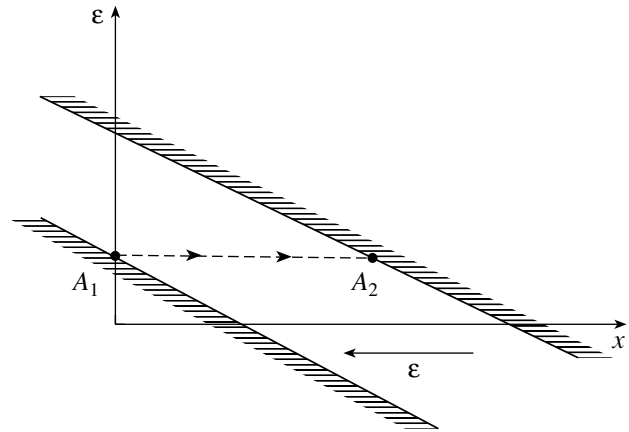


**Fig. 5.** Production of a  $e^+e^-$  pair from a vacuum as the tunneling of an electron from the lower continuum (Dirac sea) to the upper continuum ( $A_1$  and  $A_2$  are turning points).

$$= \frac{1}{2e\mathcal{E}} \left\{ p\sqrt{p^2 + m^2} - m^2 \ln(p + \sqrt{m^2 + p^2}) \right\}.$$

In the complex plane, the action functional has the branch point  $t = t_*$ , at which  $p(t_*) = im$ . Upon the circumvention around this branch point (see Fig. 6), the action functional develops an imaginary part<sup>10)</sup>  $\Delta S = i\pi m^2/2e\mathcal{E}$ , which determines the probability of pair production from a vacuum:

$$w \propto \exp\left(-\frac{2}{\hbar}\text{Im} \Delta S\right) = \exp(-\pi\mathcal{E}_{cr}/\mathcal{E}), \quad (7.3)$$

$$\mathcal{E} \ll \mathcal{E}_{cr}.$$

The generalization to the case of a variable field has the form [13]

$$w(\mathbf{p}) = P \exp\left\{-\pi\frac{\mathcal{E}_{cr}}{\mathcal{E}}\right. \quad (7.4)$$

$$\left. \times \left[\tilde{g}(\gamma) + \tilde{b}_1(\gamma)\frac{p_{\parallel}^2}{m^2} + \tilde{b}_2(\gamma)\frac{p_{\perp}^2}{m^2}\right]\right\},$$

where we now have<sup>11)</sup>

$$\tilde{g}(\gamma) = \frac{4}{\pi} \int_0^1 \chi(\gamma u) \sqrt{1 - u^2} du, \quad (7.5)$$

$$\gamma = \frac{mc\omega}{e\mathcal{E}} = \frac{\hbar\omega}{mc^2} \frac{\mathcal{E}_{cr}}{\mathcal{E}},$$

<sup>10)</sup> A nonzero contribution here comes only from the term that involves a logarithm in (7.2).

<sup>11)</sup> The functions appearing here are labeled with a tilde in order to distinguish them from (5.19).

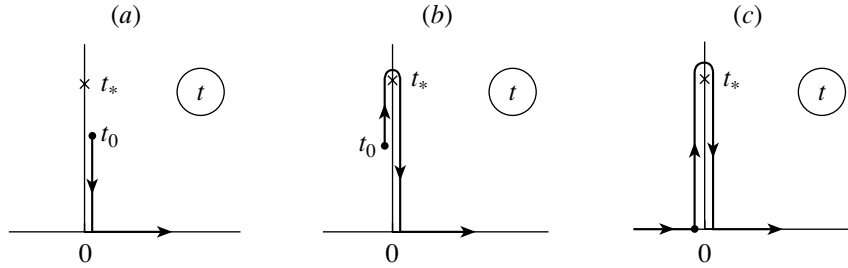


**Fig. 6.** Variation of the imaginary “time”  $t$  in the course of the subbarrier motion of an electron: (a) level of energy  $E_0$ ,  $mc^2 > E_0 > 0$ ; (b)  $0 > E_0 > -mc^2$ ; and (c) in the problem of pair production,  $E_0 = -mc^2$ .

$$\tilde{b}_1(\gamma) = -\gamma\tilde{b}'_2(\gamma), \quad \tilde{b}_2(\gamma) = \frac{2}{\pi} \int_0^1 \frac{\chi(\gamma u)}{\sqrt{1-u^2}} du.$$

As to the function  $\chi(u)$ , which is determined by the shape of the field pulse  $\varphi(t)$ , it has the same form as in the nonrelativistic theory of ionization (see Table 1). The distinction between formulas (7.5) and (5.20) stems from the different forms of the dispersion law  $\varepsilon(\mathbf{p})$  both in relativistic and in nonrelativistic mechanics. In some particular cases, including that of the monochromatic field  $\varphi(t) = \cos t$ , all functions appearing in (7.4) can be calculated analytically [13, 63].

At the present time, lasers of the infrared range are the most powerful; for them,  $\hbar\omega \ll mc^2$  and  $\gamma \ll 1$ . In this case, we have the following results for the field  $\varphi(t) = \cos t$ :

$$\tilde{g}(\gamma) = 1 - \frac{1}{8}\gamma^2 + \frac{3}{64}\gamma^4 + \dots, \quad (7.6)$$

$$\tilde{b}_1 = \frac{1}{2}\gamma^2, \quad \tilde{b}_2 = 1 - \frac{1}{4}\gamma^2.$$

For the number of  $e^+e^-$  pairs produced from a vacuum in the case where laser radiation is focused in a volume of about  $\lambda^3$  (diffraction limit), estimates were obtained in [14, 65, 66] for pulses of various duration and for lasers of the optical and x-ray ranges. Pair production induced by an elliptically polarized field was considered in [15], where analytic formulas were obtained, which were recently used in [68] to perform numerical calculations for the case of a circular polarization. The question of whether it is possible to observe experimentally the Schwinger effect for  $e^+e^-$  pairs attracted much attention in recent years [56, 65, 66].

In the simplest case of constant (in time and space) fields, the imaginary-time method yields not only the exponential (7.3) but also the exact expression for the imaginary part of the Lagrangian,<sup>12)</sup>

<sup>12)</sup>We consider only  $\text{Im } \mathcal{L}$ , which does not receive contributions from Faddeev–Popov ghosts.

which arises from the interaction of the electromagnetic field with the vacuum of charged particles (whose spin is denoted by  $s$ ). The result is

$$\text{Im } \mathcal{L} = (2s + 1) \frac{e^2}{16\pi^3} \mathcal{E}\mathcal{H} \quad (7.7)$$

$$\times \sum_{n=1}^{\infty} \frac{\sigma_n}{n} \exp\left(-\frac{n\pi\mathcal{E}_{\text{cr}}}{\mathcal{E}}\right) f_s(n\pi\mathcal{H}/\mathcal{E}),$$

$$f_s(y) = \begin{cases} 1/\sinh y, & s = 0 \\ \coth y, & s = 1/2 \\ (2\cosh 2y + 1)/3\sinh y, & s = 1, \end{cases} \quad (7.7a)$$

where  $\sigma_n = (-1)^{n-1}$  for bosons and  $\sigma_n = 1$  for fermions.

These results were obtained by Schwinger [61] for scalar and spinor electrodynamics and by Vanyashin and Terent'ev [69] for vector bosons characterized by the gyromagnetic ratio  $g = 2$ . We will apply the imaginary-time method to this problem [13, 37].

In the reference frame where the fields  $\mathcal{E}$  and  $\mathcal{H}$  are collinear, the charged-particle trajectory has the form

$$p_z = e\mathcal{E}t = \varepsilon_0 \sinh \psi, \quad \mathbf{p}_{\perp} = p_{\perp} e^{-i\varphi}, \quad (7.8)$$

$$\varepsilon = \varepsilon_0 \cosh \psi,$$

$$z = \frac{\varepsilon_0}{e\mathcal{E}} \cosh \psi, \quad x = \frac{p_{\perp}}{e\mathcal{H}} \sin \varphi,$$

$$y = \frac{p_{\perp}}{e\mathcal{H}} (\cos \varphi - 1), \quad \varepsilon_0 = \sqrt{m^2 + p_{\perp}^2}.$$

We also have ( $\tau$  is the proper time of the particle)

$$\psi = \frac{e\mathcal{E}}{m} \tau, \quad \varphi = \frac{\mathcal{H}}{\mathcal{E}} \psi = \frac{e\mathcal{H}}{m} \tau, \quad t = \frac{\varepsilon_0}{e\mathcal{E}} \sinh \psi, \quad (7.9)$$

$$S = \int^t dt \left( -m\sqrt{1-\mathbf{v}^2} + \frac{e}{2} [\mathcal{H} \times \mathbf{r}] \cdot \mathbf{v} + e\mathcal{E}z \right)$$

$$= \frac{\varepsilon_0^2}{4e\mathcal{E}} \sinh 2\psi - \frac{m^2}{2e\mathcal{E}} \psi + \frac{p_{\perp}^2}{2e\mathcal{H}} \sin \varphi.$$

The reduced action functional is given by

$$W = S - (\mathbf{p}_\perp \cdot \boldsymbol{\rho}) = S - \frac{p_\perp^2}{e\mathcal{H}} \sin \varphi. \quad (7.10)$$

The time  $t$  becomes pure imaginary and runs along the contour that circumvents the cut  $[t_0, -t_0]$ , where  $t_0 = i\varepsilon_0/e\mathcal{E}$ ,  $n$  times, the variable  $\psi$  changing monotonically from 0 to  $i n\pi$ . The contour involving  $n$  circumventions corresponds to many walks of the particle between the turning points  $A_1$  and  $A_2$  (Fig. 5). The contribution of the  $n$ th trajectory to the imaginary part of the action functional is<sup>13)</sup>

$$\text{Im } W_n(p_\perp^2) = n \frac{\pi m^2}{2e\mathcal{E}} + \frac{p_\perp^2}{2e\mathcal{H}} \sinh(n\pi\mathcal{H}/\mathcal{E}). \quad (7.11)$$

For a particle featuring a spin, the expression in (7.11) must be supplemented with the spin-dependent part of the action functional. In the semiclassical approximation, this spin-dependent part is given by [15]

$$\Delta S_{\text{spin}} = \frac{ie}{2mc} \epsilon_{\alpha\beta\lambda\mu} \int F^{\alpha\beta} u^\lambda s^\mu d\tau, \quad (7.12)$$

where  $s_\mu$  is the spin (pseudo) 4-vector, whose variation is controlled by the Bargmann–Michel–Telegdi equation [70]. In the case being considered, this equation is solved exactly [15]. This leads to expression (7.7), where  $f_s(y) = \sinh(2s+1)y/(2s+1)\sinh^2 y$ . It can easily be seen that, at  $s = 0, 1/2$ , and 1, this expression coincides with (7.7a).

Thus, the imaginary-time method makes it possible to obtain the whole series (7.7) and not only the first term corresponding to  $n = 1$ . There are special reasons for this in the present case:

- (i) The classical equations of motion do not involve gradient terms of the  $\partial_\lambda F_{\mu\nu}$  type.
- (ii) The action functional is quadratic in  $p_\perp$  for all classical trajectories and not only for  $p_\perp \ll m$ .
- (iii) The continual integral over the set of all continuous paths [7, 8] reduces to an integral over only classical trajectories [15].

Naturally, the imaginary-time method cannot lead to an exact result in fields of a more complicated configuration (if it is possible in principle to obtain an exact result, as in the case of  $\mathcal{E}(t) = \mathcal{E}_0/\cosh^2 \omega t$  [67], for example). However, the imaginary-time method is always applicable under the conditions  $\mathcal{E}_0 \ll \mathcal{E}_{\text{cr}}$  and  $\hbar\omega \ll mc^2$ , and this is the case where the problem being considered has a clear physical meaning: if  $\mathcal{E} \gtrsim$

$\mathcal{E}_{\text{cr}}$ , then it is illegitimate to disregard the feedback effect of product electrons and positrons on the external field.

It should be noted that, in the case of a constant electric field, expression (7.7) assumes the form [60, 71, 72]

$$\begin{aligned} \text{Im } \mathcal{L} &= (2s+1) \frac{e^2 \mathcal{E}^2}{8\pi^2} \\ &\times \sum_{n=1}^{\infty} \frac{\sigma_n}{n^2} \exp(-n\pi\mathcal{E}_{\text{cr}}/\mathcal{E}), \end{aligned} \quad (7.13)$$

where each spin projection appears independently of the others. The total number of pairs produced in the 4-volume  $\lambda_C^4 = (\hbar/mc)^4 \approx 7.25 \times 10^{-53} \text{ cm}^4 \text{ s}^{-1}$  is  $N_{e^+e^-} = 2\text{Im } \mathcal{L}$  (for  $\mathcal{E} \ll \mathcal{E}_{\text{cr}}$ ).

To conclude this section, it is worth emphasizing the analogy between the extremal trajectory in the imaginary-time method and instantons in quantum field theory: in either case, such solutions satisfy classical equations of motion, but the time  $t$  for a sub-barrier trajectory becomes a pure imaginary quantity. Problems associated with instantons have been considered in many studies (see, for example, [73, 74] and references therein).

## 8. CONCLUDING REMARKS

The imaginary-time method was proposed in [9] within the theory of multiphoton ionization of atoms that is induced by intense laser light. Over the past years, this method has been applied to various physics problems, including those of the production of  $e^+e^-$  pairs in a variable electric field, the ionization of an atomic level by a pulse of arbitrary shape, Lorentz ionization, and the generalization of Keldysh's theory to the relativistic case. It can be hoped that the number of such problems will increase in the future.

In the theory of ionization, the imaginary-time method is applicable under conditions (2.14), owing to which the barrier width is much larger than the characteristic bound-state size, the barrier penetrability is small, and the process in question has a multiquantum character. In the case of a variable field  $\mathcal{E}(t)$ , the imaginary-time method makes it possible to determine the penetrability of a vibrating barrier and the momentum spectrum of emitted electrons. The required solution is obtained in an especially straightforward way if classical trajectories in a given external field can be found analytically. As a rule, the application of the imaginary-time method makes it possible to calculate readily the probability of tunneling (at least with an exponential accuracy) and extends substantially the range of problems that admit an analytic treatment.

<sup>13)</sup>It should be noted that the terms proportional to  $p_\perp^2$  in (7.10) and in (7.11) differ in sign. The correct expression for the momentum spectrum is obtained only with the function  $W$  (not with  $S$ ), as in the nonrelativistic theory of ionization [37].

This article is dedicated to Yuriĭ Antonovich Simonov on the occasion of his 70th birthday. Over my years of work at the Institute of Theoretical and Experimental Physics (ITEP, Moscow) together with Simonov, I have greatly benefited from numerous discussions with him on various scientific problems. I was always impressed by the wide range of Simonov's scientific interests: from the nonrelativistic theory of the structure of light nuclei (method of  $K$  harmonics) to the ultramodern theory of quarks and gluons (method of vacuum correlation functions in QCD). I congratulate Yu.A. Simonov and heartily wish him good health, longevity, and many years of creative activity.

#### ACKNOWLEDGMENTS

I am grateful to the organizers of the 31st ITEP Winter School in Physics (February 2003) for the proposal to deliver the lecture "The imaginary-time method in the theory of atom ionization and of the production of  $e^+e^-$  pairs from a vacuum under the effect of intense laser radiation," which formed the basis of the present article. Many physicists, including B.M. Karnakov, L.P. Kotova, V.P. Kuznetsov, V.D. Mur, A.M. Perelomov, and A.V. Sergeev and the late M.S. Marinov and M.V. Terentiev, took part, at different times, in the development of the imaginary-time method. The bulk of relevant numerical calculations were performed by S.G. Pozdnyakov and A.V. Sergeev. I am deeply indebted to these colleagues, whose contribution is difficult to overestimate. Special thanks are due to A.M. Badalian, S.S. Bulanov, B.M. Karnakov, V.D. Mur, and S.V. Popruzhenko, who read the manuscript of this article, made valuable comments, and indicated some of the relevant references. The assistance of N. Igumnov and M. Markin in the preparation of the manuscript is gratefully acknowledged.

This work was supported in part by the Russian Foundation for Basic Research (project nos. 01-02-16850 and 04-02-17157).

#### APPENDIX A

##### ON THE CALCULATION OF THE PREEXPONENTIAL FACTOR

With the aid of the imaginary-time method, one can calculate not only the exponential in the tunneling probability [see Eqs. (2.12), (3.17)] but also the preexponential factor  $P$ . We will show this by considering the example of the problem where a state bound by a delta-function potential ( $Z = 0, r_c \rightarrow 0$ ) is ionized under the effect of elliptically polarized light,

$$\mathcal{E}(t) = \{\mathcal{E} \cos \omega t, \xi \mathcal{E} \sin \omega t, 0\}, \quad (\text{A.1})$$

$$-1 \leq \xi \leq 1,$$

where  $\xi$  is the ellipticity parameter, the wave propagating along the  $z$  axis. Applying the saddle-point method to the integral in (2.6), we evaluate the flux of particles (electrons) going to infinity. We have<sup>14)</sup>

$$w(\mathbf{p}) \propto |\psi(\mathbf{p}, t \rightarrow \infty)|^2 \propto C_\kappa^2 \left| \frac{\partial^2 W}{\partial t_0^2} \right|^{-1} \times \exp\{-2\text{Im} W(\mathbf{p}, t; \mathbf{r}_0, t_0)\}, \quad (\text{A.2})$$

where  $t_0 = t_0(\mathbf{p})$  is the initial instant of time [see, for example, (3.2)]. As was shown in Section 2 above,

$$\begin{aligned} \partial W / \partial t_0 &= H(t_0) - E_0 = \frac{1}{2}(\dot{\mathbf{r}}_0^2 + \kappa^2), \\ \mathbf{r}_0 &\equiv \mathbf{r}(t_0) = 0; \end{aligned}$$

therefore, we have

$$\begin{aligned} \partial^2 W / \partial t_0^2 &= \frac{\partial H}{\partial t_0} + \frac{\partial H}{\partial \dot{x}_i^{(0)}} \ddot{x}_i^{(0)} \\ &= -\dot{\mathcal{E}} \cdot \mathbf{r} + \dot{\mathbf{r}} \cdot \ddot{\mathbf{r}} \Big|_{t=t_0} = \mathcal{E}(t_0) \cdot \dot{\mathbf{r}}_0. \end{aligned} \quad (\text{A.3})$$

Considering formulas (5.2), we find for the extremal subbarrier trajectory  $\mathbf{r}_0(t)$  that

$$\begin{aligned} \dot{\mathbf{r}}_0(t) &= i\omega \frac{d\mathbf{r}}{d\tau} \\ &= \frac{\mathcal{E}}{\omega} \left\{ i \sinh \tau, \xi \left( \frac{\sinh \tau_0}{\tau_0} - \cosh \tau \right), 0 \right\}, \\ \tau &= i\omega t, \\ \frac{\partial^2 W}{\partial t_0^2} &= i \frac{\mathcal{E}^2}{\omega} \left\{ (1 - \xi^2) \sinh \tau_0 \cosh \tau_0 + \xi^2 \frac{\sinh^2 \tau_0}{\tau_0} \right\} \\ &= i \frac{\kappa \mathcal{E}}{2\gamma} [1 - \xi^2 + \xi^2 \tanh \tau_0 / \tau_0] \sinh 2\tau_0, \end{aligned} \quad (\text{A.4})$$

which is in perfect agreement with the expression obtained (by a more involved method) in [9] {see also Eqs. (6) and (7) in [50]}. In performing a comparison with the results given in [9], it should be borne in mind that the variable  $s$  used there is defined as  $s = \xi(1 - \tanh \tau_0 / \tau_0)$ .

The formulas from [9] are simplified substantially upon going over from  $s$  to the variable  $\tau_0 = \tau_0(\gamma, \xi)$ , which has a clear physical meaning in the imaginary-time method:  $\tau_0$  is the dimensionless imaginary time of subbarrier motion. The asymptotic expressions for  $\tau_0$  under the conditions  $\gamma \ll 1$  and  $\gamma \gg 1$  are given in [50]. For  $\xi^2 \ll 1$ , we have

$$\tau_0(\gamma, \xi) = \text{arcsinh } \gamma \quad (\text{A.5})$$

<sup>14)</sup>We omit here a constant factor; the easiest way to recover it is to compare the final result with the well-known expression (see [4, § 77, problem 2]) for the probability of ionization induced by a constant electric field.

$$+ \frac{1}{2\gamma} \left( 1 - \frac{\gamma}{\operatorname{arcsinh} \gamma} \right)^2 \xi^2 + \dots,$$

$$f(\gamma, \xi) = f(\gamma) + \xi^2 f_1(\gamma) + O(\xi^4), \quad (\text{A.6})$$

where  $f(\gamma)$  is the Keldysh function (3.14) and

$$f_1(\gamma) = \frac{1}{2\gamma} \left( 1 + \frac{\operatorname{arcsinh} \gamma}{\gamma} \right) - \frac{1}{\operatorname{arcsinh} \gamma}, \quad (\text{A.7})$$

so that  $f_1/f = \gamma^2/30$  for  $\gamma \ll 1$  and  $(2 \ln \gamma)^{-1}$  for  $\gamma \gg 1$ . It follows that, for a nearly linear polarization of light, the rate of level ionization is virtually independent of the ellipticity parameter  $\xi$ .

APPENDIX B

COMMENT ON THE ARTICLE  
“SEMICLASSICAL DIRAC THEORY  
OF TUNNEL IONIZATION” [62]

For the rate of ionization ( $w_r$ ) of the ground state of the hydrogen-like atom having a nuclear charge  $Z$  and occurring in constant crossed electric and magnetic fields, the authors of [62] presented the formula

$$w_r = \frac{(eF)^{1-2\varepsilon}}{2\sqrt{3}\xi\Gamma(2\varepsilon+1)} \quad (\text{B.1})$$

$$\times \sqrt{\frac{3-\xi^2}{3+\xi^2}} \left( \frac{4\xi^3(3-\xi^2)^2}{\sqrt{3}(1+\xi^2)} \right)^{2\varepsilon}$$

$$\times \exp\left( 6\mu \arcsin \frac{\xi}{\sqrt{3}} - \frac{2\sqrt{3}\xi^3}{eF(1+\xi^2)} \right)$$

(see Eq. (8) in [62a]). This equation was considered by the authors of [62] as the main result of their studies, which gives “for the first time a quantitative description of tunnel ionization of atomic ions” or “the first quantitative determination of tunneling in atomic ions in the relativistic regime” (the italics of the present author).

In connection with this claim, it is necessary to indicate the following. The above result is not new since it is completely contained in previous studies [40, 22, 23] performed (and published) much earlier. Moreover, the authors of [62] were aware of the results reported in [40, 22, 23]—they quoted these articles.

Let us consider this point in some detail. Equation (B.1) can be easily recast into the form

$$w_r = \frac{m_e c^2}{\hbar} C_\lambda^2 P \tilde{Q} \text{Exp}, \quad (\text{B.2})$$

where the exponential term Exp and the preexponential factor  $P$  coincide with the expressions obtained in [40, 22, 23]; that is,

$$\text{Exp} = \exp\left( -\frac{2\sqrt{3}\xi^3}{1+\xi^2} \frac{\mathcal{E}_{\text{cr}}}{\mathcal{E}} \right), \quad (\text{B.3})$$

$$P = \frac{1}{\xi} \sqrt{\frac{1-\xi^2/3}{3+\xi^2}} \frac{\mathcal{E}}{\mathcal{E}_{\text{cr}}}$$

{see, in particular, Eqs. (17), (35), and (50) in [23]}. In comparing these formulas with Eq. (B.1), it is necessary to take into account the following relationship between the notation in (B.1) and the notation in (B.3):

$$eF \equiv \mathcal{E}/F_{\text{cr}}, \quad F_{\text{cr}} \equiv \mathcal{E}_{\text{cr}} = 1/e, \quad \mu = Z\alpha = Z/137$$

(in relativistic units,  $\hbar = m = c = 1$ , where  $m$  is the electron mass). Here,  $\mathcal{E}$  is the electric-field strength,  $\mathcal{E}_{\text{cr}} = m_e^2 c^3 / e\hbar$  is the critical (Schwinger) field in QED [60, 61], and  $\xi$  is a convenient auxiliary variable that was introduced in [22]. This variable naturally arises in describing subbarrier motion within the imaginary-time method,

$$\xi = \left[ 1 - \frac{1}{2}\varepsilon \left( \sqrt{\varepsilon^2 + 8} - \varepsilon \right) \right]^{1/2}, \quad (\text{B.4})$$

where  $\varepsilon = E_0/m_e c^2$ ,  $E_0$  being the energy (including the electron rest mass) of the initial atomic state.

The factor  $\tilde{Q}$  in (B.2) results from taking into account the Coulomb interaction between the outgoing electron and the atomic core. It coincides with our factor<sup>15)</sup>  $Q$ ,

$$Q = \left[ \frac{2\xi^3(3-\xi^2)^2}{\sqrt{3}(1+\xi^2)} \frac{\mathcal{E}_{\text{cr}}}{\mathcal{E}} \right]^{2n} \quad (\text{B.5})$$

$$\times \exp\left( 6Z\alpha \arcsin \frac{\xi}{\sqrt{3}} \right),$$

$$\eta = Z\alpha\varepsilon/\sqrt{1-\varepsilon^2}, \quad \alpha = 1/137,$$

in the particular case of the  $1s_{1/2}$  level of the hydrogen-like atom, in which case we have

$$\varepsilon \equiv \eta = \sqrt{1-(Z\alpha)^2}, \quad \tilde{Q} \equiv Q. \quad (\text{B.6})$$

However, the expression for  $\tilde{Q}$  is applicable only under the condition that there is only one electron in the  $K$  shell of the atom, while all of the other electrons are stripped. Our formula (B.5) is much more general because it is applicable to atomic ions of an arbitrary degree of ionization if the parameters  $\varepsilon$  and  $C_\lambda^2$  are taken from independent calculations (for example, according to the Hartree–Fock–Dirac method) or directly from experimental data [compare with analogous formula (4.7) in the nonrelativistic theory of ionization].

<sup>15)</sup>This formula was derived in [23] in taking into account the Coulomb potential within semiclassical perturbation theory [11].

Further, the factor  $C_\lambda$  appearing in (B.2) is the asymptotic (for large distances from the nucleus) coefficient in the atomic wave function in the absence of external fields  $\mathcal{E}$  and  $\mathcal{H}$ . In [62], this factor was taken to be  $C_\lambda^2 = 2^{2\varepsilon-1}/\Gamma(2\varepsilon + 1)$ , which is obtained for the  $1s_{1/2}$  ground state in a purely Coulomb field and which can be found in any textbook on quantum mechanics (see, for example, [34, 75, 76]). In general, however, the coefficient  $C_\lambda$  is not expressed in terms of the energy of the state and must be determined on the basis of an independent calculation.

The majority of the formulas presented in [62], including the so-called main result (B.1), literally reproduce, in the same notation,<sup>16)</sup> the corresponding formulas from [22, 23]. The novel contribution of the authors of [62] reduces to the multiplication of the factors  $\text{Exp}$ ,  $Q$ , and  $P$ , which were obtained earlier in [22, 23, 40]. It should be emphasized that Eq. (B.1), which arises upon the application of this operation, is not physically meaningful since it does not include the spin factor  $S_\pm$  {see Eqs. (18) and (18') in [24]} associated with the spin correction that the action functional (7.12) develops in the course of the subbarrier motion of the electron. Although the phrase “Dirac theory of tunnel ionization” is present in the titles of the articles quoted in [62], the Dirac equation is not used there as a matter of fact. As can be seen from Eqs. (1), (2), and (5) in [62a], the authors of those studies assume that the bispinor  $\hat{S}$  determining the electron polarization does not change in the course of subbarrier motion—that is, they disregard spin-orbit interaction. For this reason, there is no spin factor in [62]; one should include this factor in Eq. (B.1) for this equation to describe the tunneling of a relativistic electron.

The relativistic generalization of Keldysh’s ionization theory, proposed in [41], was first considered by Nikishov and Ritus [40] for a scalar particle (without allowance for spin). In the case of constant crossed fields, the probability  $w_r$  of ionization of the  $s$  level bound by short-range forces ( $Z = 0$ ,  $Q \equiv 1$ ) was calculated in [40]. The expression obtained in [40] for  $w_r$  coincides with the results presented in [22, 23], but it is written in a different form.

The authors of [62] were aware of our studies, quoting [11], but they interpret them as “an analytical solution of the Klein–Gordon equation for  $\pi^-$  atoms in static electric and magnetic fields” [62]. In fact, no mention of  $\pi^-$  atoms was made in [22, 23]. On the contrary, it was repeatedly emphasized in [22, 23] that the objective there was to generalize the

<sup>16)</sup>For example, use is made of the variable  $\xi$  [see (B.4)] instead of the reduced energy  $\varepsilon$ .

imaginary-time method to the case of the relativistic subbarrier motion of an electron and to apply it to the theory of ionization of deep levels, including those of the  $K$  shell in heavy atoms. In order to implement experimentally ionization of  $\pi^-$  atoms, the field strength  $\mathcal{E}$  should be increased by five orders of magnitude because  $\mathcal{E}_{\text{cr}} \sim m^2$  [see Eq. (6.8) above]. Accordingly, the intensity  $J$  of laser radiation must reach fantastic values of  $J \gtrsim 10^{32}$  W/cm<sup>2</sup>, which can hardly be achievable in principle because the intensive production of  $e^+e^-$  pairs from a vacuum would screen the external field.

Apart from the results for crossed fields, formulas of the relativistic theory of ionization in a constant electric field ( $\mathcal{H} = 0$ ) are given in [62b], which were borrowed from [23] without giving appropriate references. For example, Eq. (35) in [62b] is equivalent to Eqs. (6) and (32) from [23].

Thus, the articles quoted in [62] are a mere compilation of results that were published much earlier [22, 23, 77] and which were well known to the authors of [62]. The articles in question [62] should not have been published in such journals as *Physical Review Letters* and *Journal of Physics*—there exist journals of a different kind for this. In any case, it was necessary to indicate that the formulas given there are not novel and that they were obtained by other authors rather than claiming that they were obtained “for the first time.”

Considering this situation as a flagrant violation of basic principles of scientific ethics, we decided to call the attention of the physics community to this fact.

I am grateful to S.V. Bulanov, M.I. Vysotsky, L.V. Keldysh, N.B. Narozhny, L.B. Okun, and Yu.A. Simonov for the discussion of this situation, valuable advice, and encouragement (arXiv: quant-ph/0405158 v1 26 May 2004).

*Note added in proof:* Some aspects of the imaginary-time method (including the spin correction to the tunneling probability, the calculation of the momentum spectrum of photoelectrons, and the limiting transition from the formulas given in Section 6 to nonrelativistic Keldysh’s theory) are only outlined in the present articles. For further details, the interested reader is referred to [78].

## REFERENCES

1. L. D. Landau, *Phys. Z. Sowjetunion* **1**, 88 (1932); **2**, 46 (1932); *Collected Works* (Nauka, Moscow, 1969), Vol. 1.
2. E. M. Lifshits, *Zh. Éksp. Teor. Fiz.* **8**, 930 (1938).
3. E. E. Nikitin and L. P. Pitaevskii, *Usp. Fiz. Nauk* **163** (9), 101 (1993) [*Phys.–Usp.* **36** (9), 851 (1993)].

4. L. D. Landau and E. M. Lifshits, *Quantum Mechanics: Non-Relativistic Theory* (Nauka, Moscow, 1974; Pergamon, Oxford, 1977).
5. A. M. Dykhne, Zh. Éksp. Teor. Fiz. **38**, 570 (1960) [Sov. Phys. JETP **11**, 411 (1960)]; **41**, 1324 (1961) [**14**, 941 (1961)].
6. N. B. Delone and V. P. Kraĭnov, *Atom in a Strong Light Field* (Energoatomizdat, Moscow, 1984).
7. R. P. Feynman, Rev. Mod. Phys. **20**, 367 (1948).
8. R. P. Feynman and A. R. Hibbs, *Quantum Mechanics and Path Integrals* (McGraw-Hill, New York, 1965; Mir, Moscow, 1968).
9. A. M. Perelomov, V. S. Popov, and M. V. Terent'ev, Zh. Éksp. Teor. Fiz. **50**, 1393 (1966) [Sov. Phys. JETP **23**, 924 (1966)]; **51**, 309 (1966) [**24**, 207 (1966)].
10. V. S. Popov, V. P. Kuznetsov, and A. M. Perelomov, Zh. Éksp. Teor. Fiz. **53**, 331 (1967) [Sov. Phys. JETP **26**, 222 (1967)].
11. A. M. Perelomov and V. S. Popov, Zh. Éksp. Teor. Fiz. **52**, 514 (1967) [Sov. Phys. JETP **25**, 336 (1967)].
12. L. P. Kotova, A. M. Perelomov, and V. S. Popov, Zh. Éksp. Teor. Fiz. **54**, 1151 (1968) [Sov. Phys. JETP **27**, 616 (1968)].
13. V. S. Popov, Pis'ma Zh. Éksp. Teor. Fiz. **13**, 261 (1971) [JETP Lett. **13**, 185 (1971)]; Zh. Éksp. Teor. Fiz. **61**, 1334 (1971) [Sov. Phys. JETP **34**, 709 (1971)].
14. V. S. Popov, Pis'ma Zh. Éksp. Teor. Fiz. **18**, 435 (1973) [JETP Lett. **18**, 255 (1973)]; Yad. Fiz. **19**, 1140 (1974) [Sov. J. Nucl. Phys. **19**, 584 (1974)].
15. M. S. Marinov and V. S. Popov, Yad. Fiz. **15**, 1271 (1972) [Sov. J. Nucl. Phys. **15**, 702 (1972)]; **16**, 809 (1972) [**16**, 449 (1972)].
16. M. S. Marinov and V. S. Popov, Fortschr. Phys. **25**, 373 (1977).
17. V. S. Popov, B. M. Karnakov, and V. D. Mur, Zh. Éksp. Teor. Fiz. **113**, 1579 (1998) [JETP **86**, 860 (1998)].
18. V. S. Popov, A. V. Sergeev, and A. V. Shcheblykin, Zh. Éksp. Teor. Fiz. **102**, 1453 (1992) [Sov. Phys. JETP **75**, 787 (1992)].
19. V. S. Popov and A. V. Sergeev, Phys. Lett. A **172**, 193 (1993); **193**, 165 (1994); Zh. Éksp. Teor. Fiz. **105**, 568 (1994) [JETP **78**, 303 (1994)].
20. V. S. Popov, in *New Methods in Quantum Theory*, Ed. by C. A. Tsipis *et al.* (Kluwer Acad. Publ., Dordrecht, 1996), p. 149.
21. V. S. Popov and A. V. Sergeev, Pis'ma Zh. Éksp. Teor. Fiz. **63**, 398 (1996) [JETP Lett. **63**, 417 (1996)]; Zh. Éksp. Teor. Fiz. **113**, 2047 (1998) [JETP **86**, 1122 (1998)].
22. V. S. Popov, V. D. Mur, and B. M. Karnakov, Pis'ma Zh. Éksp. Teor. Fiz. **66**, 213 (1997) [JETP Lett. **66**, 229 (1997)]; Phys. Lett. A **250**, 20 (1998).
23. V. D. Mur, B. M. Karnakov, and V. S. Popov, Zh. Éksp. Teor. Fiz. **114**, 798 (1998) [JETP **87**, 433 (1998)].
24. V. S. Popov, B. M. Karnakov, and V. D. Mur, Pis'ma Zh. Éksp. Teor. Fiz. **79**, 320 (2004) [JETP Lett. **79**, 262 (2004)].
25. B. M. Karnakov, V. D. Mur, and V. S. Popov, quant-ph/0405158 v1.
26. V. S. Popov, B. M. Karnakov, and V. D. Mur, Phys. Lett. A **229**, 306 (1997); Zh. Éksp. Teor. Fiz. **113**, 1579 (1998) [JETP **86**, 860 (1998)].
27. J. Heading, *An Introduction to Phase-Integral Methods* (Methuen, London, 1962; Mir, Moscow, 1965).
28. N. Fröman and P. O. Fröman, *JWKB Approximation* (North-Holland, Amsterdam, 1965; Mir, Moscow, 1967).
29. L. I. Ponomarev, *Lectures on the Semiclassical Approximation*, Preprint ITF Akad. Nauk USSR (Inst. Theor. Phys., Kiev, 1967).
30. A. I. Baz', Ya. B. Zel'dovich, and A. M. Perelomov, *Scattering, Reactions and Decays in Nonrelativistic Quantum Mechanics* (Nauka, Moscow, 1971), Chap. 5.
31. M. V. Berry and K. E. Mount, Rep. Prog. Phys. **35**, 315 (1972).
32. A. B. Migdal, *Qualitative Methods in Quantum Theory* (Nauka, Moscow, 1975; Benjamin, Reading, Mass., 1977).
33. V. P. Maslov and M. V. Fedoryuk, *Semi-Classical Approximation in Quantum Mechanics* (Nauka, Moscow, 1976; Reidel, Dordrecht, 1981).
34. V. M. Galitsky, B. M. Karnakov, and V. I. Kogan, *Problems in Quantum Mechanics* (Nauka, Moscow, 1992), Chap. 9 [in Russian].
35. B. M. Karnakov, V. D. Mur, and V. S. Popov, Yad. Fiz. **64**, 729 (2001) [Phys. At. Nucl. **64**, 670 (2001)].
36. V. S. Popov, V. P. Kuznetsov, and A. M. Perelomov, Preprint No. 517, ITEF (Inst. Theor. and Exp. Phys., Moscow, 1967).
37. V. S. Popov, Doctoral Dissertation in Mathematics and Physics (Inst. of Theor. and Exp. Phys., Moscow, 1974).
38. L. D. Landau and E. M. Lifshitz, *Mechanics* (Fizmatlit, Moscow, 2001; Pergamon, Oxford, 1976).
39. E. T. Whittaker, *A Treatise on the Analytical Dynamics of Particles and Rigid Bodies* (Univ. Press, Cambridge, 1927; ONTI, Moscow, 1937).
40. A. I. Nikishov and V. I. Ritus, Zh. Éksp. Teor. Fiz. **50**, 255 (1966) [Sov. Phys. JETP **23**, 168 (1966)].
41. L. V. Keldysh, Zh. Éksp. Teor. Fiz. **47**, 1965 (1964) [Sov. Phys. JETP **20**, 1320 (1964)].
42. N. B. Delone and V. P. Kraĭnov, J. Opt. Soc. Am. B **8**, 1207 (1991); V. P. Kraĭnov, J. Opt. Soc. Am. B **14**, 425 (1997).
43. V. P. Kraĭnov, W. Xiong, and S. L. Chin, Laser Phys. **2**, 467 (1992).
44. V. P. Kraĭnov and V. M. Ristich, Zh. Éksp. Teor. Fiz. **101**, 1479 (1992) [Sov. Phys. JETP **74**, 789 (1992)].
45. N. B. Delone and V. P. Kraĭnov, Usp. Fiz. Nauk **168**, 531 (1998) [Phys. Usp. **41**, 469 (1998)].

46. M. V. Ammosov, N. B. Delone, and V. P. Krařnov, Zh. Ėksp. Teor. Fiz. **91**, 2008 (1986)[Sov. Phys. JETP **64**, 1191 (1986)].
47. N. B. Delone and V. P. Krařnov, *Nonlinear Atom Ionization Induced by Laser Radiation* (Fizmatlit, Moscow, 2001)[in Russian].
48. V. S. Popov, Usp. Fiz. Nauk **169**, 819 (1999) [Phys. Usp. **42**, 733 (1999)].
49. Yu. N. Demkov and G. F. Drukarev, Zh. Ėksp. Teor. Fiz. **47**, 918 (1964)[Sov. Phys. JETP **20**, 614 (1964)].
50. V. D. Mur, S. V. Popruzhenko, and V. S. Popov, Zh. Ėksp. Teor. Fiz. **119**, 903 (2001) [JETP **92**, 777 (2001)].
51. S. P. Goreslavskiř and S. V. Popruzhenko, Zh. Ėksp. Teor. Fiz. **110**, 1200 (1996) [JETP **83**, 661 (1996)]; Laser Phys. **6**, 780 (1996); **7**, 100 (1997).
52. A. D. Sakharov, R. Z. Lyudaev, E. N. Smirnov, *et al.*, Dokl. Akad. Nauk SSSR **165**, 65 (1965)[Sov. Phys.—Dokl. **10**, 1045 (1965)].
53. A. D. Sakharov, Usp. Fiz. Nauk **88**, 725 (1966) [Sov. Phys.—Usp. **9**, 294 (1966)].
54. L. Keldysh, Multiphoton ionization by a very short laser pulse (private communication).
55. V. S. Popov, Laser Phys. **10**, 1033 (2000); Pis'ma Zh. Ėksp. Teor. Fiz. **73**, 3 (2001) [JETP Lett. **73**, 1 (2001)]; Zh. Ėksp. Teor. Fiz. **120**, 315 (2001) [JETP **93**, 278 (2001)].
56. T. Tajima and G. Mourou, Phys. Rev. ST Accel. Beams **5**, 031301 (2002).
57. M. Lopez-Cabrera, D. Z. Goodson, D. R. Herschbach, and J. D. Morgan, Phys. Rev. Lett. **68**, 1992 (1992).
58. D. M. Volkov, Z. Phys. **84**, 250 (1935); Zh. Ėksp. Teor. Fiz. **7**, 1286 (1937).
59. L. D. Landau and E. M. Lifshitz, *The Classical Theory of Fields* (Fizmatlit, Moscow, 2003; Pergamon, Oxford, 1975).
60. W. Heisenberg and H. Euler, Z. Phys. **98**, 714 (1936).
61. J. Schwinger, Phys. Rev. **82**, 664 (1951).
62. (a) N. Milosevic, V. P. Krainov, and T. Brabec, Phys. Rev. Lett. **89**, 193001 (2002); (b) J. Phys. B **35**, 3515 (2002).
63. E. Brezin and C. Itzykson, Phys. Rev. D **2**, 1191 (1970).
64. N. B. Narozhnyiř and A. I. Nikishov, Zh. Ėksp. Teor. Fiz. **65**, 862 (1973)[Sov. Phys. JETP **38**, 427 (1974)].
65. A. Ringwald, Phys. Lett. B **510**, 107 (2001).
66. V. S. Popov, Pis'ma Zh. Ėksp. Teor. Fiz. **74**, 151 (2001) [JETP Lett. **74**, 133 (2001)]; Zh. Ėksp. Teor. Fiz. **121**, 1235 (2002) [JETP **94**, 1057 (2002)]; Phys. Lett. A **298**, 83 (2002).
67. A. I. Nikishov, Nucl. Phys. B **21**, 346 (1970); N. B. Narozhnyiř and A. I. Nikishov, Yad. Fiz. **11**, 1072 (1970) [Sov. J. Nucl. Phys. **11**, 596 (1970)].
68. S. S. Bulanov, Phys. Rev. E **69**, 03460 (2004).
69. V. S. Vanyashin and M. V. Terent'ev, Zh. Ėksp. Teor. Fiz. **48**, 565 (1965)[Sov. Phys. JETP **21**, 375 (1965)].
70. V. Bargmann, L. Michel, and V. L. Telegdi, Phys. Rev. Lett. **2**, 435 (1959).
71. F. Sauter, Z. Phys. **69**, 742 (1931).
72. I. B. Khriplovich, Yad. Fiz. **65**, 1292 (2002) [Phys. At. Nucl. **65**, 1259 (2002)].
73. R. Rajaraman, *Solitons and Instantons* (North-Holland, Amsterdam, 1982; Mir, Moscow, 1985).
74. V. A. Rubakov, *Classical Gauge Fields* (Editorial URSS, Moscow, 1999)[in Russian].
75. A. I. Akhiezer and V. B. Berestetskii, *Quantum Electrodynamics* (Nauka, Moscow, 1979; Wiley, New York, 1965)
76. L. I. Schiff, *Quantum Mechanics* (McGraw-Hill, New York, 1955; Inostrannaya Literatura, Moscow, 1957).
77. B. M. Karnakov, V. D. Mur, and V. S. Popov, Yad. Fiz. **62**, 1444 (1999) [Phys. At. Nucl. **62**, 1363 (1999)].
78. V. S. Popov, Preprints Nos. 10-04, 13-04, ITĖF (Inst. Theor. and Exp. Phys., Moscow, 2004).

*Translated by A. Isaakyan*

# The Matrix Hamiltonian for Hadrons and the Role of Negative-Energy Components\*

Yu. A. Simonov\*\*

*Institute of Theoretical and Experimental Physics,  
Bol'shaya Cheremushkinskaya ul. 25, Moscow, 117259 Russia*

Received July 1, 2004

**Abstract**—The world-line (Fock–Feynman–Schwinger) representation is used for quarks in an arbitrary (vacuum and valence gluon) field to construct the relativistic Hamiltonian. After averaging the Green's function of the white  $q\bar{q}$  system over gluon fields, one obtains the relativistic Hamiltonian, which is a matrix in spin indices and contains both positive and negative quark energies. The role of the latter is studied using the example of the heavy-light meson and the standard einbein technique is extended to the case of the matrix Hamiltonian. Comparison with the Dirac equation shows good agreement of the results. For an arbitrary  $q\bar{q}$  system, the nondiagonal matrix Hamiltonian components are calculated through hyperfine interaction terms. A general discussion of the role of negative-energy components is given in conclusion.

© 2005 Pleiades Publishing, Inc.

## 1. INTRODUCTION

The quest for the Hamiltonian which contains the main features of QCD confinement and chiral symmetry breaking (CSB) has existed from the very beginning, when fundamental field-theoretical (FTh) QCD Hamiltonians were constructed in different gauges [1]. Unfortunately, (nonlocal) confinement cannot be seen in these local FTh Hamiltonians and for practical purposes another sort of Hamiltonians, effective Hamiltonians (EH), have been modeled, containing minimal relativity and string-type potentials [2]. A lot of information was obtained from these Hamiltonians, and the general agreement of calculated meson and baryon masses with experiment is impressive [3], with some exceptions for mesons (e.g., pions, scalar nonets, etc.) and for baryons (the Roper resonance and its companions,  $\Lambda(1405)$ , etc.).

The two main defects of effective Hamiltonians are the following:

(i) The clear-cut derivation from the basic QCD Lagrangian was absent and, therefore, it is not clear what are approximations and how to improve EH systematically.

(ii) Connected to that, the EH contains a large number of parameters in addition to the minimal QCD number: current quark masses and string tension (or  $\Lambda_{\text{QCD}}$ ). Typically, this additional number of parameters is more than ten for a detailed spectrum

calculation. The most important for hadron masses are constituent quark masses  $m_i$  and the overall negative constant  $C_0$  of the order of several hundred MeV.

With this number of arbitrary parameters, the QCD dynamics in hadrons cannot be fully understood and one needs another approach. This approach [it will be called the QCD string approach (SA)] was suggested more than a decade ago [4], where the SA Hamiltonian for spinless quarks was derived and Regge trajectories have been obtained for mesons [4], baryons [5], and glueballs [6]. Later on, the formalism was put on a more rigorous basis in [7] and the einbein technique [8] was used in [7] to take into account the string moment of inertia and to obtain the correct Regge slope. In [4–7], the constituent mass was defined using the einbein technique through the string tension and current quark mass; the subsequent calculation of baryon magnetic moments [9] has confirmed the validity of this approach.

Another mysterious problem—of large negative constant  $C_0$ —was understood recently in the framework of the same QCD SA and  $C_0$  was identified with the large quark self-energy term [10]. The latter is calculated through the string tension and quark current masses again without introduction of new parameters.

The spin-dependent (SD) part of the SA Hamiltonian was calculated earlier [11]. It was shown that, even for light quarks, one can calculate the leading SD terms without recurring to the  $1/M$  expansion, but using instead the lowest (quadratic) field-correlator approximation [12], which works with an accuracy of a few percent [13].

\*This article was submitted by the author in English.

\*\*E-mail: [simonov@heron.itep.ru](mailto:simonov@heron.itep.ru)

The final form of the SA Hamiltonian was used to calculate the masses of light mesons [14, 15], heavy quarkonia [16–18], heavy-light mesons [19–21], baryons [22–24], glueballs [6, 25, 26], hybrids [27–30], and gluelumps [31]; for a review, see also [32–34]. It is remarkable that, in most cases, the agreement with known experimental data and lattice data is good; however, only the minimal QCD set of parameters was used with addition of standard  $\alpha_s(Q^2)$ .

The most important exception in mesons from the agreement above was for pseudoscalars ( $\pi, K, \eta, \eta'$ ), which need the chiral dynamics, absent in the SA Hamiltonian. To overcome this discrepancy, it was realized in [35–37] that the chiral dynamics brings a new tadpole term, which should be accounted for in computation of the Nambu–Goldstone spectrum. As a result, the Gell-Mann–Oakes–Renner relation was found in [35, 36] and the quark condensate was computed [37] in terms of the SA Hamiltonian spectrum.

This connection allows to calculate the spectrum of Nambu–Goldstone mesons and their radial excitations in terms of the SA Hamiltonian spectrum, without introducing new parameters.

So far so good, but to proceed further, one should look carefully into the approximations done and understand how to improve the SA Hamiltonian systematically.

The systematic procedure of the derivation of the SA Hamiltonian is given in [4–7] and discussed later in [38–40]. It contains three typical approximations:

(i) Replacement of the Wilson loop by the minimal area expression and neglect of gluon excitation, which amounts to the neglect of mixing of a given hadron with all its hybrid excitations. As was shown in [41], the effect of mixing is indeed small, except for the cases of states almost degenerate in mass.

(ii) The use of the local Hamiltonian, which appears in the limit of small gluon correlation length  $\lambda$  (denoted as  $T_g$  in most previous publications). Since  $\lambda \cong 0.2$  fm and is much smaller than typical hadron sizes, this limit is legitimate.

(iii) The use of only the positive solution for the stationary point equations in the einbein variable, corresponding to the positive constituent quark mass. This latter approximation means neglect of the quark negative-energy states, and it is the main point of the present investigation. As a result, we shall obtain the Hamiltonian containing both positive- and negative-energy quark components and estimate quantitatively the importance of the latter.

The paper is organized as follows. In Section 2, we derive the Green's function for the  $q\bar{q}$  system and consider in Section 3 the one-body self-energy corrections for the quark and antiquark. Having fixed

that, we turn in Section 4 to the heavy-light  $q\bar{q}$  interaction and derive the corresponding  $q\bar{q}$  Hamiltonian in the full relativistic form, containing negative-energy components (NEC), and compare numerical results of the matrix Hamiltonian with those for the Dirac equation. In Section 5, the effects of NEC are derived for the general  $q\bar{q}$  system. The last section is devoted to conclusions and outlook. Appendix I is devoted to the derivation of the path integral form of the Fock–Feynman–Schwinger representation (FFSR) type, in particular, a novel first-order form of FFSR is obtained for one particle in an external non-Abelian field using the Weyl representation for  $\gamma$  matrices. Appendix 2 contains details of the self-energy correction.

## 2. THE QUARK–ANTIQUARK GREEN'S FUNCTION

We recapitulate here the steps done in derivation of the SA Hamiltonian [4, 7, 32].

One starts with the FFSR for the quark (or valence gluon) Green's function in the Euclidean external gluonic fields [34, 41], which is exact and does not contain any approximation:

$$\begin{aligned} S(x, y) &= (m + \hat{D})^{-1} \quad (1) \\ &= (m - \hat{D}) \int_0^\infty ds (Dz)_{xy} e^{-K} P_A \\ &\times \exp \left( ig \int_y^x A_\mu dz_\mu \right) P_\sigma(x, y, s), \end{aligned}$$

where  $K$  is the kinetic-energy term,

$$K = m^2 s + \frac{1}{4} \int_0^s d\tau \left( \frac{dz_\mu(\tau)}{d\tau} \right)^2, \quad (2)$$

and  $m$  is the pole mass of quark, with  $z_\mu(\tau)$  being the quark trajectory with end points  $x$  and  $y$  integrated over  $(Dz)_{xy}$ .

The factor  $P_\sigma(x, y, s)$  in (1) is generated by the quark spin (color-magnetic moment) and is equal to

$$P_\sigma(x, y, s) = P_F \exp \left[ g \int_0^s \sigma_{\mu\nu} F_{\mu\nu}(z(\tau)) d\tau \right], \quad (3)$$

where  $\sigma_{\mu\nu} = \frac{1}{4i}(\gamma_\mu\gamma_\nu - \gamma_\nu\gamma_\mu)$ , and  $P_F$  and  $P_A$  in (3) and (1), respectively, are ordering operators of matrices  $F_{\mu\nu}(A_\mu)$  along the path  $z_\mu(\tau)$ . In what follows,

the role of the operator  $P_\sigma(x, y, s)$  will be crucial, and it is convenient to rewrite  $\sigma_{\mu\nu}F_{\mu\nu}$  in  $2 \times 2$  notation:

$$\sigma_{\mu\nu}F_{\mu\nu} = \begin{pmatrix} \boldsymbol{\sigma} \cdot \mathbf{B} & \boldsymbol{\sigma} \cdot \mathbf{E} \\ \boldsymbol{\sigma} \cdot \mathbf{E} & \boldsymbol{\sigma} \cdot \mathbf{B} \end{pmatrix}, \quad (4)$$

where  $\boldsymbol{\sigma}$  are usual Pauli matrices.

The next step is the FFSR for the hadron Green's function, which for the case of the  $q\bar{q}$  meson is

$$G_{q\bar{q}}(x, y; A) = \int_0^\infty ds \int_0^\infty ds' (Dz)_{xy} (Dz')_{xy} \quad (5)$$

$$\times e^{-K-K'} \text{tr}(\Gamma(m - \hat{D})W_\sigma(x, y)\bar{\Gamma}(m' - \hat{D}')),$$

where  $\Gamma$  and  $\bar{\Gamma} = \Gamma^+$  are 1,  $\gamma_\mu, \gamma_5, (\gamma_\mu\gamma_5), \dots$ , "tr" means trace operation in both Dirac and color indices, and

$$W_\sigma(x, y) = P_A \exp \left( ig \int_{C(x,y)} A_\mu dz_\mu \right) \quad (6)$$

$$\times P_\sigma(x, y, s)P'_\sigma(x, y, s').$$

In (6), the closed contour  $C(x, y)$  is along trajectories of quark  $z_\mu(\tau)$  and antiquark  $z'_\nu(\tau')$ , and the ordering  $P_A$  and  $P_F$  in  $P_\sigma, P'_\sigma$  is universal; i.e.,  $W_\sigma(x, y)$  is the Wegner–Wilson loop with insertion of operators (4) along the contour  $C(x, y)$  at the proper places.

The FFSR Eq. (5) is exact and is a functional of gluonic fields  $A_\mu, F_{\mu\nu}$ , which contain both perturbative and nonperturbative contributions, not specified at this level.

The next step, containing an important approximation, is the averaging over gluonic fields, which yields the physical  $q\bar{q}$  Green's function  $G_{q\bar{q}}$ :

$$G_{q\bar{q}}(x, y) = \langle G_{q\bar{q}}(x, y; A) \rangle_A. \quad (7)$$

Here, the averaging is done with the usual Euclidean weight  $\exp(-\text{action})$ , containing all gauge-fixing, ghost terms; the exact form is inessential for what follows. To proceed, it is convenient to use the non-Abelian Stokes theorem [42] for the first factor on the right-hand side in (6) and to rewrite the average of (6) as

$$\langle W_\sigma(x, y) \rangle = \left\langle \exp \left[ ig \int d\pi_{\mu\nu}(z) F_{\mu\nu}(z) \right] \right\rangle \quad (8)$$

$$= \exp \left[ \sum_{n=1}^\infty \frac{(ig)^n}{n!} \int d\pi(1) \dots \int d\pi(n) \right.$$

$$\left. \times \langle \langle F(1) \dots F(n) \rangle \rangle \right],$$

where

$$d\pi_{\mu\nu}(z) = ds_{\mu\nu}(z) - i\sigma_{\mu\nu}d\tau \quad (9)$$

and  $ds_{\mu\nu}$  is the surface element. In (8), we have used the cluster expansion theorem and omitted indices of  $d\pi(k)$  and  $F(k)$ , implying  $d\pi(k) \equiv d\pi_{\mu_k\nu_k}(z) = ds_{\mu_k\nu_k}(u_k) - i\sigma_{\mu_k\nu_k}d\tau_k$  and  $F(k) \equiv F_{\mu_k\nu_k}(u_k, x_0) \equiv \Phi(x_0, u_k)F_{\mu_k\nu_k}(k)\Phi(u_k, x_0)$ , where

$$\Phi(x, y) = P \exp \left( ig \int_y^x A_\mu dz_\mu \right).$$

Equation (8) is exact and, therefore, the right-hand side does not depend on the choice of the surface, which is integrated over  $ds_{\mu\nu}(z)$ . To proceed, one makes at this point an approximation, keeping only lowest (quadratic) field correlator  $\langle \langle F(i)F(k) \rangle \rangle$ , while the surface is chosen to be the minimal area surface. As was argued in [13], using a comparison with lattice data, this approximation (sometimes called the Gaussian approximation) has an accuracy of a few percent. The factors  $(m - \hat{D})$  and  $(m' - \hat{D}')$  in (5) need special treatment in the process of averaging in (7), and, as shown in Appendix 1 of [19], one can use a simple replacement,

$$m - \hat{D} \rightarrow m - i\hat{p}, \quad p_\mu = \frac{1}{2} \left( \frac{dz_\mu}{d\tau} \right)_{\tau=s}. \quad (10)$$

With the insertion of the cluster expansion (8) and the operator  $(m - \hat{D})$  from Eq. (10) into the general expressions (5), (7), one fulfills the first step: the derivation of the physical  $q\bar{q}$  Green's function in terms of vacuum correlators  $\langle \langle F(1) \dots F(n) \rangle \rangle$ . At this point, it is important to discuss the separation of one-body (self-energy) and two-body terms in the interaction kernel (8), together with the separation of perturbative and nonperturbative contributions.

### 3. QUARK SELF-ENERGY IN THE CONFINING BACKGROUND

It is clear that, on physical grounds, it is difficult to separate out the one-body (self-energy) contributions for the quark connected by the string to the antiquark. The situation here is different in the confining QCD from the nonconfining QED, since in the latter an electron can be isolated and its self-energy is part of the renormalized electron mass operator. For a bound electron in an atom, the one- and two-body contributions to the interaction kernel can be separated in each order in  $\alpha^n$ , as is done, e.g., in the Bethe–Salpeter equation.

In the case of QCD, confinement cannot be excluded in any order of perturbative gluon exchanges

and the separation seems to be impossible in principle. Nevertheless, the world-line or FFSR (1), (5), (7) suggests a possible way of separating out the one-body contributions. It is based on distinguishing the perimeter ( $L$ ) law and area ( $S_{\min}$ ) law terms in the Wegner–Wilson loop,

$$\langle W(C) \rangle = \text{const} \cdot \exp(-C_1 L - C_2 S_{\min}), \quad (11)$$

where the one-body terms are associated with the coefficient  $C_1$ , while the two-body terms are associated with  $C_2$ . Going over from the Wegner–Wilson loop to the  $q\bar{q}$  Green's function and the  $q\bar{q}$  Hamiltonian, the situation, however, becomes more complicated, since  $\langle G_{q\bar{q}} \rangle$  is an integral over all Wegner–Wilson loops, and typical loops ( $q\bar{q}$  trajectories) have a finite average  $q\bar{q}$  separation  $\langle r \rangle$  and the same time length  $T$ , so that both perimeter and area law terms contribute terms proportional to  $T$ . At this point the FFSR is helpful, since it allows one to separate the Lorentz-invariant self-energy (SE) terms,  $\Delta m^2$ , which contribute to the Hamiltonian (see below and in [10]) as  $\Delta m^2/(2\omega)$ , where  $2\omega = dt/ds$ ,  $t$  being the physical time and  $s$ , as in (1), being the proper time. One can see that the SE terms are multiplied by the effective length of trajectory indeed,

$$\Delta H dt = \frac{\Delta m^2}{2\omega} dt \sim \Delta m^2 ds.$$

At the same time, the two-body terms in the Hamiltonian are proportional to  $\omega$  (see below and [10, 32]).

To calculate the SE terms explicitly, we shall use background perturbation theory [43, 44] with the separation of nonperturbative background field  $B_\mu$  and valence (perturbative) gluon field  $a_\mu$ , so that the total vector potential  $A_\mu$  can be written as

$$A_\mu = B_\mu + a_\mu. \quad (12)$$

The method [44] assumes the perturbative expansion in powers of  $ga_\mu$ , while  $B_\mu$  enters via nonperturbative field correlators known from lattice [45] or analytic [31] calculations. Accordingly, we separate the contributions to the quark SE (we prefer to use  $m^2$  instead of  $m$ , since  $m^2$  appears in the Hamiltonian both in the FFSR technique and after Foldy–Wouthuizen diagonalization of the Dirac operators):

$$m^2(\mu) = m_{\text{pert}}^2(\mu) + \Delta m_{\text{np}}^2(\mu) + m_{\text{int}}^2. \quad (13)$$

Here,  $m_{\text{pert}}^2(\mu)$  is the pole mass and its connection to the  $\overline{MS}$  mass is known to two loops (for a detailed discussion, see the book [46]),

$$m_{\text{pert}}^{(\text{pole})}(\mu) = \bar{m}(\bar{m}^2) \quad (14)$$

$$\times \left\{ 1 + \frac{C_F}{\pi} \alpha_s(m^{\text{pole}}) + O(\alpha_s^2) \right\},$$

while the basic nonperturbative term  $m_{\text{np}}^2$  was found in [10] (below, we shall find a correction to this term), and the mixed perturbative–nonperturbative contribution  $m_{\text{int}}^2$  is yet to be calculated. We stress that  $m^2(\mu)$  can be found in a gauge-invariant form only when it is computed inside the gauge-invariant  $q\bar{q}$  or  $3q$  Green's function, and in principle it may depend on the system where the quark is imbedded.

Since we are mostly interested in the case of light quarks, the perturbative mass evolution is small and unimportant, and the main term appears to be  $\Delta m_{\text{np}}^2$ , which we consider now.

Following [10], we consider the quadratic in  $(\sigma F)$  term in (8) and expand the exponent to make explicit the resulting SE term (which is exponentiated after all, yielding an additive contribution to the Hamiltonian). One has

$$\langle W_{\sigma\sigma'}(x, y) \rangle \cong \left\langle \left( 1 + \frac{g^2}{2} \sigma_{\mu\nu} \sigma_{\rho\lambda} \int_0^s d\tau \right. \right. \quad (15)$$

$$\left. \left. \times \int_0^s d\tau' F_{\mu\nu}(z(\tau)) F_{\rho\lambda}(z(\tau')) \right) W_0 + \dots \right\rangle,$$

where we have neglected the term proportional to  $ds_{\mu\nu} ds_{\lambda\rho}$ , since it contributes to the  $q\bar{q}$  potential, accounted for in the Hamiltonian, and not one-body SE terms; also, the mixed terms ( $\sim ds_{\mu\nu} \sigma_{\lambda\rho}$ ) contribute to the spin–orbit potentials, also taken into account in the Hamiltonian [11]. Here,  $W_0$  is the usual Wegner–Wilson loop without  $(\sigma F)$  operators. The vacuum averaging in (15) yields in the Gaussian approximation (see Appendix of the first paper in [11])

$$\langle F_{\mu\nu} F_{\rho\lambda} W_0 \rangle = \left\{ \left[ \langle F_{\mu\nu} F_{\rho\lambda} \rangle - g^2 \right. \right. \quad (16)$$

$$\left. \left. \times \int ds_{\alpha\beta} \langle F_{\mu\nu} F_{\alpha\beta} \rangle \int ds_{\gamma\delta} \langle F_{\rho\lambda} F_{\gamma\delta} \rangle \right] \langle W_0 \rangle \right\}.$$

Introducing scalar functions  $D$  and  $D_1$ , as in [12] (we omit for simplicity parallel transporters  $\Phi(u, v)$ ),

$$g^2 \langle F_{\mu\nu}(n) F_{\rho\lambda}(v) \rangle \quad (17)$$

$$= \hat{1} \left\{ (\delta_{\mu\rho} \delta_{\nu\lambda} - \delta_{\mu\lambda} \delta_{\nu\rho}) D(u - v) \right.$$

$$+ \frac{1}{2} [\partial_\mu (h_\rho \delta_{\mu\lambda} - h_\lambda \delta_{\nu\rho})$$

$$\left. + \partial_\nu (h_\lambda \delta_{\mu\rho} - h_\rho \delta_{\mu\lambda}) \right] D_1(u - v) \left. \right\}$$

with  $h_\mu = u_\mu - v_\mu$ , one has

$$\sigma_{\mu\nu} \sigma_{\rho\lambda} \langle F_{\mu\nu}(z) F_{\rho\lambda}(z') W_0 \rangle \quad (18)$$

$$= 6[D(z - z') + D_1(z - z')] - 4 \int \sigma_{\alpha\beta} ds_{\alpha\beta}(u) D(u - z) \times \int \sigma_{\gamma\delta} ds_{\gamma\delta}(v) D(v - z'),$$

where one should have in mind that, in  $ds_{\alpha\beta}$ , it is always implied  $\alpha < \beta$  both in (16) and, consequently, in (18).

Using now the identities

$$(Dz)_{xy} = (Dz)_{xu} d^4 u (Dz)_{uv} d^4 v (Dz)_{vy}, \quad (19)$$

$$\int_0^\infty ds \int_0^s d\tau_1 \int_0^{\tau_1} d\tau_2 f(s, \tau_1, \tau_2) \quad (20)$$

$$= \int_0^\infty ds \int_0^\infty d\tau_1 \int_0^\infty d\tau_2 f(s + \tau_1 + \tau_2, \tau_1 + \tau_2, \tau_2),$$

one can rewrite (5), (7) with insertion of (15) as

$$G_{q\bar{q}}(x, y) = G_{q\bar{q}}^{(0)}(x, y) \quad (21)$$

$$+ \text{tr}[\Gamma(m - \hat{D}) \Delta_{xu} \sigma_{\mu\nu} d^4 u \Delta_{uv} \sigma_{\rho\lambda} d^4 v \times \Delta_{vy} \bar{\Gamma}(m' - \hat{D}') \Delta_{yx} \langle F_{\mu\nu}(u) F_{\rho\lambda}(v) W_0 \rangle],$$

where we have defined

$$\Delta_{xu} \equiv \int_0^\infty ds e^{-K(s)} (Dz)_{xu}, \quad (22)$$

$$K(s) \equiv m^2 s + \frac{1}{4} \int_0^s \left( \frac{dz_\mu}{d\tau} \right)^2 d\tau.$$

An alternative derivation is given in [10]. Note that  $\langle W_0 \rangle$  depends on trajectories entering in  $\Delta_{zz'}$  in (21). One can now take into account that, when  $|x - u|$  is small, i.e.,  $|x - u| \lesssim T_g$ , the influence of  $\langle W_0 \rangle$  on  $\Delta_{xu}$  can be neglected, since  $\langle W_0 \rangle$  is a smooth function of its boundaries, varying when they are deformed at a scale larger than  $T_g$ , while  $\Delta_{xu}$  is singular for small  $|x - u|$ . Indeed, in this limit, neglecting the presence of  $\langle W_0 \rangle$ , one obtains

$$\Delta_{xu}^{(0)} = \frac{m}{4\pi^2} \frac{K_1(m|x - u|)}{|x - u|}. \quad (23)$$

For large  $|x - u|$ , one can use the fact that the product of the spinless quark Green's function  $\Delta_{xy}$  and that of the spinless antiquark  $\Delta_{yx}$  together with  $\langle W_0 \rangle$  yield the asymptotics of the total meson mass  $M_0$  without spin contributions and without SE corrections:

$$\int \Delta_{xy} \Delta_{yx} \langle W_0 \rangle \sim \exp(-M_0|x - y|). \quad (24)$$

Therefore, we shall use for  $\Delta_{xy}$  at large  $|x - y|$  the interpolation form

$$\Delta_{xu}(x) \cong \frac{\bar{m} K_1(\bar{m}|x|)}{4\pi^2|x|}, \quad (25)$$

$$\bar{m} = m + \tilde{M}_0, \quad \tilde{M}_0 \approx M_0/2.$$

(We do not need a high accuracy of (25), since it will enter in the small correction term.)

Now, inserting (18) into (21), one obtains the following combination:

$$J(u, v) = 6[D(u - v) + D_1(u - v)] \Delta_{uv} \quad (26)$$

$$- 4\sigma_{\alpha\beta} \sigma_{\gamma\delta}$$

$$\times \int ds_{\alpha\beta}(z) D(z - u) \int ds_{\gamma\delta}(w) D(w - v).$$

In the first term on the right-hand side of (26),  $\Delta_{uv}$  enters with the factors  $D(u - v)$  and  $D_1(u - v)$ , which fall off with small correlation length  $T_g$ .

Therefore, in [10],  $\Delta_{uv}$  was taken as  $\Delta_{uv}^{(0)}$ . Here, we tend to improve this result by taking into account the asymptotic falloff of  $\Delta_{uv}$  as in (24), (25). This can be done replacing in the free propagator by the  $\Delta_{uv}$  from (25) so that the asymptotics at both small and large distances is reproduced.

Identifying  $m_{\text{np}}^2$  from the expansion

$$(m^2 + \Delta m_{\text{np}}^2 - D^2)^{-1} = (m^2 - D^2)^{-1} \quad (27)$$

$$- (m^2 - D^2)^{-1} \Delta m_{\text{np}}^2 (m^2 - D^2)^{-1} + \dots,$$

one obtains

$$\Delta m_{\text{np}}^2 = - \int d^4 w \frac{\bar{m} K_1(\bar{m}|w|)}{4\pi^2|w|} \quad (28)$$

$$\times 6(D(|w|) + D_1(|w|)) + \sigma^2 \int \Delta_{xu} d^4(x - u).$$

We take the lattice estimate (for the quenched case [45]),  $D_1 \cong D/3$  and the relation [12]  $\sigma = \frac{1}{2} \int D(z) d^2 z$ , and obtain

$$\Delta m_{\text{np}}^2 = - \frac{4\sigma}{\pi} \varphi(t) + \frac{\sigma^2}{2(m + \tilde{M}_0)^2}, \quad (29)$$

$$t = (m + \tilde{M}_0) T_g.$$

Here,  $\varphi(t)$  is given in Appendix 2; it is normalized as  $\varphi(0) = 1$ . The first term on the right-hand side of (29) coincides with the result [10] when  $\tilde{M}_0$  is neglected [note, however, that the coefficients before  $D$  and  $D_1$  in [10] have a misprint and should be replaced by those in (26)], while the last term in (29), which is a correction to the first, is new. To understand the role of this term in creating the total mass of the meson (still without Coulomb correction and SD terms), we take the case of the heavy-light meson, i.e., when

**Table 1.** Mass eigenvalues (in GeV) and the function  $\varphi(t)$  according to Eqs. (31), (32) for different values of  $\alpha_s$ 

$\alpha_s$	$\omega_0$	$\varepsilon$	$\tilde{M}_0$	$\varphi(t)$	$\Delta M_{SE}$	$M = \tilde{M}_0 + \Delta M_{SE}$
0	0.448	0.735	0.96	0.416	-0.106	0.854
0.3	0.546	0.498	0.771	0.5	-0.105	0.666
0.39	0.594	0.407	0.704	0.525	-0.101	0.603

the quark is moving in the field of an infinitely heavy antiquark. The Hamiltonian in this case is written as in [19–21] with the SE term treated as in [10], namely,

$$H_0(\omega) = \frac{m^2 + \Delta m_{np}^2}{2\omega} + \tilde{M}_0(\omega), \quad (30)$$

where

$$\tilde{M}_0(\omega) = \frac{\omega}{2} + \varepsilon(\omega), \quad \varepsilon(\omega) = \frac{\sigma^{2/3} a(n)}{(2\omega)^{1/3}};$$

$a(0) = 2.338$ . Taking into account (29), one obtains the resulting expression for  $H_0(\omega)$ :

$$H_0(\omega) = \left( -\frac{4\sigma\varphi(t)}{\pi} + \frac{\sigma^2}{2(\tilde{M}_0 + m)^2} \right) \frac{1}{2\omega} + \tilde{M}_0(\omega). \quad (31)$$

Now  $\omega$  should be found from the equation [4, 7, 32]

$$\left. \frac{\partial H_0(\omega)}{\partial \omega} \right|_{\omega=\omega_0} = 0. \quad (32)$$

Neglecting in (32) the contribution of the SE term, one obtains the values of  $\omega_0$  and  $\tilde{M}_0(\omega_0)$ ,  $H_0(\omega_0) \equiv M$ , as in [4], which are shown in Table 1 (all masses are given in GeV).

For  $\alpha_s > 0$ , the values  $\varepsilon(\omega)$  and  $\tilde{M}_0 = \omega/2 + \varepsilon(\omega)$  have been calculated in [4] taking the color Coulomb term  $-(4/3)(\alpha_s/r)$  into account, while

$$\Delta M_{SE} = -\frac{2\sigma}{\pi\omega_0}\varphi(t)$$

and  $t = T_g \tilde{M}_0$ ,  $T_g = 1 \text{ GeV}^{-1}$ . One can see that  $\Delta M_{SE}$  is rather stable and gives a correction around 15% to the total mass. The correction of the second term on the right-hand side of (29) to the total  $\Delta m^2$  is of the order of 7% for  $m = 0$ , so that the earlier calculations made without this term in [14–18] and [22–24] would be modified by a few percent.

As the next comparison, one can take the solution of the Dirac equation for the heavy-light meson with confining and color Coulomb term present. In

**Table 2.** Masses and self-energy corrections (in GeV) for  $\sigma = 0.16 \text{ GeV}^2$  according to Eq. (31) in comparison with eigenvalues of the Dirac equation

$\alpha_s$	$\Delta M_{SE}$	$M = \tilde{M}_0 + \Delta M_{SE}$	$M_D$
0	-0.227	0.733	0.65
0.3	-0.186	0.585	0.465
0.39	-0.171	0.533	0.401

this case, the SE term is absent in the first-order Dirac Hamiltonian (in contrast to the second-order SA Hamiltonian, obtained from FFSR). The results of calculations performed in [47, 48] are shown in Table 2. In this case, to compare with the SA Hamiltonian (31), one should take  $T_g$  in  $\varphi(t)$  equal to zero, since the linear confining potential is obtained in this limit (while for  $T_g \neq 0$  there appear corrections to the linear potential calculated in [48]). Hence, in (31), one sets  $\varphi(t = 0) = 1$  and neglects as before the second correction term in brackets on the right-hand side. As a result, one obtains the masses listed in Table 2 for  $\sigma = 0.16 \text{ GeV}^2$  (all masses are given in GeV).

In the last column, the Dirac eigenvalues from [47, 48] are given to be compared with the eigenvalues of (31) in the adjacent column. One can see that Dirac eigenvalues are about 100 MeV lower. This difference can be attributed to the fact that, in the Dirac equation, both positive and negative eigenvalues (the latter corresponding to the backward-in-time motion of quark) are taken into account, while in (31) only positive values of  $\omega_0$  are considered. In the next section, we shall discuss how the negative modes (negative solutions for  $\omega_0$ ) can be included in the SA Hamiltonian.

#### 4. THE MATRIX HAMILTONIAN FOR THE HEAVY-LIGHT $q\bar{q}$ SYSTEM

We start with the Hamiltonian for the free Dirac particle  $\hat{H} = m\beta + \boldsymbol{\alpha} \cdot \mathbf{p}$ , which can be diagonalized using Foldy–Wouthuyzen (FW) procedure:

$$\hat{H} = U^+ \hat{H}_d U, \quad (33)$$

$$\hat{H}_d = \begin{pmatrix} \sqrt{\mathbf{p}^2 + m^2} & 0 \\ 0 & -\sqrt{\mathbf{p}^2 + m^2} \end{pmatrix}.$$

As is explained in detail in Appendix 1, the free

Green's function can be written in terms of  $\hat{H}_d$  as

$$S(t) = i\beta U \begin{pmatrix} \theta(t) & 0 \\ 0 & -\theta(-t) \end{pmatrix} e^{-i\hat{H}_d t} U^\dagger. \quad (34)$$

In Appendix 1, also the case of the Weyl representation is discussed for the Dirac particle in the external fields, which gives a representation similar to (34), i.e., having a diagonal Hamiltonian of the form of  $\hat{H}_d$  in the exponent for the time-dependent Green's function.

We now turn to the FFSR of the quark Green's function in the external gluonic field, written with the help of the einbein function  $\omega$  [4, 7] (this function was previously denoted as  $\mu$  in most papers):

$$S_q(x, y) = \int D\omega (D^3 z)_{\mathbf{x}, \mathbf{y}} \quad (35)$$

$$\times \exp \left[ - \int_0^T \left( \frac{m^2}{2\omega} + \frac{\omega}{2} + \frac{\omega \dot{z}_i^2}{2} \right) dt + ig \int_y^x A_\mu dz_\mu + g \int_0^T \sigma F \frac{dt}{2\omega} \right].$$

After vacuum averaging, this function can be associated with the Green's function of the heavy-light meson.

Here,  $D\omega$  is the path integration over functions  $\omega(t)$ , which in our formalism [4, 7] is calculated by the stationary point (steepest descent) method, after going over to the Hamiltonian form instead of the Lagrangian path integral form of (35), namely,

$$S_q(x, y) = \left\langle x \left| \int D\omega \exp \left[ -i \int_0^{T_M} \left( H_0(\omega) - g \frac{\sigma F}{2\omega} \right) dt_M \right] \right| y \right\rangle, \quad (36)$$

where we have changed from the Euclidean time  $t$  to the Minkowskian time  $t_M = -it$ , and

$$H_0(\omega) = \frac{m^2}{2\omega} + \frac{\omega}{2} + \frac{\mathbf{p}^2}{2\omega} + \sigma r. \quad (37)$$

Solving the Schrödinger-type equation

$$\left( \frac{\mathbf{p}^2}{2\omega} + \sigma r \right) \varphi_n = \varepsilon_n(\omega) \varphi_n, \quad (38)$$

one obtains

$$\varepsilon_n(\omega) = \frac{\sigma^{2/3}}{(2\omega)^{1/3}} a_n, \quad (39)$$

where  $a_n, n = 0, 1, 2, \dots$ , is the set of zeros of Eiry functions,  $a_0 \cong 2.338$ . As a result, for  $L = 0$ , one has the eigenvalues  $E_n^{(0)}(\omega)$  of  $H_0(\omega)$ , equal to

$$E_n^{(0)}(\omega) = \frac{m^2}{2\omega} + \frac{\omega}{2} + \frac{\sigma^{2/3}}{(2\omega)^{1/3}} a_n. \quad (40)$$

In our previous calculations of the spectrum, the stationary point in the integration over  $D\omega$  was taken at the positive solution of the equation

$$\left. \frac{\partial E_n^{(0)}(\omega)}{\partial \omega} \right|_{\omega=\omega_n^{(0)}} = 0, \quad \omega_n^{(0)} > 0. \quad (41)$$

However, there is a negative solution, at  $\omega_n = -\omega_n^{(0)}$ , which was neglected in all previous calculations.

The Hamiltonian (37) actually refers to the gauge-invariant system of a heavy-light  $q\bar{Q}$  system, where the infinitely heavy quark  $\bar{Q}$  propagates along the time axis and is located at the spatial origin.

In line with the Hamiltonian (33), we can write the total Hamiltonian of the  $q\bar{Q}$  system with the lower Dirac components as

$$\hat{H}_{q\bar{Q}} = \begin{pmatrix} h_0 & h_{+-} \\ h_{-+} & -h_0 \end{pmatrix}, \quad h_0 \varphi = E_n^{(0)} \varphi. \quad (42)$$

In  $h_0$ , the SD term  $g(\sigma F)/(2\omega)$  in the exponent of (36) does not contribute to the diagonal part of (42) for  $s$ -wave states of heavy-light mesons, except for the diagonal SE term considered in the previous section [this term can be added replacing  $m^2$  in (37), (40) by  $m^2 + \Delta m_{np}^2$ ].

Now we turn to the calculation of the terms  $h_{+-} = h_{-+}^*$ . To this end, one can use Eqs. (5), (6), (8), having in mind that, for the heavy-light meson, the Green's function of the heavy quark reduces to the parallel transporter  $\Phi(x, y)$  along a straight line and the factors  $ds'(Dz')_{xy} e^{-K'}$  are absent. Having in mind (4), one must calculate the factor

$$\langle W_{\sigma\sigma'}^{(2)}(x, y) \rangle \quad (43) \\ = \exp \left[ -\frac{g^2}{2} \int d\pi(1) d\pi(2) \langle F(1) F(2) \rangle \right].$$

In the product  $d\pi(1)d\pi(2)$ , the term  $ds(1)ds(2)$  contributes to the linear interaction and is present in  $H_0(\omega)$ ; the term  $d\tau(1)d\tau(2)$  was calculated in the previous section and in [10] and was taken into account in  $\Delta m_{\text{np}}^2$ . The mixed terms can be written as

$$\exp\left(-g^2 \int ds_{\mu\nu}(u)d\tau\right) \times \left\langle F_{\mu\nu}(u) \begin{pmatrix} \boldsymbol{\sigma} \cdot \mathbf{B} & \boldsymbol{\sigma} \cdot \mathbf{E} \\ \boldsymbol{\sigma} \cdot \mathbf{E} & \boldsymbol{\sigma} \cdot \mathbf{B} \end{pmatrix}_{z(\tau)} \right\rangle. \quad (44)$$

The diagonal terms in (44) contribute to the spin-orbit interaction, computed in [11], and vanish for the  $s$  states, while the nondiagonal terms contribute to  $h_{+-}$ ,  $h_{-+}$  and are calculated below. Writing

$$ds_{\mu\nu}F_{\mu\nu}(u) = ds_{i4}E_i(u) + ds_{ik}F_{ik} \quad (45)$$

$$= n_i d^2u E_i(u) + d\mathbf{s} \cdot \mathbf{B}, \quad \mathbf{n} = \frac{\mathbf{u}}{|\mathbf{u}|},$$

one should average this term with nondiagonal component  $\boldsymbol{\sigma} \cdot \mathbf{E}$  and neglect the last term, since the correlator (45)  $\langle B_i E_k \rangle$  is proportional to  $\partial D_1 / \partial u_l$  and small; as a result, one obtains the integral

$$\int d^2u \langle (\mathbf{n} \cdot \mathbf{E}(u)) (\boldsymbol{\sigma} \cdot \mathbf{E}(z(\tau))) \rangle \quad (46)$$

$$= \boldsymbol{\sigma} \cdot \mathbf{n} \int d^2u D(u-z) = \boldsymbol{\sigma} \cdot \mathbf{n} \sigma,$$

where we have taken into account the definition

$$\sigma = \frac{1}{2} \int d^2u D(u)$$

and the fact that  $z(\tau)$  lies on the quark trajectory, which is the boundary of the integration surface.

Finally, one must replace  $d\tau$  in (44) by  $dt$ , having in mind that upper matrix elements refer to the positive time evolution, while lower ones (corresponding to the negative-energy eigenvalues) refer to the negative (backward) time evolution, viz.,

$$\int d\tau \begin{pmatrix} a & c \\ d & b \end{pmatrix} = \begin{pmatrix} \int \frac{dt}{2\omega} a & \int \frac{dt}{2\omega} c \\ -\int \frac{dt}{2\omega} d & -\int \frac{dt}{2\omega} b \end{pmatrix}. \quad (47)$$

As a consequence, from (44) and (46), one obtains

$$h_{+-} = \frac{i\sigma}{2\omega} (\boldsymbol{\sigma} \cdot \mathbf{n}), \quad h_{-+} = -\frac{i\sigma}{2\omega} (\boldsymbol{\sigma} \cdot \mathbf{n}). \quad (48)$$

The energy eigenvalues of the matrix Hamiltonian (42) are obtained in the usual way from the equation

$$\det \begin{pmatrix} h_0 - E & h_{+-} \\ h_{-+} & h_0 - E \end{pmatrix} = 0, \quad h_0 \equiv E_n^{(0)}(\omega), \quad (49)$$

which yields

$$E = \pm \sqrt{h_0^2 + \left(\frac{\sigma}{2\omega}\right)^2}, \quad (50)$$

where  $\omega$  should be found from the condition  $\left. \frac{\partial E}{\partial \omega} \right|_{\omega=\omega_0} = 0$ , which replaces the old condition (41) and can be rewritten as

$$2h_0 h_0' - \frac{\sigma^2}{2\omega_0^3} = 0. \quad (51)$$

Writing  $h_0 = (m^2 - \Delta)/(2\omega) + M_0(\omega)$ , with  $\Delta = (4\sigma/\pi)\varphi(t)$ , one can rewrite (51) for the case  $m = 0$ ,  $T_g = 0$ ,  $\varphi \equiv 1$ :

$$\omega_0 = \bar{\omega}_0 \left\{ 1 - 2 \left( \frac{c_1}{\omega_0^2} - \Delta \right) \left( \frac{\omega_0}{\bar{\omega}_0} \right)^{4/3} \right\}^{3/4}, \quad (52)$$

where

$$c_1 = \frac{2\sigma}{\pi}, \quad \bar{\omega}_0 = \sqrt{2\sigma} \left( \frac{a}{3} \right)^{3/4}, \quad \Delta = \frac{\sigma^2}{4\omega_0^3 h_0(\omega_0)}.$$

Solving (52), one obtains for  $\sigma = 0.18 \text{ GeV}^2$

$$h_0(\omega_0) \approx 0.56 \text{ GeV}, \quad \omega_0 \approx 0.21 \text{ GeV}, \quad (53)$$

and the energy eigenvalue (50) is equal to

$$E_0 = E(\omega_0) = \pm 0.70 \text{ GeV}, \quad (54)$$

which should be compared with the Dirac eigenvalue from Table 2, recalculated for  $\sigma = 0.18 M_D$  =  $0.65\sqrt{0.18/0.16} = 0.689 \text{ GeV}$ . Thus, taking into account the matrix structure of the Hamiltonian diminishes the eigenvalue by  $\sim 0.1 \text{ GeV}$  and yields values in good agreement with an independent calculation of the Dirac equation.

It is of interest to compare this Hamiltonian with the Hamiltonian of the Dirac equation for a light quark in the static source of linear potential, considered in [47, 48]:

$$\hat{H}_D = \boldsymbol{\alpha} \cdot \mathbf{p} + \beta(m + \sigma r). \quad (55)$$

For the solution  $\psi_n(\mathbf{r})$  represented in the form [47]

$$\psi_n(\bar{r}) = \frac{1}{r} \begin{pmatrix} G_n(r)\Omega_{j\ell M} \\ iF_n(r)\Omega_{j\nu M} \end{pmatrix}, \quad (56)$$

the equation  $H_D \psi_n = \varepsilon_n \psi_n$  assumes the form

$$\begin{cases} \frac{dG_n}{dr} + \frac{\kappa}{r} G_n - (\varepsilon_n + m + \sigma r) F_n = 0, \\ \frac{dF_n}{dr} + \frac{\kappa}{r} F_n - (\varepsilon_n - m - \sigma r) G_n = 0, \end{cases} \quad (57)$$

where  $\kappa(j, l) = (j + 1/2)\text{sgn}(l - j)$ .

Equations (57) are invariant under the substitution  $(\varepsilon_n, G_n, F_n, \kappa) \leftrightarrow (-\varepsilon_n, F_n, G_n, -\kappa)$ . This means that, for every solution with  $\varepsilon_n > 0$  and  $\Psi_{\varepsilon_n}$  having the form (56), there exists another solution of the form

$$\psi_{-\varepsilon_n}(r) = \frac{1}{r} \begin{pmatrix} F_n(r)\Omega_{j'l'M} \\ iG_n(r)\Omega_{j'l'M} \end{pmatrix}, \quad (58)$$

which is characterized by  $-\varepsilon_n, -\kappa$ .

Following the idea of the FW transformation leading to (33), one can also assume that the Hamiltonian (55) can be diagonalized to the form

$$\hat{H}_D \rightarrow U^+ \begin{pmatrix} \hat{h}(\kappa) \\ -\hat{h}(-\kappa) \end{pmatrix} U,$$

where  $\hat{h}(\kappa)\varphi_n^\kappa = \varepsilon_n\varphi_n^\kappa$  and  $\hat{h}(-\kappa)\varphi_n^{-\kappa} = \varepsilon_n\varphi_n^{-\kappa}$ .

This brings us to the eigenvalue matrix (42). One special feature of this representation is that the states  $\psi_{\varepsilon_n}$  and  $\psi_{-\varepsilon_n}$  have different parities.

### 5. NEGATIVE-ENERGY STATES FOR THE $q\bar{q}$ MESONS

We are now considering the  $q\bar{q}$ -meson states made of light quarks. The Hamiltonian for positive-energy states was used repeatedly (see [32] for details) and has the form

$$H_0(\omega_1, \omega_2) = \frac{m_1^2 - \Delta_1}{2\omega_1} + \frac{m_2^2 - \Delta_2}{2\omega_2} + \frac{\omega_1 + \omega_2}{2} + \frac{\mathbf{p}^2}{2\tilde{\omega}} + \sigma r, \quad (59)$$

where  $\tilde{\omega} = \omega_1\omega_2/(\omega_1 + \omega_2)$ ,  $\Delta_i = (4\sigma/\pi)\varphi(t_i)$ , and  $t_i = (m_i + \tilde{M}_0)T_g$ . Turning now to the SD term ( $\sigma F$ ) in (8) and (35), one notes that, in addition to the one-quark corrections considered in the previous section, one has also the spin–spin term, previously treated in [11] and yielding the hyperfine interaction, namely, the term  $V_4$ . However, in the derivation, only the diagonal components of the matrix  $\langle \sigma_{\mu\nu}^{(1)} F_{\mu\nu} \sigma_{\alpha\beta}^{(2)} F_{\alpha\beta} \rangle$  have been taken into account, and now we shall look carefully into the nondiagonal terms.

From (8), one has the following contribution (note that, for the antiquark, the spin operator  $\sigma_{\mu\nu}^{(2)}$  enters with the sign opposite to  $\sigma_{\mu\nu}^{(1)}$ ):

$$\exp \left\{ -\frac{1}{2} \int_0^{s_1} d\tau_1 \int_0^{s_2} d\tau_2 g^2 \right\} \quad (60)$$

$$\times \left\langle \begin{pmatrix} \boldsymbol{\sigma}^{(1)} \cdot \mathbf{B} & \boldsymbol{\sigma}^{(1)} \cdot \mathbf{E} \\ \boldsymbol{\sigma}^{(1)} \cdot \mathbf{E} & \boldsymbol{\sigma}^{(1)} \cdot \mathbf{B} \end{pmatrix}_{z(\tau_1)} \times \begin{pmatrix} \boldsymbol{\sigma}^{(2)} \cdot \mathbf{B} & \boldsymbol{\sigma}^{(2)} \cdot \mathbf{E} \\ \boldsymbol{\sigma}^{(2)} \cdot \mathbf{E} & \boldsymbol{\sigma}^{(2)} \cdot \mathbf{B} \end{pmatrix}_{z(\tau_2)} \right\rangle,$$

and one should replace, as usual,  $d\tau_i = \pm dt_i/(2\omega_i)$ .

As a result, one obtains the following spin–spin terms in the Hamiltonian:

(i) From the product of diagonal components  $\langle \boldsymbol{\sigma}^{(1)} \cdot \mathbf{B} \boldsymbol{\sigma}^{(2)} \cdot \mathbf{B} \rangle$ , one has the usual hyperfine interaction [11, 32]

$$\hat{V}_{\text{hf}}^{(\text{diag})}(r) = \frac{\boldsymbol{\sigma}^{(1)} \cdot \boldsymbol{\sigma}^{(2)}}{12\omega_1\omega_2} \int_{-\infty}^{\infty} d\nu \quad (61)$$

$$\times \left[ 3D(r, \nu) + 3D_1(r, \nu) + 2r^2 \frac{\partial D_1}{\partial r^2}(r, \nu) \right],$$

where  $D(r, \nu) = D(\sqrt{r^2 + \nu^2})$ , and  $\mathbf{r} = \mathbf{z}_1(t) - \mathbf{z}_2(t)$  is the quark–antiquark distance, and we have used (17) to calculate  $\langle B_i(u)B_k(v) \rangle$ . Equation (61) contains both perturbative and nonperturbative contributions; the latter have been calculated in [11] and found to be much smaller than the perturbative ones, which can be easily calculated using the lowest order form of  $D_1$  [11],

$$D_1^{(\text{pert})}(x) = \frac{16}{3\pi} \frac{\alpha_s}{x^4} + O(\alpha_s^2), \quad (62)$$

which gives the standard result

$$\hat{V}_{\text{hf}}^{(\text{diag})} = \frac{8\pi\alpha_s \boldsymbol{\sigma}^{(1)} \cdot \boldsymbol{\sigma}^{(2)} \delta^{(3)}(\mathbf{r})}{9\omega_1\omega_2}. \quad (63)$$

The matrix element of (63) can be written in terms of radial wave function  $R_n(r)$ ,

$$\langle \hat{V}_{\text{hf}}^{(\text{diag})} \rangle = \frac{2\alpha_s \langle \boldsymbol{\sigma}^{(1)} \cdot \boldsymbol{\sigma}^{(2)} \rangle}{9\omega_1\omega_2} R_n^2(0) = \frac{4\alpha_s \tilde{\sigma}}{9(\omega_1 + \omega_2)} \begin{pmatrix} -3, & S = 0 \\ +1, & S = 1 \end{pmatrix}, \quad (64)$$

where  $\tilde{\sigma} \equiv \sigma + 4\alpha_s \langle r^{-2} \rangle/3$  (for more details, see Appendix 3 of [37]).

(ii) We now turn to the product of nondiagonal terms in (60), which can be written similarly to (61) as

$$\hat{V}_{\text{hf}}^{(\text{nond})}(r) = \frac{\boldsymbol{\sigma}^{(1)} \cdot \boldsymbol{\sigma}^{(2)}}{12\omega_1\omega_2} \quad (65)$$

$$\times \int_{-\infty}^{\infty} d\nu \left[ 3D + 3D_1 + (3\nu^2 + r^2) \frac{\partial D_1}{\partial r^2} \right].$$

Keeping again only the perturbative contribution, one easily obtains

$$\hat{V}_{\text{hf}}^{(\text{nond})} = -\hat{V}_{\text{hf}}^{(\text{diag})}. \quad (66)$$

Consider now the total Hamiltonian

$$\hat{H} = (H_0(\omega_1, \omega_2) + \hat{V}_{\text{hf}}^{(\text{diag})})\hat{1}_1\hat{1}_2 + \hat{V}_{\text{hf}}^{(\text{nond})}(\gamma_5)_1(\gamma_5)_2. \quad (67)$$

The energy eigenvalues can be found in the same way, as was done in the previous section:

$$E^{(\omega_1, \omega_2)} = \pm \sqrt{(H_0(\omega_1, \omega_2) + \hat{V}_{\text{hf}}^{(\text{diag})})^2 + (\hat{V}_{\text{hf}}^{(\text{nond})})^2}. \quad (68)$$

To illustrate the general result (68), we take the case of massless quarks and write the energy as

$$E(\omega) = \pm \sqrt{\left(h_0(\omega) + \frac{c_\sigma}{\omega}\right)^2 + \frac{c_\sigma^2}{\omega^2}}, \quad (69)$$

where  $h_0(\omega)$  is the eigenvalue of  $H_0(\omega_1, \omega_2)$ ,  $\omega_1 = \omega_2$ ,

$$h_0(\omega) = -\frac{\delta}{\omega} + \omega + \frac{c}{\omega^{1/3}}; \quad (70)$$

$$c = \sigma^{2/3}a(n), \quad a(0) = 2.338.$$

Also, we have defined

$$c_\sigma = \frac{2\alpha_s\tilde{\sigma}}{9} \begin{pmatrix} -3, & S=0 \\ 1, & S=1 \end{pmatrix}. \quad (71)$$

The crucial point is now that  $\omega$  is to be found, as before, from the minimum of  $E(\omega)$  (we assume that minimization of the eigenvalue  $E(\omega)$  instead of the operator Hamiltonian  $H(\omega_1, \omega_2)$  brings about a small correction, as was in the case of the one-channel Hamiltonian—see [7] and numerical analysis in the second reference of [7]). This section served as an illustration of positive–negative state mixing due to hyperfine interaction in  $\bar{q}q$  mesons. For lack of space, the detailed analysis of the corresponding change in the spectrum will be published elsewhere.

## 6. CONCLUSIONS

In this paper, a systematic discussion is started of the role of negative-energy components for quark bound states. The NEC are automatically taken into account in the one-body Dirac or Bethe–Salpeter formalism. In the latter case, however, the Bethe–Salpeter wave function contains for the  $q\bar{q}$  meson at least eight independent components and their relative role can be studied only numerically. A dedicated analysis of NEC was done in the quasipotential approximation of the Bethe–Salpeter equations [49] and

effects of NEC were found to be significant for the spectrum of mesons. Recently, another approach was introduced in [48, 50] and developed further in [51, 52], called the method of Dirac orbitals, where the quark bound state is expanded in a series of products of individual one-body Dirac states. In this case, the NEC effects are also taken into account, but other approximations are usually done (c.m. motion, higher components), which require a cross-check of all results and comparison to other formalisms.

The Hamiltonian formalism, in particular, the SA Hamiltonian, is physically transparent and mathematically simple; it reduces to the popular relativistic quark model Hamiltonian in its simplest form (when string motion is neglected), and therefore it is necessary to understand the role of NEC in the Hamiltonian form.

This is done in the present paper using the simplest bound system, the heavy-light meson, where the heavy quark plays the role of an external field, and therefore results can be compared to those of the Dirac equation. The comparison proceeds in two steps. Firstly, one takes in the Hamiltonian the one-body SE terms, which do not mix positive energy components and NEC. Here, a new correction term was obtained in Section 3, Eq. (31), in addition to the old one [10], which gives around 7% of the total. Secondly, the NEC mixing appears due to the nondiagonal matrix Hamiltonian elements. The stationary-point condition for the einbein variable  $\omega$  should now be applied to the eigenvalues of the total matrix Hamiltonian  $E(\omega)$ :

$$\hat{H} = \begin{pmatrix} h_0 & h_{+-} \\ h_{-+} & -h_0 \end{pmatrix}, \quad (72)$$

$$\det(\hat{H} - E(\omega)) = 0, \quad \frac{\partial E(\omega)}{\partial \omega} = 0.$$

The resulting stationary values  $\omega_0$  and  $E(\omega_0)$  are in good agreement with the eigenvalue of the Dirac operator  $E_D$ :

$$E(\omega_0) \cong E_D. \quad (73)$$

This procedure justifies the stationary analysis with respect to  $\omega$ , since for  $h_0(\omega)$  the stationary point does not exist for light quarks if the SE term  $-\Delta m^2/(2\omega)$  is included in  $h_0(\omega)$ , while for  $E(\omega)$  the stationary point  $\omega \equiv \omega_0$  always exists. In Section 5, the first step is done for arbitrary  $q\bar{q}$  systems, and the matrix Hamiltonian is written explicitly. The main lesson here is that NEC are mixed up by the hyperfine interaction and the doubly nondiagonal (for both quark and antiquark) terms can be calculated explicitly. Further analysis and numerous applications are relegated for lack of space to future publications.

However, even at this stage, it is clear that NEC are very important for the structure of the wave functions and eigenvalues of mesons. This is probably even more so for baryons, where NEC are responsible for the correct relativistic structure of baryon wave functions, which is clearly seen in the values of the  $g_A/g_V$  ratio [53].

ACKNOWLEDGMENTS

I am grateful to A.B. Kaidalov, I.M. Narodetsky, J.A. Tjon, M.A. Trusov, and J. Weda and members of the ITEP seminar theory group for useful discussions.

The work is supported by the Federal Program of the Russian Ministry of Industry, Science, and Technology no. 40.052.1.1.1112.

APPENDIX I

In this appendix, we shall derive several representations for the quark Green's function in the external non-Abelian field. We start with the standard FFSR as a warm-up. To this end, one writes first the proper-time representation in the Euclidean spacetime:

$$S = (m + \hat{D})^{-1} = (m - \hat{D})(m^2 - \hat{D}^2)^{-1} \quad (A.1)$$

$$= (m - \hat{D}) \int_0^\infty ds e^{-s(m^2 - \hat{D}^2)}.$$

Now one transforms (A.1) to the path integral as follows:

$$\langle x | \int_0^\infty ds e^{sD_\mu^2} | y \rangle = \langle x | e^{\varepsilon D_\mu^2(N)} | x_{N-1} \rangle \quad (A.2)$$

$$\times \langle x_{N-1} | e^{\varepsilon(D_\mu^2(N-1))} | x_{N-2} \rangle \dots \langle x_1 | e^{\varepsilon D_\mu^2(1)} | y \rangle.$$

In (A.2), the integration over all  $d^4x_1 \dots d^4x_{N-1}$  is implied and the relation  $s = \varepsilon N$  is used. Consider now one piece of the path in (A.2) and write

$$I_{n,n-1} \equiv \langle x_n | e^{\varepsilon(\partial_\mu - igA_\mu)^2} | x_{n-1} \rangle \quad (A.3)$$

$$= \langle x_n | p \rangle \frac{d^4p}{(2\pi)^4}$$

$$\times \exp \left[ \varepsilon \left( \partial_\mu - igA_\mu \left( \frac{x_n + x_{n-1}}{2} \right) \right)^2 \right]$$

$$\times \langle p | x_{n-1} \rangle = \frac{d^4p}{(2\pi)^4} \exp \left[ ip(x_n - x_{n-1}) \right.$$

$$\left. - \varepsilon \left( p_\mu - gA_\mu \left( \frac{x_n + x_{n-1}}{2} \right) \right)^2 \right].$$

Integration over  $d^4p$  in (A.3) gives

$$I_{n,n-1} = \frac{1}{(4\pi\varepsilon)^2} \quad (A.4)$$

$$\times \exp \left[ -\frac{(\Delta x)^2}{4\varepsilon} + ig\Delta x_\mu A_\mu \right],$$

$$\Delta x = x_n - x_{n-1}.$$

Insertion of (A.4) into (A.2) finally yields

$$S = (m - \hat{D}) \int_0^\infty ds e^{-sm^2} (Dz)_{xy} \exp \left[ -\frac{1}{4} \quad (A.5)$$

$$\times \int_0^s z_\mu^2 d\tau + ig \int_y^x A_\mu dz_\mu + g \int_0^s \sigma_{\mu\nu} F_{\mu\nu} d\tau \right],$$

where we have used the relation  $\hat{D}^2 = D_\mu^2 + g\sigma_{\mu\nu}F_{\mu\nu}$ .

Note that, in FFSR (A.5), the exponent contains  $\gamma$  matrices only in the spin term  $\sigma_{\mu\nu}F_{\mu\nu}$ , and moreover it commutes with  $\gamma_5$ . Therefore, in the chiral limit ( $m \rightarrow 0$ ),  $S$  is odd in  $\gamma_\mu$  irrespective of any vacuum averaging of terms containing  $A_\mu$  and  $F_{\mu\nu}$ . Hence, in this form, one cannot describe the effect of the chiral symmetry breaking and one should look for other representations, which will be a topic of other publications.

We start with the case of the free quark and write the Green's function in the energy and the time-dependent representations  $S(E)$  and  $S(t)$  (in the Minkowskian spacetime):

$$S(E) = \frac{1}{m + i\hat{p}} \quad (A.6)$$

$$= \frac{\beta}{\hat{H} - E} = \frac{\beta}{m\beta + \boldsymbol{\alpha} \cdot \mathbf{p} - E},$$

$$S(t) = \int_{-\infty}^\infty S(E) e^{-iEt} \frac{dE}{2\pi}.$$

Consider now the FW transformation of the free Hamiltonian

$$U^+ \hat{H} U = U^+ \begin{pmatrix} m & \boldsymbol{\sigma} \cdot \mathbf{p} \\ \boldsymbol{\sigma} \cdot \mathbf{p} & -m \end{pmatrix} U \equiv \hat{H}_d \quad (A.7)$$

$$= \begin{pmatrix} \sqrt{\mathbf{p}^2 + m^2} & 0 \\ 0 & -\sqrt{\mathbf{p}^2 + m^2} \end{pmatrix},$$

where

$$U = \begin{pmatrix} \cos \hat{\theta} & -\sin \hat{\theta} \\ \sin \hat{\theta} & \cos \hat{\theta} \end{pmatrix}, \quad (A.8)$$

$$U^+ = \begin{pmatrix} \cos \hat{\theta} & \sin \hat{\theta} \\ -\sin \hat{\theta} & \cos \hat{\theta} \end{pmatrix},$$

and

$$\begin{aligned} \sin 2\hat{\theta} &= \frac{\boldsymbol{\sigma} \cdot \mathbf{p}}{\sqrt{\mathbf{p}^2 + m^2}}, \\ \cos 2\hat{\theta} &= \frac{m}{\sqrt{\mathbf{p}^2 + m^2}}, \quad \hat{\theta} = \frac{1}{2} \arctan \left( \frac{\boldsymbol{\sigma} \cdot \mathbf{p}}{m} \right). \end{aligned} \quad (\text{A.9})$$

Consequently, one has

$$S(E) = \beta U \frac{1}{\hat{H}_d - E} U^+, \quad (\text{A.10})$$

$$S(t) = \frac{\beta}{2\pi} U \int_{-\infty}^{\infty} \frac{dE(\hat{H}_d + E)}{\mathbf{p}^2 + m^2 - E^2} U^+ e^{-iEt}.$$

Integrating in (A.10), one gets finally

$$S(t) = i\beta U \begin{pmatrix} \theta(t) & \\ & -\theta(-t) \end{pmatrix} U^+ \times e^{-i\sqrt{\mathbf{p}^2 + m^2}|t|}. \quad (\text{A.11})$$

Another form can be given to  $S(E)$ , using the proper-time representation:

$$\begin{aligned} S(E) &= \frac{1}{m + i\hat{p}} \\ &= i\beta \int_0^{\infty} \exp[-i(m\beta + \boldsymbol{\alpha} \cdot \mathbf{p} + ip_4)s] ds \\ &= i\beta U \int_0^{\infty} \exp[-i(\hat{H}_d + ip_4)s] ds U^+. \end{aligned} \quad (\text{A.12})$$

The form (A.12) is interesting since it contains the matrix Hamiltonian in the exponent, and we shall use it now to take into account external field  $A_\mu$ . The form (A.7) is especially convenient in the non-relativistic case, when  $|\mathbf{p}| \ll m$ , and then also  $\theta \ll 1$ , and the FW transformation is nearly diagonal. In the opposite case,  $|\mathbf{p}| \gg m$ , one needs to start from another representation of  $\gamma$  matrices, namely, the Weyl representation,

$$(E - \mathbf{p} \cdot \boldsymbol{\sigma}_W - m\gamma_0^{(W)})\psi = 0; \quad (\text{A.13})$$

$$\boldsymbol{\sigma}_W = \begin{pmatrix} \boldsymbol{\sigma} & 0 \\ 0 & -\boldsymbol{\sigma} \end{pmatrix}, \quad \gamma_0^{(W)} = \begin{pmatrix} 0 & 1 \\ 1 & 0 \end{pmatrix},$$

so that the Green's function in the Weyl representation is

$$S_W(E) = (\boldsymbol{\sigma}_W \cdot \mathbf{p} + m\gamma_0^{(W)} - E)^{-1}. \quad (\text{A.14})$$

Doing the FW transformation, one has, similarly to (A.7),

$$U_W^+ \hat{H}_W U_W \quad (\text{A.15})$$

$$= \hat{H}_d^{(W)} = \begin{pmatrix} \sqrt{\mathbf{p}^2 + m^2} \frac{\boldsymbol{\sigma} \cdot \mathbf{p}}{|\mathbf{p}|} & 0 \\ 0 & -\sqrt{\mathbf{p}^2 + m^2} \frac{\boldsymbol{\sigma} \cdot \mathbf{p}}{|\mathbf{p}|} \end{pmatrix},$$

where

$$U_W = \begin{pmatrix} \cos \theta_W & -\sin \theta_W \\ \sin \theta_W & \cos \theta_W \end{pmatrix} \equiv e^{-it_2 \theta_W}, \quad (\text{A.16})$$

$$\theta_W = \frac{1}{2} \arctan \frac{m\boldsymbol{\sigma} \cdot \mathbf{p}}{\mathbf{p}^2},$$

and  $t_2 \equiv \sigma_2$  is the Pauli matrix in the helicity indices.

We now use the proper-time representation for  $S_W(E)$ ,

$$S_W(E) \quad (\text{A.17})$$

$$= \left\langle x \left| \int_0^{\infty} ds \exp[is(\boldsymbol{\sigma}_W \cdot \mathbf{P} + m\gamma_0^{(W)} + iP_4)] \right| y \right\rangle,$$

where  $\mathcal{P}_\mu = \frac{1}{i}\partial_\mu - gA_\mu$ , and split the interval  $(x, y)$  into  $N$  steps as in (A.2),  $N\varepsilon = s$ . One has

$$I_{n,n-1}^{(W)} \quad (\text{A.18})$$

$$\begin{aligned} &\equiv \left\langle x_n \left| \exp[i\varepsilon(\boldsymbol{\sigma}_W \cdot \mathbf{P} + m\gamma_0 + iP_4)] \right| x_{n-1} \right\rangle \\ &= \int \frac{d^4 p}{(2\pi)^4} e^{ip(x_n - x_{n-1})} U_W(\theta_W(n)) \\ &\quad \times \exp[i\varepsilon(\hat{H}_d^{(W)}(n) + iP_4(n))] U_W^+(\theta_W(n)). \end{aligned}$$

As in (A.3), one can write  $\mathcal{P}_\mu = p_\mu - gA_\mu$  and integrate over  $d^4 p$ , representing the square-root terms in  $\hat{H}_d^{(W)}$  through the einbein function  $\mu(x_4)$ ,

$$e^{i\varepsilon\sqrt{\mathbf{p}+m^2}} \quad (\text{A.19})$$

$$\sim \int d\mu_n \exp \left[ i \left( \frac{\mathbf{p}^2 + m^2}{2\mu_n} + \frac{\mu_n}{2} \right) \varepsilon \right];$$

one can also use the identity

$$e^{ia\boldsymbol{\sigma} \cdot \mathbf{n}} = e^{ia \frac{(1 + \boldsymbol{\sigma} \cdot \mathbf{n})}{2}} + e^{-ia \frac{(1 - \boldsymbol{\sigma} \cdot \mathbf{n})}{2}}. \quad (\text{A.20})$$

Now the integration over  $d^4 p$  yields

$$\begin{aligned} I_{n,n-1}^{(W)} &= \int d\mu_n \left( \frac{\mu_n}{2\pi\varepsilon} \right)^2 U_W(\theta_W(n)) \\ &\quad \times e^{igA_\mu \Delta x_\mu} G(n) U_W^+(\theta_W(n)), \end{aligned} \quad (\text{A.21})$$

where we have defined the diagonal matrix  $G(n)$  with elements

$$\begin{aligned}
 G_{++}(n) &= \exp \left\{ -\Delta x_4 \right. & (A.22) \\
 &\times \left. \left[ \frac{\mu}{2}(\dot{\mathbf{x}}^2 + 1) + \frac{m^2}{2\mu} \right] \right\} \theta(\Delta x_4) \\
 &\times \frac{1 + \boldsymbol{\sigma} \cdot \mathbf{n}}{2} + \exp \left\{ \Delta x_4 \left[ \frac{\mu}{2}(\dot{\mathbf{x}}^2 + 1) + \frac{m^2}{2\mu} \right] \right\} \\
 &\times \theta(-\Delta x_4) \frac{1 - \boldsymbol{\sigma} \cdot \mathbf{n}}{2}, \\
 G_{--}(n) &= \exp \left\{ -\Delta x_4 \left[ \frac{\mu}{2}(\dot{\mathbf{x}}^2 + 1) + \frac{m^2}{2\mu} \right] \right\} \\
 &\times \theta(\Delta x_4) \frac{1 - \boldsymbol{\sigma} \cdot \mathbf{n}}{2} \\
 &+ \exp \left\{ \Delta x_4 \left[ \frac{\mu}{2}(\dot{\mathbf{x}}^2 + 1) + \frac{m^2}{2\mu} \right] \right\} \\
 &\times \frac{1 + \boldsymbol{\sigma} \cdot \mathbf{n}}{2} \theta(-\Delta x_4),
 \end{aligned}$$

and  $\dot{\mathbf{x}} = \Delta \mathbf{x} / \Delta x_4$ ,  $\Delta x_\mu = (x_n - x_{n-1})_\mu$ , while  $\mathbf{p}$  residing in  $\theta_W$  is  $\mathbf{p} = \mu \dot{\mathbf{x}}$ .

APPENDIX 2

The function  $\varphi(t)$ ,  $t \equiv m/\delta$ , defined in Eq. (29), can be written as (note the difference in definitions here and in [10])

$$\varphi(t) = t \int_0^\infty z^2 dz K_1(tz) e^{-z}, \quad (A.23)$$

where  $K_1$  is the Macdonald function,  $K_1(x)(x \rightarrow 0) \approx 1/x$ , so that, for  $t = 0$ , one obtains

$$\varphi(0) = 1. \quad (A.24)$$

For  $t > 0$ , the integration in (A.23) yields two different forms; for  $t < 1$ ,

$$\begin{aligned}
 \varphi(t) &= -\frac{3t^2}{(1-t^2)^{5/2}} & (A.25) \\
 &\times \ln \frac{1 + \sqrt{1-t^2}}{t} + \frac{1+2t^2}{(1-t^2)^2},
 \end{aligned}$$

while for  $t > 1$  one has, instead,

$$\begin{aligned}
 \varphi(t) &= -\frac{3t^2}{(t^2-1)^{5/2}} & (A.26) \\
 &\times \arctan(\sqrt{t^2-1}) + \frac{1+2t^2}{(1-t^2)^2}.
 \end{aligned}$$

For large  $t$ , one has the following limiting behavior:

$$\varphi(t) = \frac{2}{t^2} - \frac{3\pi}{2t^3} + O\left(\frac{1}{t^4}\right). \quad (A.27)$$

For small  $t$ , one obtains, expanding the right-hand side of (A.25),

$$\begin{aligned}
 \varphi(t) &= 1 + t^2 \left( 4 - 3 \ln \frac{2}{t} \right) & (A.28) \\
 &+ t^4 \left( \frac{7}{4} - \frac{15}{2} \ln \frac{2}{t} \right) + O(t^6).
 \end{aligned}$$

Some numerical values are useful in applications:

$$\varphi(0.175) \cong 0.88, \quad \varphi(1.7) \cong 0.234, \quad \varphi(5) \cong 0.052.$$

REFERENCES

1. R. Jackiw, Rev. Mod. Phys. **52**, 661 (1980); T. D. Lee, *Particle Physics and Introduction to Field Theory* (Harwood, New York, 1981); Yu. A. Simonov, Yad. Fiz. **41**, 1311 (1985) [Sov. J. Nucl. Phys. **41**, 835 (1985)].
2. D. P. Stanley and D. Robson, Phys. Rev. D **21**, 3180 (1980); J. Carlson, J. Kogut, and V. R. Pandharipande, Phys. Rev. D **27**, 233 (1983); J. L. Basdevant and S. Boukraa, Z. Phys. C **28**, 413 (1985); J. M. Richard and P. Taxil, Phys. Lett. B **128B**, 453 (1983); Ann. Phys. (N.Y.) **150**, 263 (1983).
3. S. Godfrey and N. Isgur, Phys. Rev. D **32**, 189 (1985); S. Capstick and N. Isgur, Phys. Rev. D **34**, 2809 (1986).
4. Yu. A. Simonov, Phys. Lett. B **226**, 151 (1989); Z. Phys. C **53**, 419 (1992); Yad. Fiz. **54**, 192 (1991) [Sov. J. Nucl. Phys. **54**, 115 (1991)].
5. Yu. A. Simonov, Phys. Lett. B **228**, 413 (1989); M. Fabre de la Ripelle and Yu. A. Simonov, Ann. Phys. (N. Y.) **212**, 235 (1991).
6. Yu. A. Simonov, Phys. Lett. B **249**, 514 (1990); Preprint TPI-MINN-90/19-T.
7. A. Yu. Dubin, A. B. Kaidalov, and Yu. A. Simonov, Phys. Lett. B **323**, 41 (1994); Yad. Fiz. **56**, (12), 213 (1993) [Phys. At. Nucl. **56**, 1745 (1993)]; V. L. Morgunov, A. V. Nefediev, and Yu. A. Simonov, Phys. Lett. B **459**, 653 (1999).
8. A. M. Polyakov, *Gauge Fields and Strings* (Harwood Acad., New York, 1987); A. Yu. Dubin, Pis'ma Zh. Èksp. Teor. Fiz. **56**, 565 (1992) [JETP Lett. **56**, 545 (1992)]; Yu. S. Kalashnikova and A. V. Nefediev, Yad. Fiz. **60**, 1333 (1997) [Phys. At. Nucl. **60**, 1389 (1997)]; **61**, 871 (1998) [**61**, 785 (1998)].
9. B. O. Kerbikov and Yu. A. Simonov, Phys. Rev. D **62**, 093016 (2000).
10. Yu. A. Simonov, Phys. Lett. B **515**, 137 (2001).
11. Yu. A. Simonov, Nucl. Phys. B **324**, 67 (1989); A. M. Badalian and Yu. A. Simonov, Yad. Fiz. **59**, 2247 (1996) [Phys. At. Nucl. **59**, 2164 (1996)].

12. H. G. Dosch, Phys. Lett. B **190**, 177 (1987); Yu. A. Simonov, Nucl. Phys. B **307**, 512 (1988); for a review see A. Di Giacomo, H. G. Dosch, V. I. Shevchenko, and Yu. A. Simonov, Phys. Rep. **372**, 319 (2002); hep-ph/0007223.
13. Yu. A. Simonov, Pis'ma Zh. Éksp. Teor. Fiz. **71**, 187 (2000) [JETP Lett. **71**, 127 (2000)]; V. I. Shevchenko and Yu. A. Simonov, Phys. Rev. Lett. **85**, 1811 (2000).
14. A. M. Badalian, B. L. G. Bakker, and Yu. A. Simonov, Phys. Rev. D **66**, 034026 (2002).
15. A. M. Badalian and B. L. G. Bakker, Phys. Rev. D **66**, 034025 (2002); hep-ph/0202246.
16. A. M. Badalian, V. L. Morgunov, and B. L. G. Bakker, Yad. Fiz. **63**, 1722 (2000) [Phys. At. Nucl. **63**, 1635 (2000)].
17. A. M. Badalian and B. L. G. Bakker, Phys. Rev. D **64**, 114010 (2001).
18. A. M. Badalian and B. L. G. Bakker, Phys. Rev. D **67**, 071901 (2003); hep-ph/0302200.
19. Yu. A. Simonov, Z. Phys. C **53**, 419 (1992).
20. Yu. S. Kalashnikova, A. V. Nefediev, and Yu. A. Simonov, Phys. Rev. D **64**, 014037 (2001).
21. Yu. S. Kalashnikova and A. V. Nefediev, Phys. Lett. B **492**, 91 (2000); hep-ph/0008242.
22. Yu. A. Simonov, Phys. Rev. D **65**, 116004 (2002).
23. Yu. A. Simonov, Yad. Fiz. **66**, 363 (2003) [Phys. At. Nucl. **66**, 338 (2003)].
24. I. M. Narodetskii and M. A. Trusov, Yad. Fiz. **65**, 949 (2002) [Phys. At. Nucl. **65**, 917 (2002)].
25. A. B. Kaidalov and Yu. A. Simonov, Phys. Lett. B **477**, 163 (2000).
26. A. B. Kaidalov and Yu. A. Simonov, Yad. Fiz. **63**, 1507 (2000) [Phys. At. Nucl. **63**, 1428 (2000)].
27. Yu. A. Simonov, in *Proceedings of the Workshop on Physics and Detectors for DAΦNE, Frascati, 1991*; Nucl. Phys. B (Proc. Suppl.) **23B**, 283 (1991); Nuovo Cimento A **107**, 2629 (1994).
28. Yu. S. Kalashnikova and Yu. B. Yufryakov, Phys. Lett. B **359**, 175 (1995); Yu. Yufryakov, hep-ph/9510358.
29. Yu. S. Kalashnikova and D. S. Kuzmenko, Yad. Fiz. **64**, 1796 (2001) [Phys. At. Nucl. **64**, 1716 (2001)]; **66**, 988 (2003) [**66**, 955 (2003)]; hep-ph/0203128; hep-ph/03022070.
30. Yu. A. Simonov, *QCD: Confinement, Hadron Structure and DIS*, in *Proceedings of the International Conference "I.Ya. Pomeranchuk and Physics at the Turn of Centuries"*, Moscow, 2003.
31. Yu. A. Simonov, Nucl. Phys. B **592**, 350 (2001); M. Eidemueller, H. G. Dosch, and M. Jamin, Nucl. Phys. B (Proc. Suppl.) **86**, 421 (2000).
32. Yu. A. Simonov, in *QCD: Perturbative or Nonperturbative*, Ed. by L. Ferreira *et al.* (World Sci., Singapore, 2001); hep-ph/9911237.
33. Yu. A. Simonov, Yad. Fiz. **66**, 2088 (2003) [Phys. At. Nucl. **66**, 2038 (2003)]; hep-ph/0210309.
34. Yu. A. Simonov and J. A. Tjon, Ann. Phys. (N.Y.) **300**, 54 (2002).
35. Yu. A. Simonov, Yad. Fiz. **67**, 868 (2004) [Phys. At. Nucl. **67**, 846 (2004)]; hep-ph/0302090.
36. S. N. Fedorov and Yu. A. Simonov, Pis'ma Zh. Éksp. Teor. Fiz. **78**, 67 (2003) [JETP Lett. **78**, 57 (2003)]; hep-ph/0306216.
37. Yu. A. Simonov, Yad. Fiz. **67**, 1050 (2004) [Phys. At. Nucl. **67**, 1027 (2004)]; hep-ph/0305281.
38. Yu. A. Simonov, Yad. Fiz. **67**, 571 (2004) [Phys. At. Nucl. **67**, 553 (2004)]; hep-ph/0306310.
39. Yu. A. Simonov, hep-ph/0310031.
40. Yu. A. Simonov, Yad. Fiz. **64**, 1959 (2001) [Phys. At. Nucl. **64**, 1876 (2001)]; hep-ph/0110033.
41. Yu. A. Simonov and J. A. Tjon, Ann. Phys. (N.Y.) **228**, 1 (1993).
42. M. Halpern, Phys. Rev. D **19**, 517 (1979); I. Aref'eva, Theor. Math. Phys. **43**, 353 (1980); N. Bralic, Phys. Rev. D **22**, 3090 (1980); Yu. A. Simonov, Yad. Fiz. **50**, 213 (1989) [Sov. J. Nucl. Phys. **50**, 134 (1989)]; M. Hirayama and S. Matsubara, Prog. Theor. Phys. **99**, 691 (1998); hep-th/9712120.
43. B. S. De Witt, Phys. Rev. **162**, 1195, 1239 (1967); J. Honerkamp, Nucl. Phys. B **48**, 269 (1972); G. 't Hooft, Nucl. Phys. B **62**, 444 (1973); Lect. at Karpacz, Acta Univ. Wratislaviensis **368**, 345 (1976); L. F. Abbot, Nucl. Phys. B **185**, 189 (1981).
44. Yu. A. Simonov, Yad. Fiz. **58**, 113 (1995) [Phys. At. Nucl. **58**, 107 (1995)]; Pis'ma Zh. Éksp. Teor. Fiz. **57**, 513 (1993) [JETP Lett. **57**, 525 (1993)]; Lect. Notes Phys. **479**, 139 (1997).
45. A. Di Giacomo and H. Panagopoulos, Phys. Lett. B **285**, 133 (1992); A. Di Giacomo, E. Meggiolaro, and H. Panagopoulos, Nucl. Phys. B **483**, 371 (1997); M. D'Elia, A. Di Giacomo, and E. Meggiolaro, Phys. Lett. B **408**, 315 (1997).
46. F. J. Yndurain, *The Theory of Quark and Gluon Interactions*, 3rd ed. (Springer, Berlin, 1999).
47. V. D. Mur, V. S. Popov, Yu. A. Simonov, and V. P. Yurov, Zh. Éksp. Teor. Fiz. **105**, 3 (1994) [J. Exp. Theor. Phys. **78**, 1 (1994)];
48. Yu. A. Simonov and J. A. Tjon, Phys. Rev. D **62**, 014501 (2000).
49. P. C. Tiemeijer and J. A. Tjon, Phys. Rev. C **48**, 896 (1993).
50. Yu. A. Simonov, Yad. Fiz. **62**, 2087 (1999) [Phys. At. Nucl. **62**, 1932 (1999)]; hep-ph/9912383.
51. Yu. A. Simonov, J. A. Tjon, and J. Weda, Phys. Rev. D **65**, 094013 (2002).
52. J. A. Tjon and J. Weda, Yad. Fiz. **68**, 621 (2005) [Phys. At. Nucl. **68**, 591 (2005)]; hep-ph/0403177.
53. Yu. A. Simonov and M. A. Trusov (in preparation).